A STUDY OF THE IONIZATION PROPERTIES OF HYDROGEN

IN THE PRESENCE OF RELATIVELY STRONG

MAGNETOSTATIC FIELDS

By

JAMES RUSSELL McDOUGAL

Bachelor of Science
University of Kansas
Lawrence, Kansas
1952

Master of Science
Tohoku University
Sendai, Japan
1957

Submitted to the faculty of the Graduate College
of the Oklahoma State University
in partial fulfillment of the requirements
for the degree of
DOCTOR OF PHILOSOPHY
May, 1968

Name: James Russell McDougal   Date of Degree: May, 1968

Institution: Oklahoma State University Location: Stillwater, Oklahoma

Title of Study: A STUDY OF THE IONIZATION PROPERTIES OF HYDROGEN IN
THE PRESENCE OF RELATIVELY STRONG MAGNETOSTATIC FIELDS

Pages in Study: 311   Candidate for Degree of Doctor of Philosophy

Major Field: Electrical Engineering

Scope of Study: The objective of this study is to present an engineering
orientated investigation into the ionization properties of hydrogen
in the presence of a relatively strong magnetostatic field (i.e.,
approximately 0.6 to 5 kilogauss) with rf excitation over the
frequency range of 2 to 30 MHz. The method of study involves an
analysis based upon solutions to the Lorentz Force Equation, the
design and construction of an experimental system and apparatus for
taking data in the framework of this theory, and the tabulation and
analysis of the experimental results obtained from this system.
The experimental work is carried out at reduced pressures, varying
approximately from one to six millimeters of mercury.

Findings and Conclusions: Certain values of magnetic intensity are found
to be optimum in the sense that their application allows a minimal
degree of ionization to be maintained in the gas with the least
magnitude of rf excitation. This is explained as the result of a
resonance phenomenom which was predicted in the analysis. An ex-
tensive data mapping of these optimum magnetic intensity values
throughout the range of excitation frequencies is given and compared
with the theory. Reasonable agreement is found at the lower excita-
tion frequencies, but it is concluded that the theory is not adequate
to predict conditions at the higher excitation frequencies. It is
hoped that the results of this study may be of aid to those search-
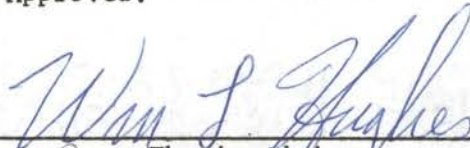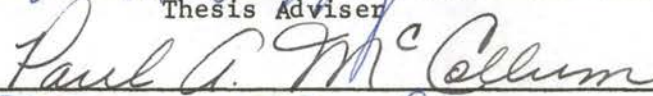ing for new and improved methods of energy conversion.

ADVISER'S APPROVAL _____

A STUDY OF THE IONIZATION PROPERTIES OF HYDROGEN
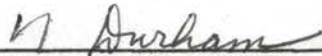
IN THE PRESENCE OF RELATIVELY STRONG

MAGNETOSTATIC FIELDS

Thesis Approved:

_____

Thesis Adviser

_____

_____

_____

Dean of the Graduate College

ii

PREFACE

Ionization phenomena of various and sundry sort have been studied for many years. Sir J. J. Thomson in his <u>Conduction of Electricity Through Gases</u> (1928) (1) quotes references dating well back into the 19th Century. This is understandable since such phenomena, generally speaking, exhibits striking effects. One finds literally reams of literature relating to detailed observations of the glow seen in gaseous discharge tubes, and I must admit that even after working with ionization cells for a period of three years there still exists an aura of excitement at the instant in an experiment when the glow first appears. This area has long been very much the exclusive domain of the experimental physicist, but fortunately for the rest of us recent advances in technology, the exploration of space, and increasing concern with the conservation of the earth's dwindling sources of energy have all given the study of ionization phenomena a practical significance which it did not previously enjoy. With the promise of practical and economic benefits to be ultimately obtained, the engineer gains his excuse, and with luck, the money necessary for entering this exciting and extremely complicated field.

This thesis attempts to present an engineering orientated study, for which the incentive came from fuel cell research, of the ionization properties of hydrogen in the presence of a relatively strong magnetostatic field with rf excitation. It cumulates in the presentation of an Optimum Magnetic Intensity Mapping of Hydrogen. Here, the optimum

magnetic intensity is that value of applied magnetostatic field which allows a minimal degree of ionization to be continuously maintained in the gas with the least magnitude of rf excitation. The mapping presented in Chapter V of this thesis covers the measurement of optimum magnetic intensity throughout the range of 2 to 30 MHz in excitation frequencies as a function of the parameters pressure, applied voltage, and current through the ionization cell. All measurements were performed at reduced pressures, varying approximately from one to six millimeters of mercury. It is hoped that this information may aid in the conception of new and improved methods of energy conversion.

TABLE OF CONTENTS

LIST OF TABLES

LIST OF FIGURES

CHAPTER I

INTRODUCTION

Townsend's Theory of Ionization

Interest in ionization became strong at about the turn of the

century in connection with investigations into the basic structure of

matter. One of the earliest investigations, and one which set a

pattern for the interpretation of results which is employed to this

present day was reported by J. S. Townsend[1] in 1900. Townsend conducted

his experiment with air in an evacuated glass tube at pressures of

2 and 8 mm Hg in which parallel plane electrodes had been installed,

somewhat as shown in Figure 1 below. Townsend observed that at these
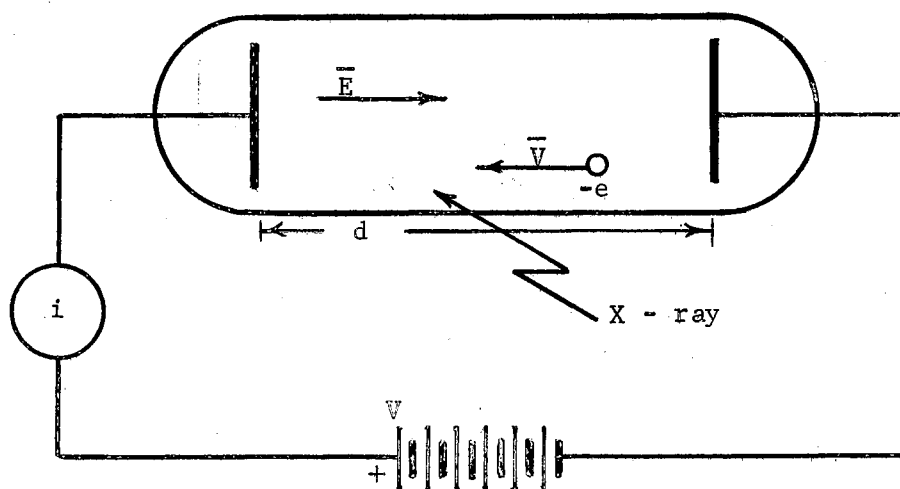
Figure 1. Townsend's Experiment

---

[1]J. S. Townsend, Nature, 62:340 (1900).

pressures and with applied electric intensities, V/d, up to about 10 volts per centimeter, the total current measured was due to the electrons produced through ionization by the X-rays. At greater applied electric intensities, Townsend observed that the current increased and he based his explanation of this phenomenon upon an argument of essentially the following nature.

Suppose that n electrons in moving a distance dx in the gas produce α ndx others, where α is a constant depending upon the applied electric intensity and pressure.

Then,

$$dn = \alpha n dx, \qquad (1.1)$$

or

$$\frac{dn}{n} = \alpha dx \qquad (1.2)$$

which integrates to give

$$n = K\epsilon^{\alpha x} \qquad (1.3)$$

where ϵ is the base of natural logarithms. At x = 0, the number of electrons will be those produced by the X-rays, say n_o. Inserting this initial condition, Equation (3) is written

$$n = n_o \epsilon^{\alpha x} \qquad (1.4)$$

and the total number of electrons produced in traveling the distance between the electrodes, d, will be:

$$N = \int_o^d n_o \epsilon^{\alpha x} dx = \frac{n_o}{\alpha} (\epsilon^{\alpha d} - 1). \qquad (1.5)$$

The total number of electrons produced by the X-rays alone is obtained by setting $\alpha = 0$ in the above integral, in which case integration gives

$$N' = n_o d \qquad (1.6)$$

and we may combine Equation (5) and (6) to write:

$$\frac{N}{N'} = \frac{1}{\alpha d} \left(e^{\alpha d} - 1 \right). \tag{1.7}$$

Now, assuming all of the carriers to have the same charge and travel with the same velocity, which would be the case for electrons in the absence of a space charge, Equation (7) may be written as

$$\frac{i}{i_o} = \frac{1}{\alpha d} \left(e^{\alpha d} - 1 \right). \tag{1.8}$$

in terms of current. Townsend based his interpretations upon an equation of the form of (8) above. However, in more modern work it is customary to note that Equation (8) approaches the limit

$$i = i_o e^{\alpha d} \tag{1.9}$$

as the separation, d, between the electrodes becomes very small. As this is, of necessity (i.e., in order to obtain the desired degree of uniformity in the applied electric field), sufficiently close to the usual case in practice, most references[2,3,4] refer to Equation (9) as Townsend's equation. The constant α is called the Townsend ionization coefficient, or simply ionization coefficient. It is usually measured by varying the electrode spacing and pressure in such a manner as to maintain a constant ratio of electric intensity to pressure, E/P. The ionization coefficient is then determined as the slope of the curve obtained by plotting the logarithm of the measured values of current versus the electrode spacing at a specified value of E/P.

In a broad sense, Townsend's equation is generally considered to apply up to the point where the gas breaks down, although the equation

[2] M. A. Harrison and R. Geballe, Phys. Rev., 91:1 (1953).

[3] D. J. Rose, Phys. Rev., 104:273 (1956).

[4] D. J. DeBitetto and L. H. Fisher, Phys. Rev., 104:1213 (1956).

requires modification[5] if the finer details are to be taken into
account. Contemporary studies[6] with crossed static electric and magnetic
fields also follow this basic pattern, with the addition of a constant
magnetic field to pressure ratio, H/P. Apparently, the Townsend
equation with extensions and modifications can be used to accurately
predict the point of breakdown, the so-called sparking potential, of
some gases.[7] Basically, however, it is to be considered as an adequate
description of phenomena observed prior to breakdown.

The Franck and Hertz Experiment

Another experiment of historical interest which has continued to
influence the pattern of ionization research to the present day is that
performed with a triode gas tube by Franck and Hertz[8] in 1914. These
investigators constructed a triode gas tube filled with mercury vapor
as shown in the schematic diagram of Figure 2. The vapor pressure in
the tube and the distances between tube elements were adjusted so that
the mean free path was considerably smaller than the distance between
cathode and grid and somewhat greater than the distance between grid
and anode. As shown in the figure; the grid was made slightly
positive, e.g., 0.5 volts, with respect to the anode so as to produce

---

[5] D. J. DeBitetto and L. H. Fisher, *Phys. Rev.*, 104:1213 (1956).

[6] S. C. Haydon and A. G. Robertson, Proc. 5th International Conf. on Ionization Phenomena in Gases, 75 (1961).

[7] D. J. DeBitetto and L. H. Fisher, *Phys. Rev.*, 111:390 (1958).

[8] J. Franck and G. Hertz, *Phys. Ges.*, 16:12 (1914); *Phys. Zeits*, 17:409 (1916); also discussion in H. E. White, *Introduction to Atomic Spectra*, McGraw-Hill (1934), p. 92.
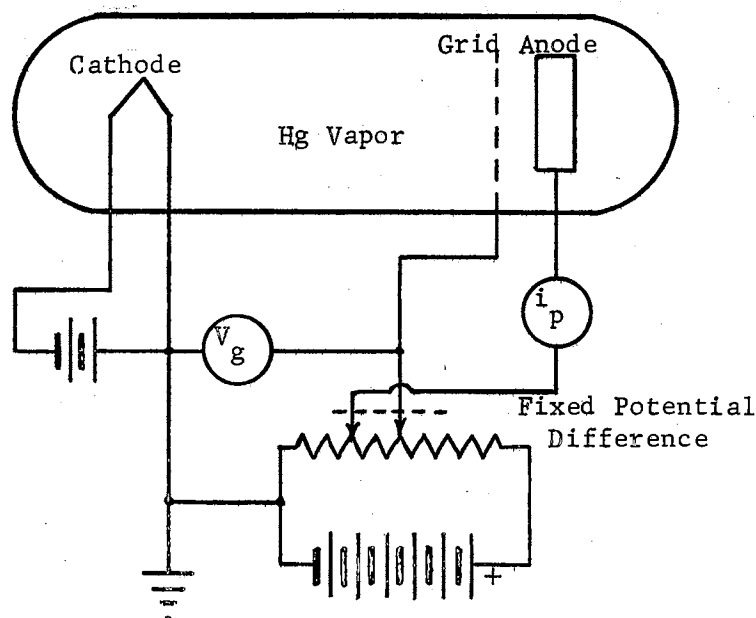
Figure 2. The Franck and Hertz
Experiment

a negative potential gradient in the region between the grid and the

anode. Then, for small values of V_g, few of the electrons emitted by

the cathode could reach the anode because the energy they had acquired

in traversing the region between the cathode and grid was too low,

consequently the anode current, i_p, was small. For large V_g, many

more of the electrons were able to reach the anode due to the greater

energy acquired in traveling between cathode and grid, consequently

i_p was large. As the grid voltage, V_g, was increased, Franck and Hertz

measured a plate current, i_p, as shown in Figure 3. In the region

labeled 0 to A on the curve, i_p increased as would be predicted on the

basis of the increasing energy acquired by the electrons. In the

region labeled A to B some of the electrons (i.e., those emitted from

the cathode with greater energy) had acquired sufficient energy to

collide inelastically with Hg atoms near the grid, giving up all of
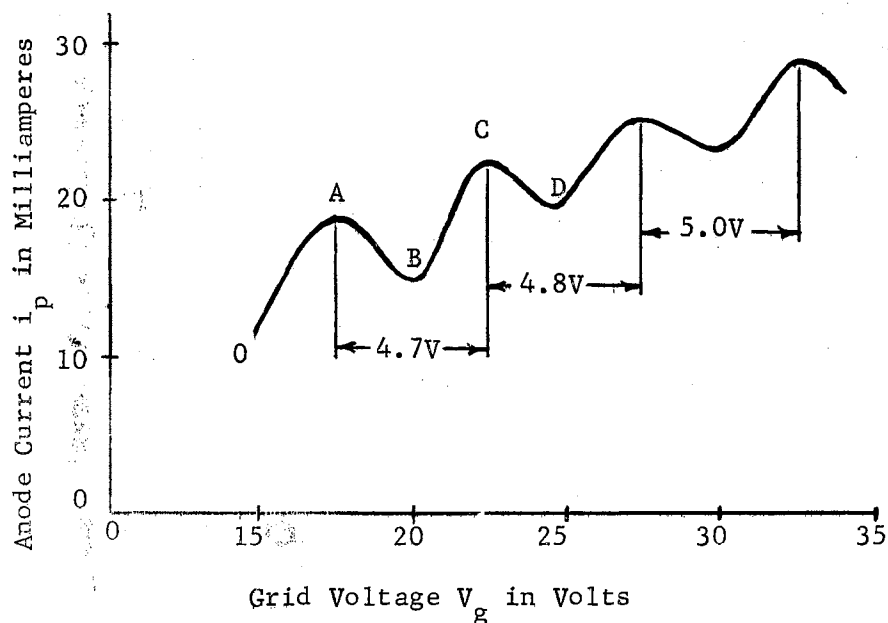
Figure 3. Sketch of the Measured Results of
Franck and Hertz

their energy and consequently were unable to reach the anode, hence

i_p decreased. In the region B to C the electrons acquired sufficient

energy after collision to reach the anode and i_p increased. In the

region C to D the electrons have collided with the Hg atoms both well

in front of the grid and then near it, consequently could not reach

the anode and i_p again decreased. Throughout the remainder of the

curve the process described above was repeated with additional

collisions in the region between cathode and grid.

The essentially constant potential difference between successive

peaks of the curve demonstrated that the Hg atoms absorbs energy only

in specified amounts. This potential difference is the amount of

energy, in electron volts, required to raise a valence electron from

the ground state to the next higher level and is called the first

excitation potential. A more refined apparatus than that employed by

Franck and Hertz allows one to determine the energy required to com-
pletely strip an electron from a nucleus giving the first ionization
potential. Contemporary apparatus[9] uses refined electrode systems such
as electron-guns, etc., but the principle remains the same as that
employed by Franck and Hertz.

<div align="center">

The Engineering Need for Further Studies

in Ionization

</div>

As stated previously, the experiments of Townsend and Franck and
Hertz have set the basic pattern for the investigations into the nature
of ionization phenomena which followed. Each of these is a collision
experiment, however, the respective results apply to different realms
in the subdivisions of matter. As determined by experiment, the
Townsend ionization coefficient is essentially a macroscopic idea; it
describes the pre-breakdown growth of ion formations in an aggregate
of molecules constituting a gas. On the other hand, excitation and
ionization potentials are microscopic in character, apply to single
atoms and molecules, and are very closely related to atomic structure.
As evidenced by the references quoted up to this point, there is a
wealth of Townsend ionization coefficient data available in the litera-
ture, and virtually any physics handbook will give ionization and
excitation potentials for the elements and many compounds. However,
in the engineering considerations related to non-conventional and
esoteric energy sources where ionized gases are involved, ionization
data of a different nature may be desired. Here the concern may not

---

[9]See, for example, E. W. Rothe, et. al, Phys. Rev., 125:582 (1962).

be primarily with the fundamental structure of matter, nor with conditions leading up to breakdown in the gas, but rather with the problem of economically producing ions in the gas at some steady rate in a specified environment. Of course, ionization potentials, Townsend coefficients, etc., should relate rather directly to this problem, but as this environment becomes more complicated it becomes increasingly more difficult to determine the nature of such relations. Almost invariably reactions with external force fields are involved and this would appear to place such considerations in the realm of that which is called plasma physics. Indeed, the general subject matter of plasma physics does treat the interactions of ionized gases with external force fields, especially electromagnetic fields, in great theoretical detail, but this treatment appears to be normally carried out largely neglecting any experimental necessity to excite the gas. Of course, this is natural in that the plasma physicist is usually treating, at least tacitly, aggregates of ionized particles which have been inadvertently created (i.e., so far as man's intentions are concerned) by the forces of nature.

The ionization study to be discussed on the following pages of this report arose out of attempts to construct a gaseous fuel cell in which a magnetostatic field was to replace the electrolyte. This consideration fixed both the gases to be investigated and the environment in which ionization was to be maintained. In the fuel cell application, the gases of interest are hydrogen and oxygen. The simpler gas, hydrogen, was selected to initiate the study and the remainder of this paper will be devoted to the discussion of the findings with this gas.

CHAPTER II

ANALYSIS

The Initial Assumptions and Solution

of the Lorentz Force Equation

From the published results[1] of mass spectrographic analysis of

Linde commerical tank hydrogen, i.e., 99.6 per cent H_2, which is the

gas employed in conducting this study, one must conclude that the

hydrogen phenomena is intimately associated with the physics of the

hydrogen molecule. The hydrogen molecule, considering that it is the

simplest of all molecules, turns out to be remarkably complex.[2] Con-

sequently, the quantum mechanics of the molecule has been discarded in

an initial attempt at analysis, using its literature[2] only as a guide

to the type of ions to be expected, and taking resort to a much simpler

form of theory. This approach has severe limitations, of course, in

that the simpler theory can never be completely, or for that matter

even satisfactorily, descriptive; but it is hoped that the knowledge

gained in continuing the analysis will eventually lead to the incorpora-

---

[1]D. J. Bitetto and L. H. Fisher, Phys. Rev., 104:1213 (1956).

[2]E. Teller, Z. Physik, 61:458 (1930): W. Hettler and F. London, Z. Physik, 46:47 (1927), 47:835 (1928), 51:805 (1929); S. C. Wang, Phys. Rev., 31:579 (1928); A. S. Coolidge and H. M. James, J. Chem. Phys., 1:825 (1933); C. A. Coulson, Trans. Faraday Soc., 33:1473 (1937); also, for an over-all summary account, see J. C. Slater, Quantum Theory of Matter, 1951.

tion of enough of the quantum mechanical ideas to build a sufficiently descriptive theory.

Starting with the common assumption[3] that inelastic collision of charged with uncharged particles is the primary mechanism of ionization produced in a gas under the influence of an applied electric field, the motion of charged particles in an environment more or less approximating the physical conditions inside the ionization cells employed in this investigation will be studied. Neglecting the flow of gas through the cell, it is assumed that the motion of an average charged particle in the absence of any collisions will obey the Lorentz force equation, i.e., assuming non-relativistic motion

$$\frac{d\overline{V}_o}{dt} = \frac{q}{m} (\overline{E} + \overline{V}_o \times \overline{B})$$ (2.1)

where $\overline{E}$ is the electric intensity, $\overline{B}$ is the magnetic intensity, and $\overline{V}_o$ is the velocity of an average particle of mass m and charge q. Consider the case where $\overline{B}$ is uniform, independent of time, and $\overline{E}$ is uniform and alternating with angular frequency ω,

$$\overline{E} = \overline{E}_o e^{j\omega t}.$$ (2.2)

So long as non-relativistic motion is assumed, the effect of the induced magnetic intensity may be neglected with respect to that of the applied electric intensity since for a plane wave in free space the ratio

$$\left| \frac{\overline{E}}{\overline{V} \times \overline{B}} \right| = c/v$$

where c is the velocity of light and $|\overline{V}| = v$ is the velocity of a

---

[3]M. A. Harrison and R. Geballe, *Phys. Rev.*, 91:1 (1953); L. Gould and L. W. Roberts, *The Breakdown of Air at Microwave Frequencies*, Microwave Assoc., Inc., MA-1 (1955);L. Gould, NAVSHIPS INDEX NO. NE-111616 (1956)

charged particle under the influence of the fields. Resolve the electric intensity vector into components parallel and perpendicular to the applied magnetic intensity. Denoting the components,

$$\bar{E} \text{ parallel to } \bar{B} \text{ as } \bar{E}_{11}, \text{ and}$$

$$\bar{E} \text{ perpendicular to } \bar{B} \text{ as } \bar{E}_{1},$$

and substituting Equation 2.2 into Equation 2.1, the equation

$$\frac{d\bar{V}_{o}}{dt} = \frac{q}{m} (\bar{E}_{o} e^{j\omega t} + \bar{V}_{o} \times \bar{B}) = \frac{q}{m} (\bar{E}_{11} + \bar{E}_{1} + \bar{V}_{o} \times \bar{B}) \qquad (2.3)$$

is obtained. Guided by the knowledge that the equation

$$\frac{d\bar{V}}{dt} = \frac{q}{m} \bar{V} \times \bar{B} , \qquad (2\text{-}4)$$

where $\bar{B}$ is uniform, independent of time, has solution

$$\bar{V} = \bar{V}_{11} + \bar{\Omega} \times r_{g} \qquad (2\text{-}5)$$

where $\bar{\Omega} = -q/m \; \bar{B}$ is the vector angular velocity, $\bar{r}_{g}$ is the radius of gyration, and $|\bar{\Omega}| = \omega_{g}$, the frequency of gyration, assume a solution to Equation (3) of the form

$$\bar{V}_{o} = a_{o} \bar{E}_{11} + a_{1} \bar{E}_{1} + a_{2} \bar{E}_{1} \times \bar{\Omega} . \qquad (2\text{-}6)$$

Here, in general, the a's are functions of time. Substituting Equation 2.6 into Equation 2.3 one obtains the following set of simultaneous differential equations in time for the solution of the coefficients:

$$\dot{a}_{o} + j \omega a_{o} = q/m$$

$$\dot{a}_{1} + j \omega a_{1} - \omega_{g}^{2} a_{2} = q/m \qquad (2\text{-}7)$$

$$\dot{a}_{2} + j \omega a_{2} + a_{1} = 0$$

Delcroix[4] gives the following integrations for Equations 2.7, which, of course, may be readily checked by direct substitution.

Case 1. $\omega = 0$

$$a_o = \left(\frac{q}{m} \right) t$$

$$a_1 = 0$$

$$a_2 = -q/m \; \omega_g^{\,2}$$

Case 2. $\omega \neq 0$ and $\omega \neq \omega_g$

$$a_o = -(q/m) \; j/\omega$$

---

[4]J. L. Delcroix, *Introduction to the Theory of Ionized Gases*, Interscience Publishers, 1960, Chapter 5.

No constants of integration appear in these solutions due to the method of obtaining the complete solution. Delcroix derives a super-position theorem considering $\overline{V}$ as the total velocity of a particle obeying the Lorentz force equation. Then it is assumed that $\overline{V} = \overline{V}_o + \overline{V}_1$, where $\overline{V}_o$ is the average velocity of a group of particles, all of charge q and mass m. The velocity $\overline{V}_1$ is added to account for the particular particle in question. Delcroix breaks this system down into two vector differential equations,

$$\frac{d\overline{V}_o}{dt} = \frac{q}{m} \left(\overline{E} + \overline{V}_o \; x \; \overline{B} \right)$$

$$\frac{d\overline{V}_1}{dt} = \frac{q}{m} \; \overline{V}_1 \; x \; \overline{B}$$

Initial conditions for a particular particle are contained in the integration of this latter equation. An estimate of gas flow velocity based upon the hydraulics of the system is of the order of 10 meters per second. As we shall see in Chapter V, calculated particle velocities range from approximately 10 to 10 x 10^6 meters per second; and it is believed that the important phenomena is associated with the higher particle velocities. For this reason, it is assumed that initial conditions may be neglected here.

$$a_1 = (q/m) \; j\omega(\omega_g^2 - \omega^2)$$

$$a_2 = -(q/m)/(\omega_g^2 - \omega^2)$$

Case 3. $\omega = \omega_g$

$$a_o = -(q/m) \; j/\omega$$

$$a_1 = (q/2m\omega) \; (\omega t - j)$$

$$a_2 = (q/2m\omega) \; jt$$

The above form of analysis is extremely limited since among the
many aspects of the phenomena which are neglected, no accounting is
made for the effects of pressure or collision frequency. Nevertheless,
much of the observed phenomena appears to be qualitatively deducible
in terms of the solutions obtained above. This is discussed below in
terms of Cases 1, 2, and 3 and related to the experimental data of
Chapter V. Furthermore, it appears that, to a first-order approximation
at least, the collision frequency (or mean free path) effects may be
inserted into the calculations as an "afterthought."

Development and Discussion of the

Solutions for the Various Cases

Case 1. ($\omega = 0$): For this case with static applied electric
intensity, from the solution for a_o, charged particles are uniformly
accelerated in the $\overline{E}_{11}$ direction with opposite directions for electrons
and positive ions. From the solution for a_1 there is no motion in the
direction of $\overline{E}_1$. However, there is motion in the direction of $\overline{E} \times \overline{B}$.
Denoting this by $\overline{V}_D$, for drift velocity,

$$\overline{V}_D = a_2 \ \overline{E}_1 \ \times \ \overline{\Omega} = (q/m)^2 \ \frac{\overline{E}_1 \ \times \ \overline{B}}{\omega_g^2} \qquad (2.8)$$

and since $\omega_g = q/m \ | \ B \ |$, Equation 2.8 may be written as

$$\overline{V}_D = \frac{\overline{E} \ \times \ \overline{B}}{\overline{B}^2} \qquad (2.9)$$

where $\overline{B}^2 = \overline{B} \ . \ \overline{B}$. This velocity is independent of the quantity q/m and will, therefore, be the same for both the electrons and ions. Then, if ionization is produced primarily by a collision process, it is seen that the application of $\overline{E}_{11}$ alone would require the same energy to maintain ionization as when there is no $\overline{B}$ applied because the motion is not affected by $\overline{B}$ in this case. If $\overline{E}_1$ alone were applied, the movement of electrons and ions in the $\overline{E} \times \overline{B}$ direction would, in general, be in a direction parallel to the electrodes and, consequently, might not be so rapidly removed from the cell by the electrodes as in the usual case of no applied $\overline{B}$. For this reason the $\overline{E}_1$ orientation might require less applied $\overline{E}$ in order to maintain ionization in certain circumstances. However, the static $\overline{E}$ case is of lesser interest in this investigation since it is a generally accepted fact[5] that ionization occurs much more readily under the influence of rf fields.

Case 2. ($\omega \neq 0$, $\omega \neq \omega_g$): This is the case which is more generally applicable to the measured data presented in Chapter V of this report. Delcroix[6] discusses this case in terms of tensor mobilities and tensor conductivities, but it appears to more aptly suit the purpose at hand

---

[5] See, for example, A. B. Cambel, Plasma Physics and Magnetofluid-Mechanics, McGraw-Hill (1963), p. 92.

[6] J. L. Delcroix, Introduction to the Theory of Ionized Gases, Interscience Publishers (1960) Chapter 5.

to avoid this nuisance by considering first $\bar{E}_{11}$ only and next $\bar{E}_{1}$ only

as the directions of applied electric intensity.

(a) $\bar{E}_{11}$ only: The solution becomes:

$$\left.\begin{array}{l} \bar{V}_{11} = -j \ q/m\omega \ \bar{E}_{11} \\[2ex] \bar{V}_{1} = a_1 \ \bar{E}_{1} = 0 \\[2ex] \bar{V}_{D} = a_2 \ \bar{E}_{1} \times \bar{\Omega} = 0 \end{array}\right\} \tag{2.10}$$

There is movement in the $\bar{E}_{11}$ direction alone. Suppose there was no applied $\bar{B}$. The Lorentz force equation becomes

$$\frac{d\bar{V}_{o}}{dt} = q/m \ \bar{E}_{o} \ e^{j\omega t} \tag{2.11}$$

and integrating, the solution

$$\bar{V}_{o} = q/m \ \bar{E}_{o} \int e^{j\omega t} dt = -j \ q/m\omega \ \bar{E} + K \tag{2.12}$$

is obtained. It is seen that in the case of $\bar{E}_{11}$ the applied $\bar{B}$ has no affect upon the motion. Consequently, one would expect the same energy to be required in order to maintain ionization as when no $\bar{B}$ is applied. The experimental evidence indicates that it is at least as difficult to maintain ionization with $\bar{E}_{11}$ as when no $\bar{B}$ is applied, and perhaps the application of $\bar{B}$ renders ionization more difficult to perform.

(b) $\bar{E}_{1}$ only: This represents the normal orientation employed throughout the study and is experimentally found to be that in which ionization is most easily maintained. The solutions become:

$$\bar{V}_{11} = a_0 \bar{E}_{11} = 0$$

$$\bar{V}_1 = a_1 \bar{E}_1 = j\omega(q/m)/(\omega_g^2 - \omega^2) \bar{E}_1 \quad . \tag{2.13}$$

$$\bar{V}_D = a_2 \bar{E}_1 \times \bar{\Omega} = (q/m)^2 \frac{\bar{E}_1 \times \bar{B}}{(\omega_g^2 - \omega^2)}$$

Now, if $\omega_g^2 \gg \omega^2$, then Equations 2.13 become

$$\bar{V}_1 \cong j \, \omega/\omega_g^2 \, (q/m) \, \bar{E}_1$$

$$\bar{V}_D \cong (q/m)^2 \frac{\bar{E}_1 \times \bar{B}}{\omega_g^2} = \frac{\bar{E} \times \bar{B}}{\bar{B}^2} \quad . \tag{2.14}$$

On the other hand, if $\omega_g^2 \ll \omega^2$, then Equations 2.13 become

$$\bar{V}_1 \cong -j/\omega \, (q/m) \, \bar{E}_1$$

$$\bar{V}_D \cong - (q/m)^2 \frac{E_1 \times B}{\omega^2} \quad . \tag{2.15}$$

Now, from a consideration of the literature[7] of the hydrogen molecule, it may be presumed that three types of charged particles are present in the cell when ionization is taking place; namely, these are negative electrons e, positively ionized hydrogen atoms H^+, and singly ionized hydrogen molecules H^+. In addition, there is the reaction $H_2^+ + H_2 \rightarrow H_3^+ + H$ which frequently occurs between a slow molecular ion and the hydrogen molecule, so that H_3^+ may also be present. The angular frequency of gyration, ω_g, for all particles is given by the equation

[7] E. Teller, Z. Physik, 61:458 (1930): W. Hettler and F. London, Z. Physik, 46:47 (1927), 47:835 (1928), 51:805 (1929); S. C. Wang, Phys. Rev., 31:579 (1928); A. S. Coolidge and H. M. James, J. Chem. Phys., 1:825 (1933); C. A. Coulson, Trans. Faraday Soc., 33:1473 (1937); also for an over-all summary account, see J. C. Slater, Quantum Theory of Matter, 1951.

$$\omega_g = q/m \, |\bar{B}| \quad . \tag{2.16}$$

Upon substitution of the applicable values for q and m, Equation 2.16 becomes:

(i) for an electron, e:

$$\omega_{g_e} = 17.6 \times 10^4 \, |\bar{B} \text{ (kg)}| \text{ mega-radian/sec.}, \tag{2.17}$$

or

$$f_{g_e} = 28 \, |\bar{B} \text{ (kg)}| \text{ GH}_z \tag{2.18}$$

(ii) for H^+:

$$\omega_{gH}^+ = 9.6 \, |\bar{B} \text{ (kg)}| \text{ mega-radian/sec.}, \tag{2.19}$$

or

$$f_{gH}^+ = 1.53 \, |\bar{B} \text{ (kg)}| \text{ MH}_z \tag{2.20}$$

(iii) and for H_2^+:

$$f_{gH_2}^+ \doteq 0.77 \, |\bar{B} \text{ (kg)}| \text{ MH}_z \tag{2.21}$$

From Equation 2.17 it is seen that Equations 2.14 should always hold for the electron throughout the frequency range of this investigation. However, as $\bar{B}$ and the frequency are varied, conditions for the ions H^+ and H_2^+ will range through Equations 2.13 to 2.15, with the "exact" Equations 2.13 being the more generally applicable. From Equations 2.13 (approximations 2.14 and 2.15 also give the same result), the ratio of magnitude of drift to perpendicular velocities is found to be

$$\left| \frac{\bar{V}_D}{\bar{V}_1} \right| = \frac{q}{\omega m} \, |\bar{B}| \quad . \tag{2.22}$$

Upon substitution of the applicable values for q and m, Equation 2.22 may be written:

(iv) for e:

$$\left| \frac{\bar{V}_D}{\bar{V}_1} \right| = \frac{2.8 \times 10^4}{f \ (MH_z)} \left| \bar{B} \ (kg) \right| , \qquad (2.23)$$

(v) for H^+:

$$\left| \frac{\bar{V}_D}{\bar{V}_1} \right|_{H^+} = \frac{1.53}{f \ (MH_z)} \left| \bar{B} \ (kg) \right| , \qquad (2.24)$$

(vi) and for H_2^+:

$$\left| \frac{\bar{V}_D}{\bar{V}_1} \right|_{H_2^+} \doteq \frac{0.77}{f \ (MH_z)} \left| \bar{B} \ (kg) \right| . \qquad (2.25)$$

Reference to the experimental data (presented in Chapter V) shows $\left| \bar{B} \right|$ values ranging from approximately 0.6 to 5 kilogauss and $f \ (MH_z)$ ranging from 2 to 30. Then, the minimum ratio for an electron, $\left| \bar{V}_D/\bar{V}_1 \right|$, ranges from approximately 10^4 to 10^3; and it is concluded that $\bar{V}_D$, within the attending assumptions in its derivation, should be the ruling velocity so far as concerns electrons (ratio of diameter to spacing of the electrodes in the cell is approximately 10). This is not, however, the case with the ions H^+ and H_2^+. As seen by Equations 2.24 and 2.25, the frequencies and applied magnetic intensities employed in the experimental investigation are of such magnitudes as to sensitively affect the $\left| \bar{V}_D/\bar{V}_1 \right|$ ratios for the ions. On this basis, one would predict that observed phenomena which is essentially independent of frequency and magnetic intensity must be due to an electron-atom, and/or molecule collision mechanism, while that phenomena which is

sensitive to variations in frequency and/or magnetic intensity must be
the result of an ion-atom, and/or molecule collision mechanism.
Again, refer to Chapter V. It is noted that the data for the lower
values of optimum magnetic intensity is essentially independent of
frequency and is nearly constant in magnetic intensity. Further, an
effect not explained by this simple theory, this data is essentially
constant with respect to mass flow and cell pressure. One concludes
that this data perhaps represents the effect of an electron-atom,
molecule collision mechanism and that the collision frequency for
electrons may tend to remain constant over the range of pressures
employed. On the other hand, the data for higher values of optimum
magnetic intensity varies radically with both frequency and pressure;
magnetic intensity is no longer an essential constant. Then, one
concludes that this data probably represents the result of an ion-
atom, molecule collision mechanism and that the collision frequency
for ions is likely more affected by the pressure.

Case 3. $(\omega = \omega_g)$: This is the condition of gyromagnetic
resonance. Equation 2.13 would indicate infinite perpendicular and
drift velocities for this condition; but, going back to the solutions
for the a's determined for the special case of resonance, one finds
that this is not strictly true.

(a) $\overline{E}_{11}$ only: The solutions become:

$$\overline{V}_{11} = a_o \overline{E}_{11} = -q/m \; j/\omega \; \overline{E}_{11}$$

$$\overline{V}_1 = \overline{V}_D = 0$$

(2.26)

and no effect is observed due to the applied $\overline{B}$. As a matter of fact, Equations 2.26 are identical to Equations 2.10, this case when $\omega \neq \omega_g$, so that one would predict no gyromagnetic resonance effects when the electric intensity is applied in the parallel direction.

(b) $\overline{E}_1$ only: The solutions become:

$$\overline{V}_{11} = 0$$

$$\overline{V}_1 = q/2\omega m \; (\omega t - j) \; \overline{E}_1$$

$$\overline{V}_D = -j \; (q/m)^2 \; t/2\omega \; \overline{E} \times \overline{B}$$

(2.27)

and it is observed that the velocities become infinite only as t approaches infinity. In cases where particle and/or other collisions do not severely limit the growth of these velocity components with time, relativistic effects would soon become important thereby nullifying the initial assumptions in this analysis.

CHAPTER III

EXPERIMENTAL SYSTEM AND EQUIPMENT

The General Nature of the Experimental System

The general nature of the experimental system is illustrated in
the block diagram of Figure 4. Linde commerical tank hydrogen is
inletted into the system as shown at the bottom of the figure. The gas
passes through a mass flow transducer for a measurement of mass flow
(Hastings model LF-300 Mass Flow Meter) on to a servo-driven variable
leak (Granville Phillips Series 213). The variable leak is controlled
so as to maintain constant pressure in the system by means of a
Granville Phillips Company Automatic Pressure Controller with its feed-
back loop connected to a modified Pirani Gauge (Consolidated Vacuum
Corporation type GP-110). From the variable leak, the gas flows into
the cell, which contains the electrodes for producing ionization, and
then on to the vacuum pump (Welch Scientific Company Model 1397) from
which it is exhausted into the outer atmosphere. Gauge tubes No. 3
and 4 are symmetrically located at approximately 18 inches, respectively,
from the outlet and inlet to the cell. The mean of these two gauge
tube readings, as indicated by the vacuum gauge (Hastings type VT-4
and/or type VT-6), is taken to be the pressure inside the cell. The
function of gauge tube No. 1 and its associated vacuum gauge (Hastings
type VT-4 and/or type VT-6) is to provide an indication of the vacuum
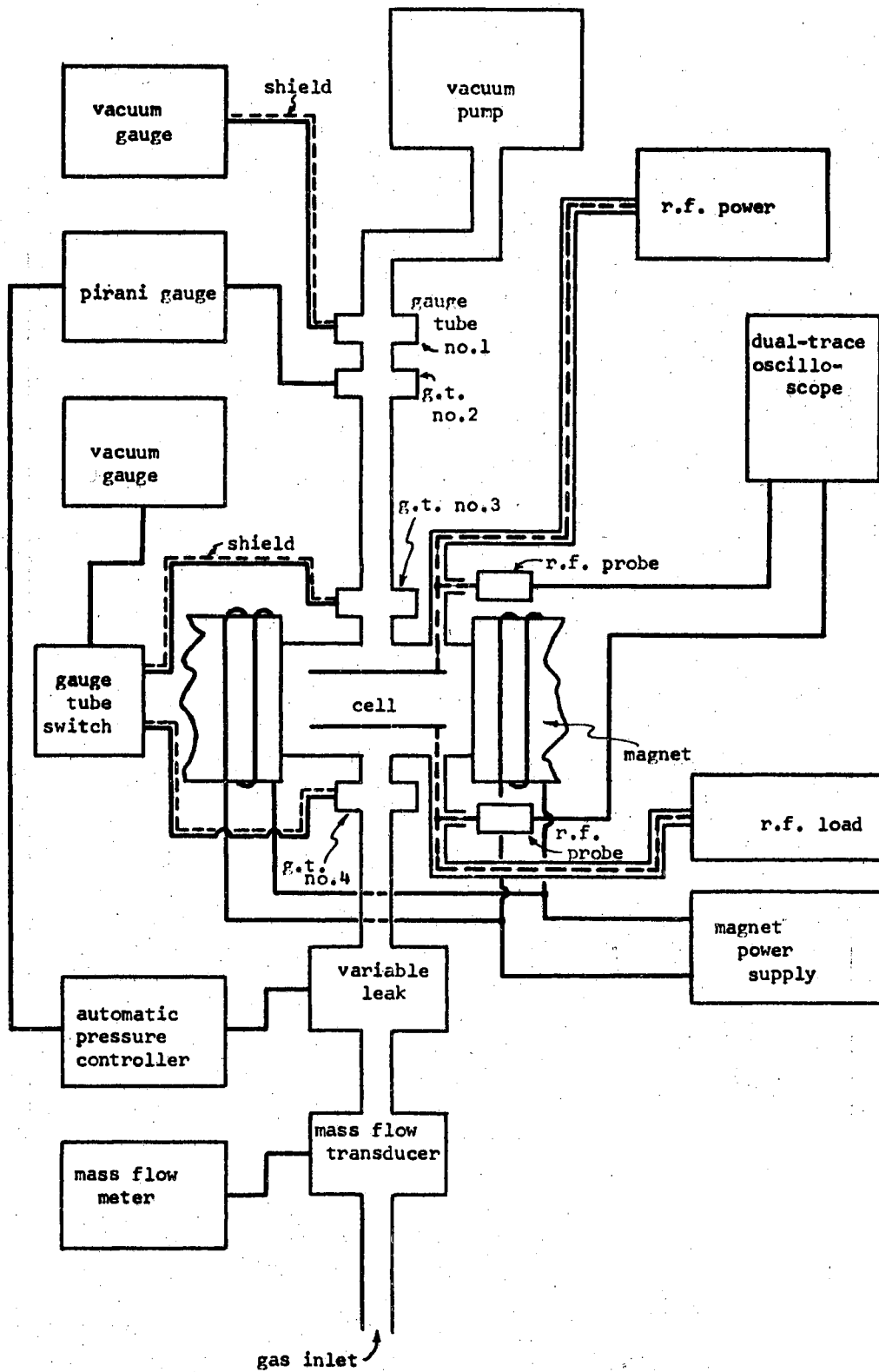system performance.

21

Figure 4. Block Diagram of the Experimental Setup

As shown in the diagram, the cell is located between the pole pieces of an electromagnet (Harvey-Wells Corporation Model L-76V), the magnetic intensity of which can be varied by means of varying the output current of the magnet power supply (Harvey-Wells Corporation Model UR1050). The electromagnet is calibrated for the applicable gap by means of a Radio Frequency Laboratories Model 1295A Gaussmeter.

In the early stages of the study an E. F. Johnson Company Viking II amateur transmitter was employed as the rf supply and is referred to in this paper as the "old rf supply." However, due to its limitations, it was replaced by the combination of a Technical Material Corporation PAL-1KW Linear Amplifier and a Hewlett-Packard Company Model 606A HF Signal Generator. This combination gives continuous coverage of the 2 to 32 MH_z frequency range with continuously variable output up to one KW maximum. From the transmitter, the rf power is fed through a coaxial cable to the electrodes of the cell. Samples of the rf voltage applied to the electrodes and rf current through the cell are picked up through rf probes and displayed on a dual-trace oscilliscope. A camera may be used to record the oscilloscope traces of voltage and current.

A photograph of the system described above is shown in Figure 5a. From left to right the equipment shown: dual-trace oscilloscope with camera; magnet with cell in place and magnet power supply immediately below, Hastings vacuum gauges, gauge tube switch gear, variable leak, and mass flow transducer are mounted in the black rack; the larger cabinet in front of the black rack is the automatic pressure controller, the smaller cabinet on top is the mass flow meter, and the other cabinet on top is the Pirani gauge; and the rf power source is shown adjacent to the table in the extreme right of the picture. A close-up of a
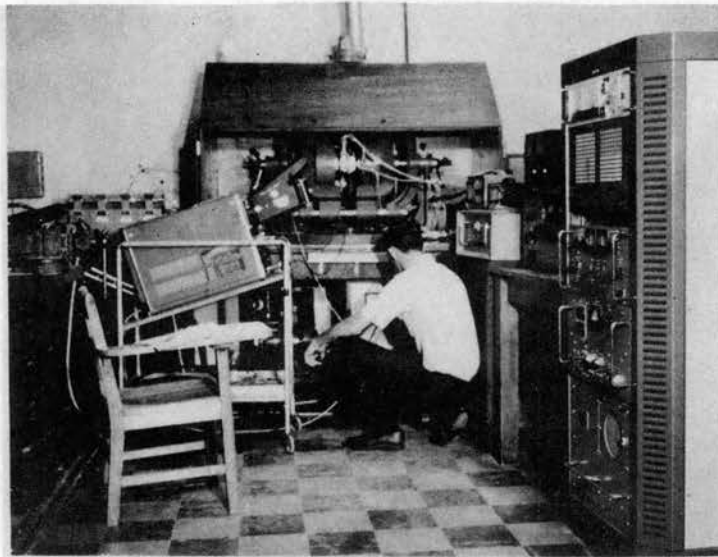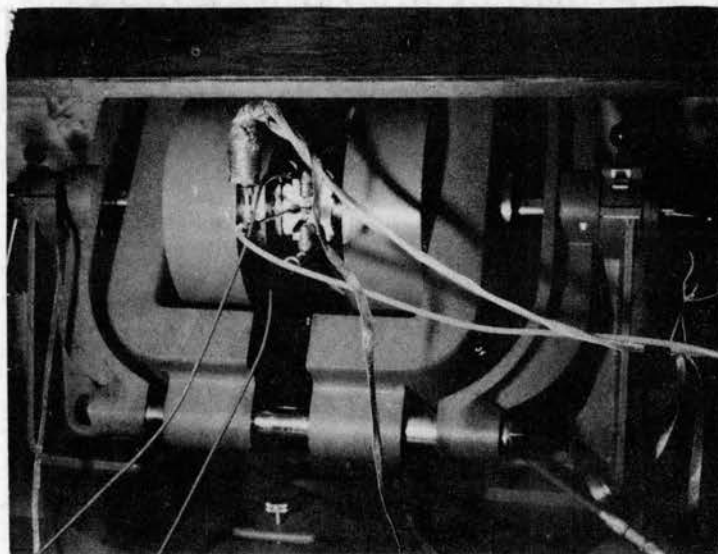
Figure 5a. Photograph of the Over-All System

Figure 5b. Cell in Operation

Figure 5. Photographs of the Experimental System

"typical" cell (the aluminum cell with secondary electrodes discussed in the following paragraph) in operation is shown in Figure 5b.

Evolution of the Ionization Cell

The ionization cells passed through several stages of development before satisfactory cells were produced. The difficulties inherent in the design were manifold, but were chiefly concerned with the problem of obtaining a suitable combination of electrical and mechanical properties along with the capability of maintaining the required vacuum. The dimensions and properties of the Harvey-Wells Corporation electromagnet used in the study necessarily limited the geometry of the ionization cells employed. The pole faces are $6\frac{1}{2}$ inches in diameter which means that the dimensions of the cell must be somewhat less than this in order to obtain the desired uniformity of field. Also, for this same reason it is essential that the cells be constructed entirely of non-ferrous materials. As can be seen by referring to Figure 85, in the Appendix, pole gaps of the order of $3\frac{1}{2}$ inches allow the magnet to attain a magnetic intensity in the vicinity of 5 kilogauss, consequently this dimension was taken as an approximate parameter. When vacuum joints and fittings are taken into account, this selection restricts the electrodes in a symmetrical plane electrode geometry to circular discs of approximately 1 3/4 inches in diameter. This in turn limits the electrode spacing to something of the order of 0.2 inch, or less, in order to obtain a reasonable degree of uniformity in the applied electric field.

Cell bodies of plexiglass were tried early in the study. The appearance and construction of one of these cells is shown in the two
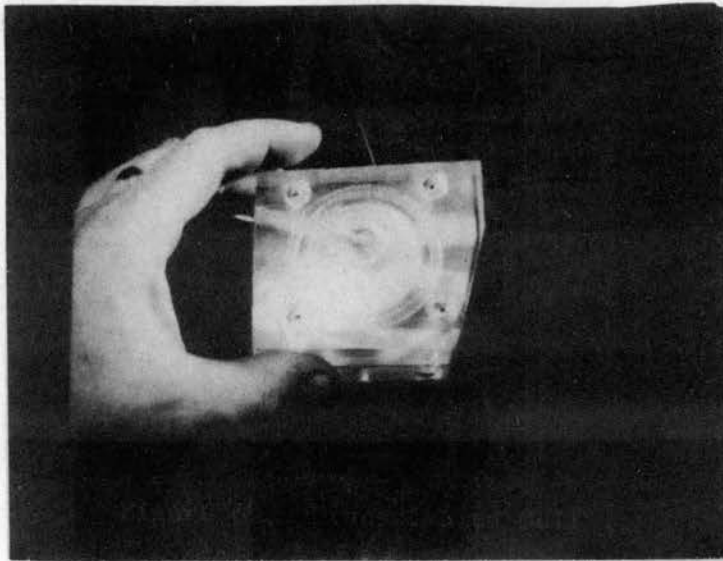
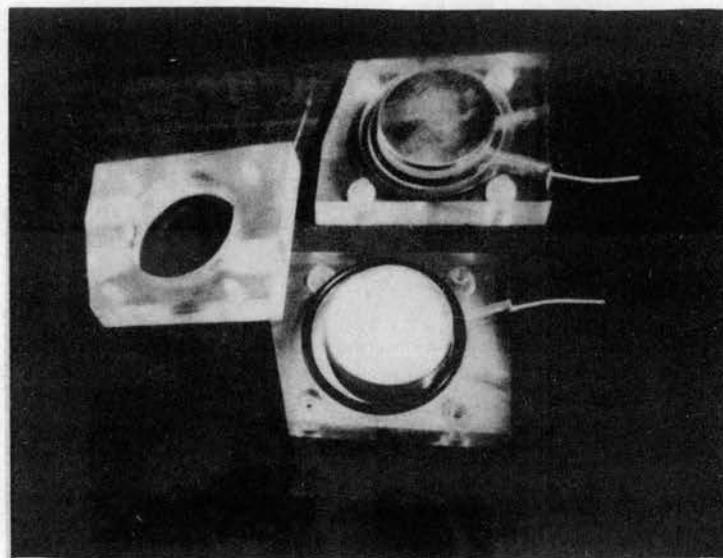Figure 6a. Assembled Cell

Figure 6b. Disassembled Cell

Figure 6. Photographs of an Early Model
Plexiglass-Bodied Ionization Cell

photographs of Figure 6. This form of design proved to be unuseable

for several reasons. First, as shown in the photographs, the electrodes

were balanced fed which led to a severe balance to unbalance transfor-

mation problem in operating the cell. However, this defect was not so

apparent at this stage of the study because the plexiglass cell bodies

failed so rapidly in operation due to the heat generated inside the

cell with ionization taking place that its full effect was not realized.

Another defect in this design was the use of "O" rings to obtain the

vacuum seal, as shown in the photograph of Figure 6 b. While these

were totally satisfactory for the purpose of obtaining the seal, the

"O" rings, being compressible, made it virtually impossible to either

maintain a precise positioning of the electrodes or to determine

accurately the spacing after assembly. The immediate problem being the

failure of the plexiglass cell bodies to withstand the heat of operation,

it was decided to construct the cell body from teflon. The previous

electrode dimensions and material (approximately 1.70 inch diameter

brass discs) were retained, as was the balanced feed geometry, but the

"O" ring seals were discarded. Instead, the mating surfaces were

tediously ground together with rottenstone (decomposed siliceous lime-

stone) and water to form a vacuum tight joint. Although this procedure

required considerable painstaking effort, the results proved superior

in operation in every way to the use of the "O" rings. This cell,

referred to elsewhere in this paper as the "old teflon cell", is shown

in the two photographs of Figure 7. It proved to be wholly satisfactory

from the mechanical standpoint, but left much to be desired in the way

of electrical design. The principal source of electrical difficulties

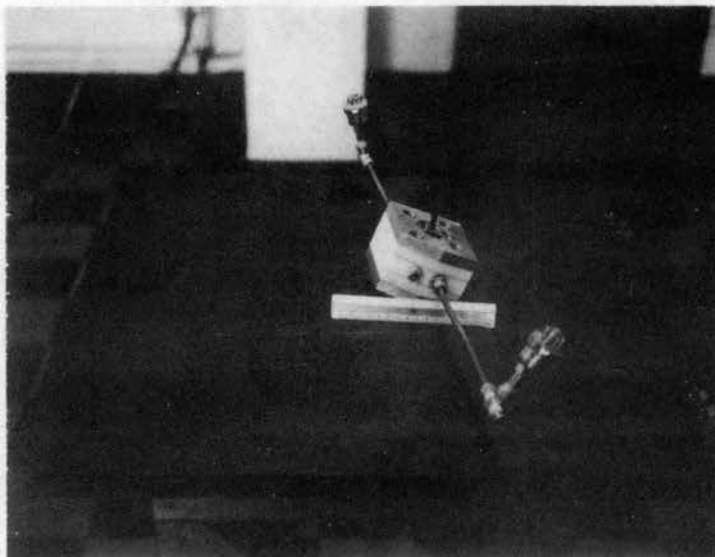in the design was the balanced feed geometry. The radiation from
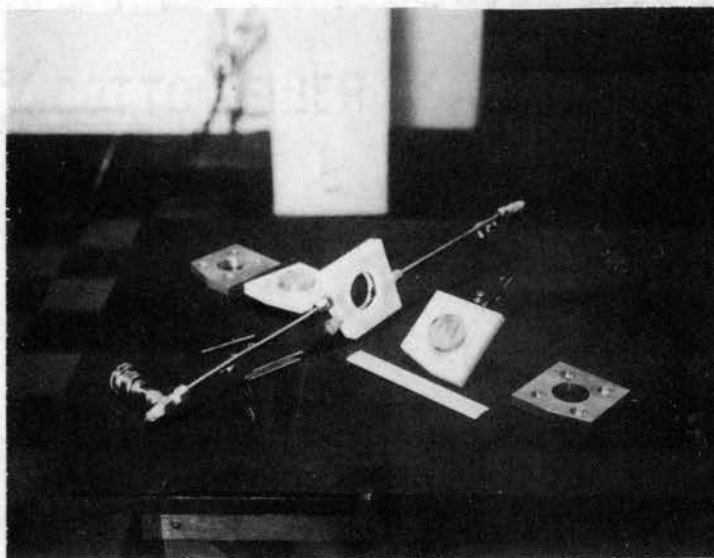
Figure 7a.   Assembled Cell

Figure 7b.   Disassembled Cell

Figure 7.   Photographs of the Old Teflon Cell,
Scale Shown is a 6-inch Engineer's
Scale

unbalanced currents on the parallel two-wire transmission line feeding

the cell was so severe as to preclude data taking at frequencies above

7 MH$_z$. An air-core balun transformer was constructed and found to

satisfactorily reduce the stray radiation from the transmission line,

but its use prevented the direct measurement of the phase relationship

between the applied voltage and through the cell. Consequently, the

next step in cell development was to redesign so as to have coaxial

rf connections to the cell, thereby eliminating the parallel two-wire

line.

The cell resulting from the modification of the "old teflon cell"

to incorporate coaxial rf connections is shown in the exploded view of

Figure 8. The dimensions of this cell, hereafter referred to as the

"teflon cell", are shown in the shop drawing of Figure 9. The

secondary electrodes for sampling drift components of current, as

discussed in the following chapter, were added to the cell at this stage

of evolution. The primary electrodes were, as in the previous cells,

1.70 inch diameter brass discs. The teflon cell, as shown in

Figures 8 and 9 and also in the photograph of Figure 34 in the following

chapter, was the first reasonably successful ionization cell produced

during the study. Its use figured prominently in the conceptive stages

of the experimental study; however, there were still troublesome

deficiencies in the electrical design. The "open" nature of the design

did not offer complete rf shielding so that again there was trouble

from stray rf currents at the higher frequencies, say 15 MH$_z$ and

above. This difficulty was eliminated at last in the final stage of

development which resulted in the aluminum-bodies cell, hereafter

referred to as the "aluminun cell", shown in the shop drawing of
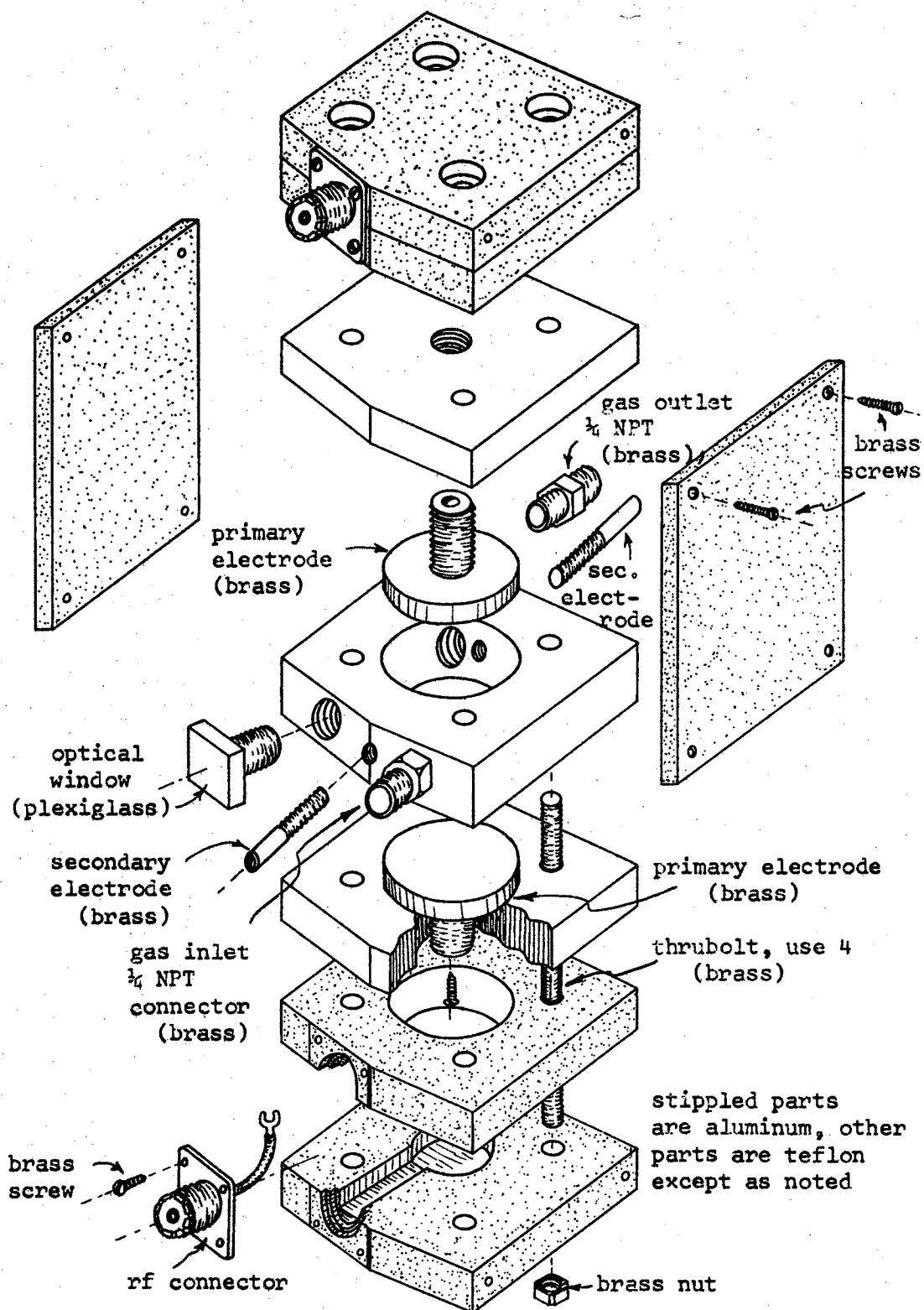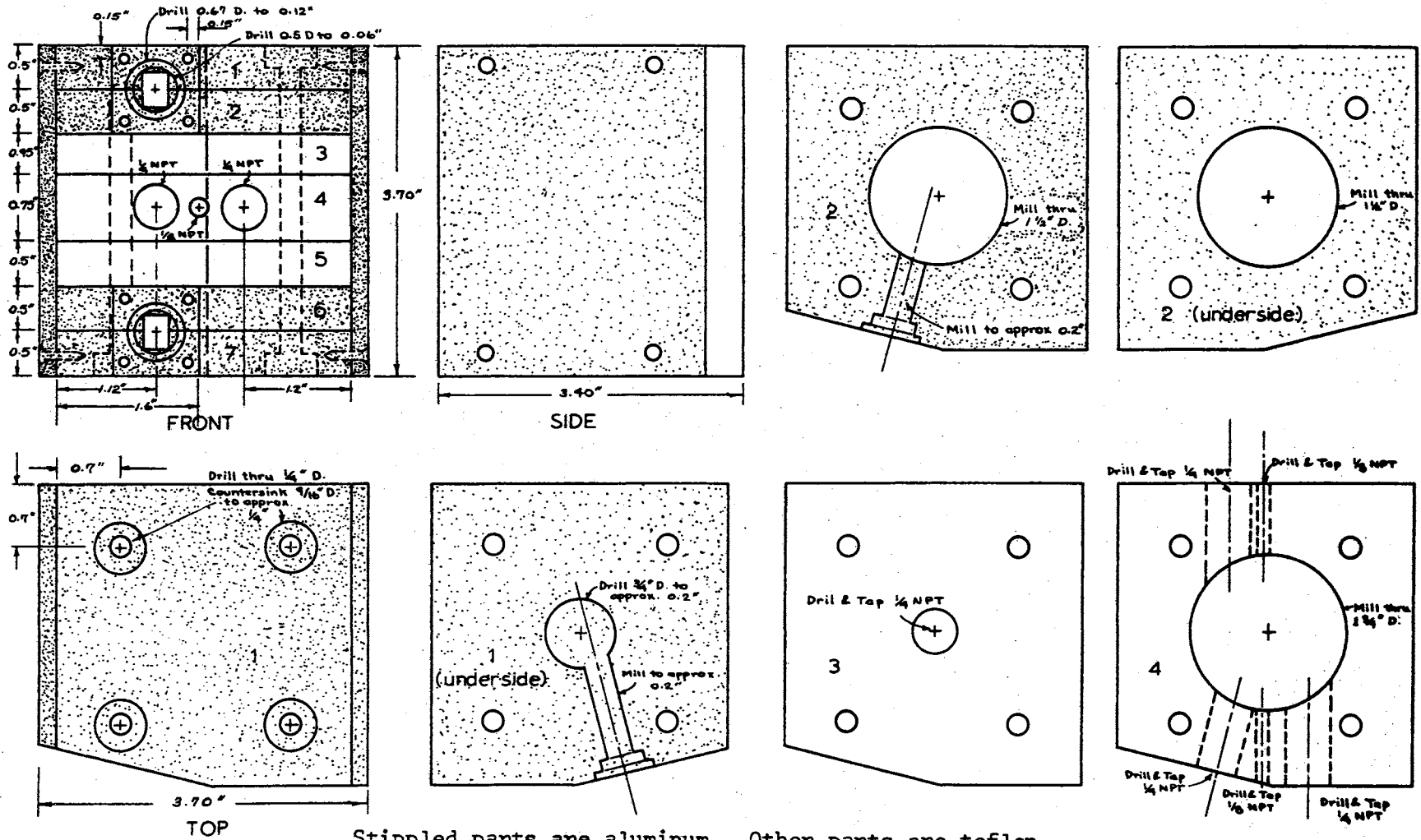
Figure 8. An Exploded View of the Teflon Cell

Stippled parts are aluminum. Other parts are teflon.

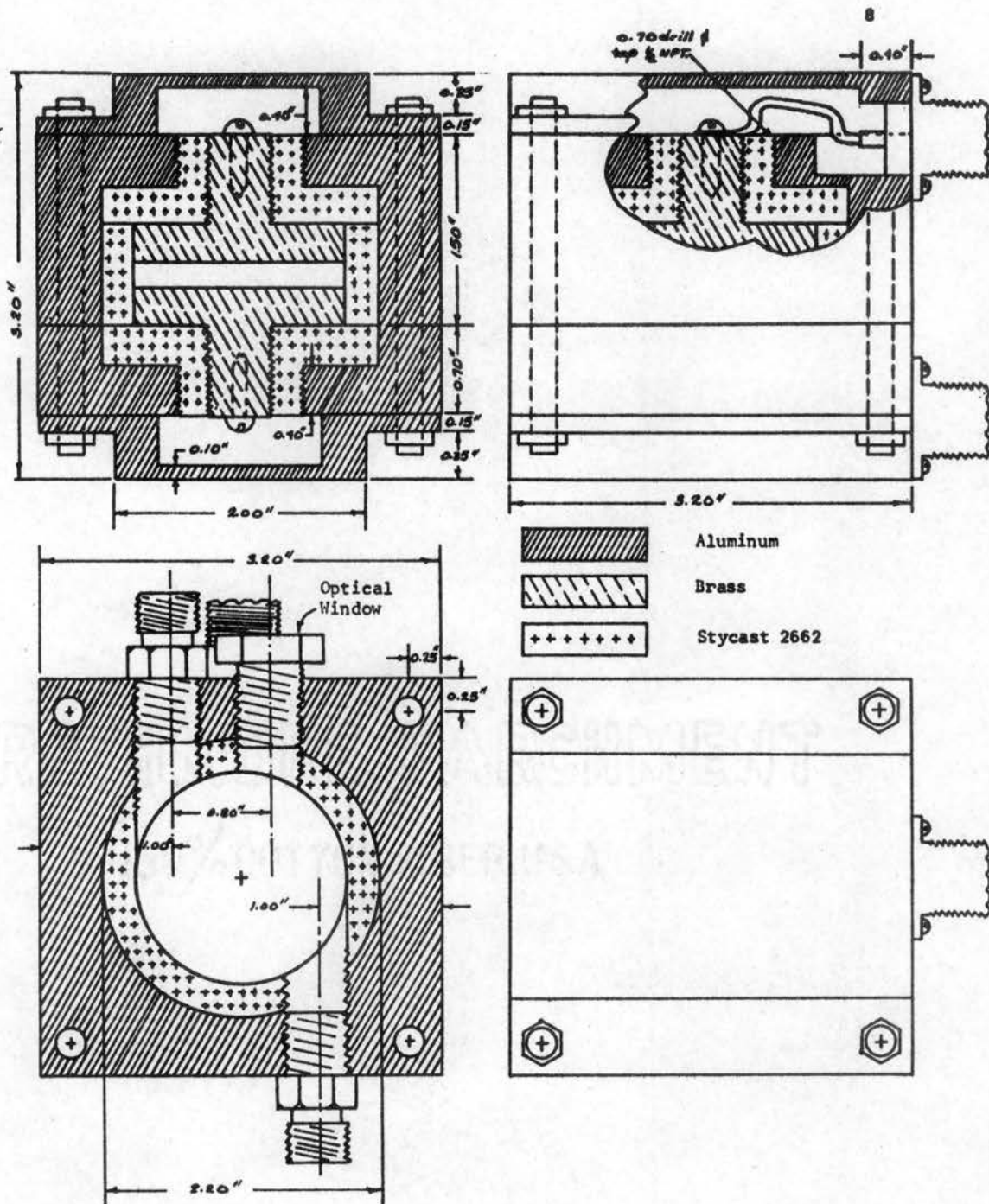Figure 9.   Shop Drawing of the Teflon Cell

Figure 10.   Shop Drawing of the Aluminum Cell

Figure 10. In addition to totally enclosing the cell within an aluminum shell, this design offers the additional feature of a guard ring structure around the electrodes which insures a greater uniformity in the applied electric intensity. The construction of the insulating parts, which also must function as vacuum seals, around the electrodes in this cell constituted something of a problem. Teflon was tried initially, but it was difficult to machine the parts so as to obtain the essential vacuum tightness. Furthermore, this material had a tendency to break down in the intense field regions inside the cell, especially around the guard ring structure, and cause severe etching of electrodes and cell body. After some experimentation, a casting resin (Emerson & Cuming, Inc. Stycast 2662) was found to offer a satisfactory solution. Two of the aluminum-bodied cells were constructed to almost identical dimensions, except that one of these carried secondary electrodes similar to those of the teflon cell shown in Figure 8, while the other one did not have these additional electrodes. The primary electrodes were, in all of the above cell designs, 1.70 inch diameter discs of brass and the spacing between electrodes varied, as listed in Chapter V, from approximately 2 to 6 millimeters.

CHAPTER IV

GENERAL NATURE OF THE OBSERVED PHENOMENA

General Experimental Observations

Certain effects are observed experimentally with hydrogen in the system and the cell in operation. These are as follows:

(a) In general, the rf energy available is not sufficient to produce deionization glow (and consequently ionization or excitation) with no static magnetic field applied.

(b) Application of the magnetic field in a direction parallel to the rf electric field has no apparent effect, but application in the perpendicular direction has the striking effect described below.

(c) With the rf field applied and applying the static magnetic field in the perpendicular direction, one observes a value of magnetic field intensity at which a glow appears in the window of the cell. Increasing the magnetic intensity while holding the rf voltage fixed will cause the glow to become more intense to a point, after which further increasing the magnetic field causes the glow to become increasingly faint until it is finally extinguished. Within the range of the magnet's capability, further increasing the magnetic intensity causes the glow to appear again with the above observations

34

being repeated. Values of applied magnetic field such that glow intensity is a maximum for a fixed rf field will hereafter be referred to as the optimum magnetic field intensity.

(d) As the rf electric field intensity is varied, the values of optimum magnetic field intensity will shift somewhat but are quite evident so long as the glow is maintained. Under the condition of the minimum rf field intensity which will maintain a steady glow, current and voltage traces as viewed on the oscilloscope are essentially sinusoidal and displaced·in phase by 90 degrees. A photograph of typical traces under these conditions is shown in Figure 11 (photograph shown was taken at $f = 3.5$ MH$_z$, MF = 30 std. cc/min., $\bar{B} = 0.85$ Kg). As the output of the rf source is increased, the glow becomes more and more intense, and the current trace becomes nonsinusoidal as shown in the photograph of Figure 12. As shown, the voltage waveform remains sinusoidal under both conditions.

As a consequence of these observations, an experimental mapping of the optimum magnetic field under the condition of a minimum steady de-ionization glow (i.e., ideally, minimum rf applied electric intensity required to maintain ionization) as a function of pressure, magnetic intensity, applied rf voltage, and applied electric intensity was initiated. The results of this undertaking are presented in detail in the following chapter of this paper.
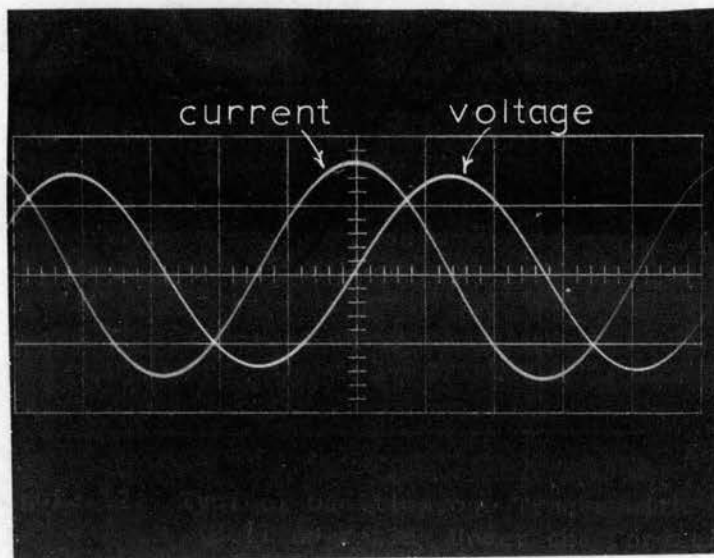
Figure 11. Typical Oscilloscope Traces with
Cell Operating Under the Condition
of Minimum Deionization Glow
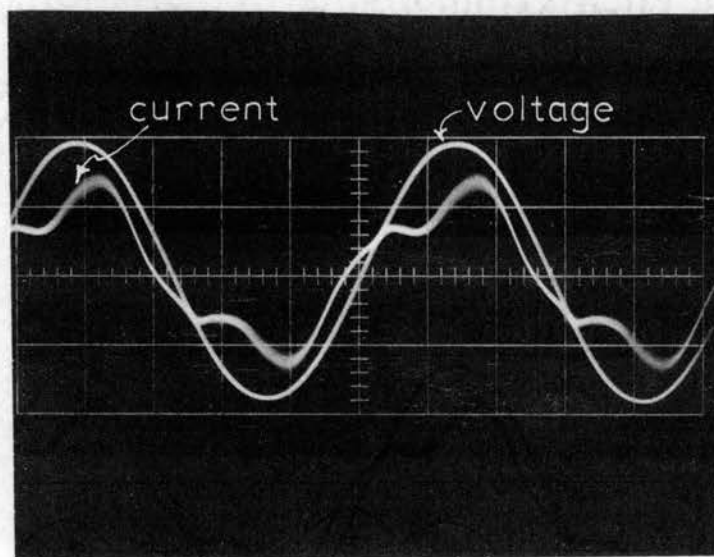
Figure 12. Typical Oscilloscope Traces with
Cell Operating Under the Condition
of Intense Deionization Glow

Essential Nature of the Measured Data

The essential nature of the measured data is displayed in the three-dimensional plot of Figure 13. Figure 13 shows a three-dimensional plot of the electric intensity values versus optimum magnetic intensity and the cell pressure. The measured current through the cell is also shown. Due to its essentially total reactive character, hereafter the cell current in this measurement will be referred to as the charging current. Now as viewed in Figure 13, the electric intensity and charging current values lie in planes of intersection defined by curves of cell pressure versus optimum magnetic intensity. These curves can and probably should be idealized by straight lines. Figure 14 shows such an idealization of the cell pressure versus optimum magnetic intensity data given in Figure 13. Along each of these lines a new variable has been defined; γ_1 along the line of lower optimum magnetic intensity values and γ_2 along the line of higher optimum magnetic intensity values. Note that the same linear scale has been picked for γ_1 and γ_2 as is used in plotting magnetic intensity and pressure, and the zero pressure axis has been selected as the reference for defining γ_1, γ_2 equal to zero. Although little use of this technique is made in this paper, one can easily convert the scale of the γ-values to either optimum magnetic intensity or cell pressure readings by writing the equations for the γ-lines. For example, in the case at hand one finds by graphical analysis:

(a) Along the γ_1 line:

$$B \ (Kg) = 0.52 + 0.43 \ \gamma_1 \qquad\qquad (4.1)$$

$$P \ (mm. \ Hg.) = 1.066 \ \gamma_1 \qquad\qquad (4.2)$$
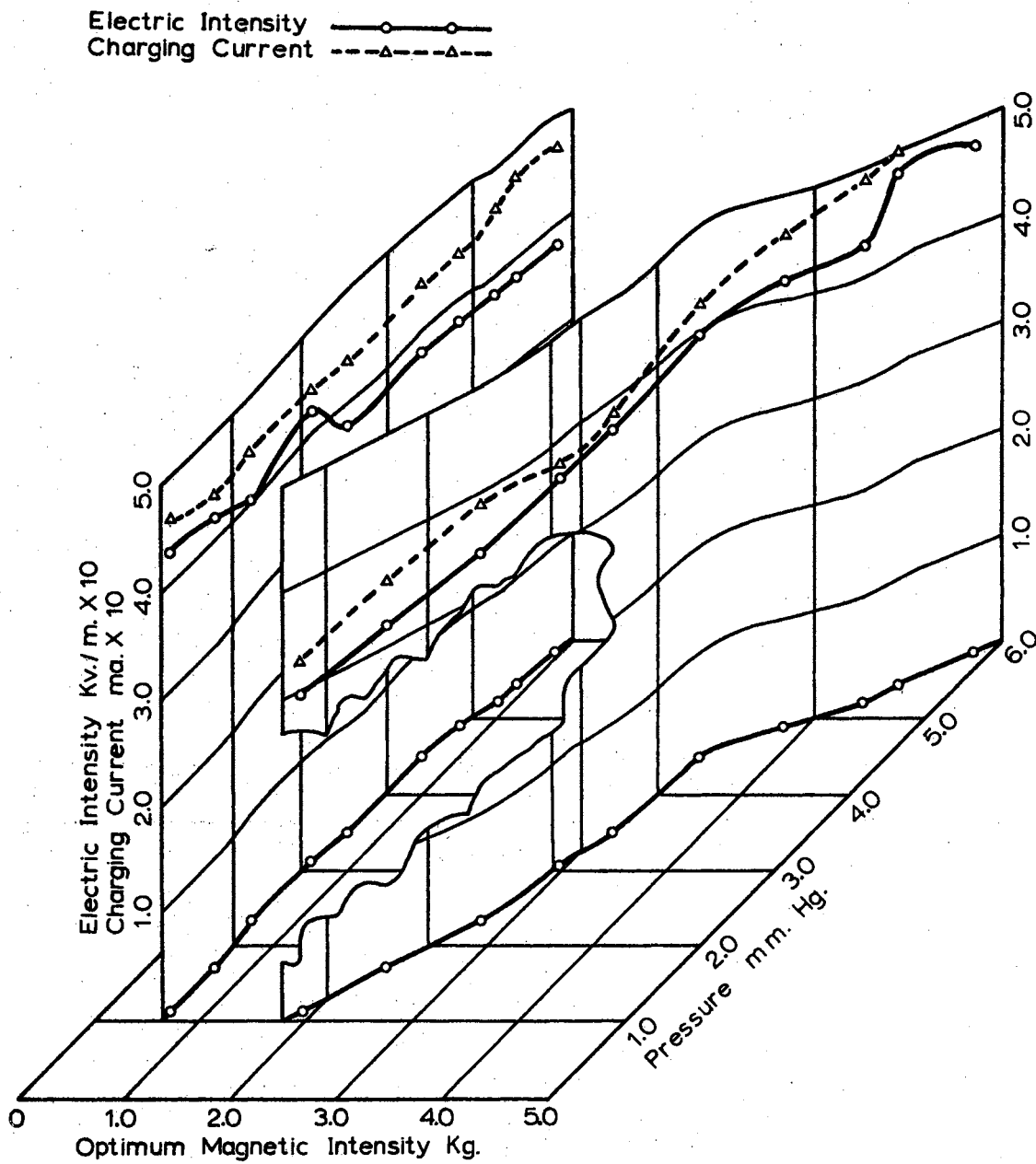
Figure 13. Three-Dimensional Plot of Applied Electric Intensity
and Charging Current Versus the B-p Plane
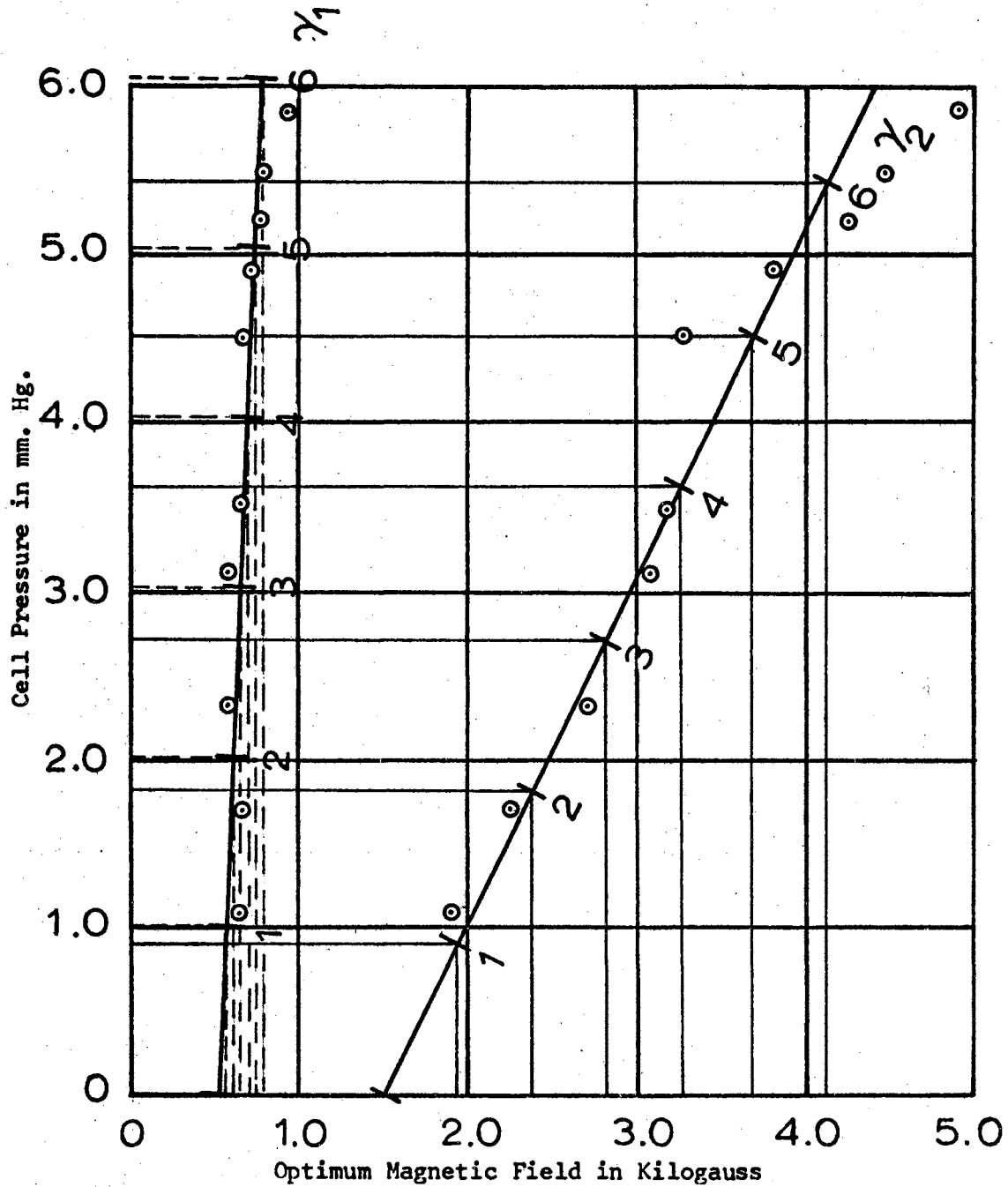
Figure 14. A Plot of Cell Pressure Versus Optimum Magnetic
            Field for Hydrogen at 7 MH_z Defining the γ_1
            and γ_2 Lines

(b) Along the γ_2 line:

$$B \text{ (Kg)} = 1.50 + 0.45 \ \gamma_2 \tag{4.3}$$

$$P \text{ (mm. Hg.)} = 0.90 \ \gamma_2 \tag{4.4}$$

Then it appears that the three-dimensional nature of the measured, as well as calculated, data can be better displayed on two-dimensional charts by plotting values relative to the lower optimum magnetic intensity versus γ_1 and values relative to the higher magnetic intensity versus γ_2. Then equations like Equations 4.1 through 4.4 above can be employed to translate specific γ values into magnetic intensity and pressure. Figure 15 shows such a plot of electric intensity and charging current versus γ_1. Note that if these values were plotted against the magnetic field intensity, all points would fall nearly together. On the other hand, a plot versus pressure would be nearly equivalent to the graph shown. Again, a plot versus mass flow results in a nonlinear distortion of the abscissa due to the nonlinear relation between mass flow and pressure. Figure 16 shows a similar plot of electric intensity and charging current corresponding to the higher optimum magnetic field values plotted against γ_2. Note that in this case, relative to the graph shown, plotting against mass flow, pressure, or optimum magnetic intensity would distort the figure. This method of presentation will be further applied to computed data in Chapter V of this thesis.

Secondary Electrode Measurements

As indicated in Chapter II of this thesis, applied field values are such throughout the measurements that the drift component of velocity of the electrons should be governed by the equation
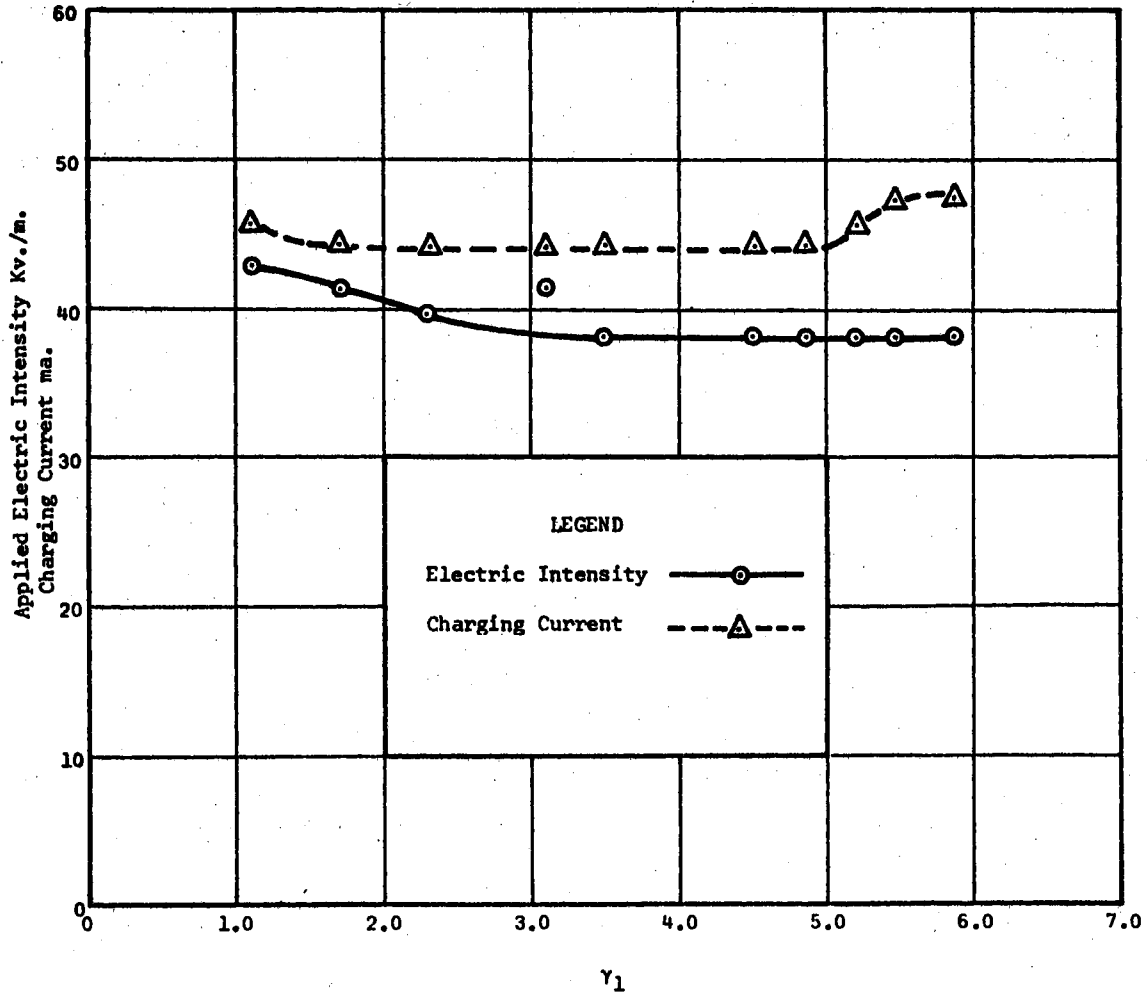
Figure 15. Electric Intensity and Charging Current
Corresponding to the Lower Optimum Magnetic
Intensity Values at 7 MH$_z$ Plotted Against
the γ_1 Variable
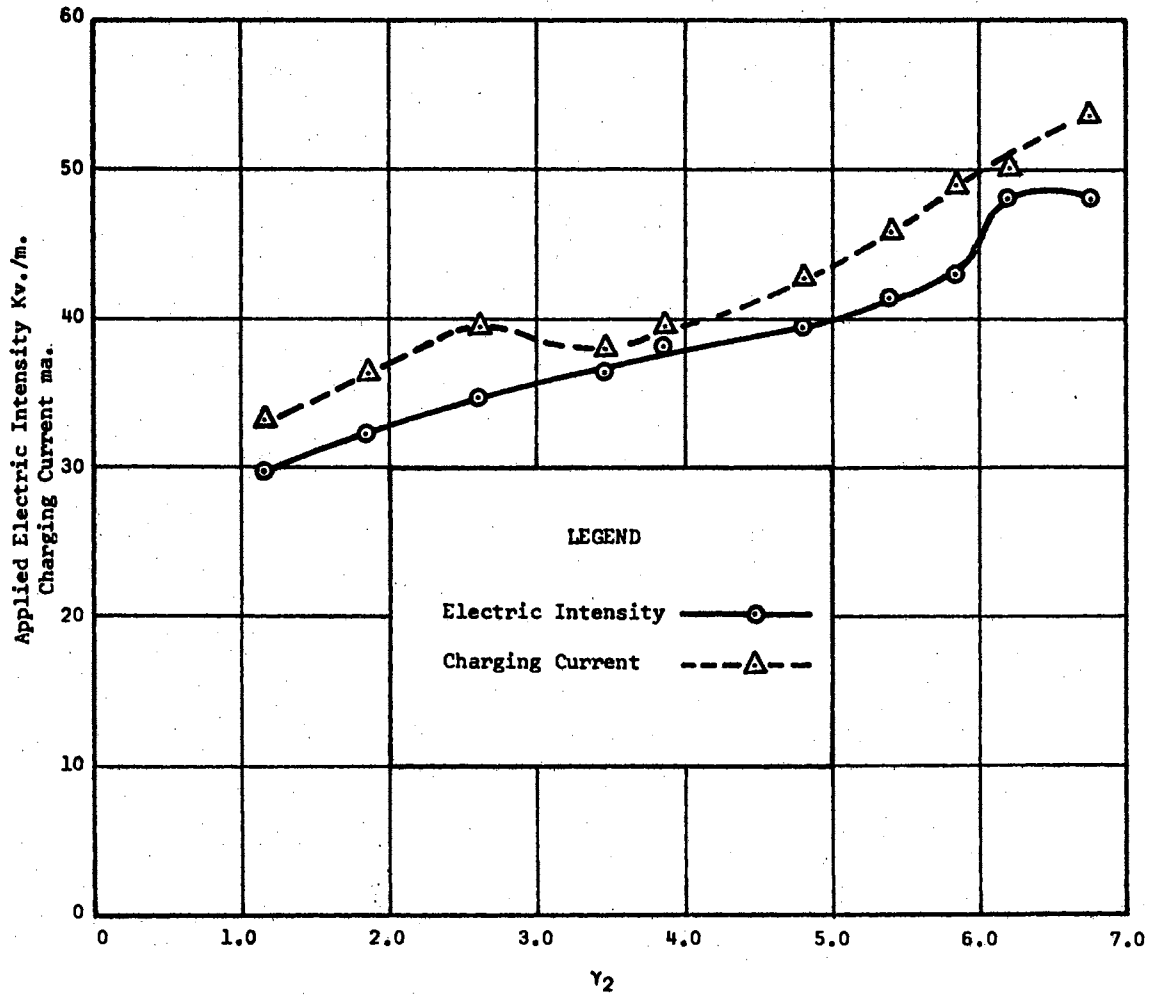
Figure 16. Electric Intensity and Charging Current Corresponding to the Higher Optimum Magnetic Intensity Values at 7 MH_z Plotted Against the γ_2 Variable

$$V_D \approx \frac{\overline{E} \times \overline{B}}{\overline{B}^2} \quad . \tag{4.5}$$

In the experimental system, values of the magnetic intensity $\overline{B}$ are always such that the minimum $|\overline{V}_D/\overline{V}_1|$ ratio for the electrons is of the order of 10^3 to 10^4; i.e., it is predicted that the electron motion is essentially in the direction perpendicular to the plane containing $\overline{E}$ and $\overline{B}$. Further, Equation 4.5 indicates that the magnitude of this velocity should be nearly independent of frequency. However, these conditions do not apply to the ions. The experimental values of ω and $\overline{B}$ are such as to indicate velocity directions and magnitudes which are, generally speaking, somewhat sensitive to variations in both $\overline{B}$ and ω.

In view of the above considerations, it appeared that information of very pertinent character concerning the ionization processes could be found by sampling the drift velocity components. These cannot be measured directly, of course, but it was reasoned that measuring the voltage buildup due to particle bombardment on electrodes placed in the direction of the drift velocity components should give relative data. This was the purpose of the secondary electrodes as shown in the exploded view of the teflon cell in Figure 8. A pictorial diagram of the electrode and applied field configurations is shown in Figure 17. The secondary electrodes are of brass, approximately 3/16-inch in diameter, and are threaded into the teflon body of the cell as far as is feasible without running the risk of electrically shorting the primary electrodes. As recorded previously, the primary electrodes to which the rf voltage is applied are also of brass, approximately 1.70 inches in diameter. For the case of the secondary electrode
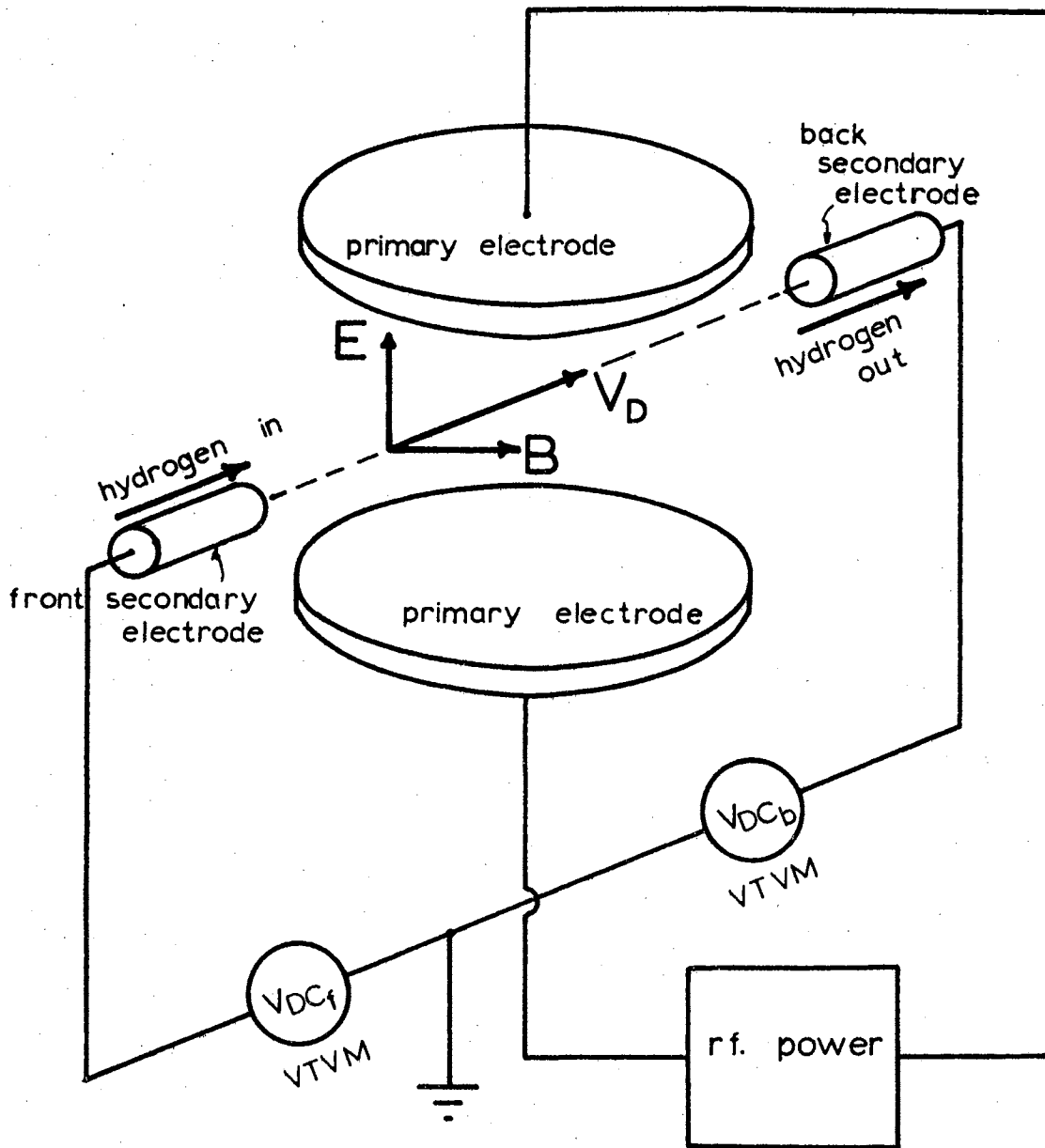
Figure 17. Cell Geometry

measurements discussed below, the primary electrode spacing was 0.169 inch. In Figure 17 this spacing between primary electrodes has been shown greatly exaggerated in order to be able to indicate the appropriate field and velocity directions. Actually, the diameter of the secondary electrodes is slightly greater than the spacing between primary electrodes.

Since experimental data taken with two primary electrodes at 7 MH_z had been the more extensively analyzed and discussed in previous reports, this frequency was selected for the initial measurements taken with secondary electrodes in order to enable comparison with the results of the previous work. The experimental system was exactly the same as that shown in Figures 4 and 5, with the exception of the addition of equipment to view and measure the potentials developed on the secondary electrodes. The electrical connections are shown in Figure 18. Referring to Figure 17, note that the secondary electrode labeled "front" is located adjacent to the hydrogen inlet while the one labeled "back" is located adjacent to the hydrogen outlet. That is, the gas flow velocity is directed from the front toward the back secondary electrode. In Figure 18, two vacuum tube voltmeters are shown connected so as to measure the respective secondary electrode voltages with respect to ground, and a dual trace oscilloscope is connected to enable one to view the nature of the voltages developed. Under the condition of optimum applied static magnetic intensity with minimal rf excitation, these voltages were always found to be as nearly pure dc as could be ascertained from the traces displayed on the oscilloscope. Their essential character remained dc at all other levels of rf excitation and values of $\bar{B}$ investigated, but when
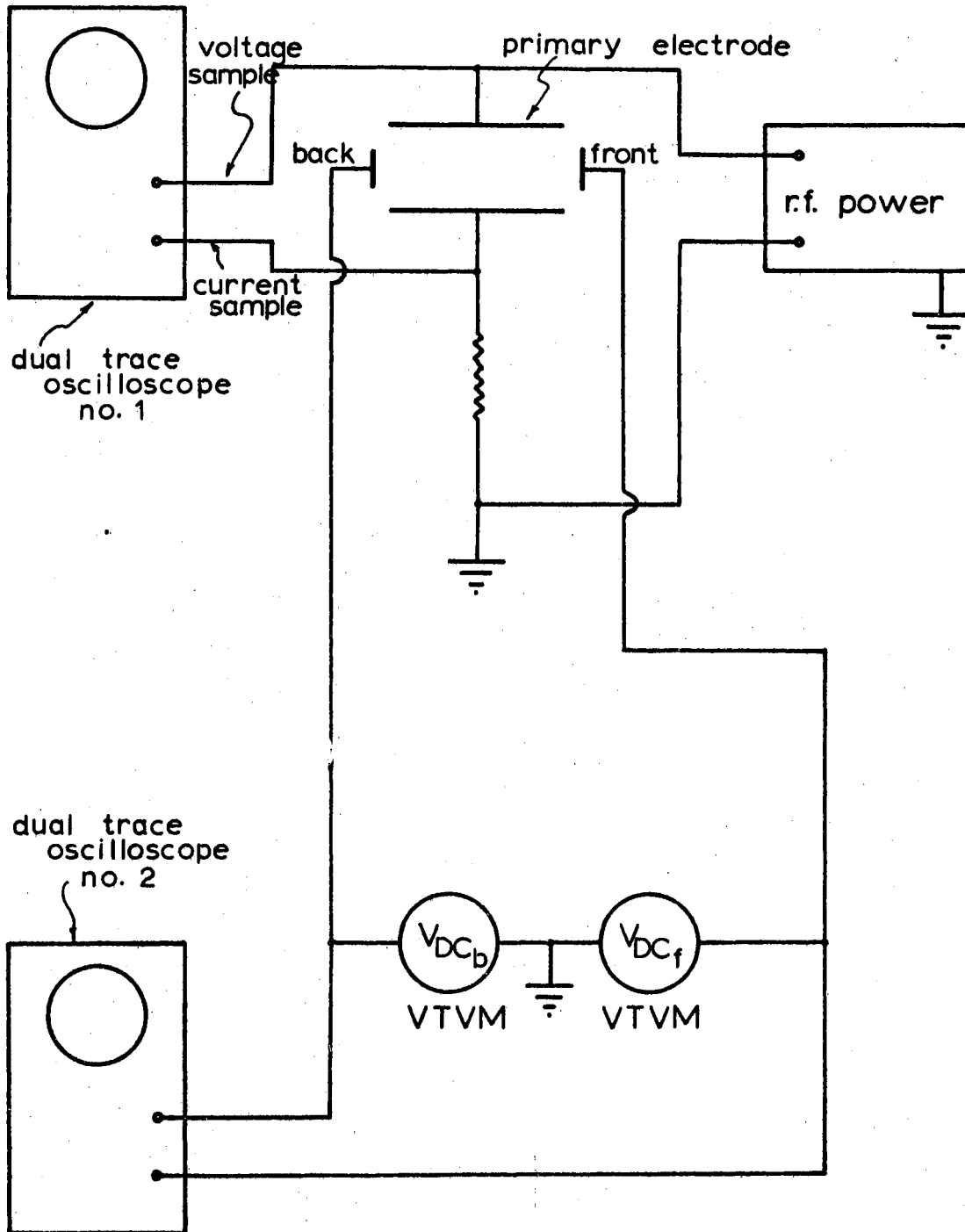
Figure 18. Electrical Circuit Showing Added Connections for Measuring the Voltages Developed at the Secondary Electrodes

conditions were such as to produce an observed flicker in the deioni-
zation glow, this would result in an apparently periodic trace of widely
varying waveforms superimposed upon the dc. The level of this "flicker
trace" was generally considerably lower than that of the dc, its wave-
form never approached anything remotely similar to a sinusoid, and its
period was always observed to be considerably greater than that of the
applied rf frequency.

The dc potentials, as observed on the two vacuum-tube voltmeters,
prove to be effective indicators of the optimum magnetic field intensity.
With the rf level held constant, the dc voltages developed on the
secondary electrodes peak quite sharply as the magnetic field is
varied through its optimum value as indicated by observing the glow
intensity. That is, as near as one can determine with the present
experimental setup, the points of maximum deionization glow and the
peak dc levels developed on the secondary electrodes coincide.

This data at 7 MH_z was taken in the manner of that reported
previously, with the addition of the secondary electrode measurements.
A plot of the cell pressure versus the optimum magnetic intensity
is shown in Figure 19. This plot follows the procedure established of
idealizing this data to γ_1 and γ_2 lines. Figure 20 shows a plot of
the dc voltages measured with respect to ground on the secondary
electrodes along the γ_1 line. The γ_1 line corresponds to the lower
values of optimum B. As the cell is operated, the secondary electrodes
blacken slightly on portions of their surfaces. Since this discolora-
tion requires some effort with metal polish to remove, it is believed
to be the result of a slight oxidation rather than the deposit of
foreign matter. Reference to the point in Figure 20 where the
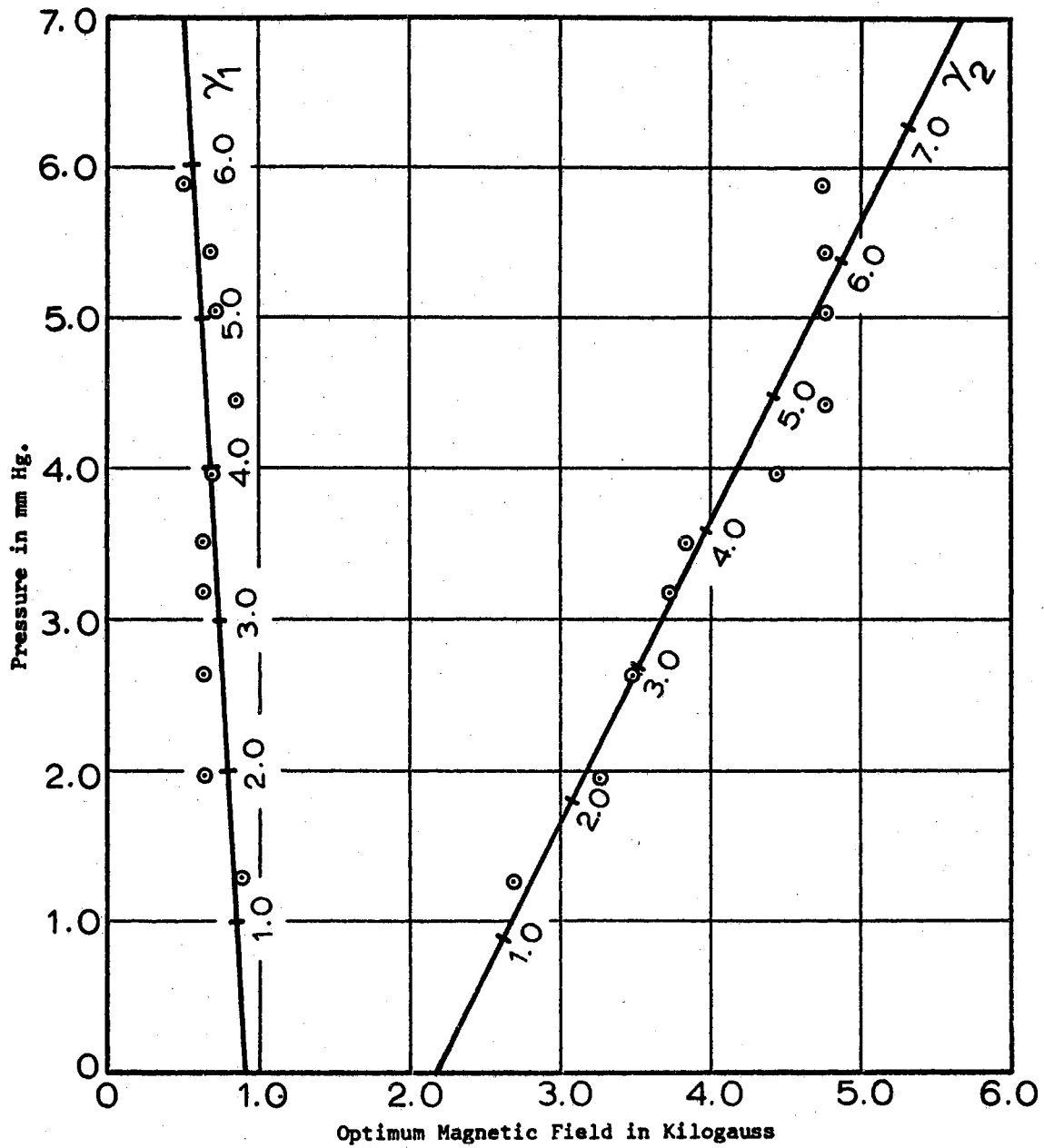
Figure 19. Cell Pressure Versus Optimum Magnetic Field with
Idealization to the γ_1 and γ_2 Lines for the
Teflon Cell with Hydrogen at 7 MH$_z$
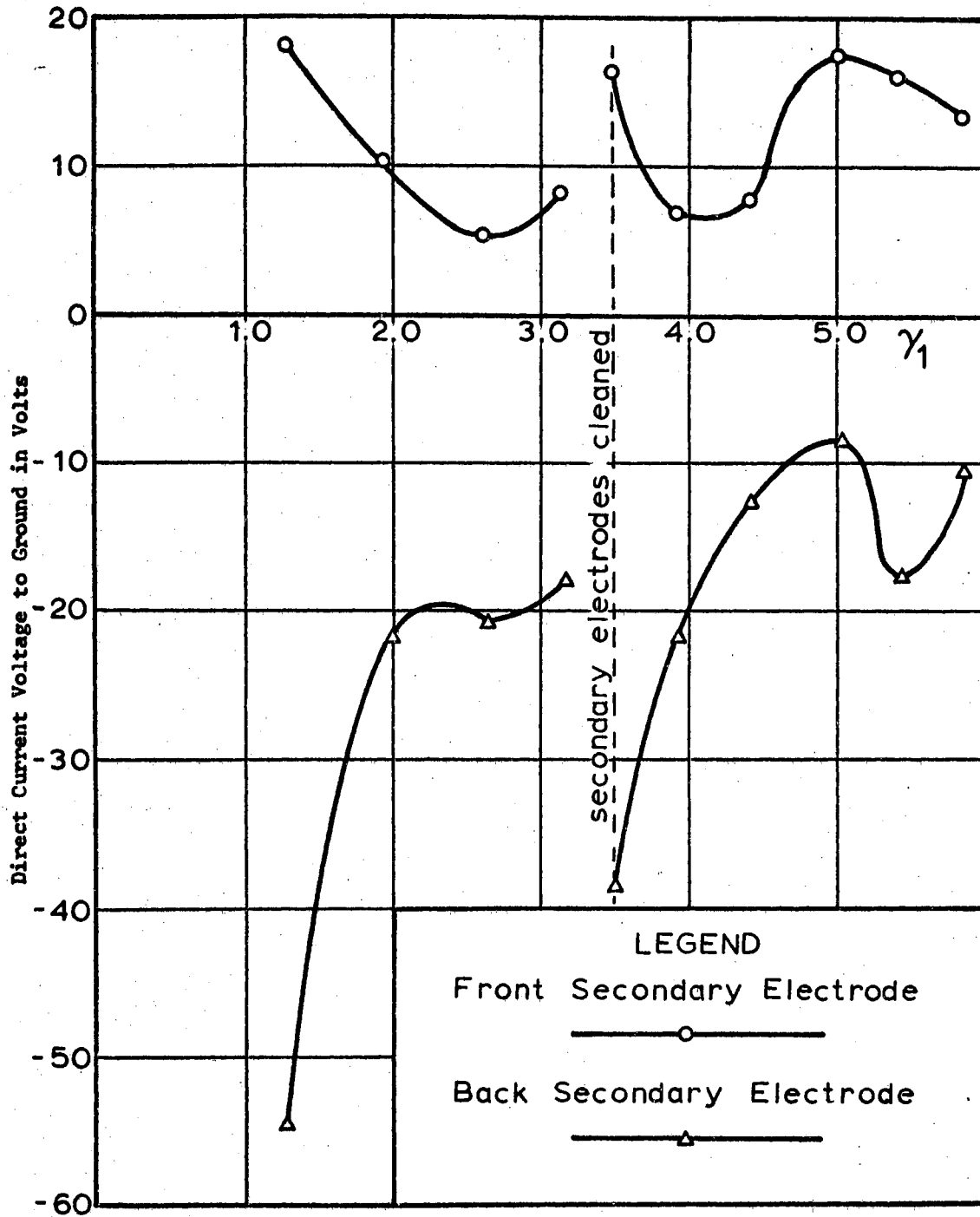
Figure 20. The DC Voltage Developed on the Secondary Electrodes
Along the γ_1 Line

electrodes were cleaned vividly illustrates the effect. The dc voltages developed on the secondary electrodes are greatly reduced by any amount of discoloration, no matter how faint. Consequently, this data is impossible to repeat unless one insures that the secondary electrodes are always maintained in the same condition. This would appear to necessitate cleaning and polishing these electrodes prior to each measurement, a procedure which the construction of the cell would not tolerate. For this reason, the data was taken by employing the scheme of alternately measuring successive points along the γ_1 and γ_2 lines so as to obtain comparative data. The plot of the voltages measured on the secondary electrodes along the γ_2 line is shown in Figure 21.

In Chapter II, as a result of the analysis, it has been proposed that an electron collision mechanism is primarily responsible for the ionization at lower values of optimum $\bar{B}$, i.e., along the γ_1 line, and that an atomic ion, H^+, collision mechanism is the principle mode of ionization at the higher optimum $\bar{B}$ values, i.e., along the γ_2 line. While this experiment cannot identify the ionization mechanisms, reference to Figures 20 and 21 does establish that ionization along the γ_1 line is a phenomenon which is distinctly different from that produced along the γ_2 line. The higher dc voltages developed at the secondary electrodes along the γ_1 line, as shown in Figure 20, would tend to indicate a mechanism associated with the more mobile particles, i.e., the electrons with their high q/m ratio. The higher potential developed at the back electrode can be explained by its location; it is adjacent to the hydrogen outlet. Hence, the gas flow velocity would tend to direct the larger number of charged particles in its direction. Our simple theory does not, however, explain why the
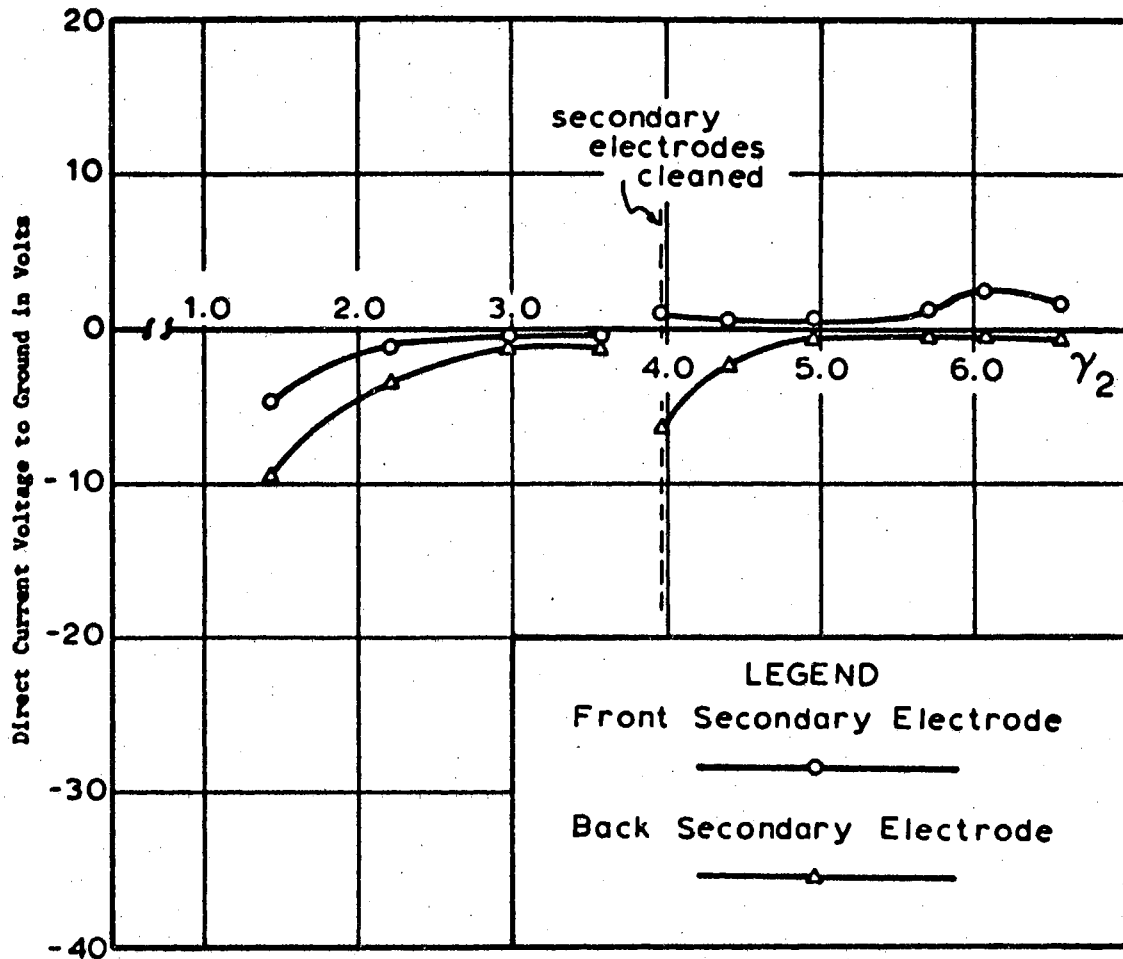
Figure 21.   The DC Voltages Developed on the Secondary
Electrodes Along the γ_2 Line

potentials should be of opposite polarity, i.e., the potential
developed on the front electrode positive and that on the back electrode
negative with respect to ground everywhere along the γ_1 line. Refer
to Equations 2.13 in Chapter II for the drift velocity. Along the γ_1
line the angular frequency of gyration for the electron is many times
greater than that of the applied rf, but the opposite is the case for
the atomic and molecular ions so that $\overline{V}_D$ for the ions in the system
is in the opposite direction to that for the electrons. A like
condition exists for the perpendicular velocity components (again,
see Equations 2.13 in Chapter II). That this effect may influence the
situation with respect to the sign of the secondary electrode potentials,
is substantiated by reference to Figure 21. Here, along the γ_2 line,
the conditions described above still apply to the electrons and molecular
ions, but the atomic ions undergo gyromagnetic resonance. Prior to
resonance, their velocity components are directed opposite to those of
the electrons, but after resonance the directions are reversed. In
Figure 21, we note that a potential reversal occurs on the front
electrode and that the potentials remain opposite from that point on.
This occurs in the vicinity of the predicted gyromagnetic resonance
of the atomic hydrogen ions.

The problem of contamination precluded the possibility of making
extensive meaningful measurements with the secondary electrodes.
However, their use in the measurements decribed above, coupled with
periodic monitoring of the potentials developed on them as the
experimental optimum magnetic intensity mapping progressed did aid in
establishing a definite conclusion with respect to the minimum
deionization glow condition. The basic experimental observation is

that with deionization glow present in the cell, dc potentials are developed on the secondary electrodes. This is true no matter how weak the glow intensity. However, in the absence of any glow there was never any observable secondary electrode potentials irrespective of any other conditions. On the basis of these observations it was concluded that the presence of the glow is essential to establishing any substantial ordered motion of charge carriers. In these terms, the minimum glow condition described at the beginning of this section may be interpreted as the result of the minimum rf excitation which will maintain ordered motion of carriers. All of the optimum magnetic intensity data presented in this paper was taken under this condition.

Effects of Variations in Primary Electrode Spacing

An effort was made to correlate the measurements made employing the teflon cell with those taken with the aluminum cell. The data was taken with different primary electrode spacings in the two cells, but with careful attention to insure that the frequencies were the same. The electrode spacing for the aluminum cell was 0.002794 meters, and it was 0.00208 meters for the teflon cell. Refer to Figures 22 and 25. We note that the γ lines as determined for the two cells at a frequency of 7 MH_z fall at essentially the same place. Now, refer to Figures 28 and 31. Here we note that the γ_1 lines fall in essentially the same place, but there is a substantial deviation in the slope of the γ_2 lines. Further, note that the γ lines for the aluminum-bodied cell at 8 MH_z have remained practically the same as at 7 MH_z. In other words, only the γ_2 line for the teflon-bodied cell has radically shifted in going from 7 to 8 MH_z. One would
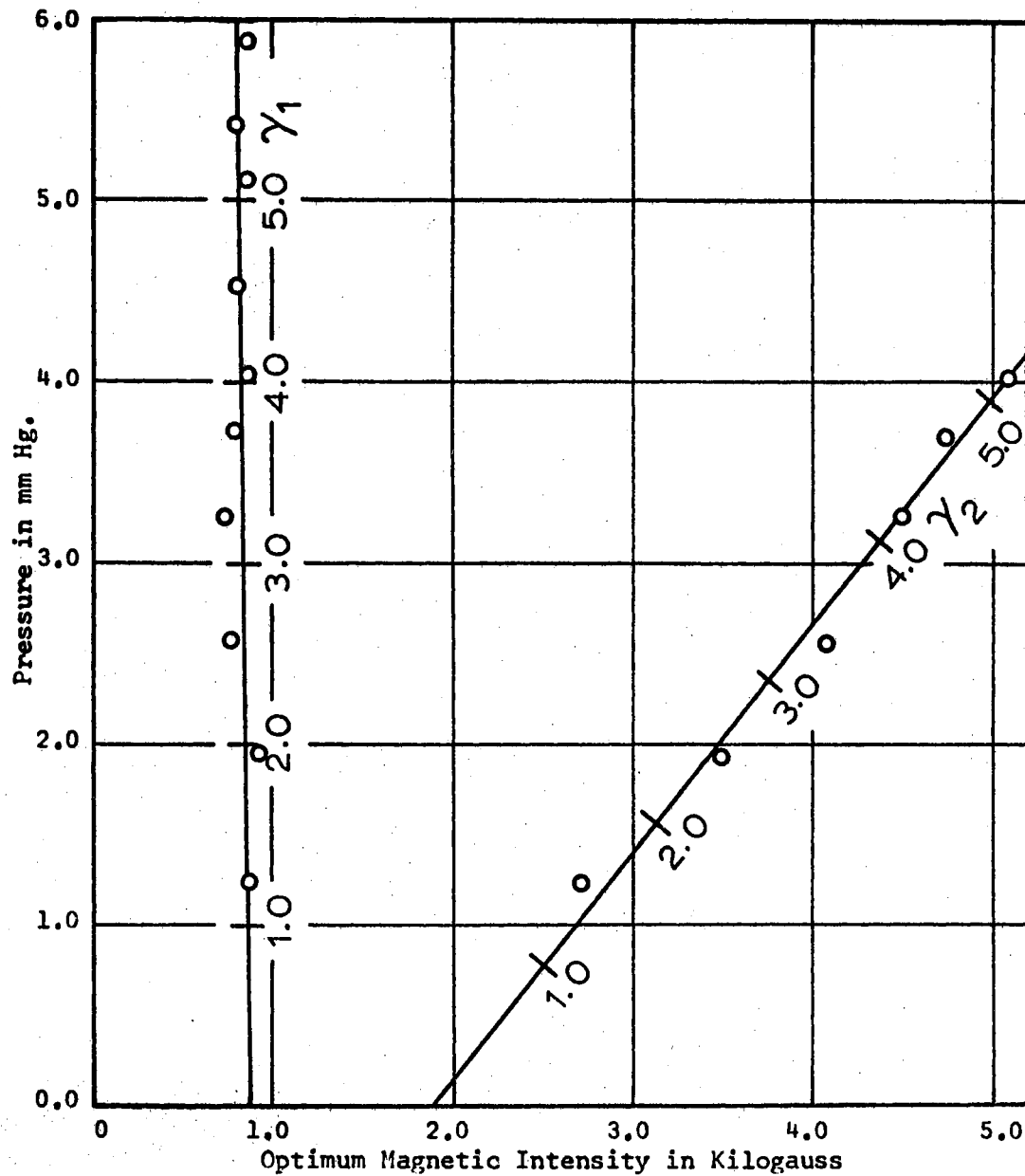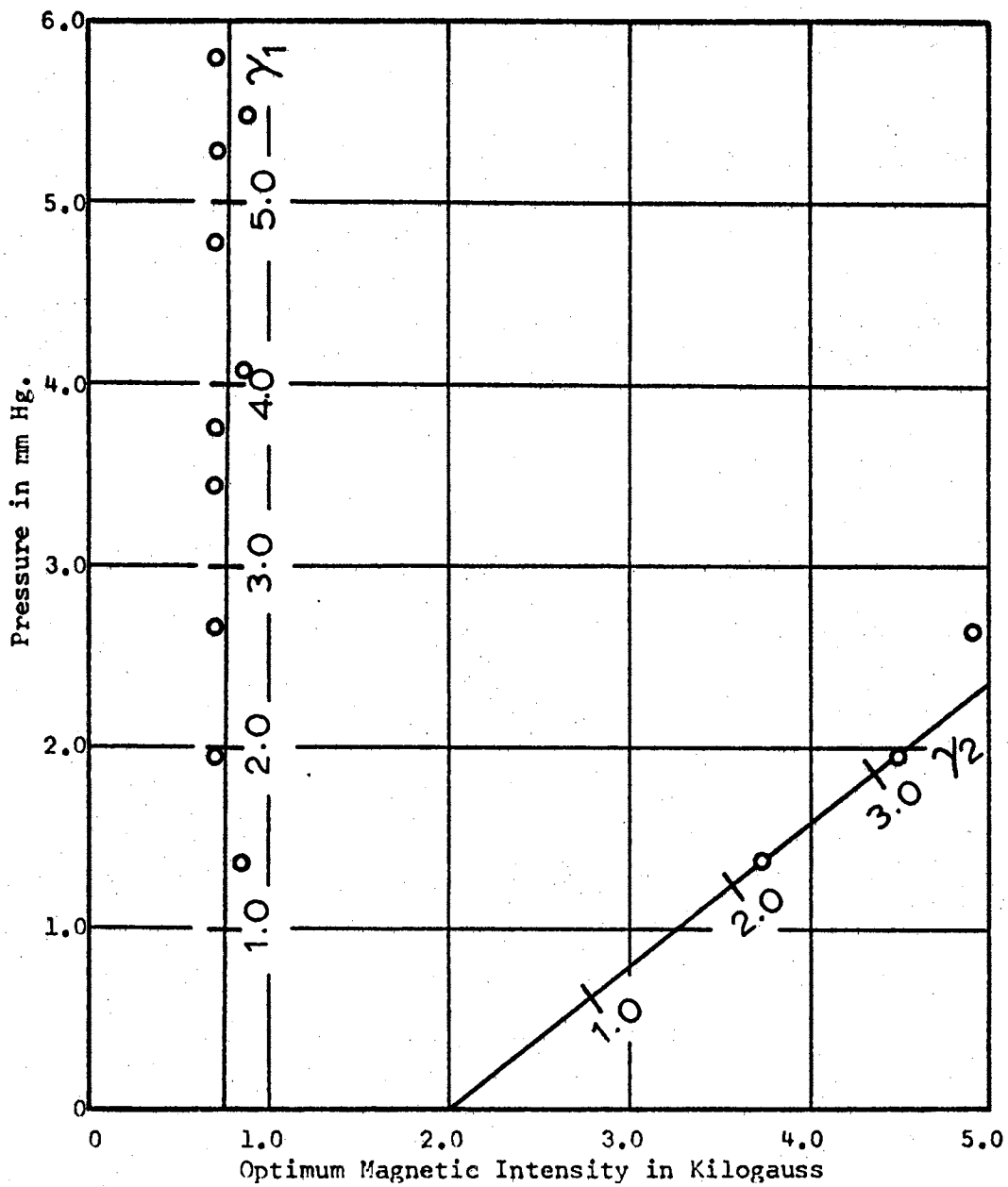
Figure 22. A Plot of Cell Pressure Versus Optimum Magnetic
Field for Hydrogen at 7 MH$_z$ Showing Data
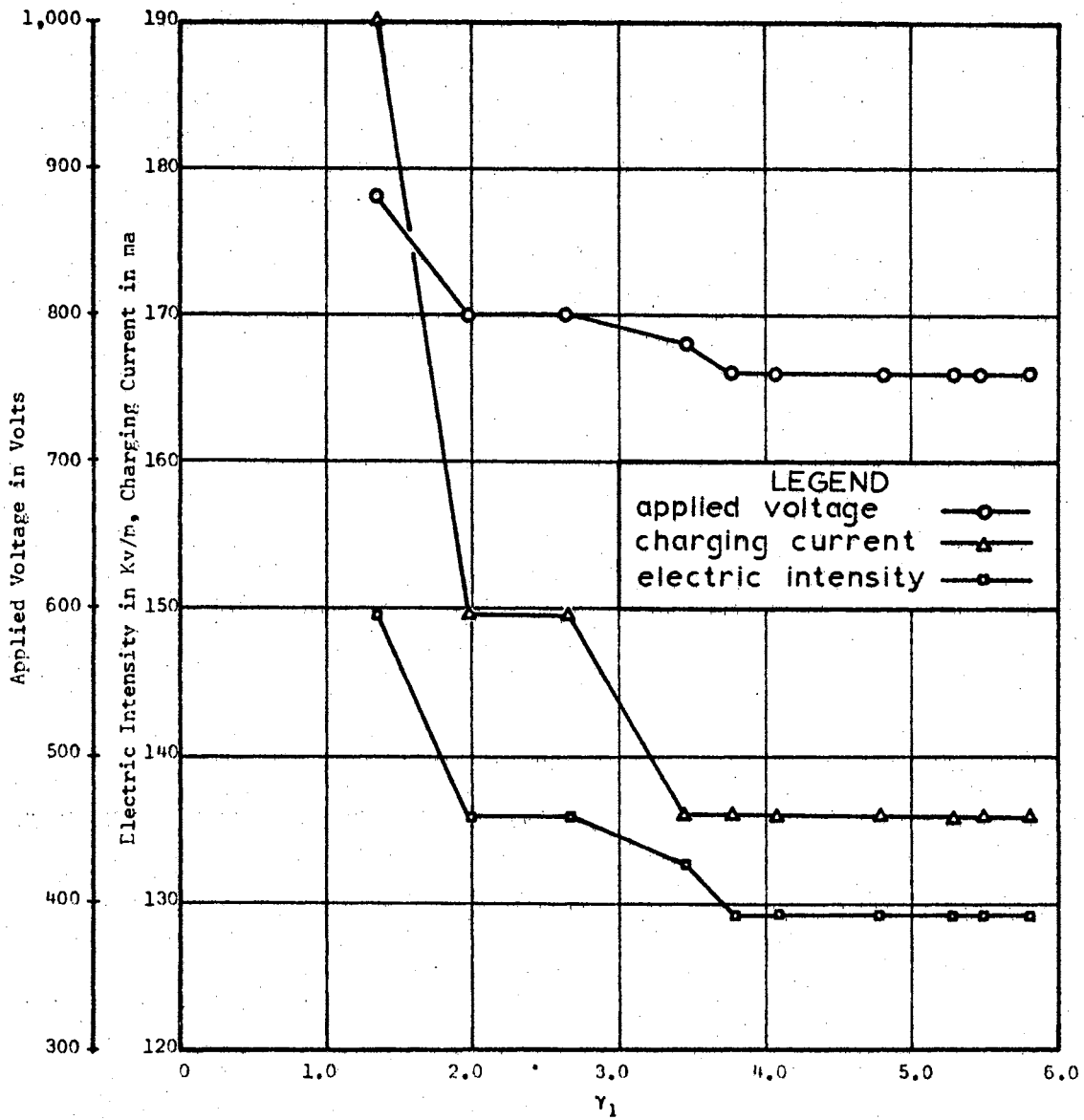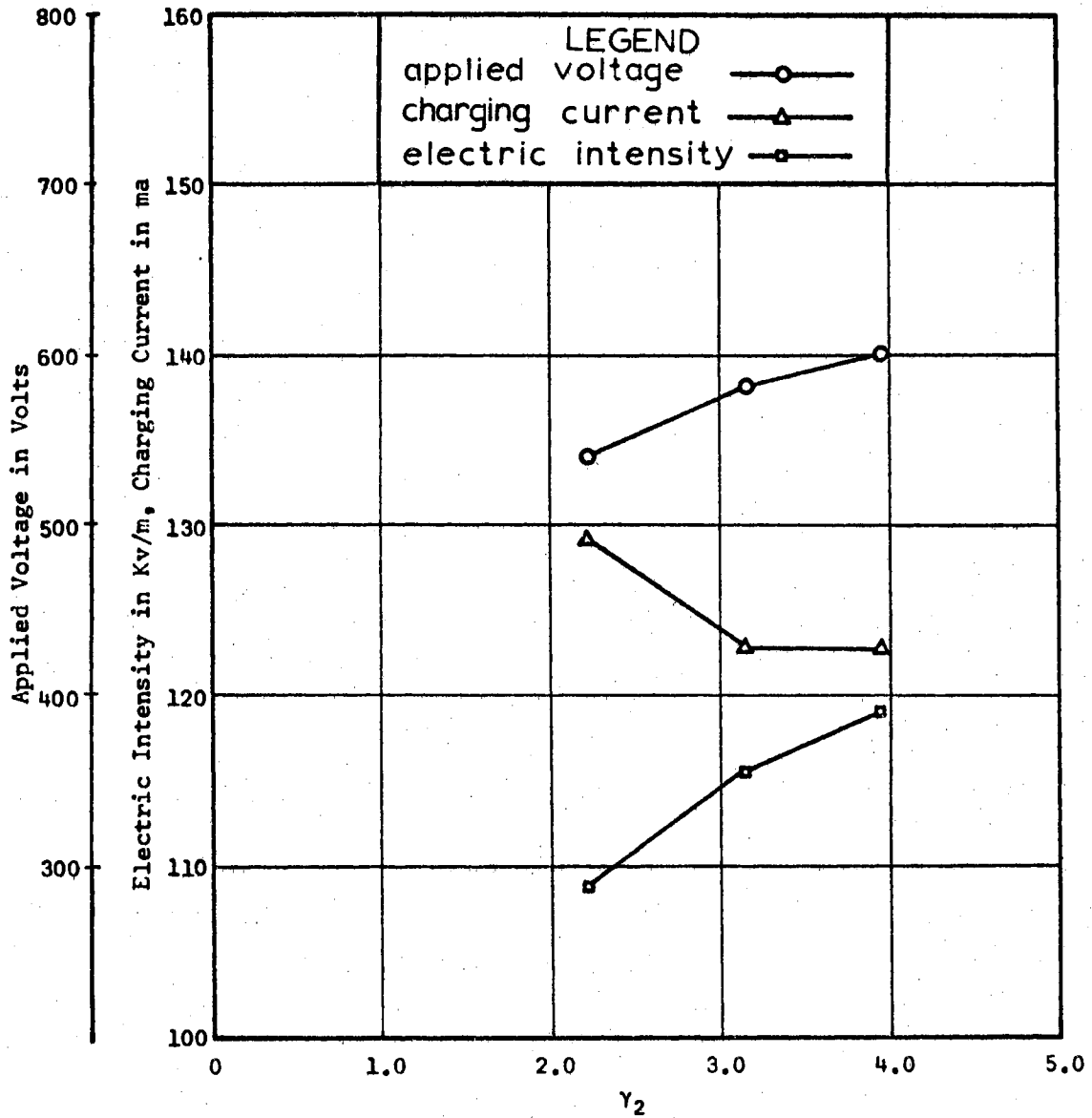Obtained Employing the Aluminum Cell
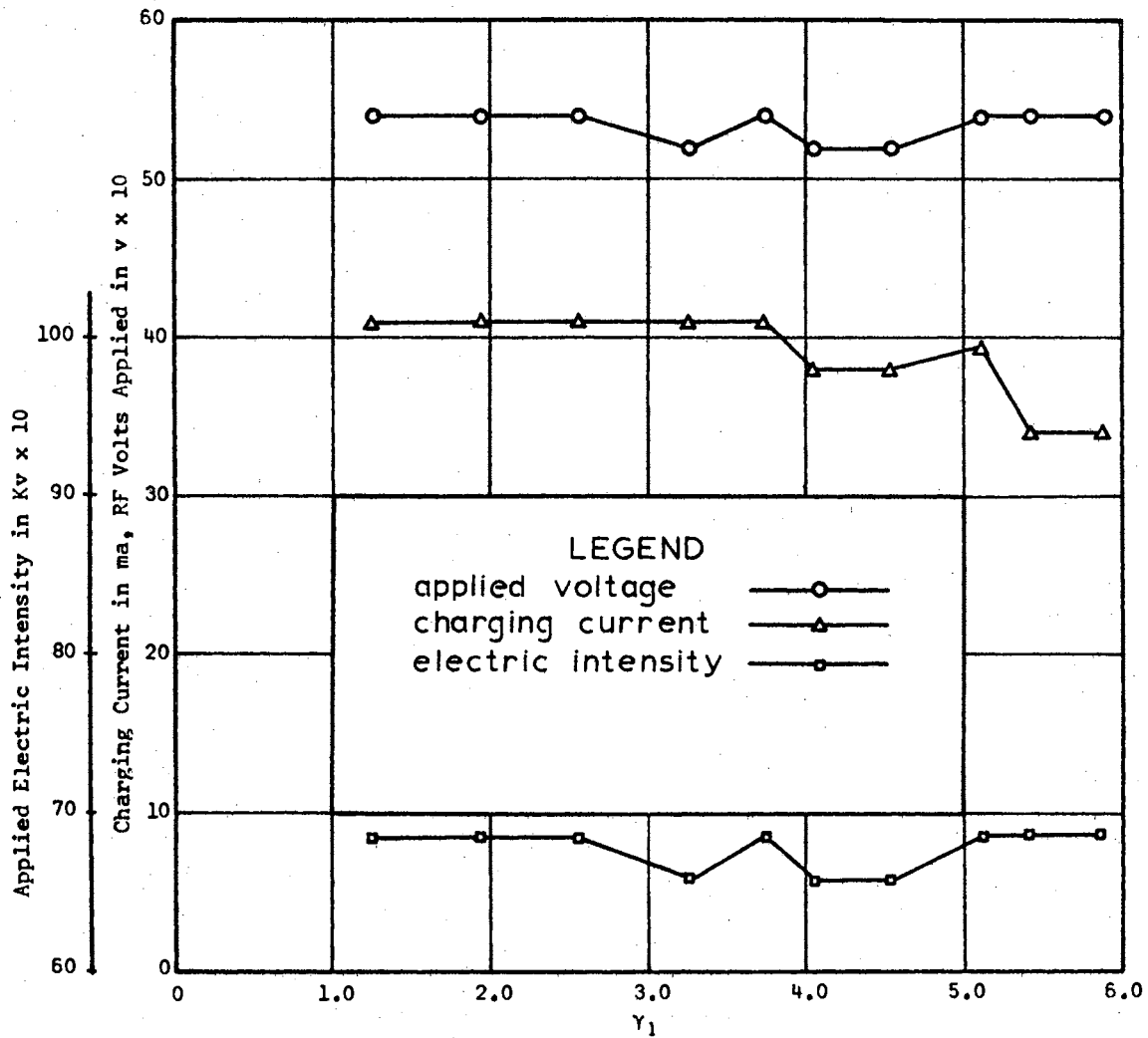
Figure 23. Applied Voltage, Charging Current, and Electric
Intensity Corresponding to the Lower Magnetic
Intensity Values at 7 MH$_z$ Shown Plotted
Against the γ_1 Variable for the Aluminum Cell
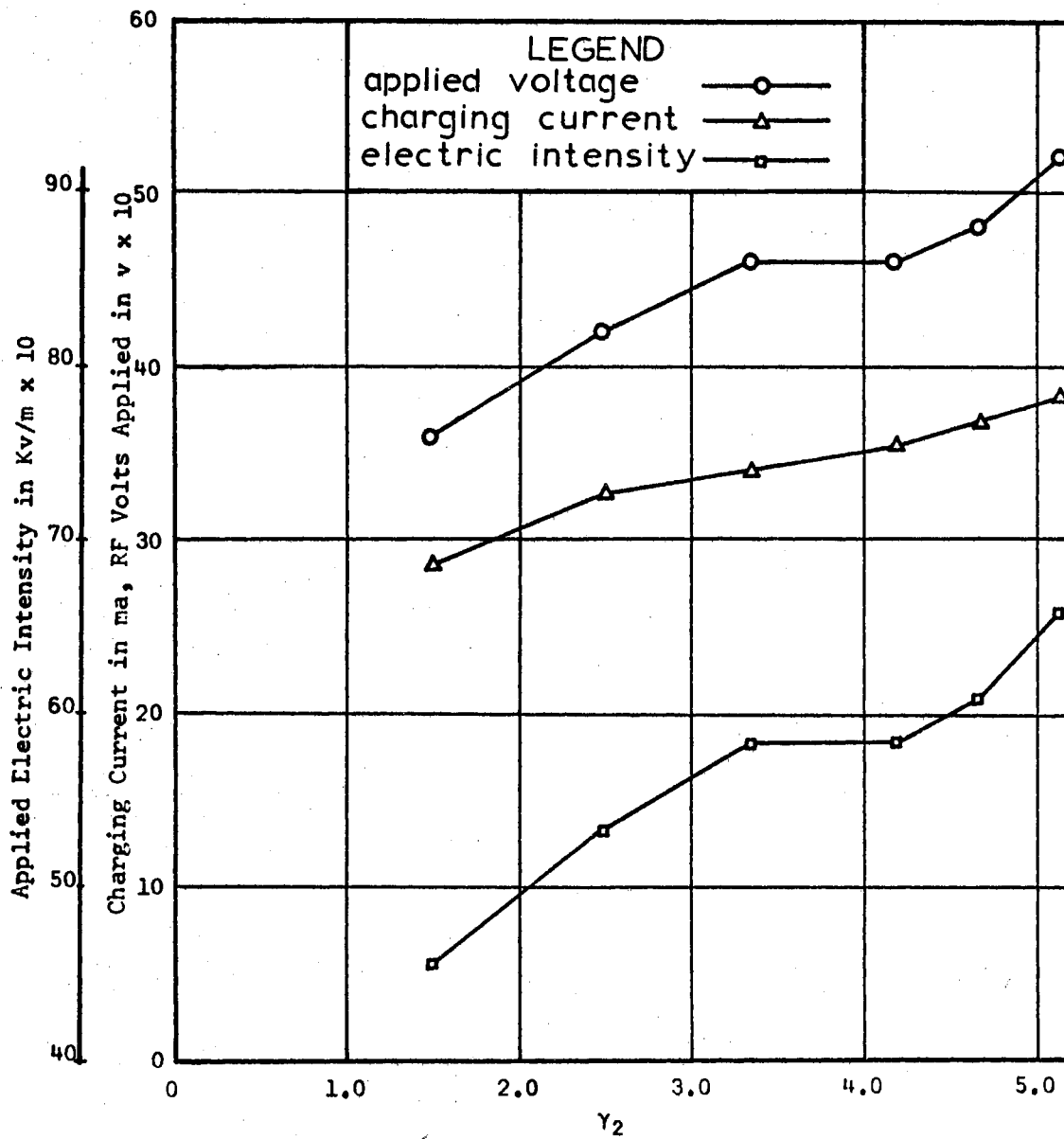
Figure 24. Applied Voltage, Charging Current, and Electric
Intensity Corresponding to the Higher Magnetic
Intensity Values at 7 MH$_z$ Shown Plotted
Against the γ_2 Variable for the Aluminum Cell
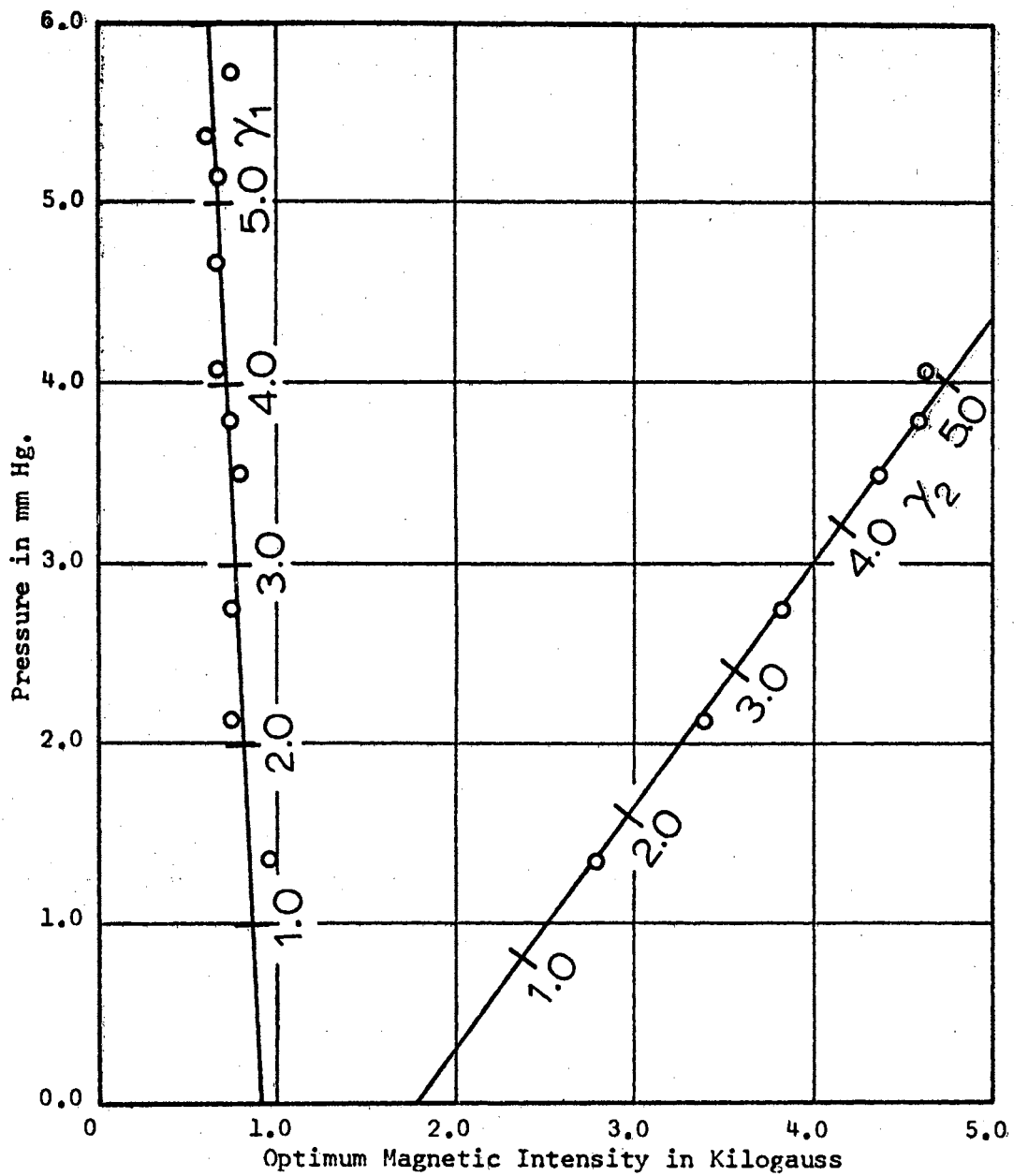
Figure 25. A Plot of Cell Pressure Versus Optimum Magnetic
Field for Hydrogen at 7 MH$_z$ Showing Data Obtained
Employing the Teflon Cell
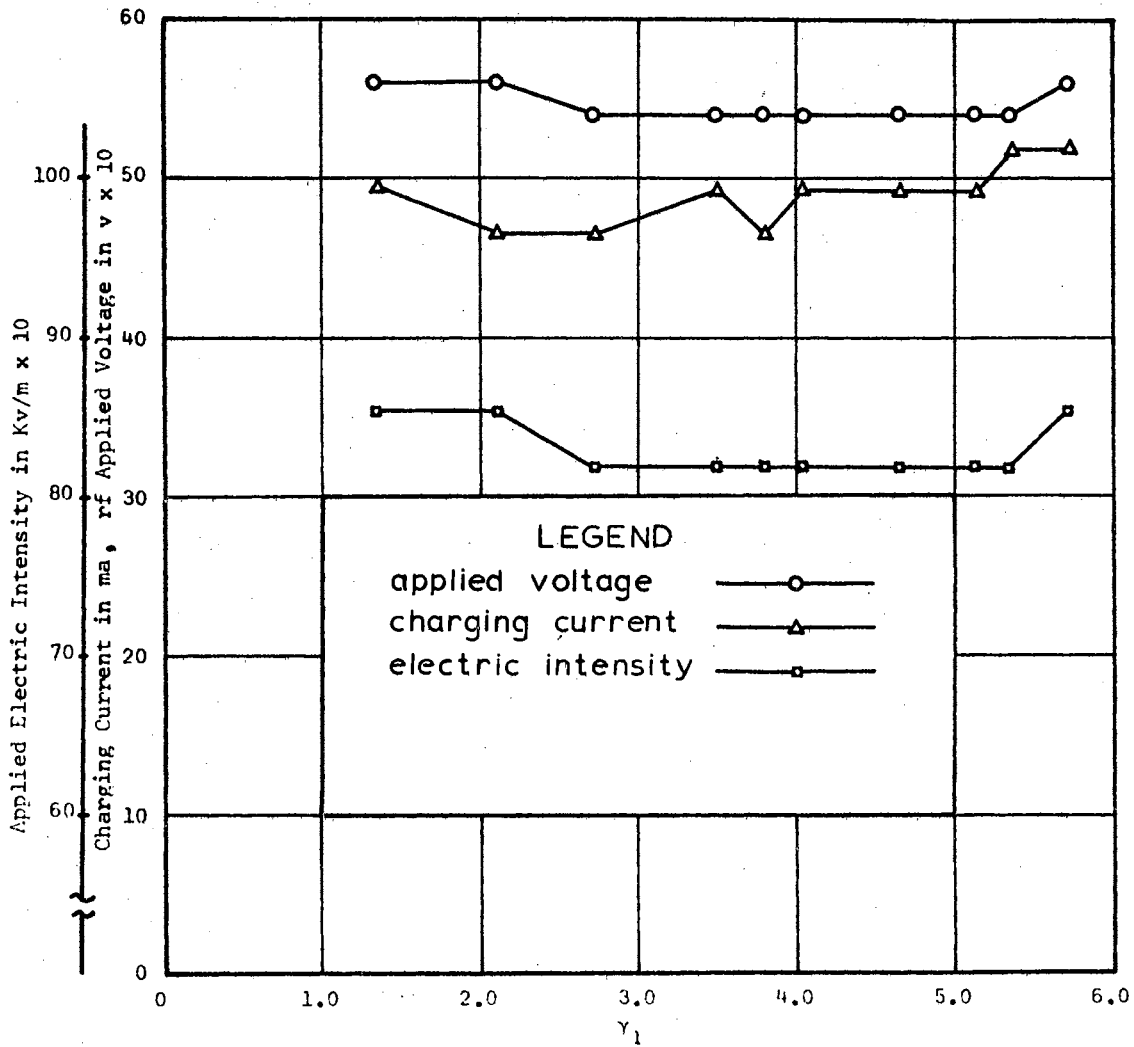
Figure 26. Applied Voltage, Charging Current, and Electric Intensity Corresponding to the Lower Magnetic Intensity Values at 7 MH_z Shown Plotted Against the γ_1 Variable for the Teflon Cell
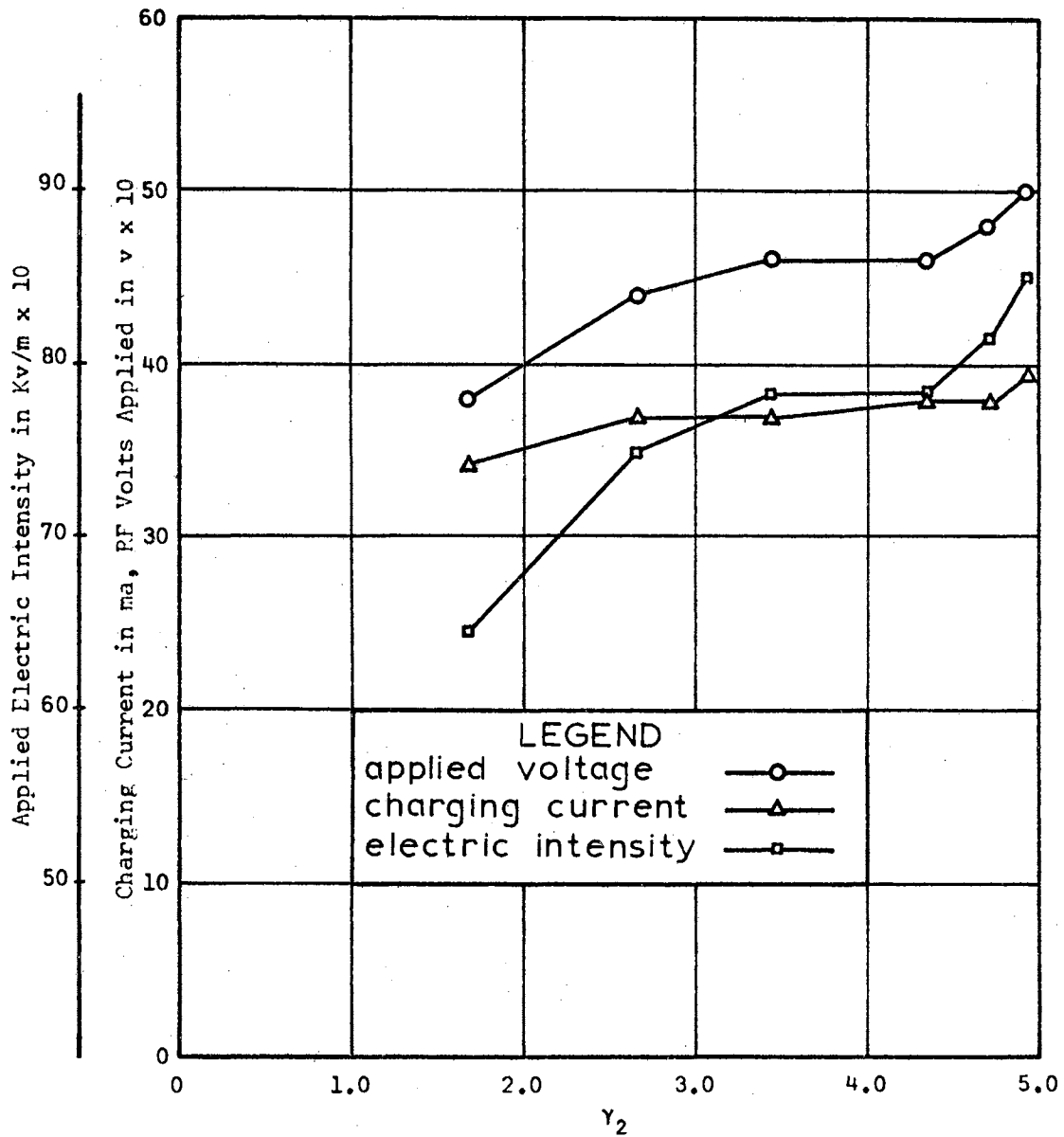
Figure 27. Applied Voltage, Charging Current, and
Electricity Corresponding to the Higher
Magnetic Intensity Values at 7 MH_z Shown
Plotted Against the γ_2 Variable for the
Teflon Cell

expect the field structure in the teflon-bodied cell to be more

subject to change with frequency than that of the aluminum-bodied cell.

This is because the teflon-bodied cell is of more "open" design, while

the aluminum-bodied cell is carefully shielded and incorporates a

guard ring structure. On the basis of these observations it is

concluded that these deviations are probably due to a small frequency

difference in the two sources. It also became evident that larger

variations with respect to frequency are to be expected in an "open"

structure like the teflon-bodied cell.

Refer to Figures 23, 24, 26 and 27. Note that at 7 MH_z the values

of applied voltage and charging current are essentially the same for

the two cells despite the difference in electrode spacing. The

applied electric intensity is calculated by dividing the applied

voltage by the electrode spacing. Consequently it appears at quite

different levels for the two cells. This would infer, on the basis

of the previously presented theory, that while all other things were

nearly equal, the particle velocities in the teflon-bodied cell were

much larger than in the aluminum-bodied cell. This, of course, is

not reasonable. Now, refer to Figures 29, 30, 32 and 33. At 8 MH_z

we noted above that the slopes of γ_2 lines were quite different for

the two cells, and here we see that this evidently implies quite

different applied voltage and charging current characteristics.

Again, refer to the 7 MH_z curves, Figures 22 through 27. The

γ line, applied voltage, and charging current data for the two cells

are essentially the same despite the fact that the electrode spacings

were considerably different. Since the data is taken under conditions

where the applied voltage and current through the cell are 90 degrees
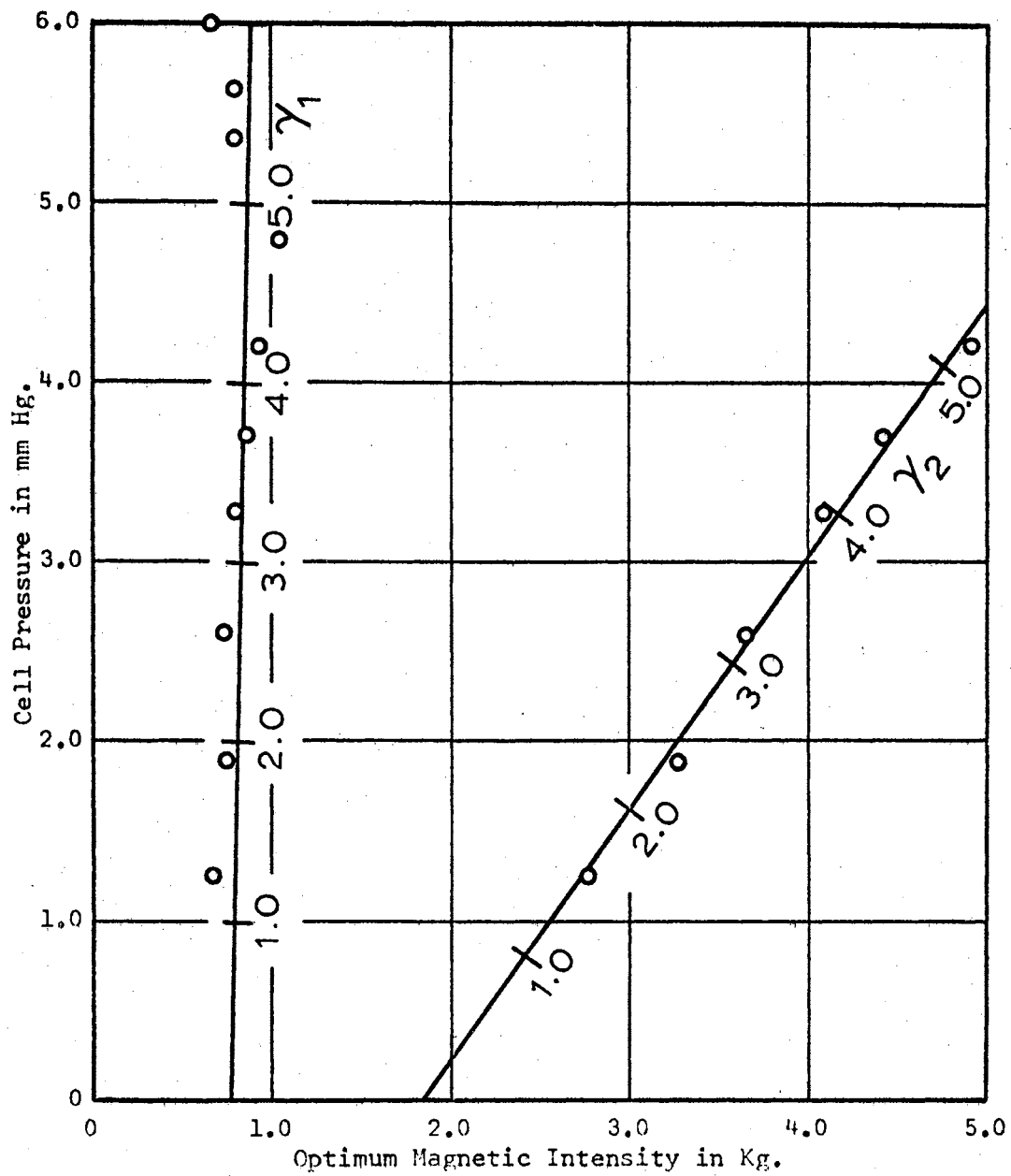
Figure 28. A Plot of Cell Pressure Versus Optimum Magnetic
Field for Hydrogen at 8 MH$_z$ Showing Data Obtained
Employing the Aluminum Cell
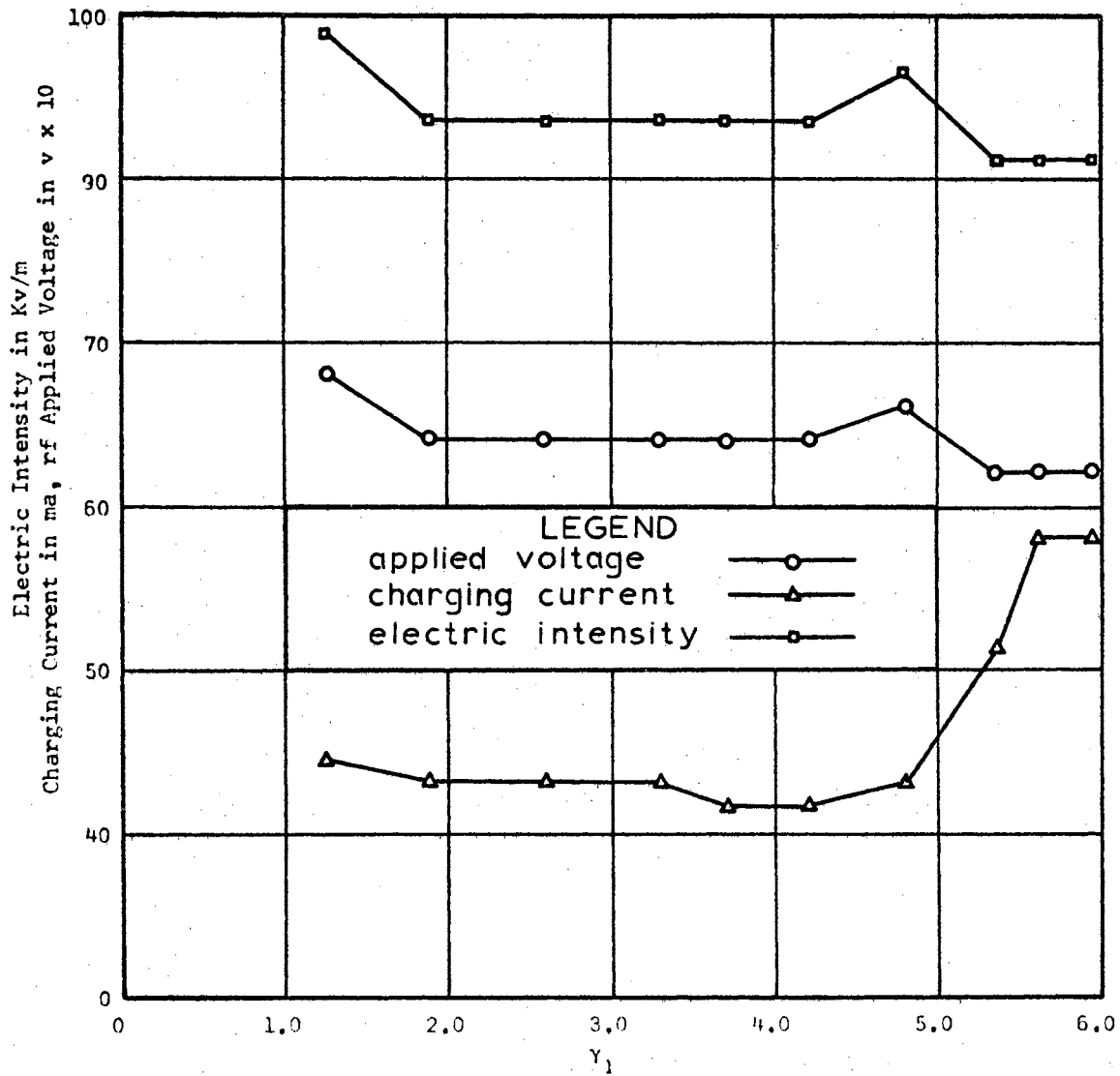
Figure 29. Applied Voltage, Charging Current, and Electric Intensity Corresponding to the Lower Magnetic Intensity Values at 8 MH_z Shown Plotted Against the γ_1 Variable for the Aluminum Cell
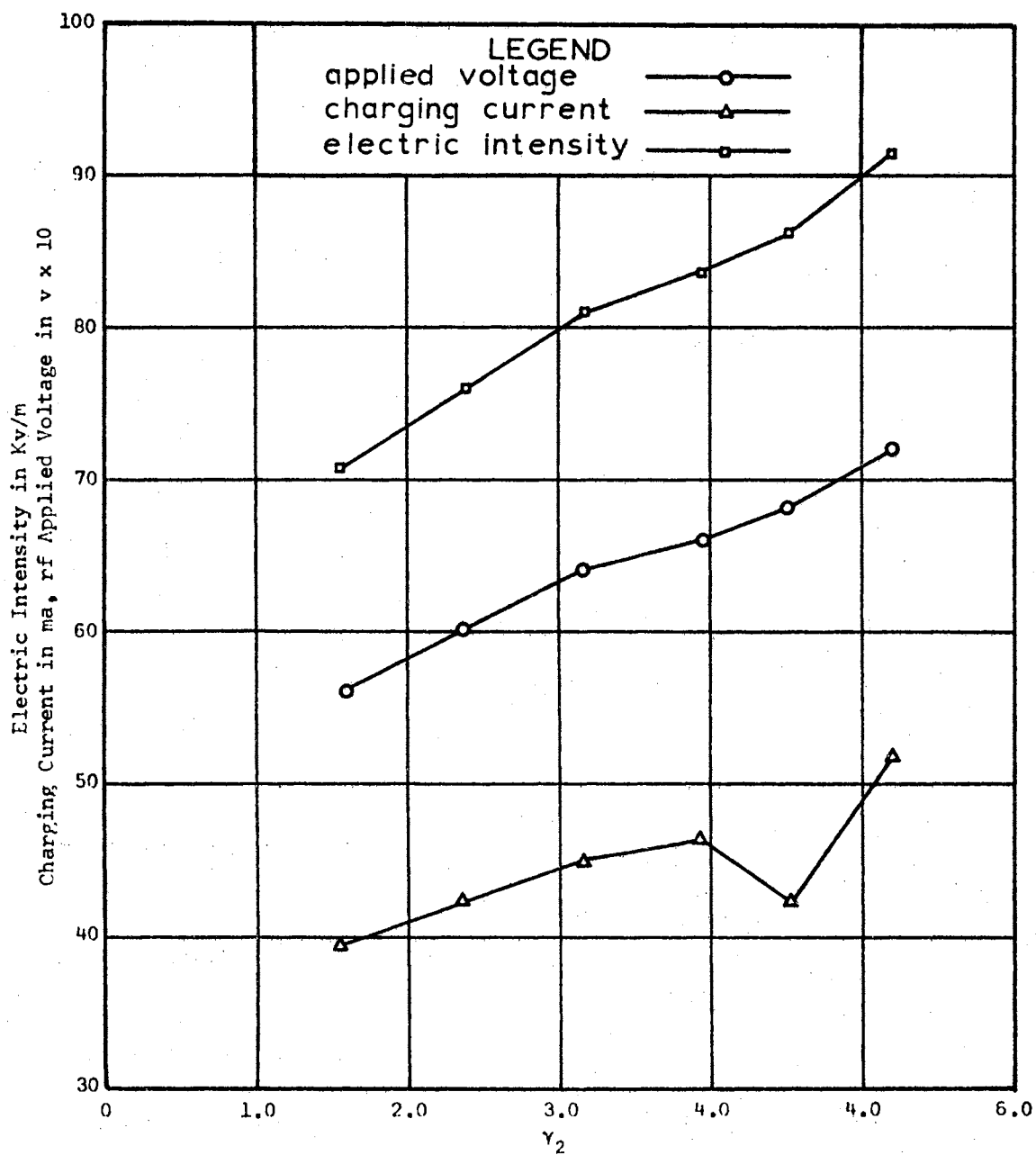
Figure 30. Applied Voltage, Charging Current, and Electric
Intensity Corresponding to the Higher Magnetic
Values at 8 MH$_z$ Shown Plotted Against the Y_2
Variable for the Aluminum Cell

Figure 31. A Plot of Cell Pressure Versus Optimum Magnetic
Field for Hydrogen at 8 MH$_z$ Showing Data
Obtained Employing the Teflon Cell

Figure 32. Applied Voltage, Charging Current, and Electric
Intensity Corresponding to the Lower Magnetic
Intensity Values at 8 MH$_z$ Shown Plotted
Against the γ_1 Variable for the Teflon Cell

Figure 33. Applied Voltage, Charging Current, and Electric Intensity Corresponding to the Higher Magnetic Intensity Values at 8 MH_z Shown Plotted Against the Y_2 Variable for the Teflon Cell
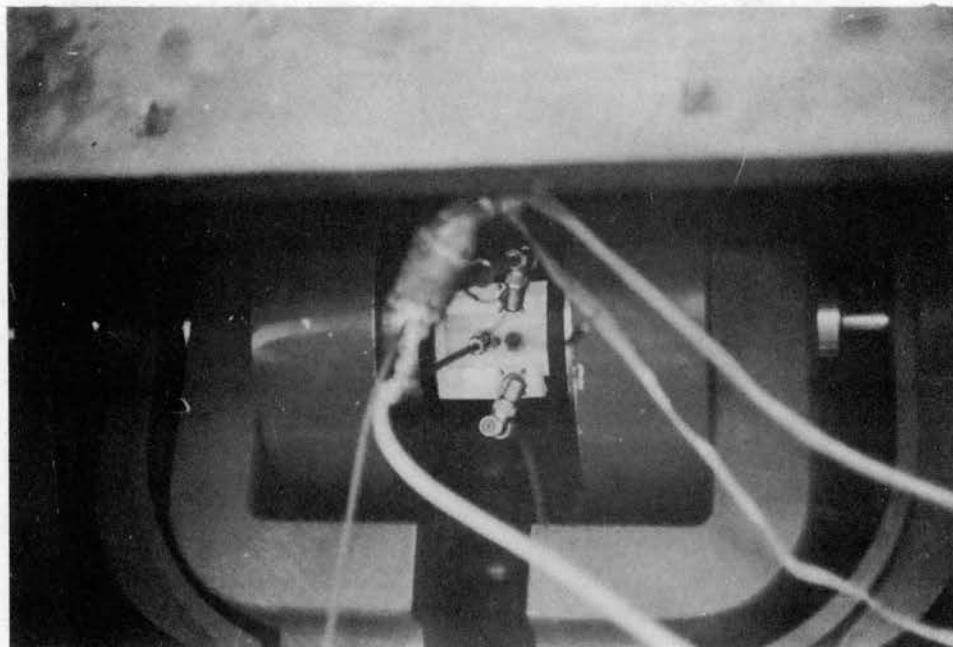
Figure 34. A Photograph Showing the Teflon Cell Installed
the Electromagnet
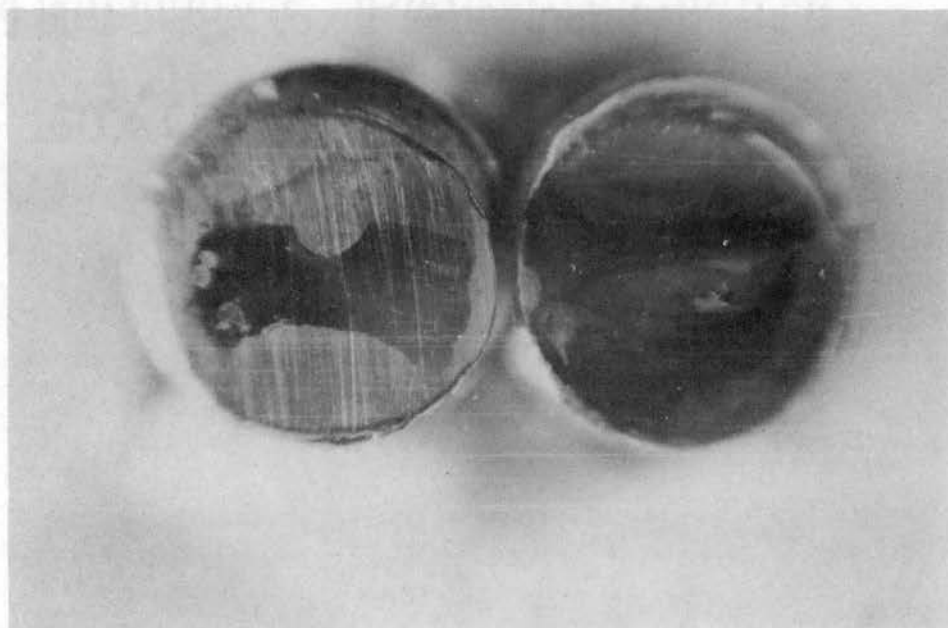
Figure 35. A Photomacrograph Showing the Darkening which
Appeared on the Secondary Electrode Surfaces
(Actual Size is 3/16 Inch Diameter) Upon
Removal from the Teflon-Bodied Cell
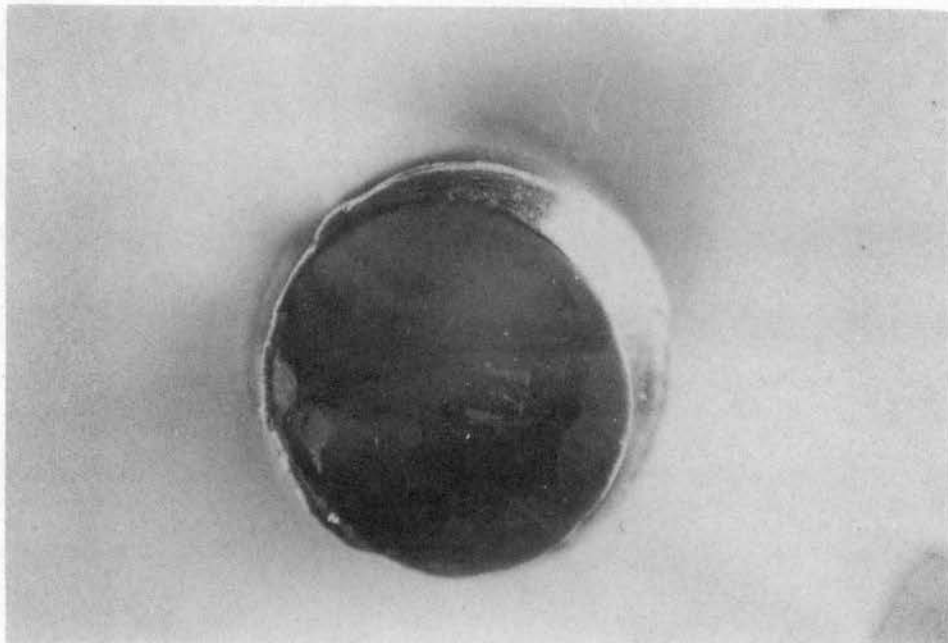
Figure 36. A Photomacrograph Showing an Enlarged View of
the Back Secondary Electrode Alone
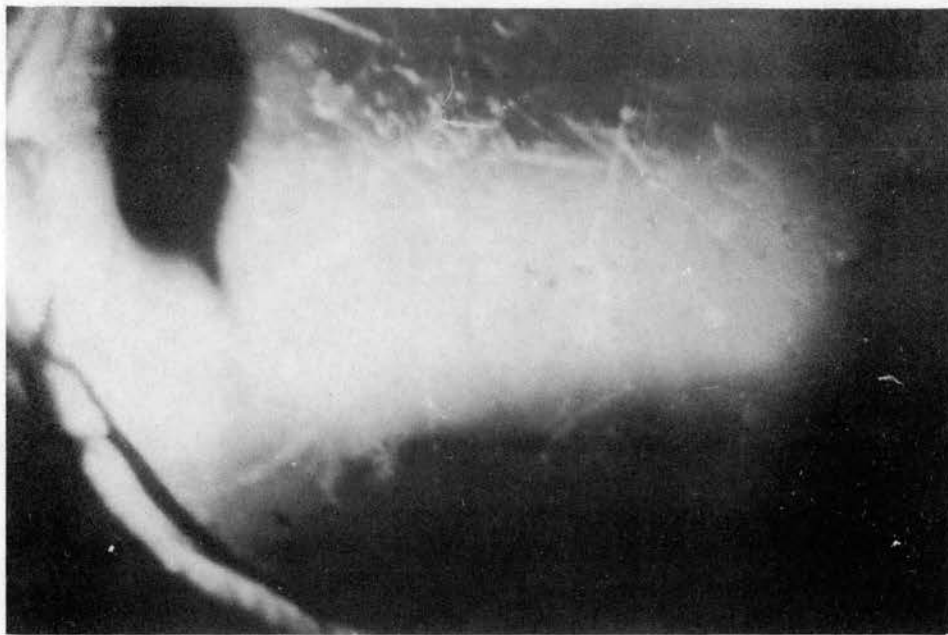
Figure 37. A Photomacrograph Showing the Deionization Glow
as it Appears in the Cell Window

out of phase, so far as can be determined by the dual-trace oscilloscope, and hence we refer to this current as the charging current, the ratio of applied voltage to charging current represents the capacitative reactance of the cell. The indication from the 7 MH_z data is that this reactance, and hence the capacitance of the two cells, did not change with electrode spacing. It is believe that this effect can only be explained in terms of a space-charge layer, or layers, lying in the region between the primary electrodes which tend to become thicker with increased electrode spacing. Velocity computations and the photomacrographs of Figures 36 and 37 tend to support this view. Velocity computations based upon the previously reported theory and the applied electric intensity computation have consistently given lower kinetic energies than required to produce ionization by collision. This could be justified in terms of space charge. Figures 36 and 37 suggest the nature of such a space charge. Figure 36 is a photomacrograph of the face of the back electrode (3/16 inch diameter actual size) as it appeared upon removal from the teflon-bodied cell at the conclusion of the data taking. This is the secondary electrode which is least disturbed by adjacent attachments to the cell. Note that the darkened portions of the surface, which indicate regions of particle bombardment, tend to describe two lines separated by a region in which no darkening occurred. This indicates layers of ordered particle activity parallel and adjacent to the surfaces of the primary electrodes and that these layers are separated by a central layer in which no such ordered activity occurs. It is believed that this central region represents the space-charge region. Figure 37 is a photomacrograph of the deionization glow as viewed through the cell window.

Much difficulty was experienced in obtaining this photograph due to
vibrations and mechanical restrictions; consequently, it leaves much
to be desired in clarity. However, note that the glow fades out to
give two dark layers which are a fraction of a millimeter in thickness
at the surfaces of the primary electrodes. These dark layers
correspond at least approximately to the darkened lines shown on the
surface of the back secondary electrode in Figure 36.

Voltage and Current Traces at 2 MH_z

In the previous paragraphs of this Chapter, much mention has
been made of the fact that the applied voltage and current through the
cell were both linear and 90 degrees out of phase (so far as could be
determined by the methods employed to measure) under the minimum
glow condition where data was taken. However, this condition did
not quite hold true at 2 MH_z. An example of the phenomenon observed
at this frequency is illustrated in Figures 38 and 39. Figure 38
shows that voltage and current waveforms were linear and 90 degrees out
of phase with no gas in the cell. Figure 39 shows the voltage and
current waveforms with gas flowing into the cell at 20 std. cc/m and
under the best minimum glow condition which could be obtained. Note
that although the phase displacement appears to be essentially the
same as before, a non-linearity has been introduced into the current
waveform. This condition tended to become slightly more prominant
with increasing mass glow. All of the 2 MH_z data presented in the
following section was taken under the condition described above.
However, this effect disappeared quite rapidly with increasing frequency.
The data at 8 MH_z and above was taken under the previously described

conditions with current and voltage waveforms as illustrated in

Figure 11.
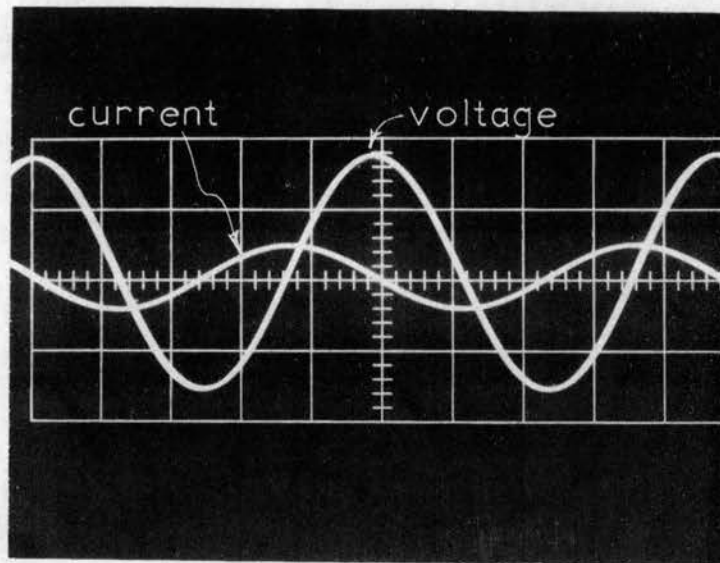
Figure 38. Voltage and Current Traces as
Observed at 2 MH$_z$ with no Gases
in the Cell
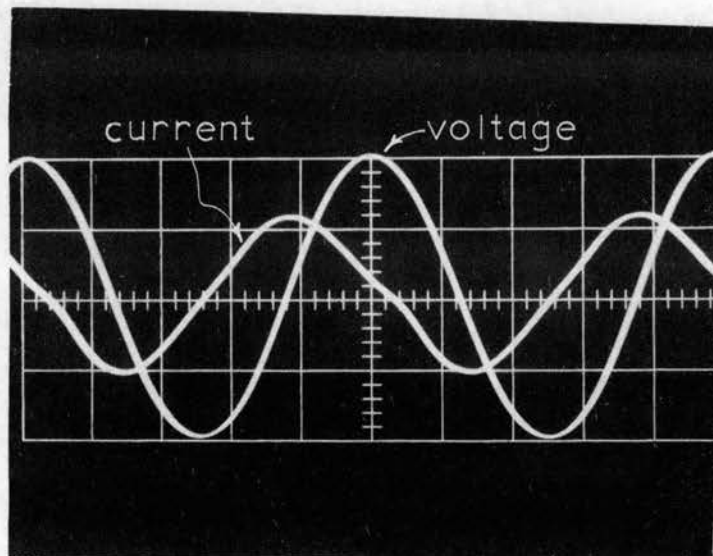
Figure 39. Voltage and Current Traces as
Observed at 2 MH$_z$ with a Mass
Flow of 20 std. cc/min Under
the Condition of Best Obtain-
able Minimum Glow

CHAPTER V

AN OPTIMUM MAGNETIC INTENSITY MAPPING OF HYDROGEN

This chapter presents the optimum magnetic intensity mapping of

hydrogen discussed in the preceding chapters of this thesis. The

results of all measurements taken throughout the course of the study

are given, listed by frequency, starting at 2 MH_z, in chronological

order. This approach adds considerable bulk to the thesis, however,

after much thought was deemed essential in order to show as clearly

as possible the true nature of the measured phenomena and the

extent to which agreement was and was not found with the predictions

of the analysis. For example, reference to the 3.5 MH_z data contained

in Figures 44 through 46 gives a comparison between the old teflon

cell, with its relatively unshielded open structure and balanced

feed geometry, and the fully shielded, coaxially fed aluminum cell

with a guard ring structure. It is seen that there is relatively

little difference between the results from the two cells at this low

frequency, so long as the electrode spacing is nearly the same;

consequently one might assume a relative freedom from precise geometric

considerations in the design of some device employing these results

in this frequency region. The extensive data presented for 7 MH_z

also serves a like purpose. Comparing Figures 53 and 54 with

Figure 55, one notes a much more pronounced difference between the

data obtained from these two cells even though the electrode spacing

is nearly the same. This would indicate the need for more care in the geometric design of devices operating in this frequency region. Also, the effects of varying the electrode spacing are more thoroughly investigated at the 7 MH_z and 8 MH_z frequencies. And so the list continues. Where the objective of a study is to determine the experimental bases of devices not yet conceived, one is quite helpless in deciding which data are superfluous.

In obtaining the data presented in this chapter the optimum magnetic intensities were determined by experimental observation, as discussed in Chapter IV, while holding the cell pressure at some constant value. After the optimum magnetic intensity was determined at minimum glow, this condition was held while the applied voltage and charging current measurements were made. This raw data was then processed on the IBM 7040 digital computer as discussed in the Appendix. At the same time, computations of the charged particle velocities were made in accordance with the analysis of Chapter II, Equations 2.13 through 2.21. This computer program is given in Table I of the Appendix. All of the graphs shown in this chapter were drawn by a combination of the IBM 1620 digital computer with disc storage and the Calcomp 565 automatic plotter with liquid ink conversion. It was found essential to use india ink in order to obtain satisfactory photographic reproduction. The γ-lines of the graphs shown in this chapter were all computed as a least squares fit to the appropriate sets of points by the IBM 1620 as a portion of the plotting program. Slightly over 40 hours actual computer time was required in order to plot the graphs. This program is given in Table III of the Appendix.

The caption information listed on the graphs employs the following

key:

      D - is the primary electrode spacing in meters.

      Aluminum Cell - refers to the Aluminum Cell as shown in the shop

           drawing of Figure 10.

      Aluminum Cell No. 2 - refers to the nearly identical cell with

           secondary electrodes.

      Old Teflon Cell - refers to the first model teflon-bodied cell

           with balanced-line fed primary electrodes.

      Teflon Cell - refers to the Teflon Cell as shown in Figures 8

           and 9.

      Old rf Source - refers to the E. F. Johnson Company Viking II

           amateur transmitter employed early in the study.

Where no mention is made with respect to the rf source, the combination

of the Technical Material Corporation Pal - 1KW Linear Amplifier and

Hewlett-Packard Company Model 606 A HF Signal Generator was used.

The greater credibility is to be given to data taken with either of

the Aluminum Cells and the linear amplifier - signal generator

combination.
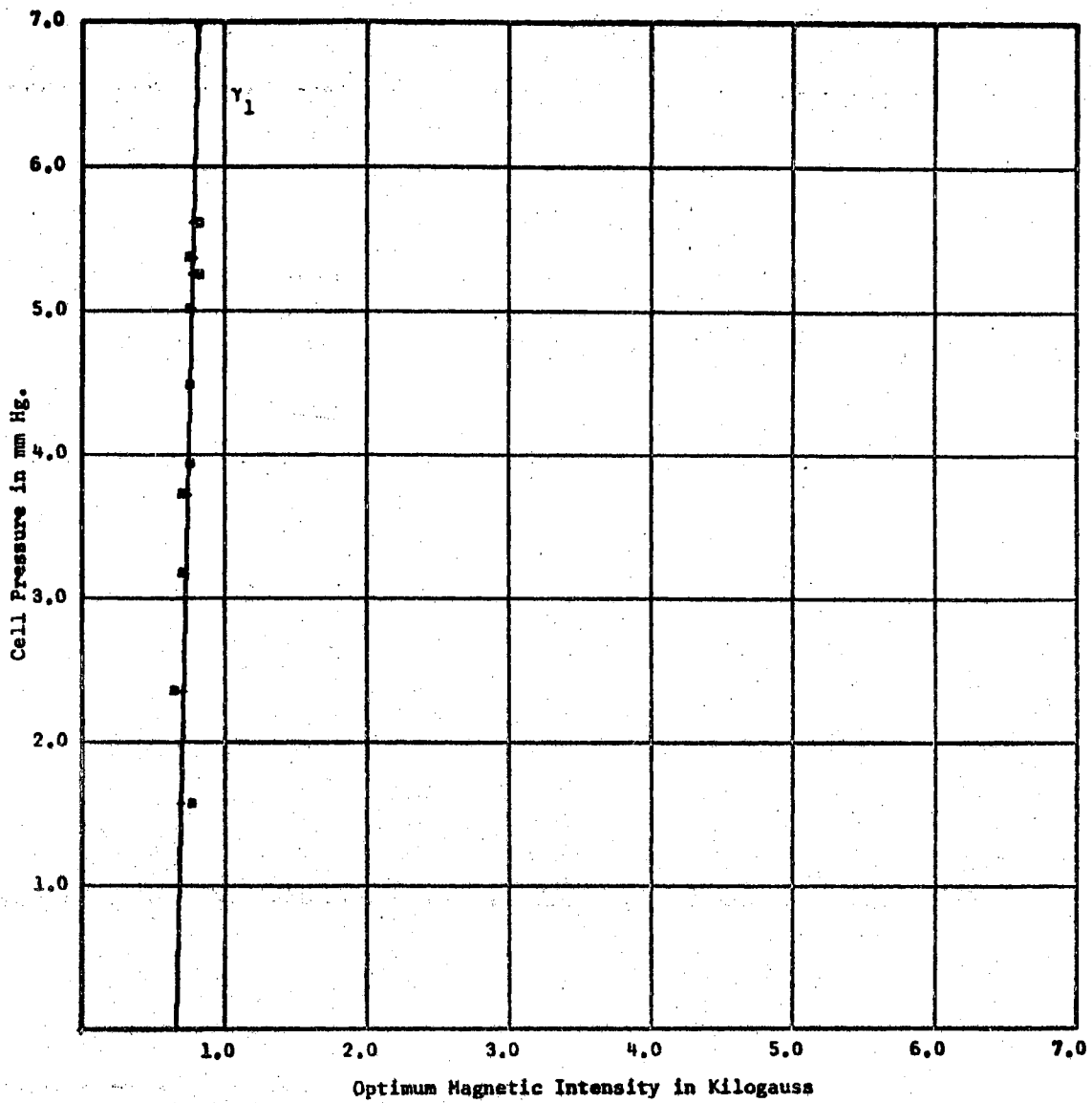
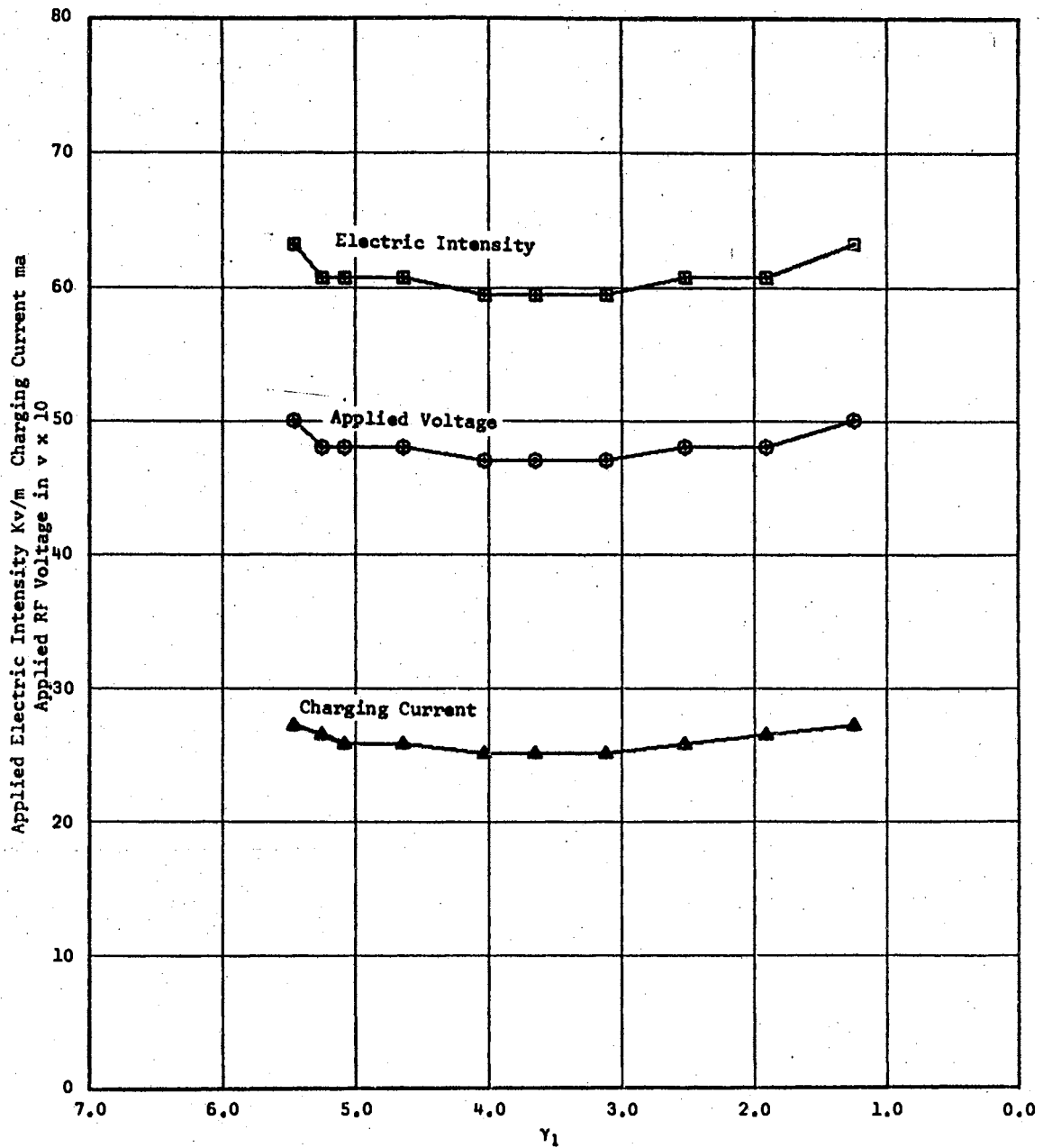Figure 40a. Data taken June 27, 1966 at 2 MH$_z$ with the Aluminum Cell, D = 0.002794 meters.
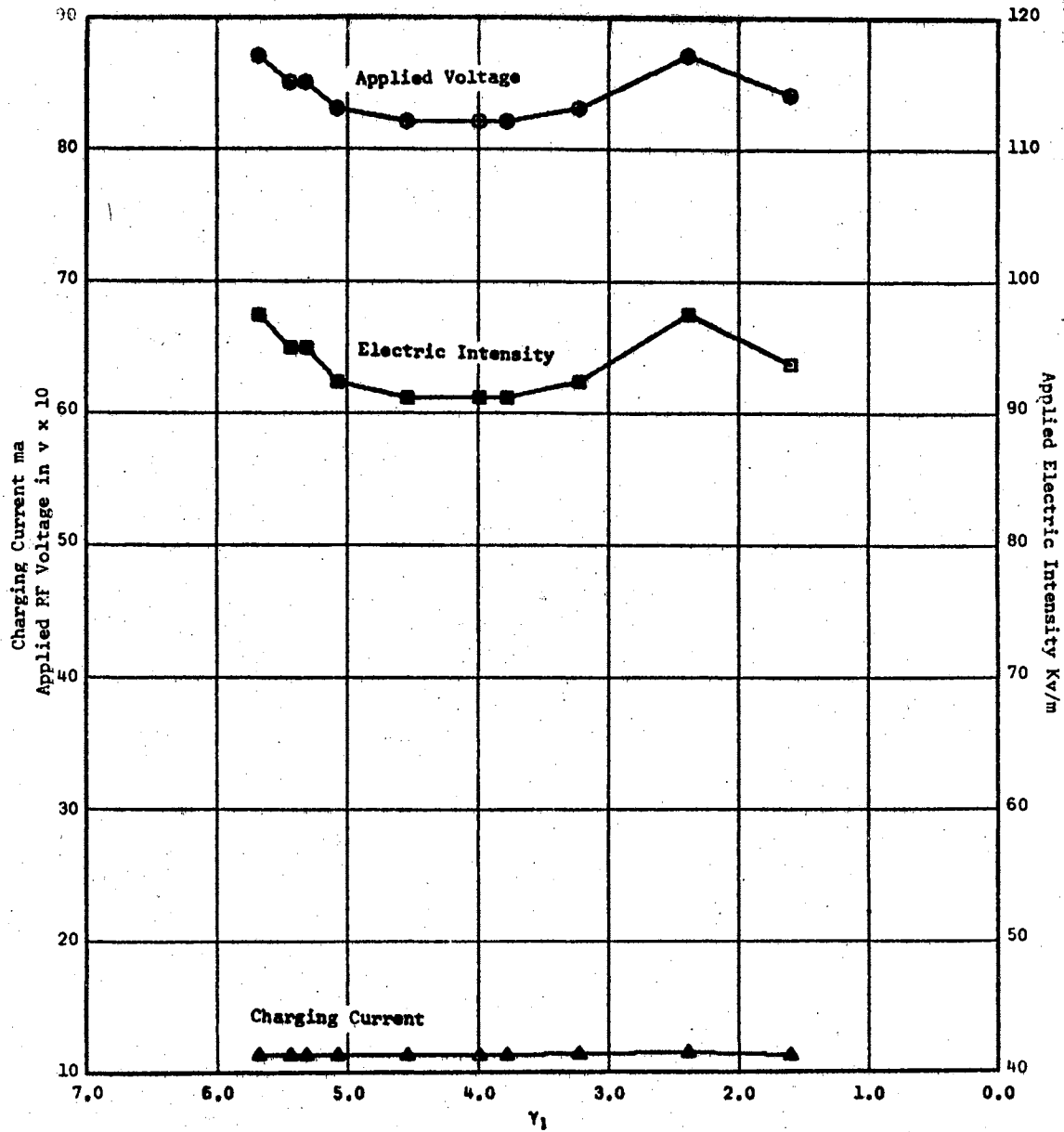
Figure 40b.   Data taken June 27, 1966 at 2 MH$_z$ with the
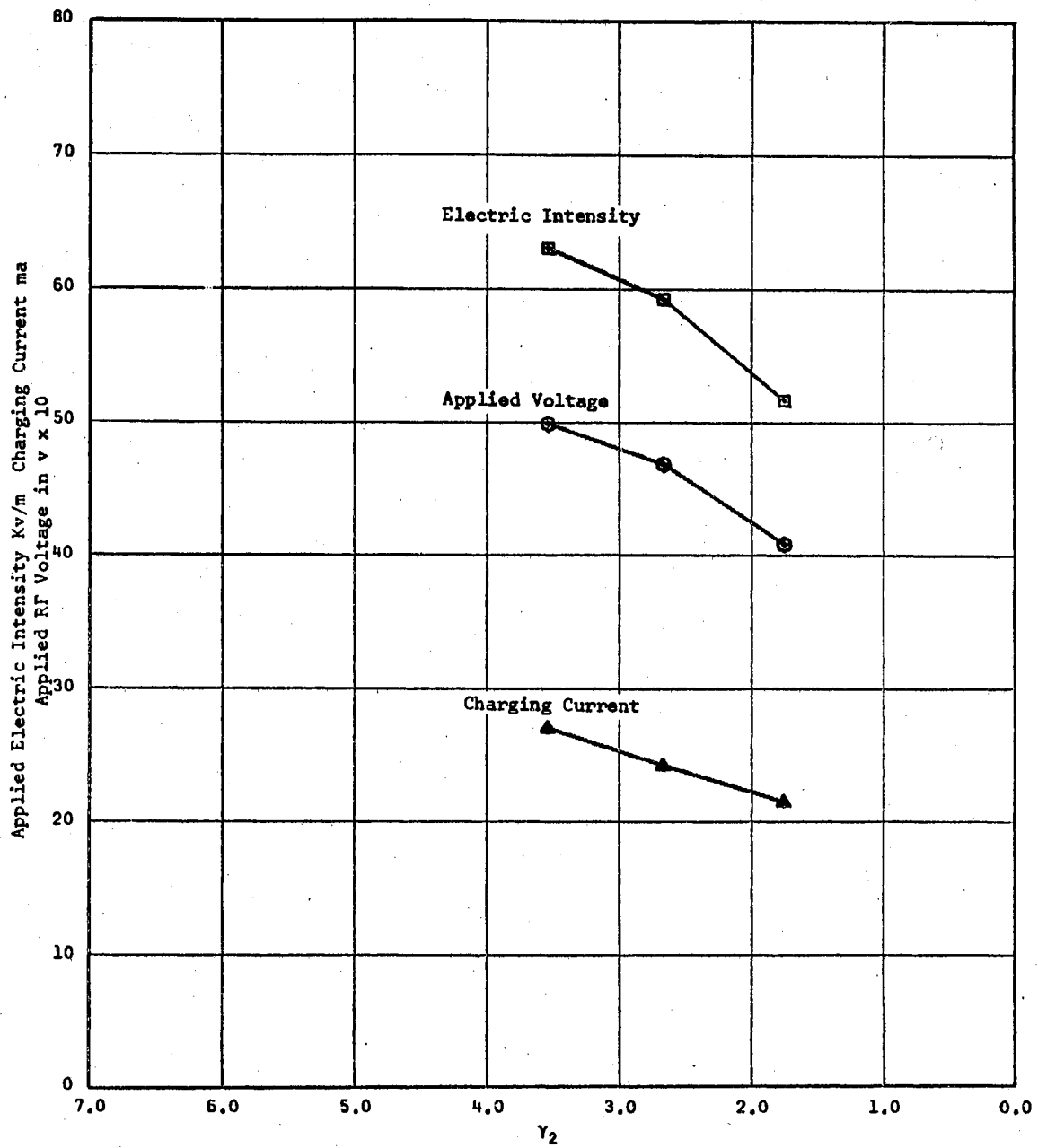Aluminum Cell, D = 0.002794 meters
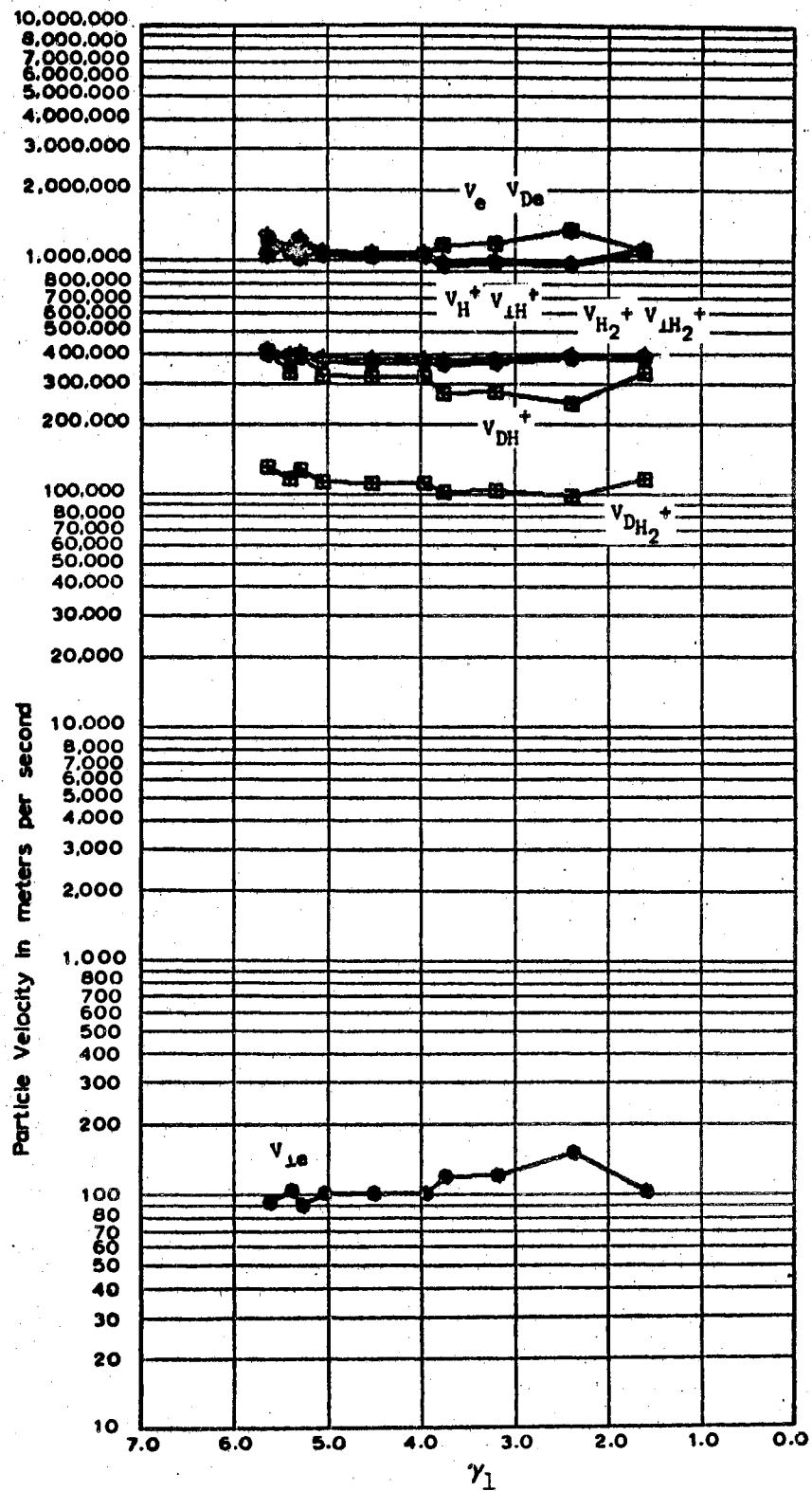
Figure 40c. Data taken June 27, 1966 at
2 MH$_z$ with the Aluminum Cell,
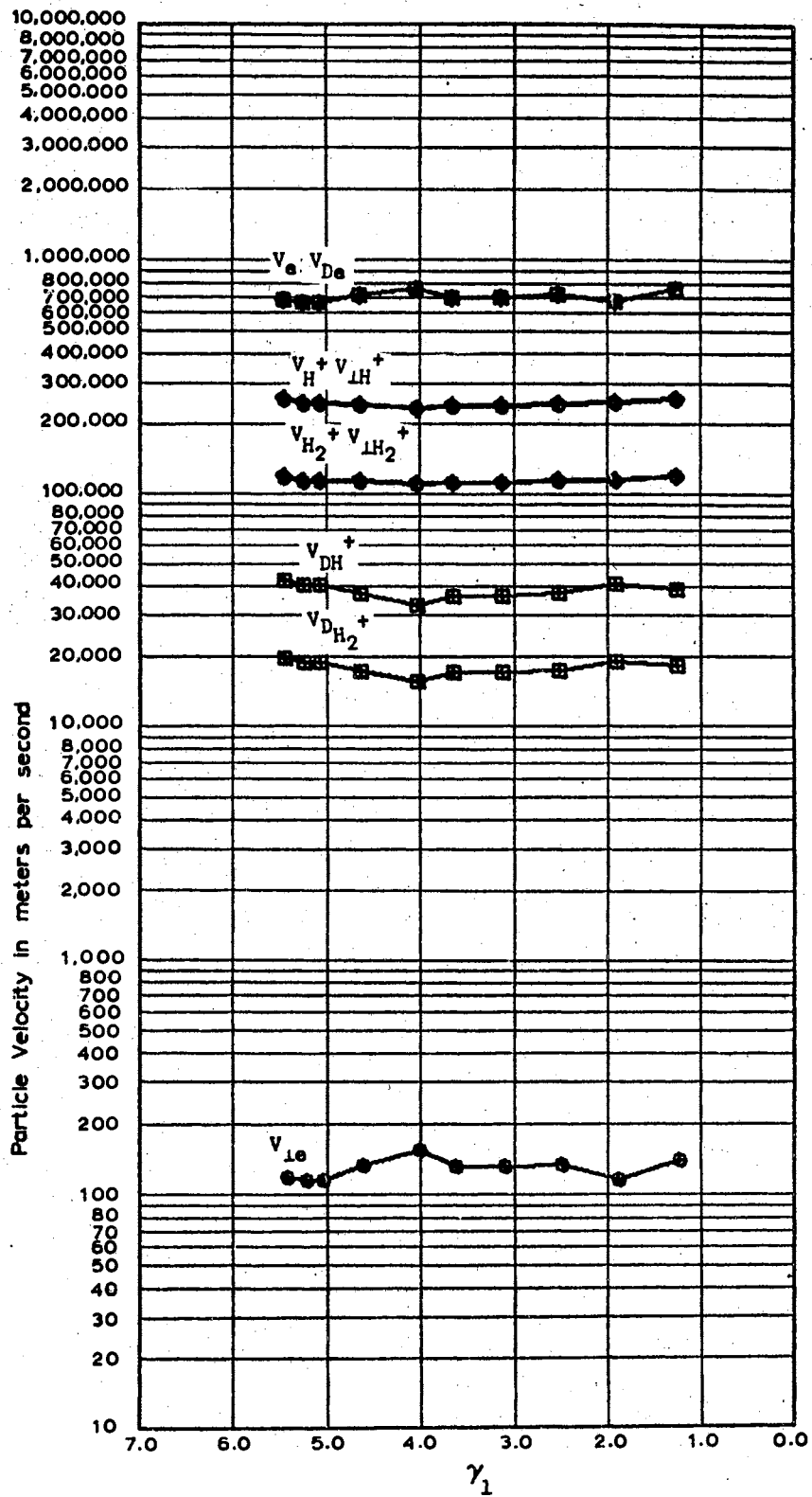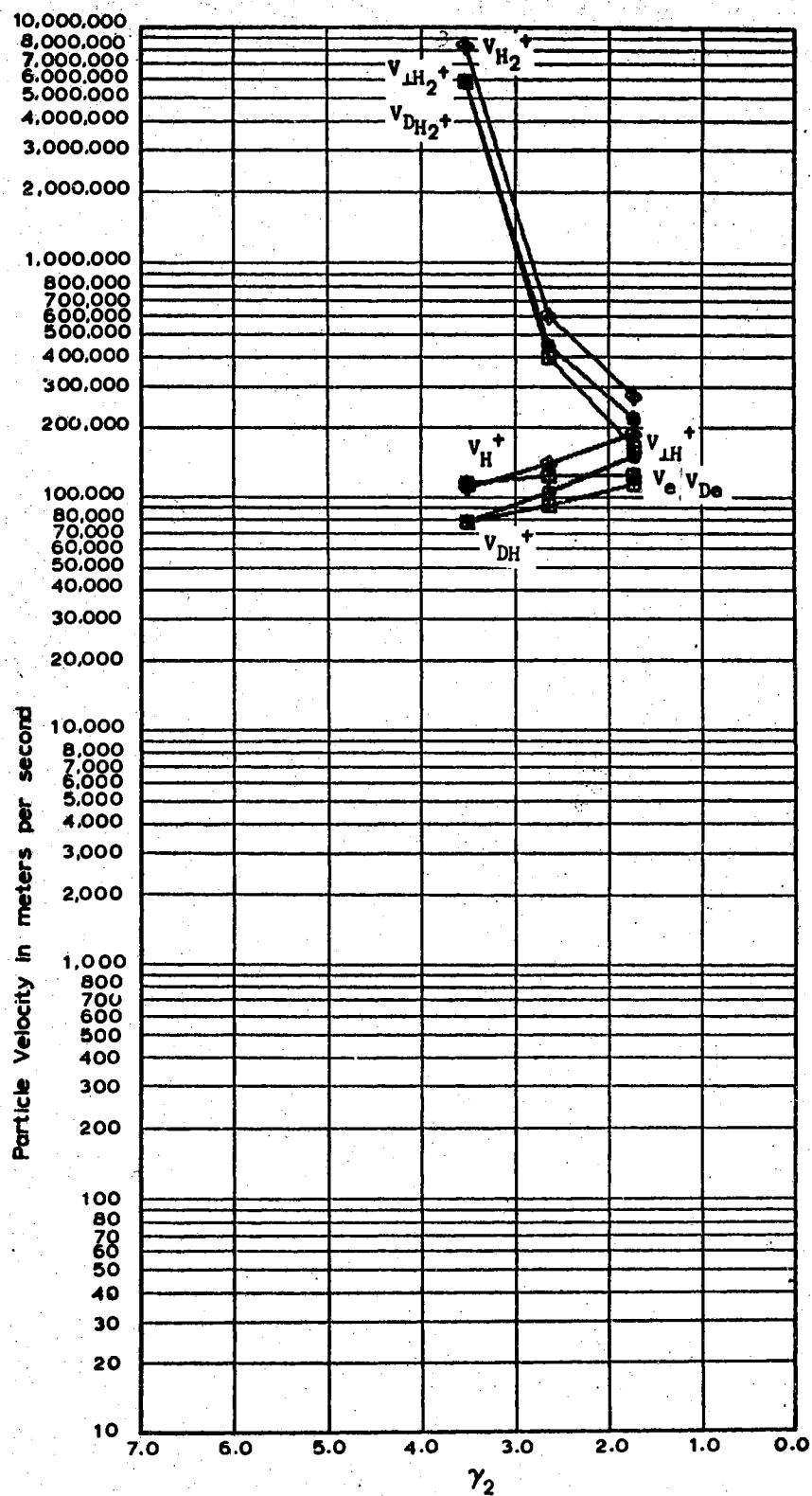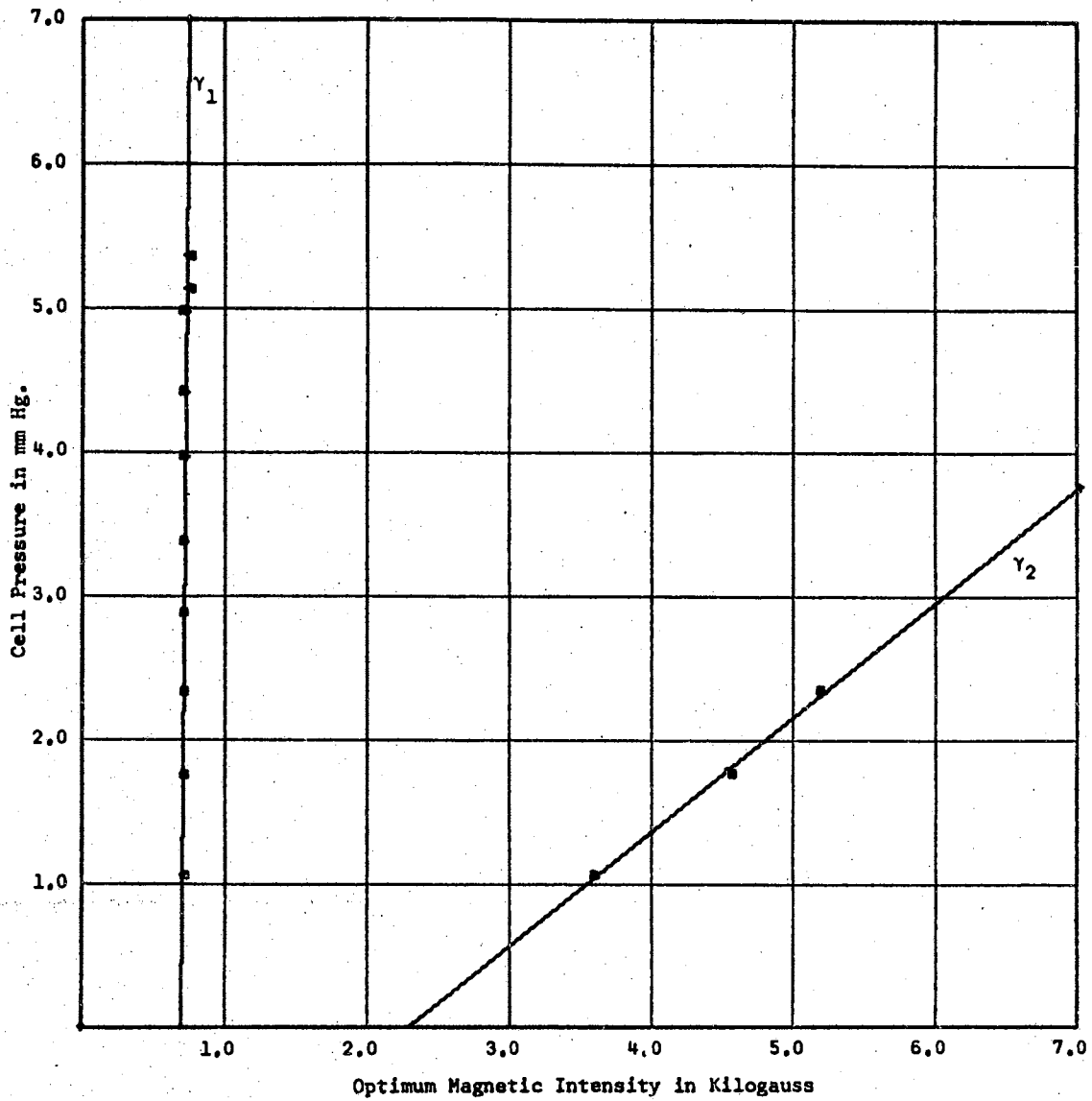D = 0.002794 meters
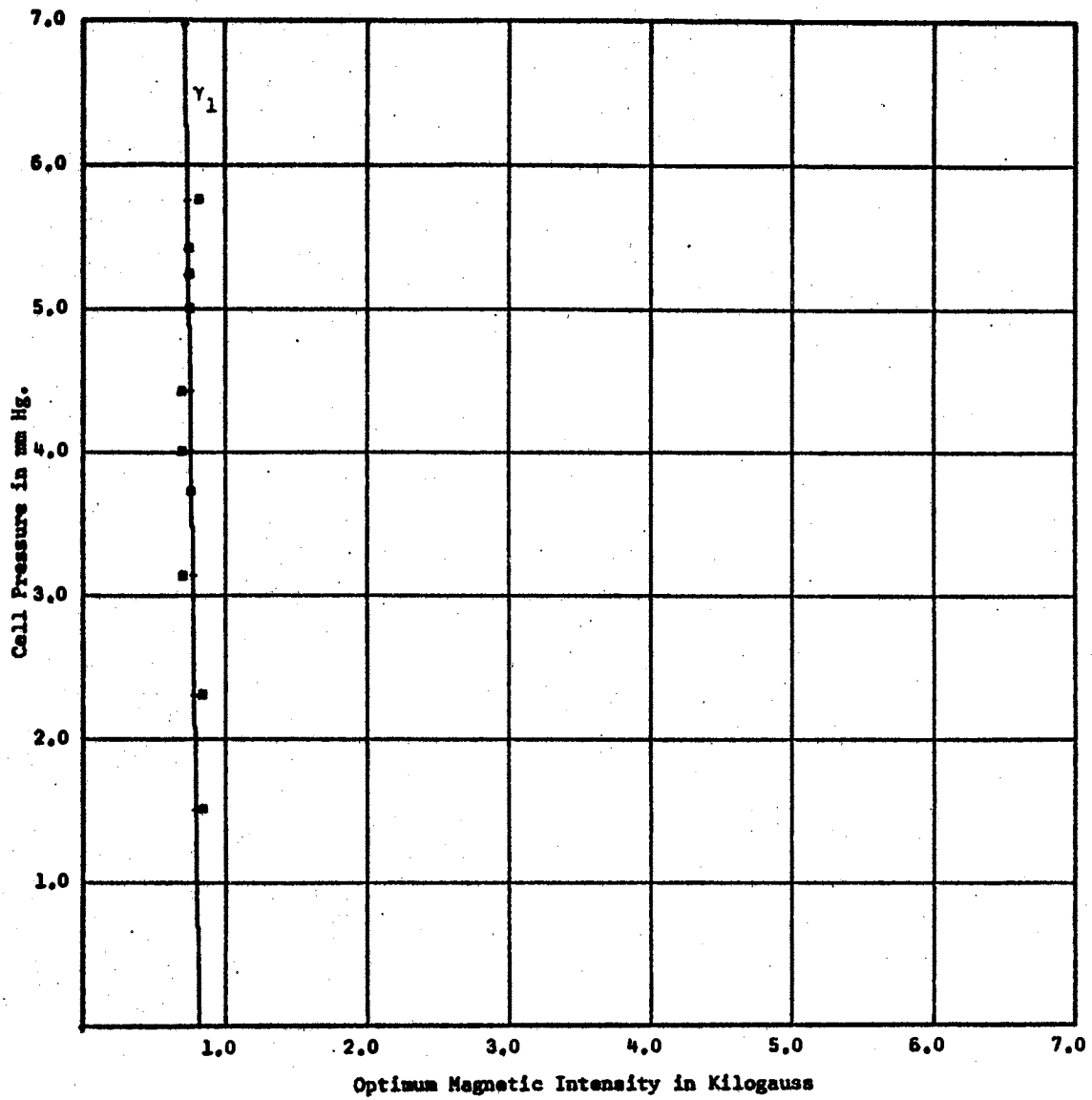
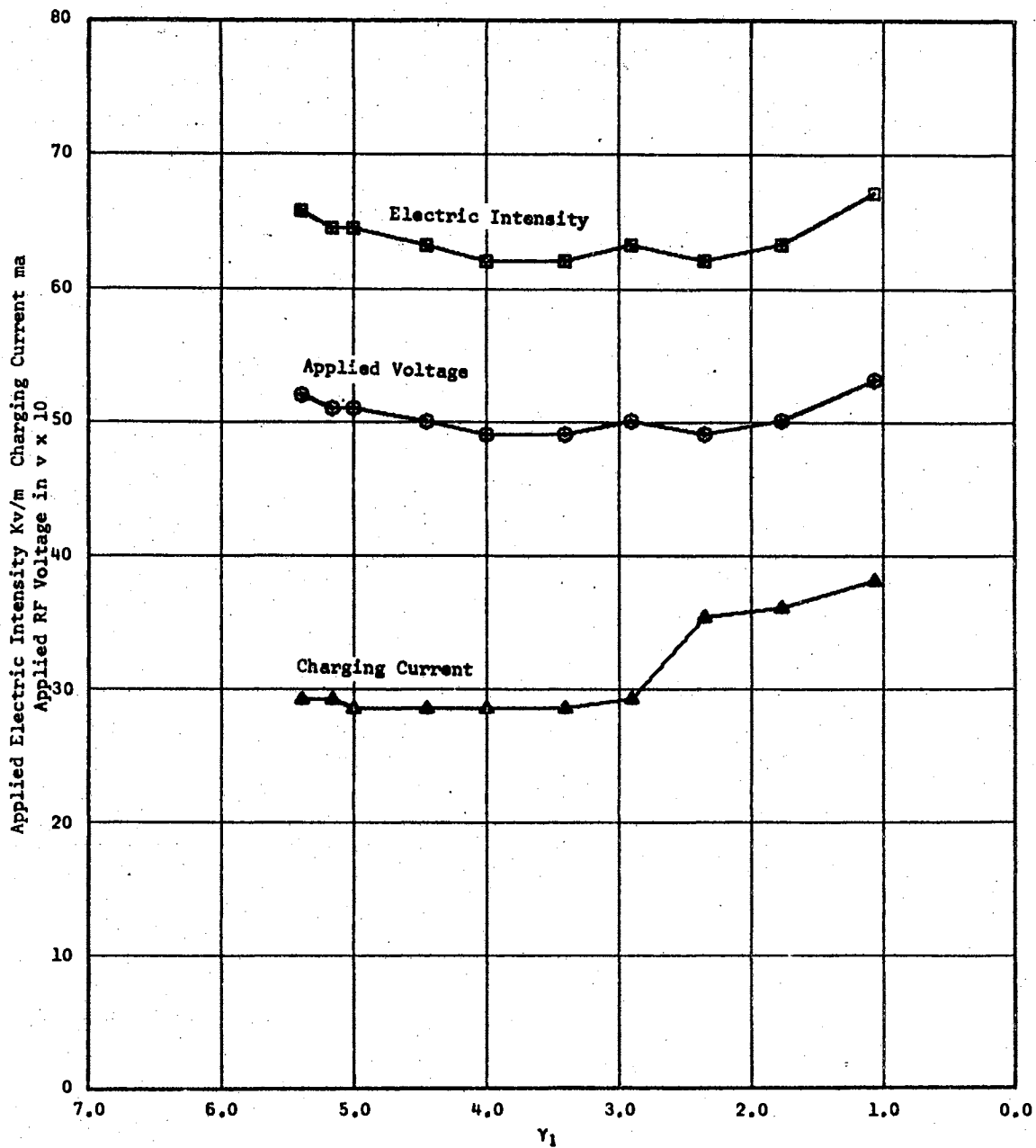Figure 41a. Data taken June 30, 1966 at 2 MH_z with the Aluminum Cell, D = 0.002794 meters
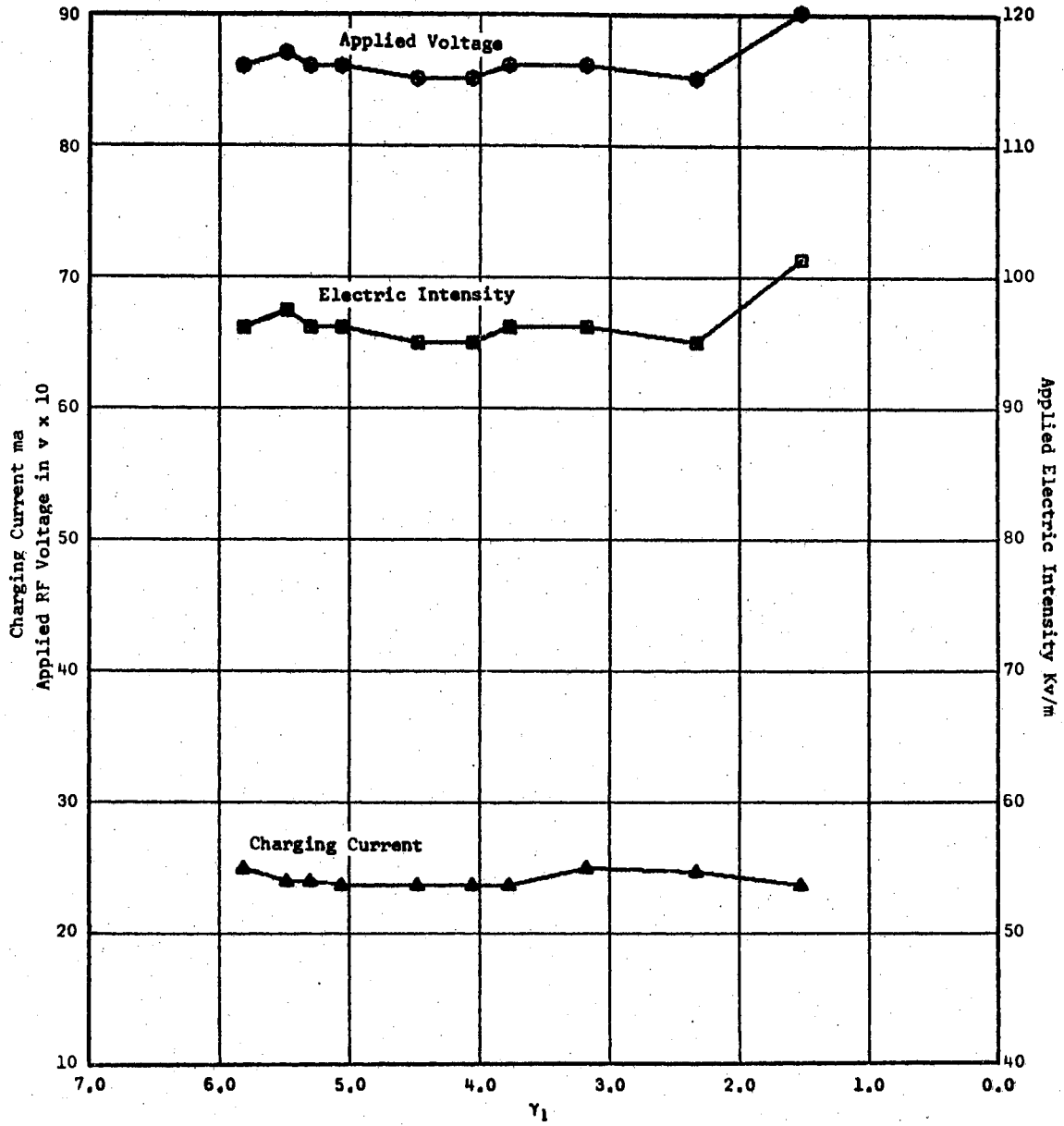
Figure 41b. Data taken June 30, 1966 at 2 MH$_z$ with the
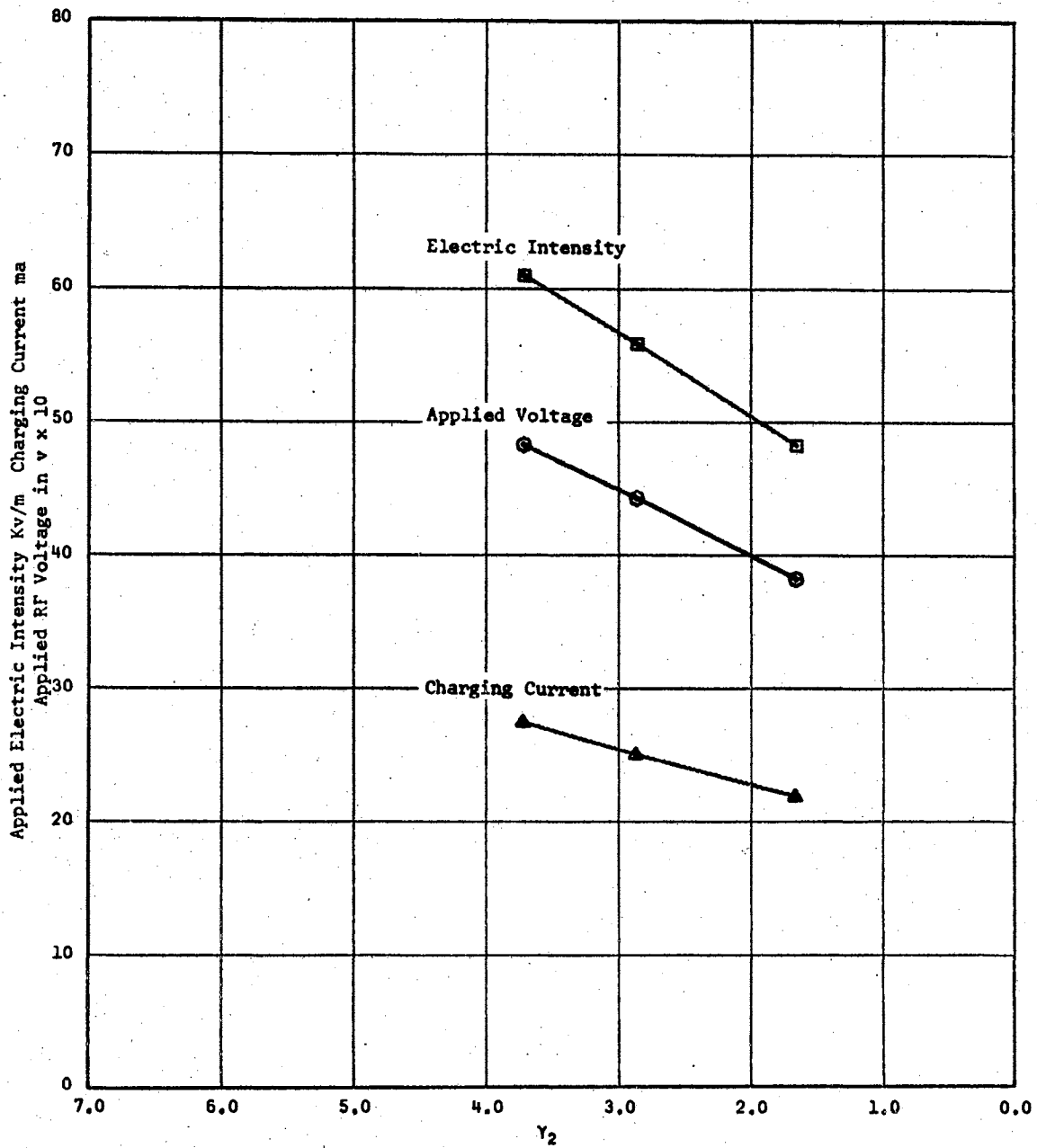Aluminum Cell, D = 0.002794 meters
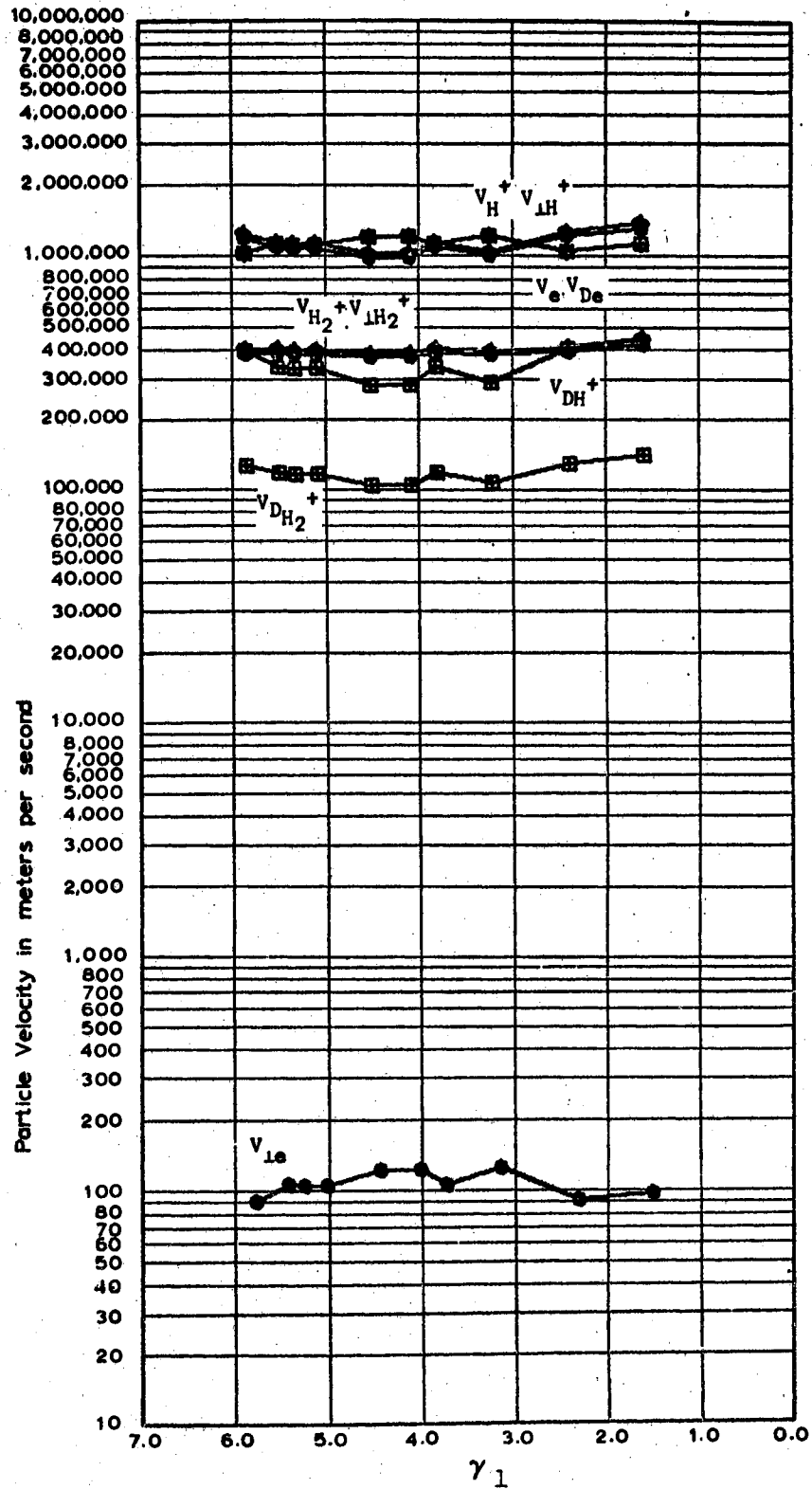
Figure 41c. Data taken June 30, 1966 at 2
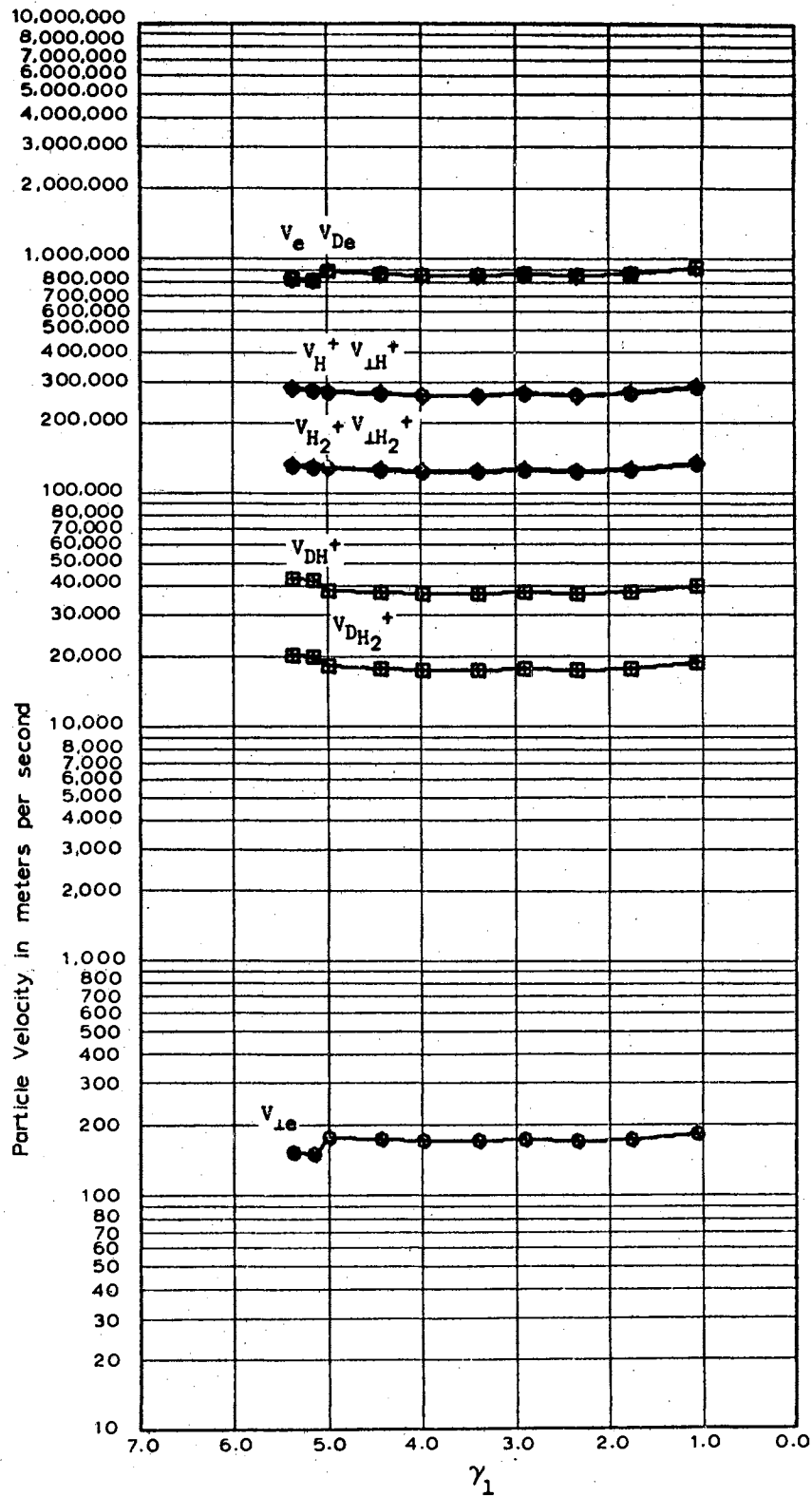MH$_z$ with the Aluminum Cell,
D = 0.002794 meters
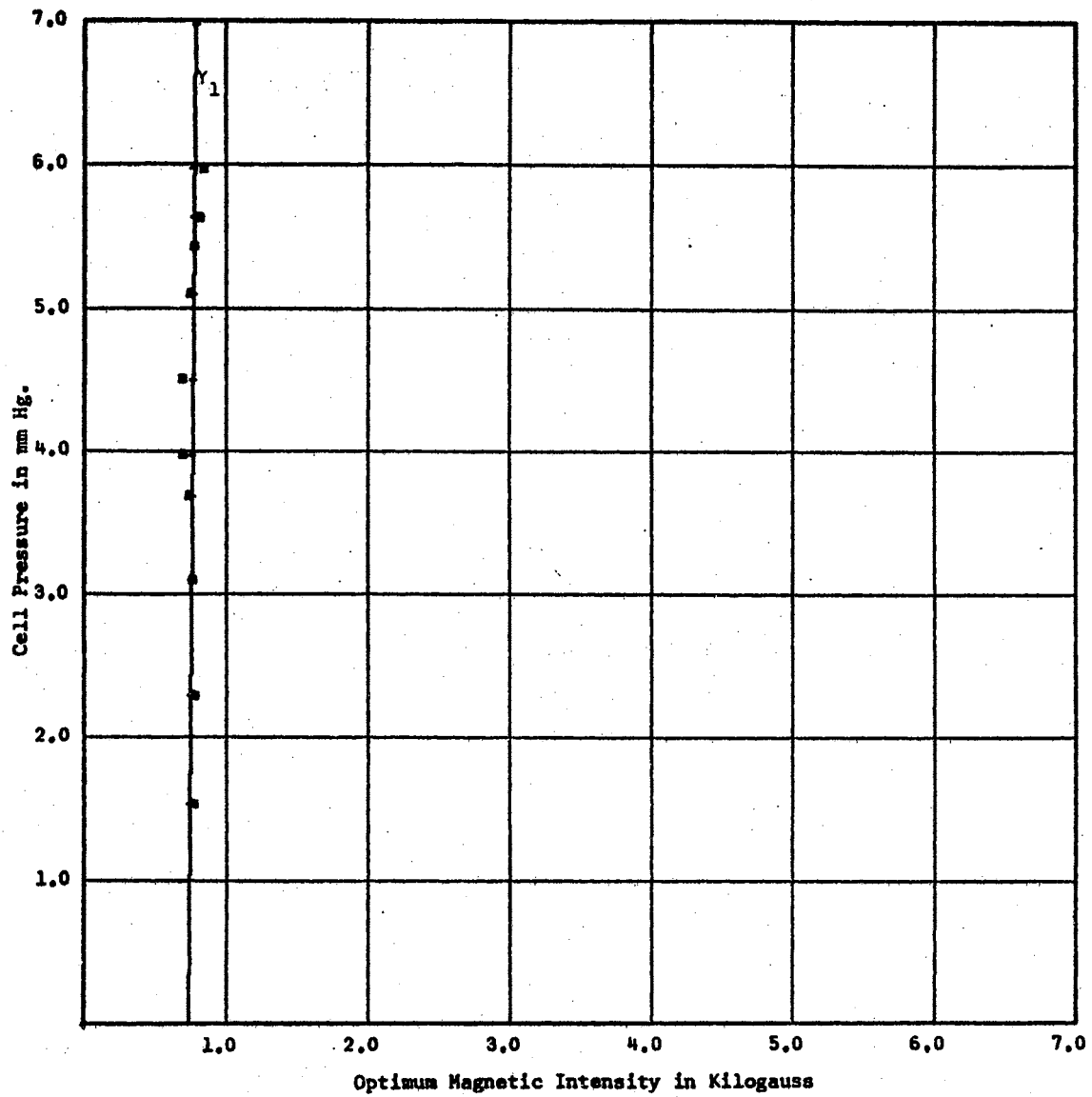
Figure 42a. Data taken July 2, 1966 at 3 MH_z with the Aluminum Cell, D = 0.002794 meters
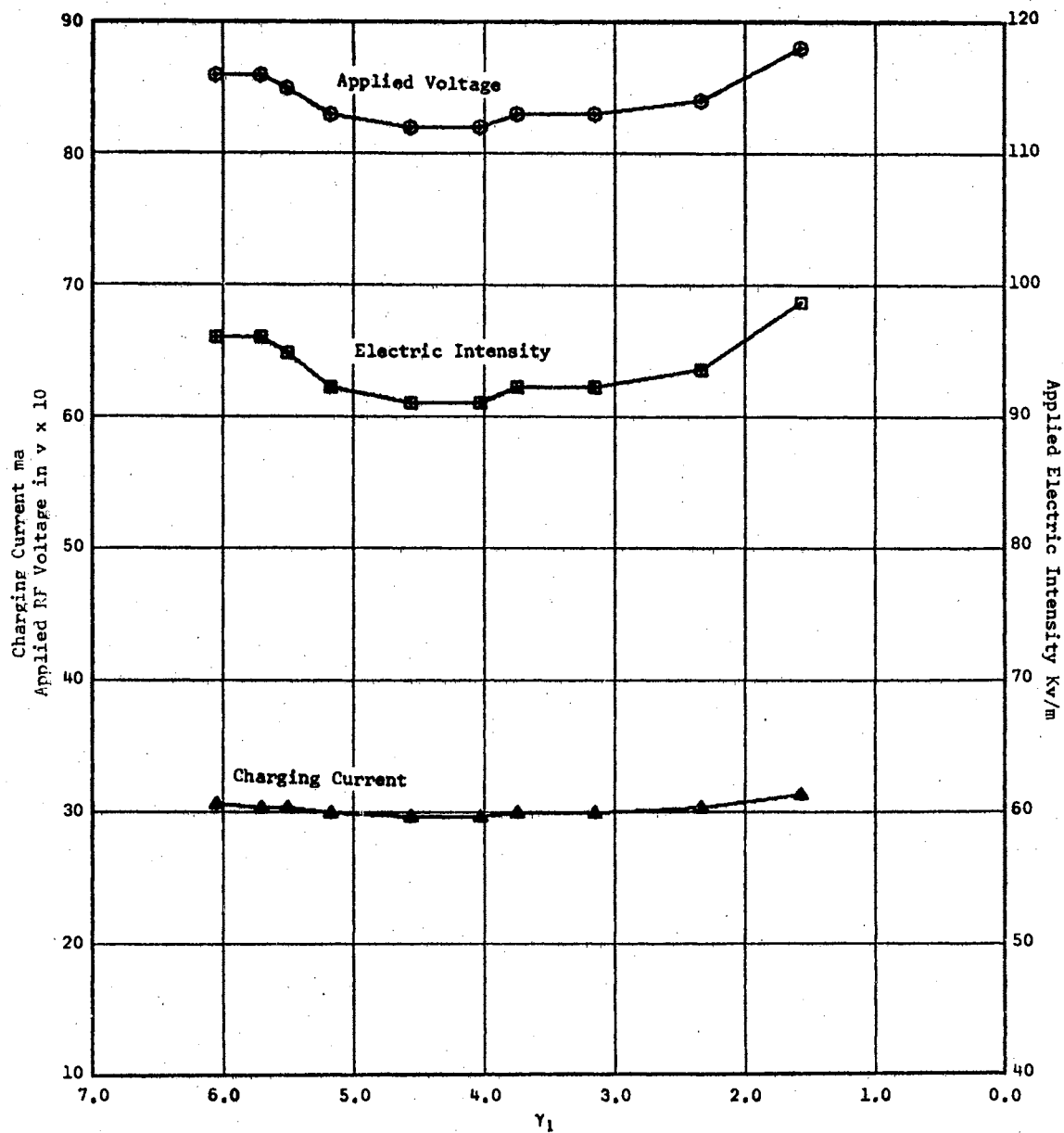
Figure 42b. Data taken July 2, 1966 at 3 MH_z with the
Aluminum Cell, D = 0.002794 meters
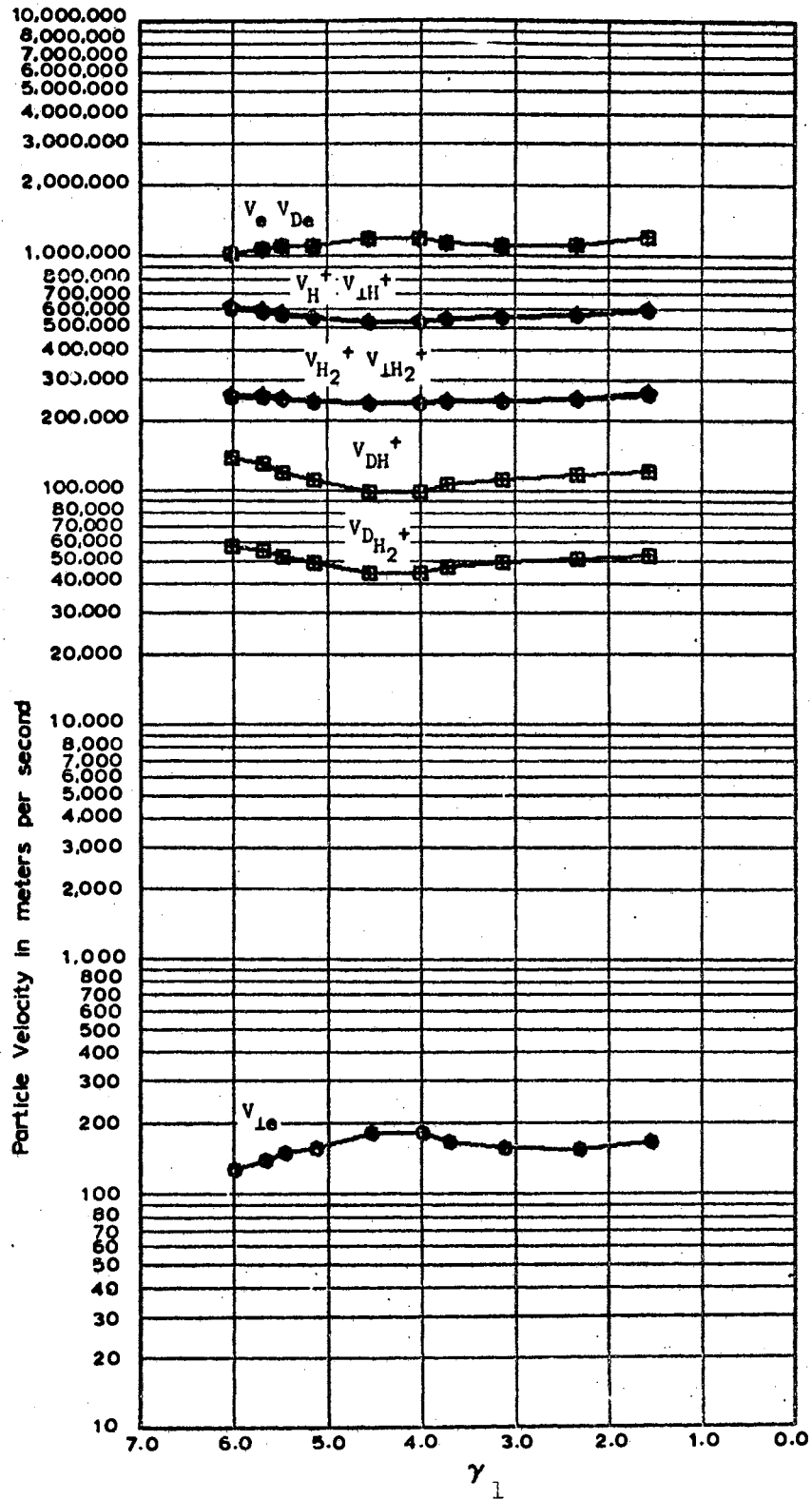
Figure 42c. Data taken July 2, 1966 at
3 MH$_z$ with the Aluminum Cell,
D = 0.002794 meters
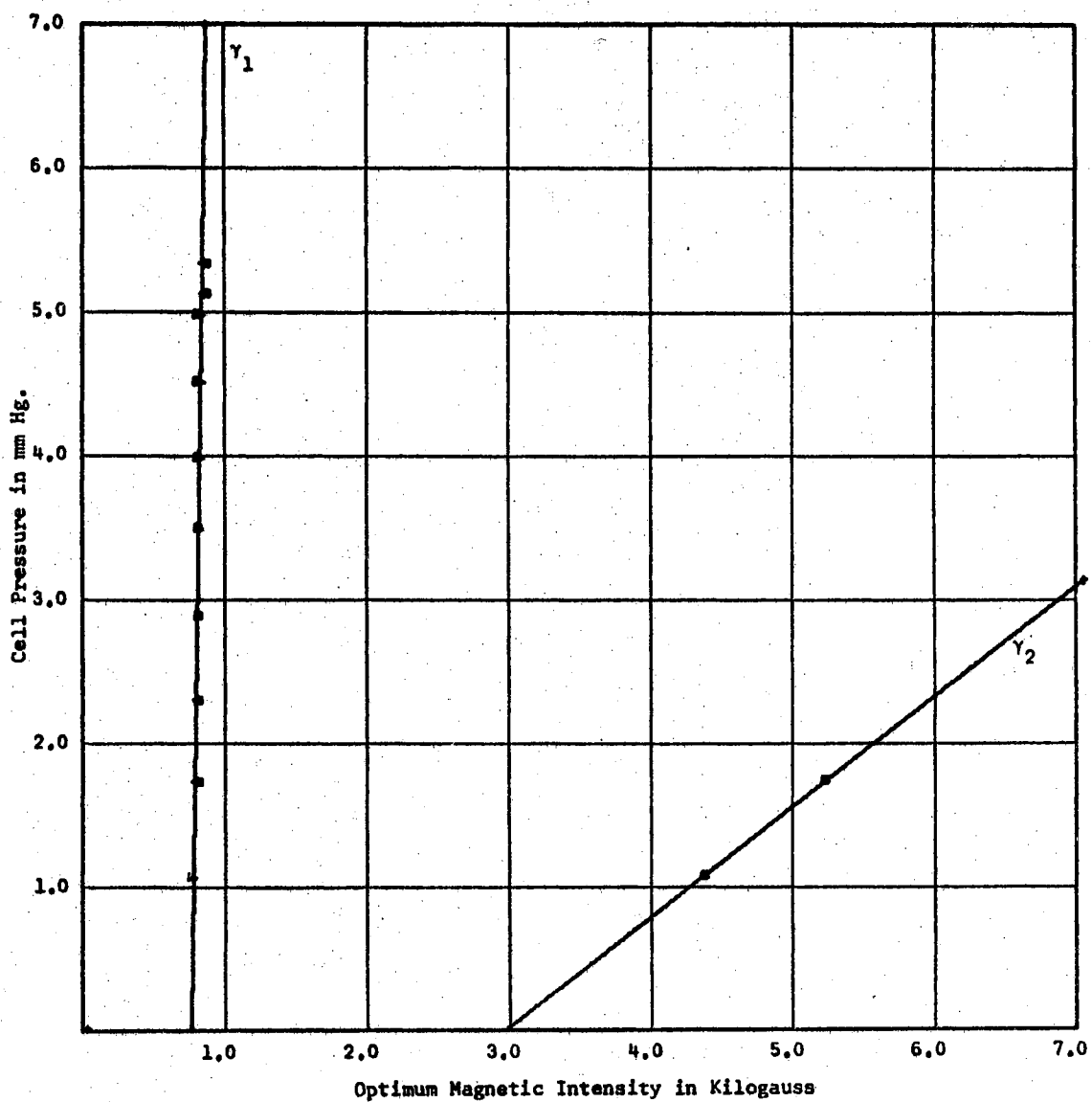
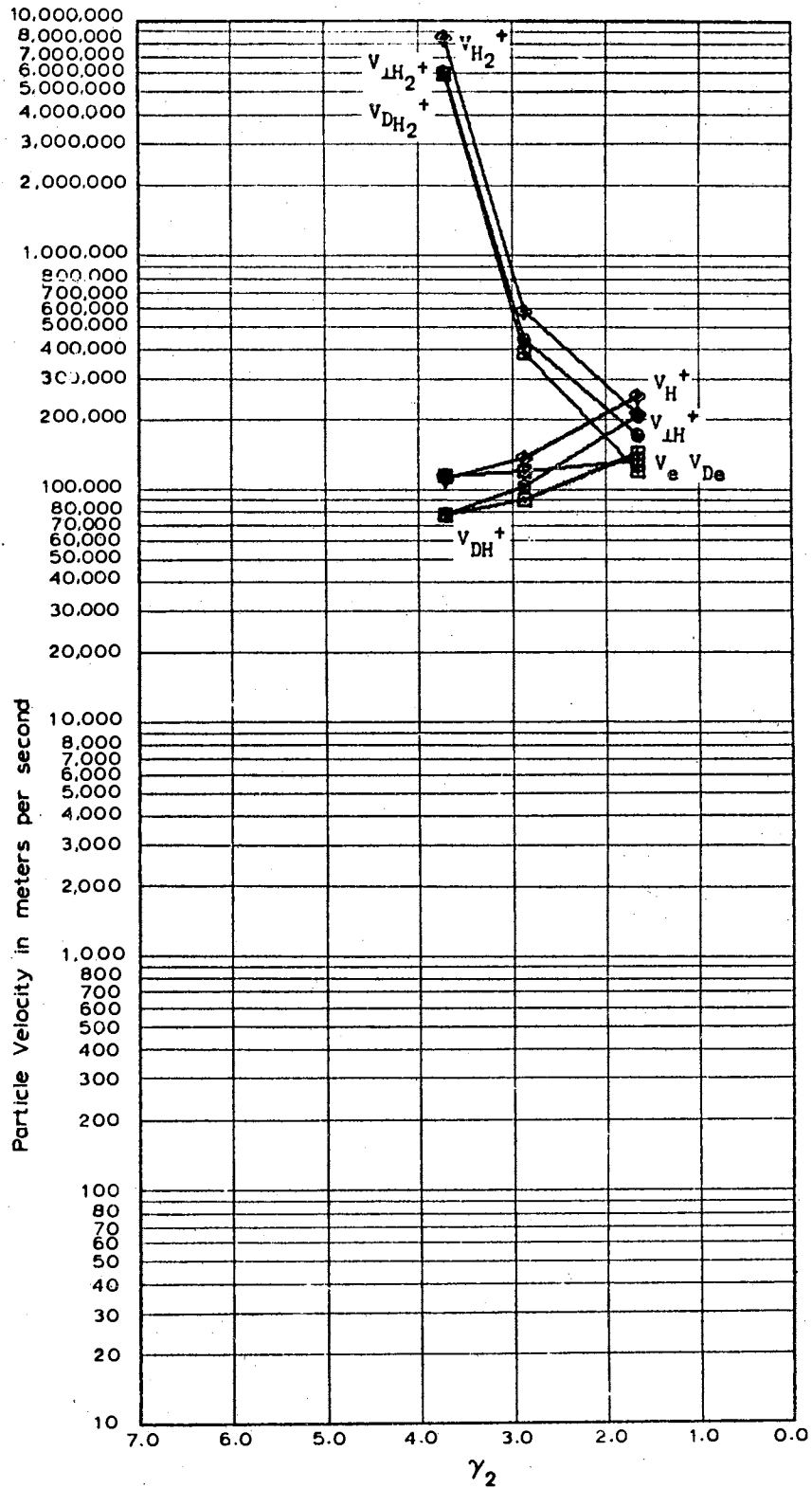Figure 43a. Data taken August 24, 1966 at 3 MH_z with the Aluminum Cell, D = 0.002794 meters
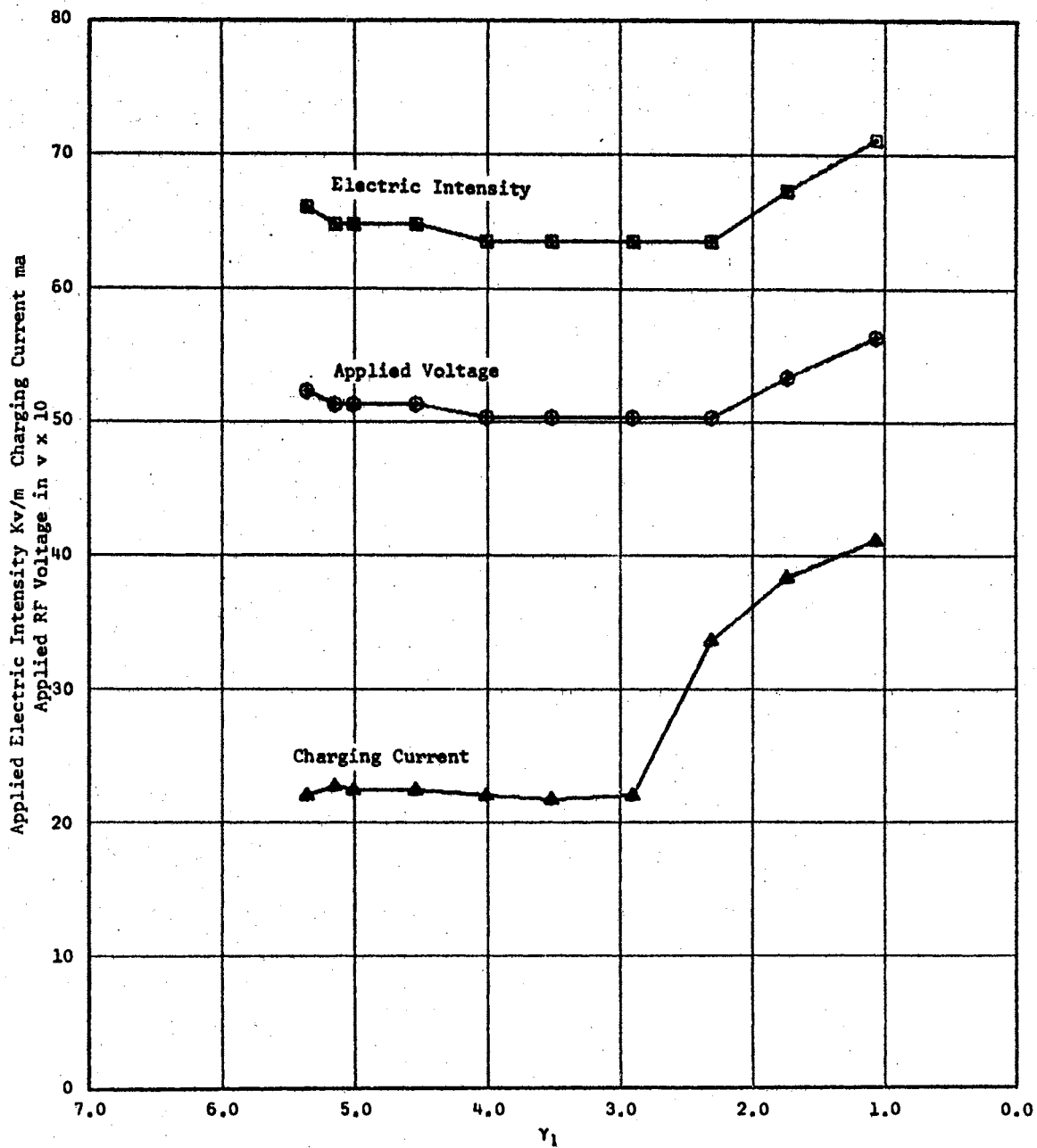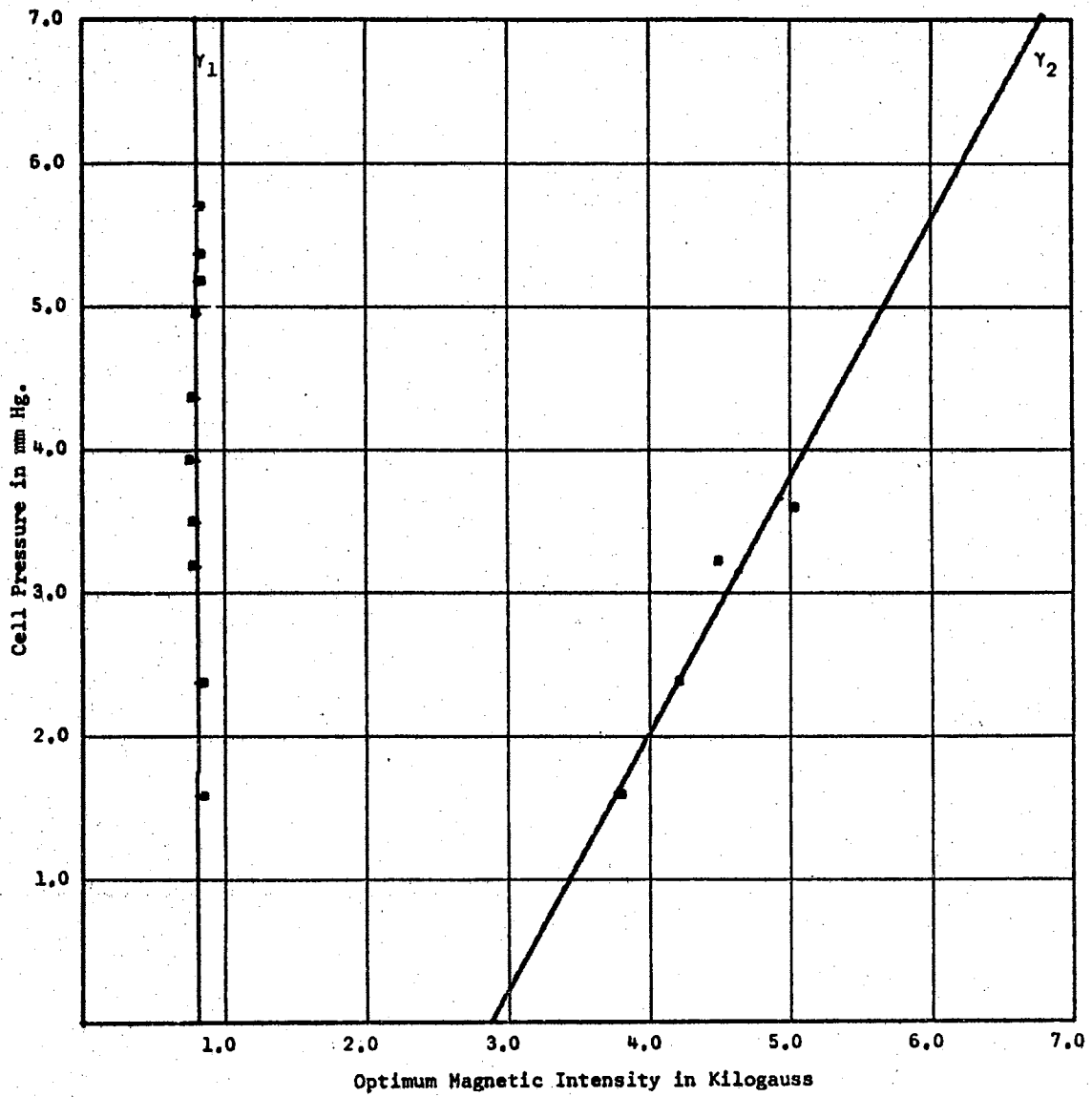
Figure 43b. Data taken August 24, 1966 at 3 MH$_z$ with the Aluminum Cell, D = 0.002794 meters
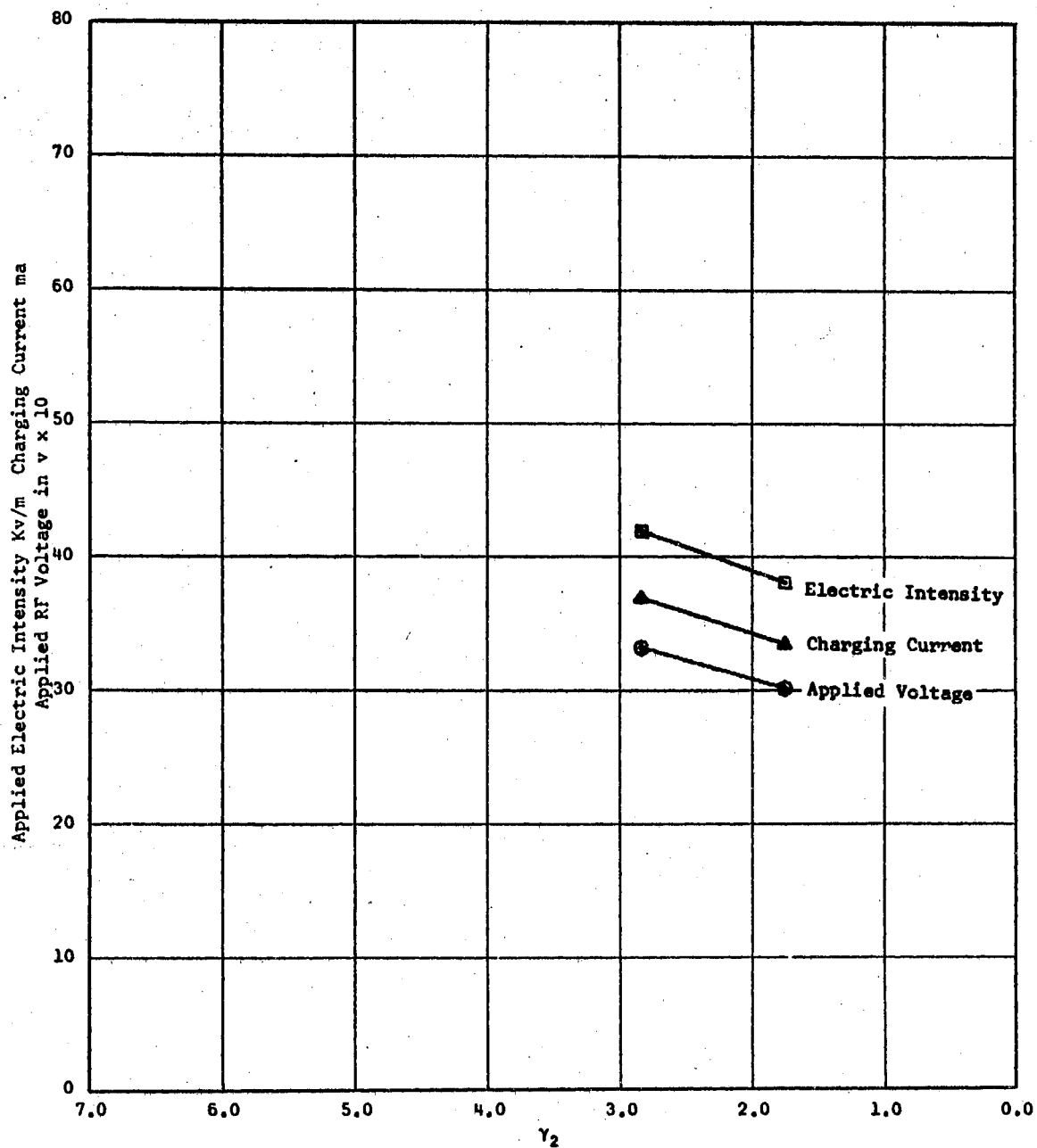
Figure 43c. Data taken August 24, 1966 at 3 MH$_z$ with the
Aluminum Cell, D = 0.002794 meters
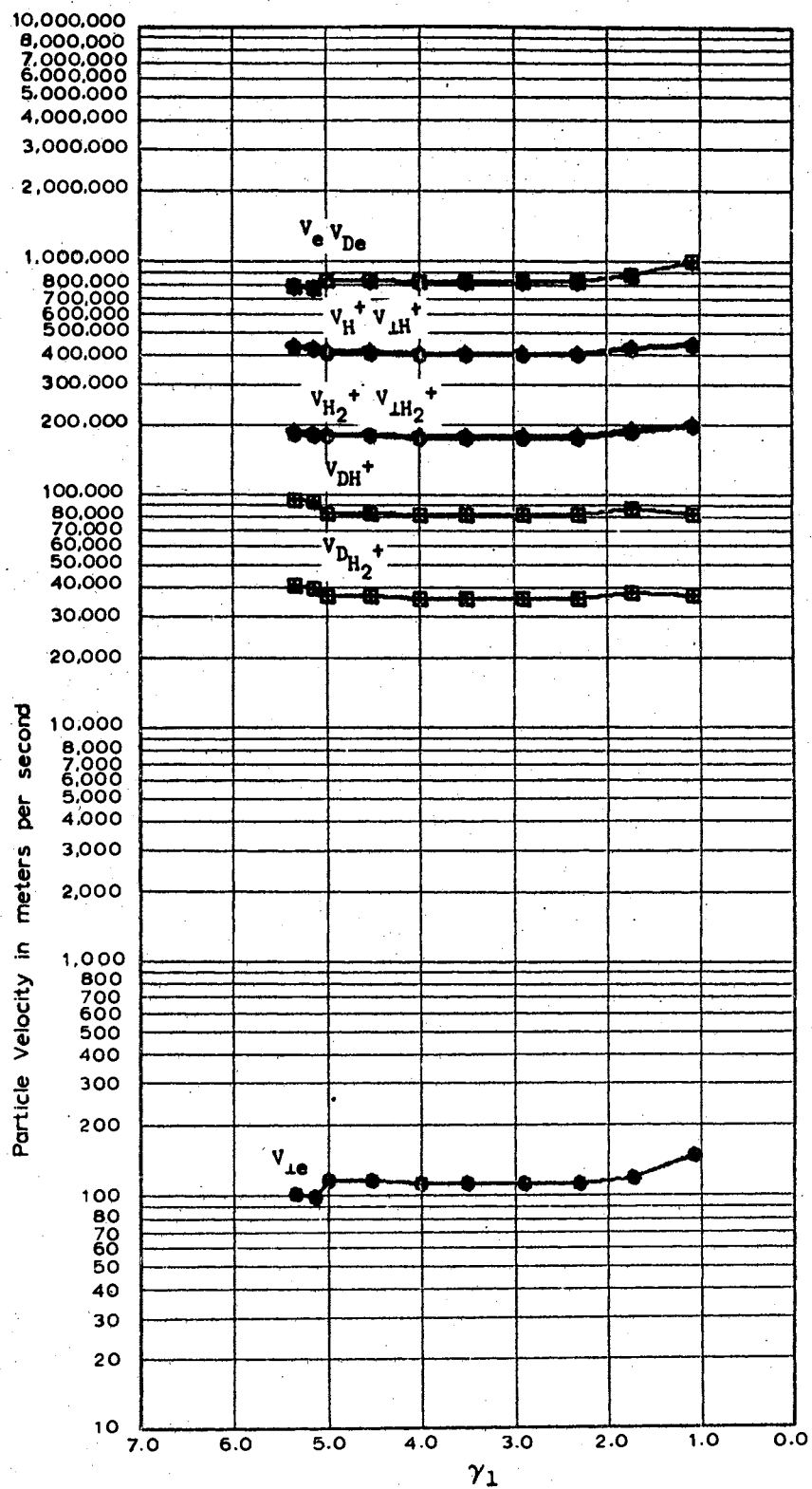
Figure 43d. Data taken August 24, 1966 at
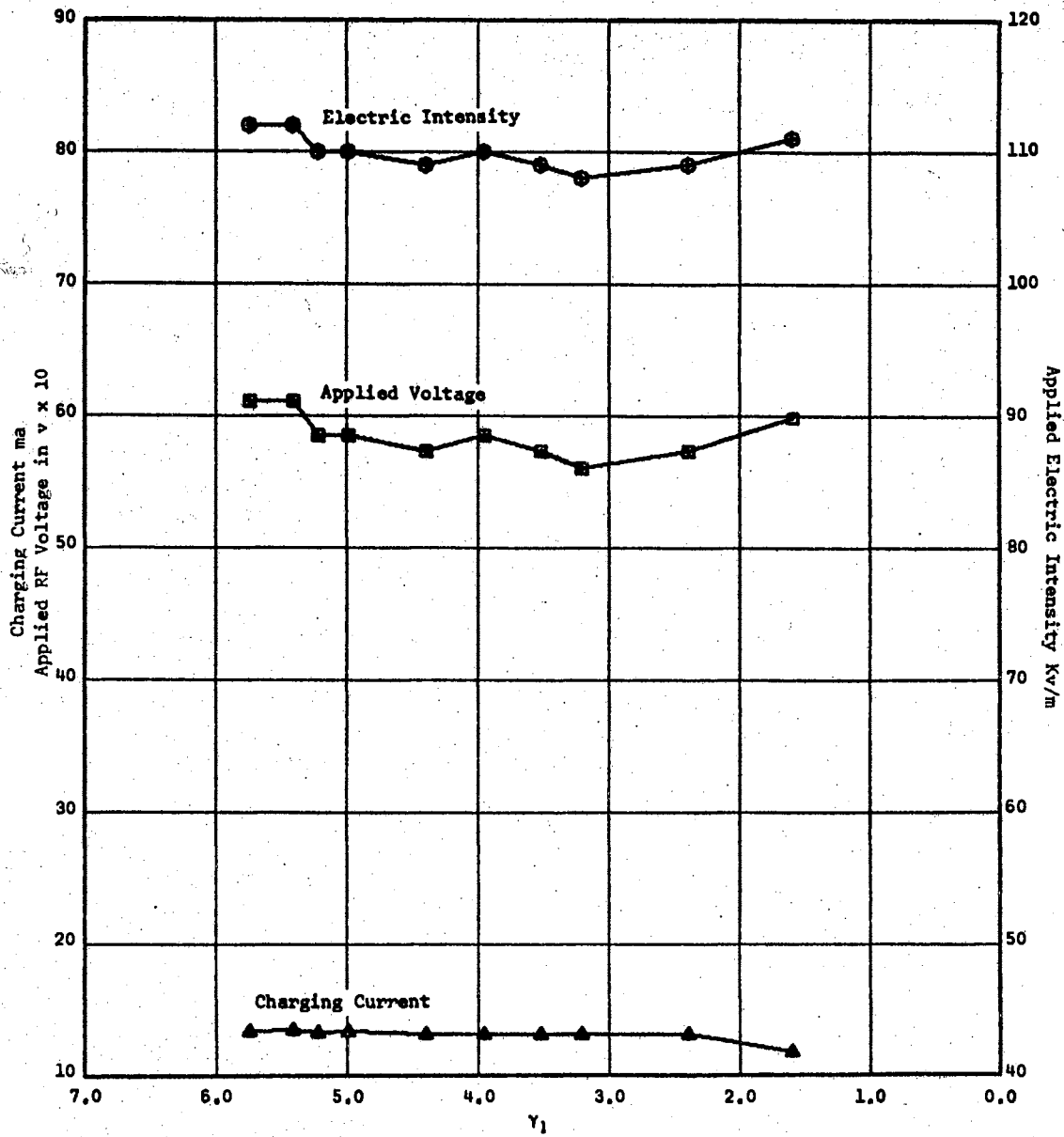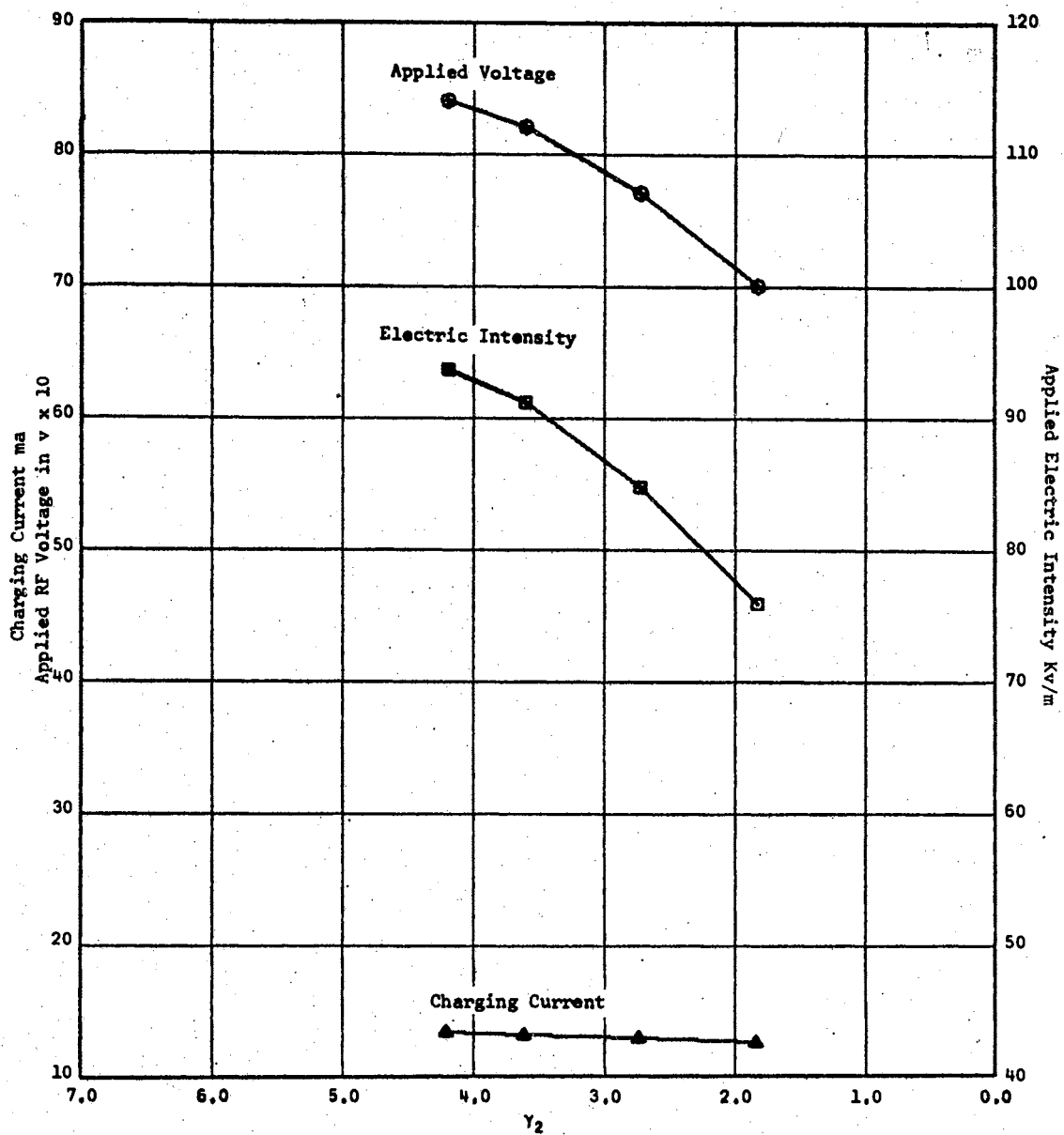3 MHz with the Aluminum Cell,
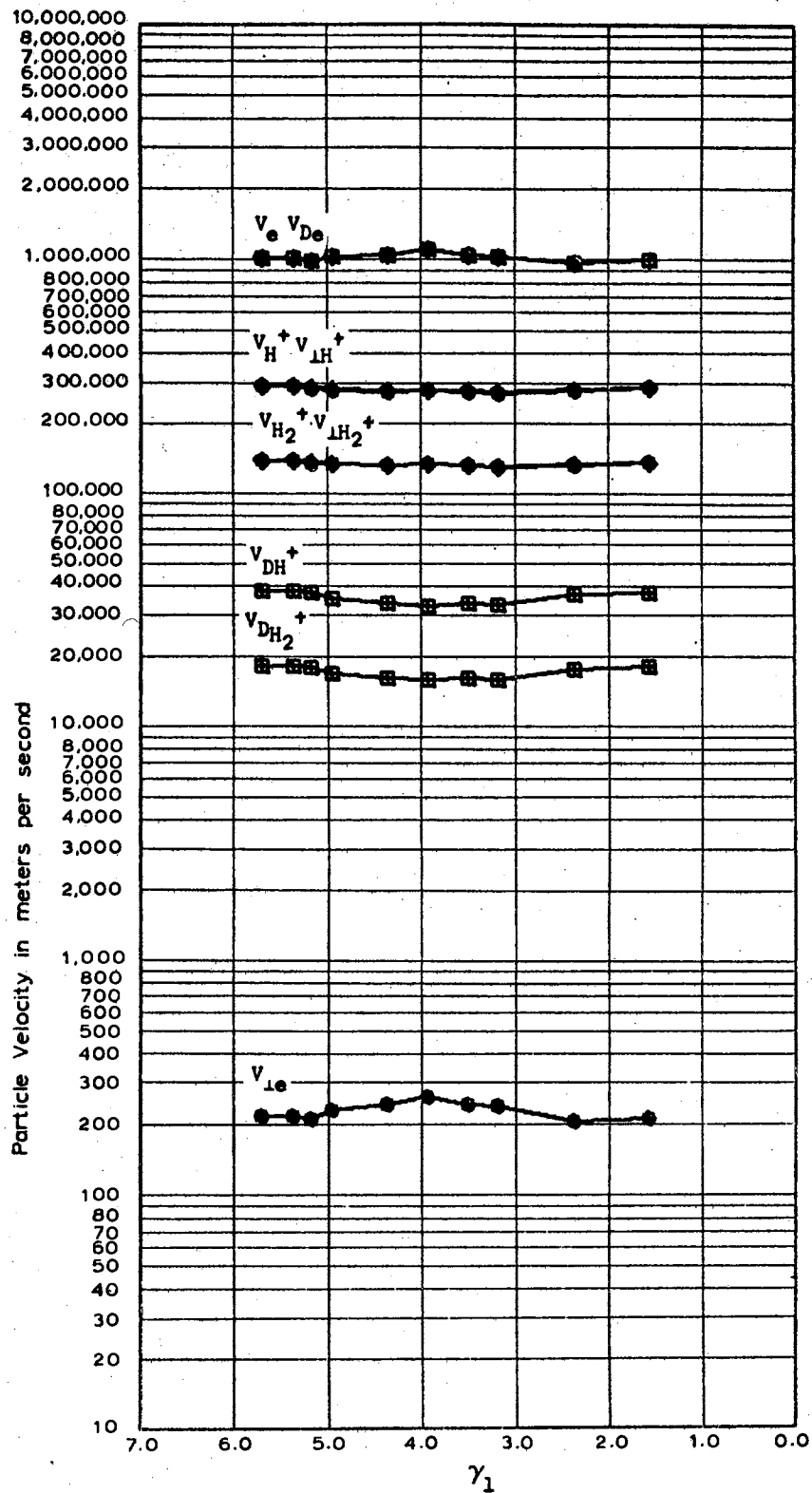D = 0.002794 meters
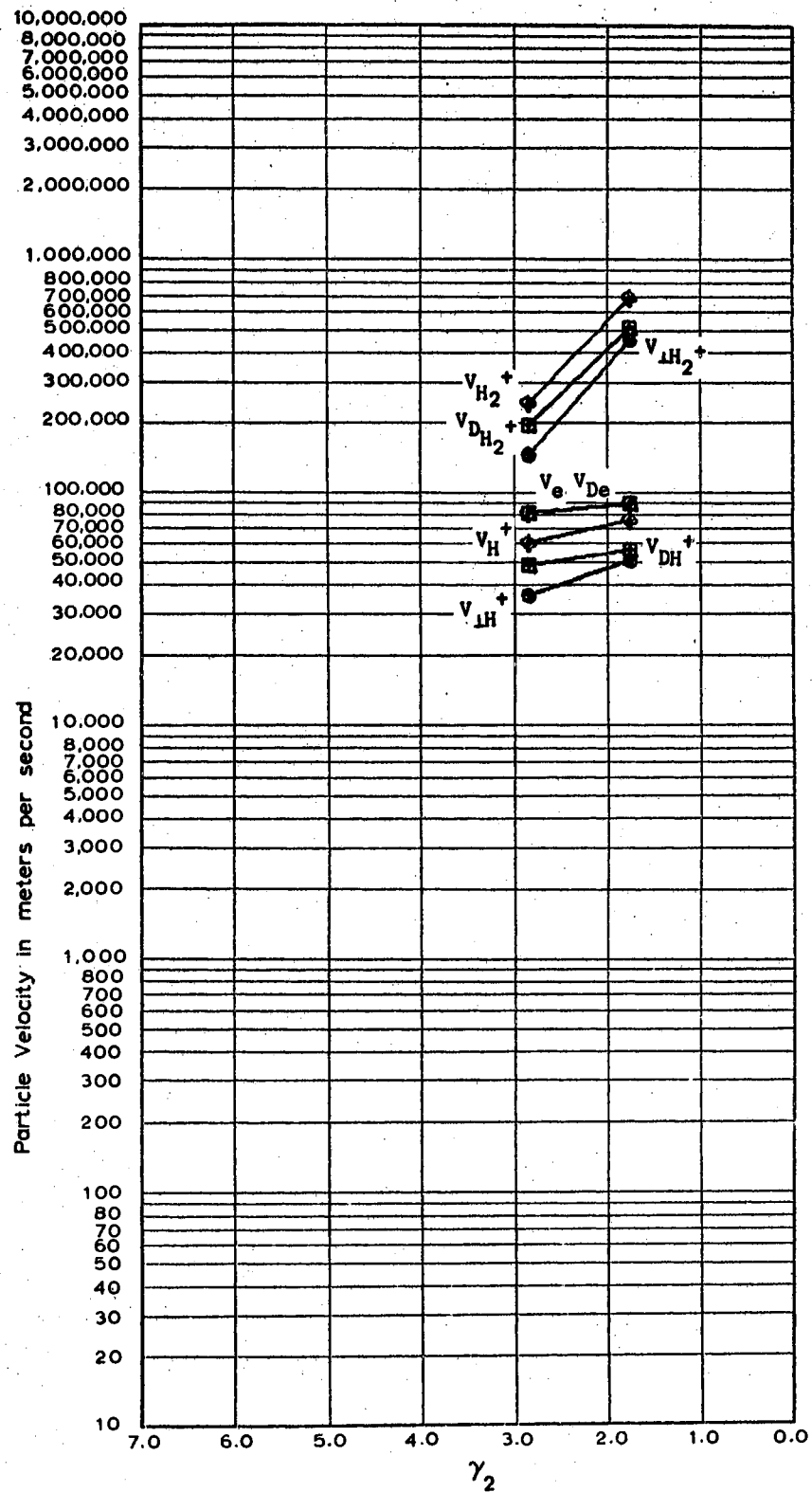
Figure 43e. Data taken August 24, 1966 at
3 MH$_z$ with the Aluminum Cell,
D = 0.002794 meters
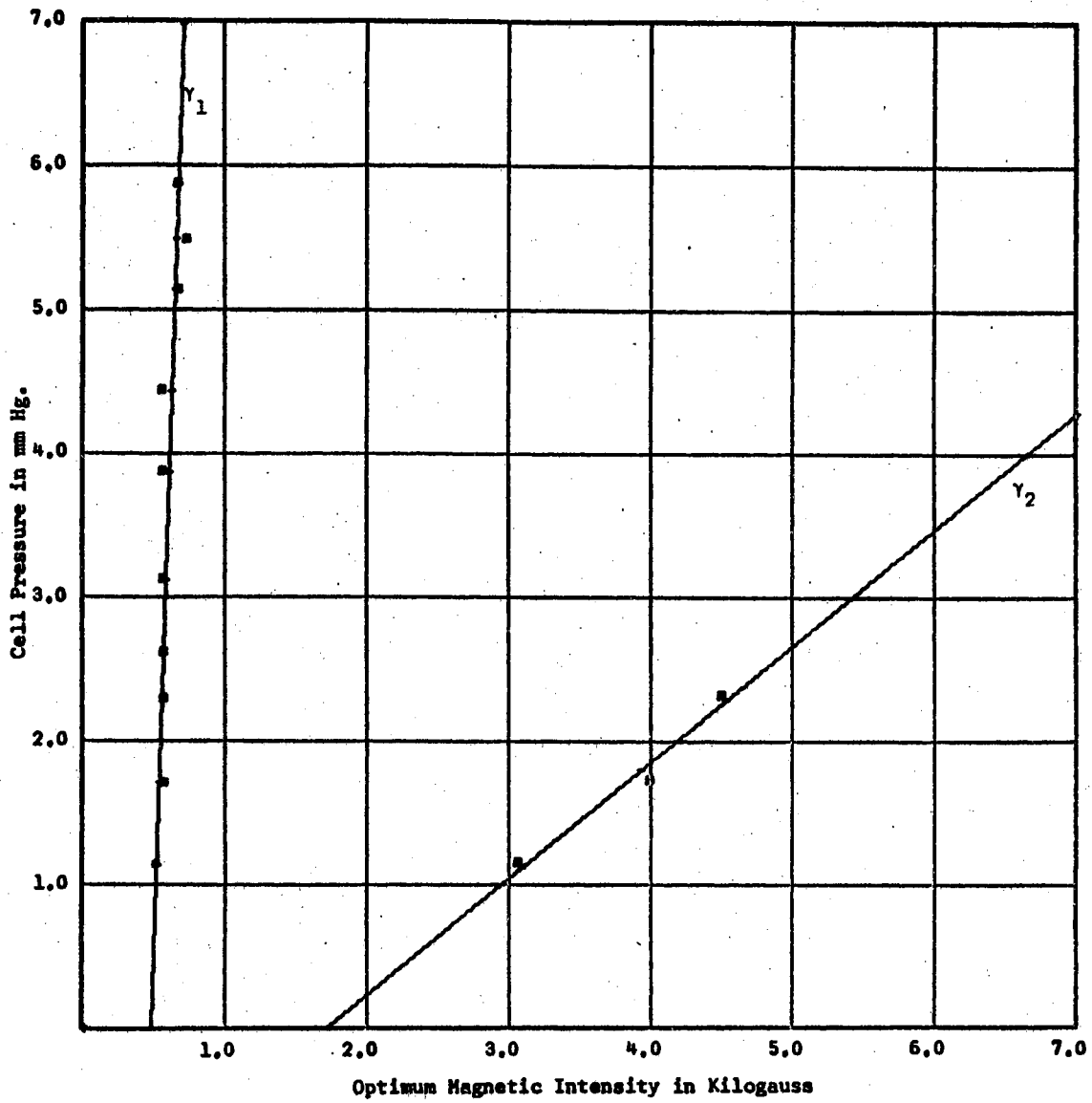
Figure 44a.   Data taken April 15, 1965 at 3.5 MH_z with the Old
Teflon Cell and Old rf Source, D^z= 0.004292 meters
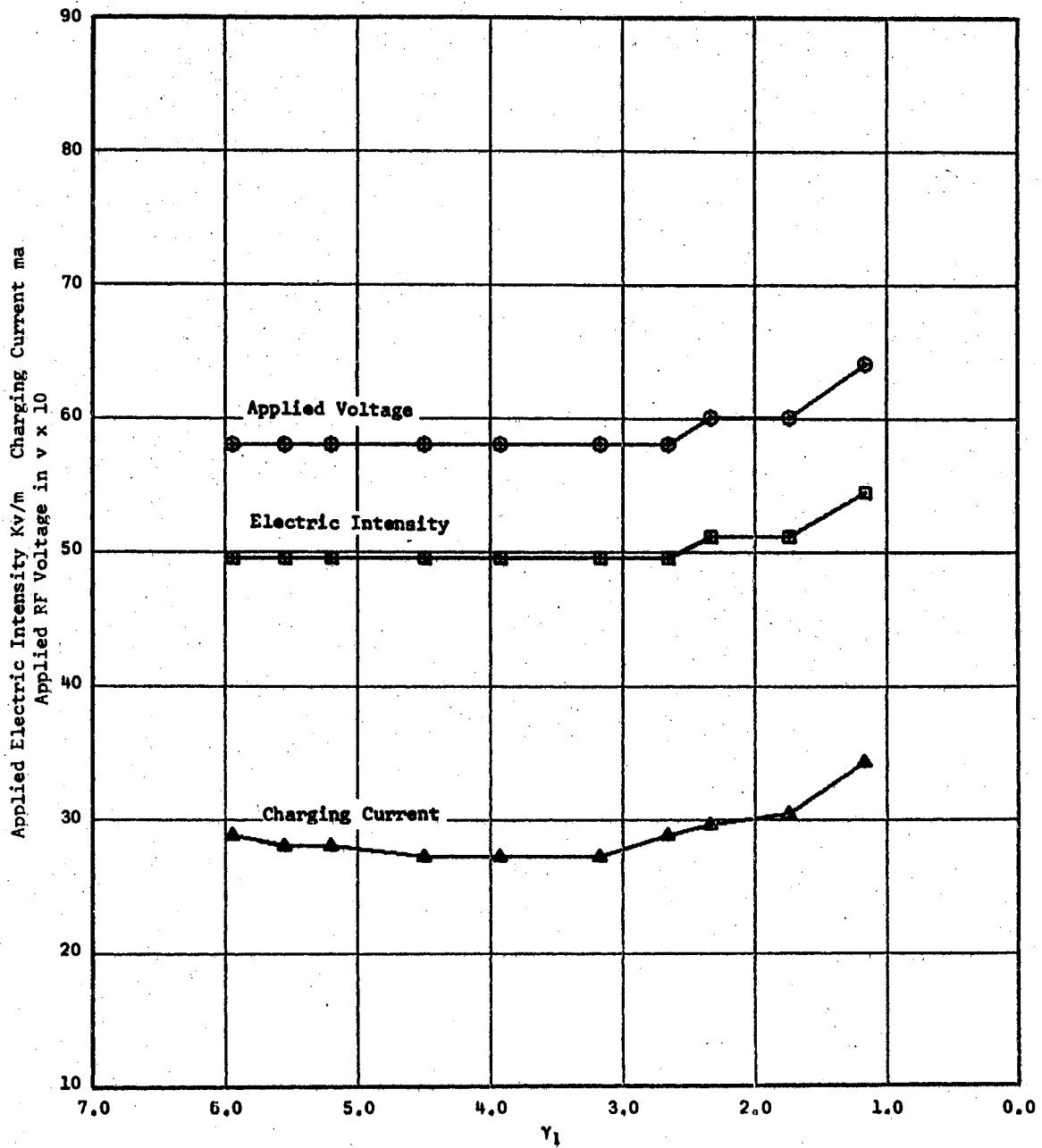
Figure 44b. Data taken April 15, 1965 at 3.5 MH$_z$ with the Old
Teflon Cell and Old rf Source, D^z = 0.004292 meters
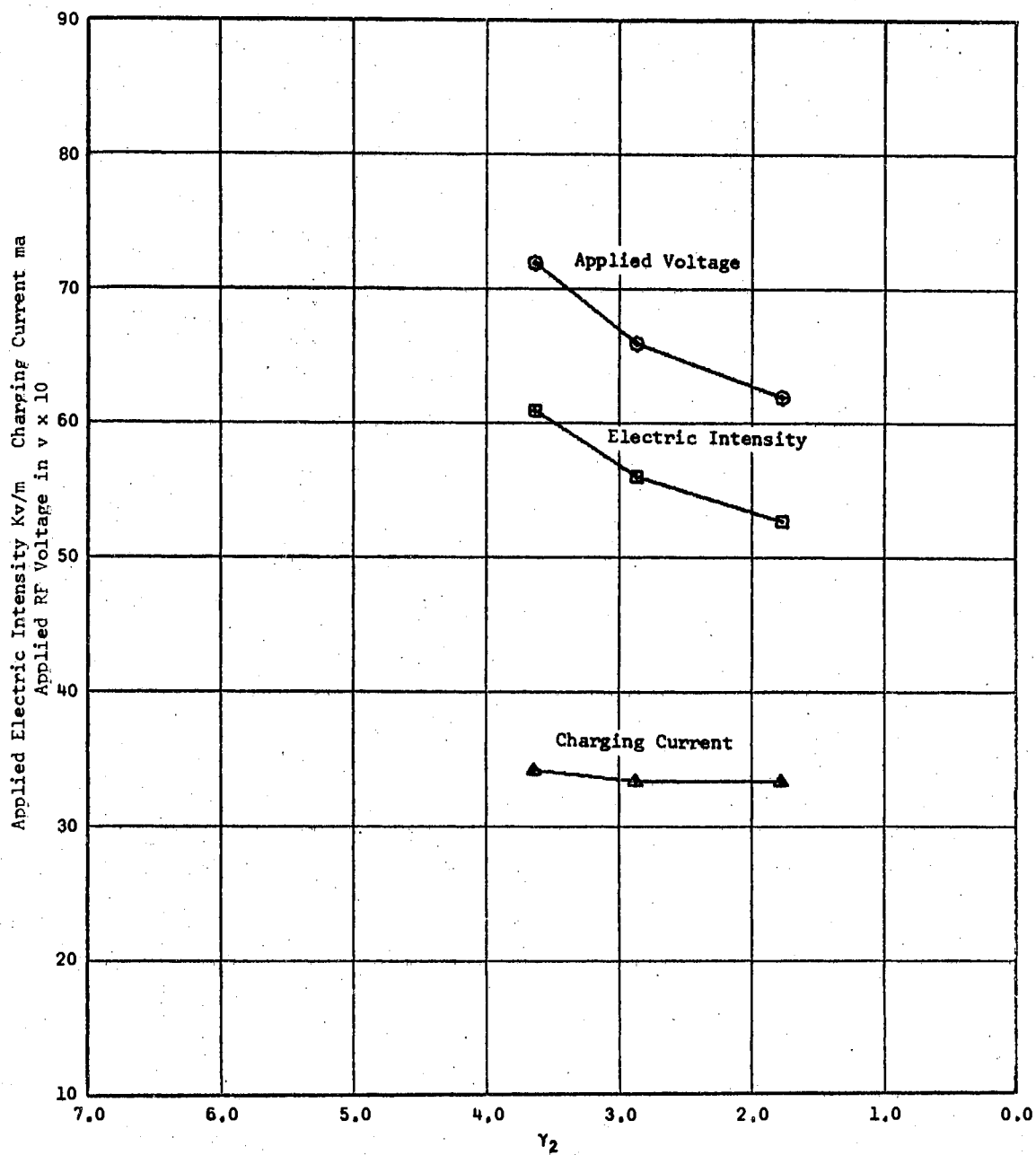
Figure 44c. Data taken April 15, 1965 at 3.5 MH$_z$ with the Old
Teflon Cell and Old rf Source, D^z = 0.004292 meters
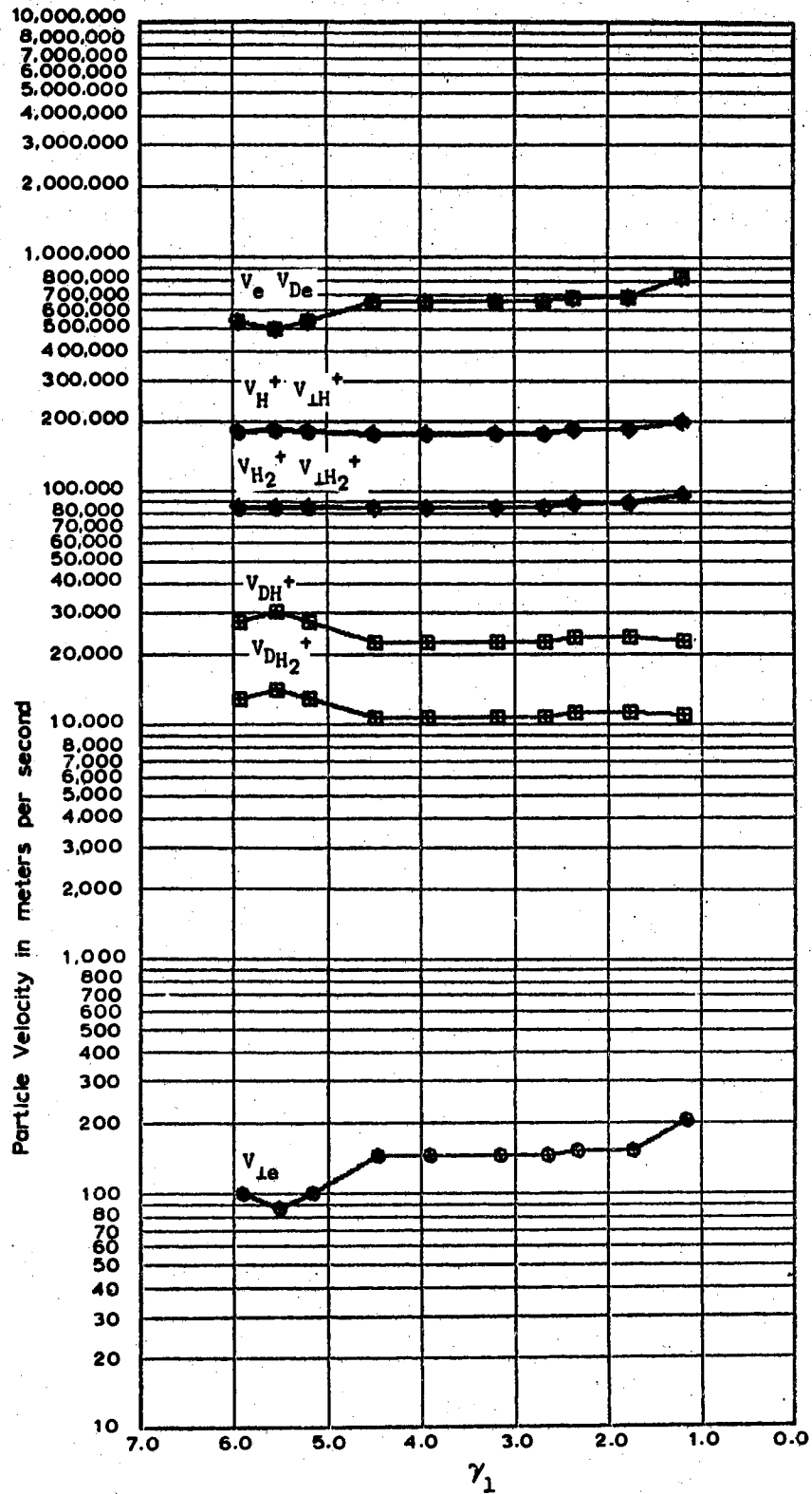
Figure 44d. Data taken April 15, 1965 at
3.5 MH$_z$ with the Old Teflon
Cell and Old rf Source, D =
0.004292 meters
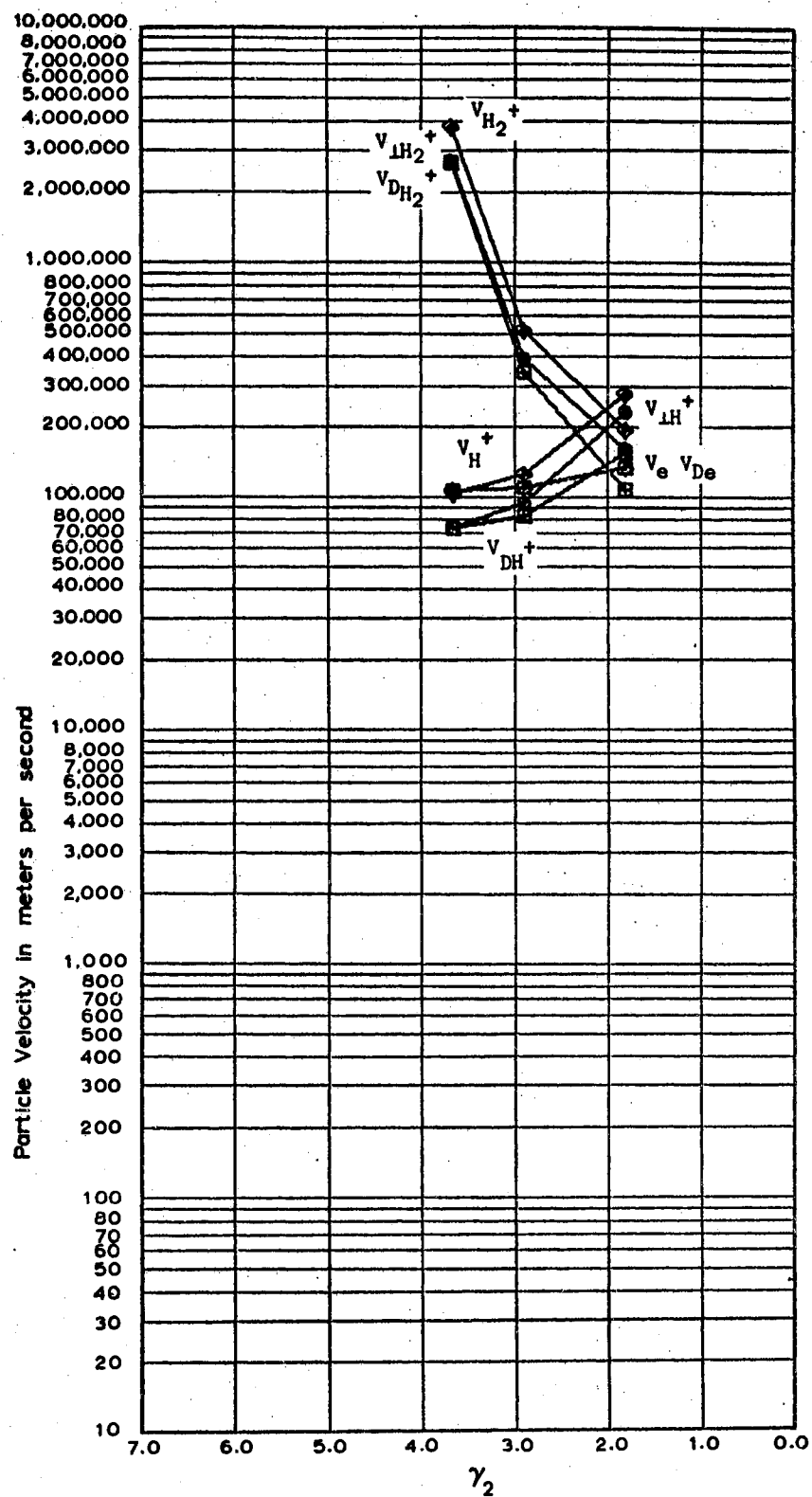
Figure 44e. Data taken April 15, 1965 at 3.5 MH_z with the Old Teflon Cell and Old rf Source, D = 0.004292 meters
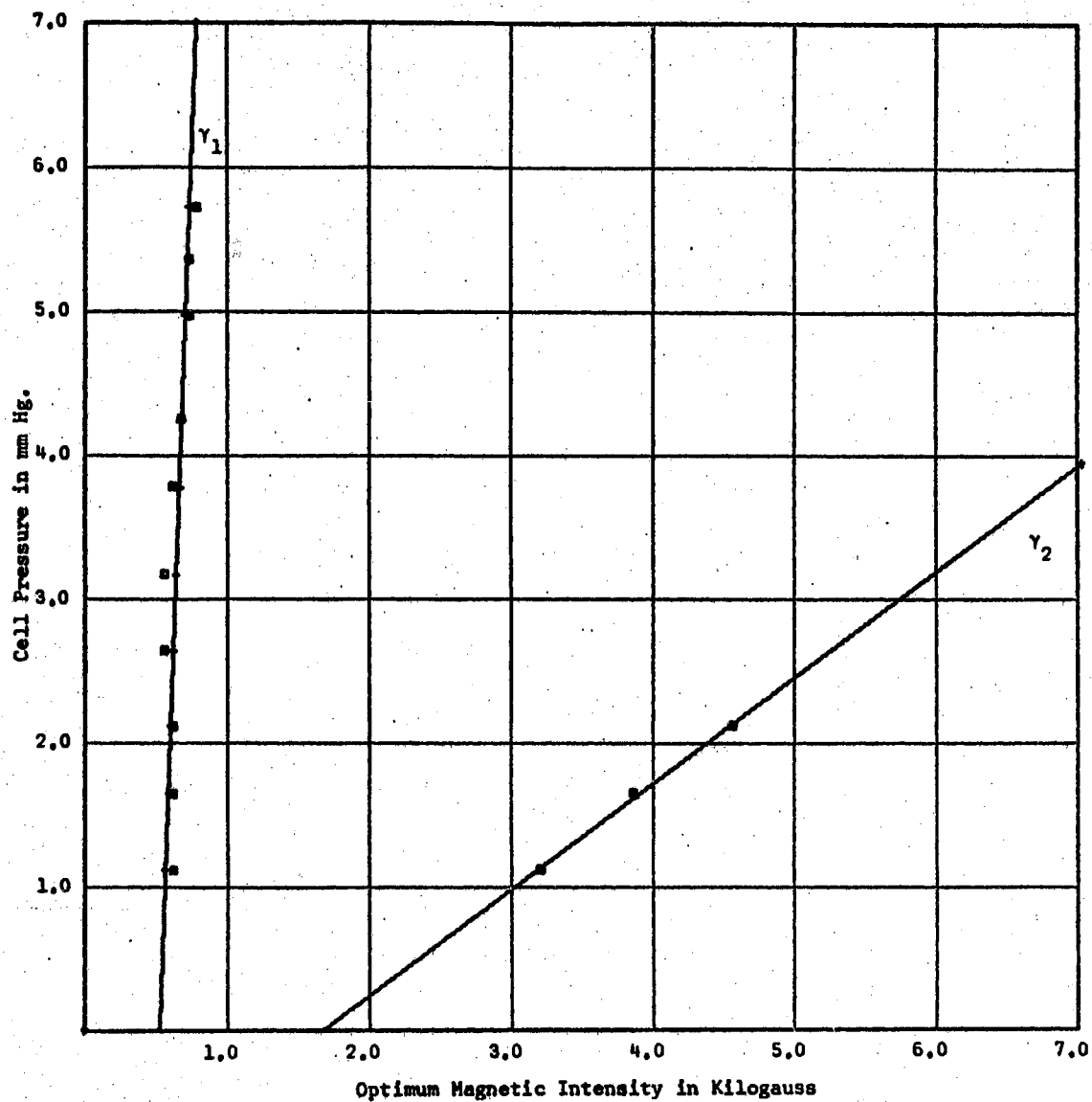
Figure 45a.   Data taken April 20, 1965 at 3.5 MH$_z$ with the Old
              Teflon Cell and Old rf Source, D $\cong$ 0.004292 meters
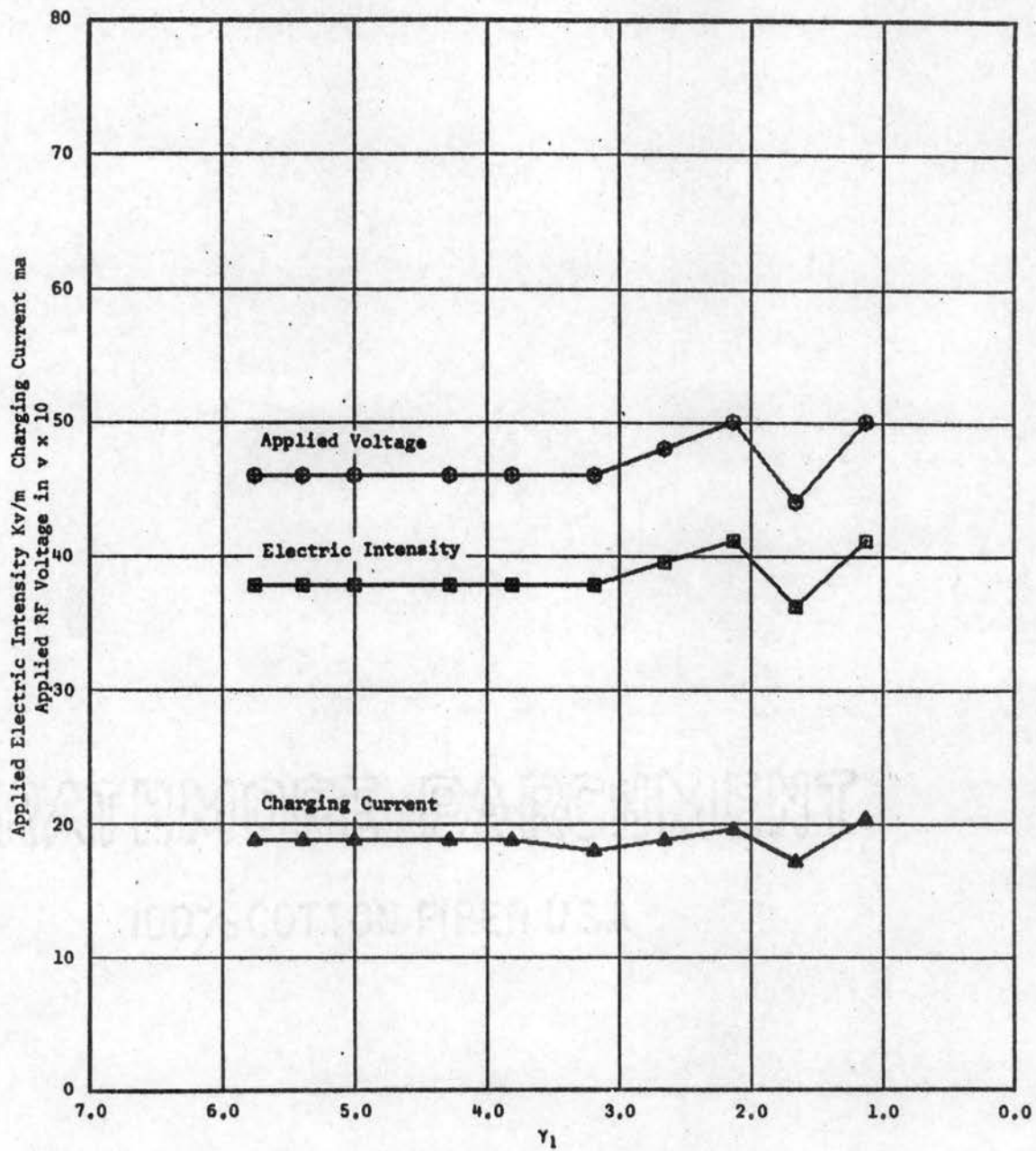
Figure 45b. Data taken April 20, 1965 at 3.5 MH_z with the Old Teflon Cell and Old rf Source, D^z = 0.004292 meters
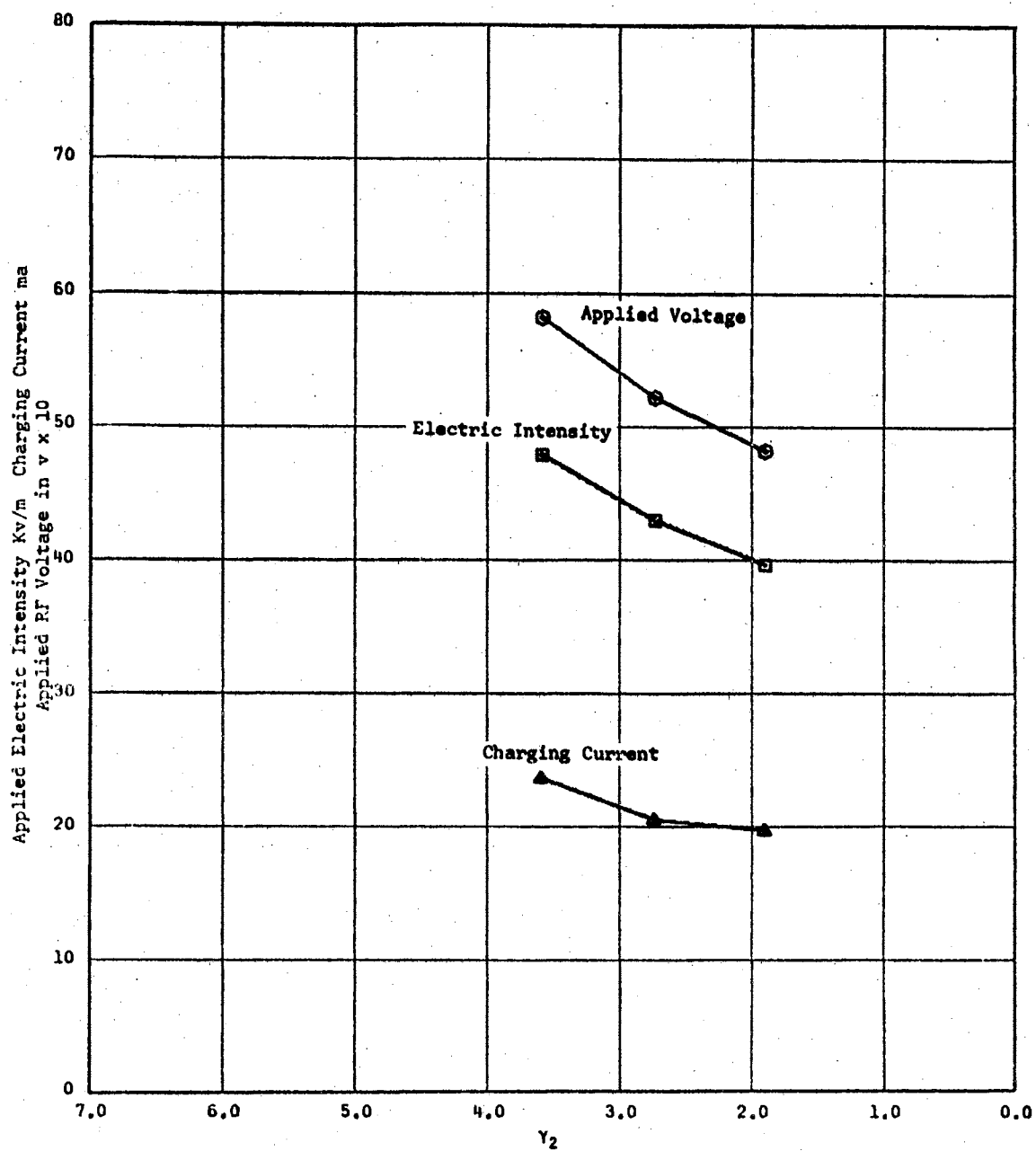
Figure 45c.   Data taken April 20, 1965 at 3.5 MH$_z$ with the Old
Teflon Cell and Old rf Source, D $\cong$ 0.004292 meters
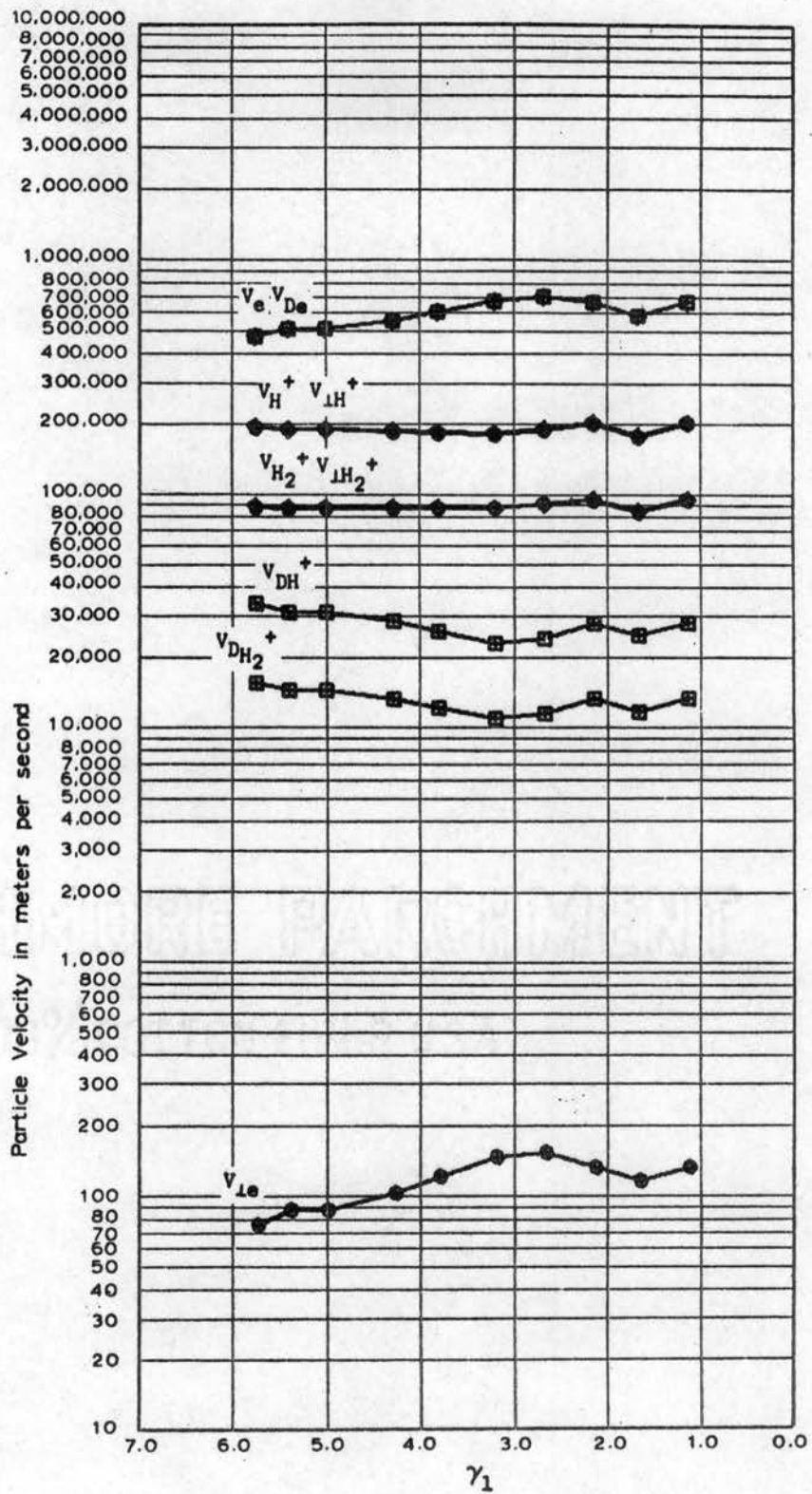
Figure 45d. Data taken April 20, 1965 at 3.5 MH$_z$ with the Old Teflon Cell and Old rf Source, D = 0.004292 meters
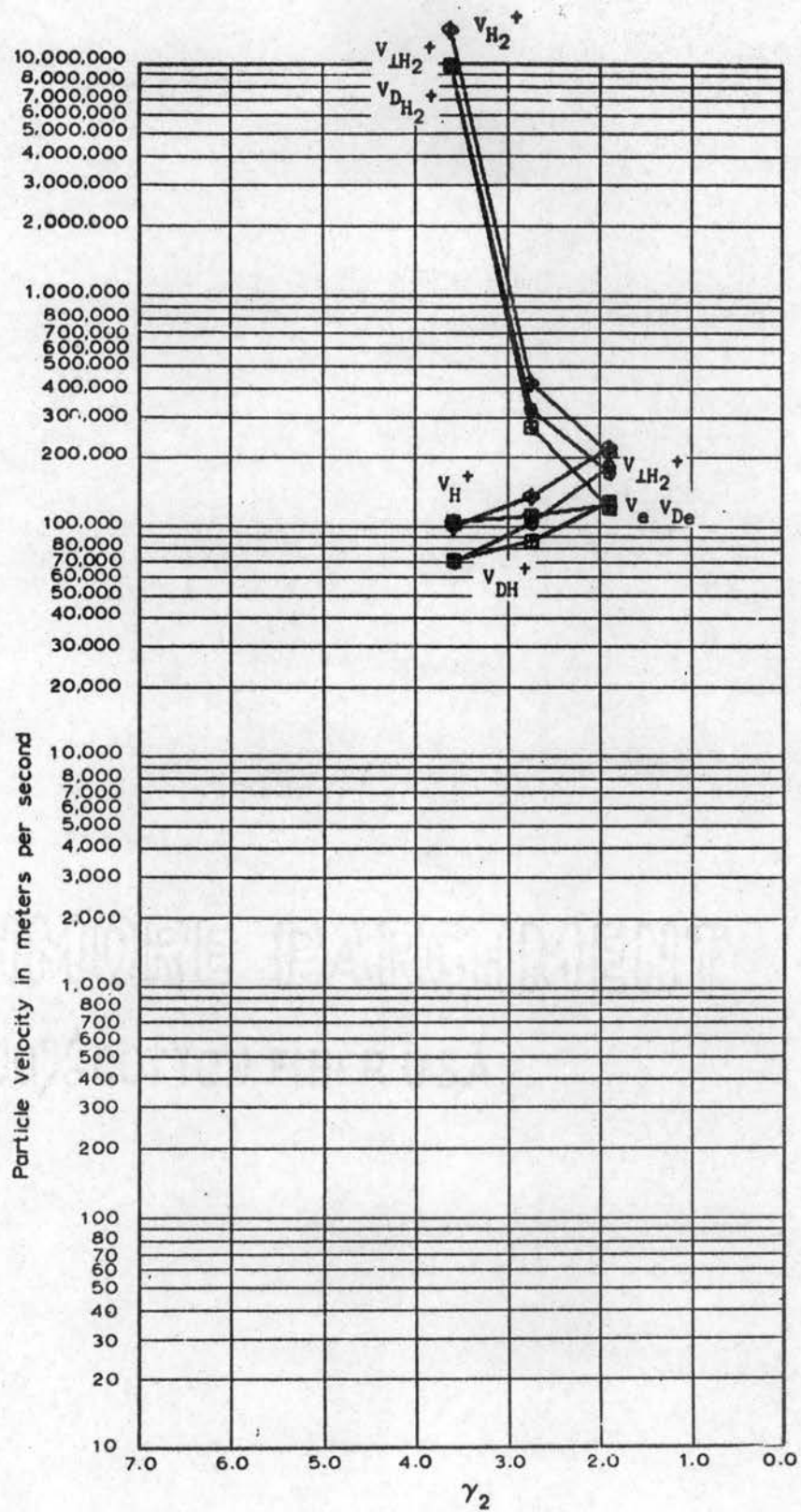
Figure 45e. Data taken April 20, 1965 at
3.5 MH$_z$ with the Old Teflon
Cell and Old rf Source, D =
0.004292 meters
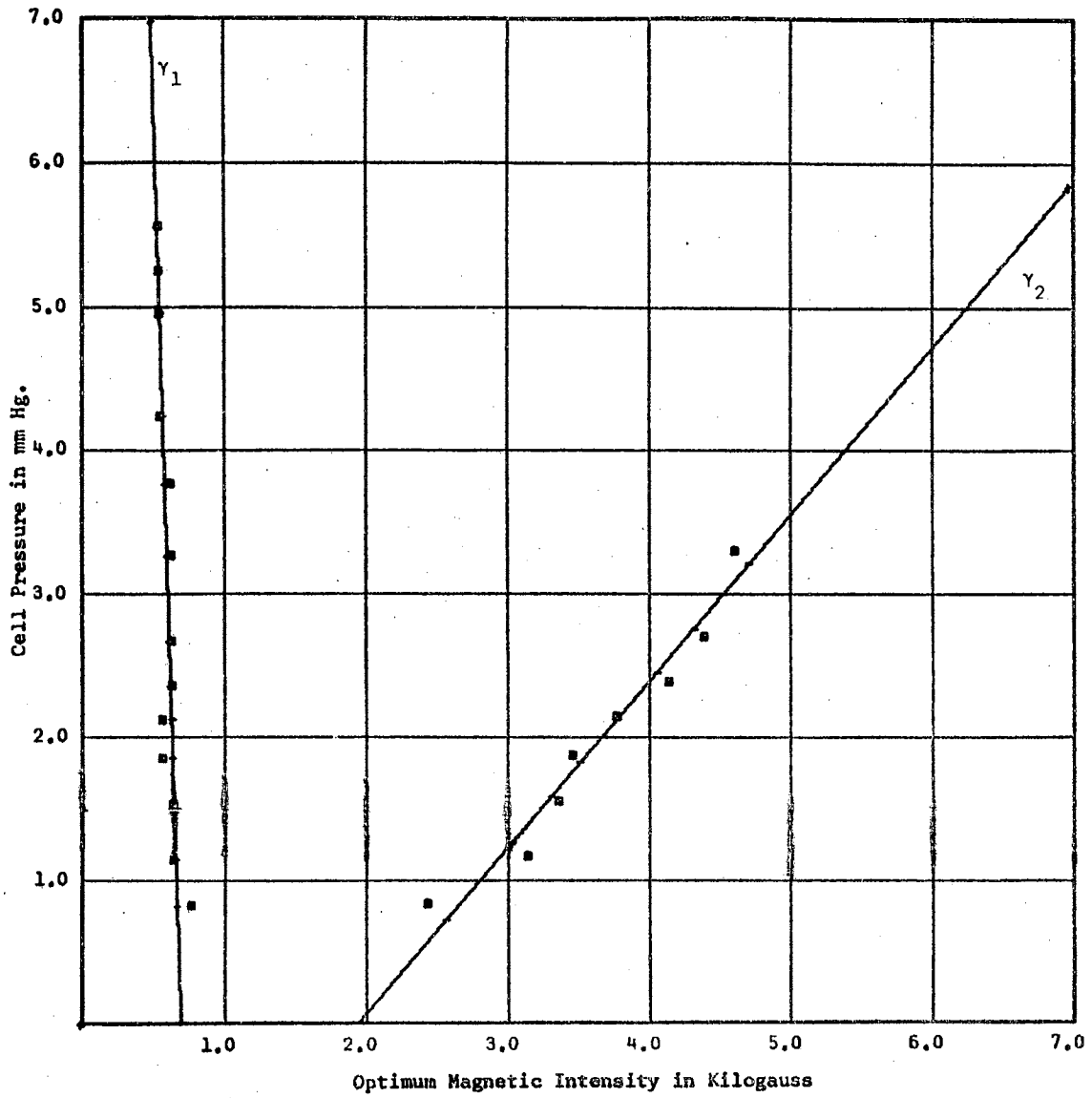
Figure 46a. Data taken August 16, 1965 at 3.5 MH$_z$ with the
Aluminum Cell and Old rf Source, D^z= 0.003937 meters
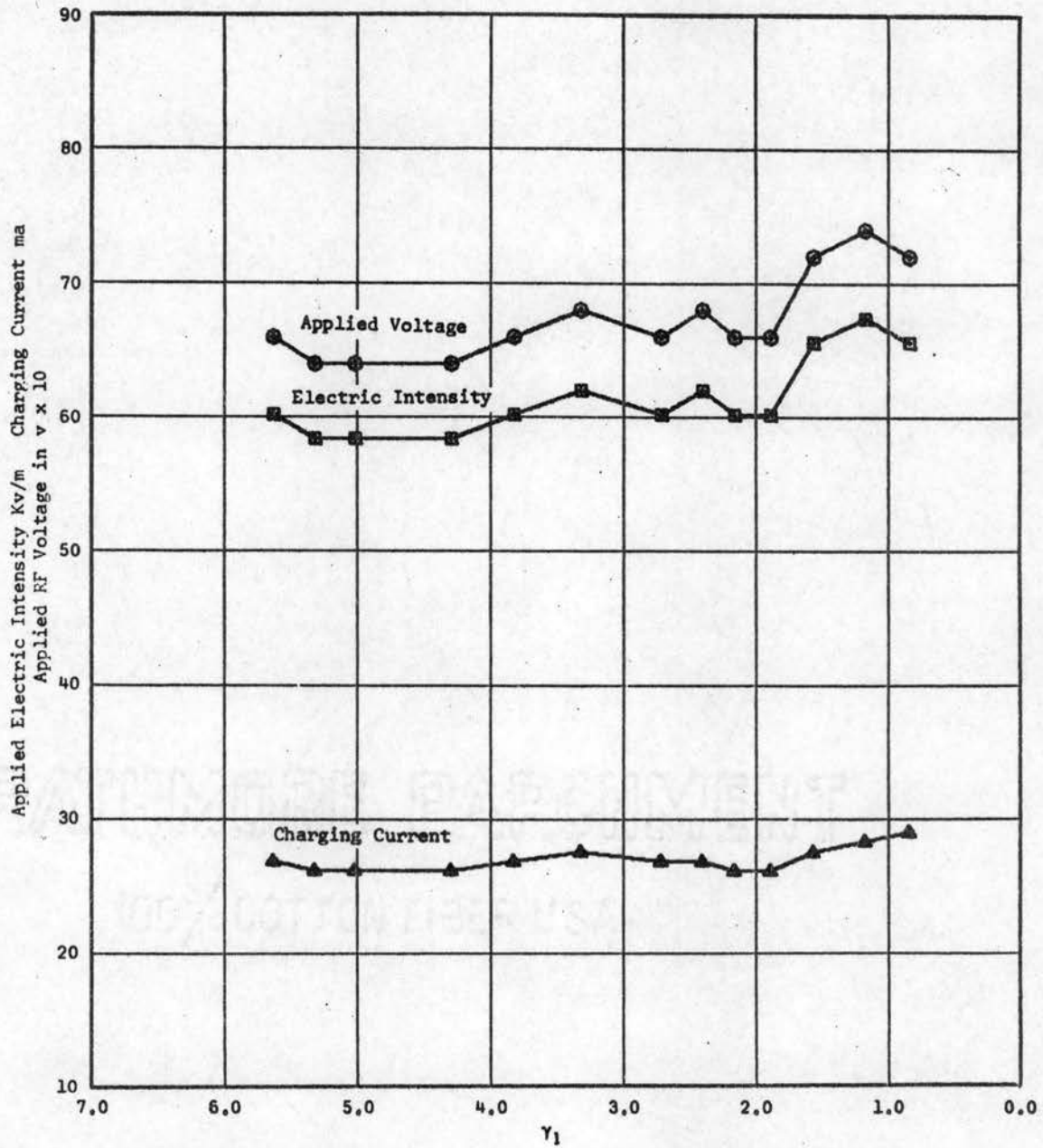
Figure 46b. Data taken August 16, 1965 at 3.5 MH with the Aluminum Cell and Old rf Source, D^2 = 0.003937 meters
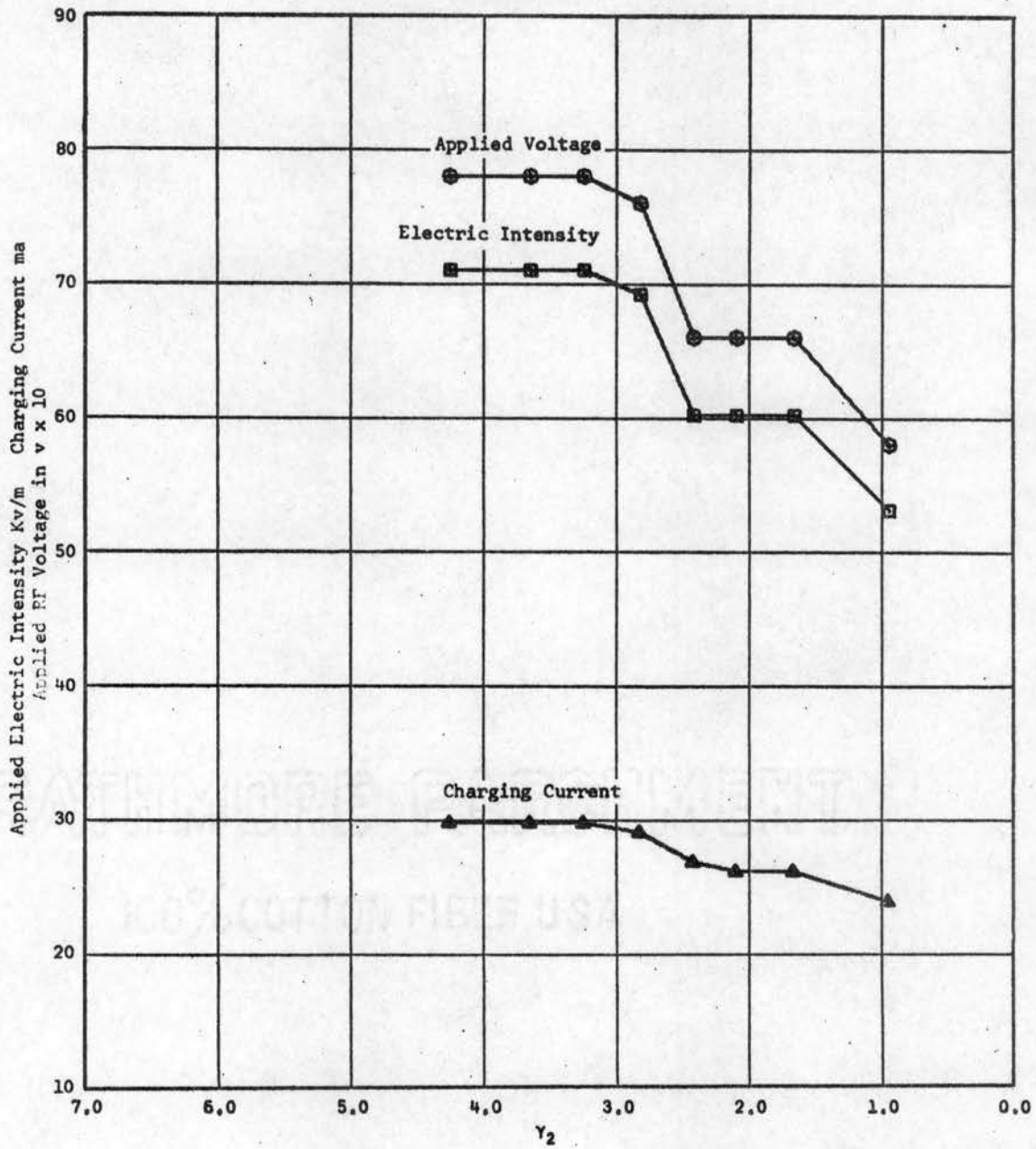
Figure 46c.   Data taken August 16, 1965 at 3.5 MH_z with the
Aluminum Cell and the Old rf Source, D = 0.003937
meters
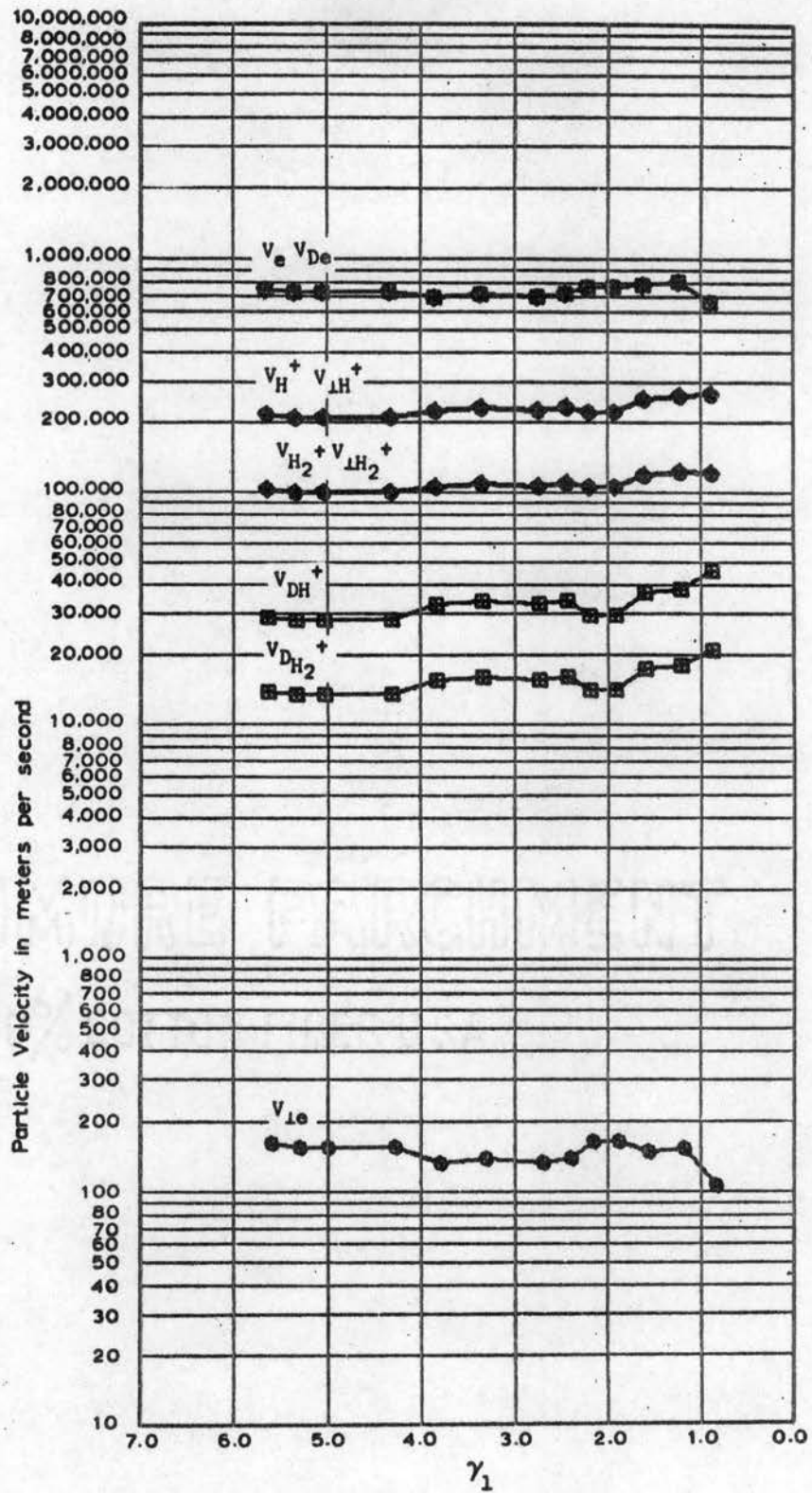
Figure 46d. Data taken August 16, 1965 at 3.5 MH$_z$ with the Aluminum Cell and Old rf Source, D = 0.003937 meters
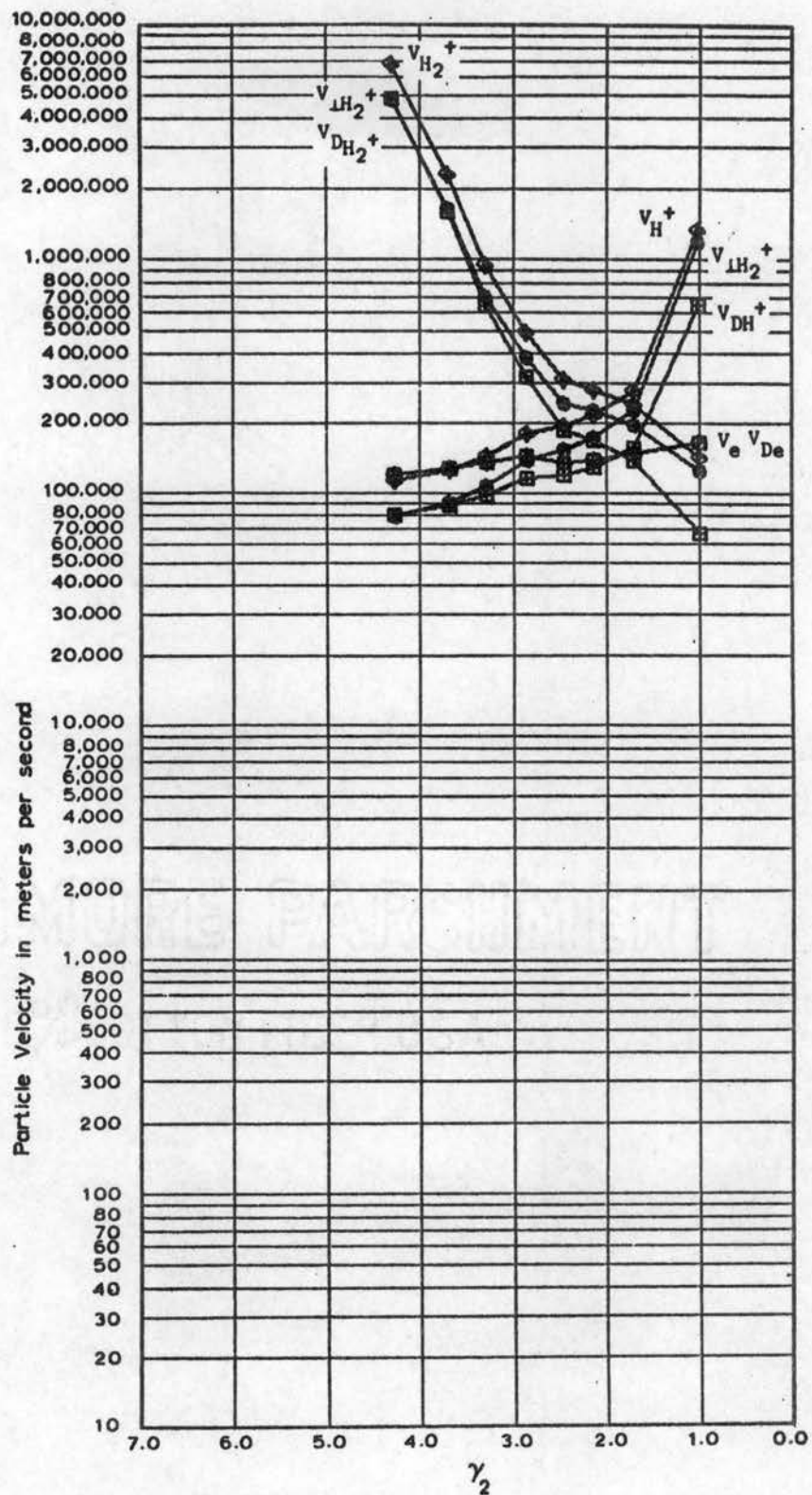
Figure 46e. Data taken August 16, 1965 at 3.5 MH$_z$ with the Aluminum Cell and Old rf Source, D = 0.003937 meters
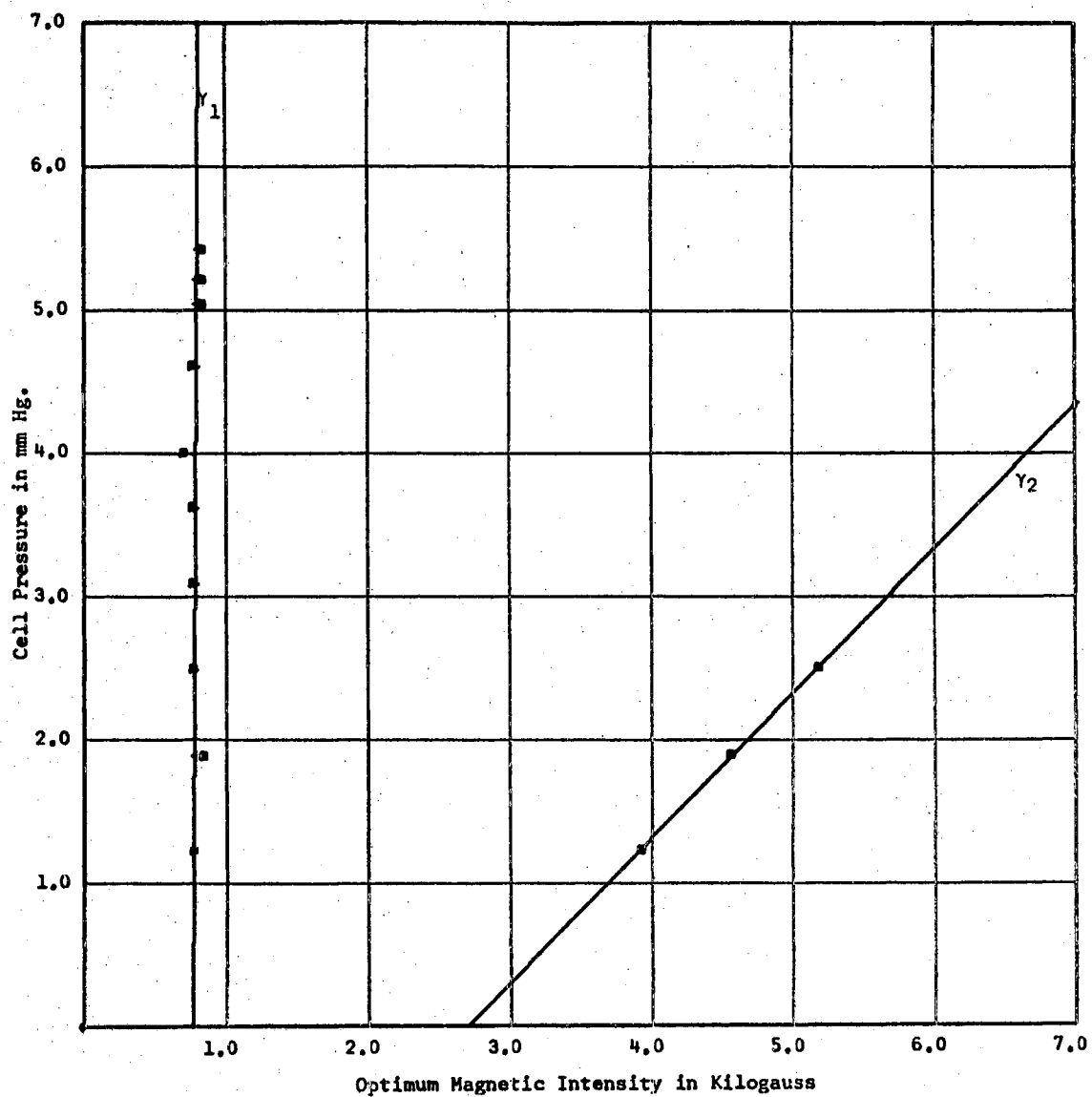
Figure 47a. Data taken August 9, 1966 at 4 MH_z with the Aluminum Cell, D = 0.002794 meters

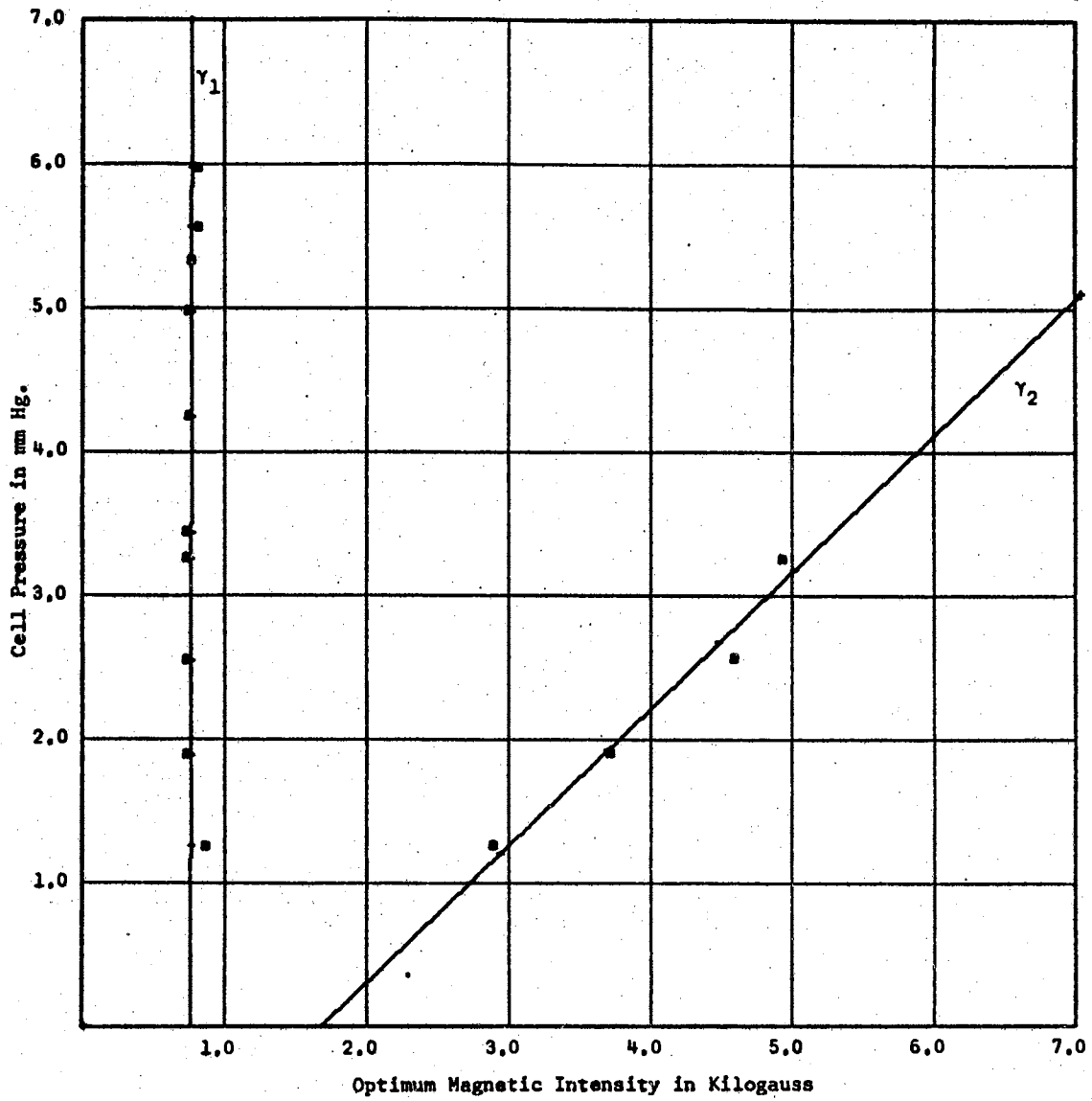Figure 47b. Data taken August 9, 1966 at 4 MH_z with the Aluminum Cell, D = 0.002794 meters
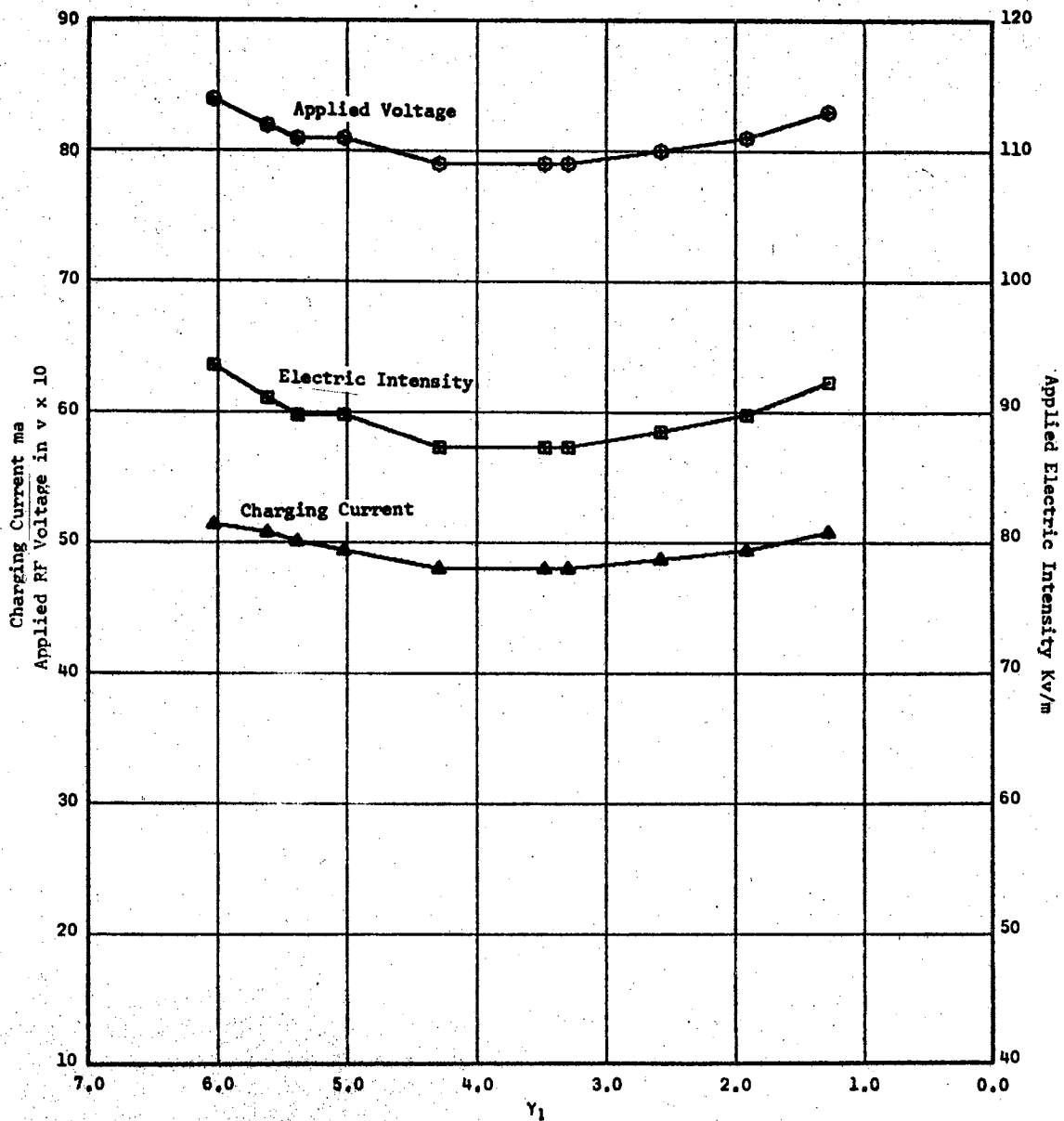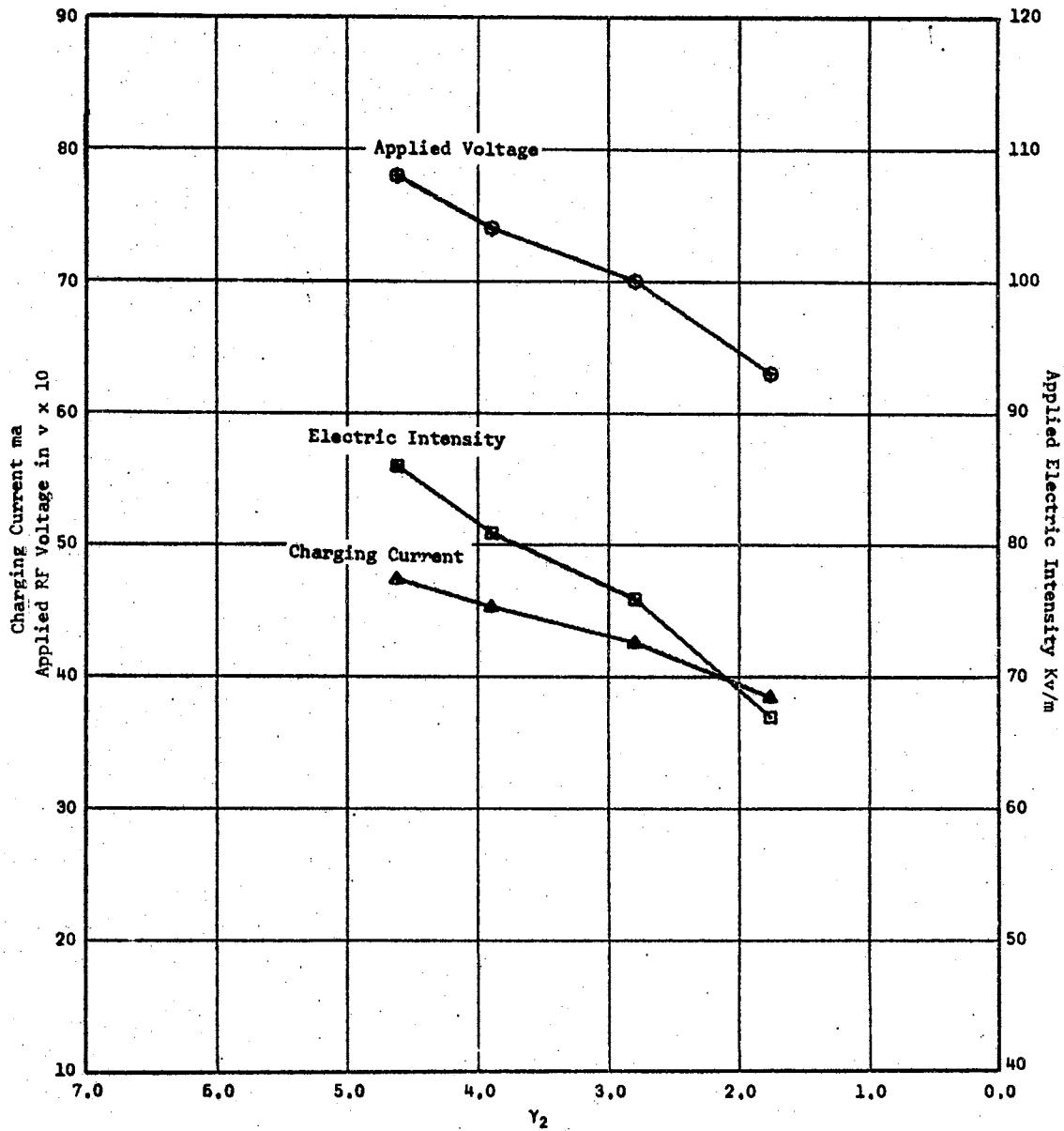
Figure 47c. Data taken August 9, 1966 at 4 MH$_z$ with the Aluminum Cell, D = 0.002794 meters

Figure 47d. Data taken August 9, 1966 at 4
MH$_z$ with the Aluminum Cell,
D = 0.002794 meters

Figure 47e. Data taken August 9, 1966 at 4
MH with the Aluminum Cell,
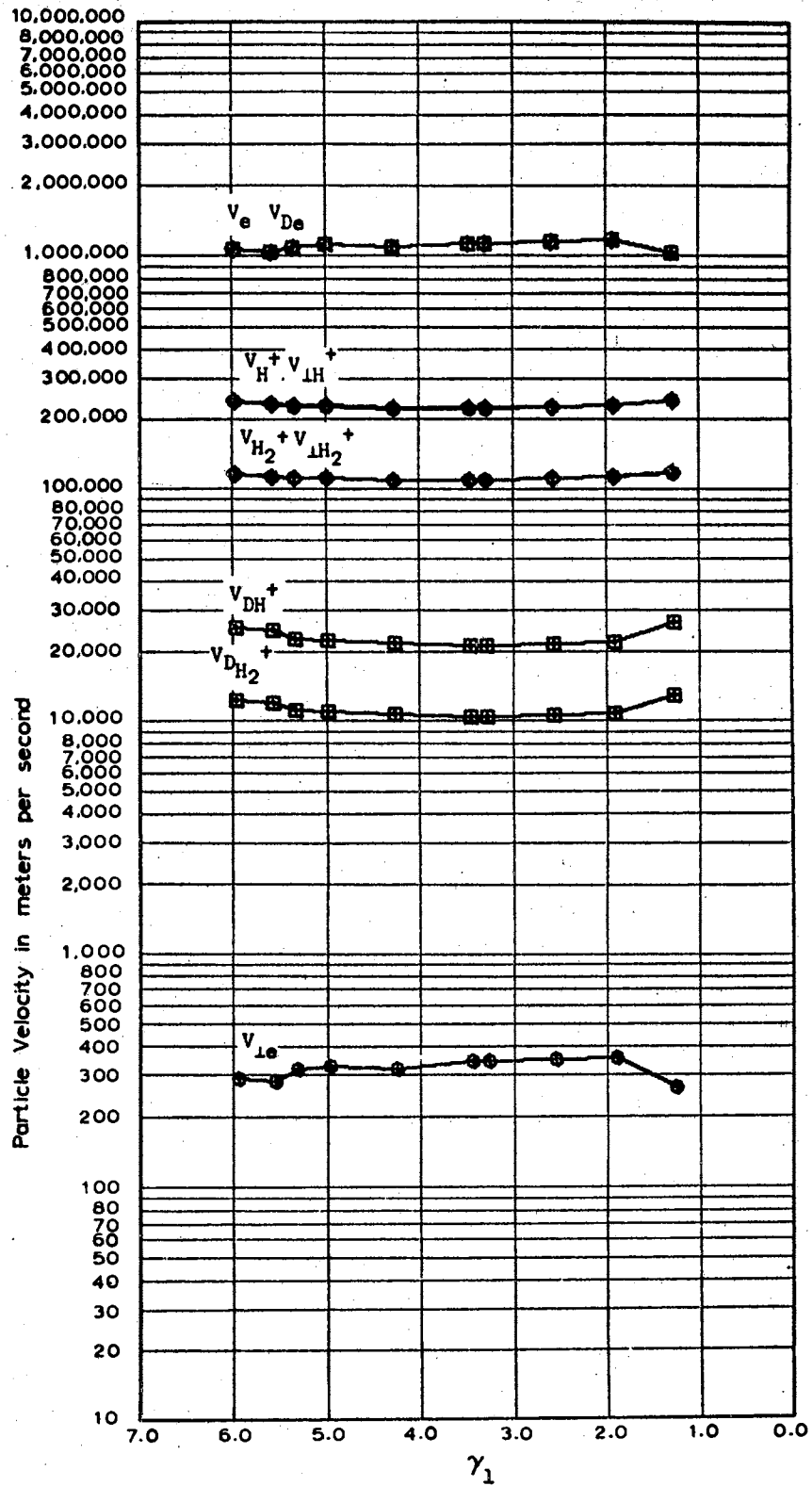b ≡ 0.002794 meters

Figure 48a. Data taken August 23, 1966 at 4 MH_z with the Aluminum Cell, D = 0.

Figure 48b. Data taken August 23, 1966 at 4 MI with the
Aluminum Cell, D = 0.002794 meters

Figure 48c. Data taken August 23, 1966 at 4 MH$_z$ with the
Aluminum Cell, D = 0.002794 meters

Figure 48d. Data taken August 23, 1966 at
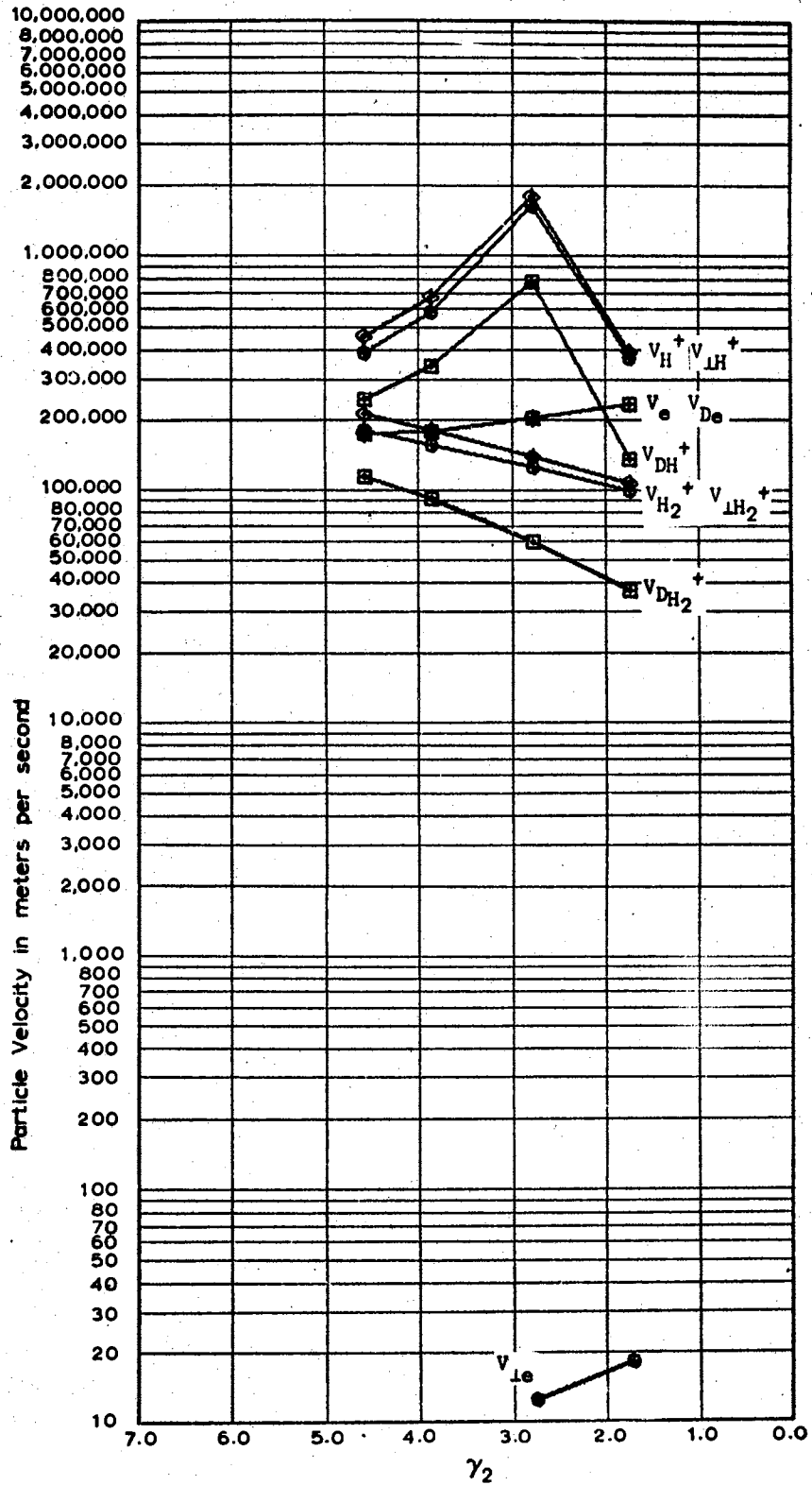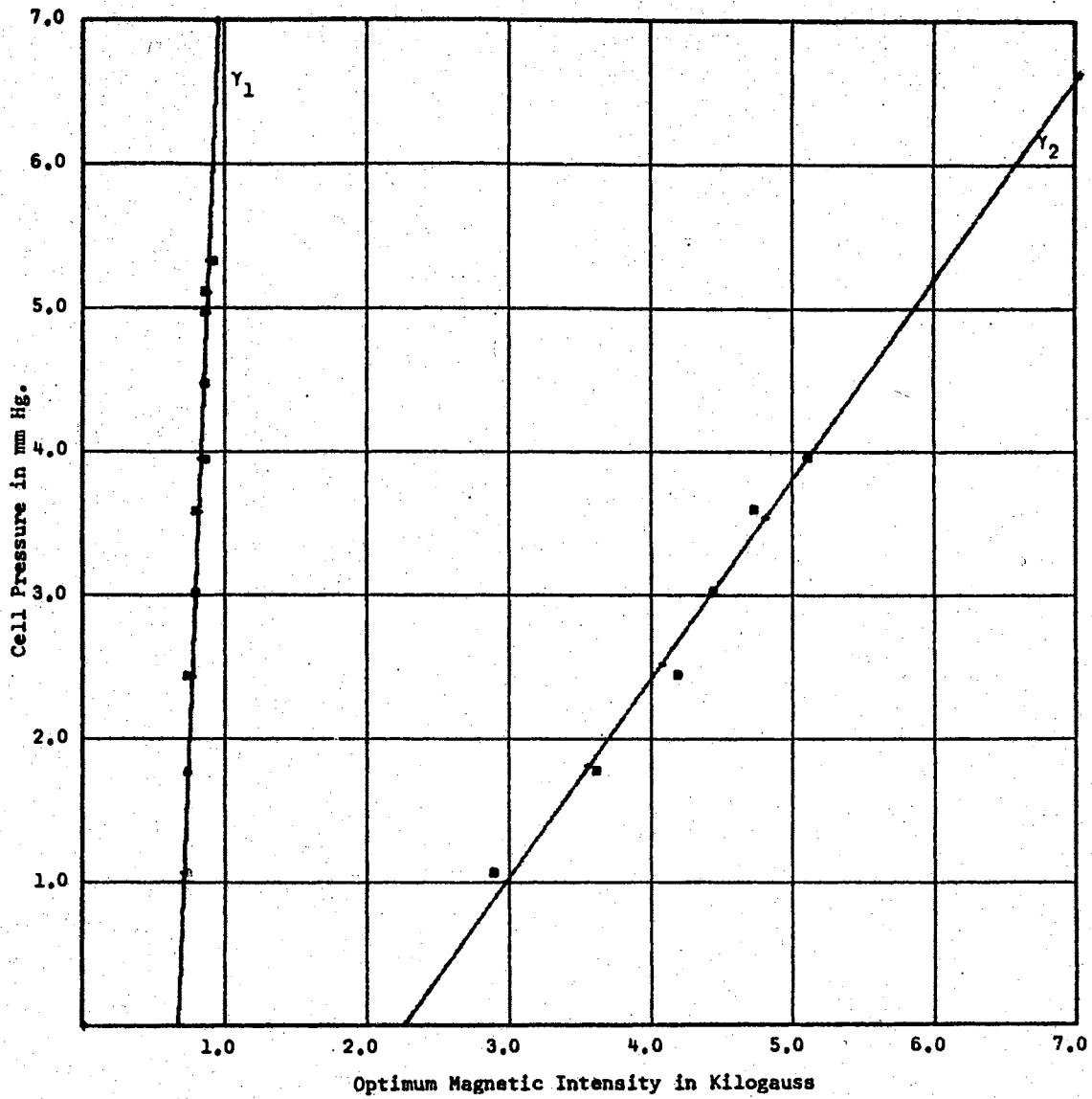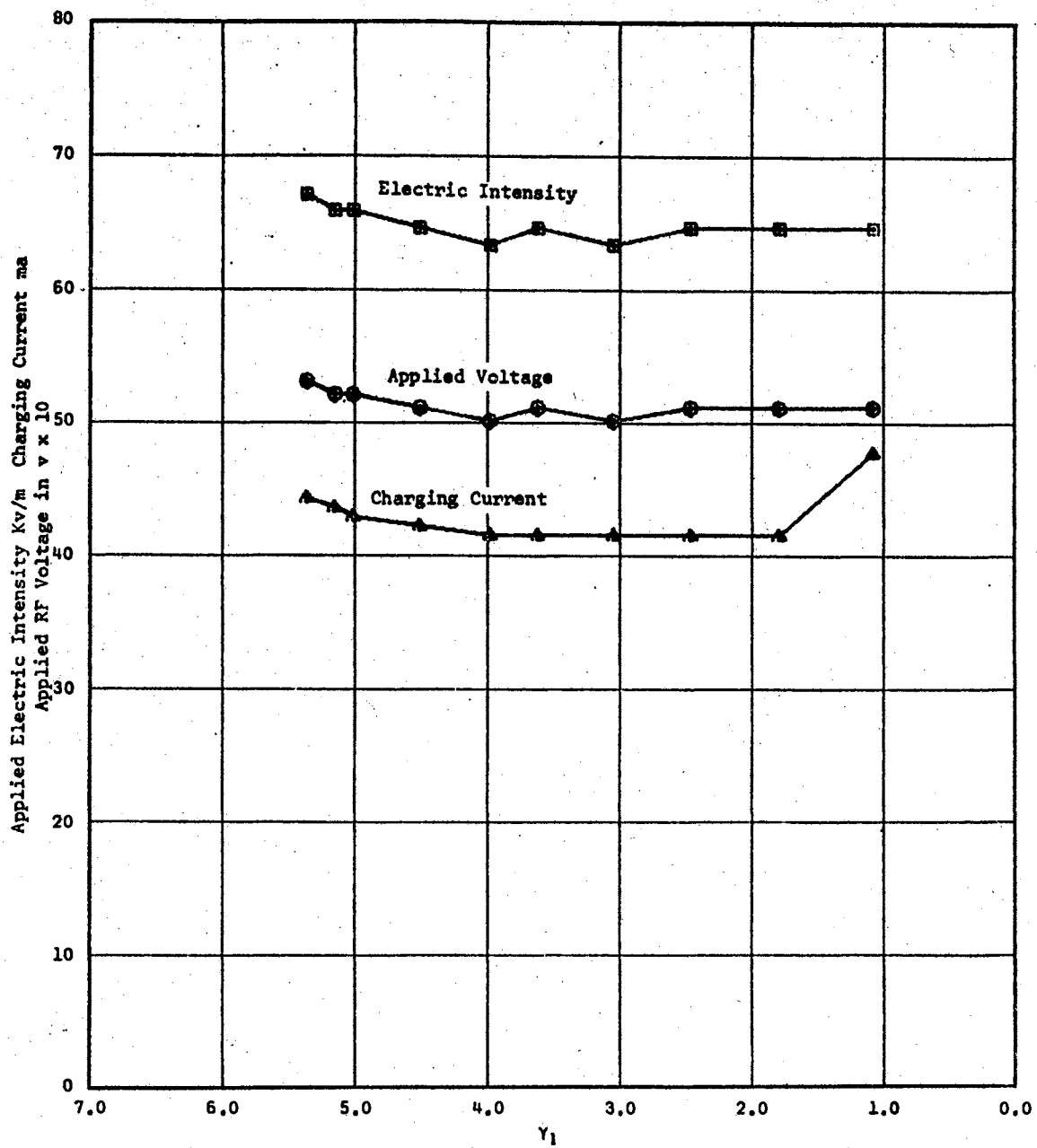4 MH$_z$ with the Aluminum Cell,
D = 0.002794 meters

Figure 48e. Data taken August 23, 1966 at 4
MH$_z$ with the Aluminum Cell,
D = 0.002794 meters

Figure 49a.   Data taken June 24, 1966 at 5 MH$_z$ with the Aluminum
Cell, D = 0.002794 meters

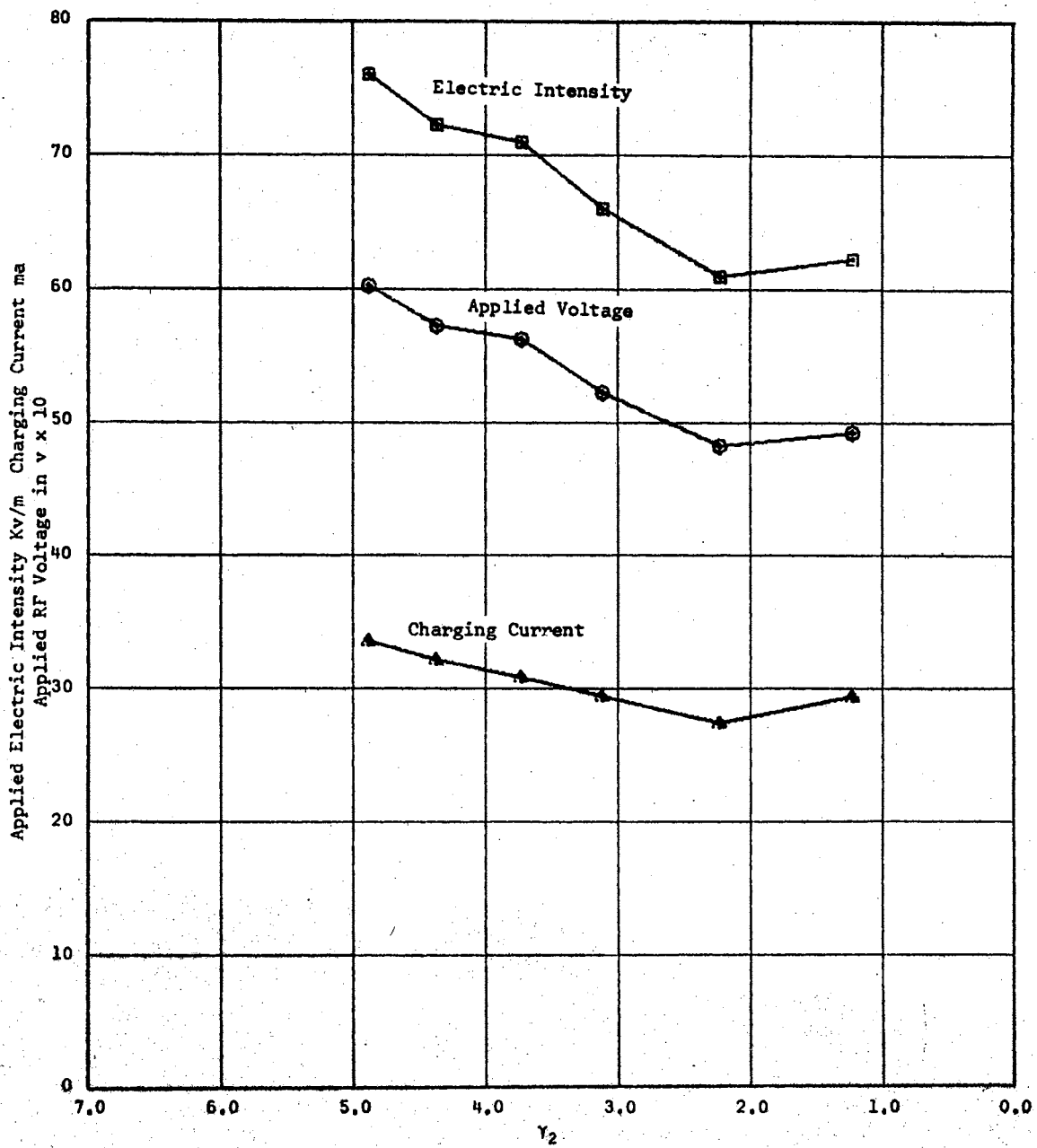Figure 49b. Data taken June 24, 1966 at 5 MH$_z$ with the Aluminum Cell, D = 0.002794 meters

Figure 49c. Data taken June 24, 1966 at 5 MH$_z$ with the
Aluminum Cell, D = 0.002794 meters

Figure 49d.   Data taken June 24, 1966 at 5
MH$_z$ with the Aluminum Cell,
D $\cong$ 0.002794 meters

Figure 49e. Data taken June 24, 1966 at 5
MH with the Aluminum Cell,
$D \stackrel{z}{=} 0.002794$ meters
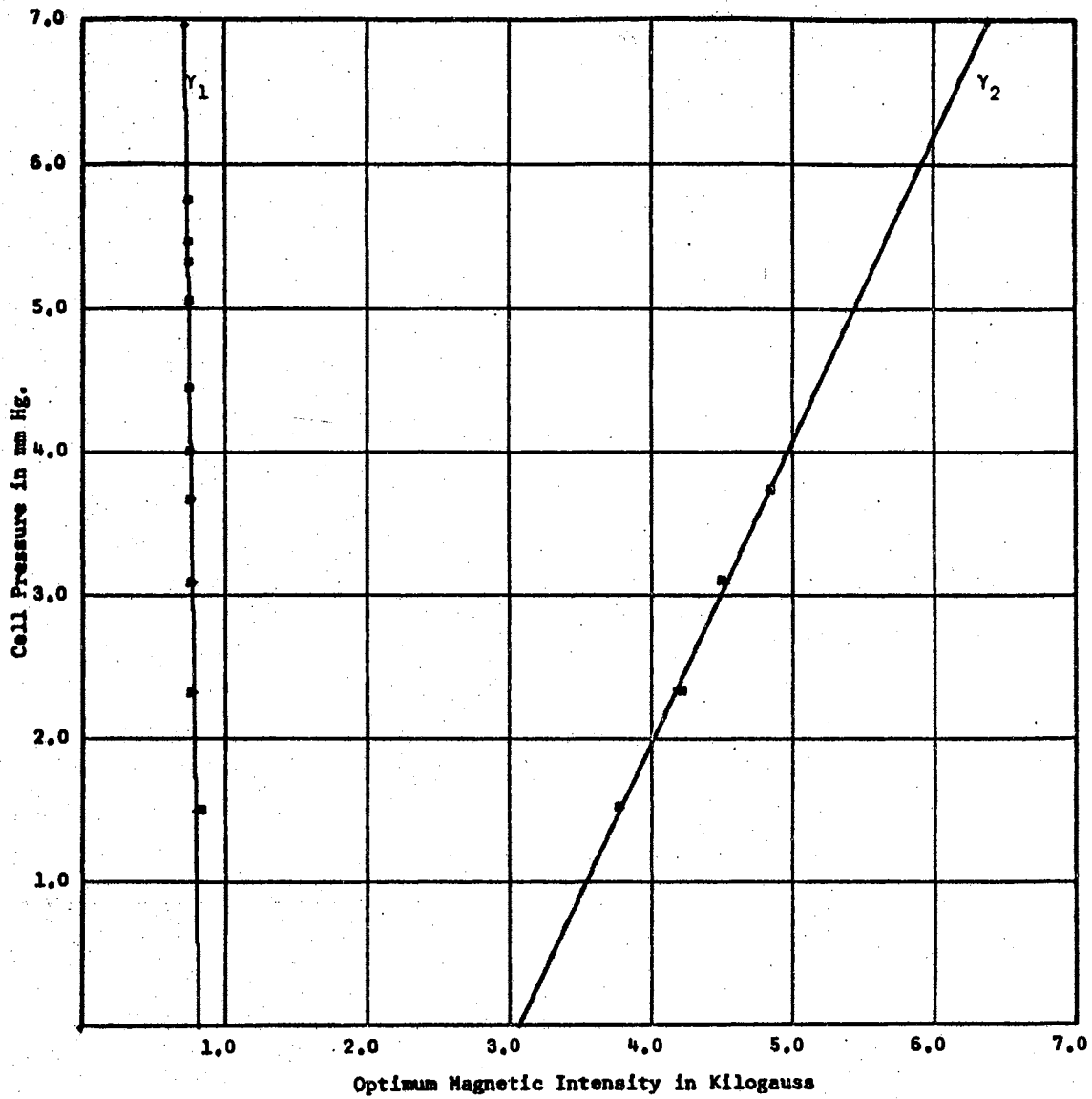
Figure 50a.   Data taken June 29, 1966 at 5 MH$_z$ with the Aluminum
Cell, D = 0.002794 meters
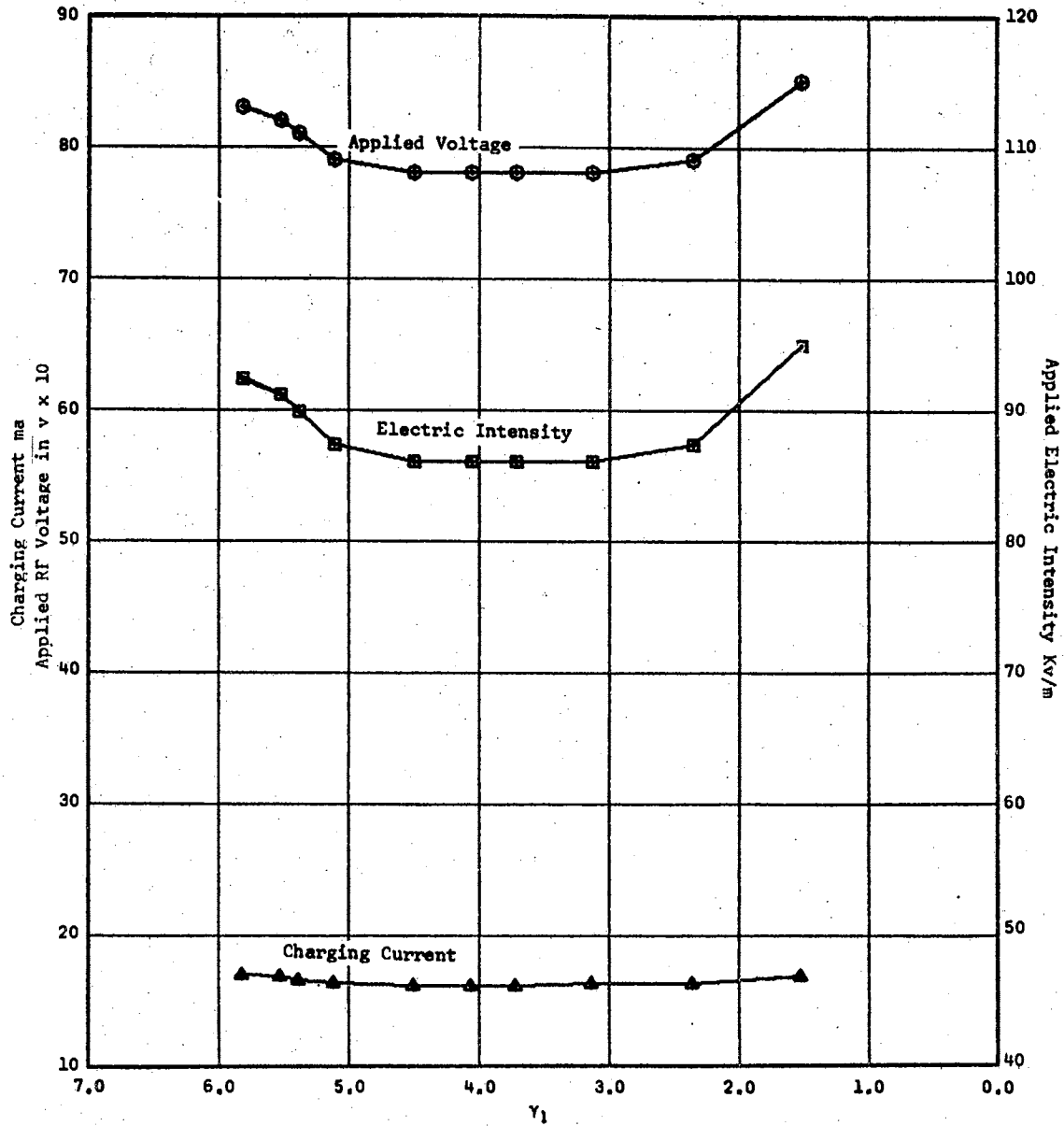
Figure 50b. Data taken June 29, 1966 at 5 MH_z with the Aluminum Cell, D = 0.002794 meters
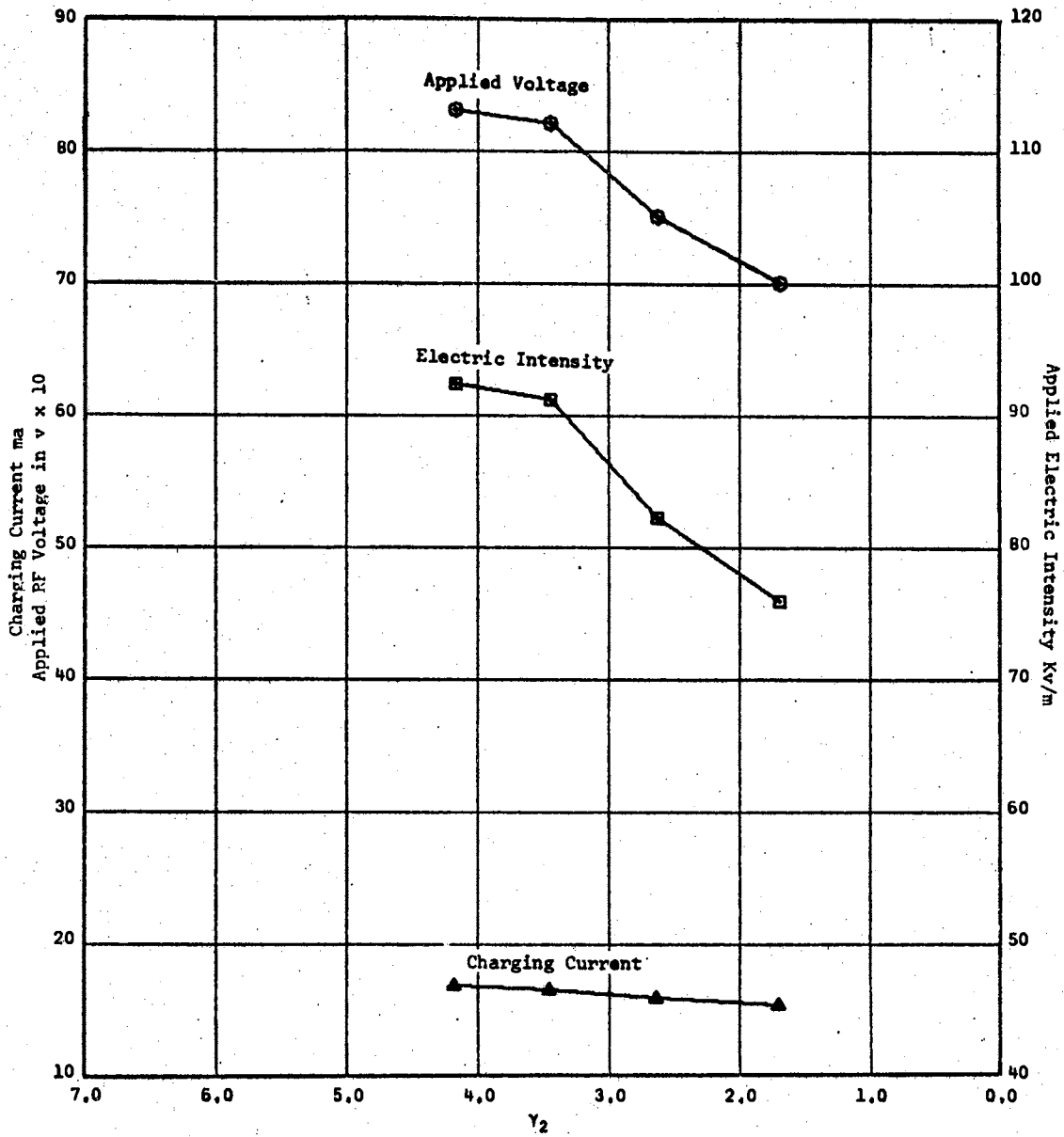
Figure 50c. Data taken June 29, 1966 at 5 MH$_z$ with the
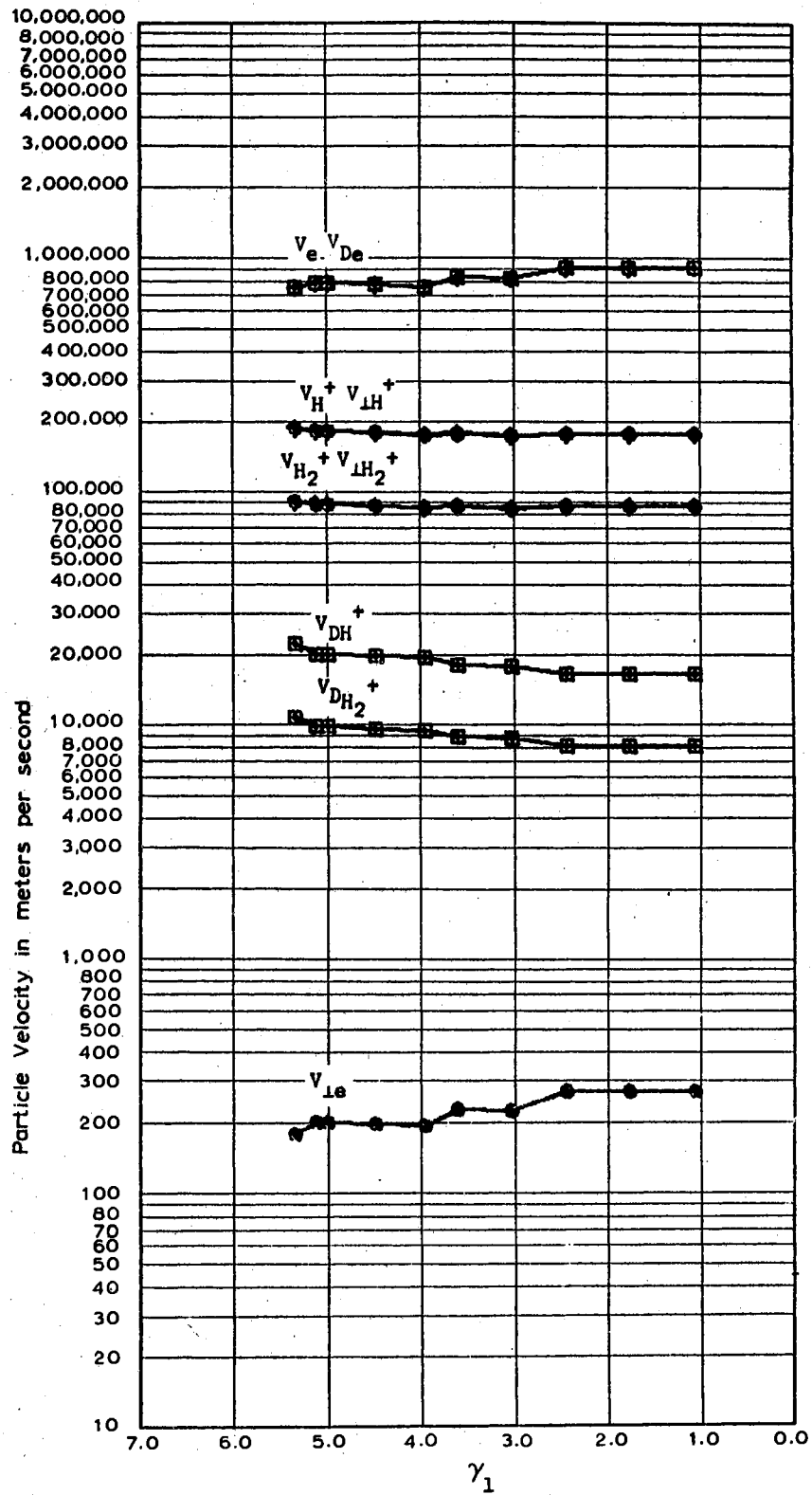Aluminum Cell, D = 0.002794 meters
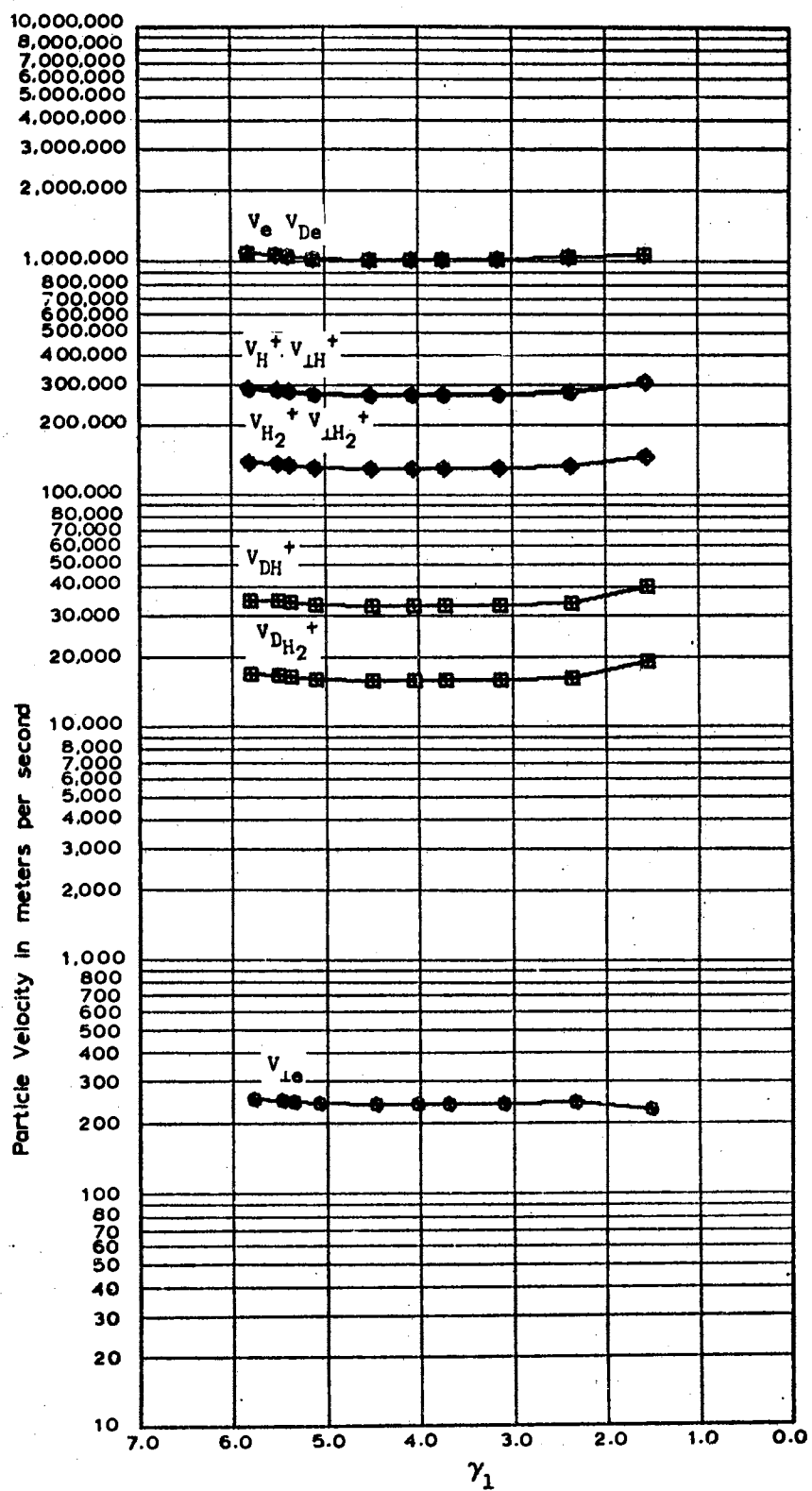
Figure 50d. Data taken June 29, 1966 at 5
MH with the Aluminum Cell,
D ≅ 0.002794 meters
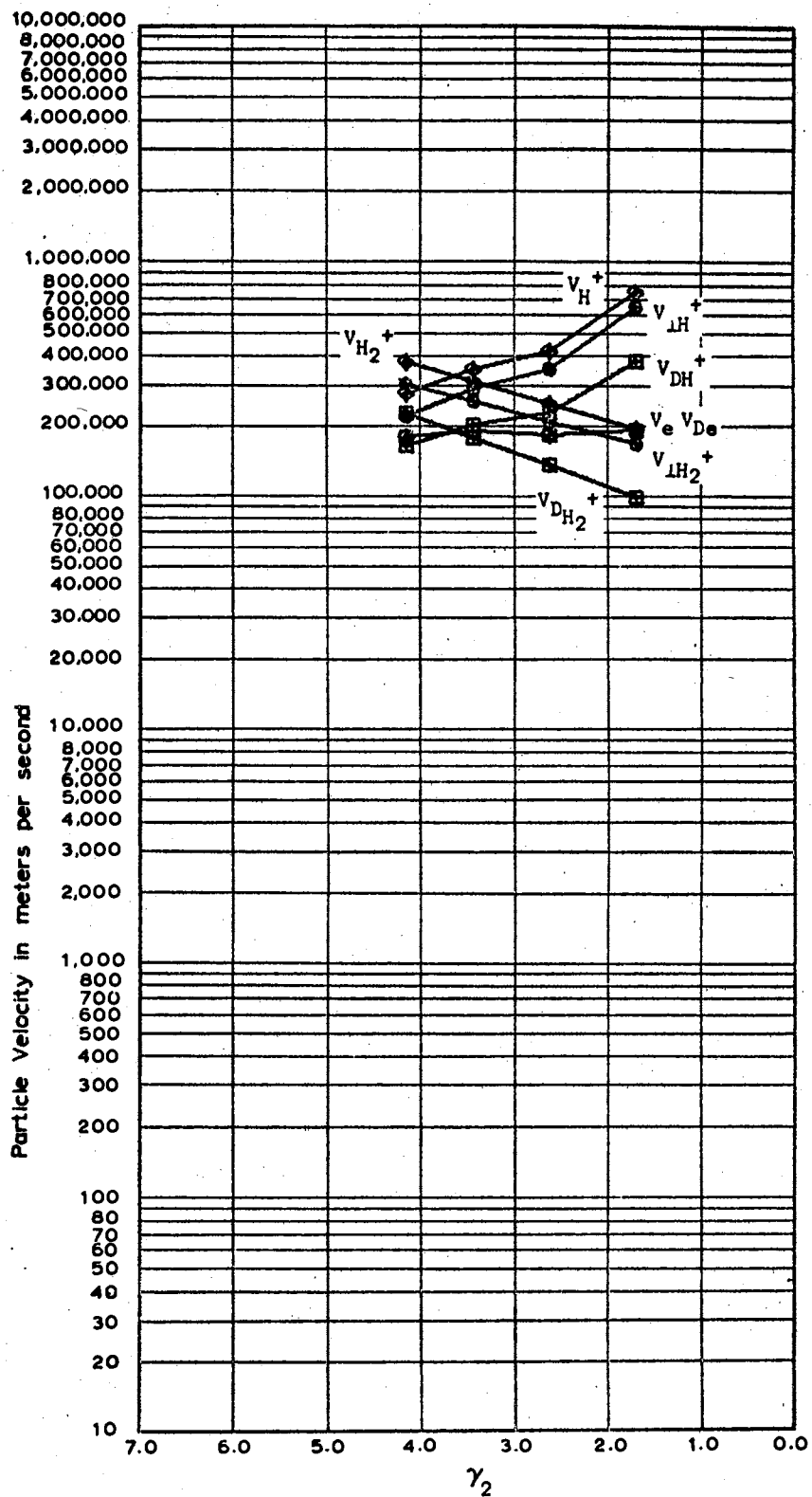
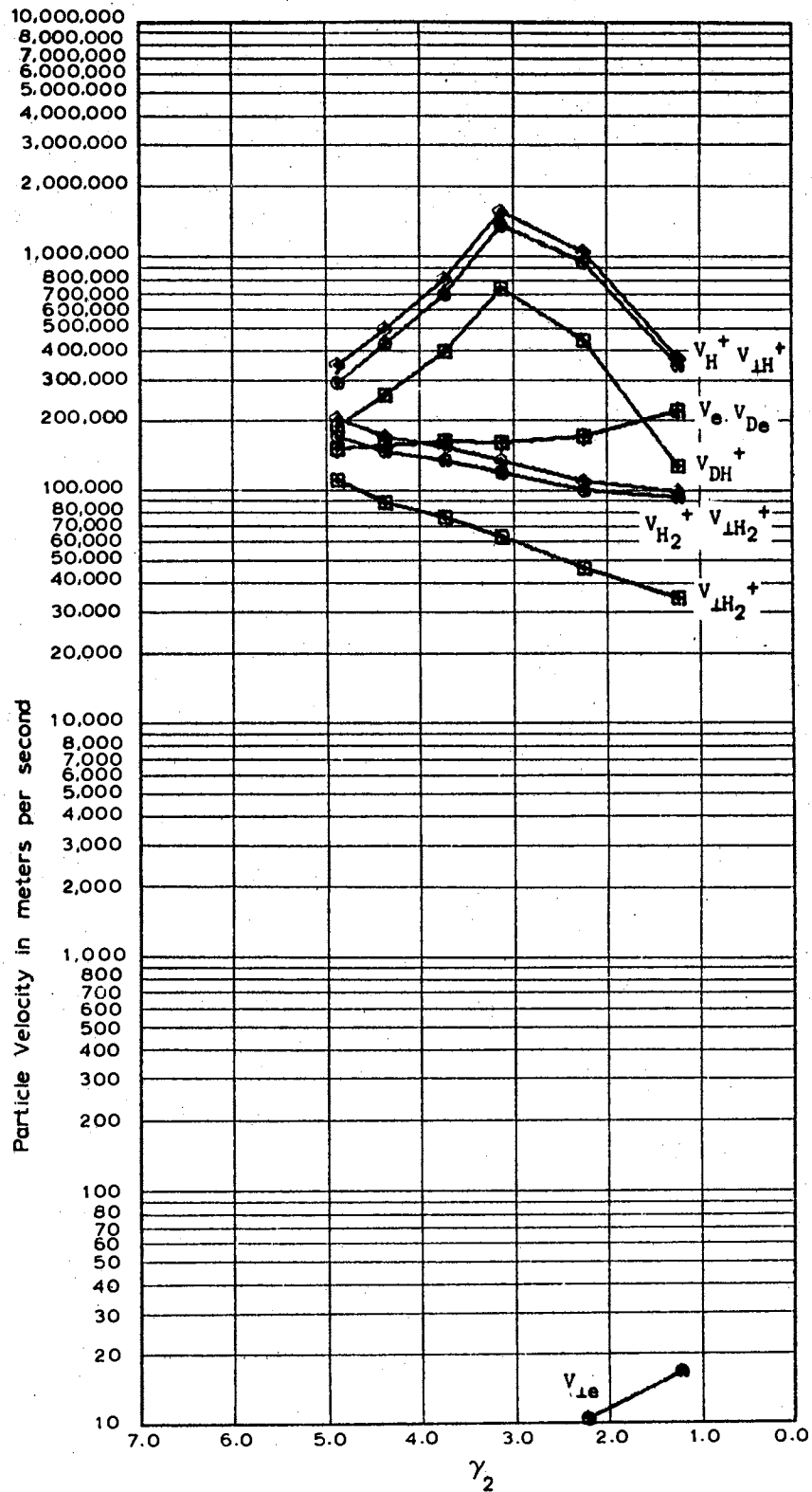Figure 50e. Data taken June 29, 1966 at 5
MH with the Aluminum Cell,
D $\stackrel{z}{=}$ 0.002794 meters

Figure 51a. Data taken July 9, 1966 at 6 MH_z with the Aluminum
Cell, D = 0.002794 meters

Figure 51b. Data taken July 9, 1966 at 6 MH$_z$ with the Aluminum Cell, D = 0.002794 meters

Figure 51c. Data taken July 9, 1966 at 6 MHz with the Aluminum Cell, D = 0.002794 meters

Figure 51d. Data taken July 9, 1966 at 6 MH$_z$ with the Aluminum Cell, D = 0.002794 meters

Figure 51e. Data taken July 9, 1966 at 6
MH with the Aluminum Cell,
D = 0.002794 meters

Figure 52a. Data taken August 18, 1966 at 6 MH$_z$ with the
Aluminum Cell, D = 0.002794 meters

Figure 52b. Data taken August 18, 1966 at 6 MH_z with the
Aluminum Cell, D = 0.002794 meters

Figure 52c. Data taken August 18, 1966 at 6 MH$_z$ with the Aluminum Cell, D = 0.002794 meters

Figure 52d. Data taken August 18, 1966 at 6
MH with the Aluminum Cell,
D ≅ 0.002794 meters

Figure 52e. Data taken August 18, 1966 at 6
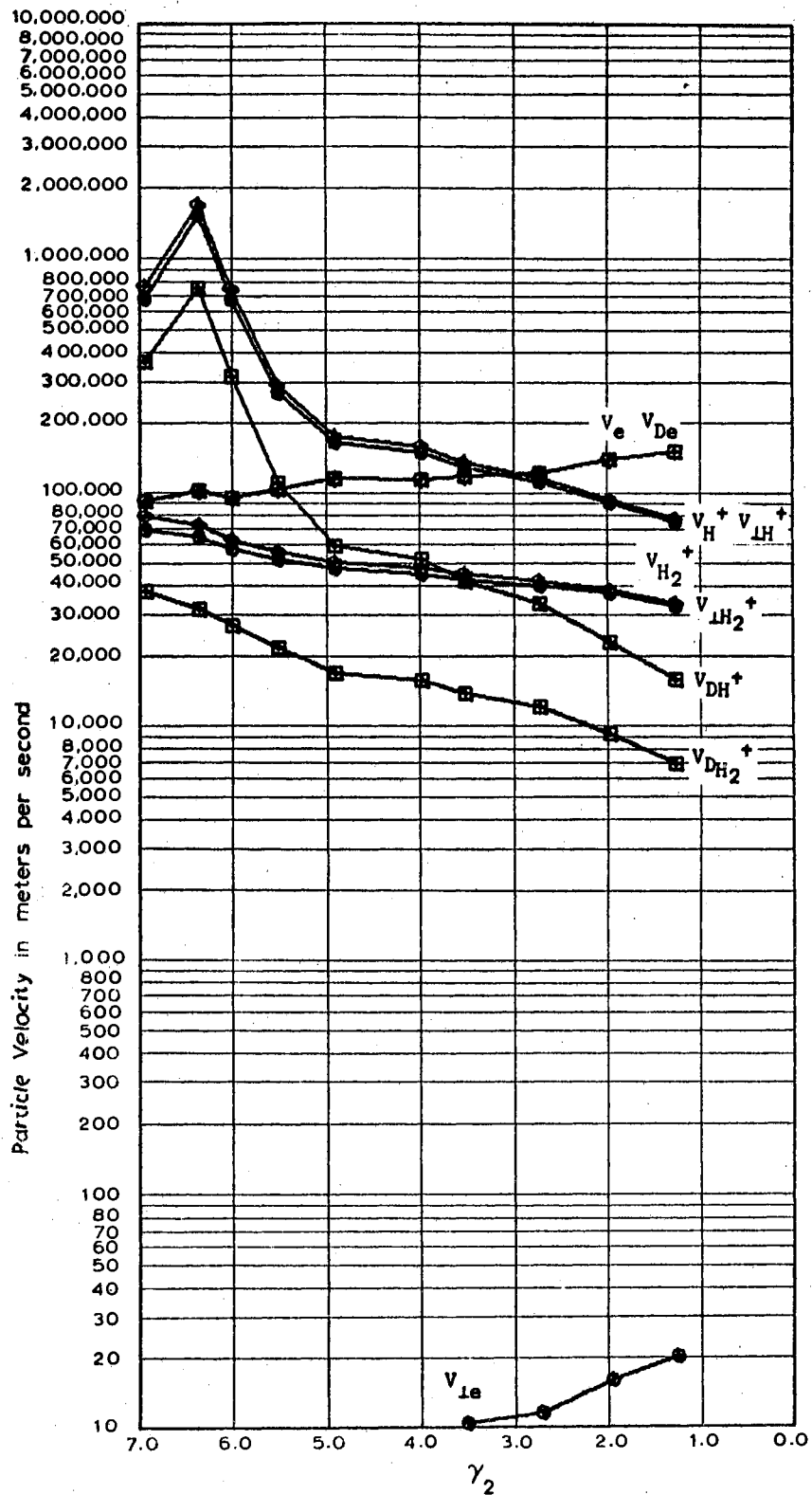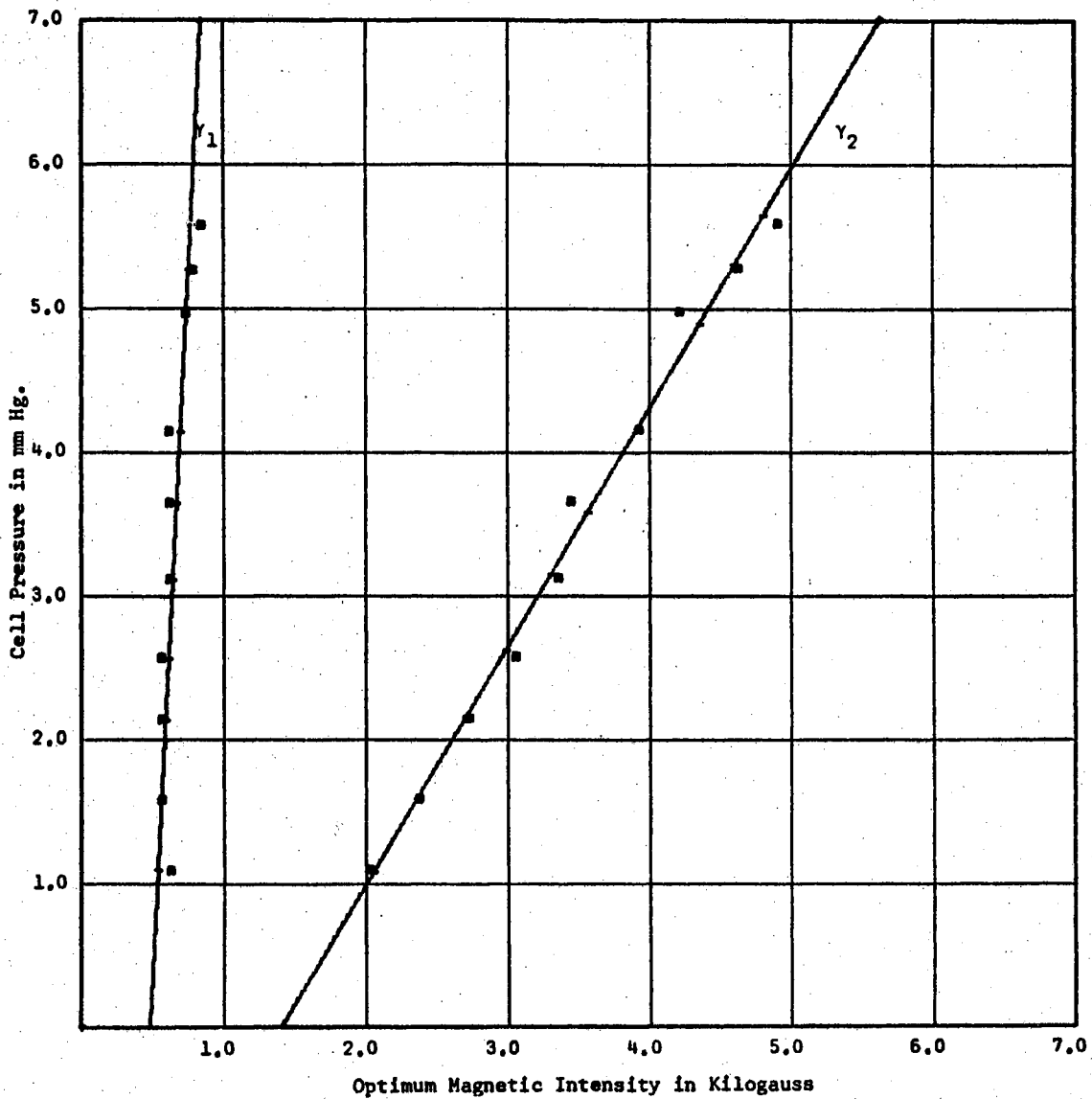MH$_z$ with the Aluminum Cell,
D ≅ 0.002794 meters
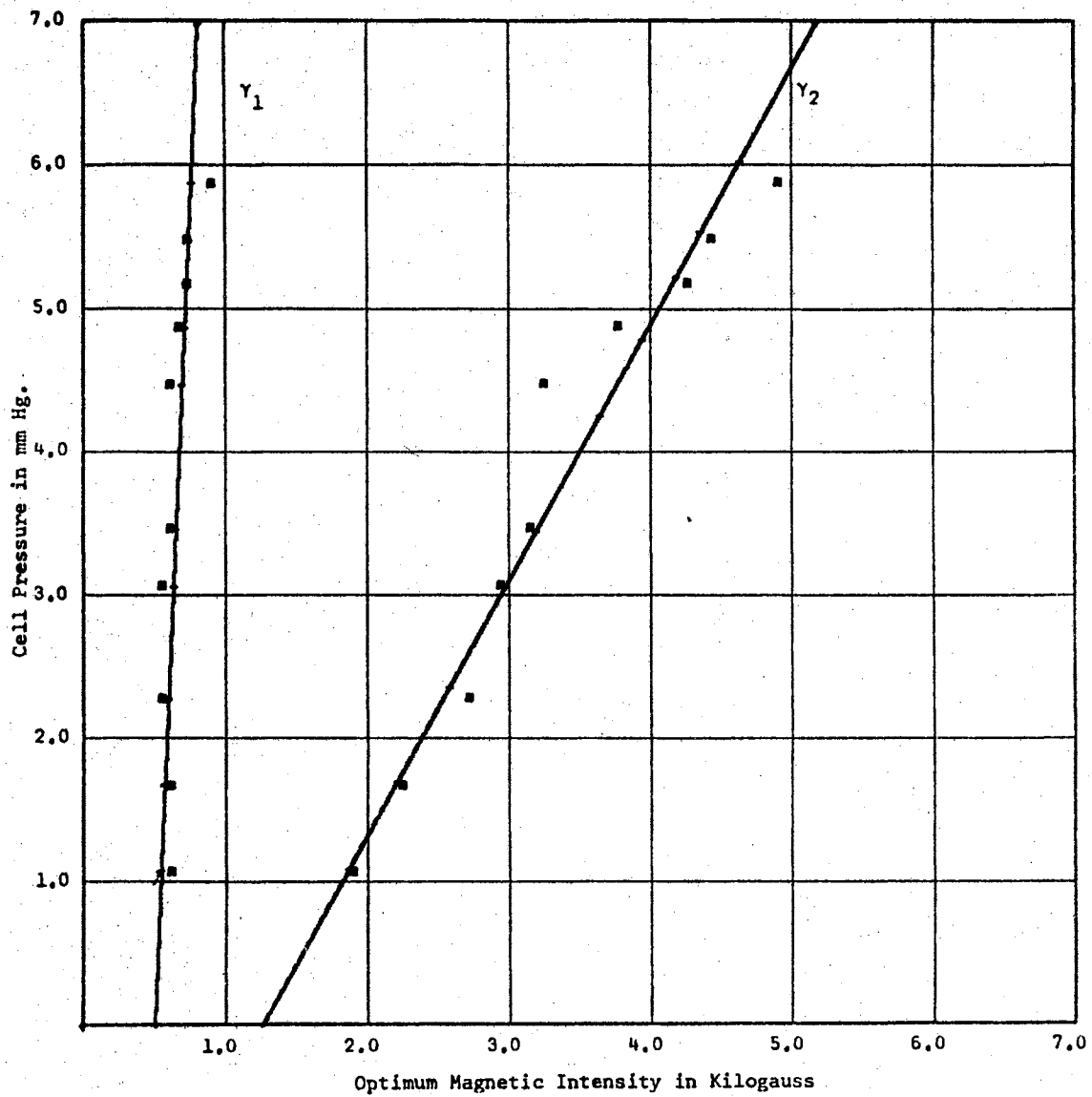
Figure 53a.   Data taken April 13, 1965 at 7 MH$_z$ with the Old
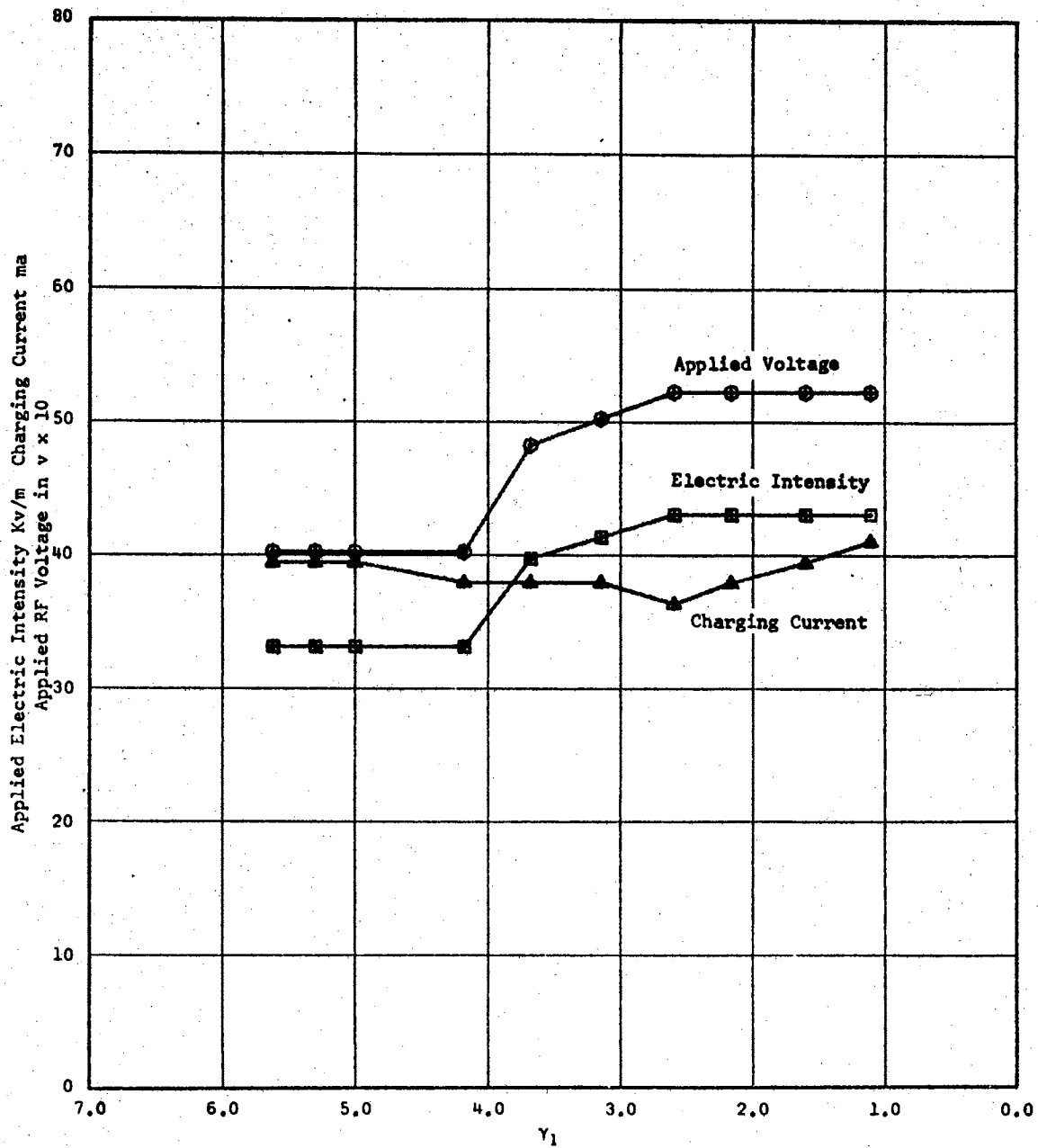Teflon Cell and Old rf Source, $\bar{D}$ = 0.004292 meters
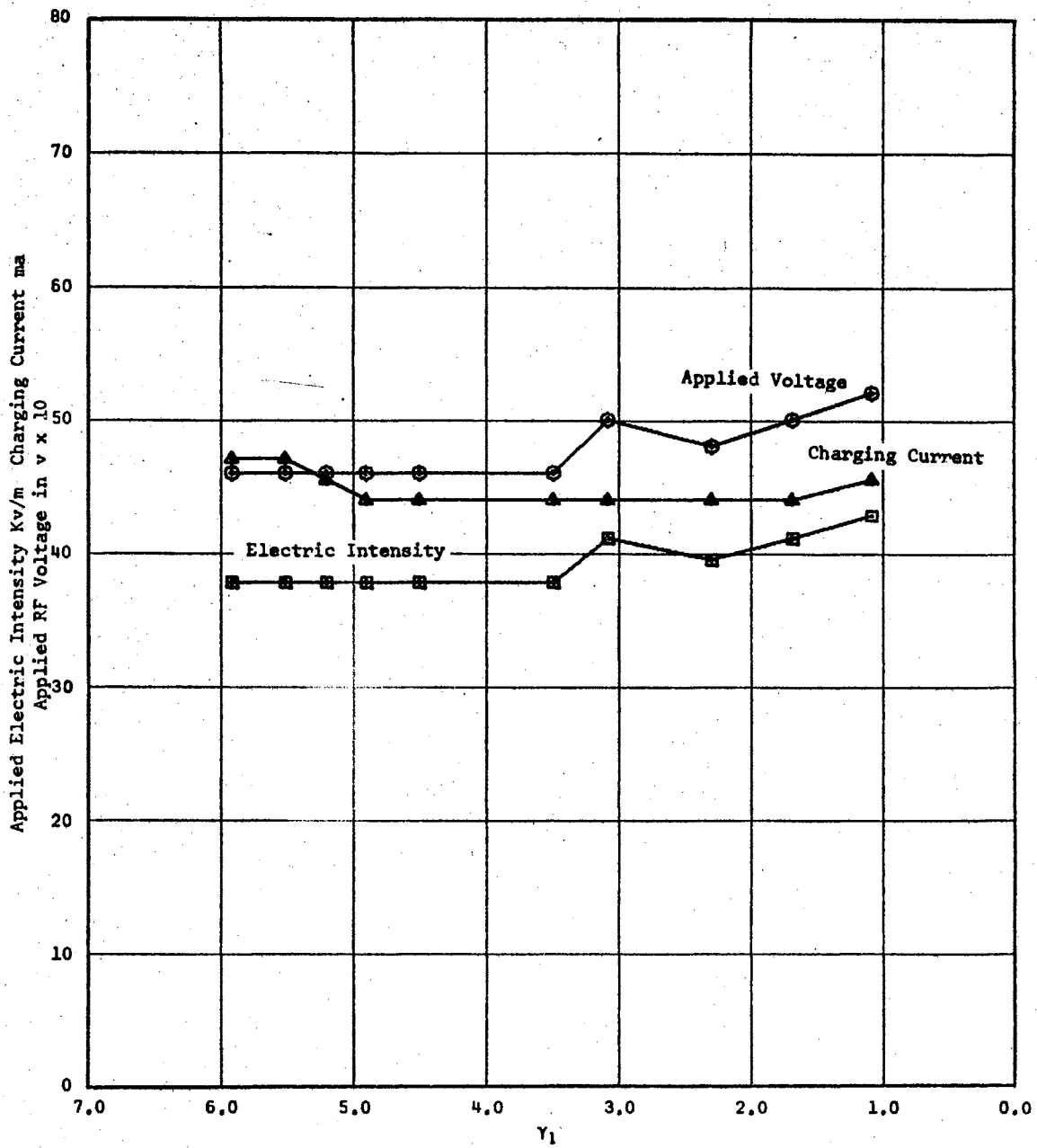
Figure 53b. Data taken April 13, 1965 at 7 MH$_z$ with the Old
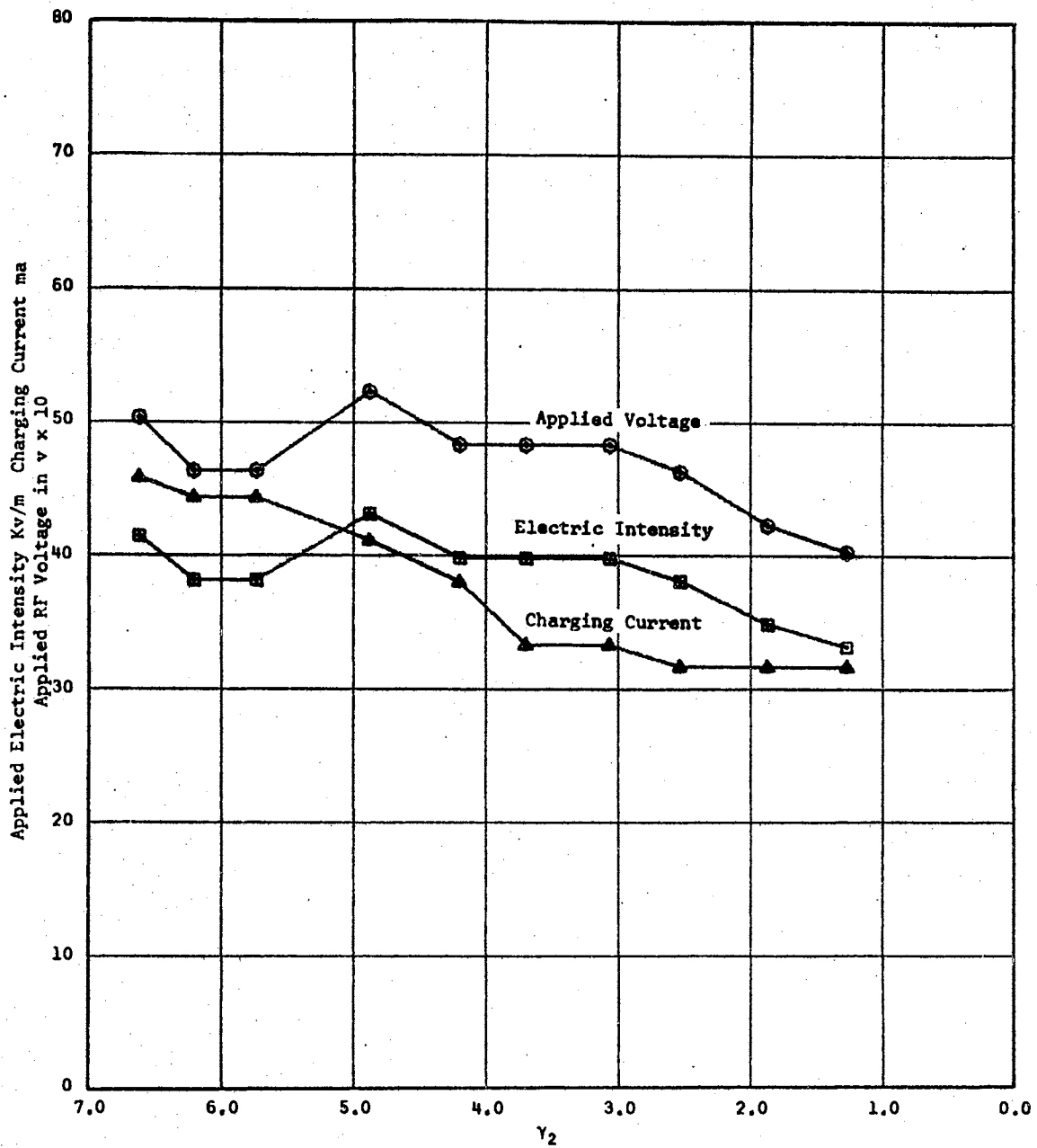Teflon Cell and Old rf Source, D = 0.004292 meters
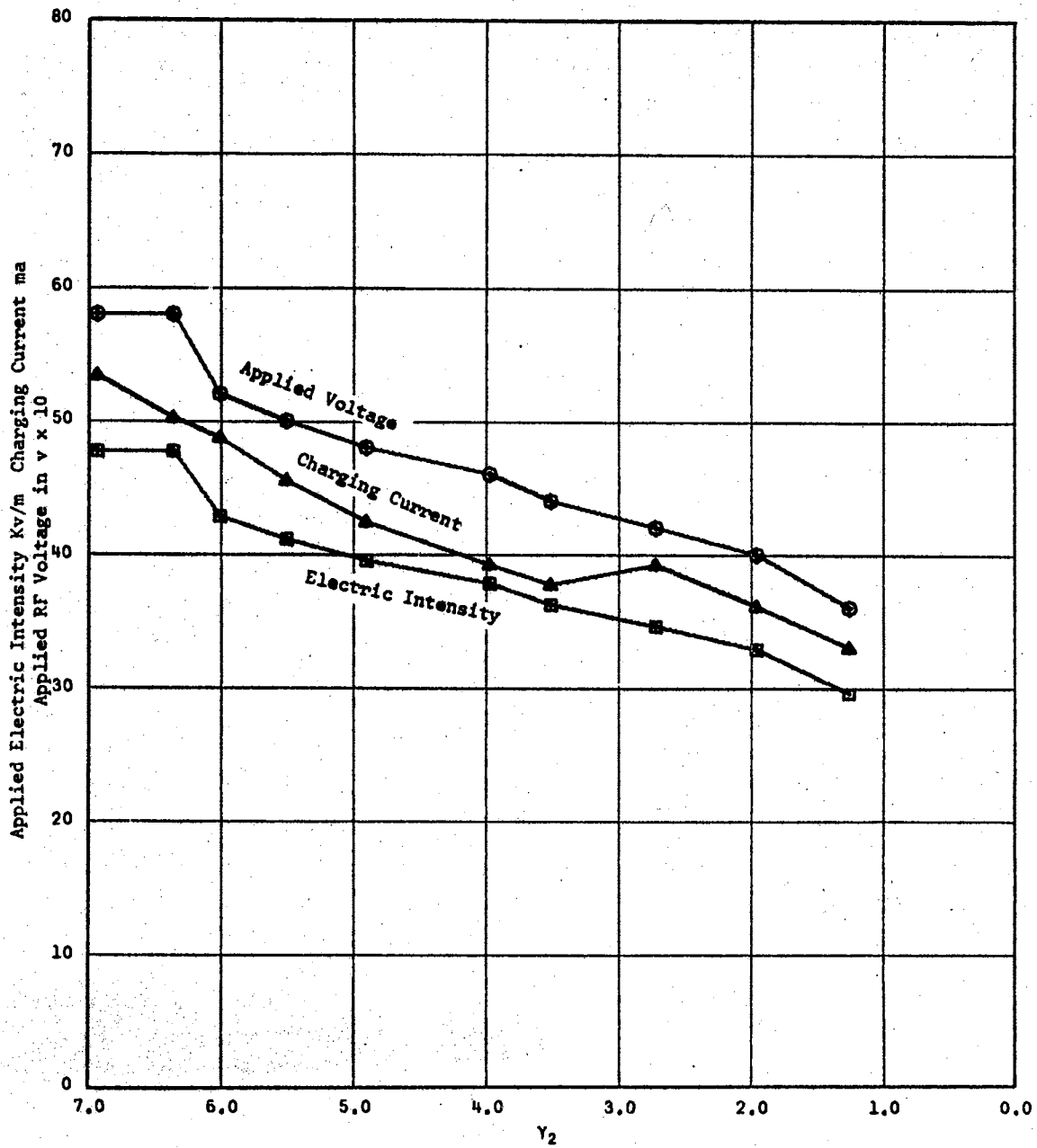
Figure 53c. Data taken April 13, 1965 at 7 MH$_z$ with the Old
Teflon Cell and Old rf Source, D̄ = 0.004292 meters
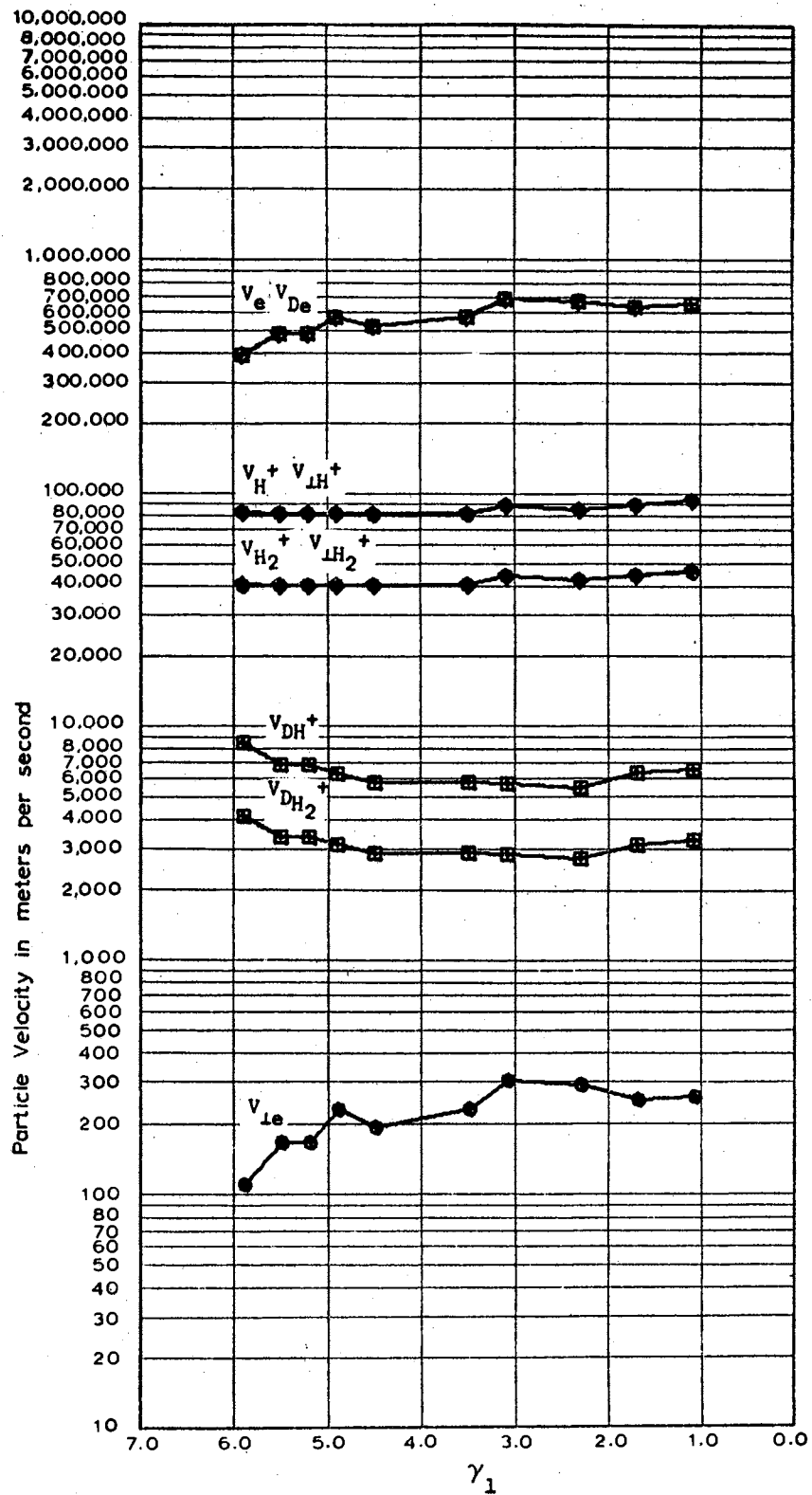
Figure 53d. Data taken April 13, 1965 at 7 MH$_z$ with the Old Teflon Cell and Old rf Source, D = 0.004292 meters

Figure 53e. Data taken April 13, 1965 at 7
MH$_z$ with the Old Teflon Cell
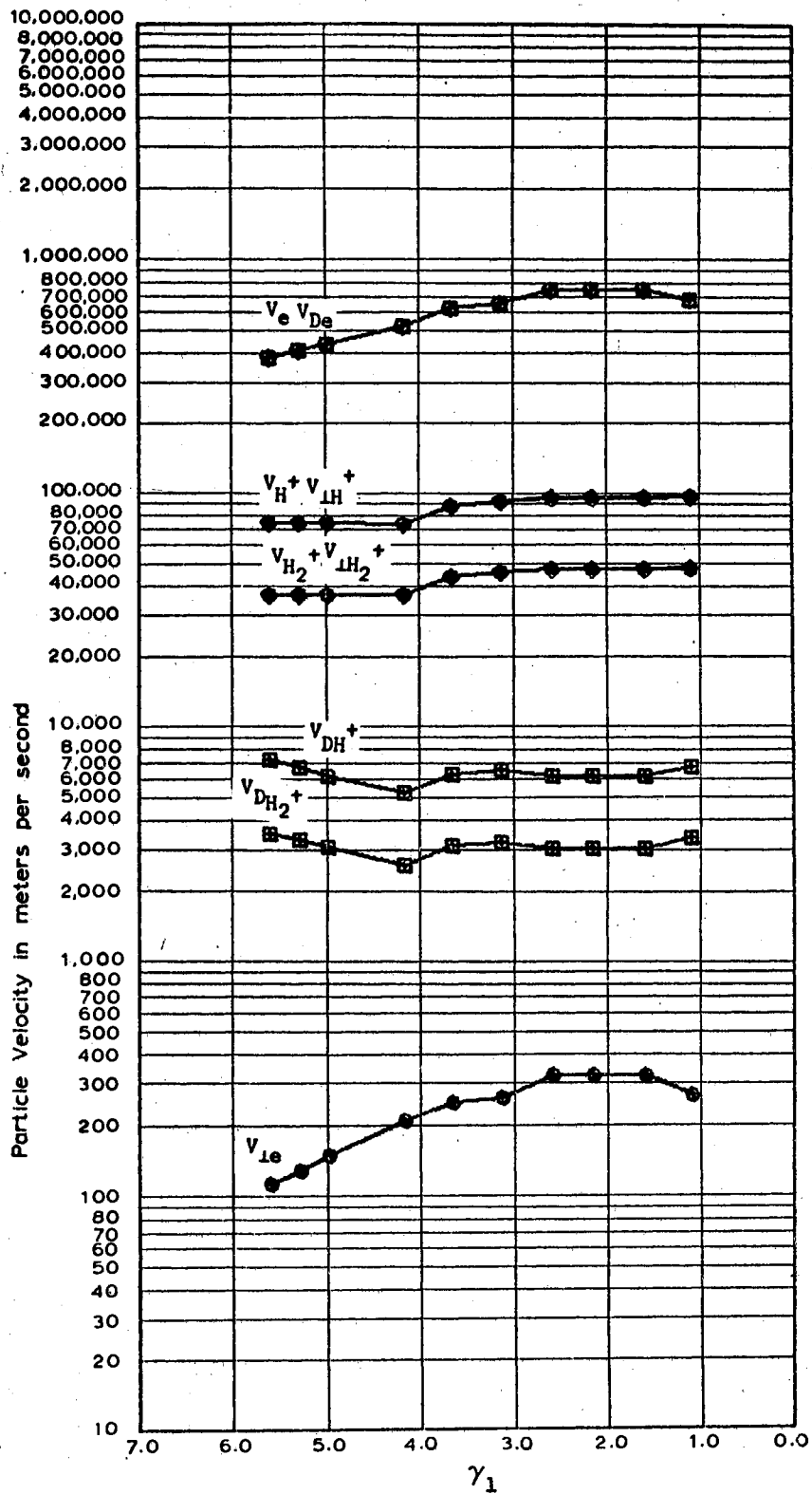and Old rf Source, D =
0.004292 meters

Figure 54a. Data taken April 16, 1965 at 7 MH$_z$ with the Old
Teflon Cell and Old rf Source, D = 0.004292 meters

Figure 54b. Data taken April 16, 1965 at 7 MH with the Old
Teflon Cell and Old rf Source, δ = 0.004292 meters

Figure 54c. Data taken April 16, 1965 at 7 MH with the Old
Teflon Cell and Old rf Source, $\vec{D}$ = 0.004292 meters

Figure 54d. Data taken April 16, 1965 at 7 MH$_z$ with the Old Teflon Cell and Old rf Source, D = 0.004292 meters
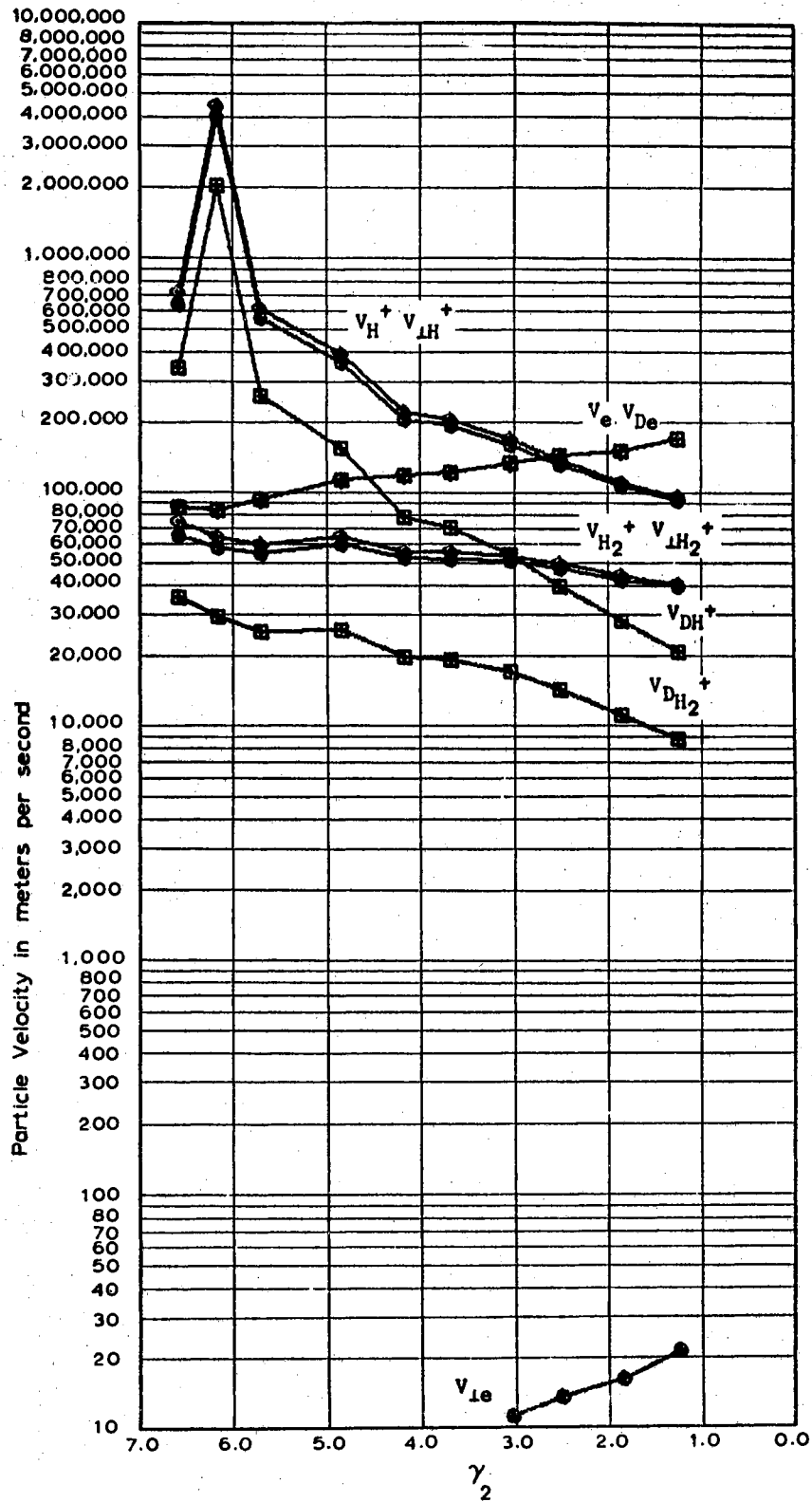
Figure 54e. Data taken April 16, 1965 at 7
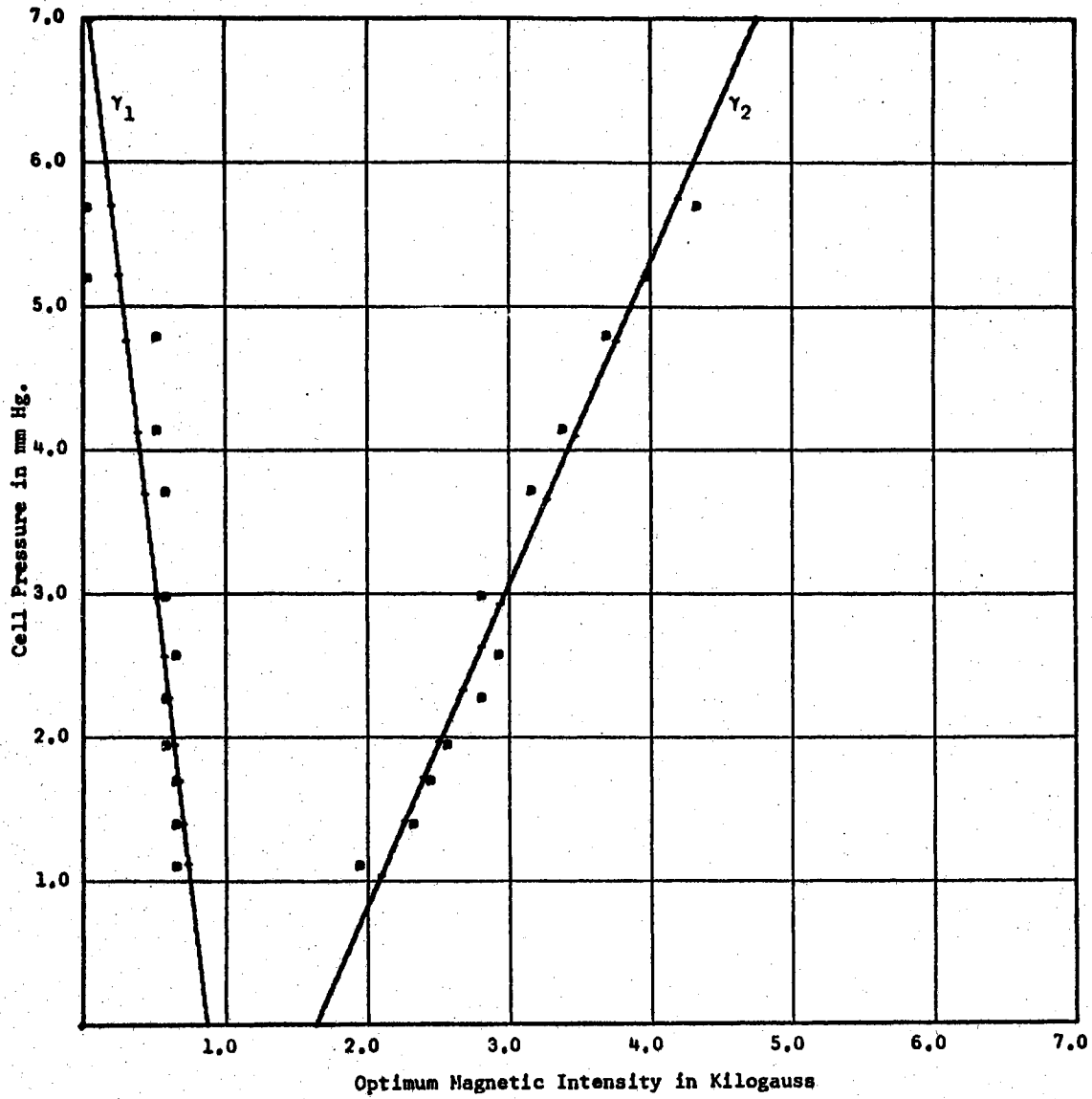MH$_z$ with the Old Teflon Cell
and Old rf Source, D =
0.004292 meters

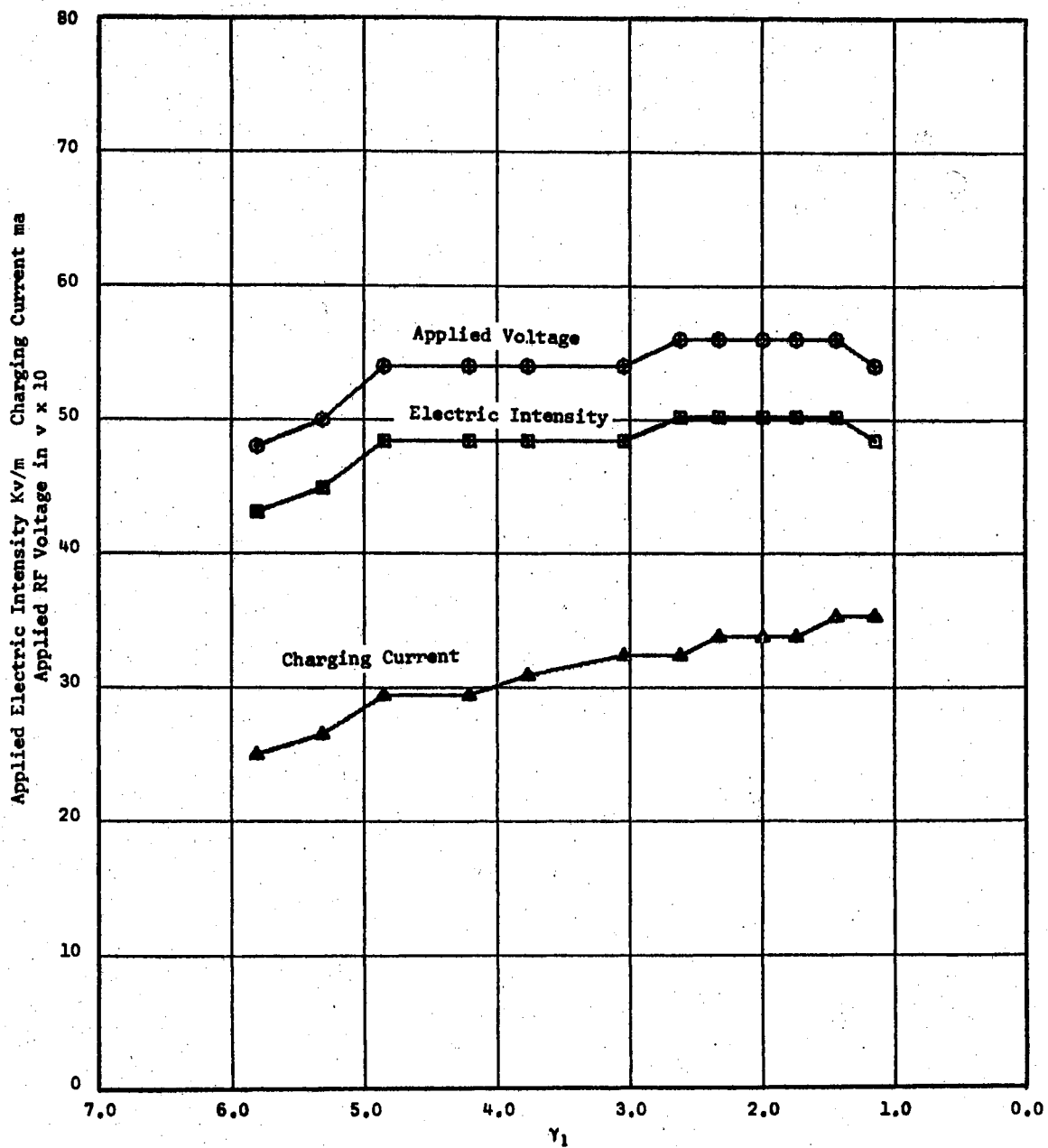Figure 55a. Data taken September 1, 1965 at 7 MH$_z$ with the Aluminum Cell and Old rf Source, D^z= 0.003937 meters

Figure 55b. Data taken September 1, 1965 at 7 MH$_z$ with the Aluminum Cell and Old rf Source, D^z = 0.003937 meters
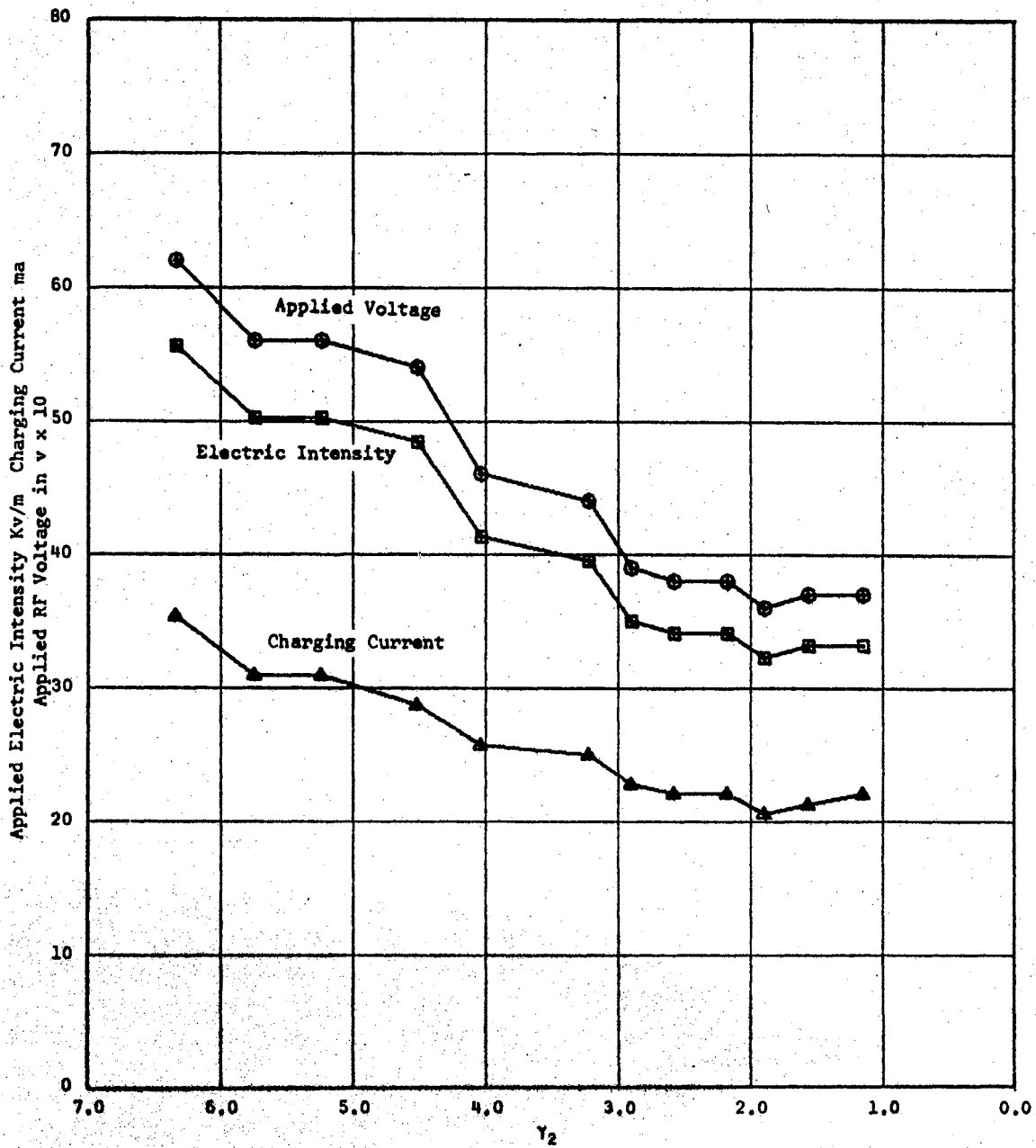
Figure 55c. Data taken September 1, 1965 at 7 MH$_z$ with the Aluminum Cell and Old rf Source, D^z= 0.003937 meters
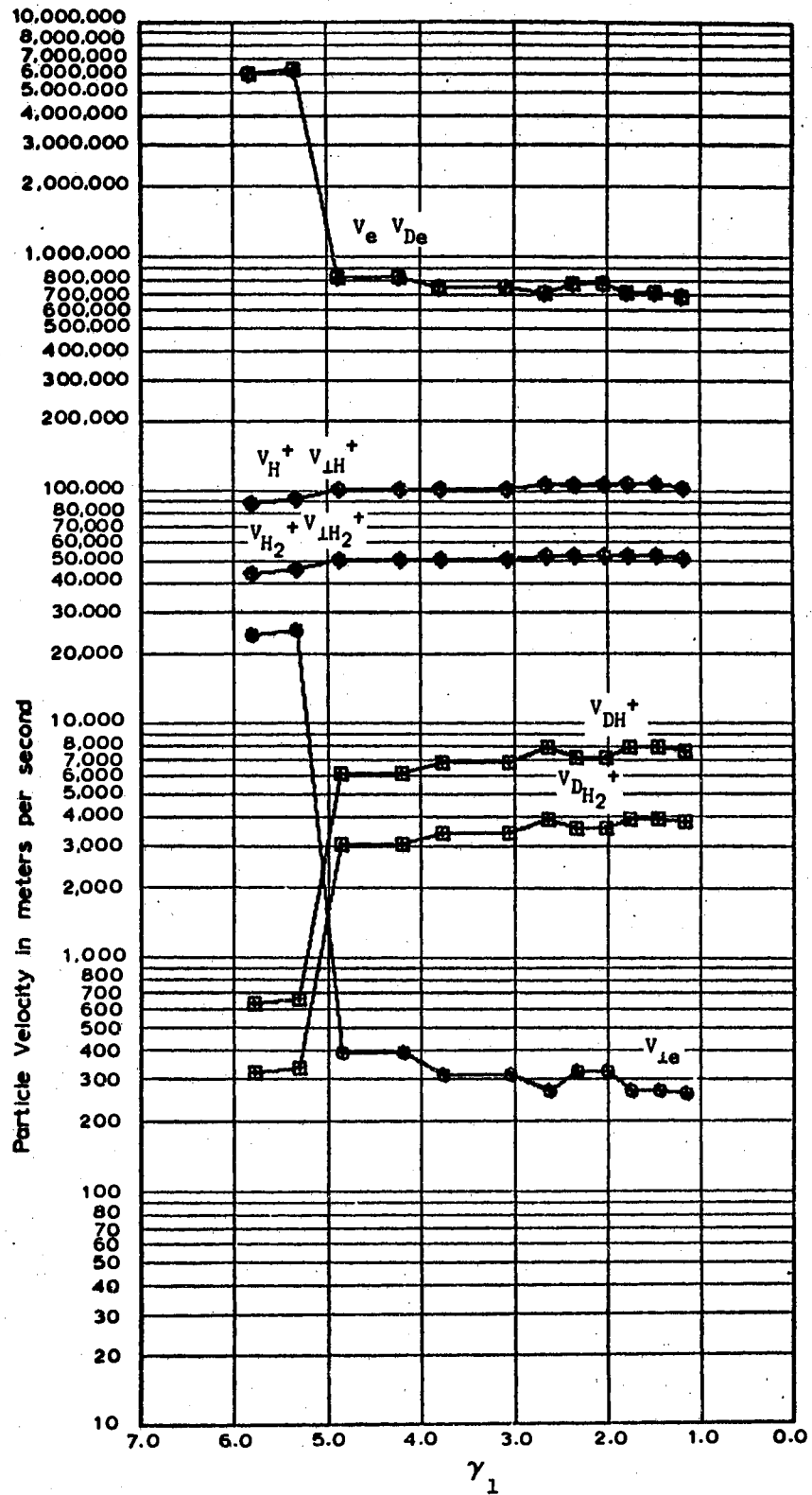
Figure 55d. Data taken September 1, 1965 at
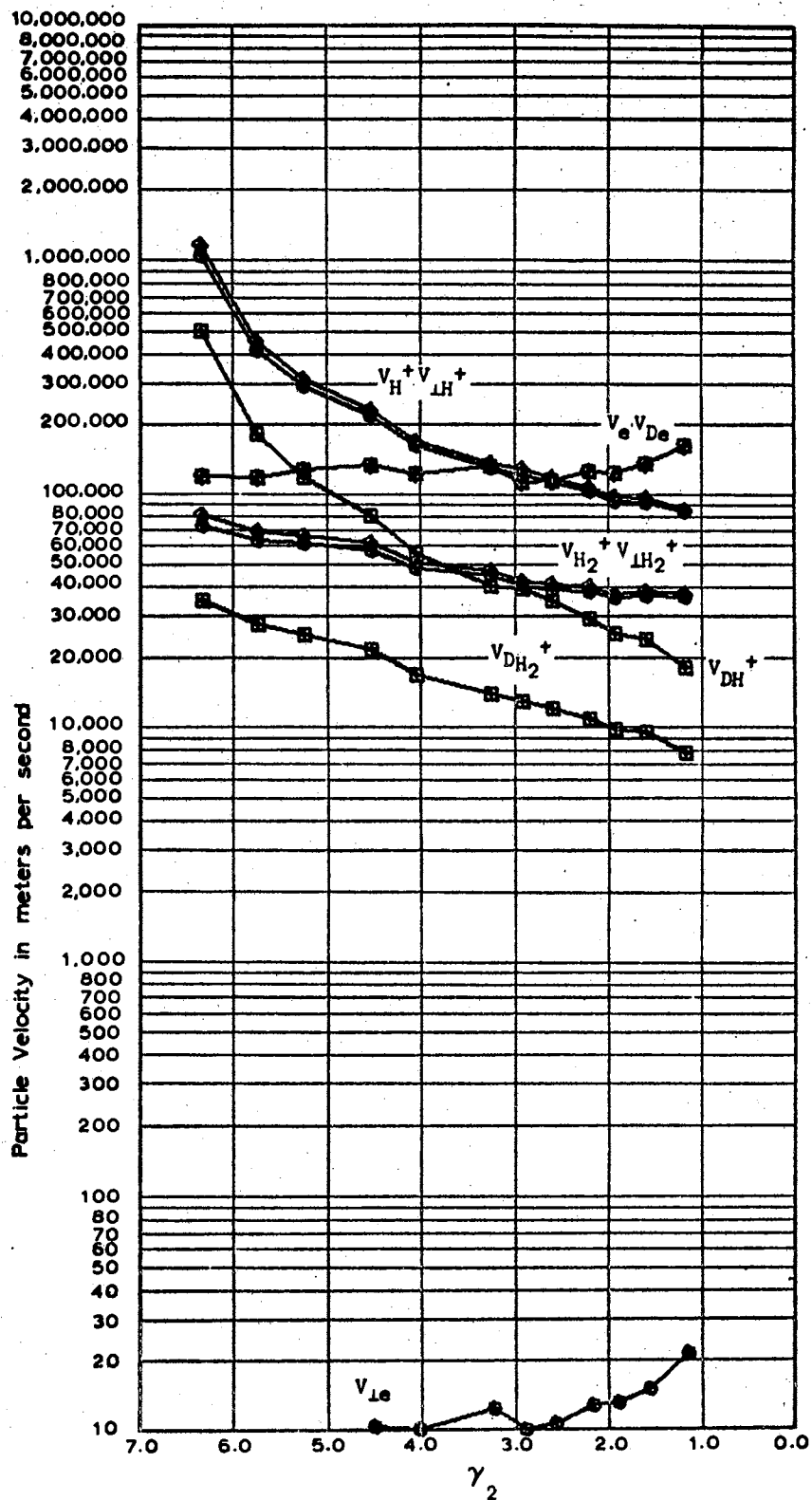7 MH$_z$ with the Aluminum Cell
and Old rf Source, D = 0.003937
meters

Figure 55e. Data taken September 1, 1965 at
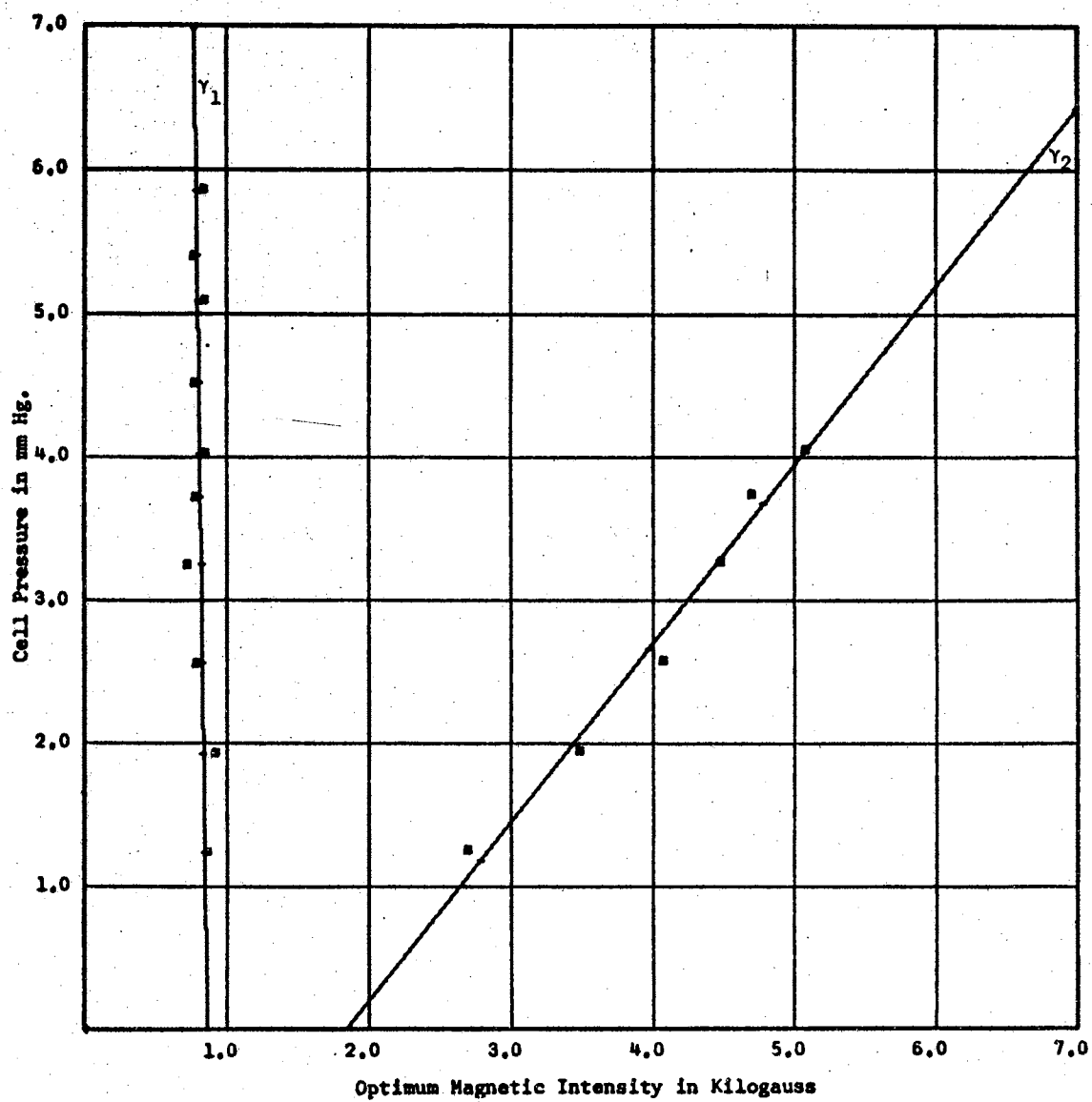7 MH$_3$ with the Aluminum Cell
and Old rf Source, D =
0.003937 meters

Figure 56a. Data taken March 2, 1966 at 7 MH_z with the Aluminum
Cell, D = 0.007902 meters

Figure 56b. Data taken March 2, 1966 at 7 MH_z with the Aluminum
Cell, D = 0.007902 meters

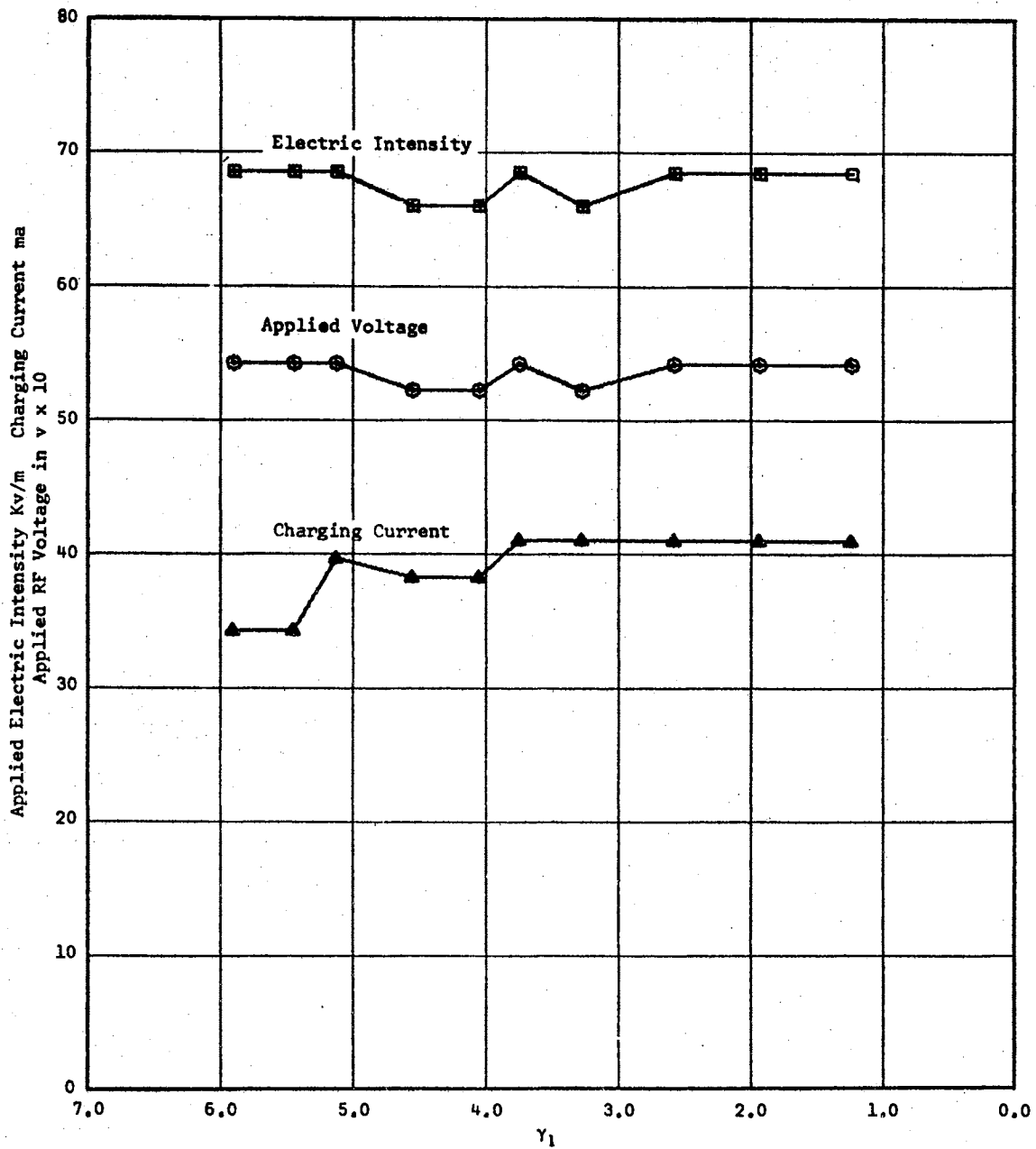Figure 56c.   Data taken March 2, 1966 at 7 MH$_z$ with the Aluminum
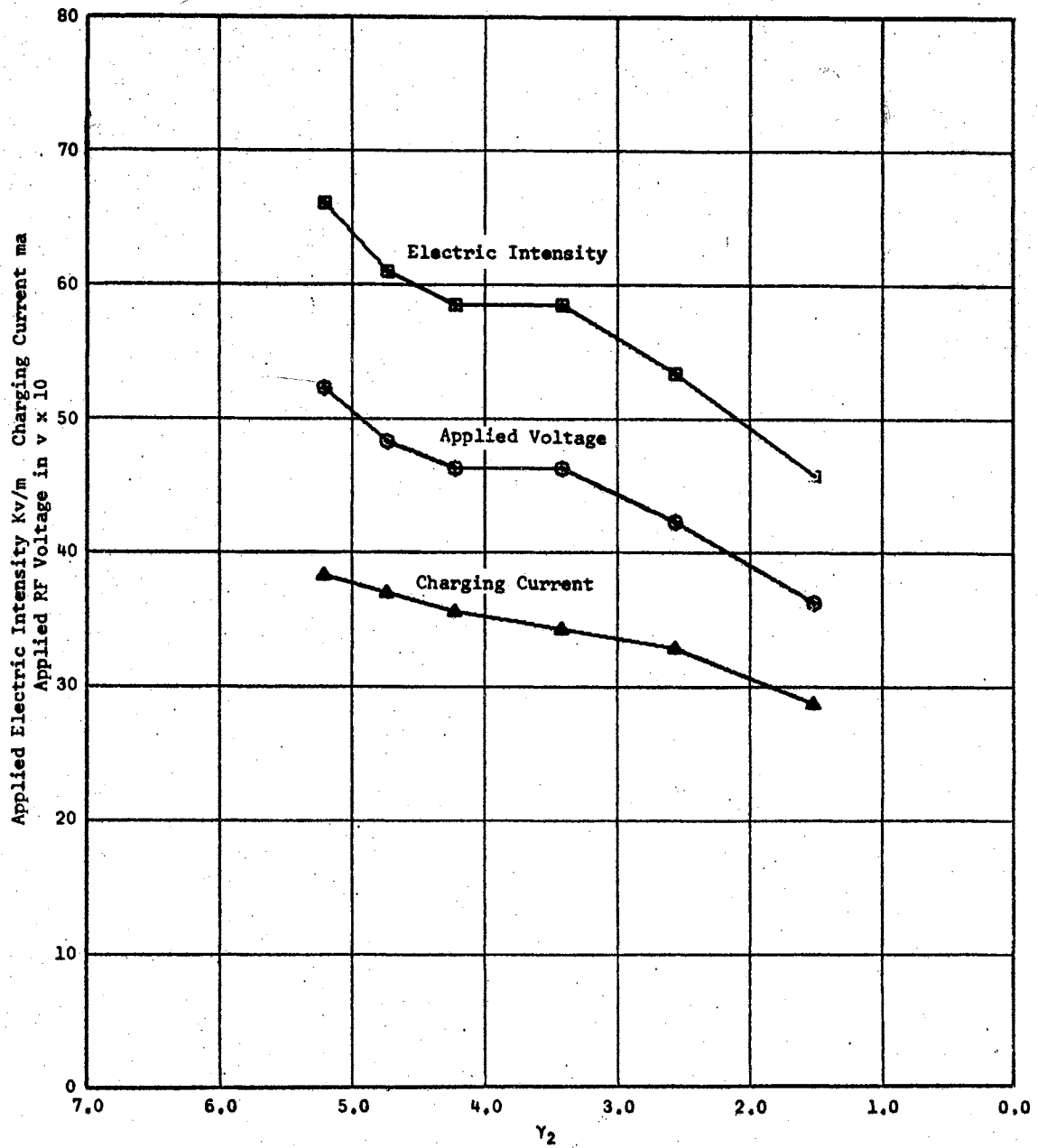Cell, D = 0.007902 meters

Figure 56d. Data taken March 2, 1966 at 7
MH$_z$ with the Aluminum Cell,
D = 0.007902 meters

Figure 56e. Data taken March 2, 1966 at 7
MH with the Aluminum Cell,
D ≅ 0.007902 meters

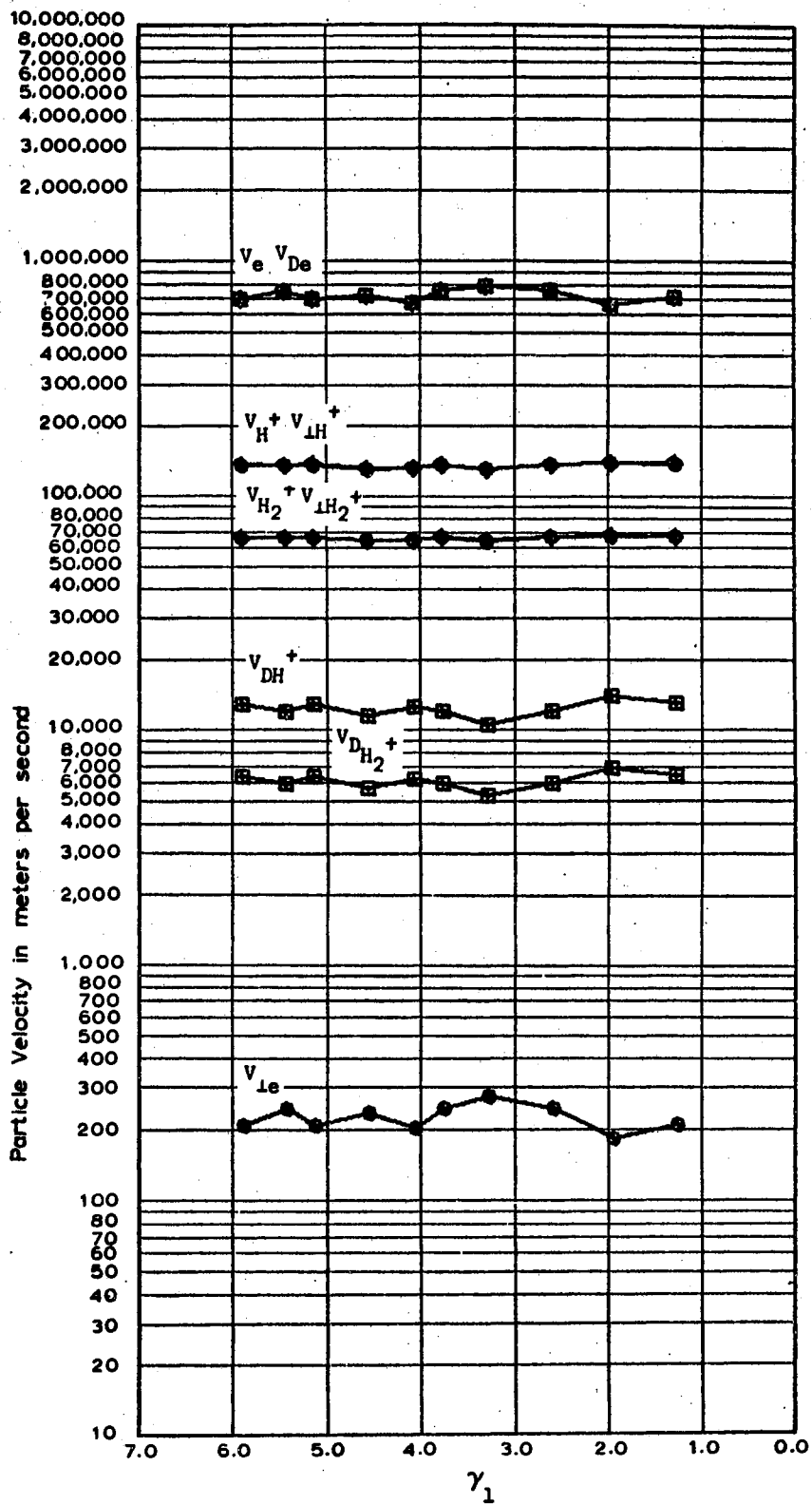Figure 57a. Data taken March 2 and 4, 1966 with the Teflon Cell,
D = 0.005879 meters
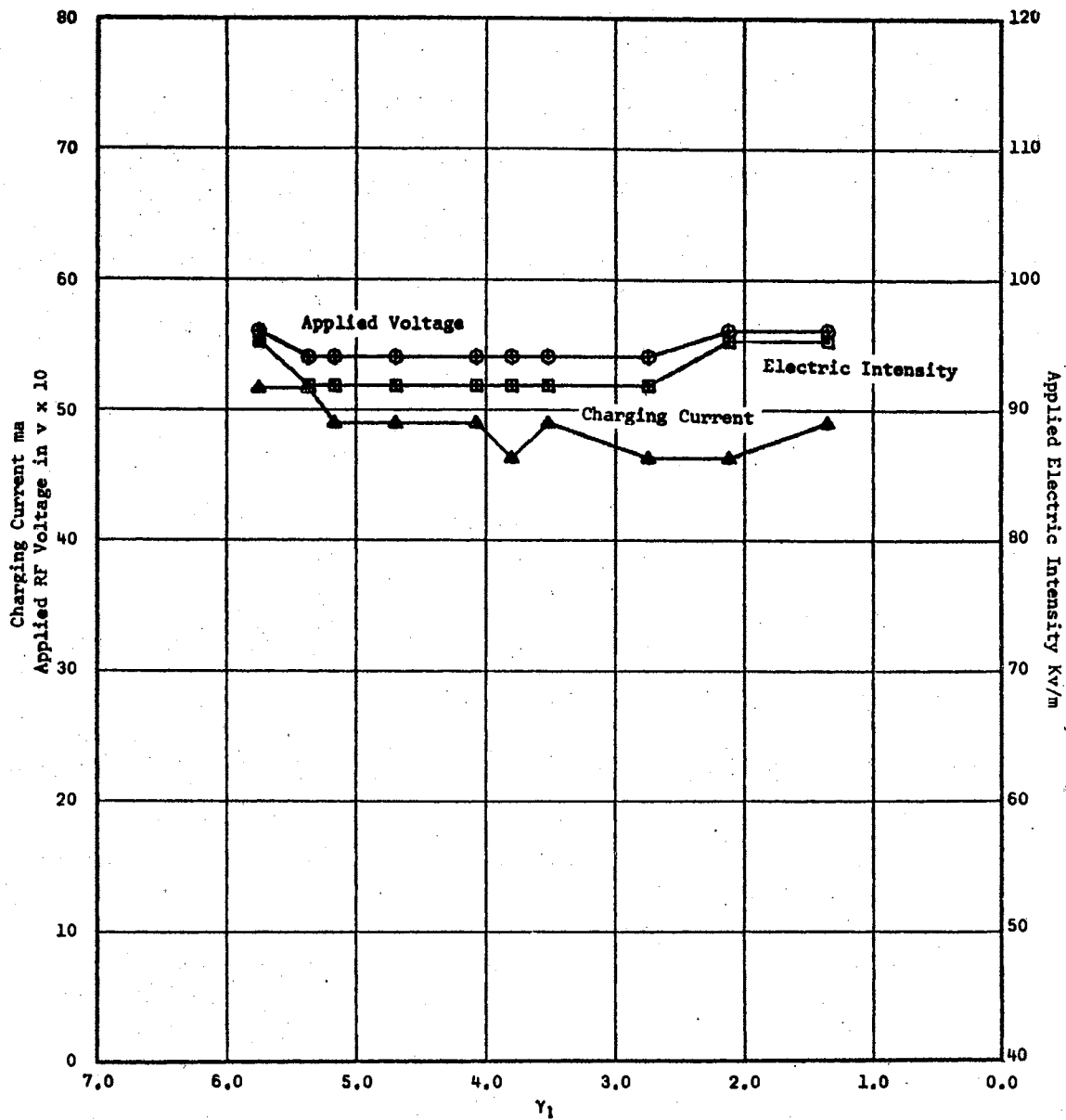
Figure 57b.   Data taken March 2 and 4, 1966 with the Teflon
Cell, D = 0.005879 meters
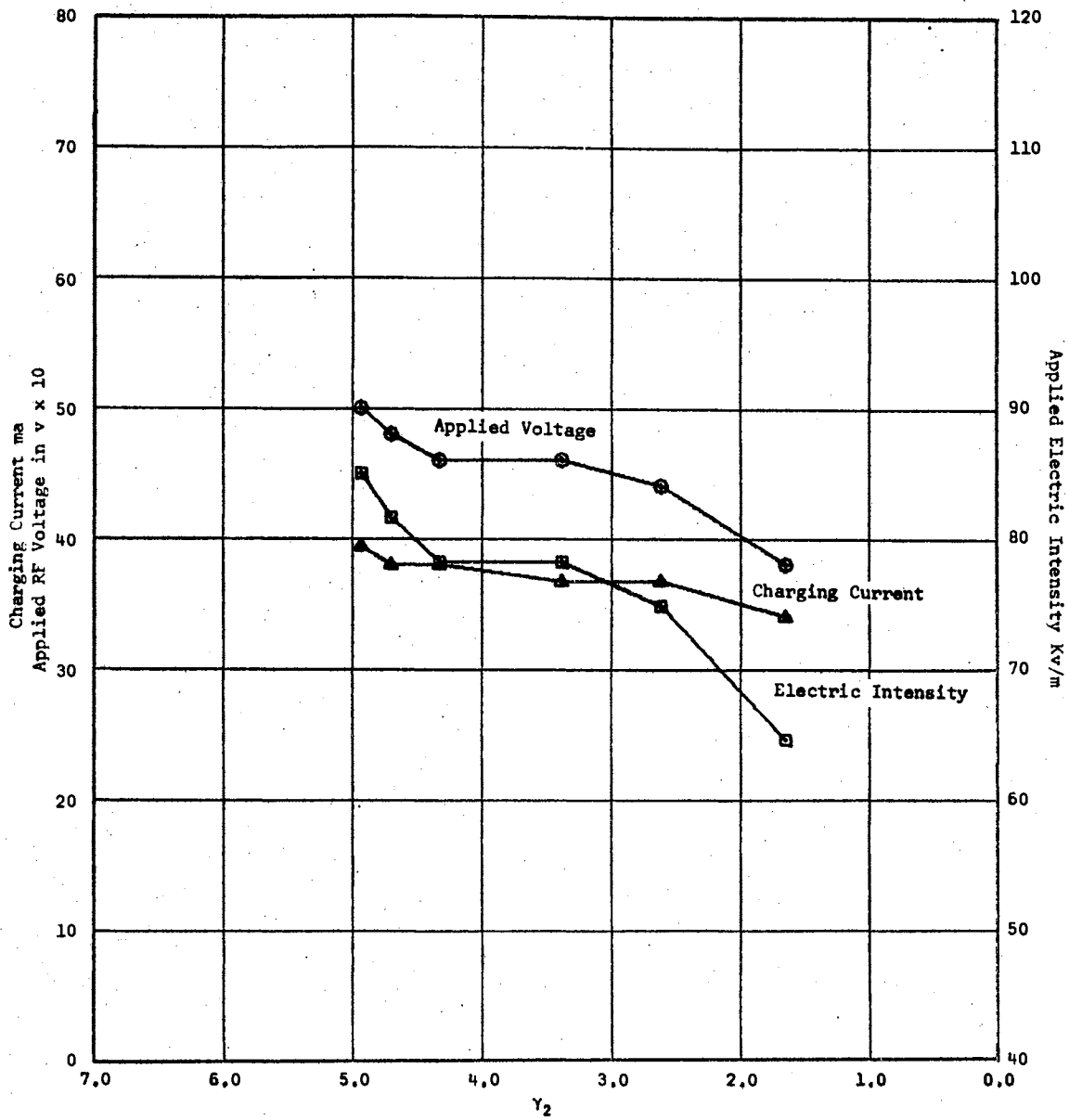
Figure 57c.   Data taken March 2 and 4, 1966 with the Teflon
Cell, D = 0.005879 meters
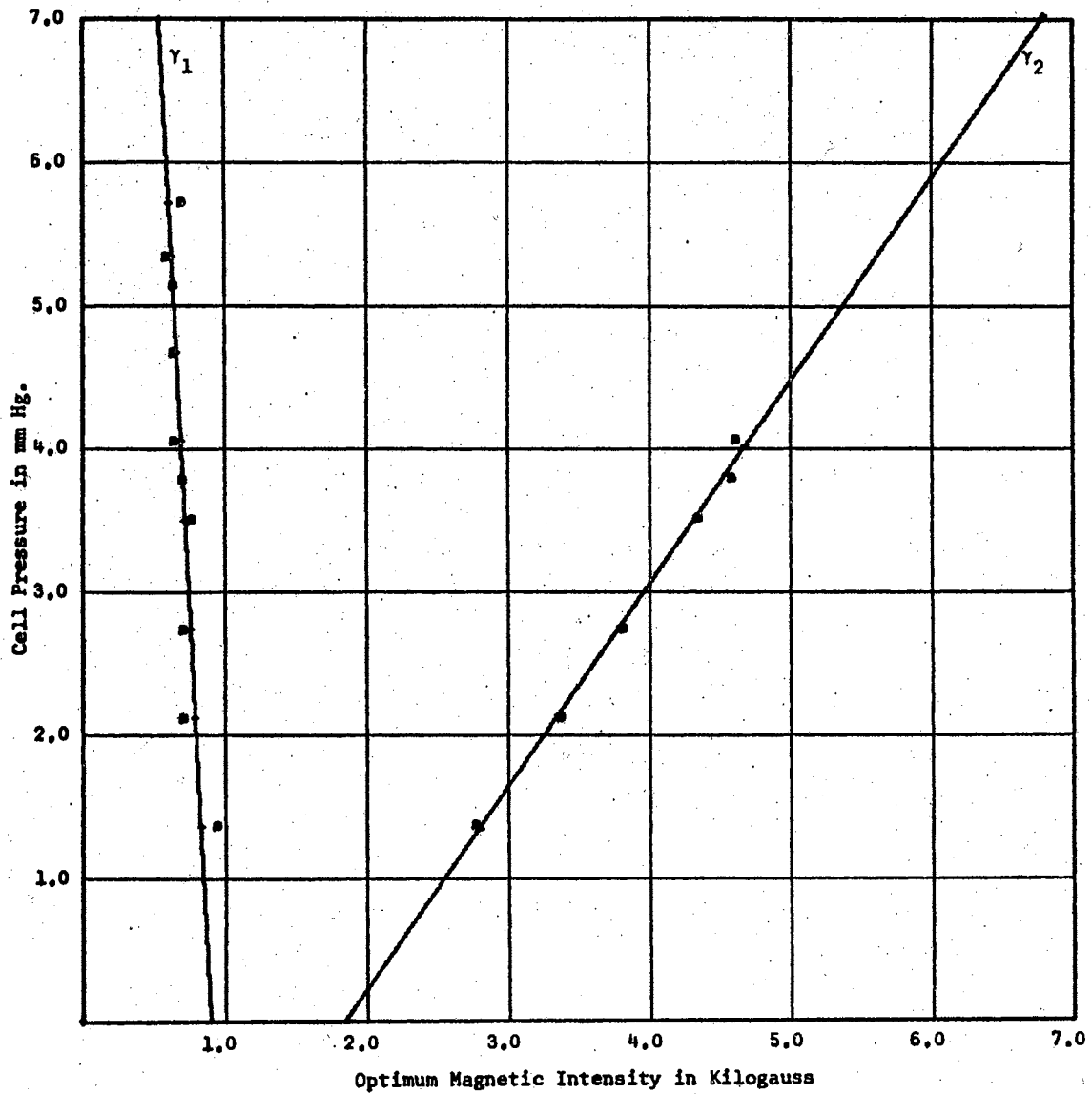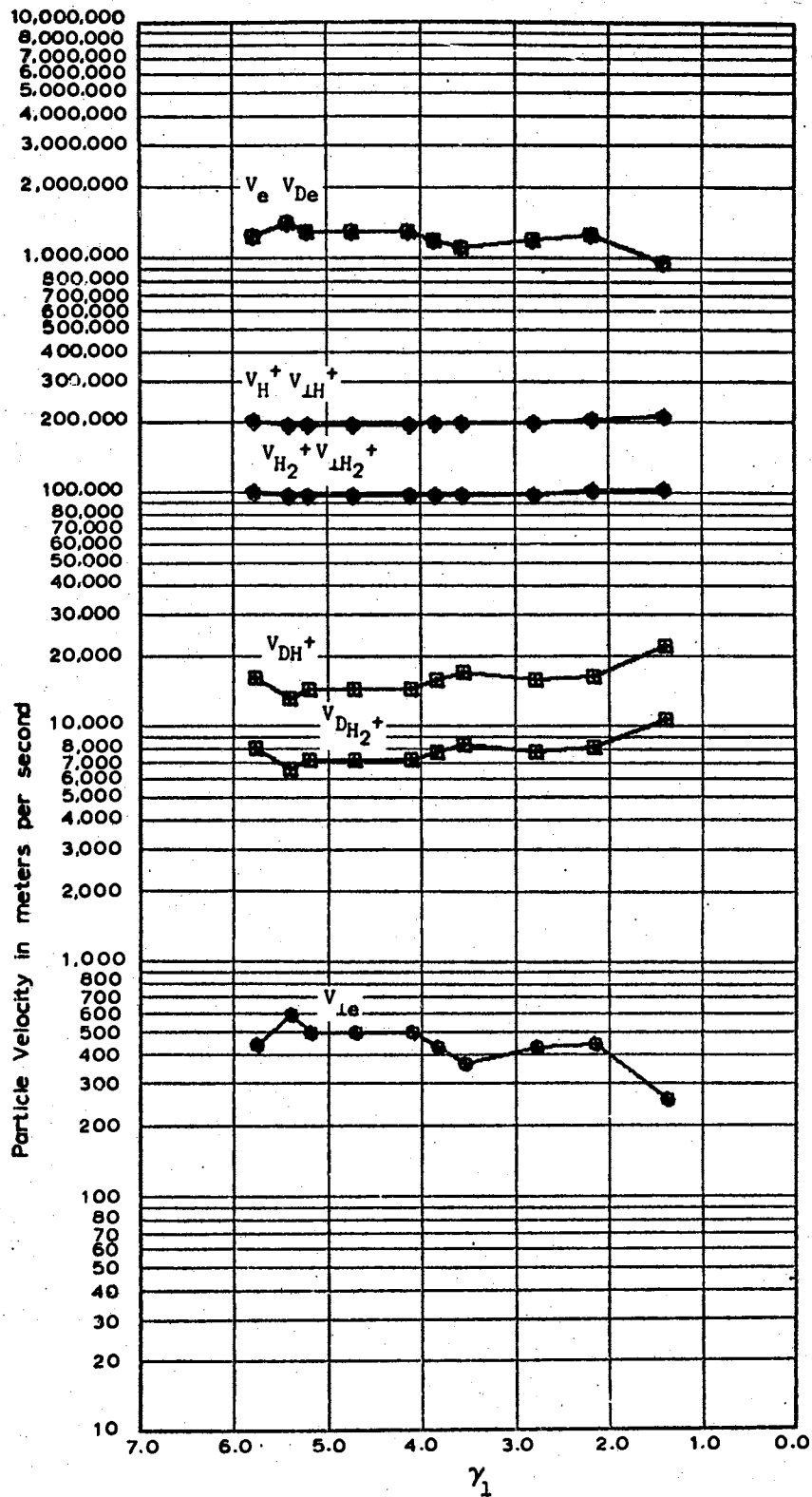
Figure 57d.   Data taken March 2 and 4, 1966
with the Teflon Cell, D =
0.005879 meters
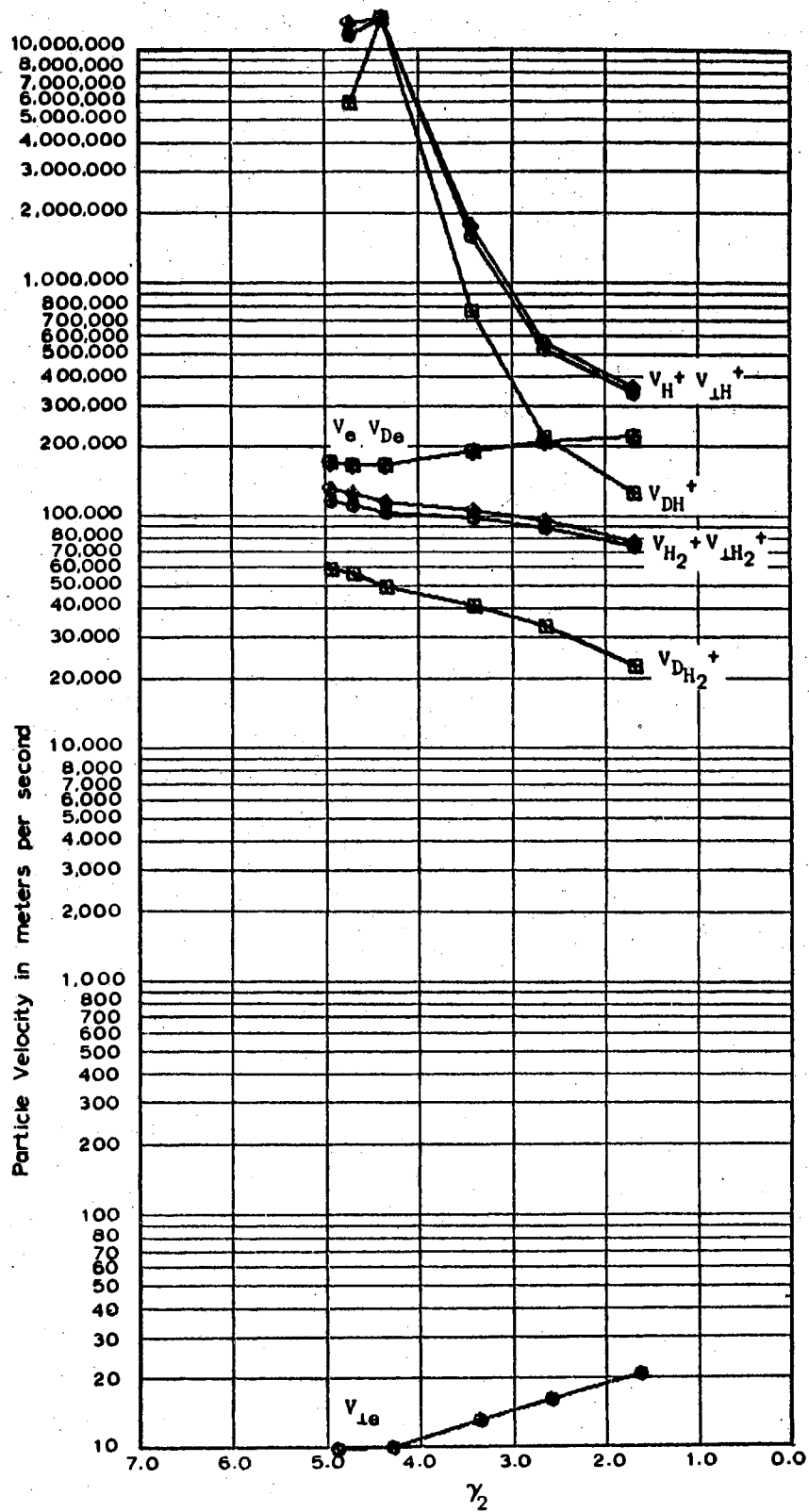
Figure 57e. Data taken March 2 and 4, 1966
with the Teflon Cell, D =
0.005879 meters
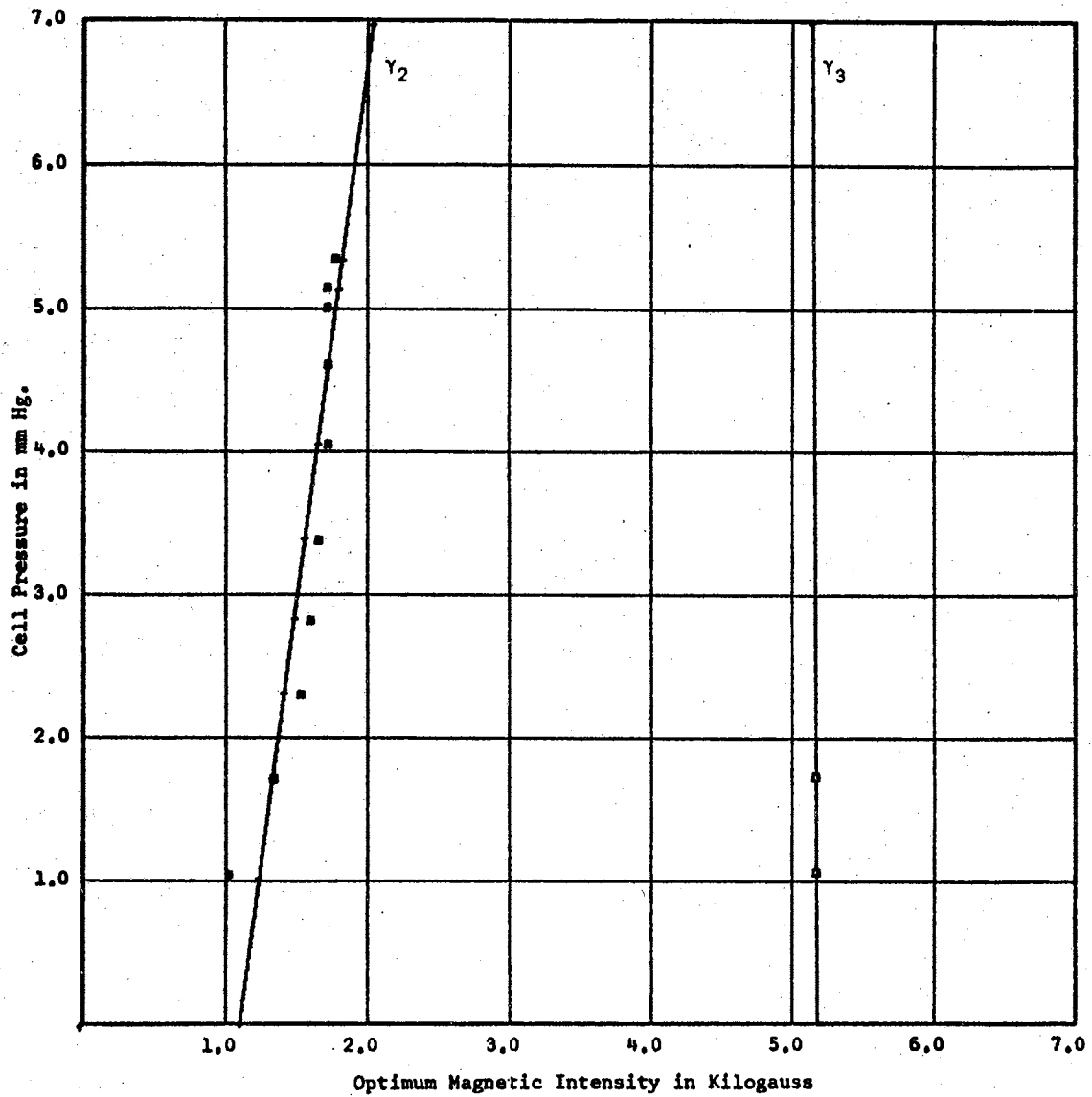
Figure 58a.   Data taken September 2, 1966 at 7 MH_z with the
Aluminum Cell No. 2, D = 0.005931 meters
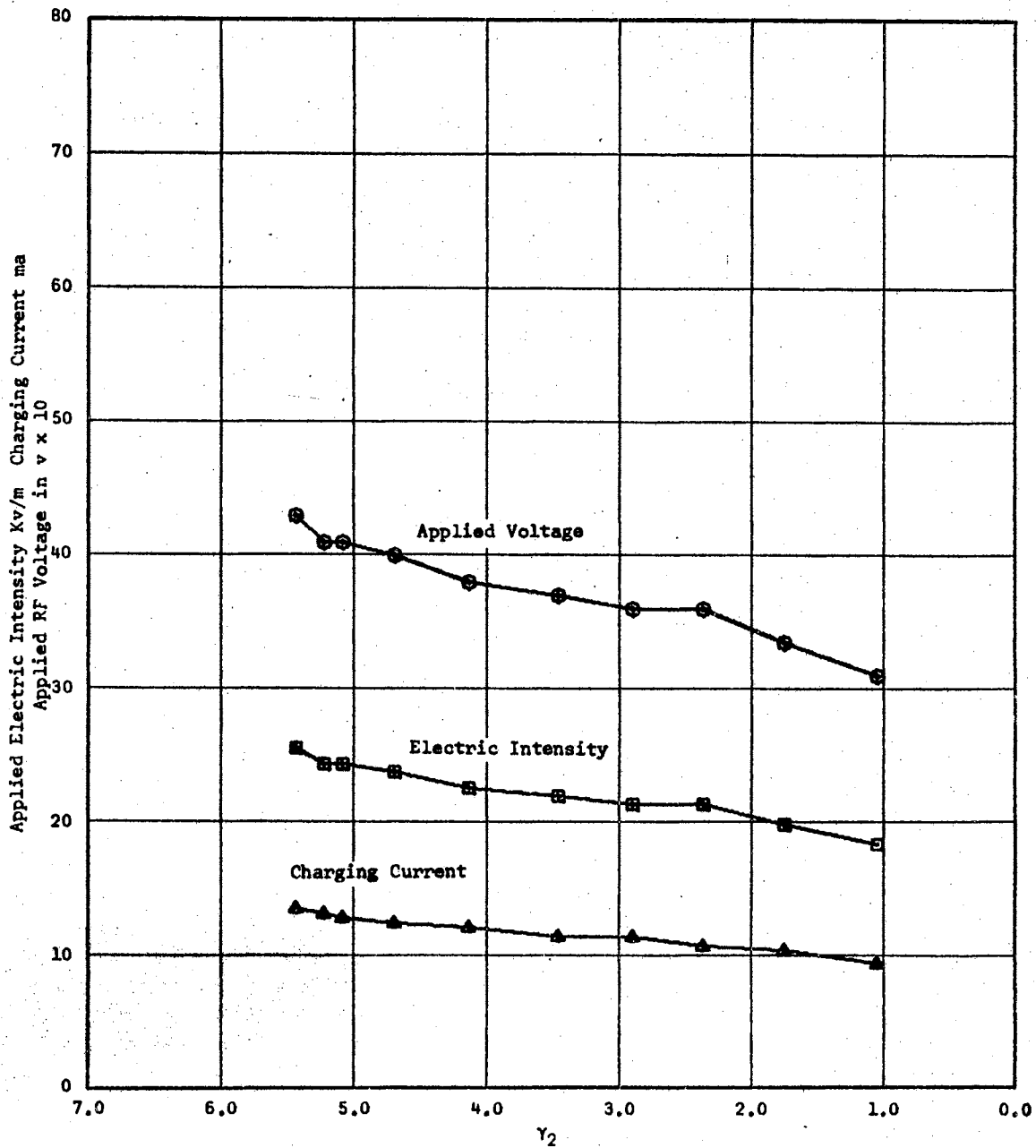
Figure 58b. Data taken September 2, 1966 at 7 MH$_z$ with Aluminum
Cell No. 2, D = 0.005931 meters
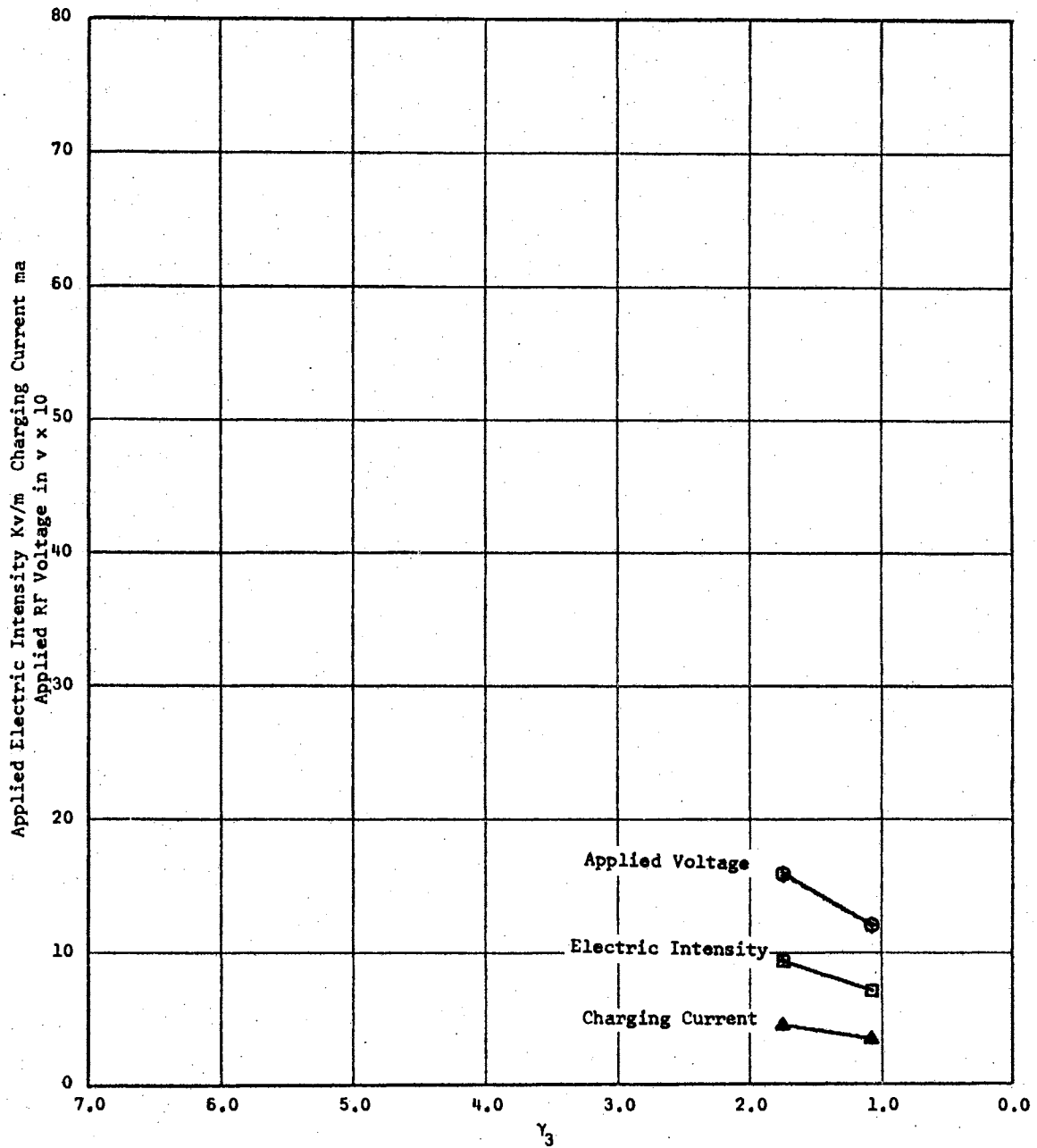
Figure 58c. Data taken September 2, 1966 at 7 MH$_z$ with Aluminum
Cell No. 2, D = 0.005931 meters
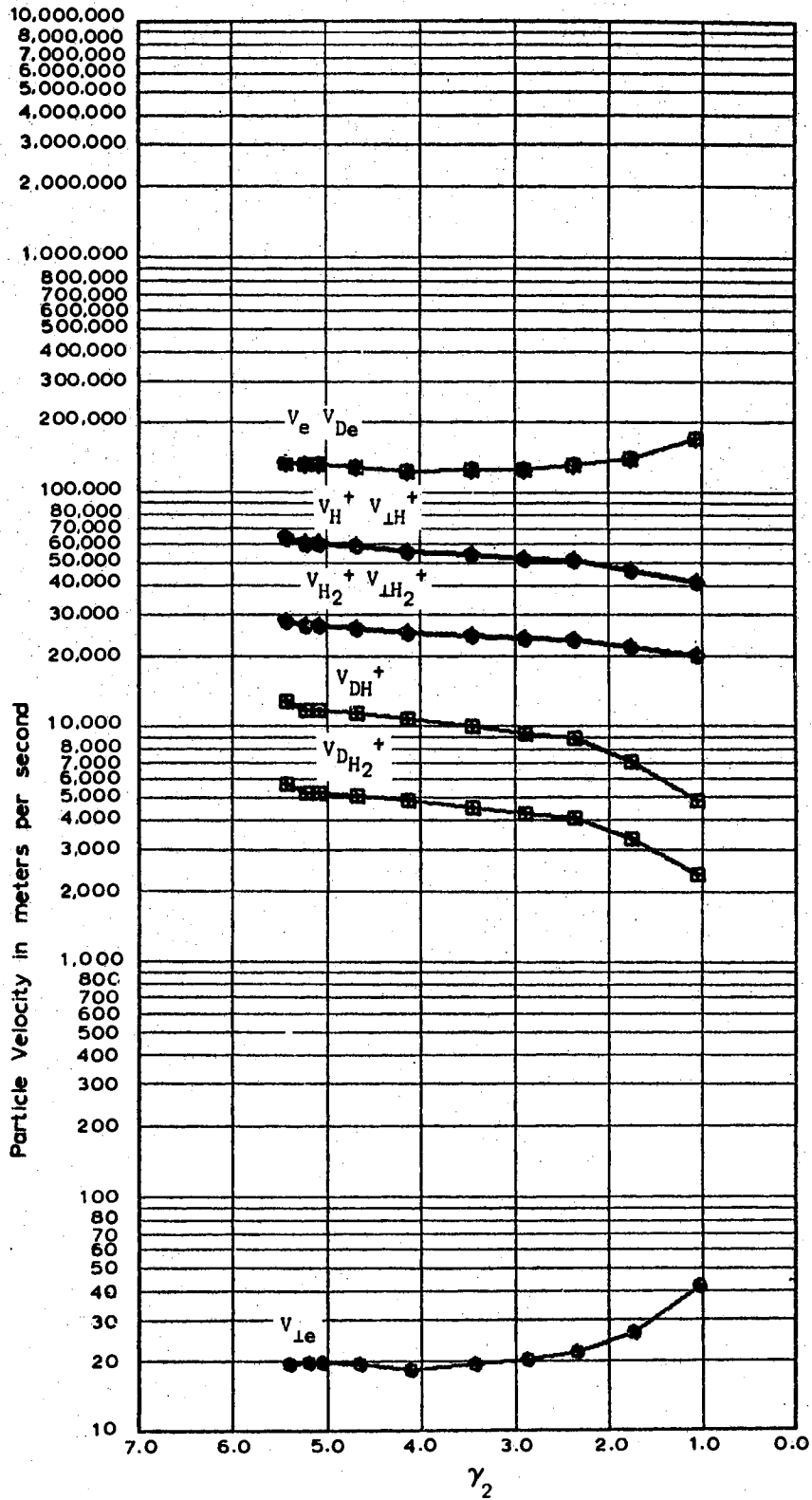
Figure 58d. Data taken September 2, 1966 at
7 MH$_z$ with Aluminum Cell No.
2, D^z= 0.005931 meters
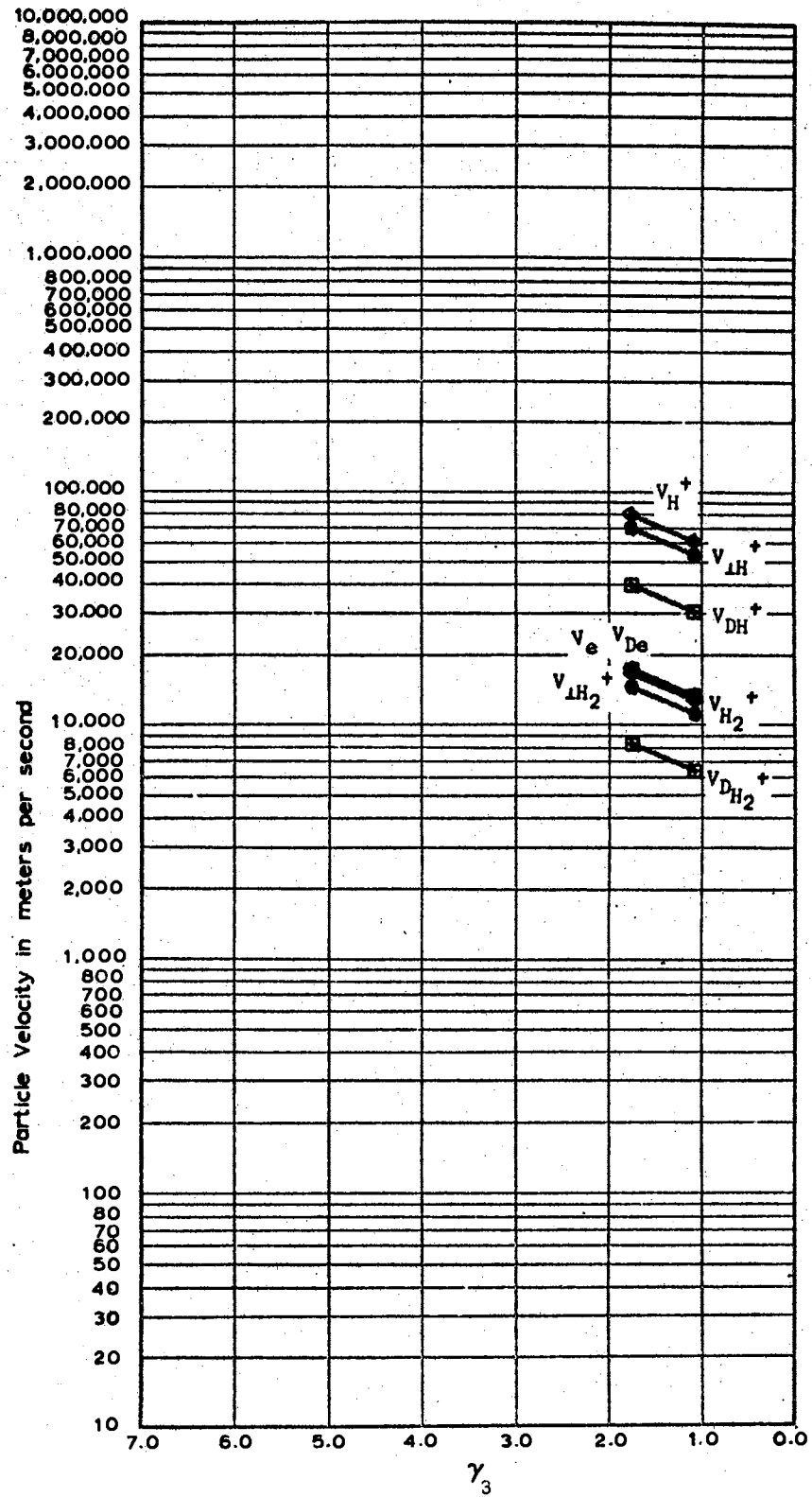
Figure 58e.   Data taken September 2, 1966 at
7 MH with Aluminum Cell No.
2, D^Z = 0.005931 meters
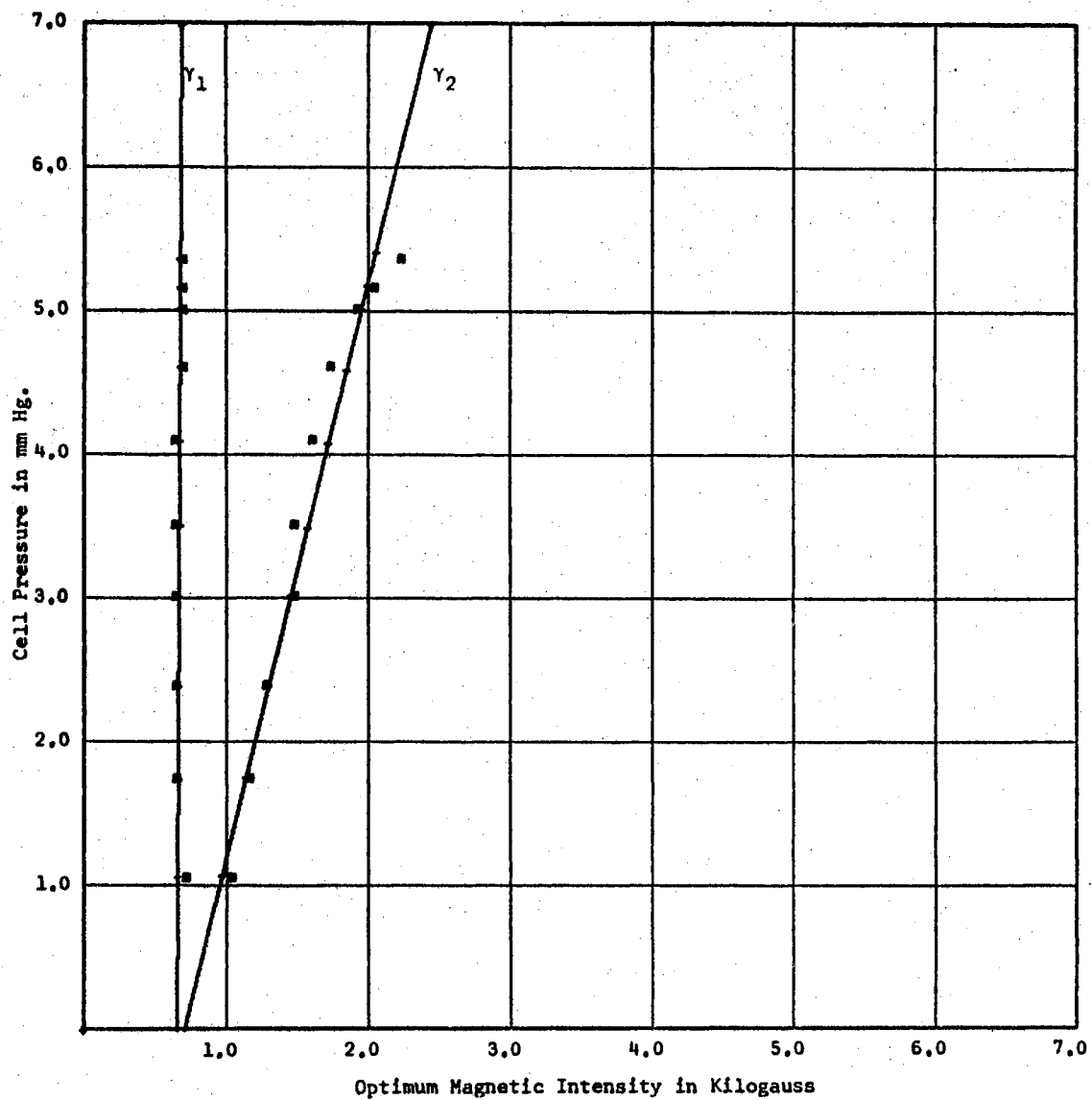
Figure 59a.   Data taken September 7, 1966 at 7 MH_z with Aluminum
              Cell No. 2, D = 0.005931 meters
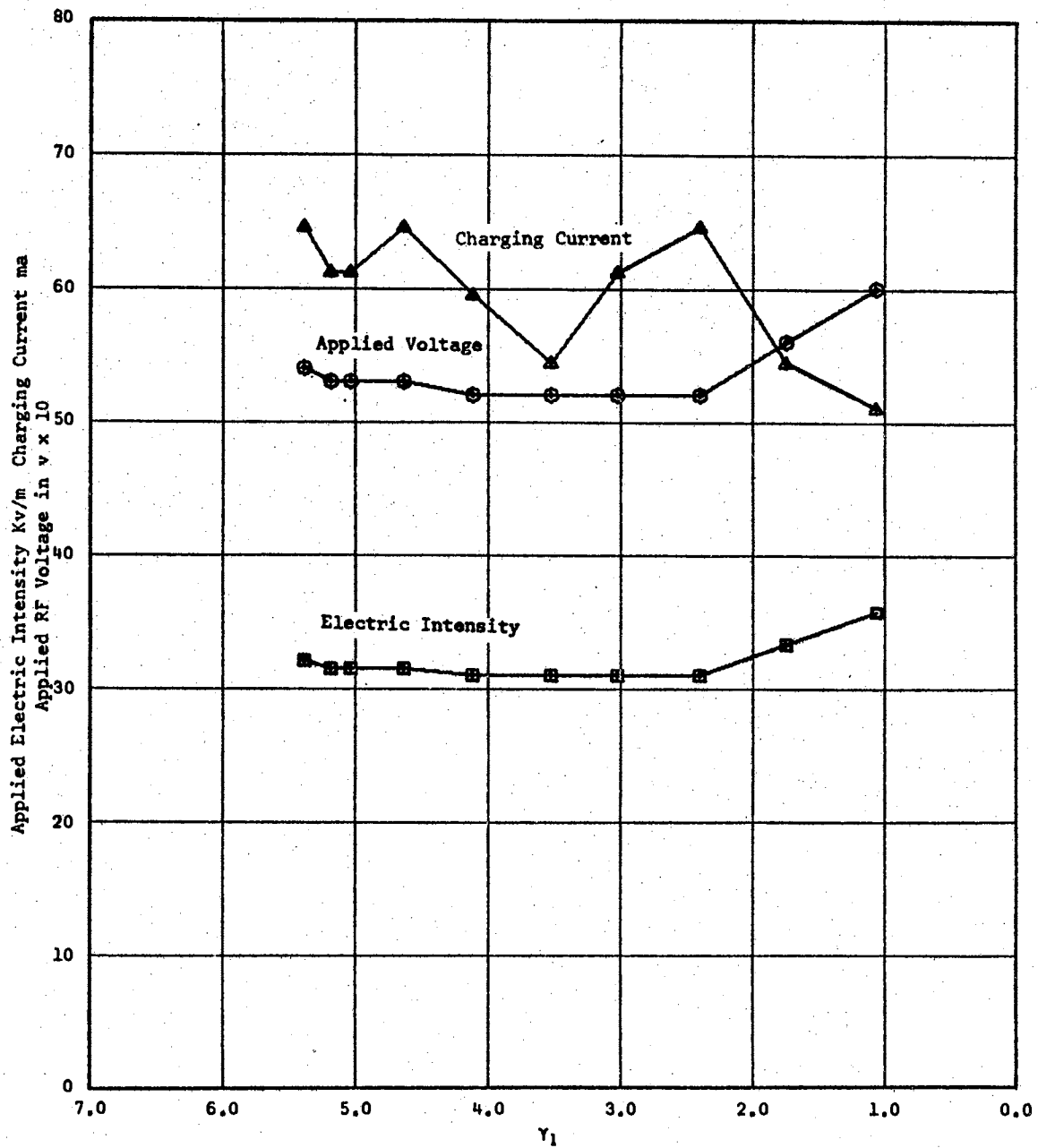
Figure 59b. Data taken September 7, 1966 at 7 MH$_z$ with Aluminum Cell No. 2, D = 0.005931 meters
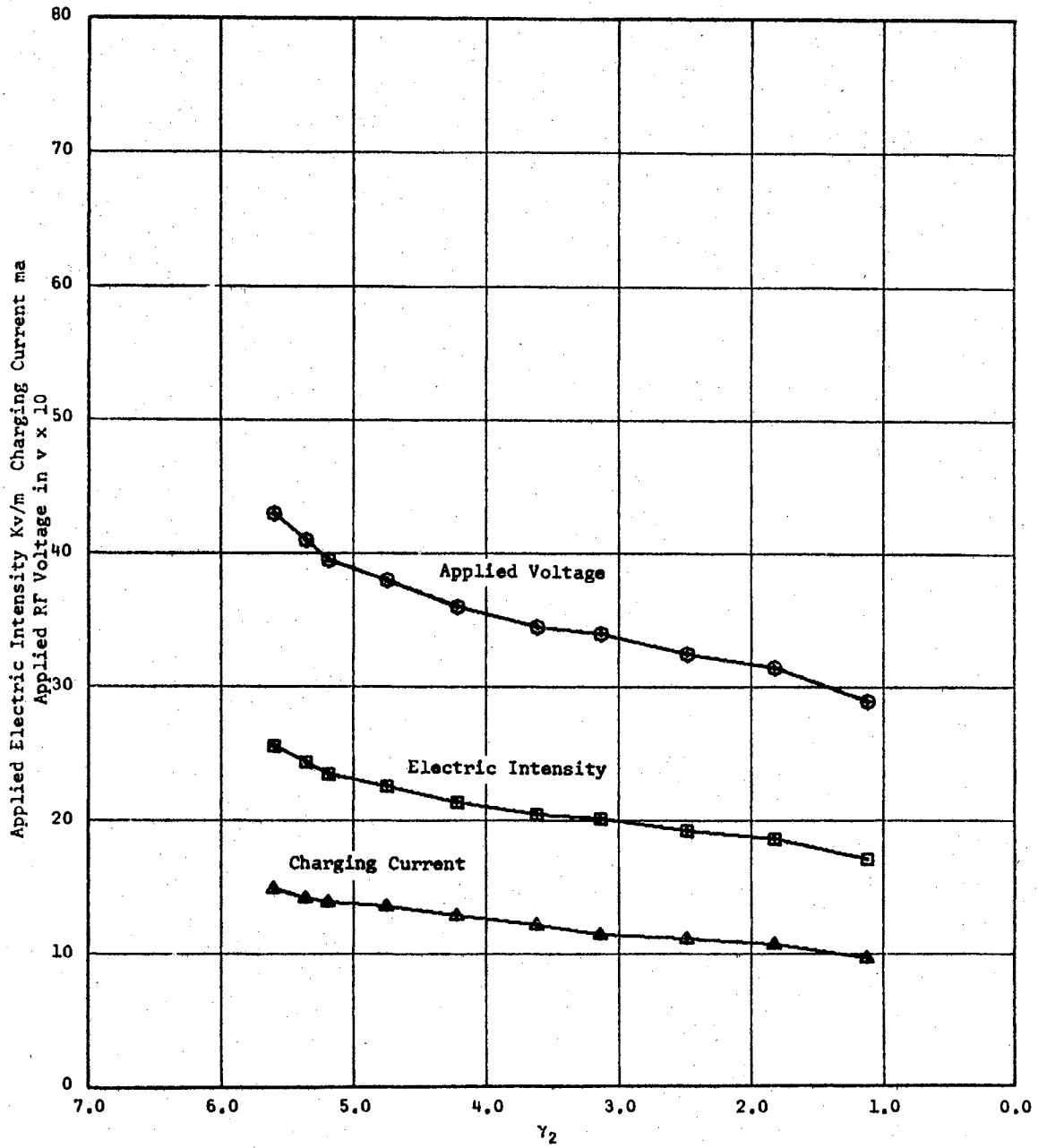
Figure 59c. Data taken September 7, 1966 at 7 MH_z with Aluminum
Cell No. 2, D = 0.005931 meters
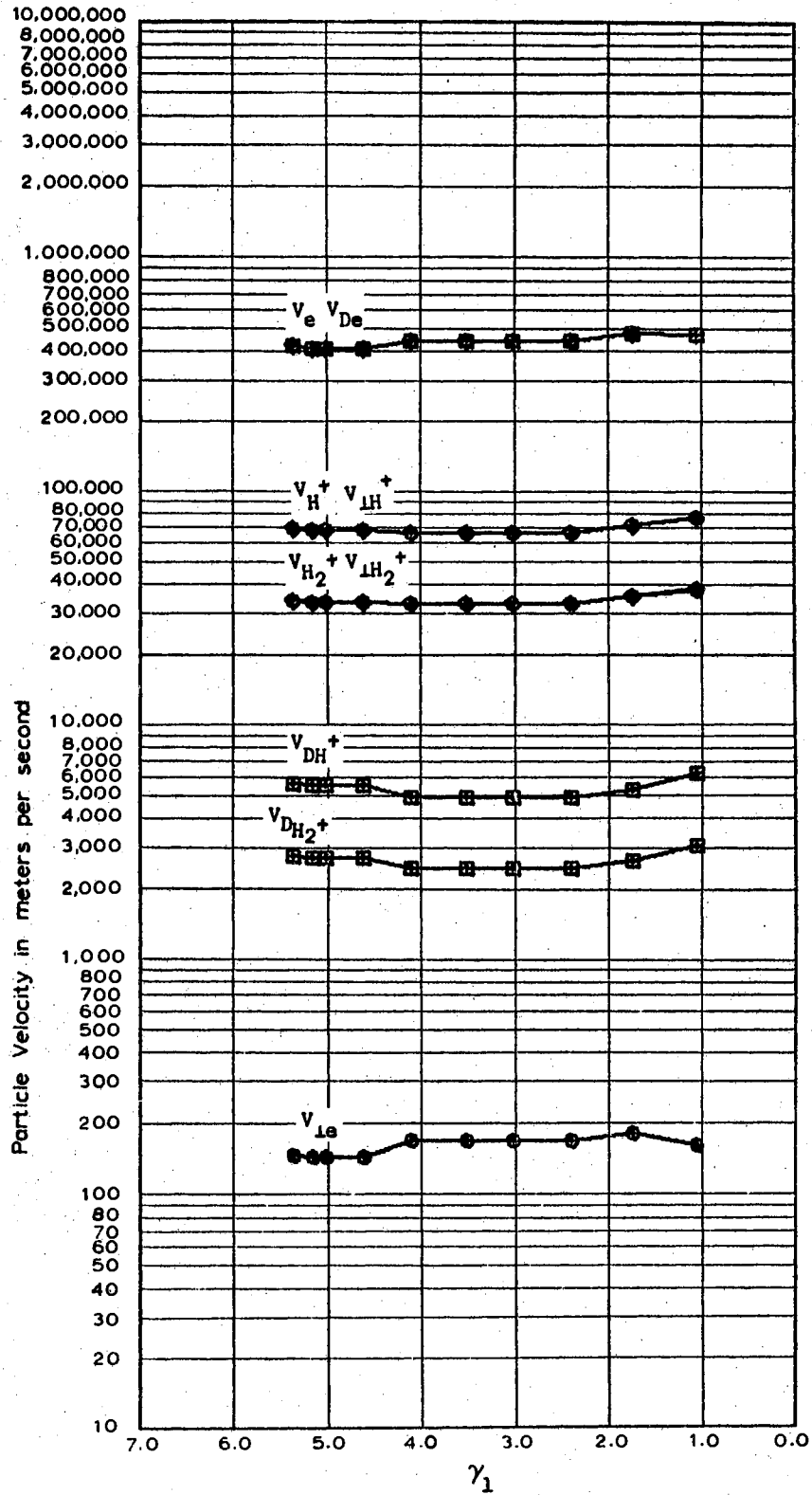
Figure 59d.   Data taken September 7, 1966 at
7 MH$_z$ with Aluminum Cell No.
2, D^z= 0.005931 meters
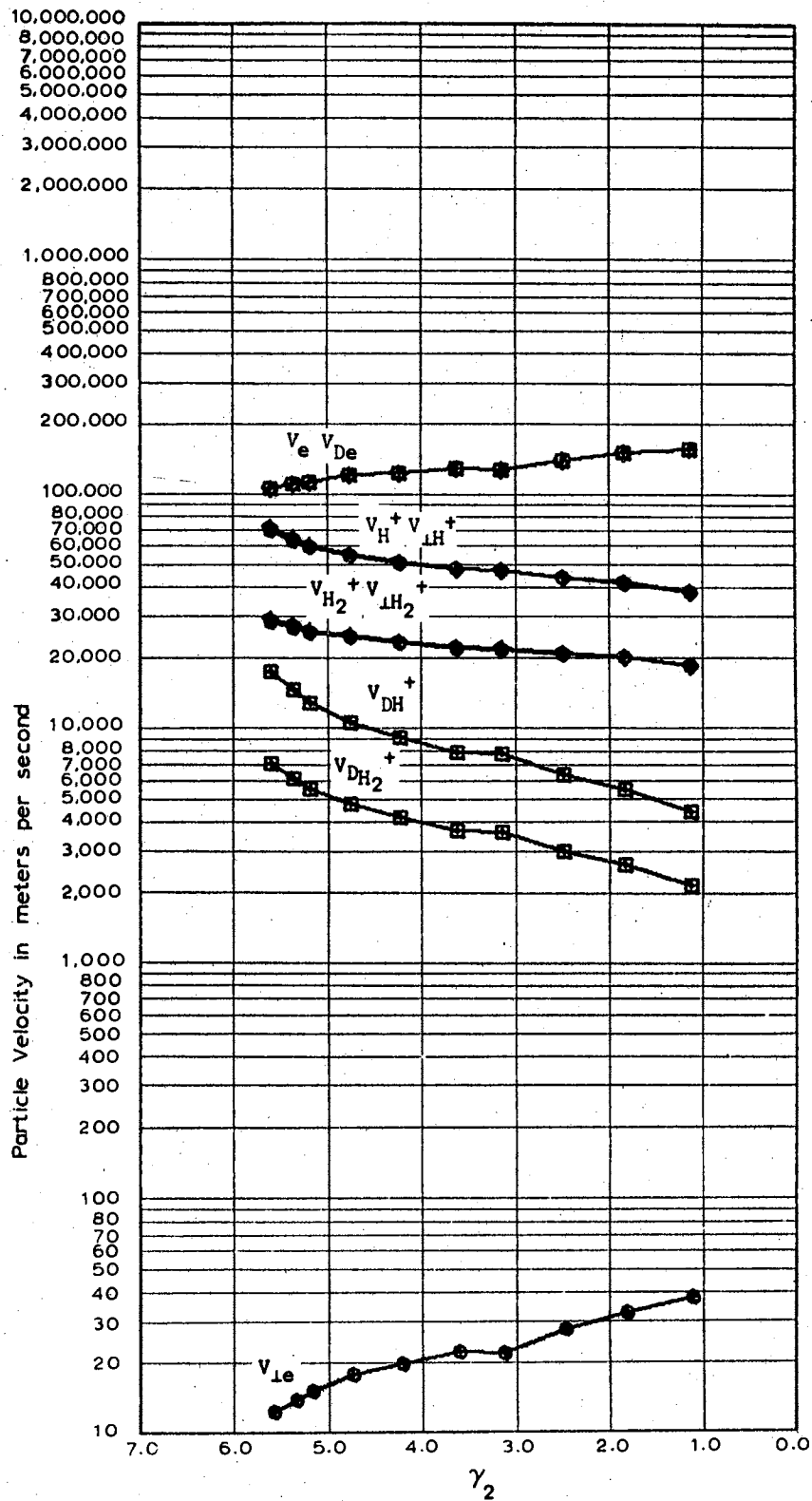
Figure 59e. Data taken September 7, 1966 at
7 MH with Aluminum Cell No.
2, D^z = 0.005931 meters
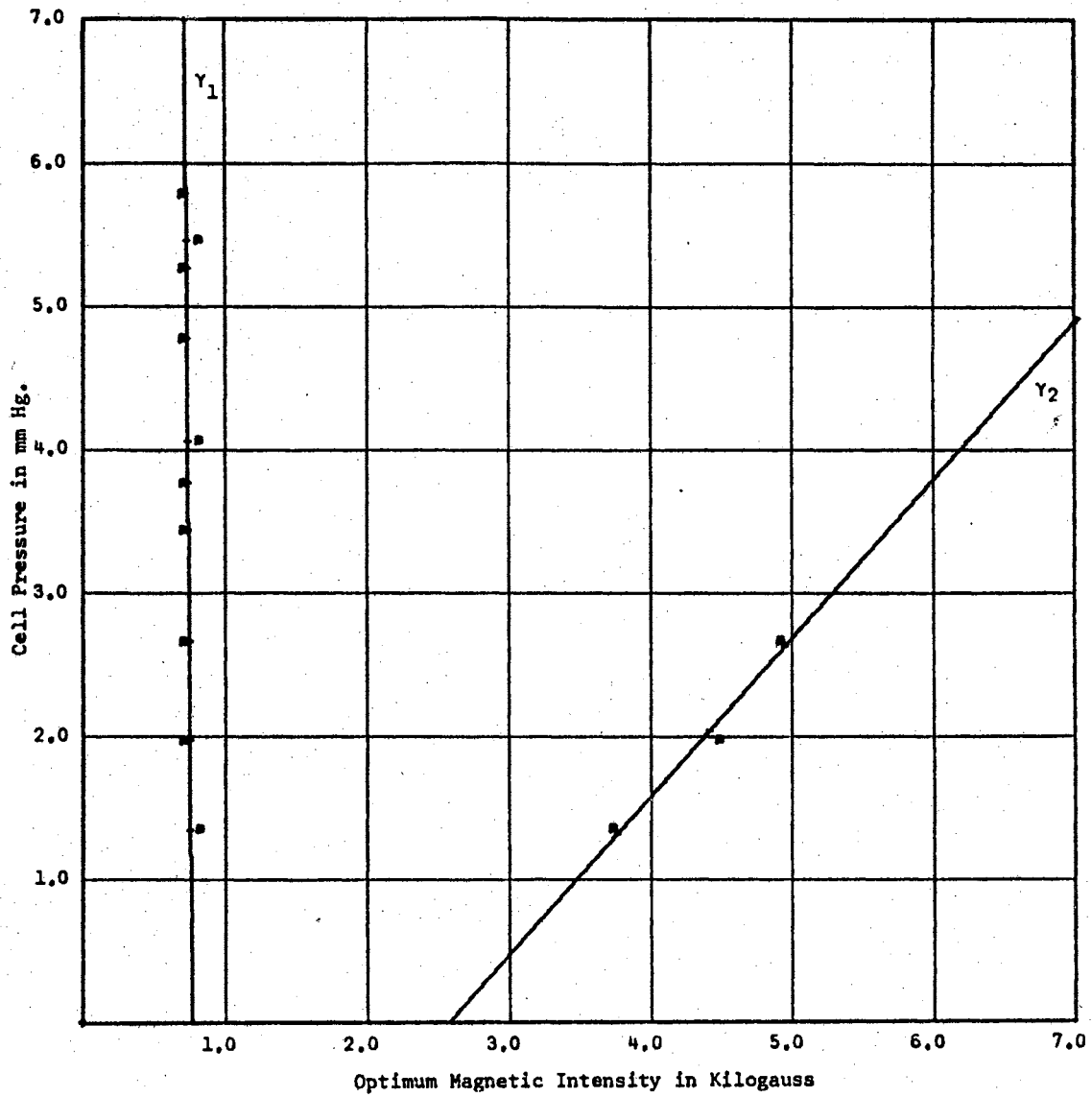
Figure 60a.   Data taken April 29, 1966 at 8 MH_z with the Teflon
Cell, D = 0.00208 meters
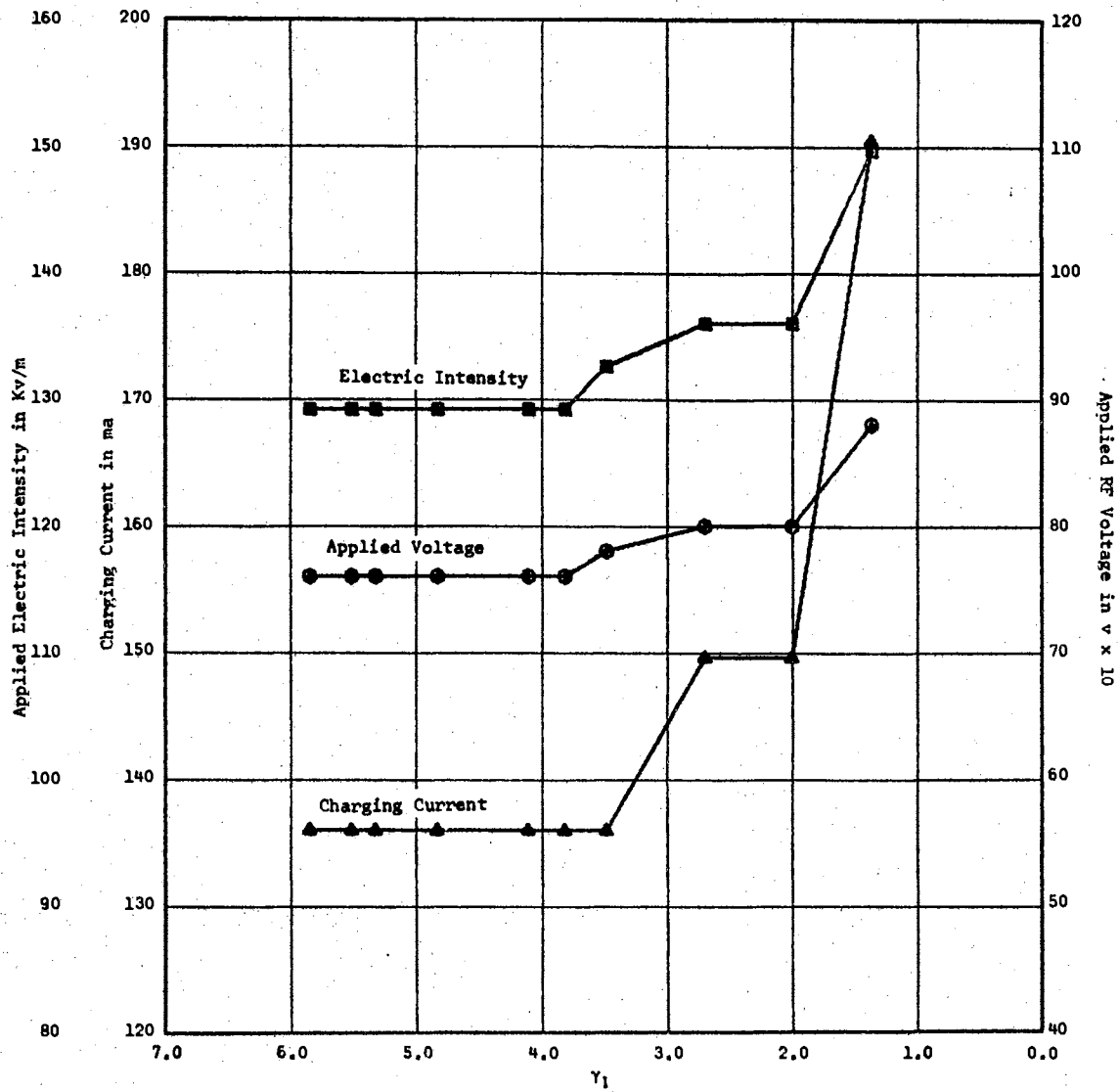
Figure 60b. Data taken April 29, 1966 at 8 MH$_z$ with the Teflon Cell, D = 0.00208 meters^2
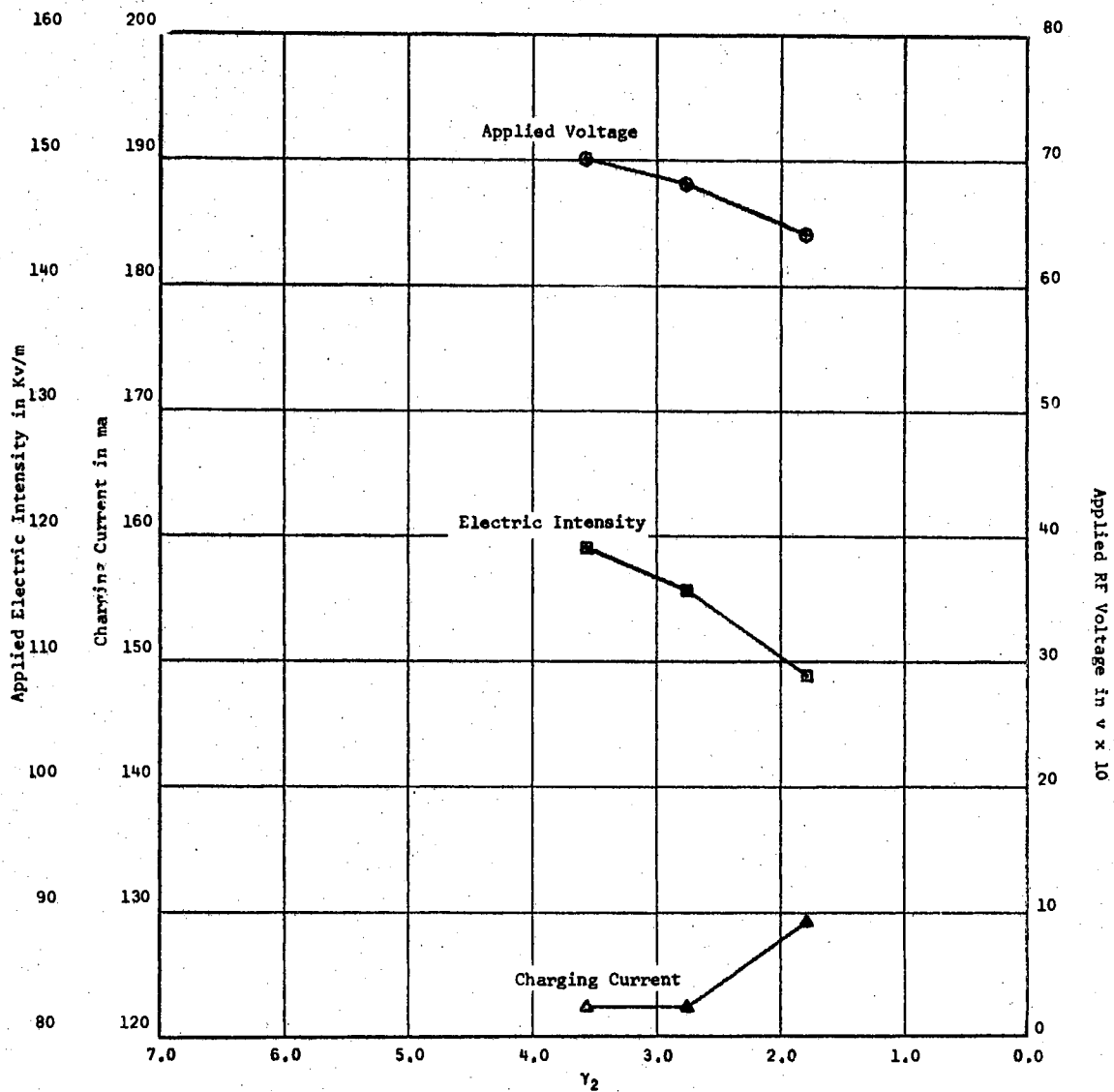
Figure 60c. Data taken April 29, 1966 at 8 MH$_z$ with the
   Teflon Cell, D = 0.00208 meters
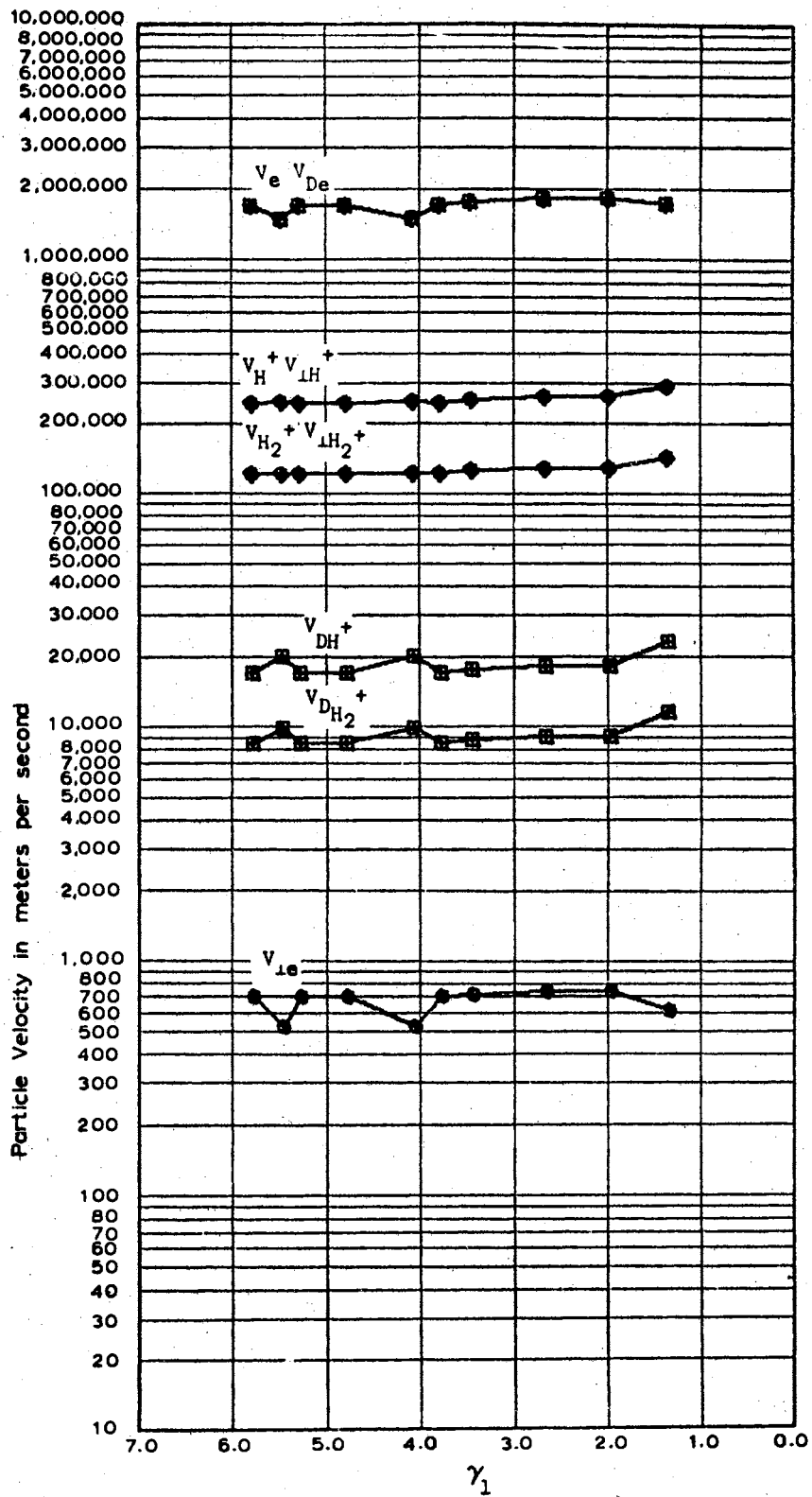
Figure 60d. Data taken April 29, 1966 at 8 MH$_z$ with the Teflon Cell, D = 0.00208 meters
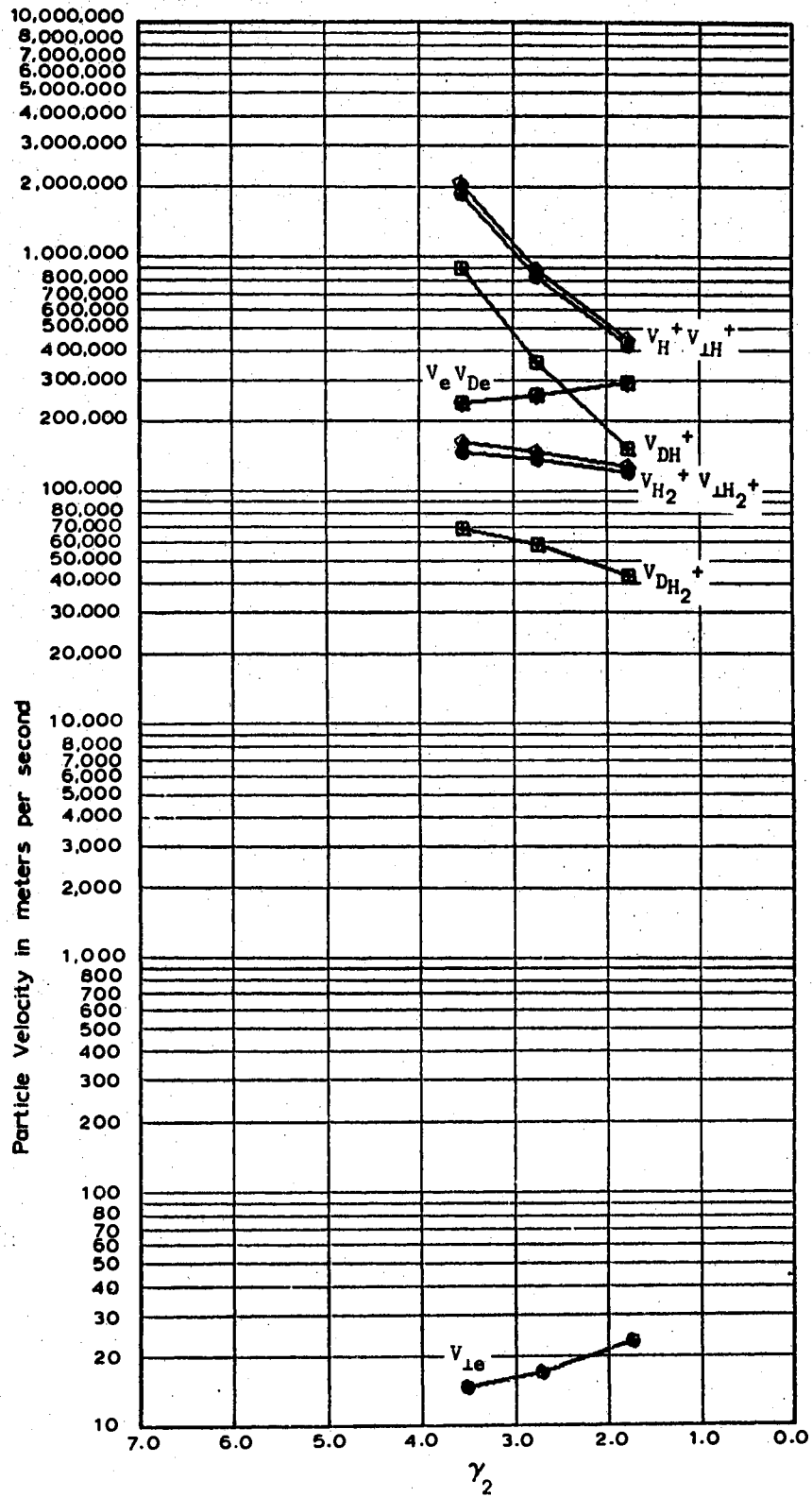
Figure 60e. Data taken April 29, 1966 at 8 MH$_z$ with the Teflon Cell, D = 0.00208 meters
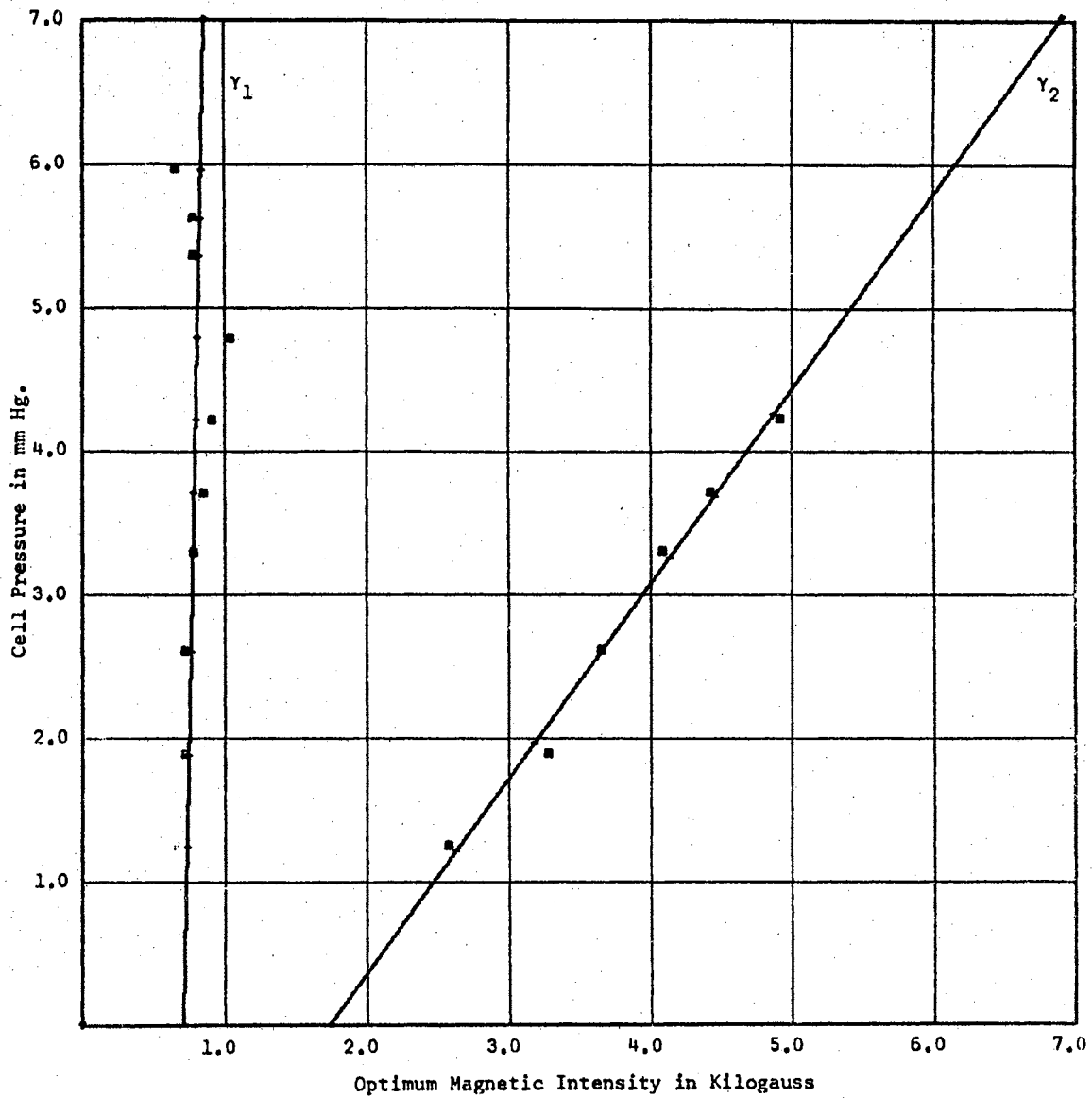
Figure 61a.   Data taken May 2, 1966 at 8 MH$_z$ with the Aluminum Cell, D = 0.002794 meters

Figure 61b. Data taken May 2, 1966 at 8 MH_z with the Aluminum
Cell, D = 0.002794 meters

Figure 61c. Data taken May 2, 1966 at 8 MH$_z$ with the Aluminum Cell, D = 0.002794 meters

Figure 61d. Data taken May 2, 1966 at 8 MH$_z$
with the Aluminum Cell, D =
0.002794 meters

Figure 61e. Data taken May 2, 1966 at 8 MH$_z$
with the Aluminum Cell, D =
0.002794 meters

Figure 62a. Data taken May 24, 1966 at 8 MH_z with the Aluminum Cell, D = 0.002794 meters

Figure 62b. Data taken May 24, 1966 at 8 MH$_z$ with the Aluminum Cell, D = 0.002794 meters

Figure 62c. Data taken May 24, 1966 at 8 MH$_z$ with the Aluminum Cell, D = 0.002794 meters

Figure 62d. Data taken May 24, 1966 at 8 MH$_z$ with the Aluminum Cell, D = 0.002794 meters

Figure 62e. Data taken May 24, 1966 at 8 MH$_z$ with the Aluminum Cell, D = 0.002794 meters

Figure 63a. Data taken July 20, 1966 at 9 MH$_z$ with the Aluminum Cell, D = 0.002794 meters

Figure 63b. Data taken July 20, 1966 at 9 MH$_z$ with the Aluminum Cell, D = 0.002794 meters

Figure 63c. Data taken July 20, 1966 at 9 MH$_z$ with the Aluminum
Cell, D = 0.002794 meters

Figure 63d. Data taken July 20, 1966 at 9
MH with the Aluminum Cell,
D ≅ 0.002794 meters

Figure 63e. Data taken July 20, 1966 at 9
MH$_z$ with the Aluminum Cell,
D $\cong$ 0.002794 meters

Figure 64a. Data taken August 17, 1966 at 9 MH_z with the Aluminum
Cell, D = 0.002794 meters

Figure 64b. Data taken August 17, 1966 at 9 MH$_z$ with the Aluminum
Cell, D = 0.002794 meters

Figure 64c. Data taken August 17, 1966 at 9 MH$_z$ with the Aluminum Cell, D = 0.002794 meters

Figure 64d. Data taken August 17, 1966 at 9 MH$_z$ with the Aluminum Cell, D = 0.002794 meters

Figure 64e. Data taken August 17, 1966 at
9 MH with the Aluminum Cell,
D = 0.002794 meters

Figure 65a. Data taken May 26, 1966 at 10 MH_z with the Aluminum Cell, D = 0.002794 meters

Figure 65b. Data taken May 26, 1966 at 10 MH$_z$ with the Aluminum
Cell, D = 0.002794 meters

Figure 65c. Data taken May 26, 1966 at 10 MH$_z$ with the
Aluminum Cell, D = 0.002794 meters

Figure 65d. Data taken May 26, 1966 at 10
MH$_z$ with the Aluminum Cell,
D $\cong$ 0.002794 meters

Figure 65e. Data taken May 26, 1966 at 10
MH with the Aluminum Cell,
D ≅ 0.002794 meters

Figure 66a. Data taken June 16, 1966 at 10 MH_z with the Aluminum
Cell, D = 0.002794 meters

Figure 66b.   Data taken June 16, 1966 at 10 MH$_z$ with the
Aluminum Cell, D = 0.002794 meters

Figure 66c.   Data taken June 16, 1966 at 10 MH$_z$ with the
Aluminum Cell, D = 0.002794 meters

Figure 66d. Data taken June 16, 1966 at 10 MHz with the Aluminum Cell, D ≡ 0.002794 meters

Figure 66e. Data taken June 16, 1966 at 10 MH$_Z$ with the Aluminum Cell, D $\cong$ 0.002794 meters
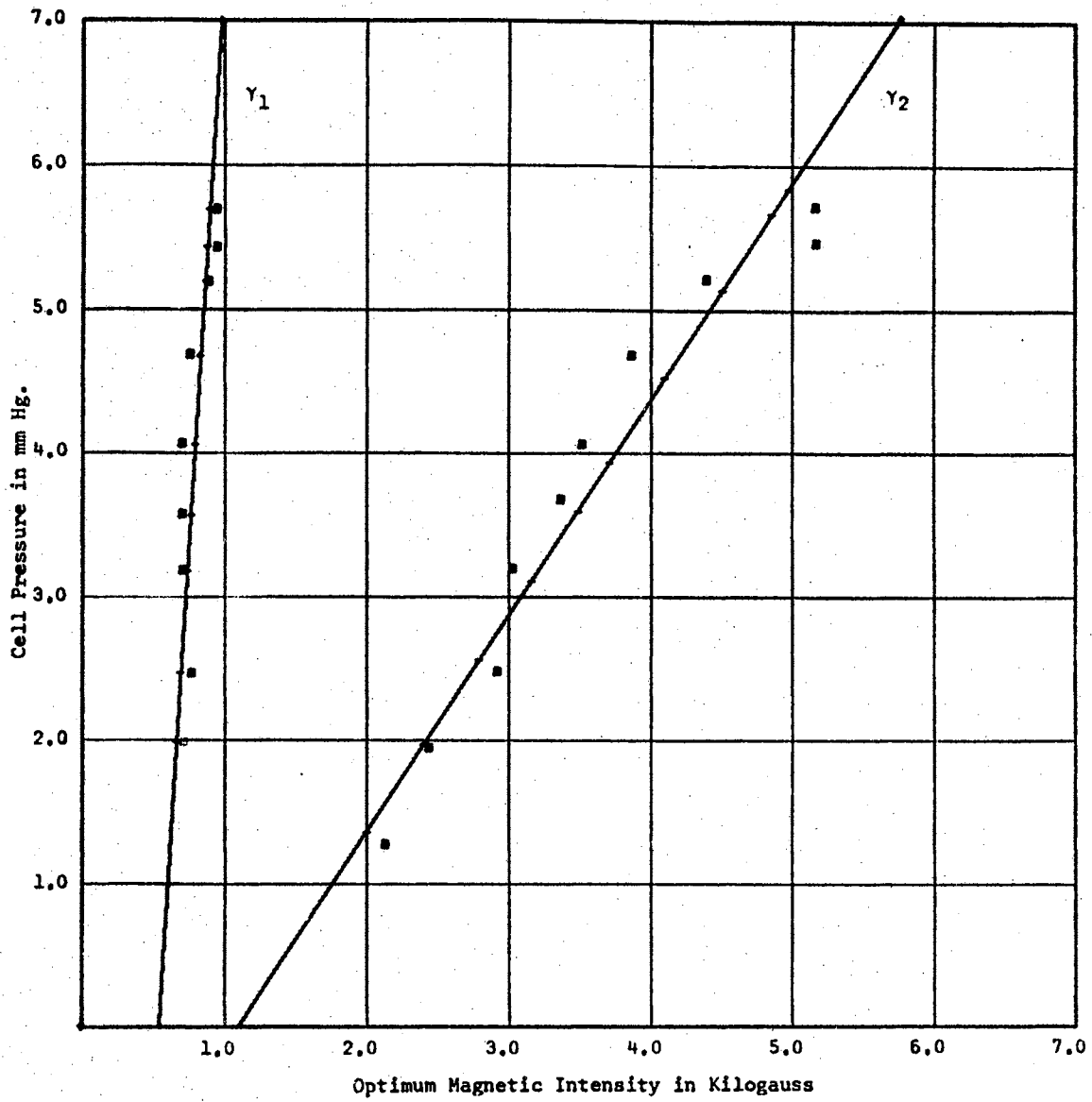
Figure 67a.   Data taken July 22, 1966 at 11 MH_z with the Aluminum
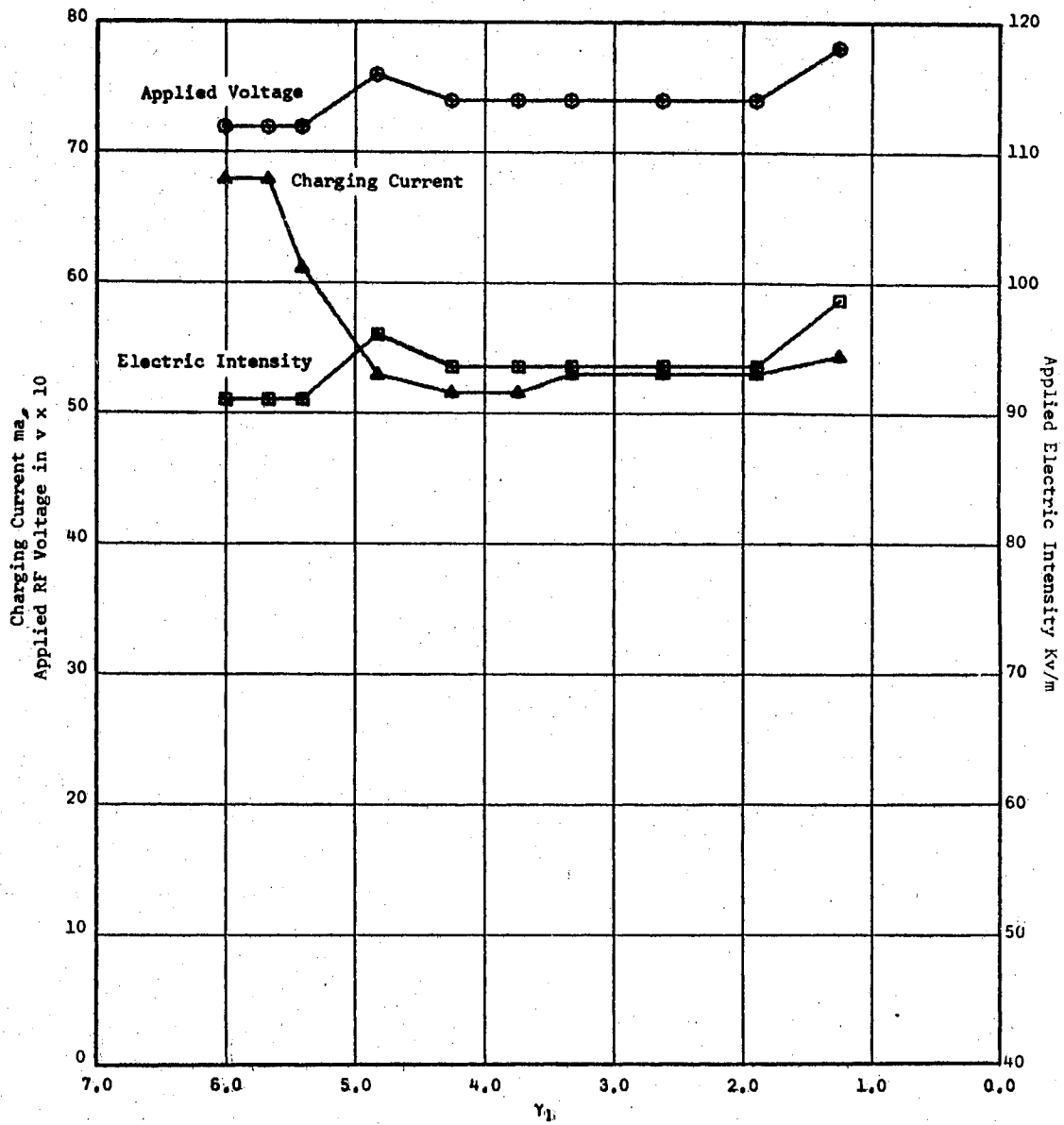   Cell, D = 0.002794 meters
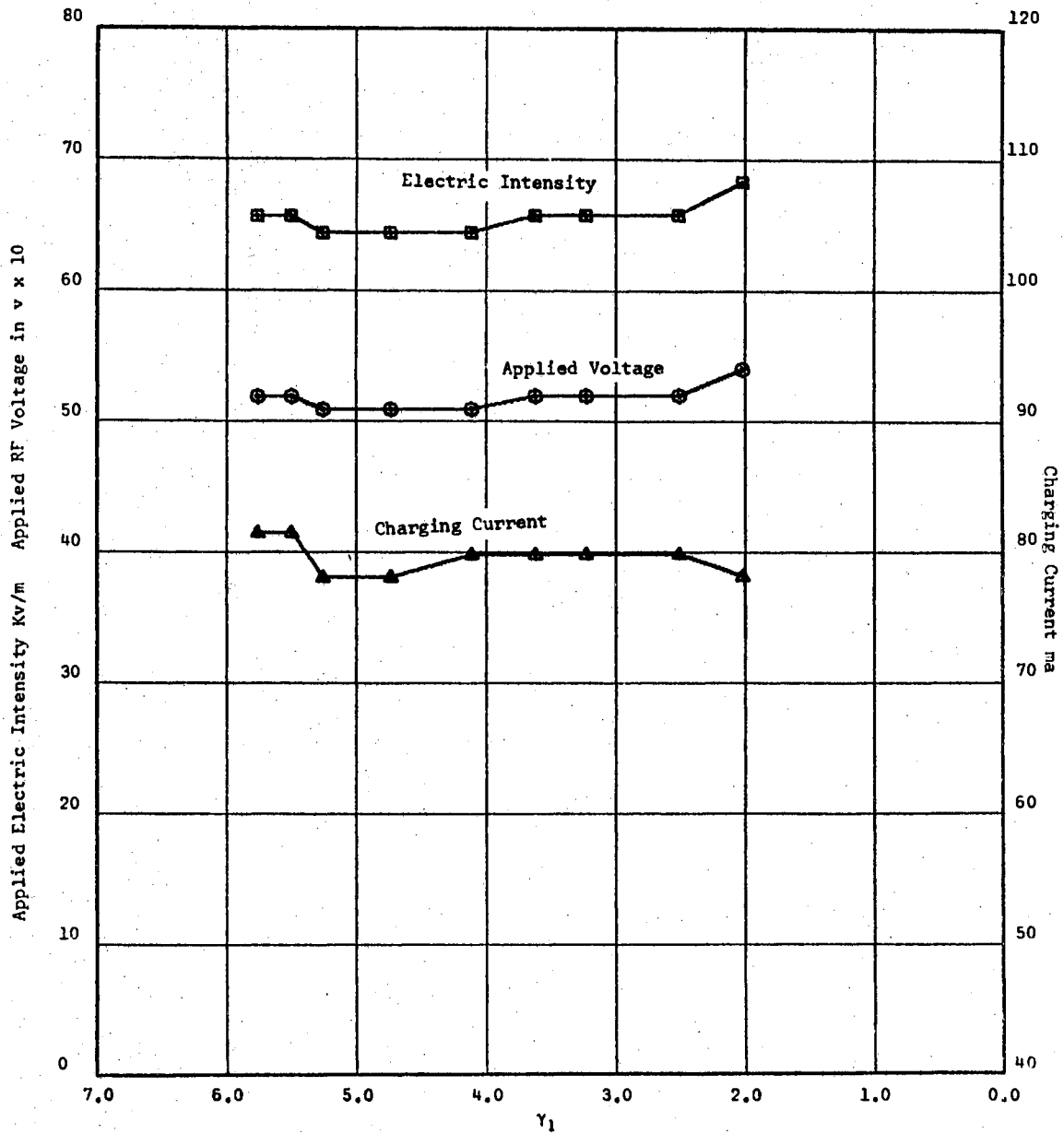
Figure 67b. Data taken July 22, 1966 at 11 MH_z with the
Aluminum Cell, D = 0.002794 meters
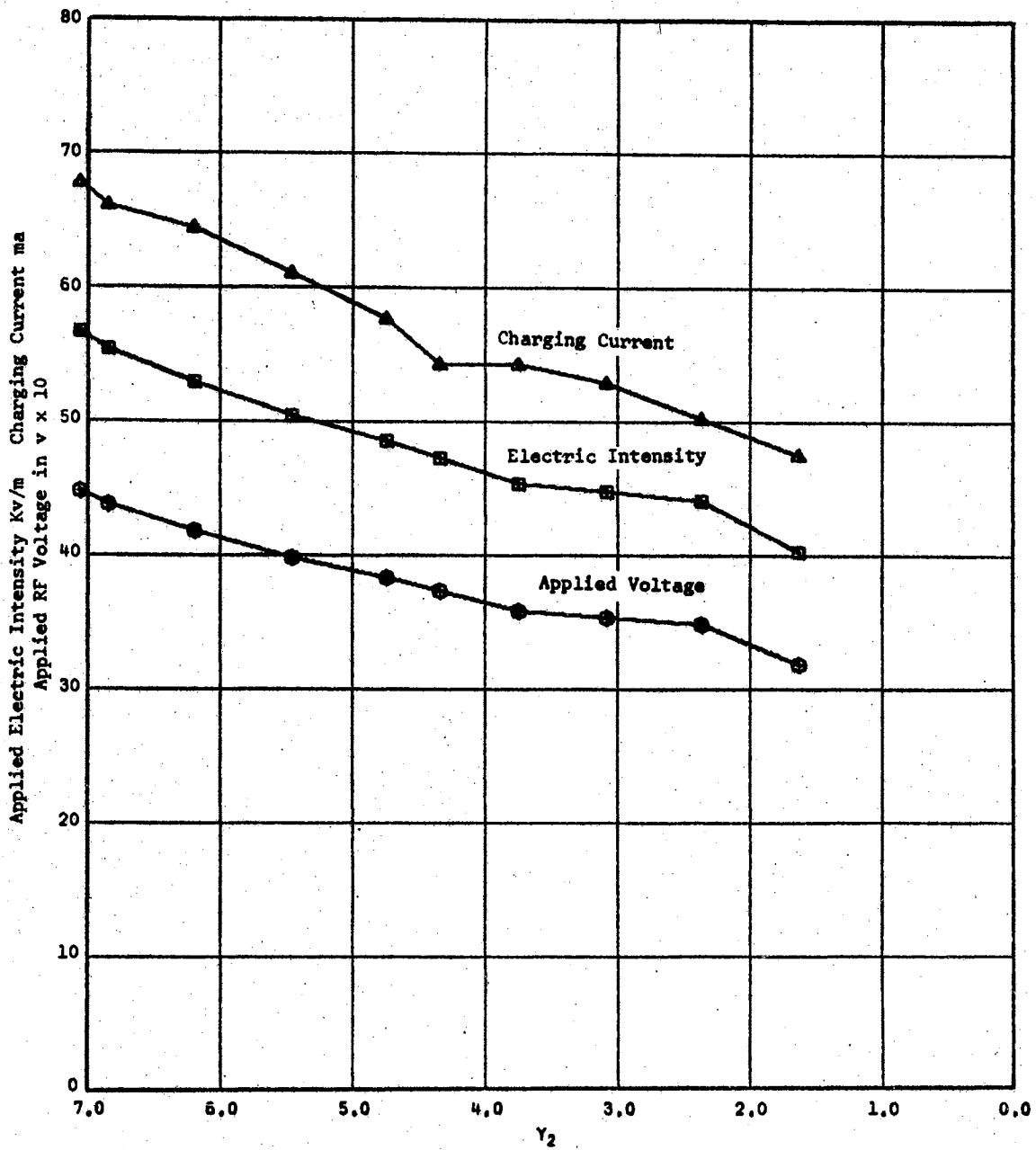
Figure 67c. Data taken July 22, 1966 at 11 MH$_z$ with the Aluminum Cell, D = 0.002794 meters

Figure 67d. Data taken July 22, 1966 at 11
MH with the Aluminum Cell,
$D \cong 0.002794$ meters

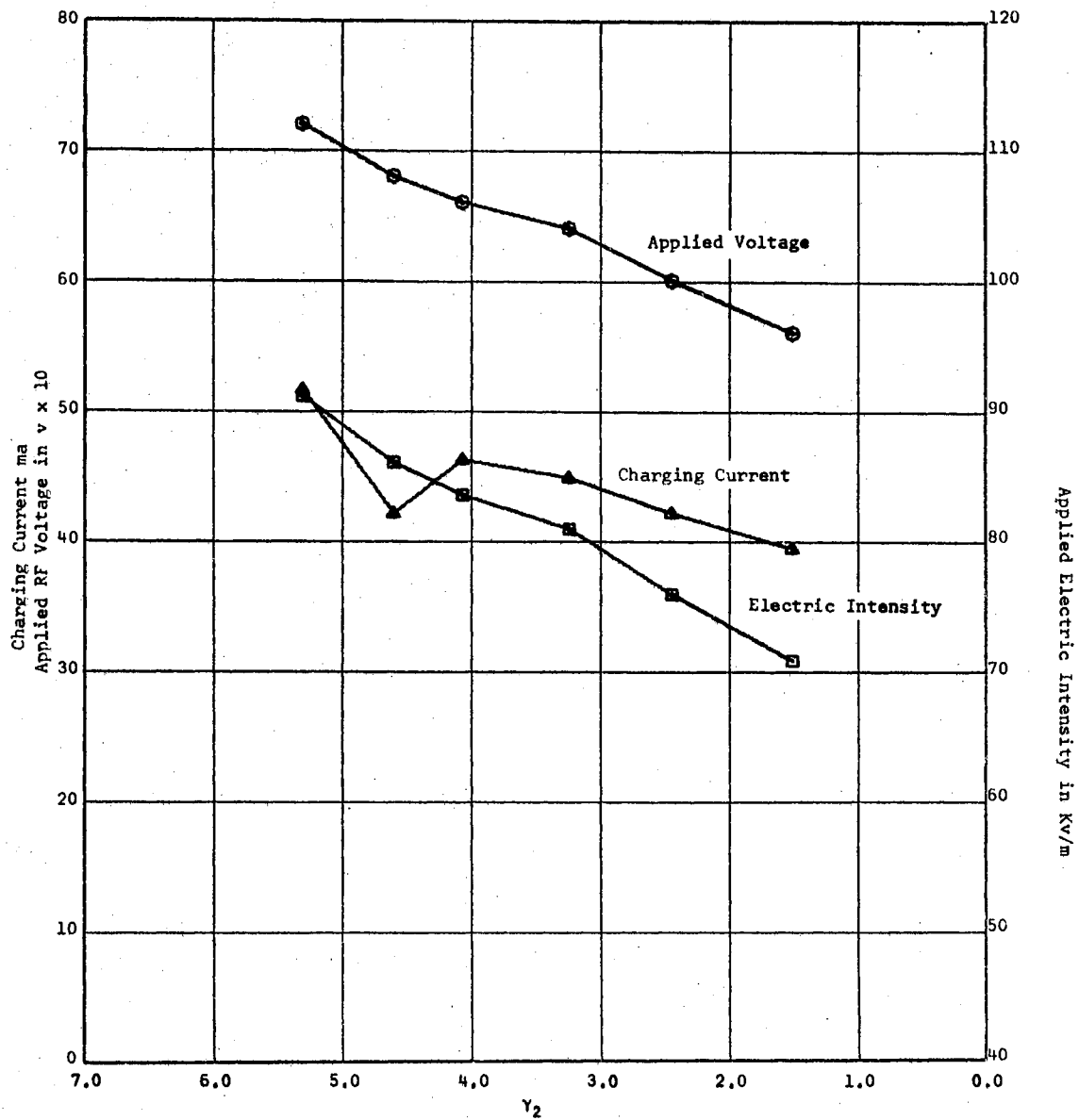Figure 67e. Data taken July 22, 1966 at 11
MH with the Aluminum Cell,
D $\stackrel{z}{=}$ 0.002794 meters

Figure 68a. Data taken August 11, 1966 at 11 MH$_z$ with the
Aluminum Cell, D = 0.002794 meters

Figure 68b. Data taken August 11, 1966 at 11 MH_z with the Aluminum Cell, D = 0.002794 meters

Figure 68c. Data taken August 11, 1966 at 11 MH$_z$ with the
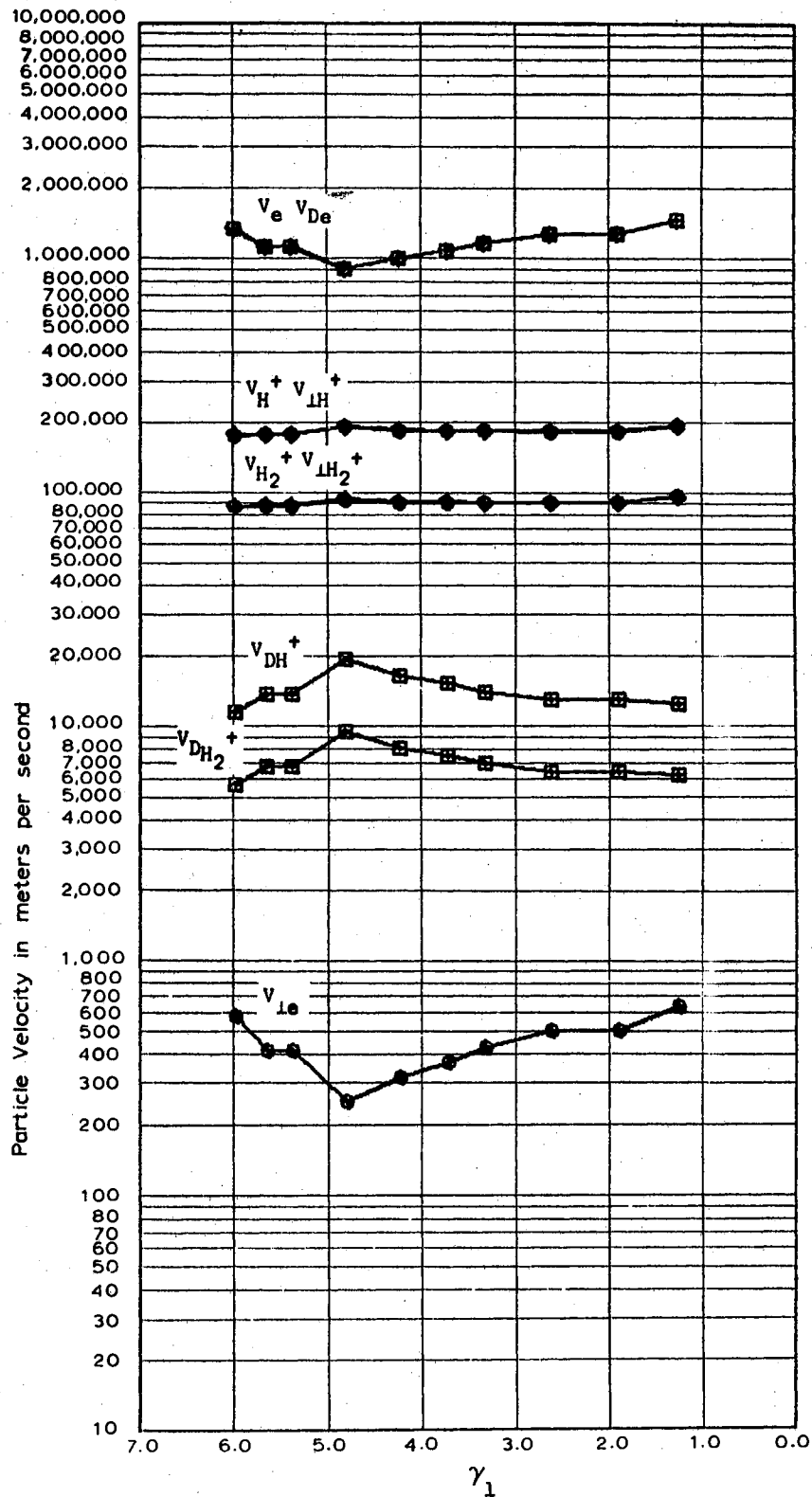Aluminum Cell, D = 0.002794 meters

Figure 68d. Data taken August 11, 1966 at 11 MH$_Z$ with the
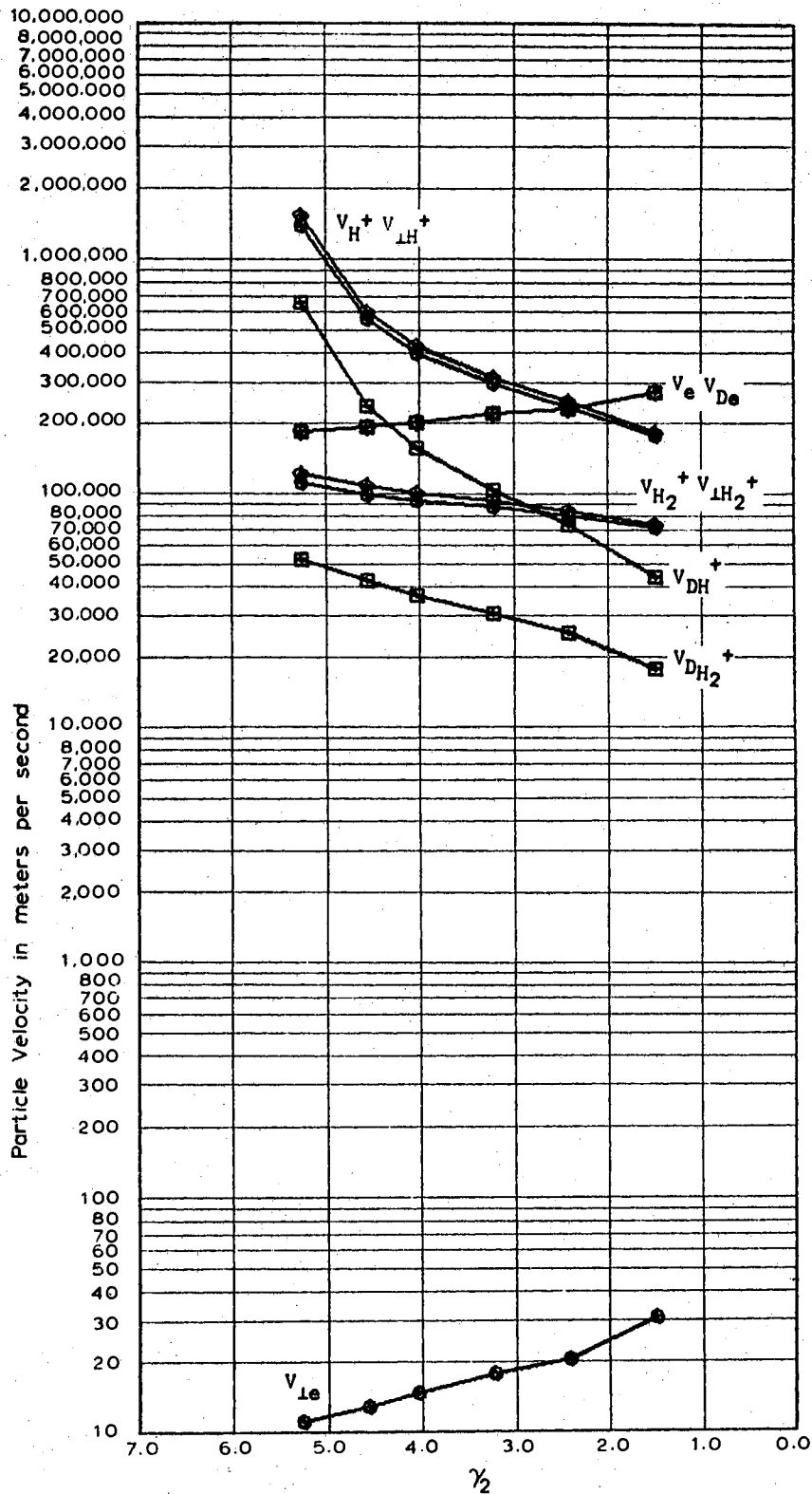Aluminum Cell, D = 0.002794 meters

Figure 68e. Data taken August 11, 1966 at
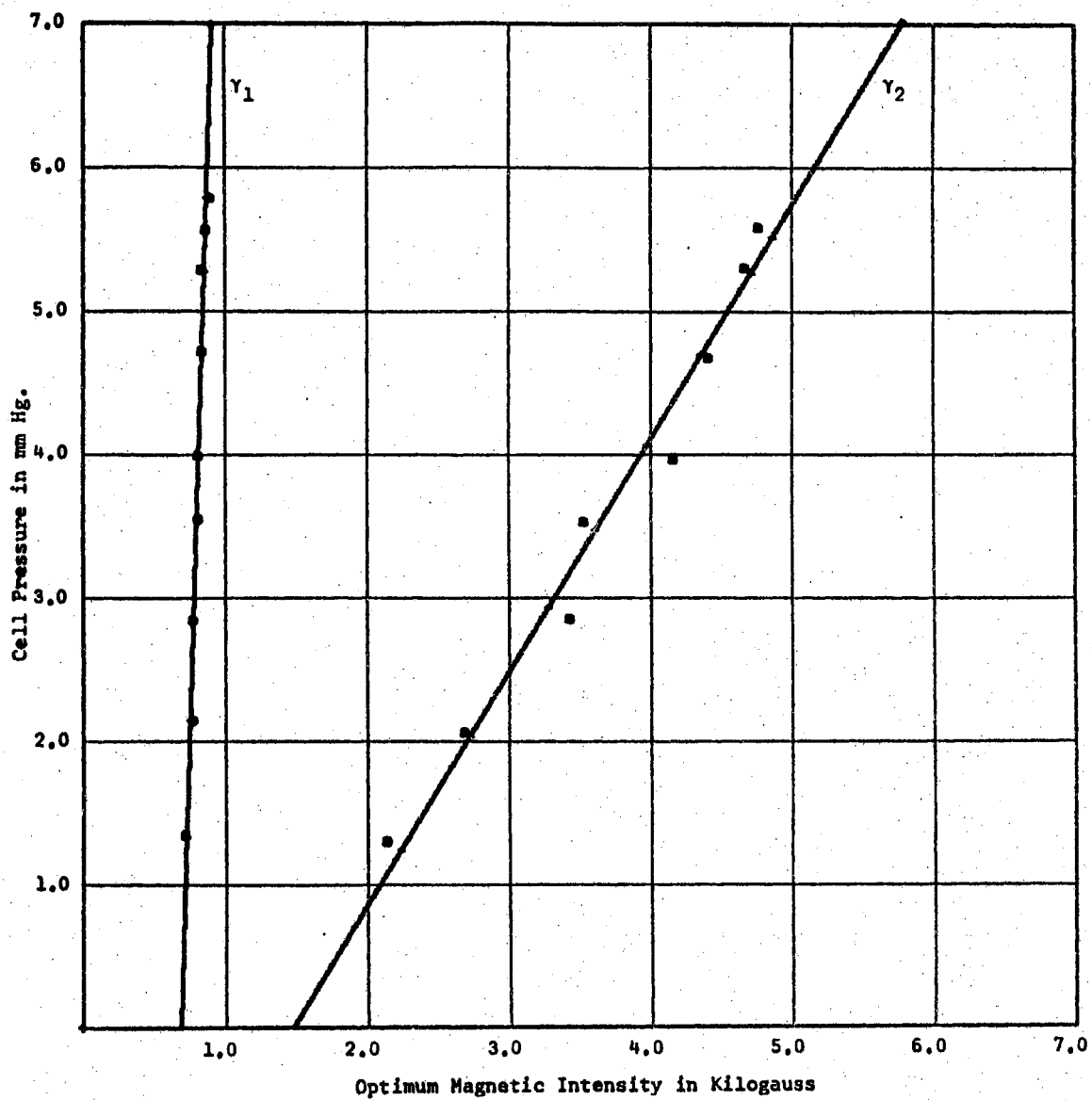11 MH$_z$ with the Aluminum Cell,
D = 0.002794 meters

Figure 68f. Data taken August 11, 1966 at
11 MH_z with the Aluminum Cell,
D = 0.002794 meters

Figure 68g. Data taken August 11, 1966 at
11 MH with the Aluminum Cell,
$D = 0.002794$ meters

Figure 69a. Data taken July 14, 1966 at 12 MH_z with the Aluminum Cell, D = 0.002794 meters
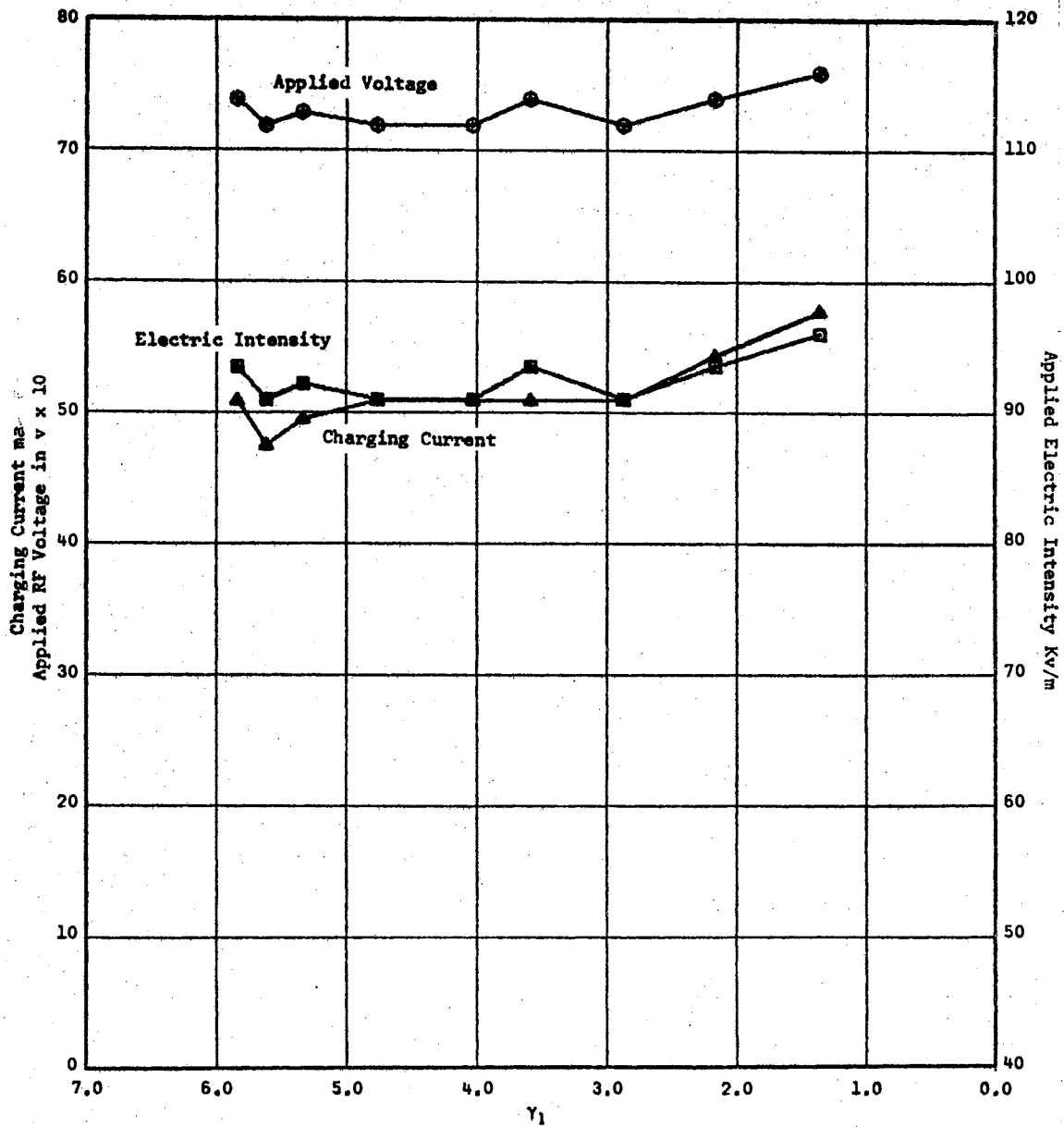
Figure 69b.   Data taken July 14, 1966 at 12 MH with the
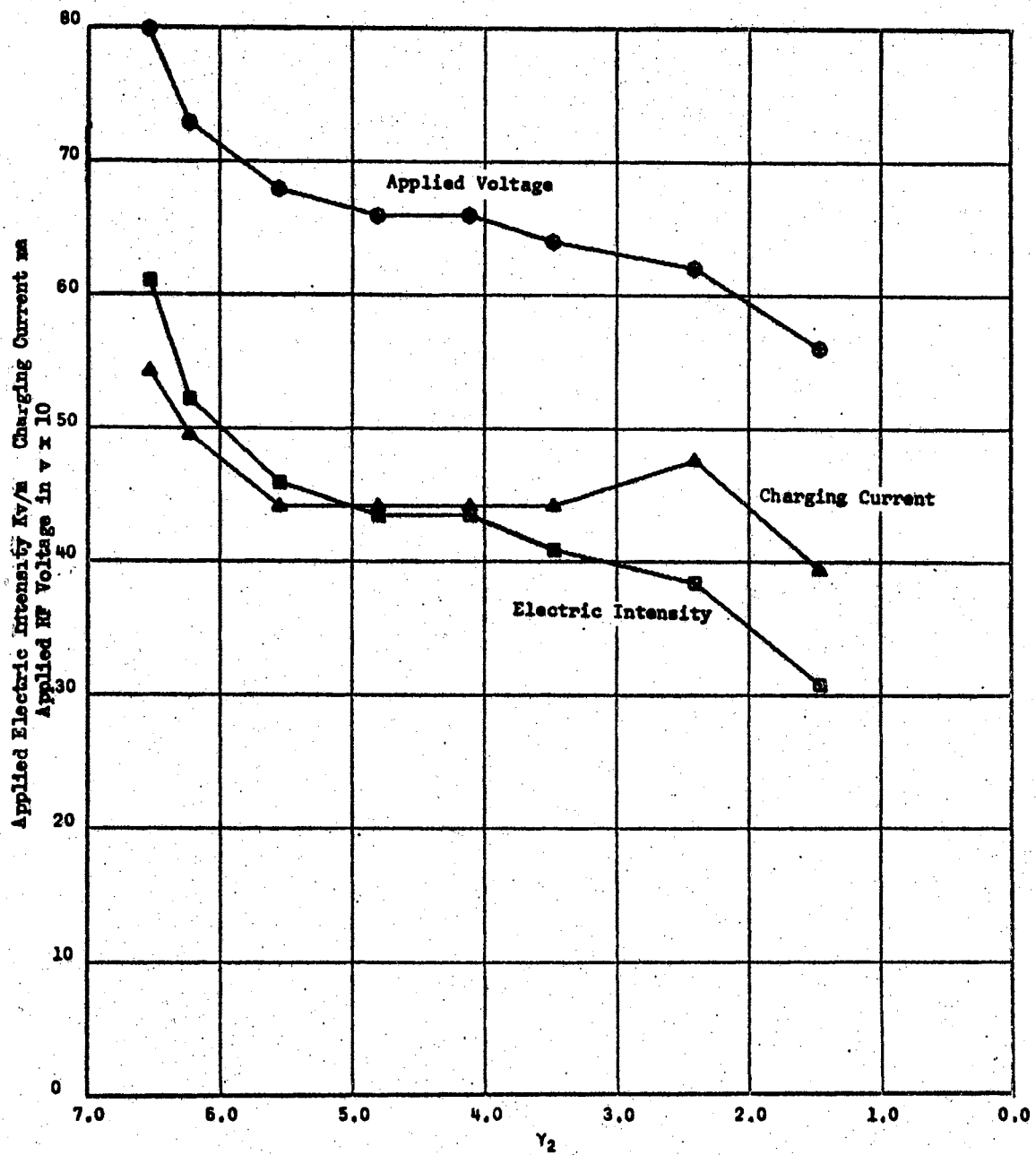Aluminum Cell, D = 0.002794 meters

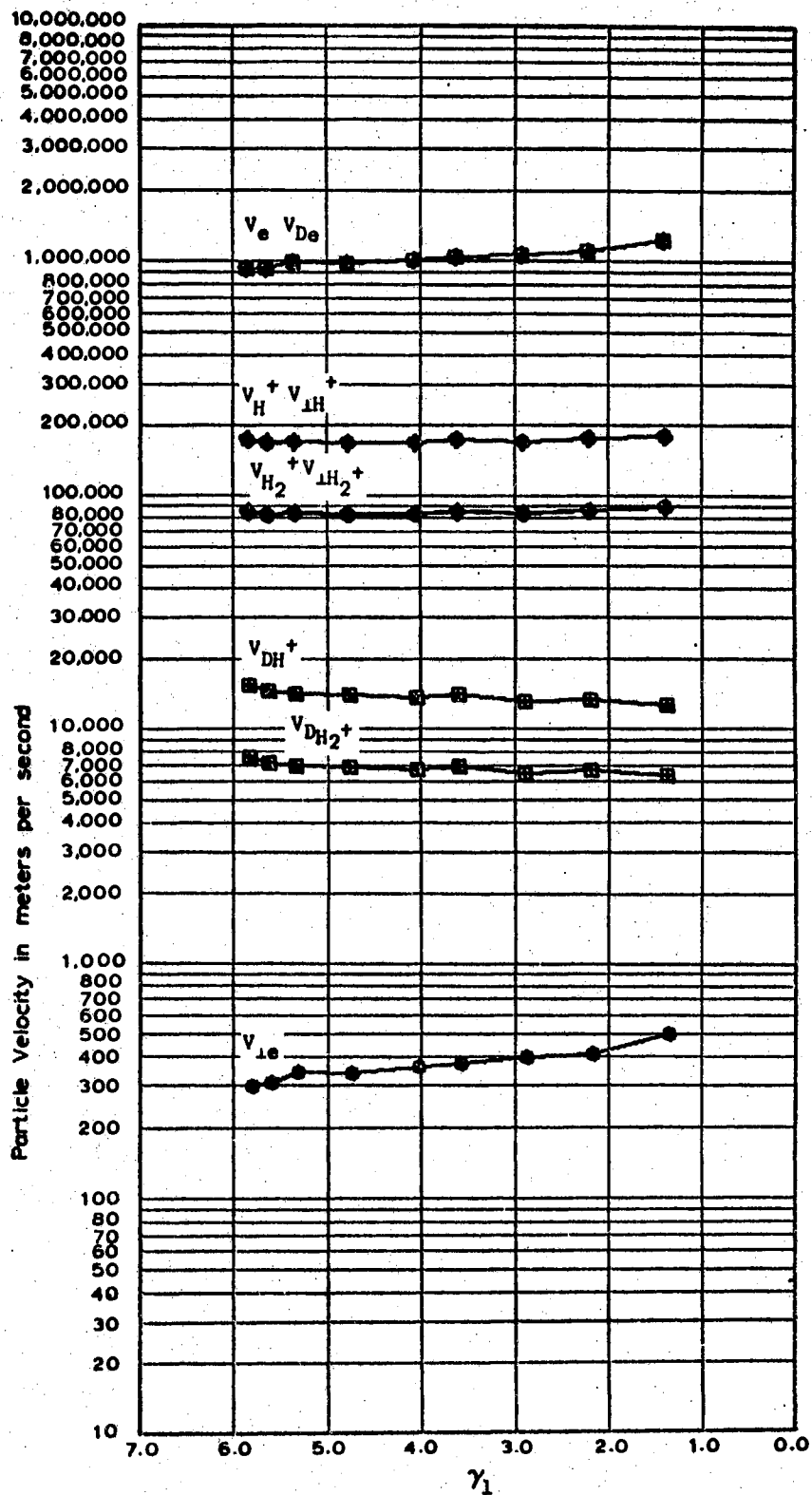Figure 69c.   Data taken July 14, 1966 at 12 MH$_z$ with the Aluminum Cell, D = 0.002794 meters

Figure 69d. Data taken July 14, 1966 at 12 MH$_z$ with the
Aluminum Cell, D = 0.002794 meters

Figure 69e. Data taken July 14, 1966 at 12
MH$_z$ with the Aluminum Cell,
D ≅ 0.002794 meters
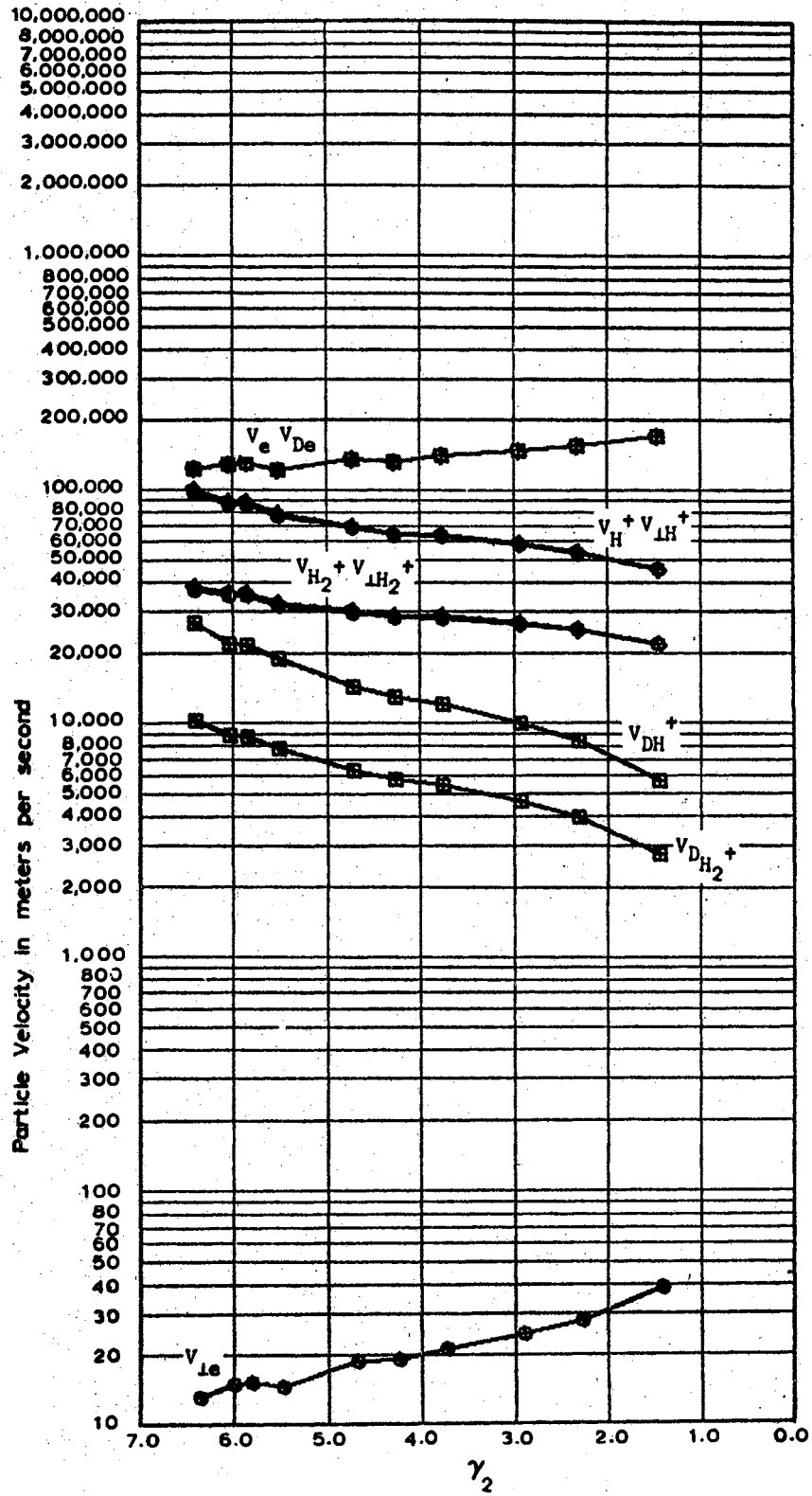
Figure 69f. Data taken July 14, 1966 at 12 MH$_z$ with the Aluminum Cell, D = 0.002794 meters
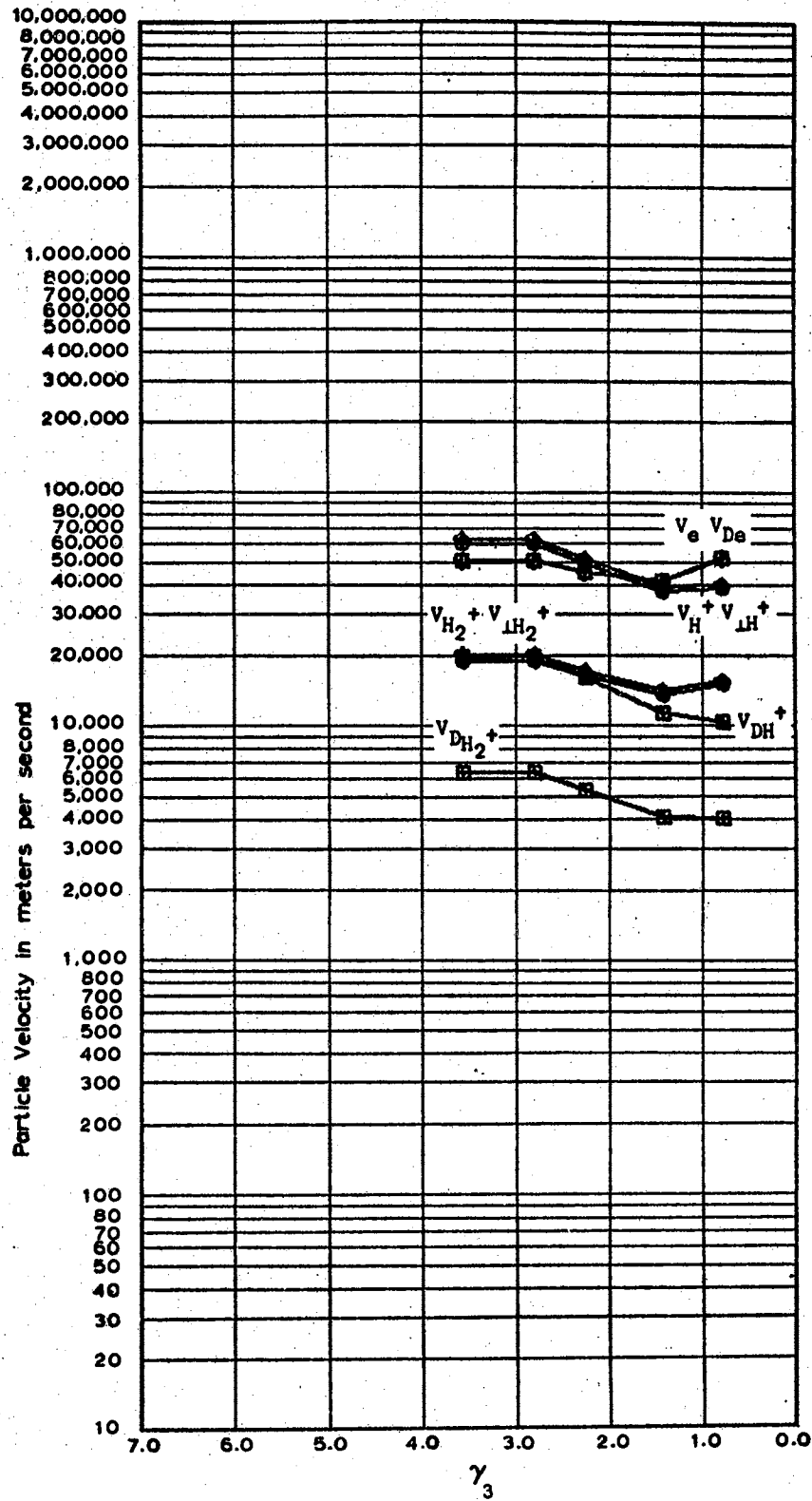
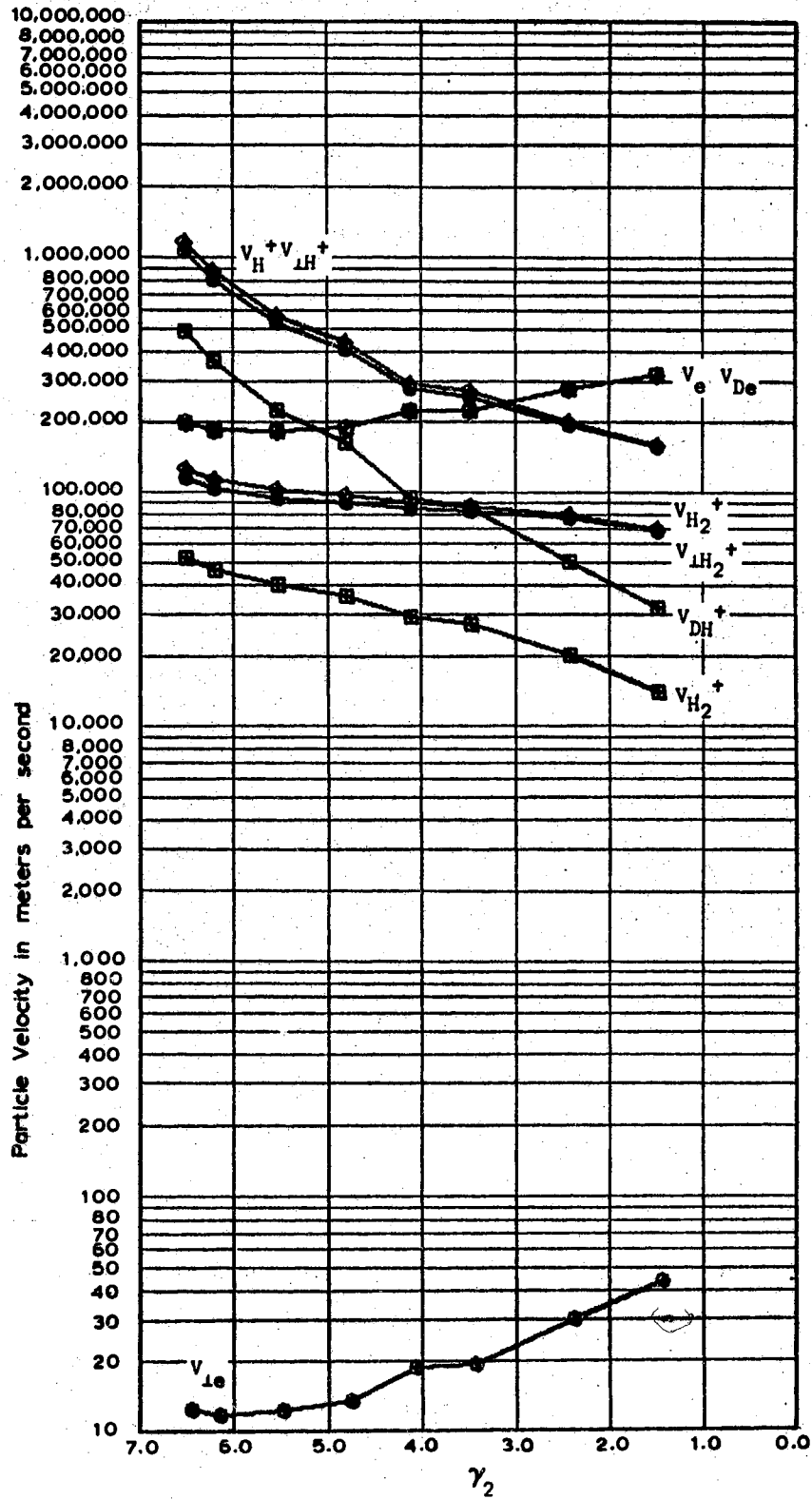Figure 69g. Data taken July 14, 1966 at 12 MH$_z$ with the Aluminum Cell, D = 0.002794 meters
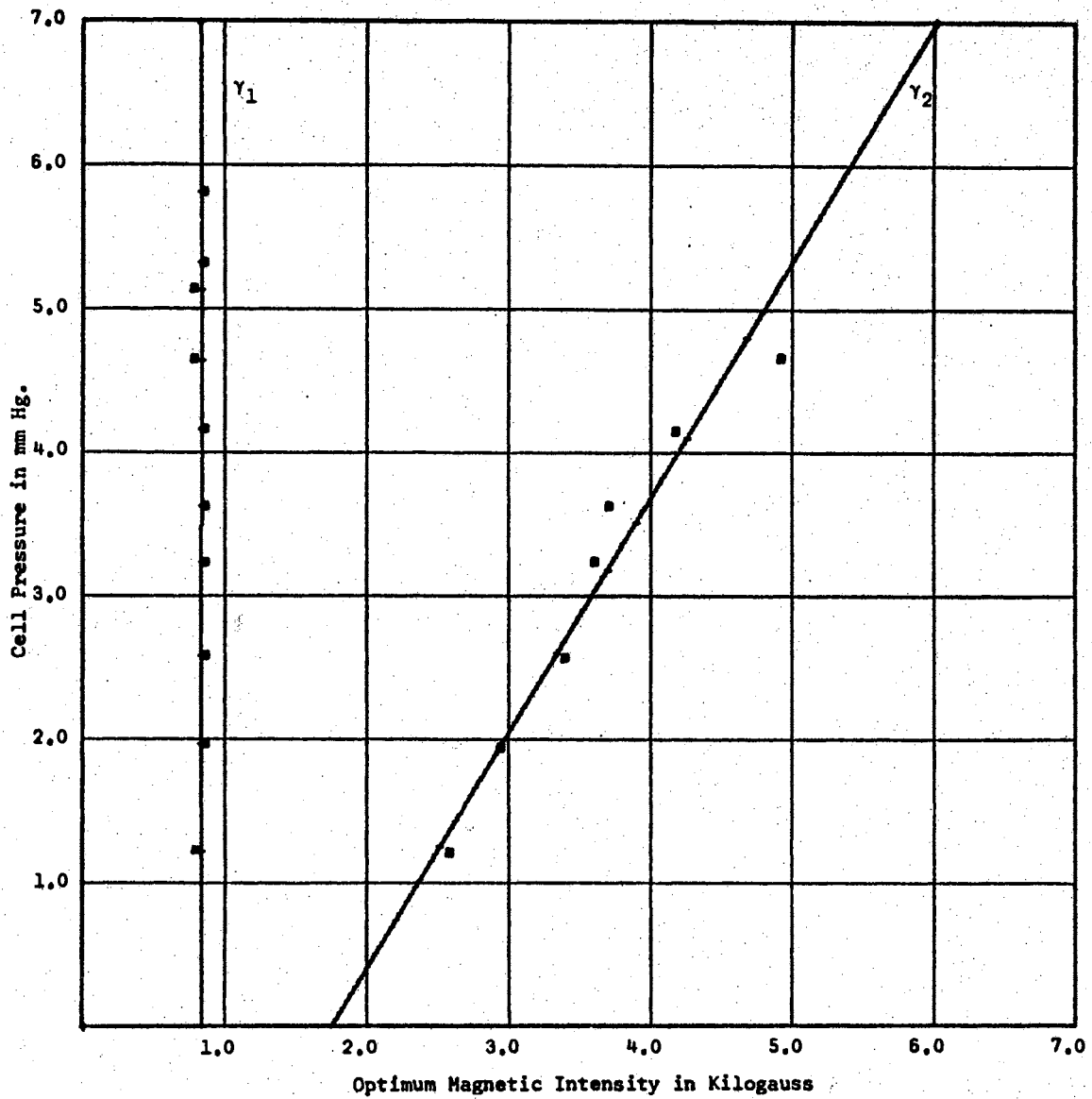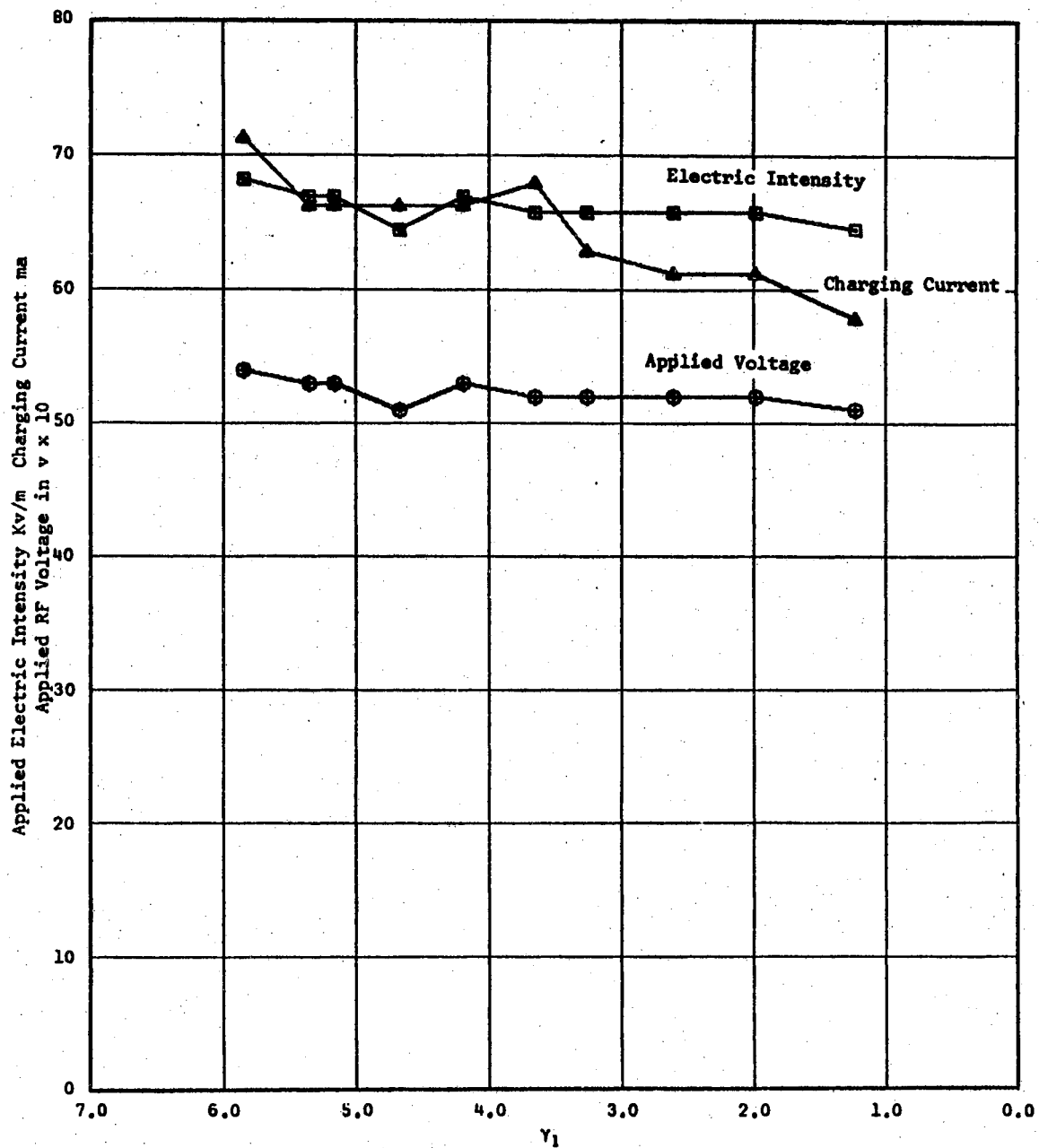
Figure 70a. Data taken August 1, 1966 at 12 MH$_z$ with the
Aluminum Cell, D = 0.002794 meters
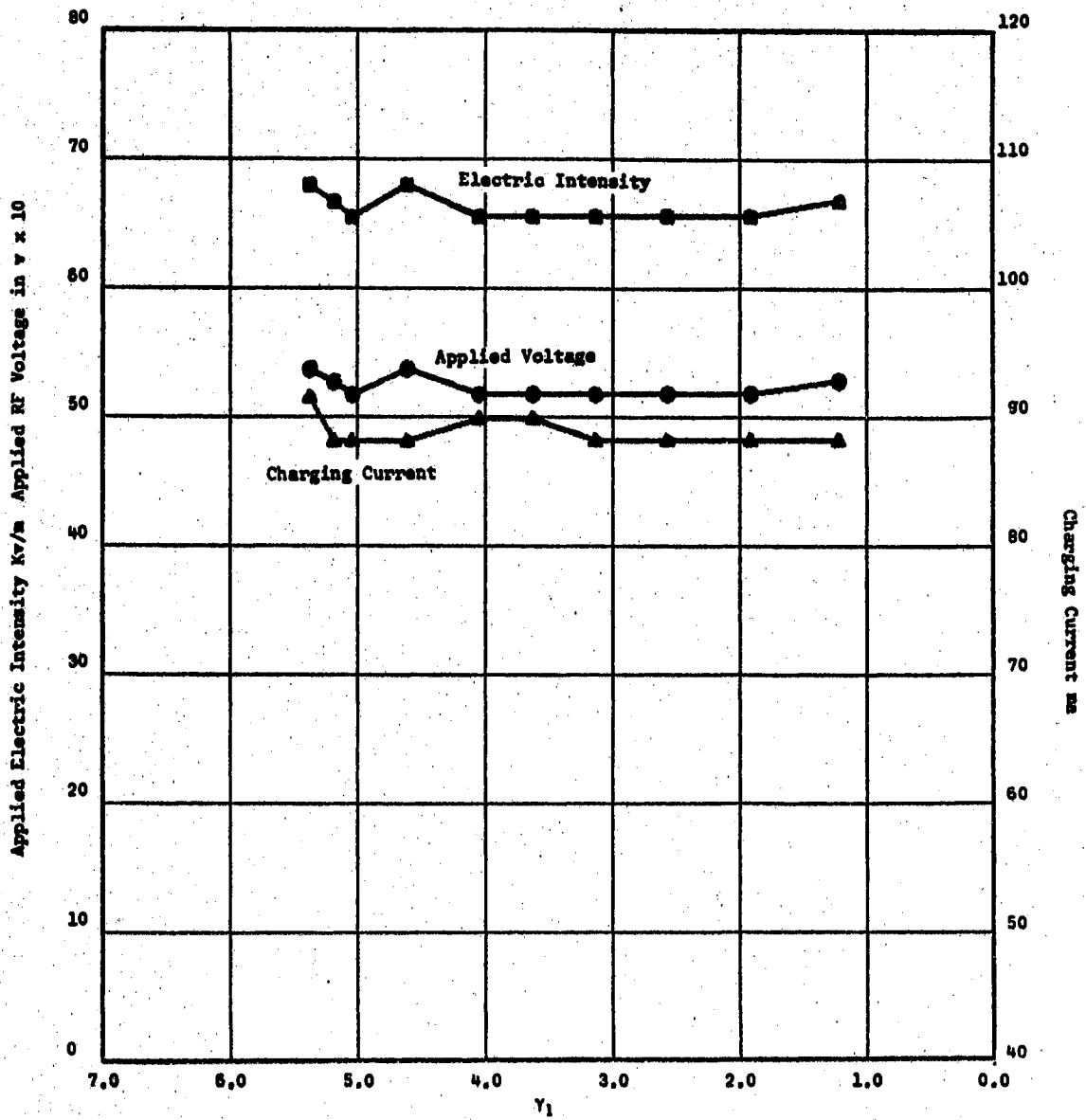
Figure 70b. Data taken August 1, 1966 at 12 MH$_z$ with the
Aluminum Cell, D = 0.002794 meters
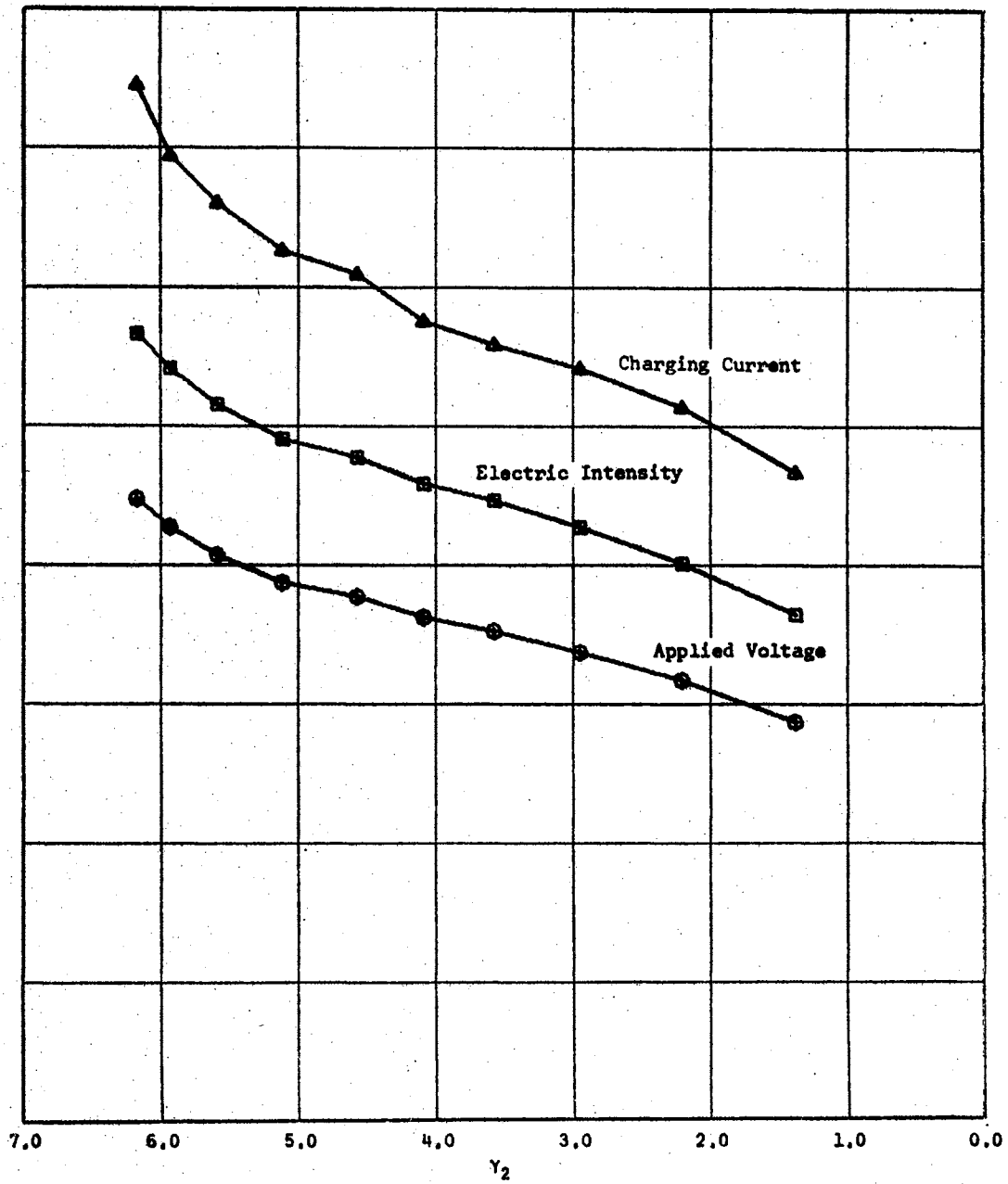
Figure 70c. Data taken August 1, 1966 at 12 MH$_z$ with the Aluminum Cell, D = 0.002794 meters
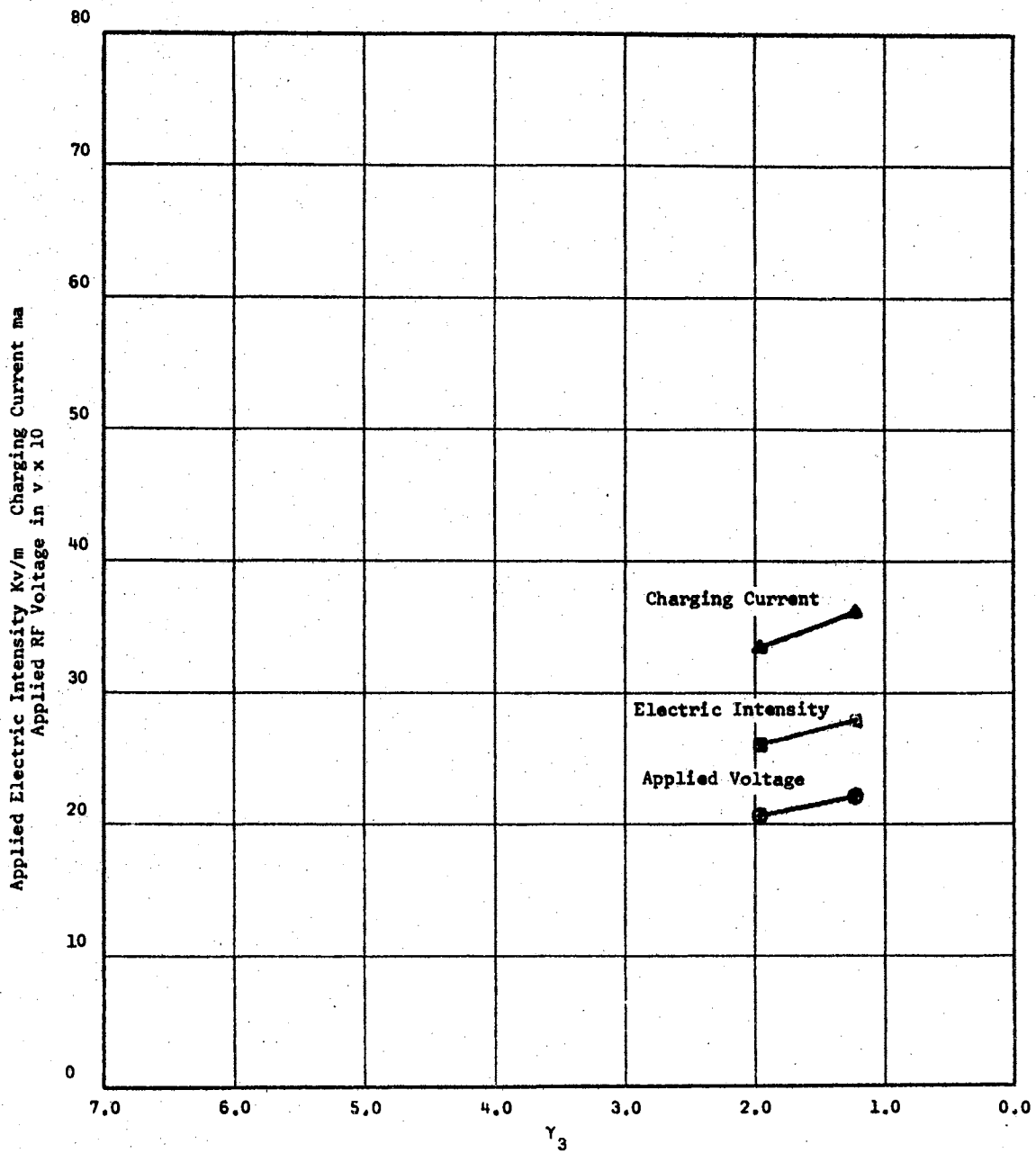
Figure 70d. Data taken August 1, 1966 at 12 MH$_z$ with the Aluminum Cell, D = 0.002794 meters
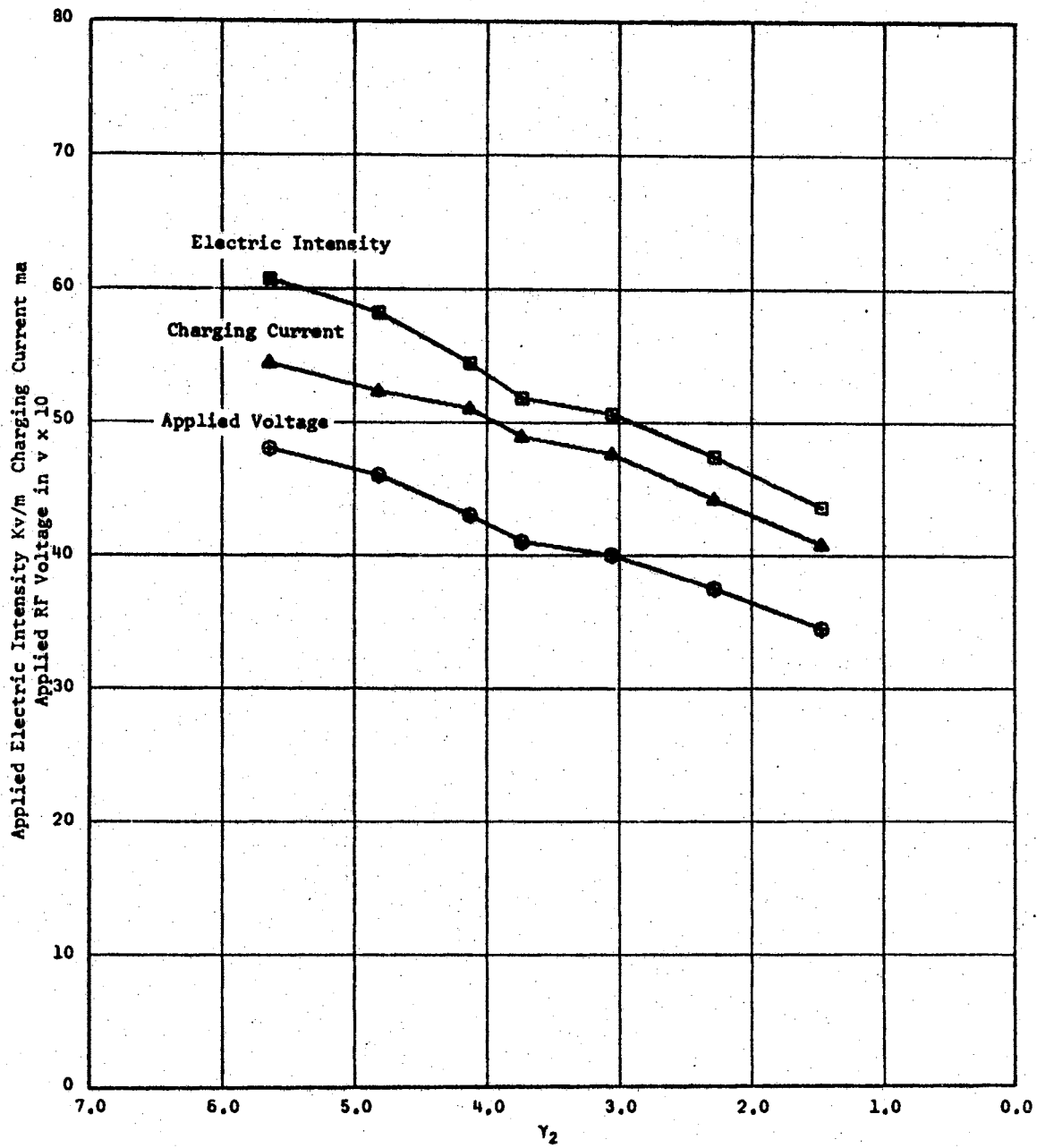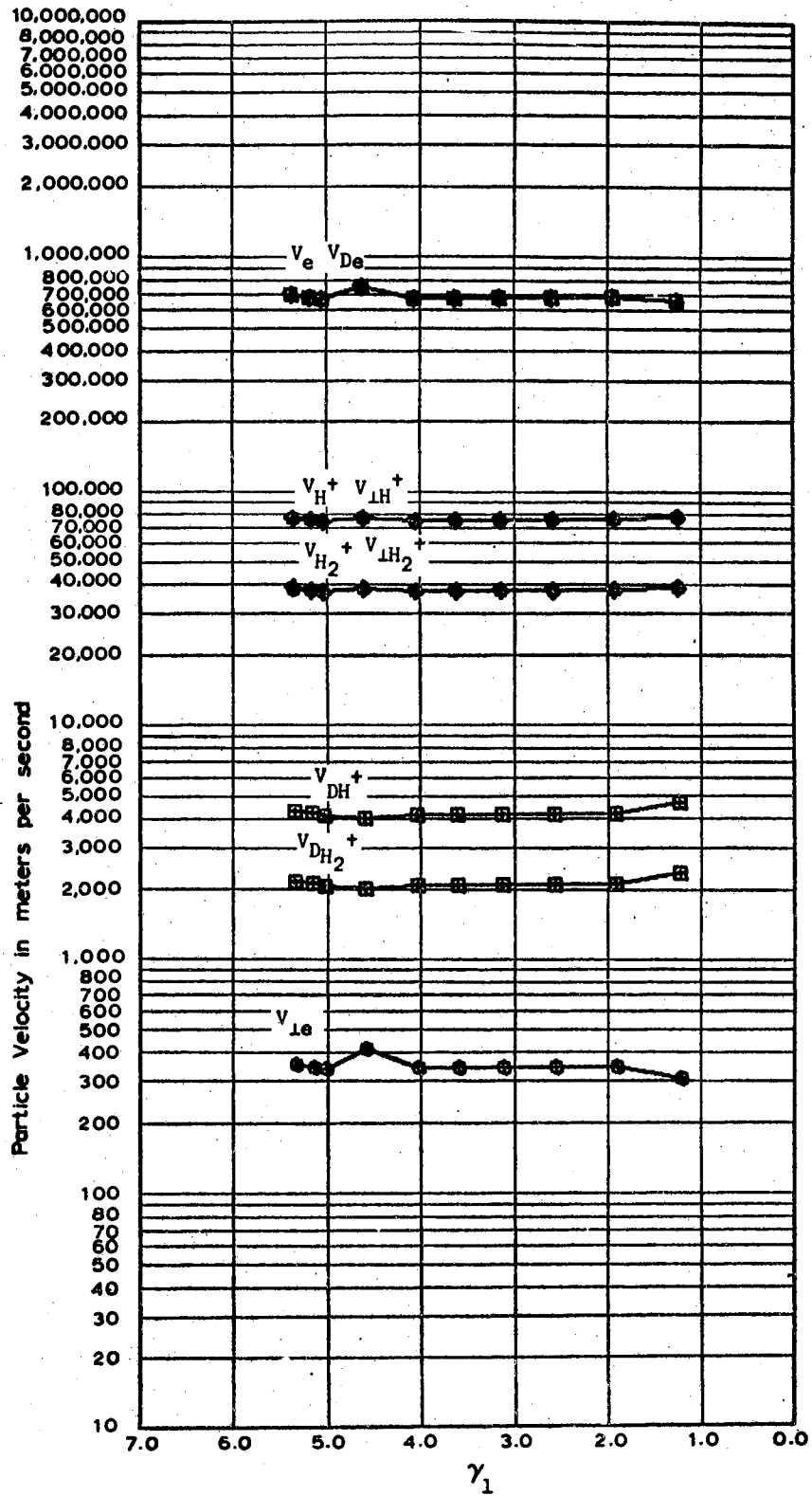
Figure 70e. Data taken August 1, 1966 at
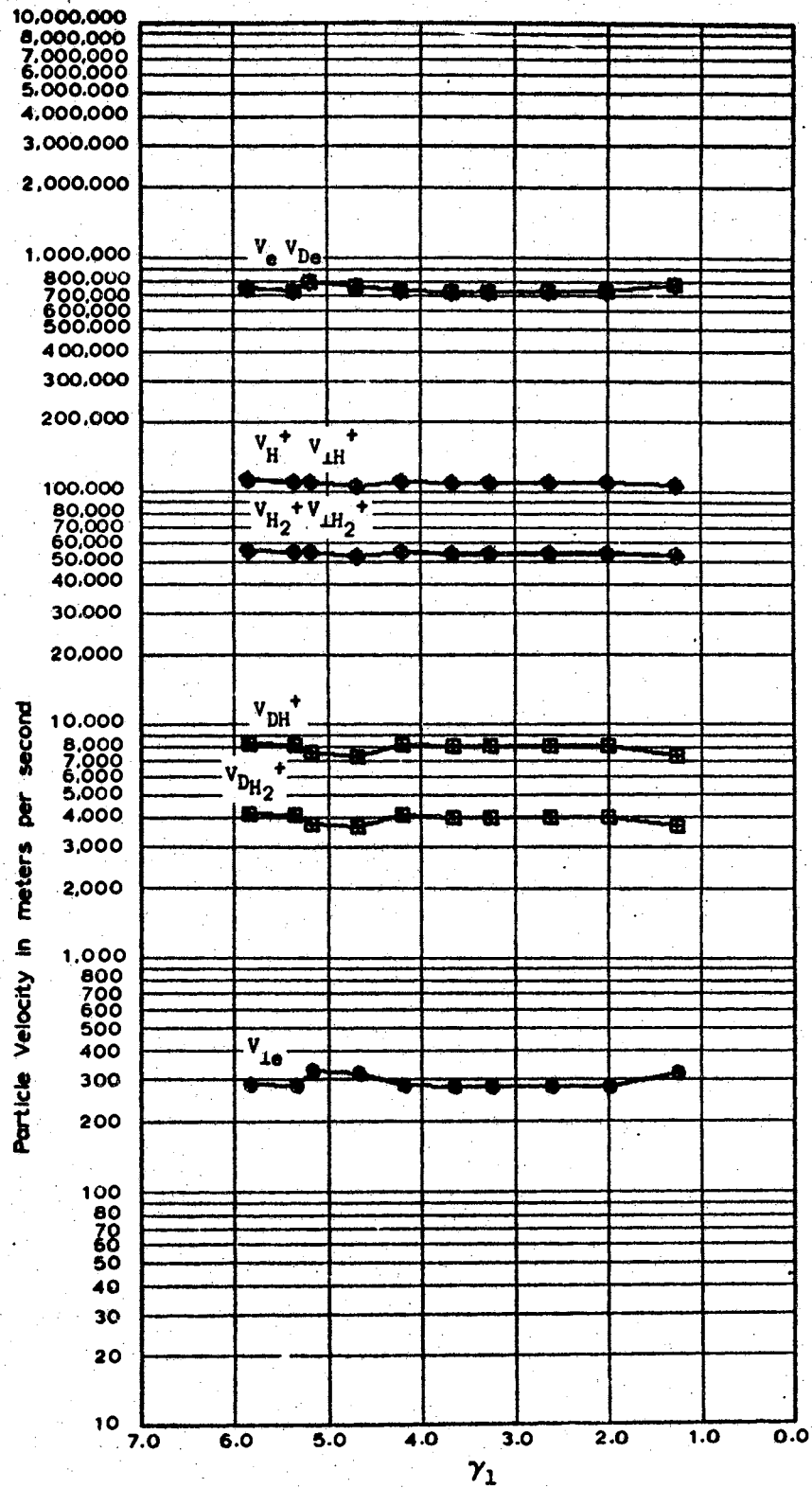12 MH_z with the Aluminum Cell,
D = 0.002794 meters

Figure 70f. Data taken August 1, 1966 at 12
MH$_Z$ with the Aluminum Cell,
D $\cong$ 0.002794 meters

Figure 70g. Data taken August 1, 1966 at 12 MH$_z$ with the Aluminum Cell, D $\cong$ 0.002794 meters
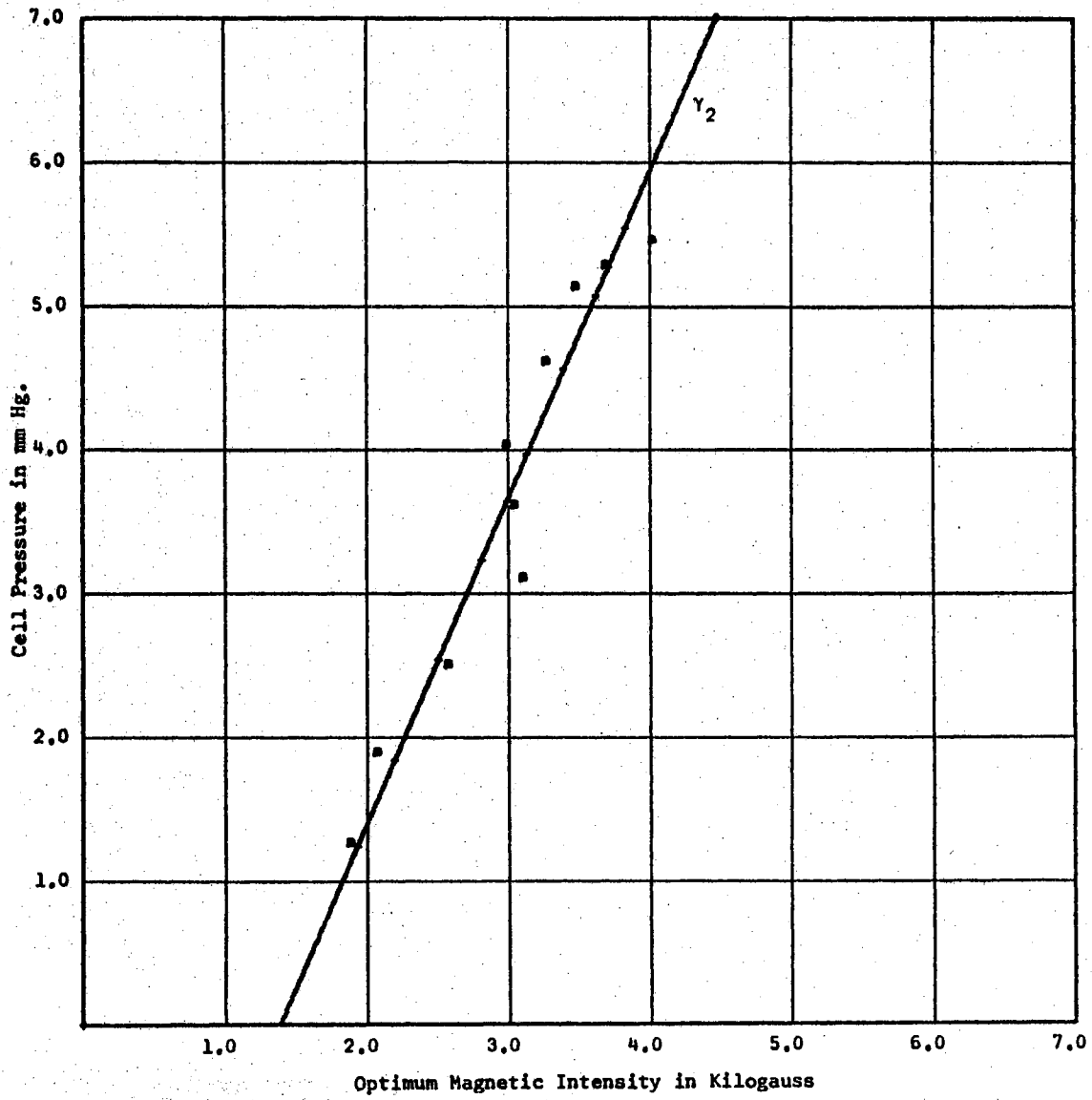
Figure 71a. Data taken July 29, 1966 at 13 MH$_z$ with the Aluminum
Cell, D = 0.002794 meters
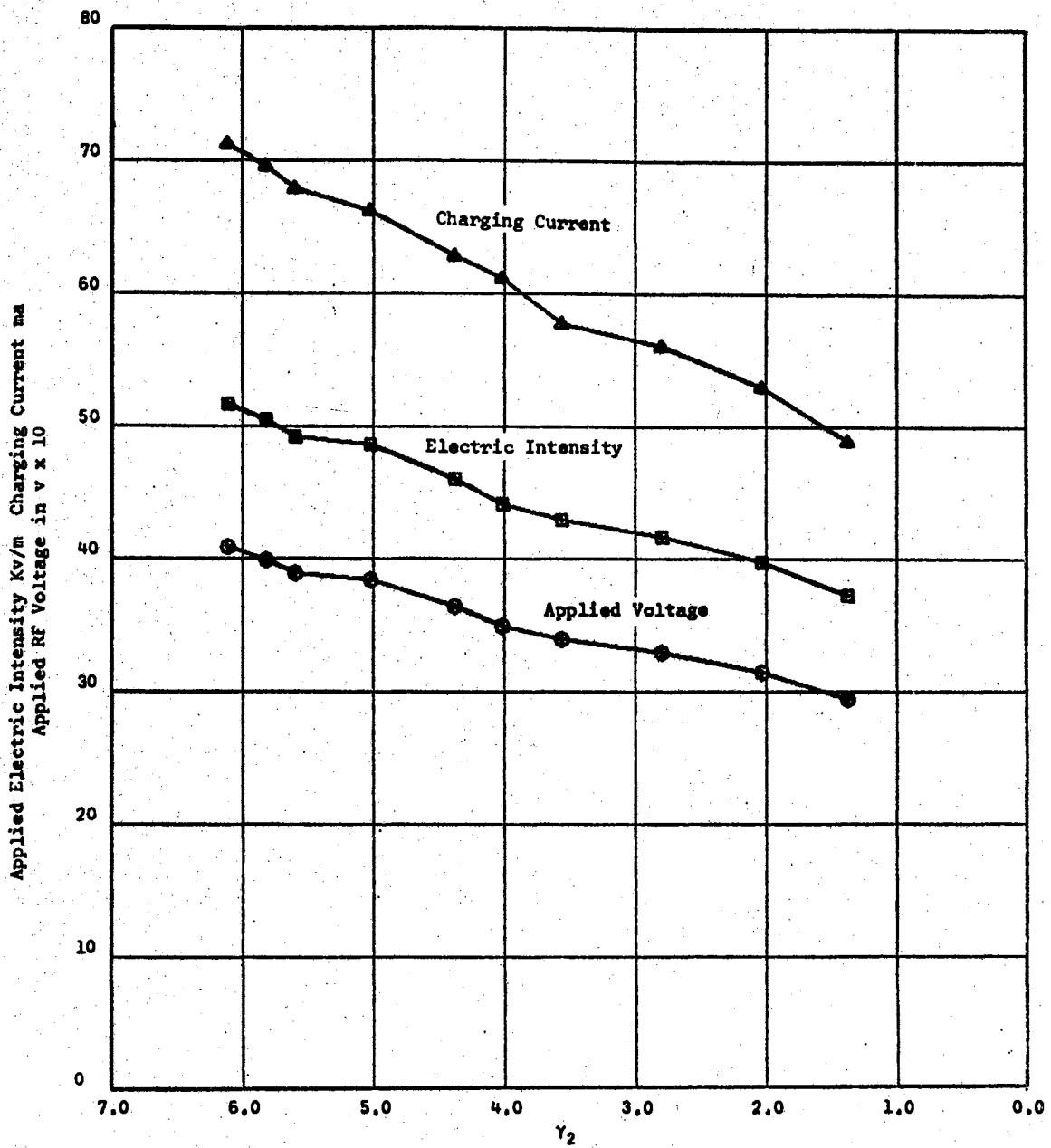
Figure 71b. Data taken July 29, 1966 at 13 MH$_z$ with the
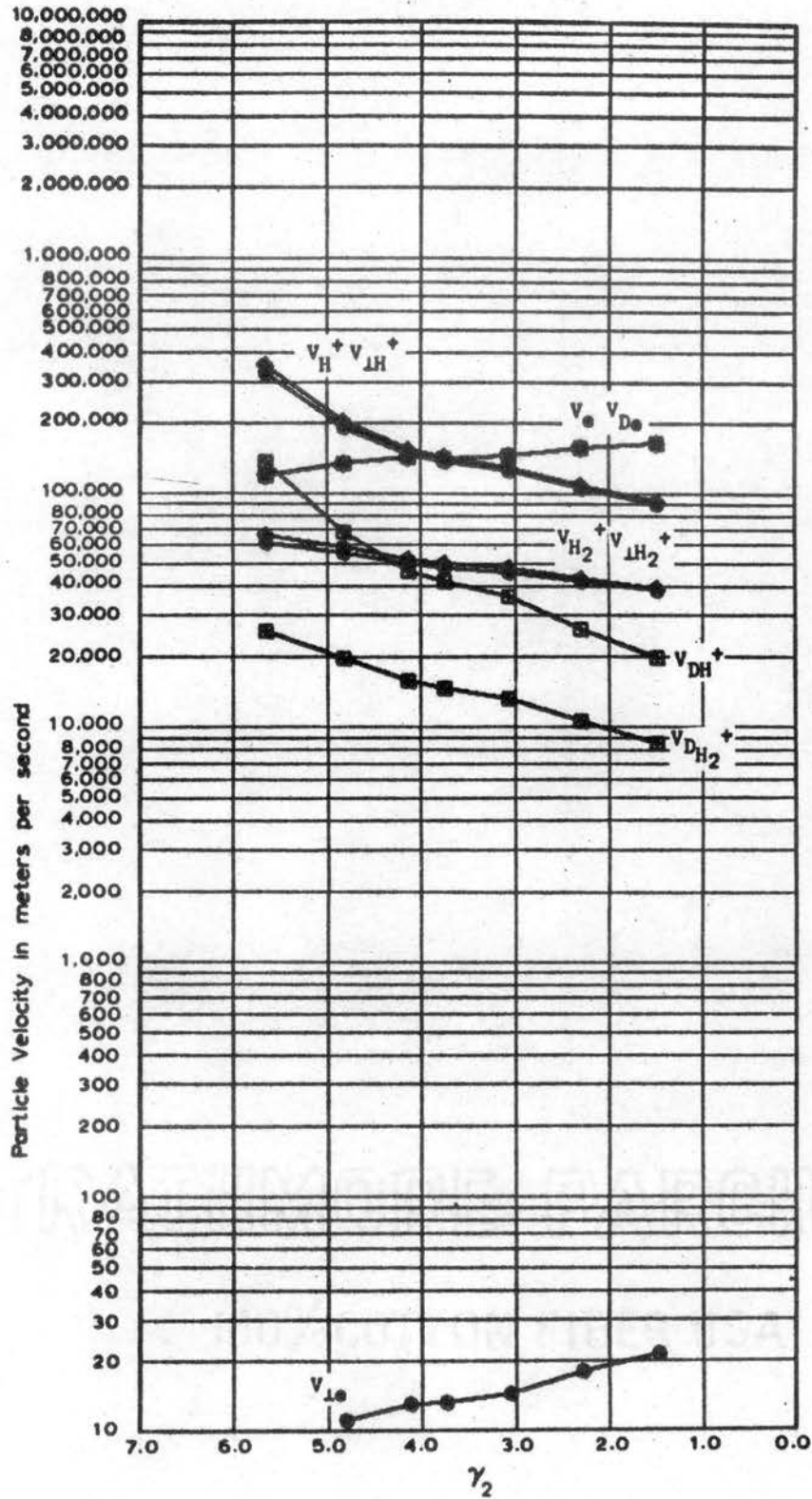Aluminum Cell, D = 0.002794 meters
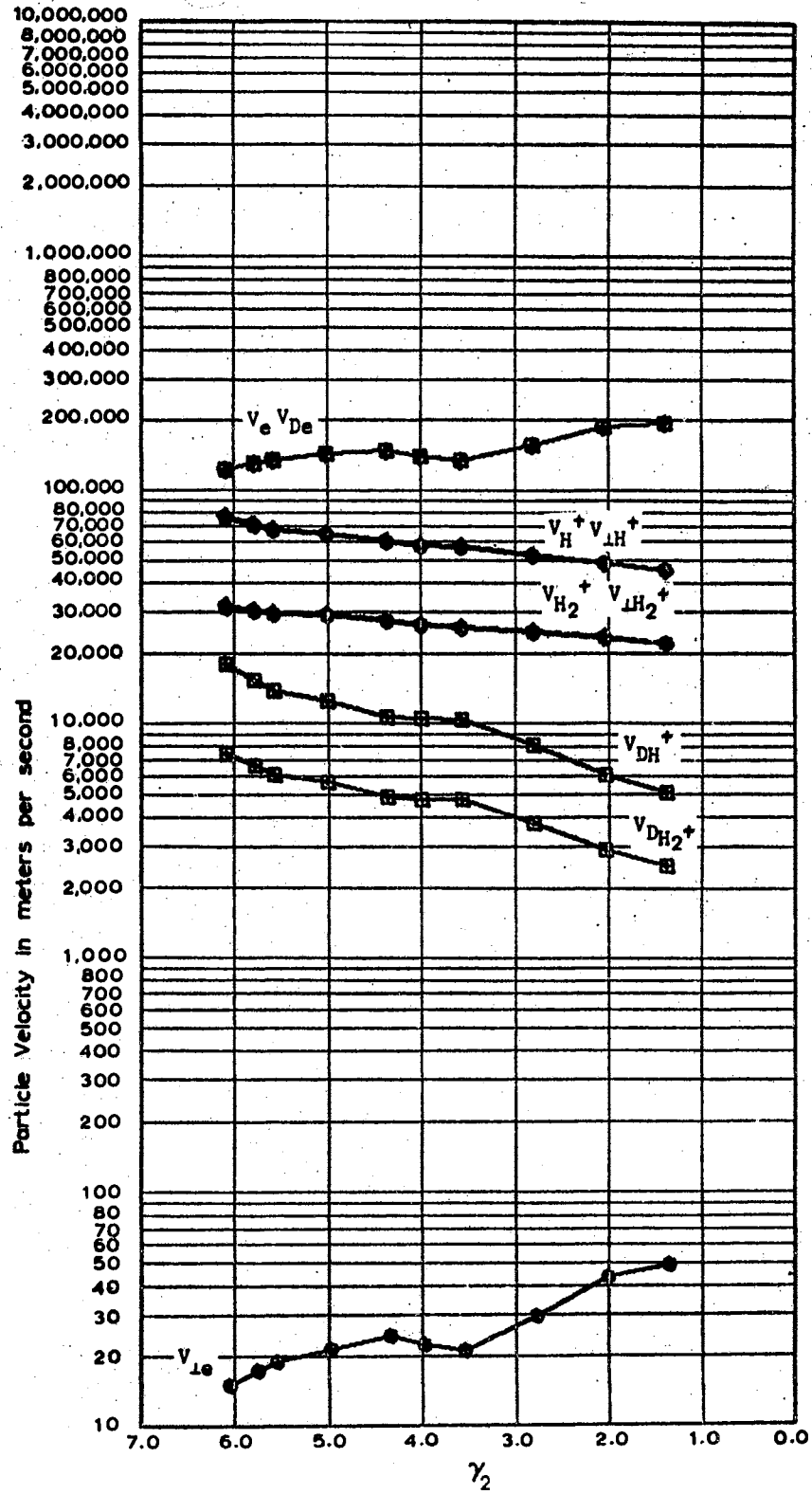
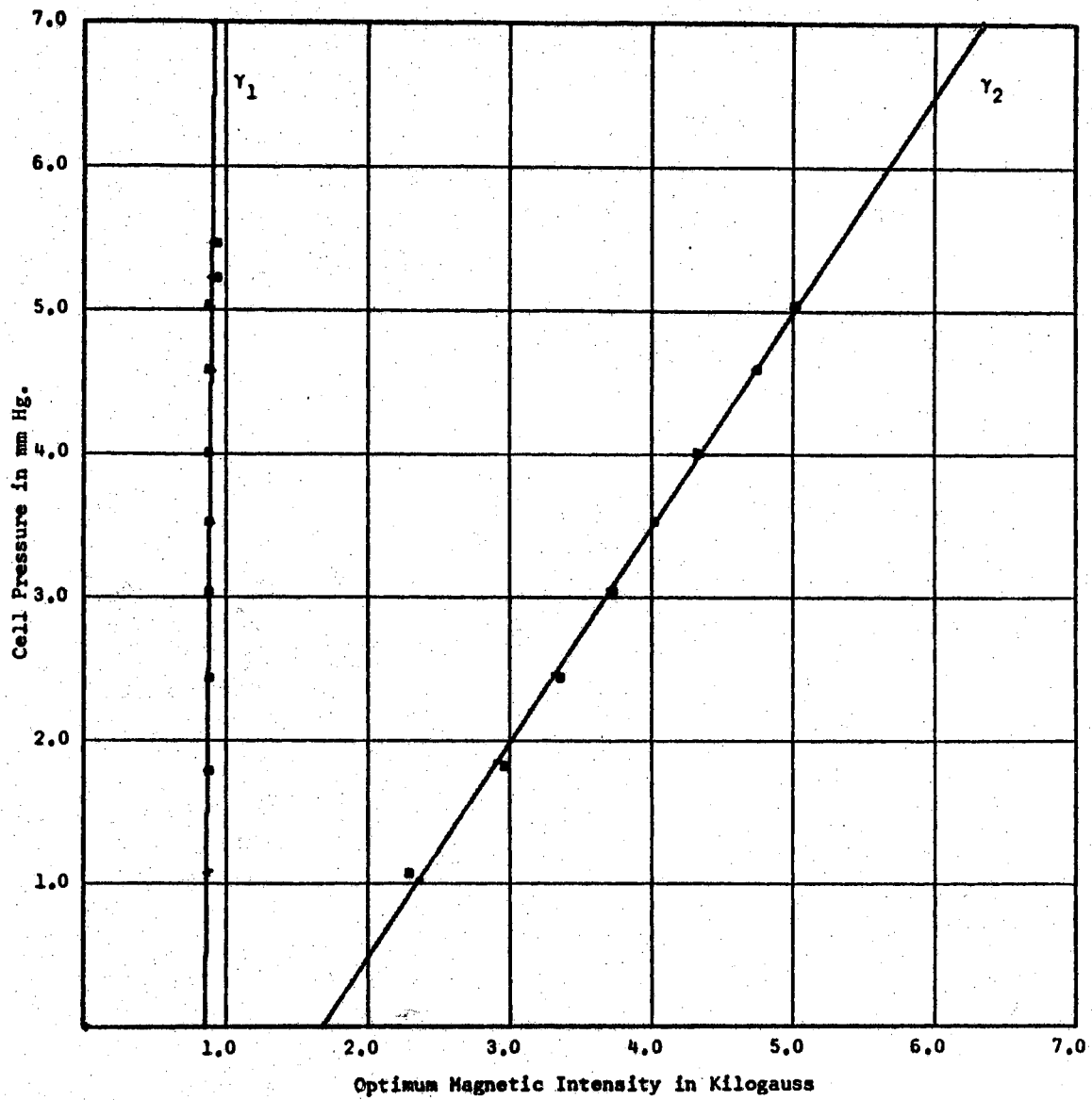Figure 71c. Data taken July 29, 1966 at 13 MH$_z$ with the Aluminum Cell, D = 0.002794 meters
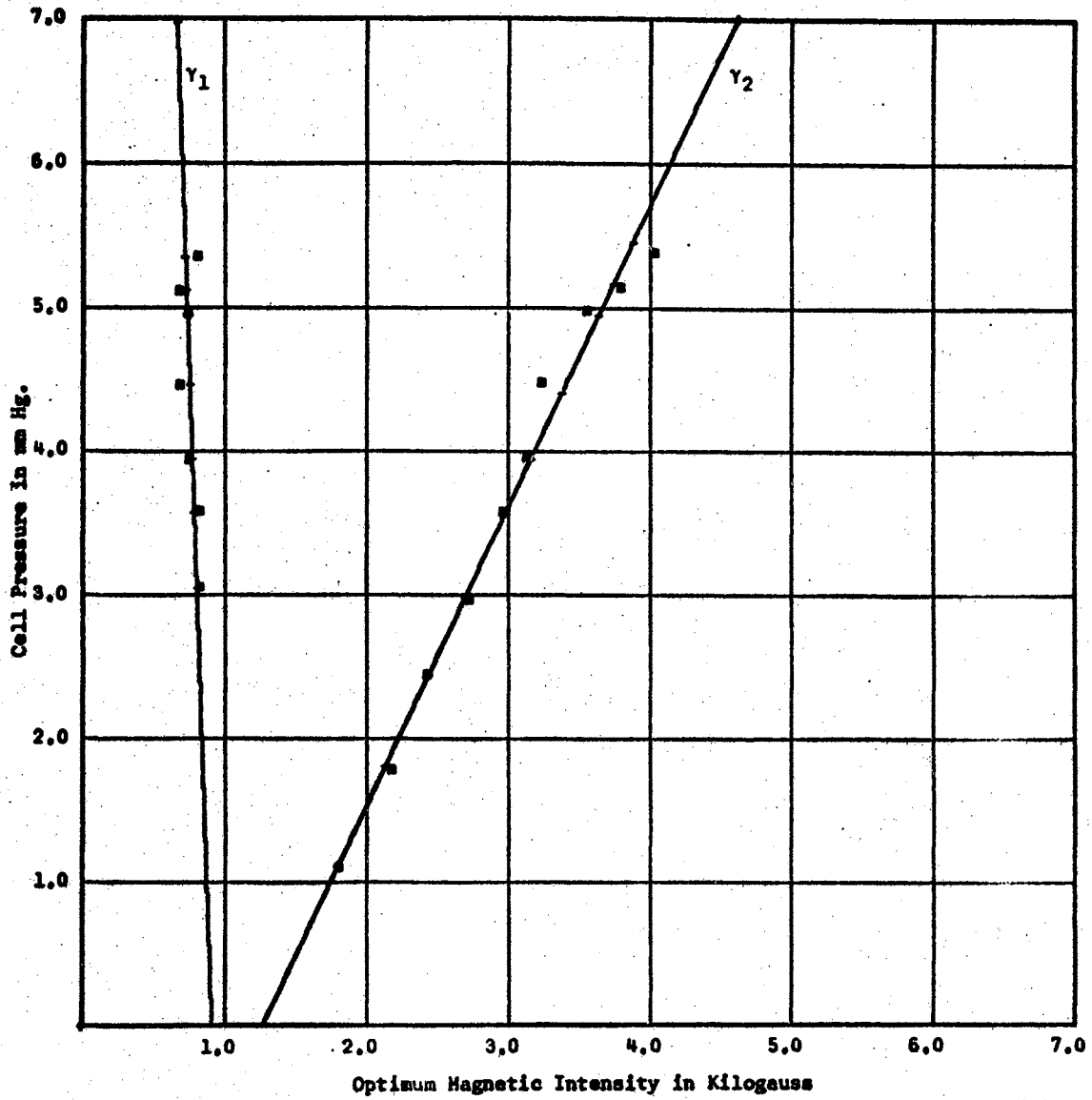
Figure 72a. Data taken August 22, 1966 at 13 MH_z with the Aluminum Cell, D = 0.002794 meters
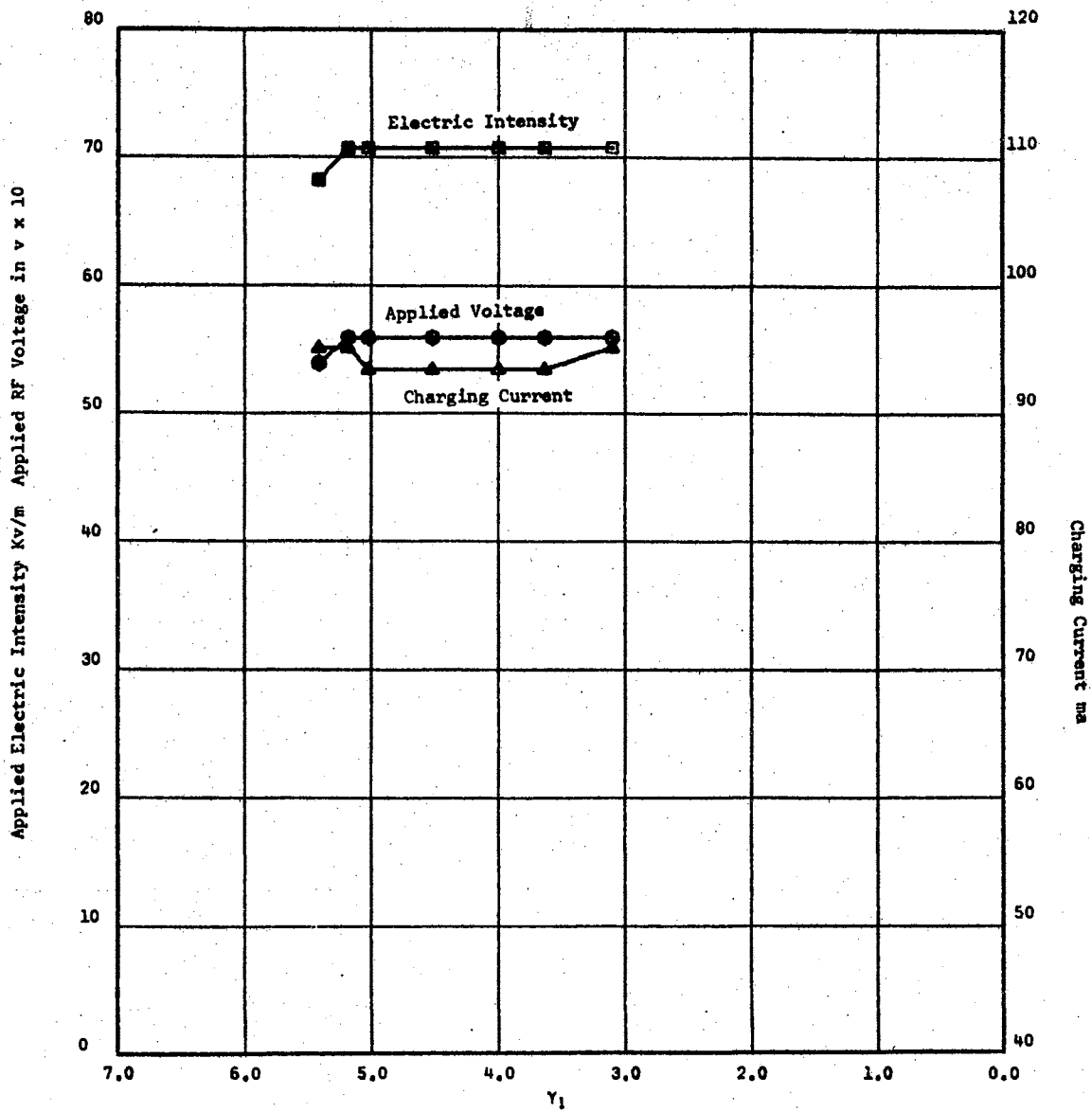
Figure 72b. Data taken August 22, 1966 at 13 MH$_z$ with the Aluminum Cell, D = 0.002794 meters
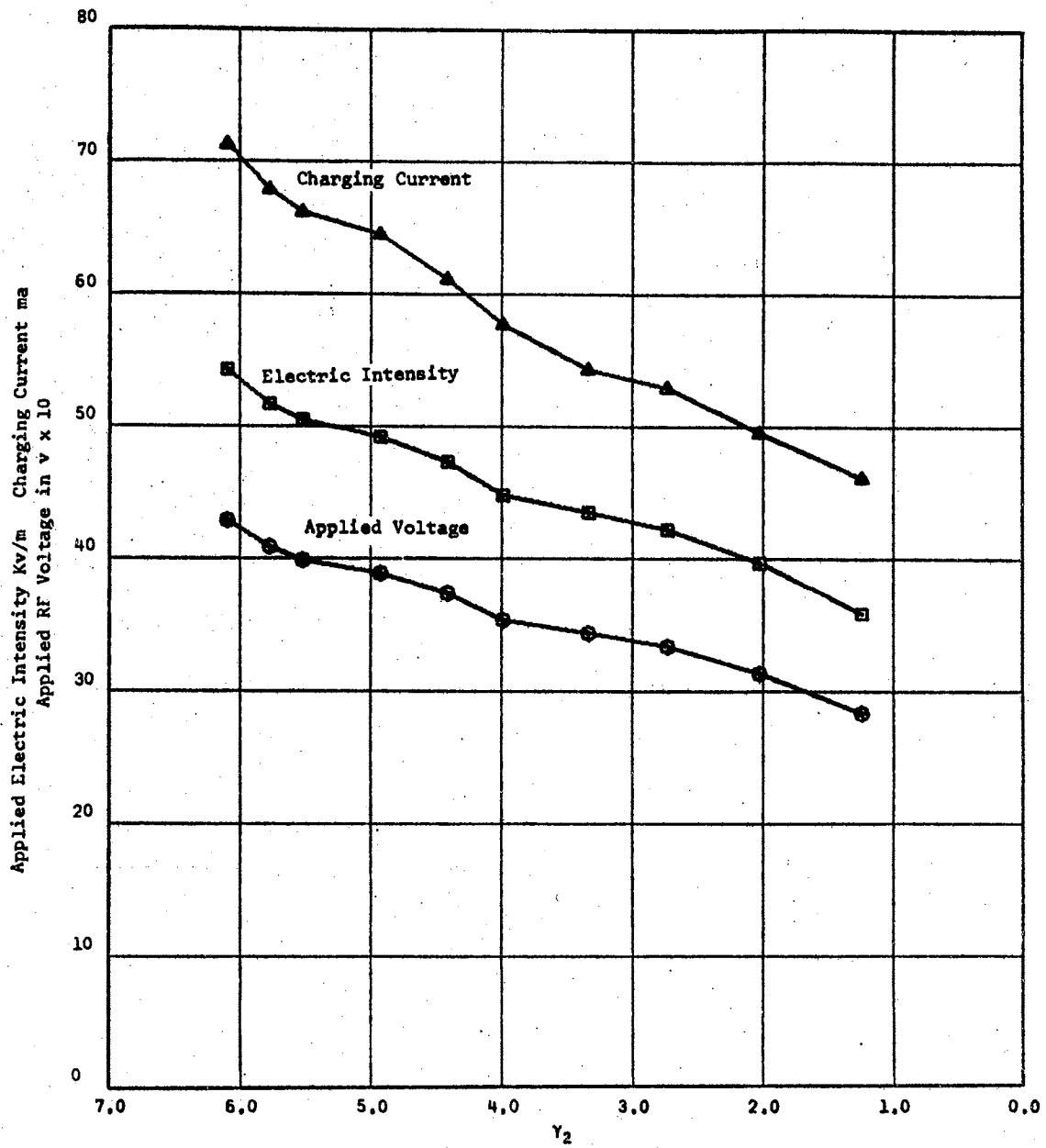
Figure 72c. Data taken August 22, 1966 at 13 MH$_z$ with the Aluminum Cell, D = 0.002794 meters
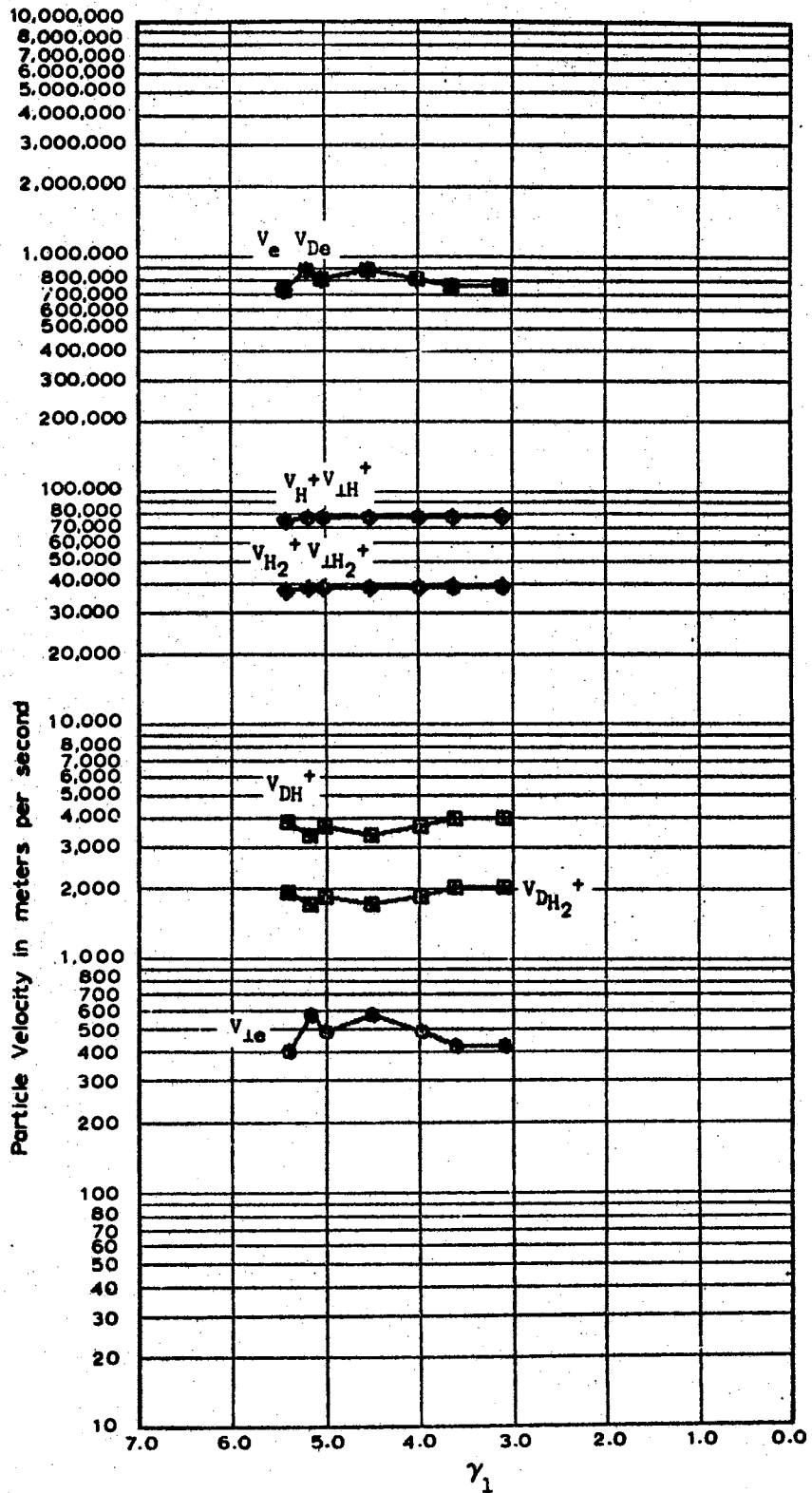
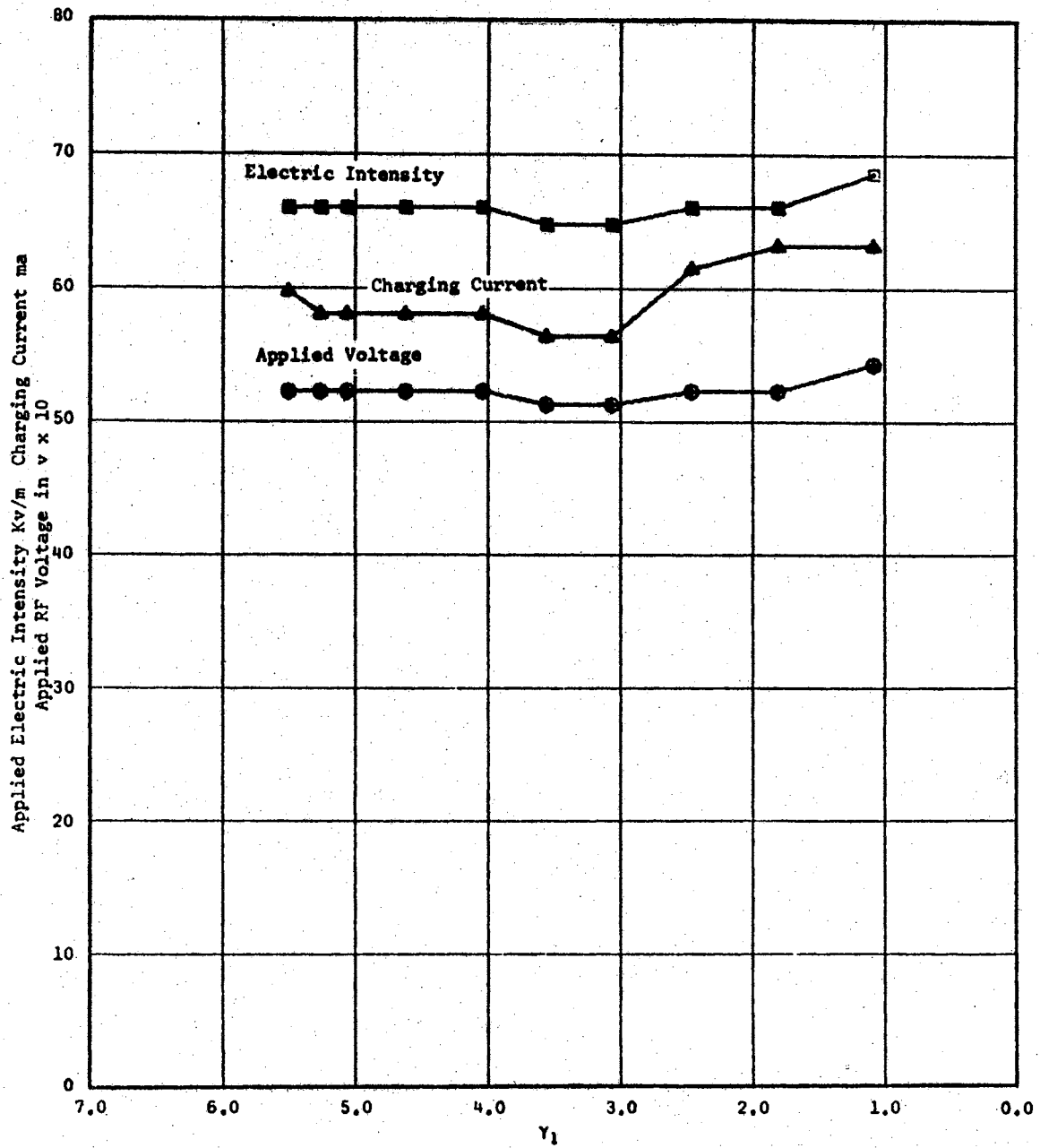Figure 72d. Data taken August 22, 1966 at 13 MH_z with the Aluminum Cell, D = 0.002794 meters
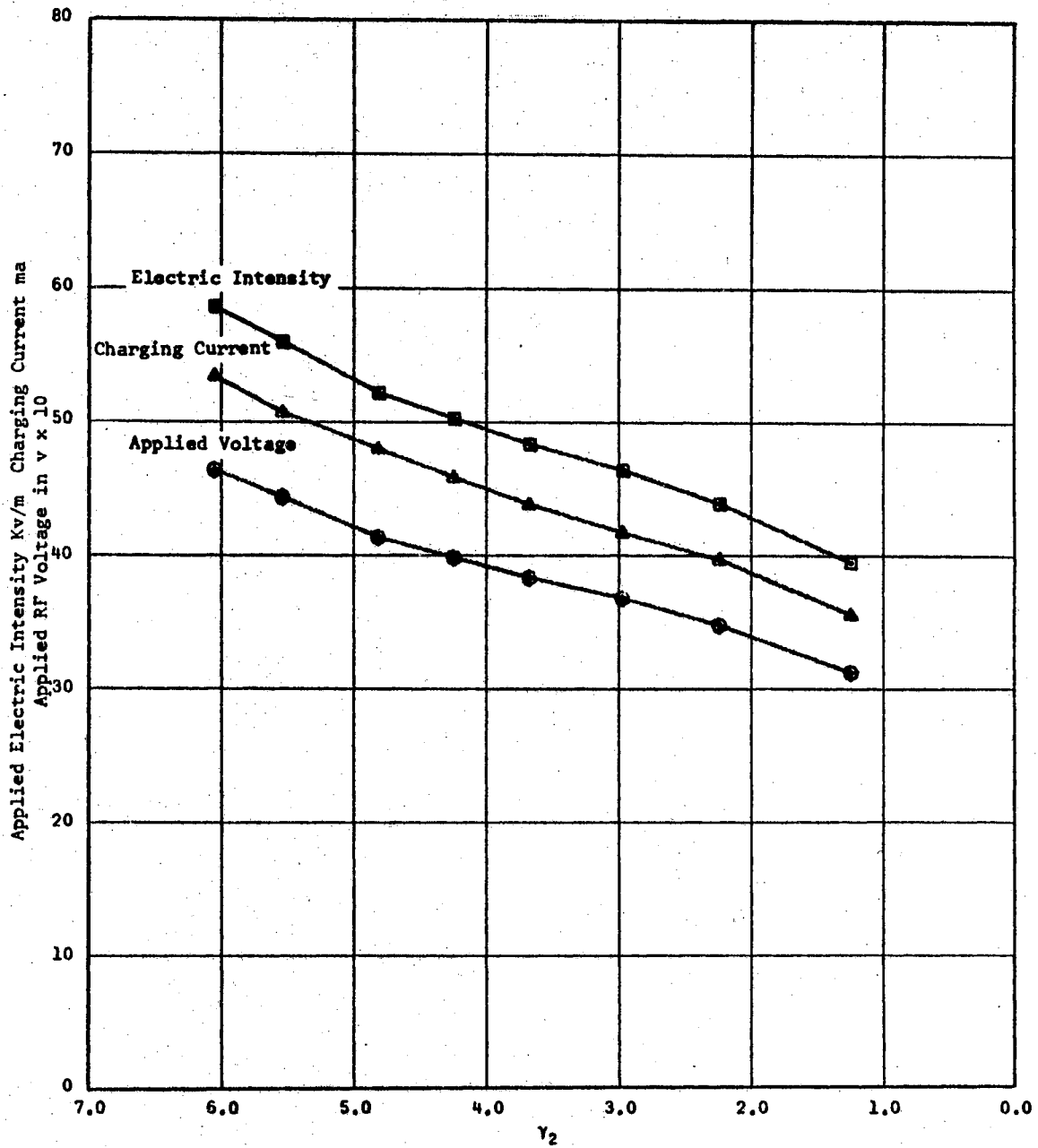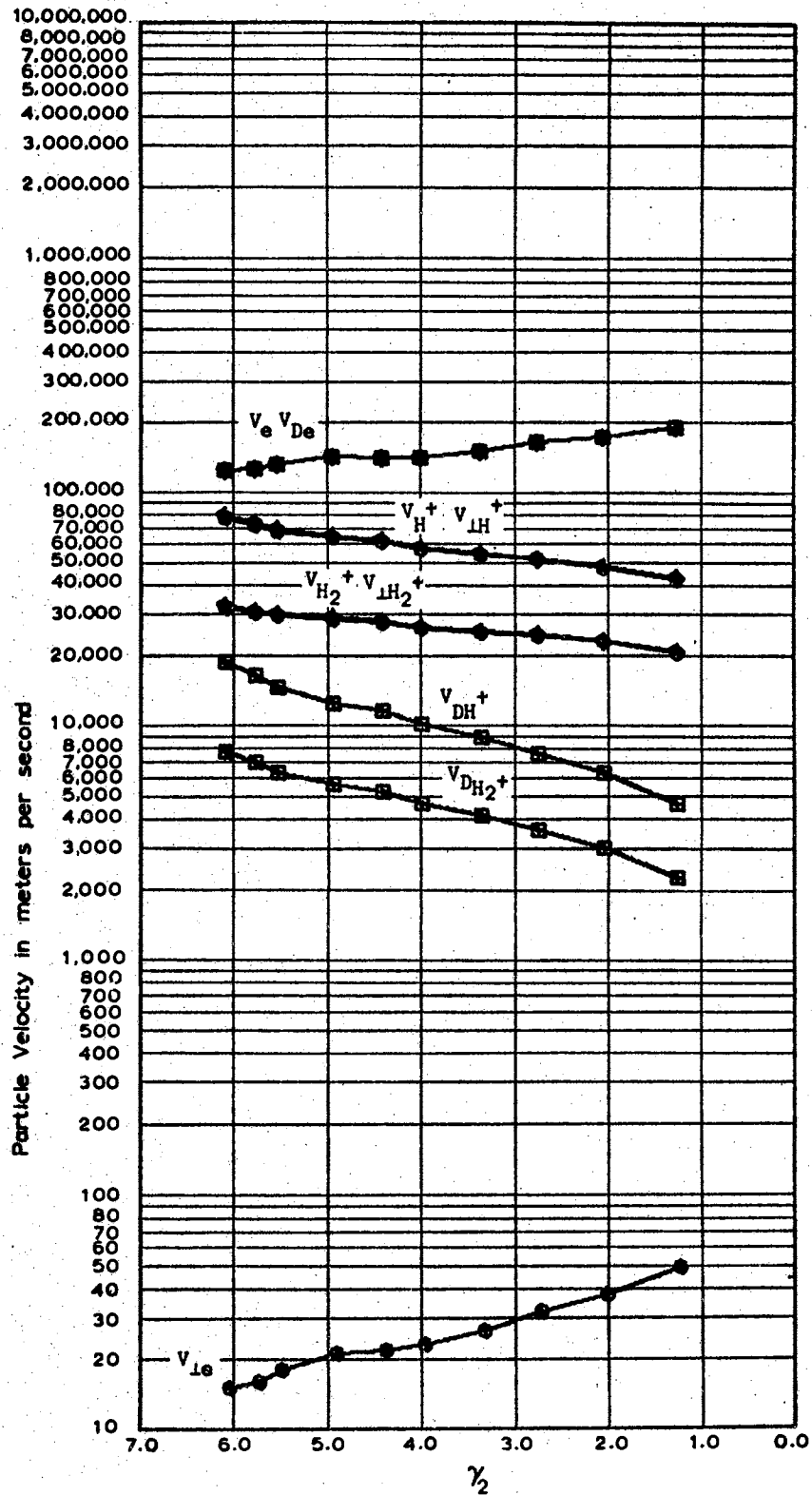
Figure 72e. Data taken August 22, 1966 at 13 MH$_z$ with the Aluminum Cell, D = 0.002794 meters
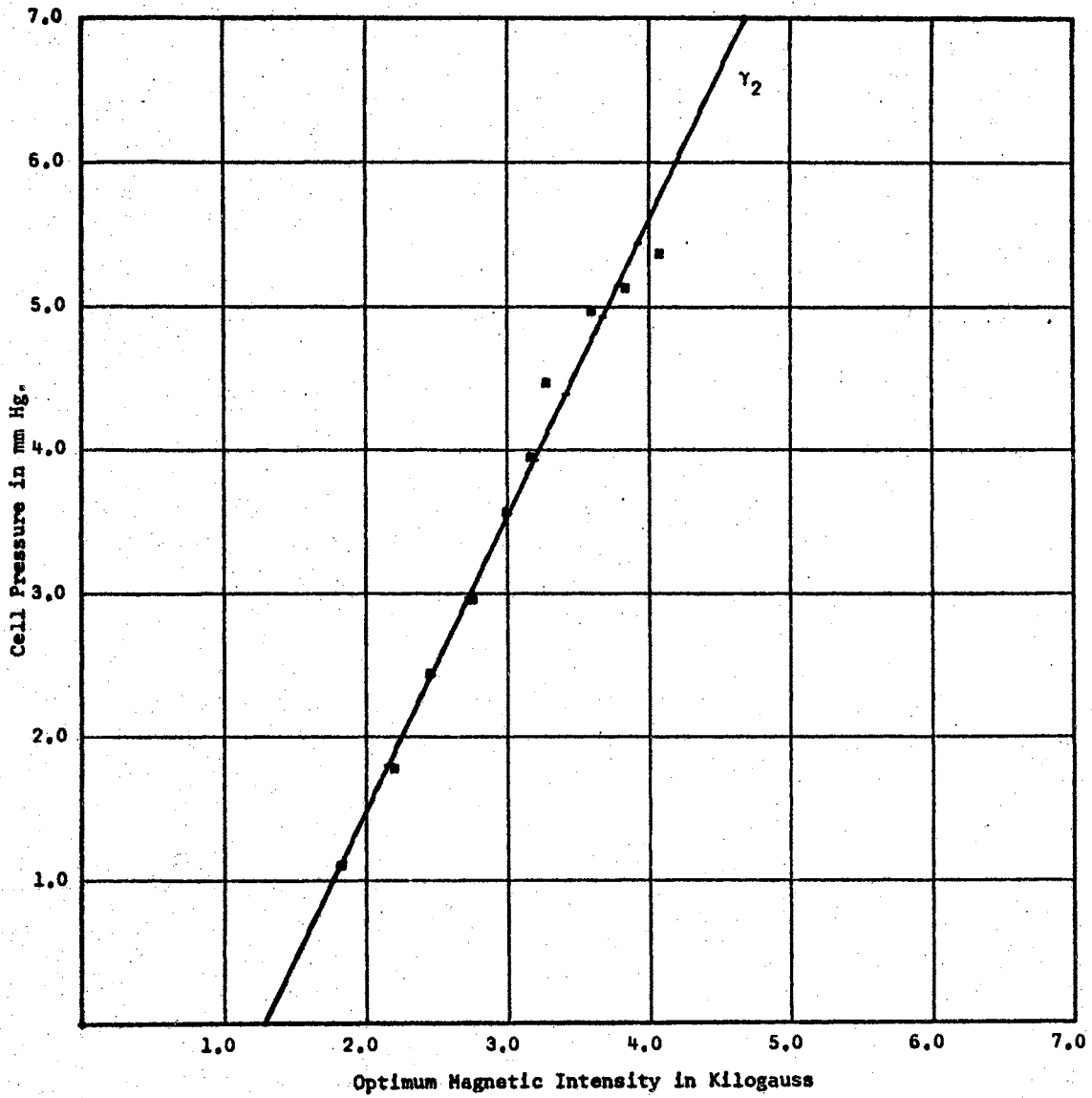
Figure 73a. Data taken August 22, 1966 at 13 MH_z with the Aluminum Cell, D = 0.002794 meters
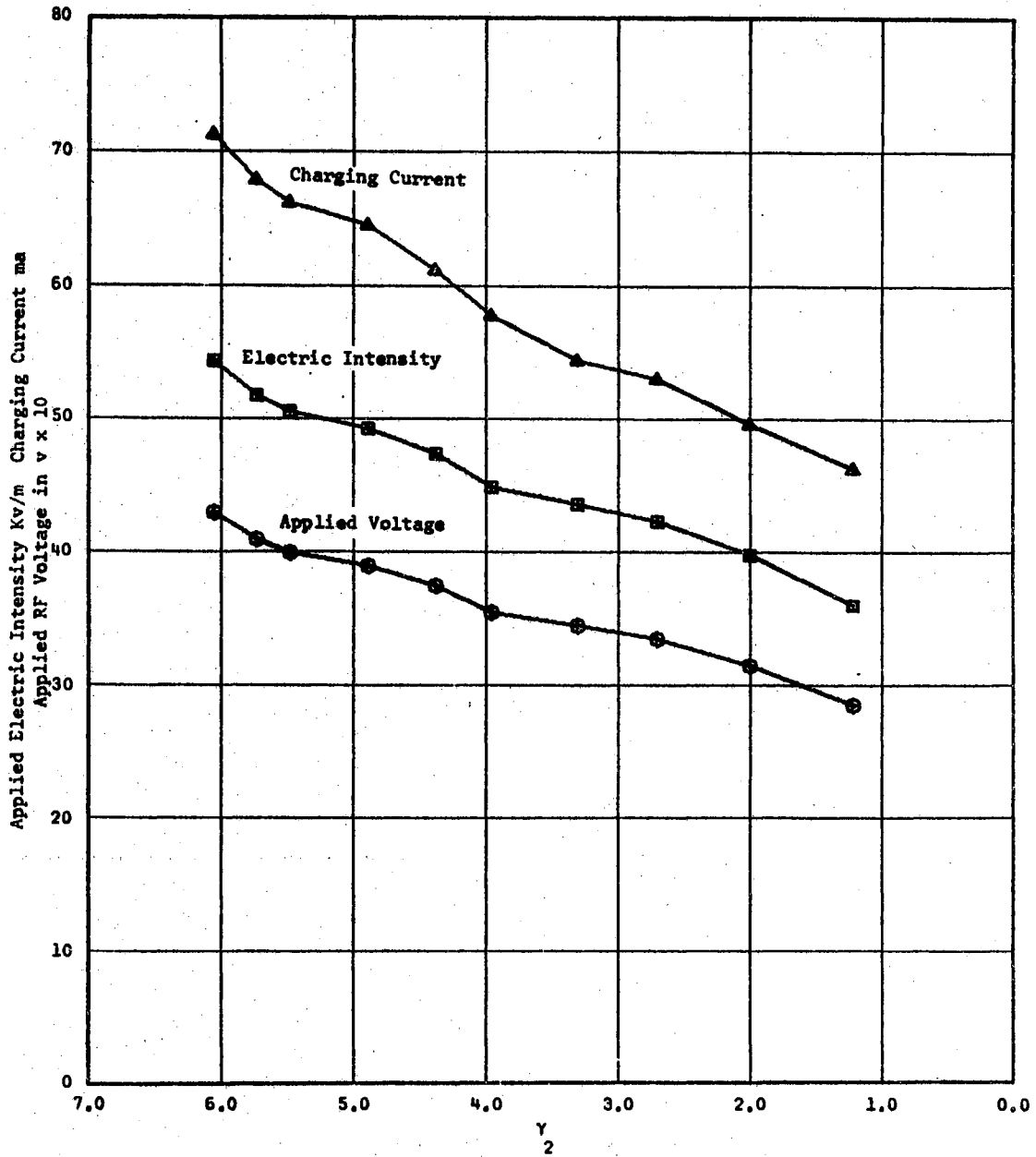
Figure 73b. Data taken August 22, 1966 at 13 MH$_z$ with the
Aluminum Cell, D = 0.002794 meters
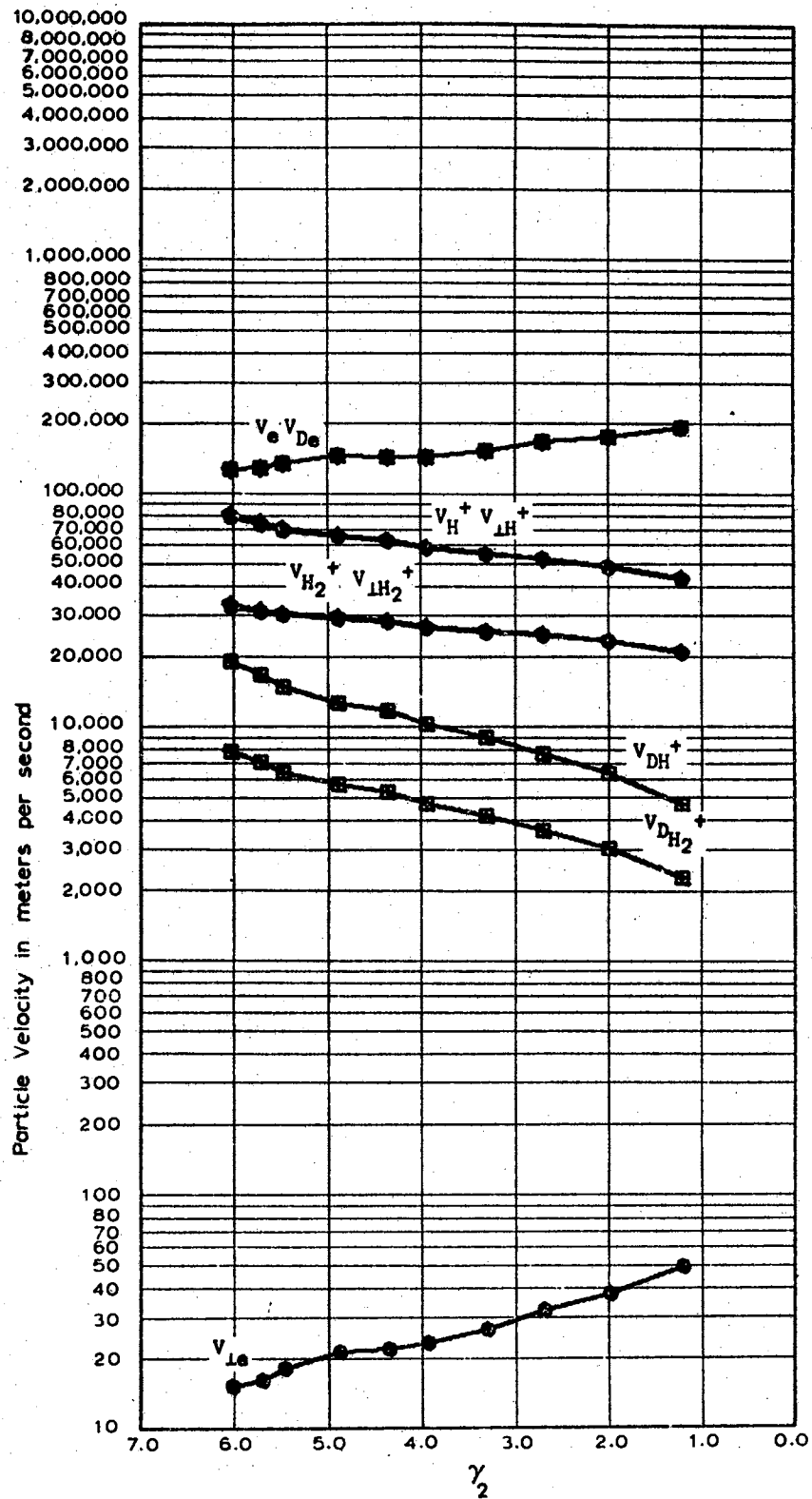
Figure 73c. Data taken August 22, 1966 at 13
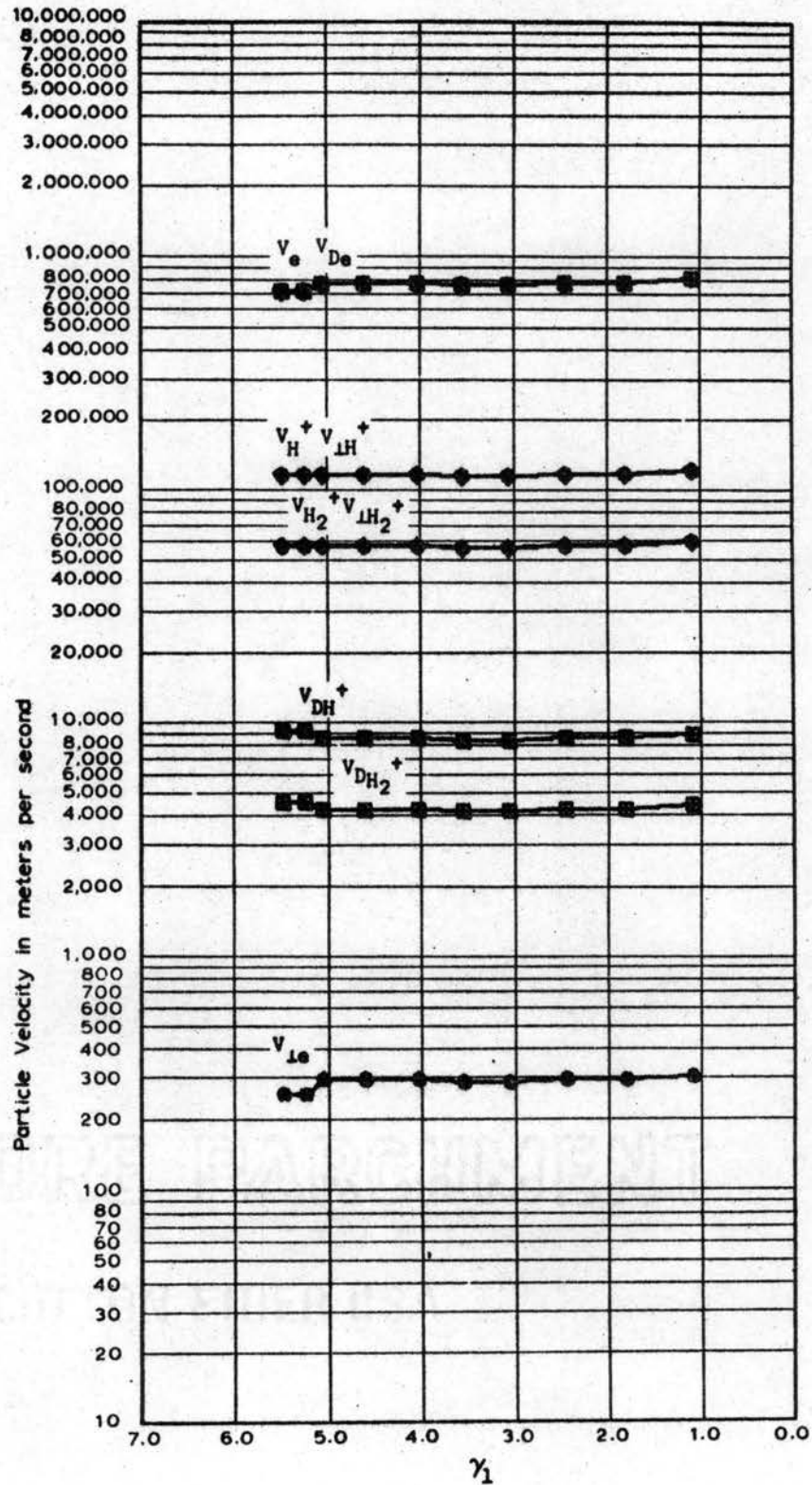MH with the Aluminum Cell,
D ≅ 0.002794 meters
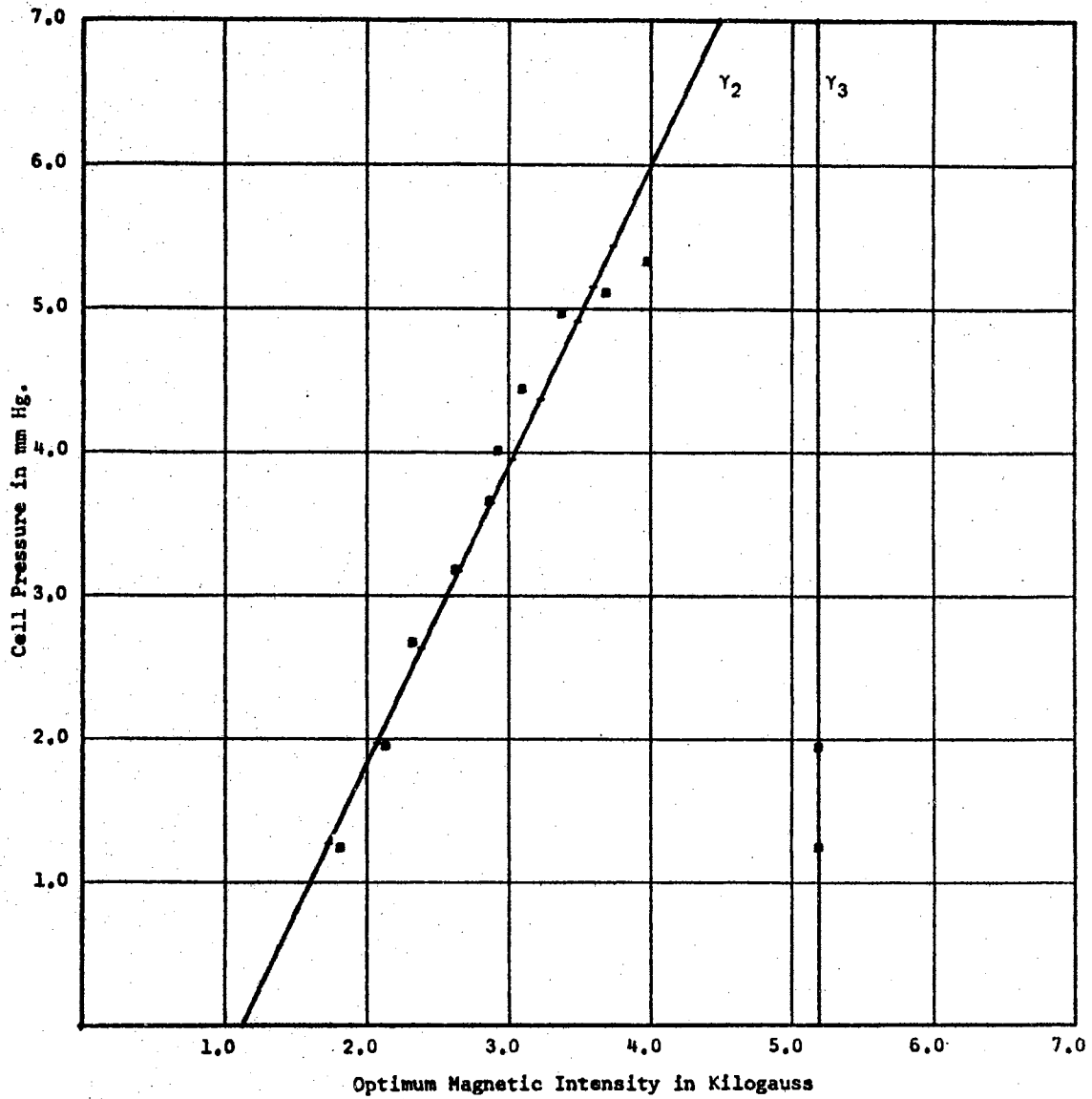
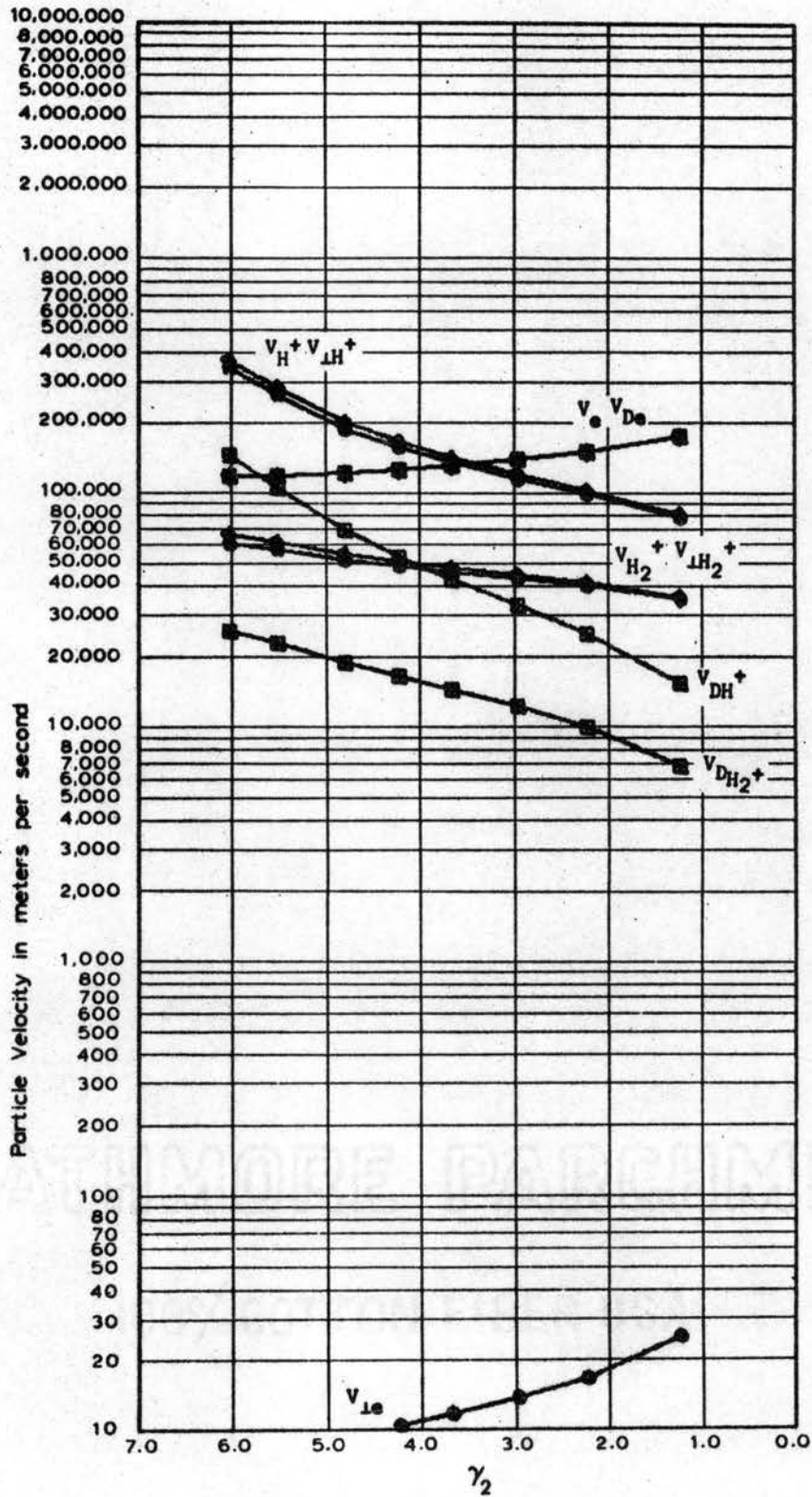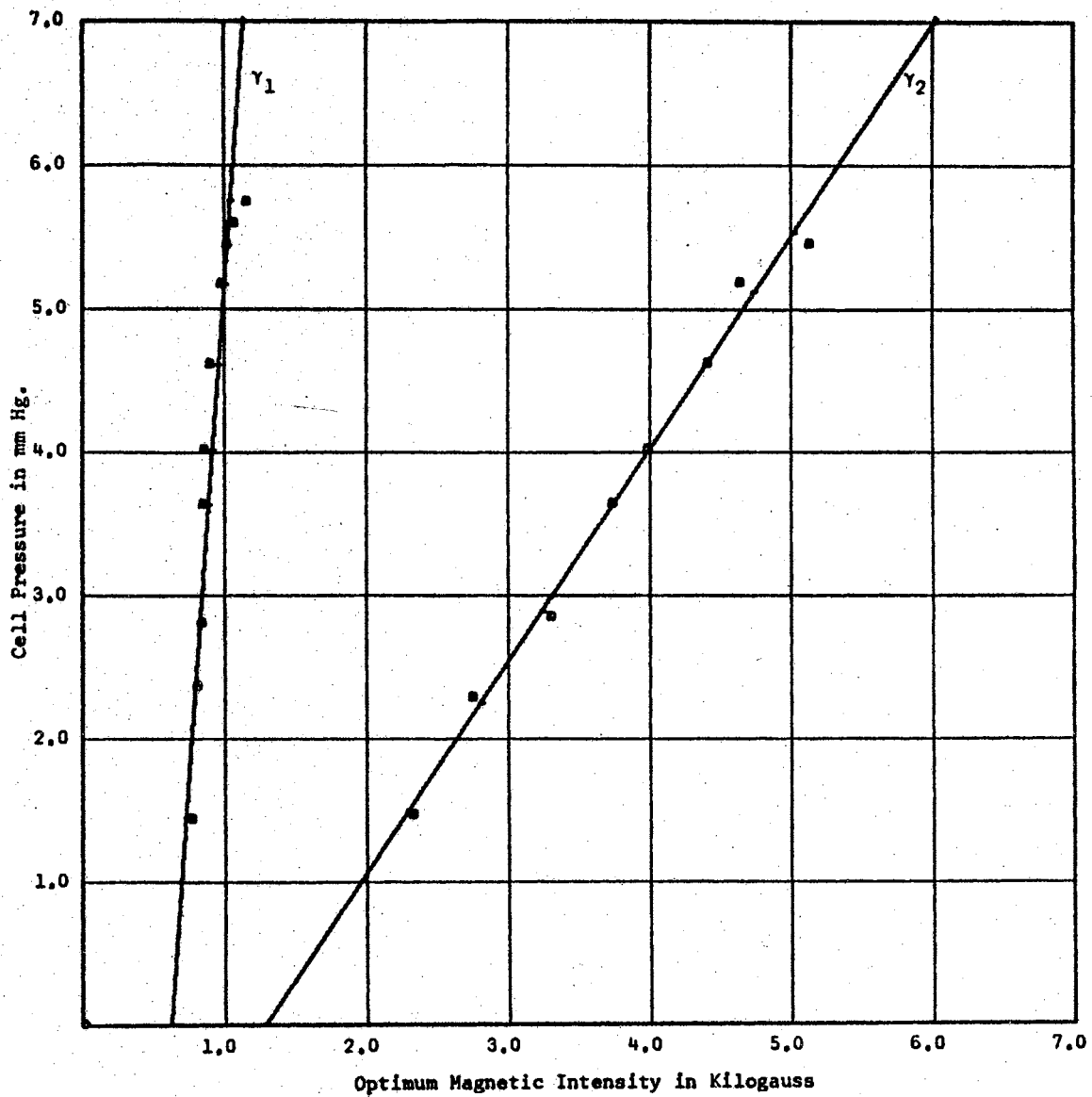Figure 74a. Data taken August 8, 1966 at 14 MH_z with the Aluminum Cell, D = 0.002794 meters
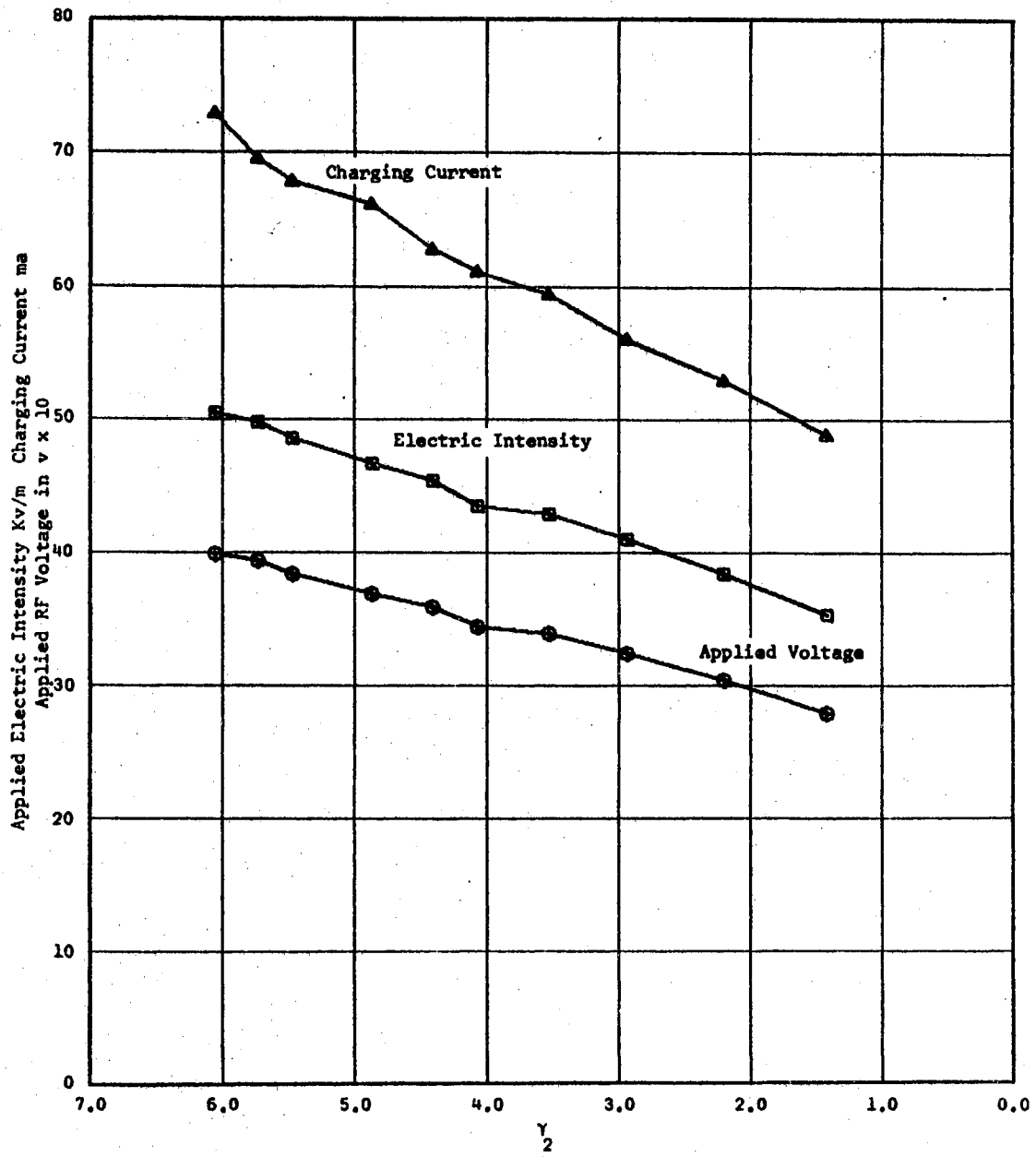
Figure 74b. Data taken August 8, 1966 at 14 MH$_z$ with the
Aluminum Cell, D = 0.002794 meters

Figure 74ε. Data taken August 18, 1966 at 14 MH$_z$ with the
Aluminum Cell, D = 0.002794 meters
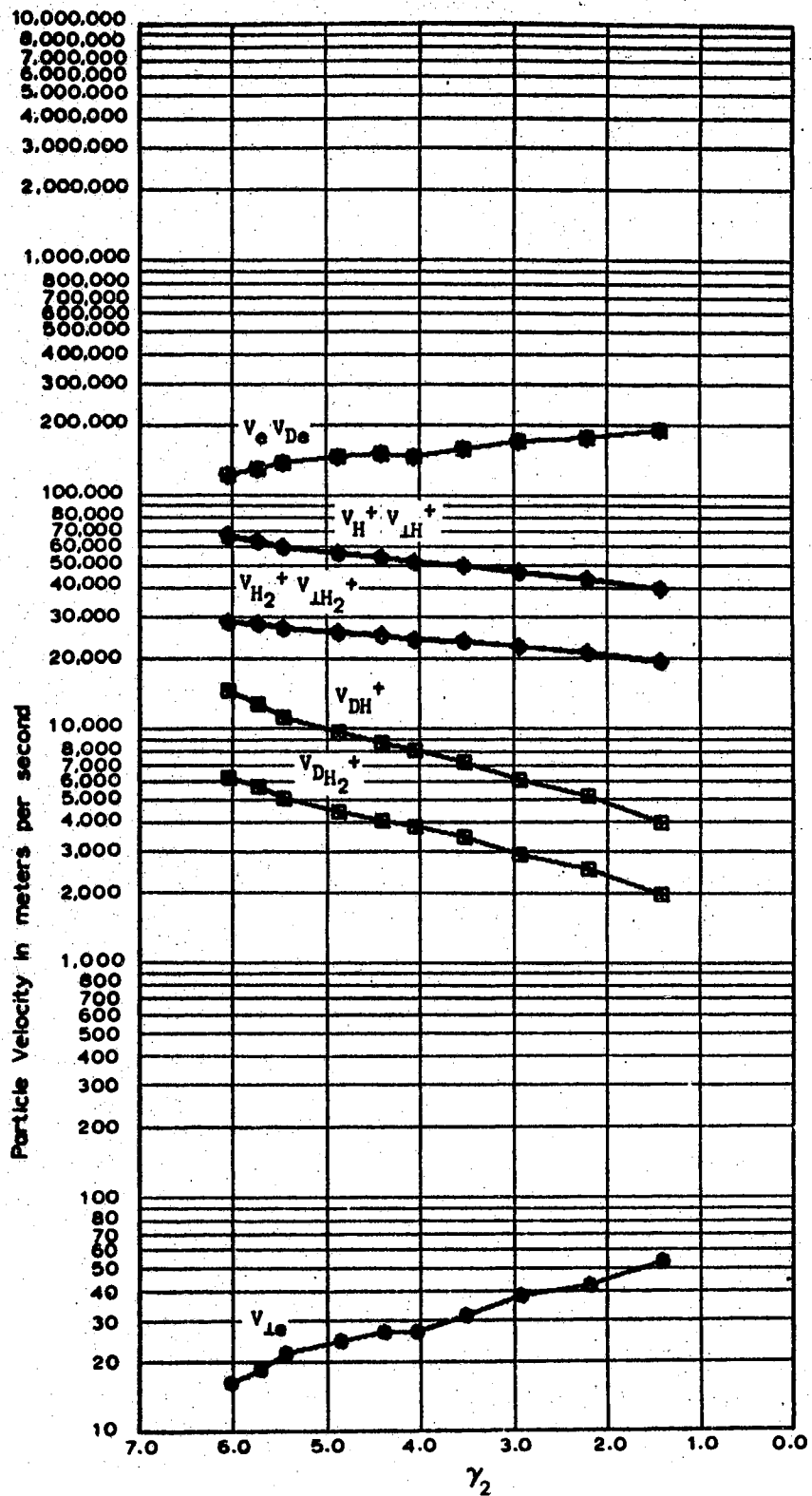
Figure 74d. Data taken August 8, 1966 at 14 MH$_z$ with the Aluminum Cell, D = 0.002794 meters
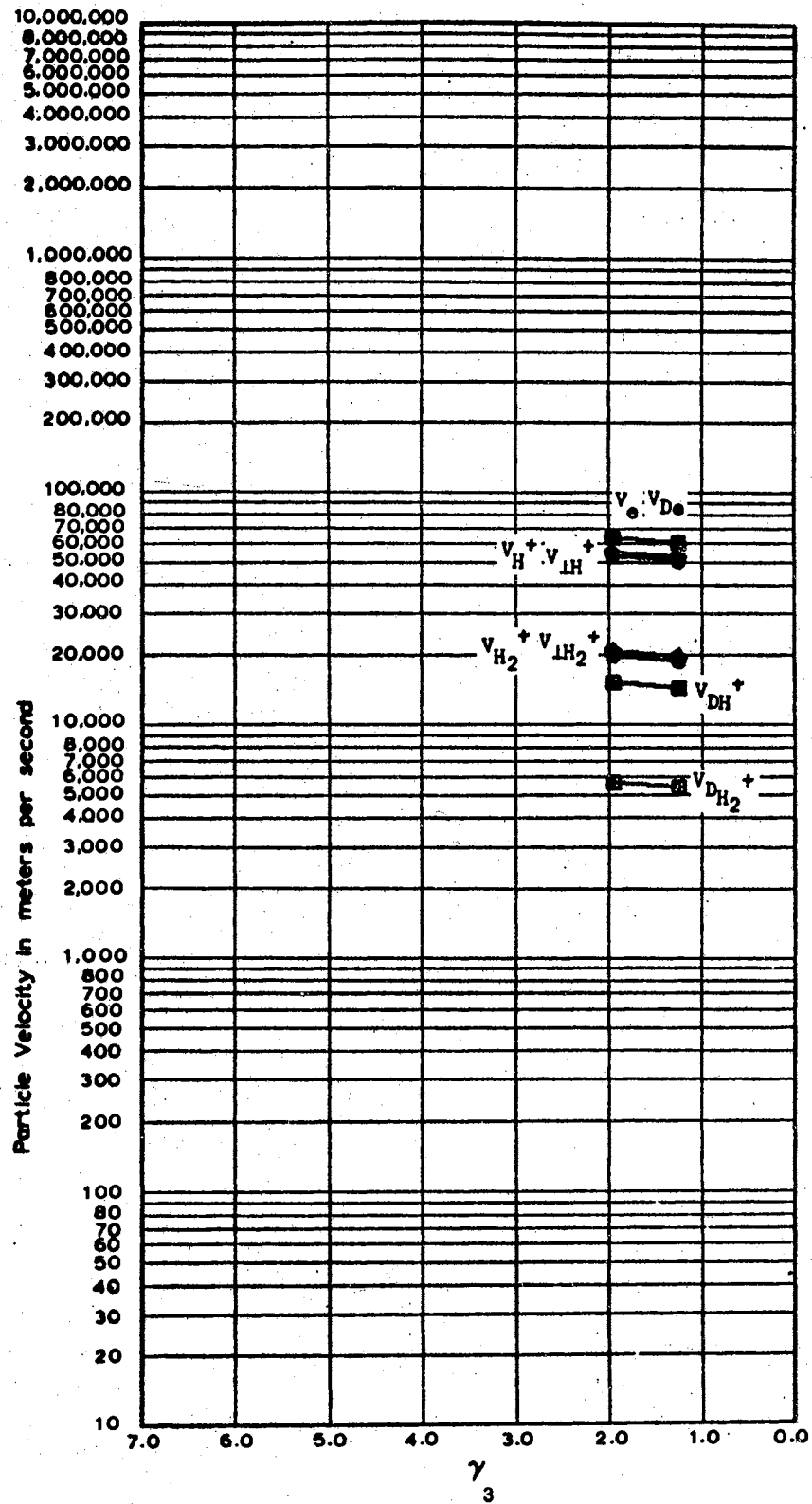
Figure 74e. Data taken August 8, 1966 at 14
MH with the Aluminum Cell,
D ≅ 0.002794 meters
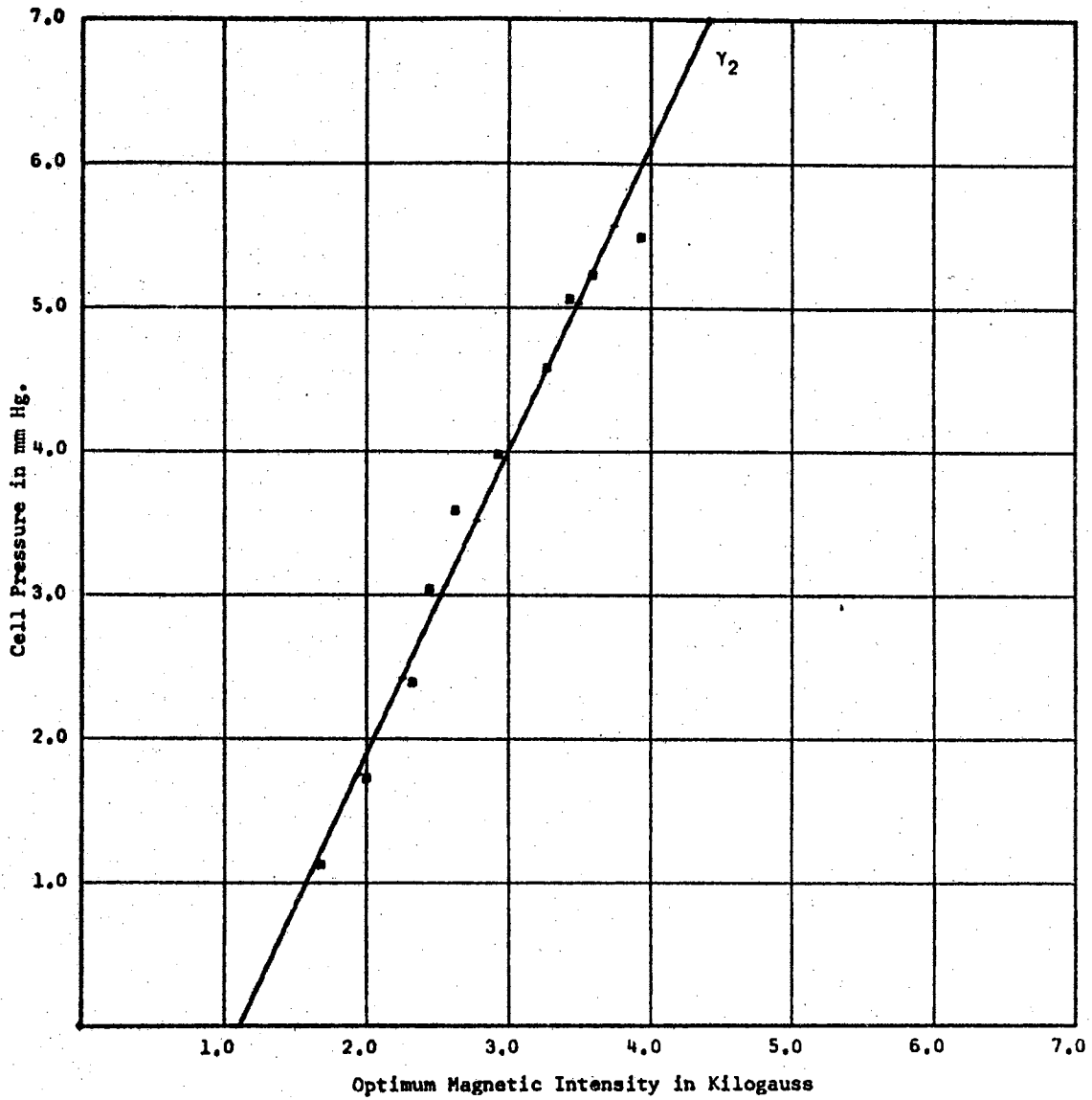
Figure 75a. Data taken August 15, 1966 at 14 MH_z with the Aluminum
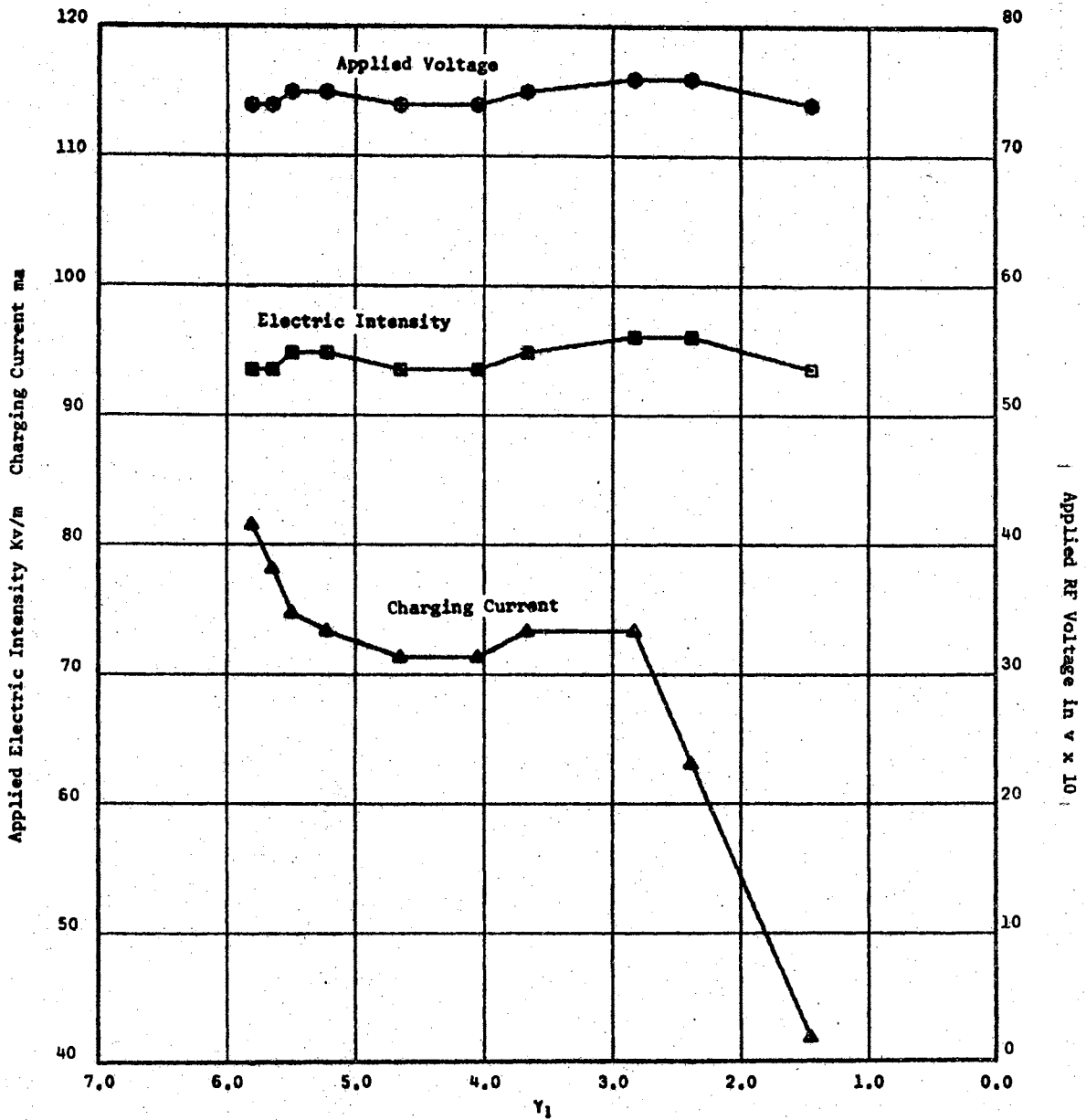Cell, D = 0.002794 meters
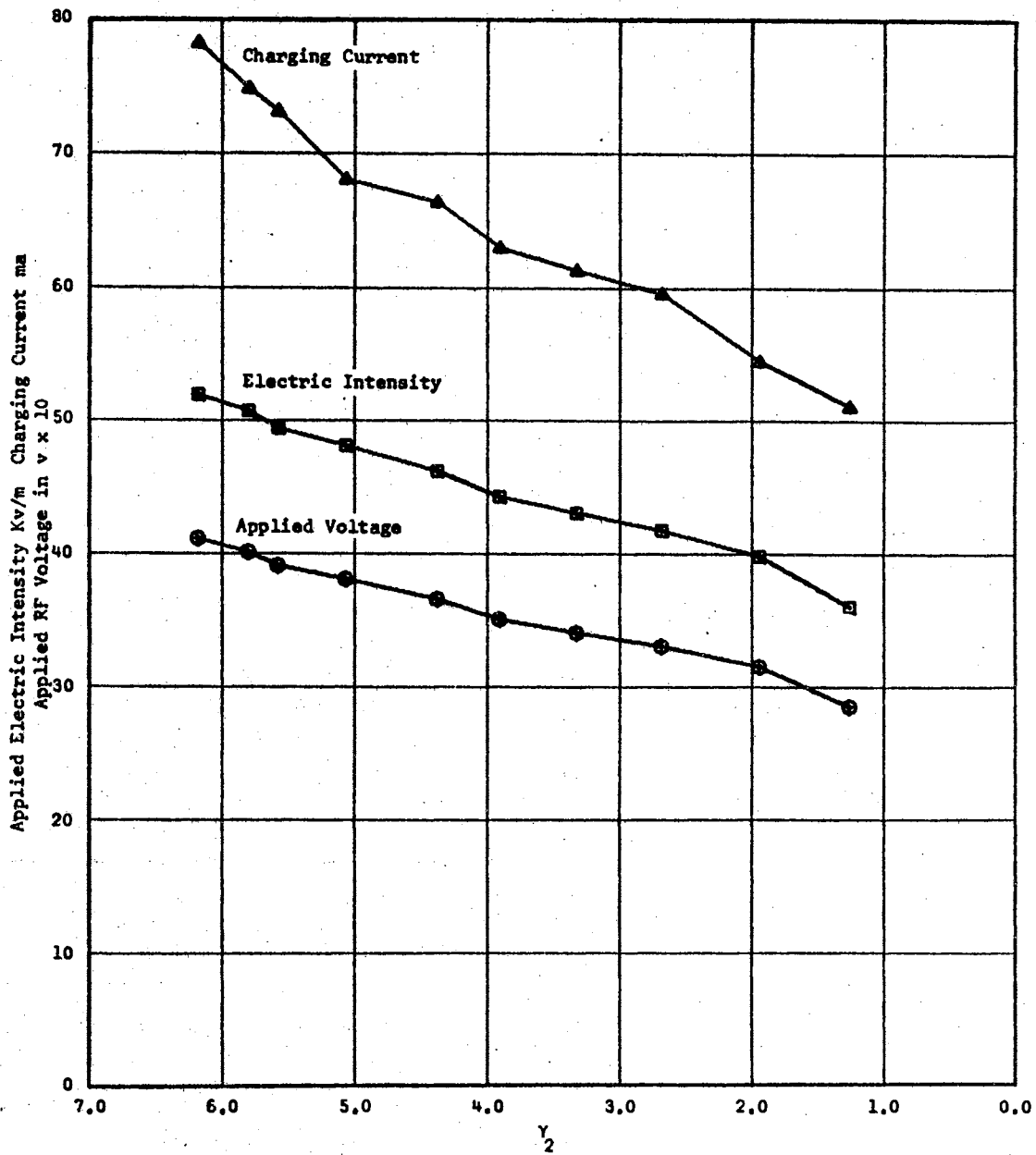
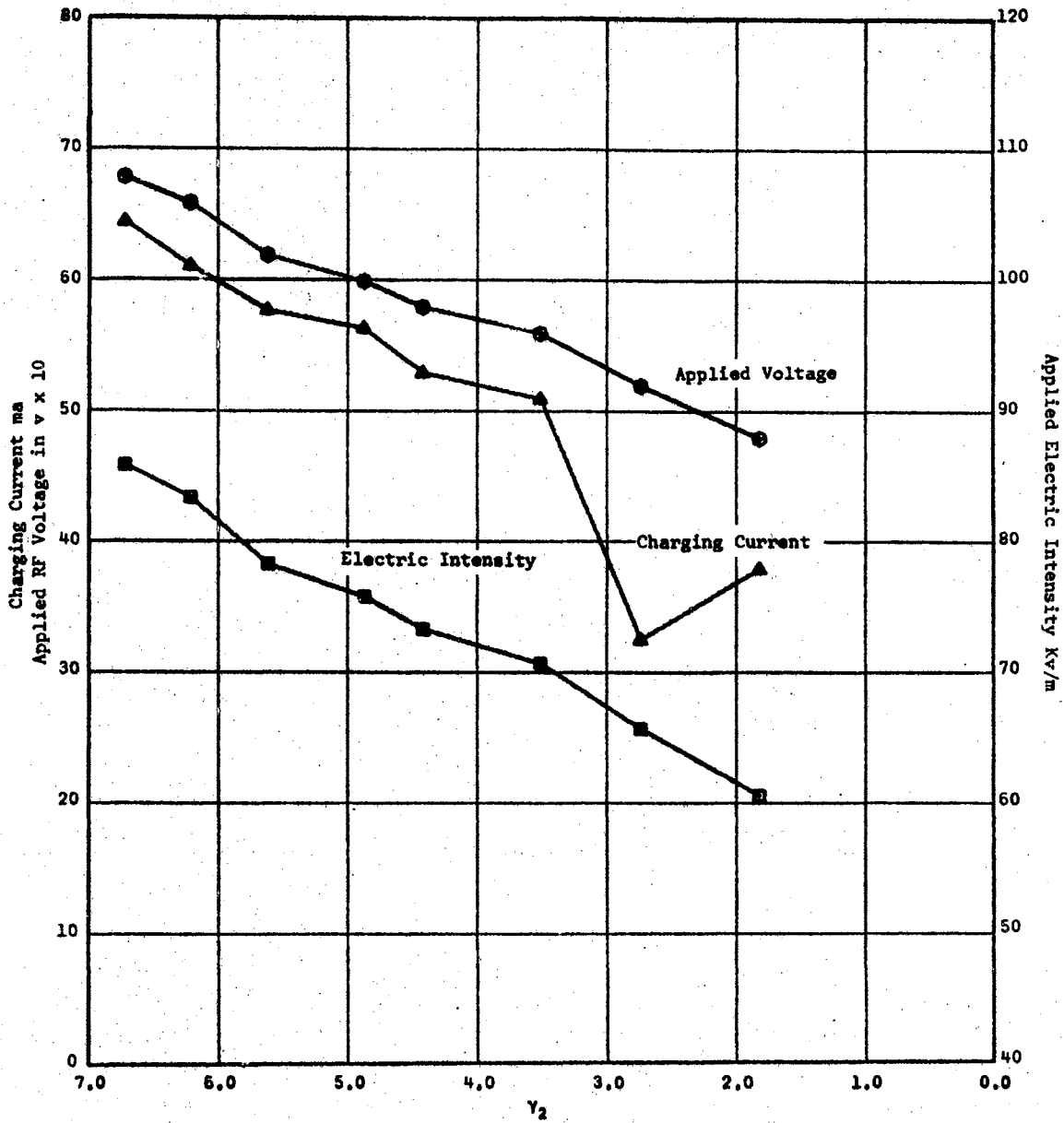Figure 75b. Data taken August 15, 1966 at 14 MH_z with the Aluminum Cell, D = 0.002794 meters
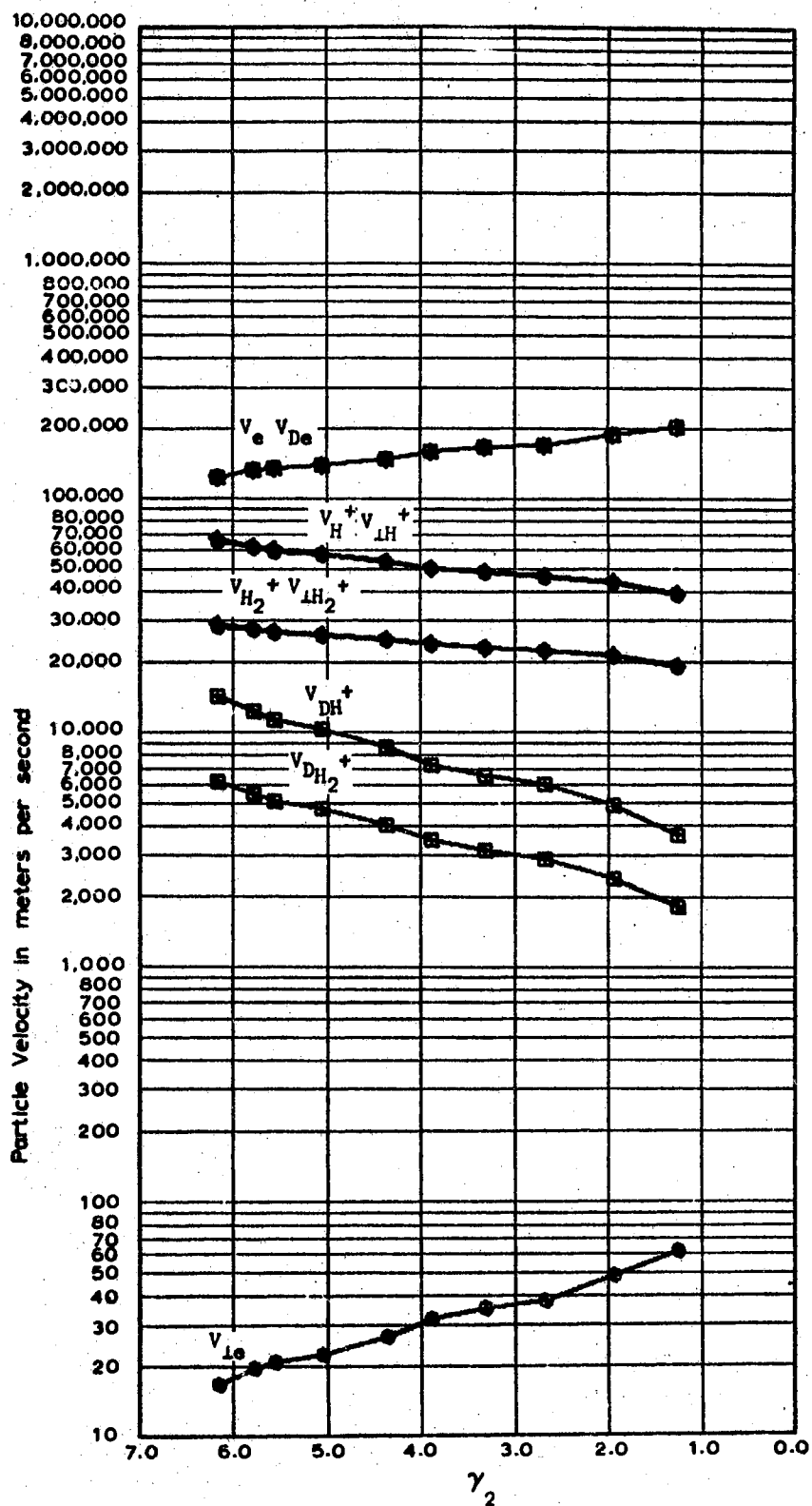
Figure 75c. Data taken August 15, 1966 at
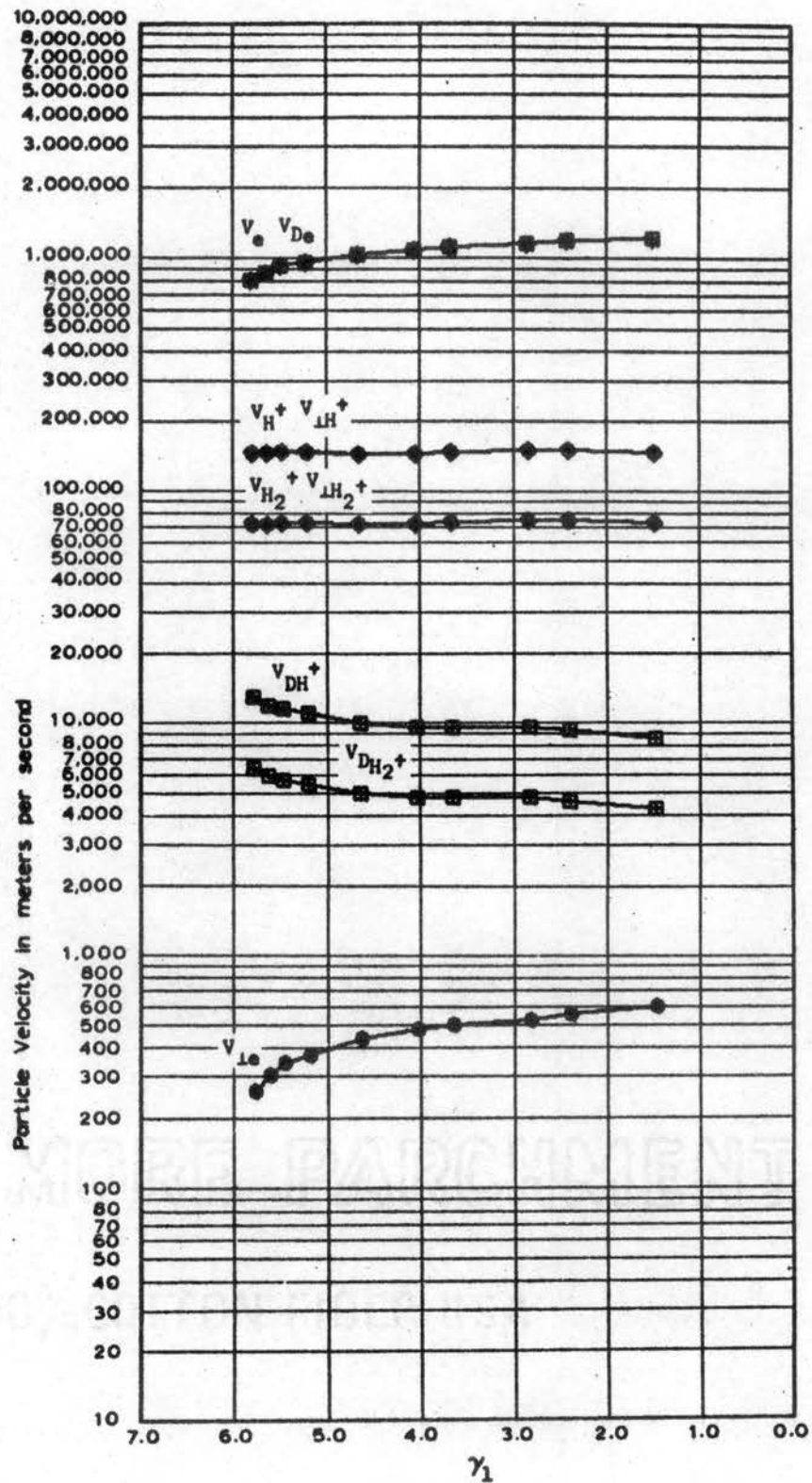14 MH$_z$ with the Aluminum Cell,
D = 0.002794 meters
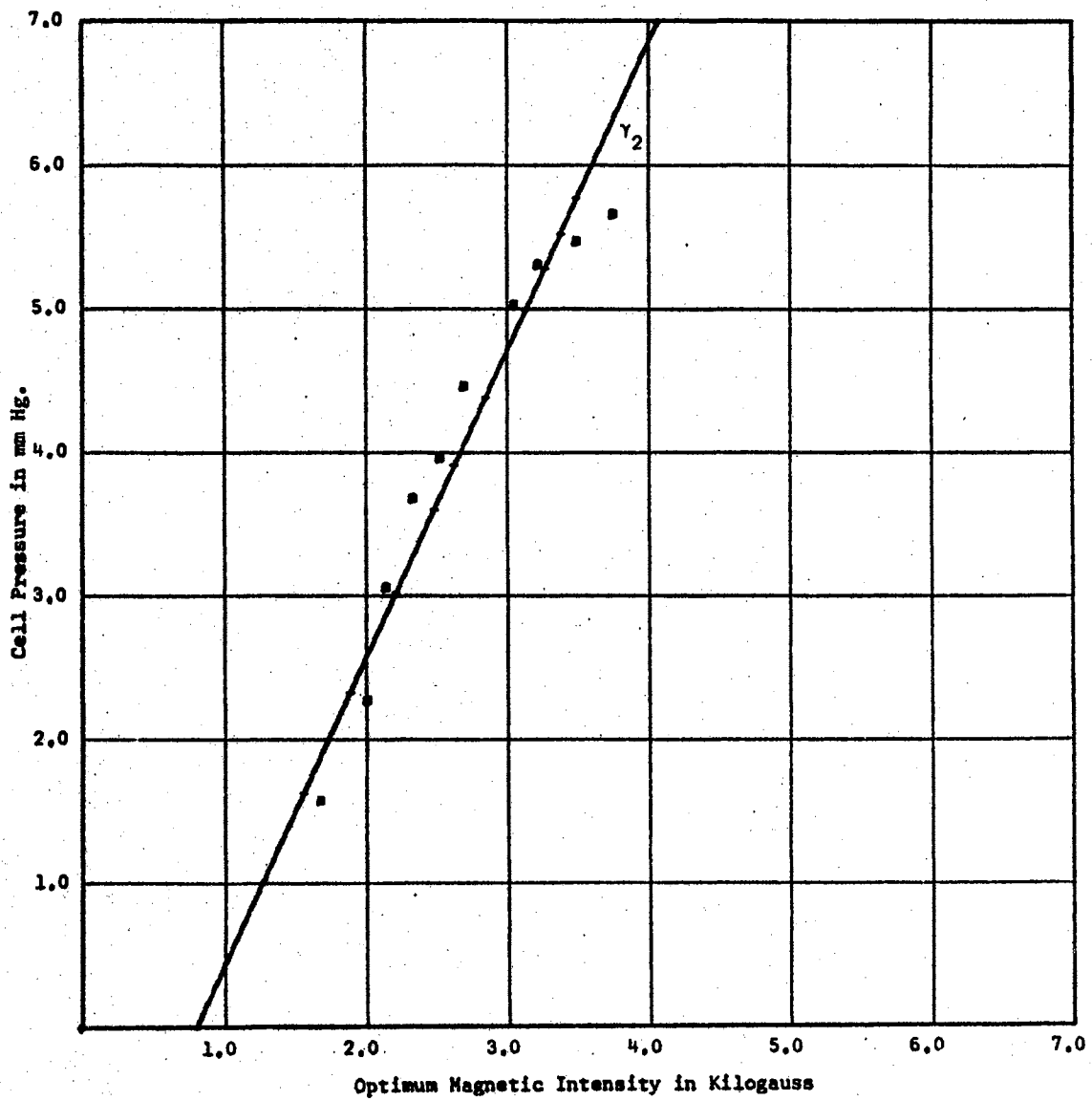
Figure 76a. Data taken June 15, 1966 at 15 MH_z with the Aluminum Cell, D = 0.002794 meters
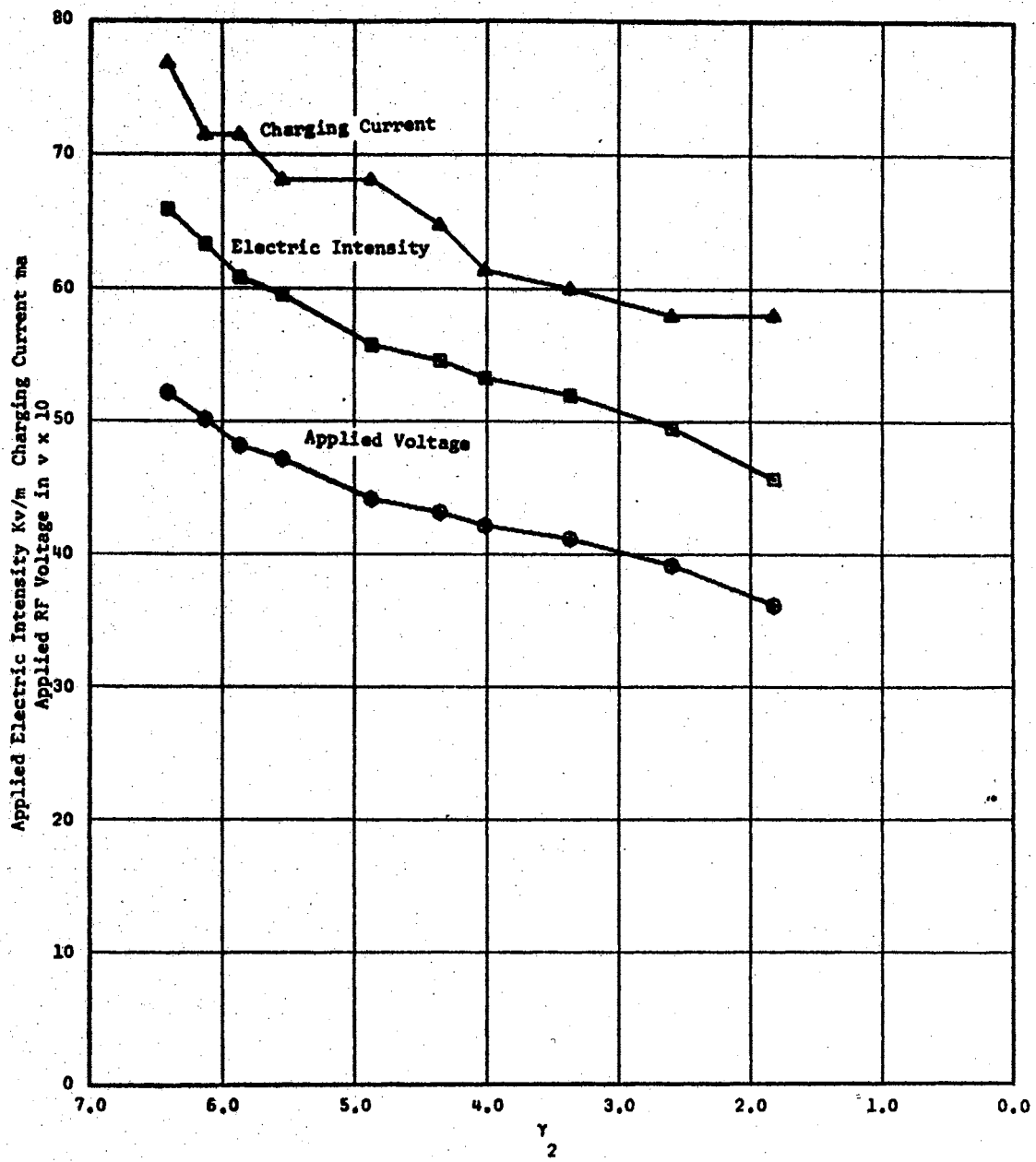
Figure 76b. Data taken June 15, 1966 at 15 MH$_z$ with the Aluminum Cell, D = 0.002794 meters
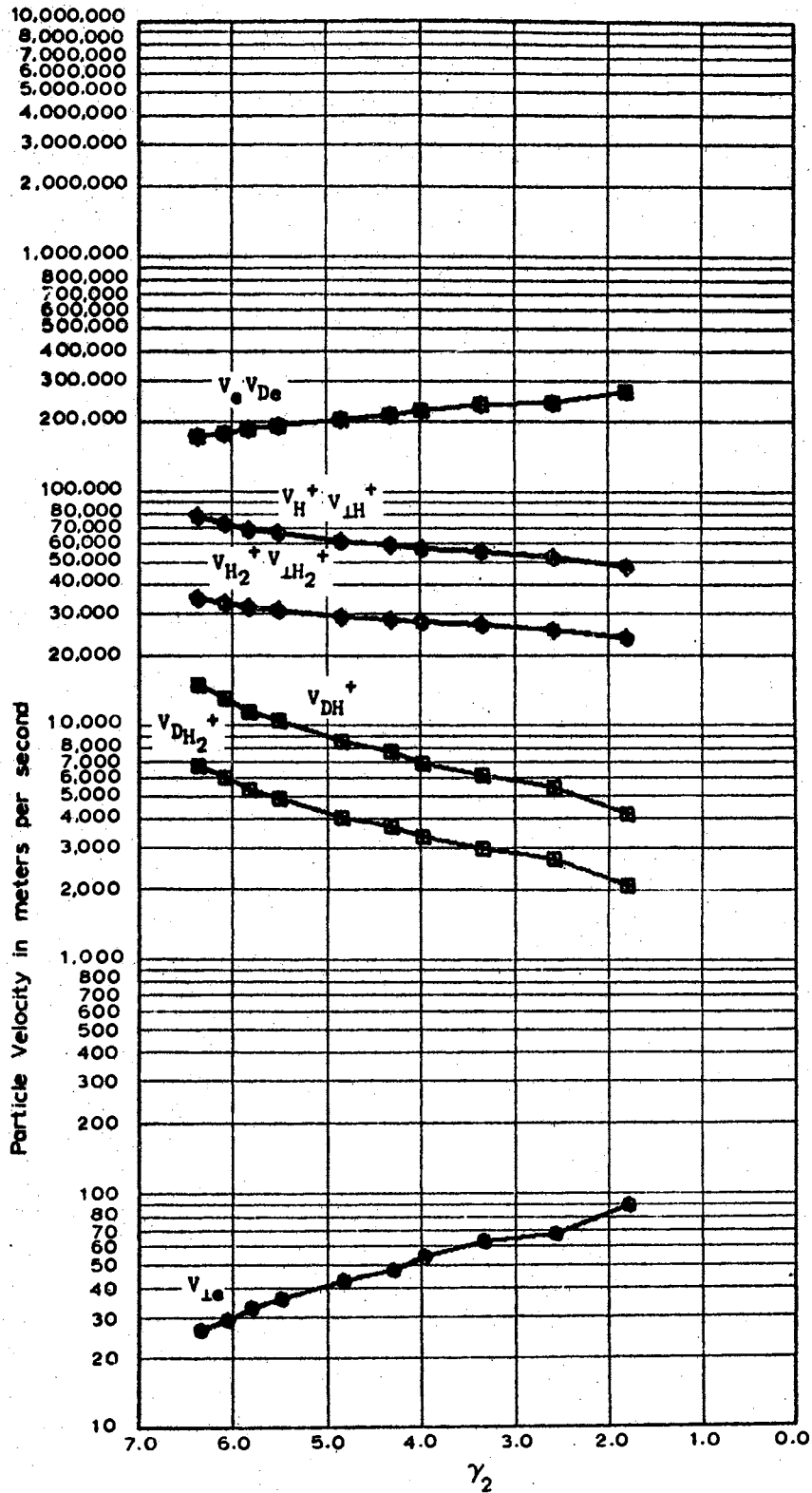
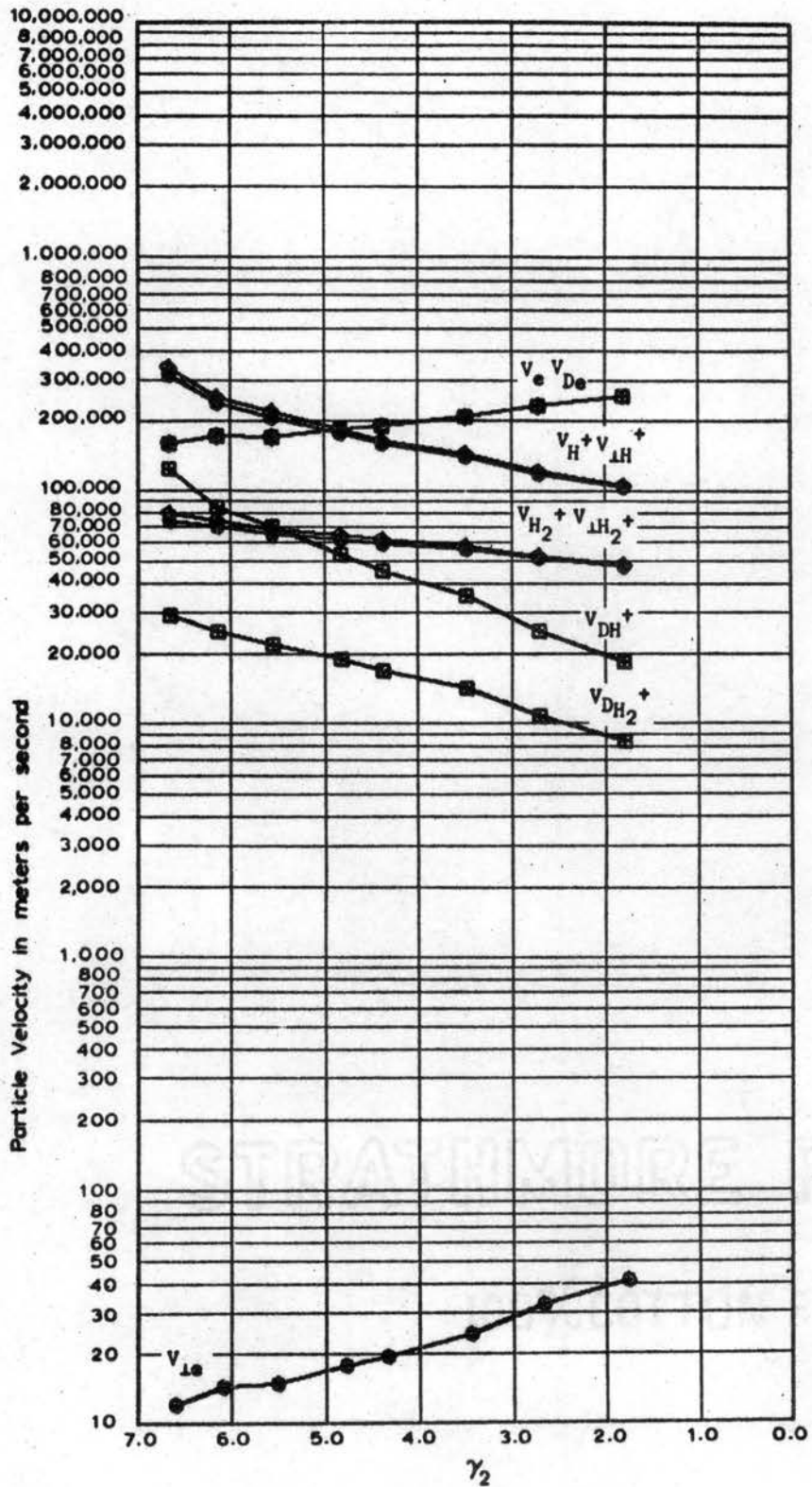Figure 76c. Data taken June 15, 1966 at 15 MH$_z$ with the Aluminum Cell, D $\cong$ 0.002794 meters
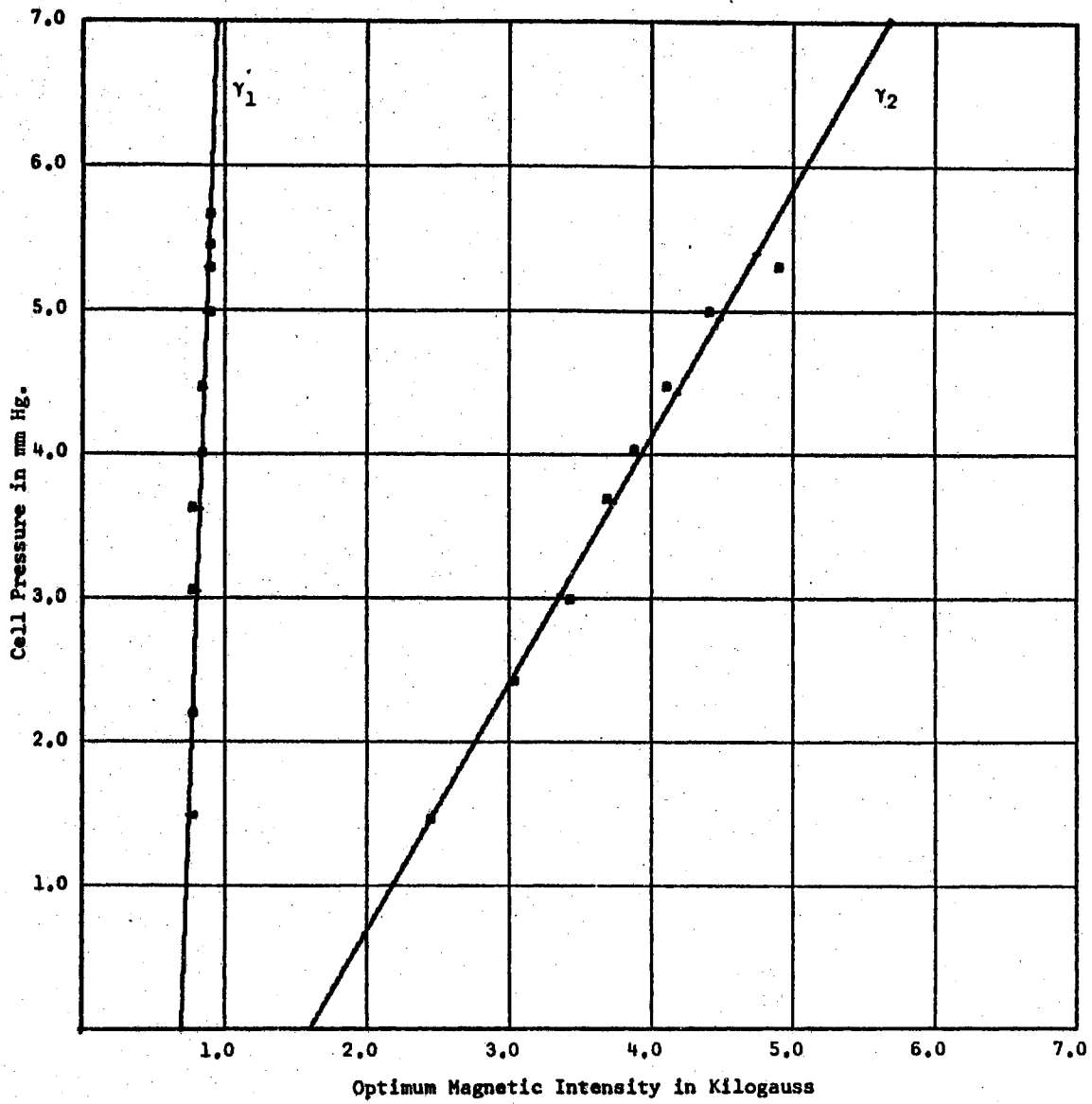
Figure 77a. Data taken June 20, 1966 at 15 MH$_z$ with the Aluminum
Cell, D = 0.002794 meters
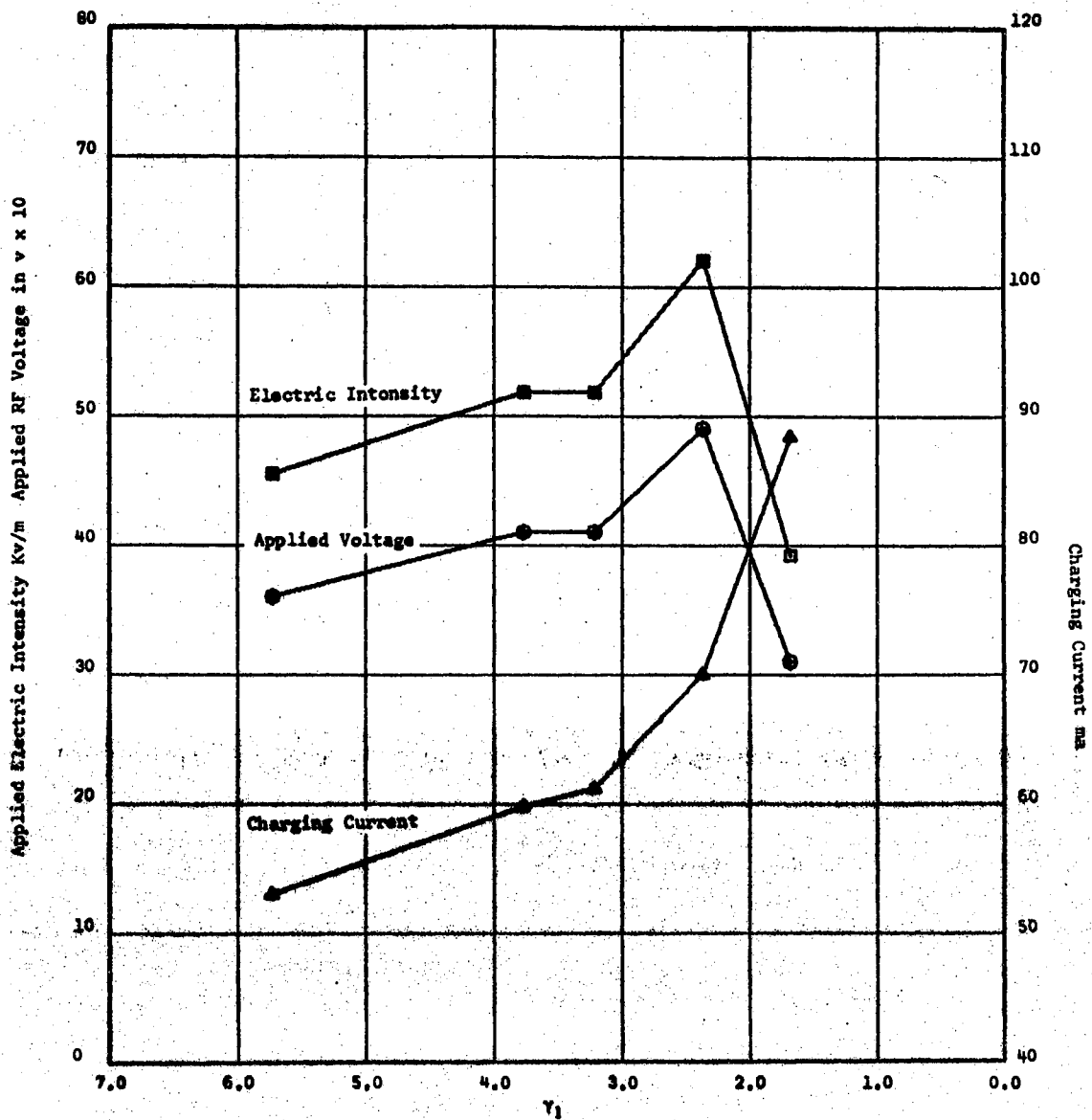
Figure 77b. Data taken June 20, 1966 at 15 MH$_z$ with the Aluminum Cell, D = 0.002794 meters
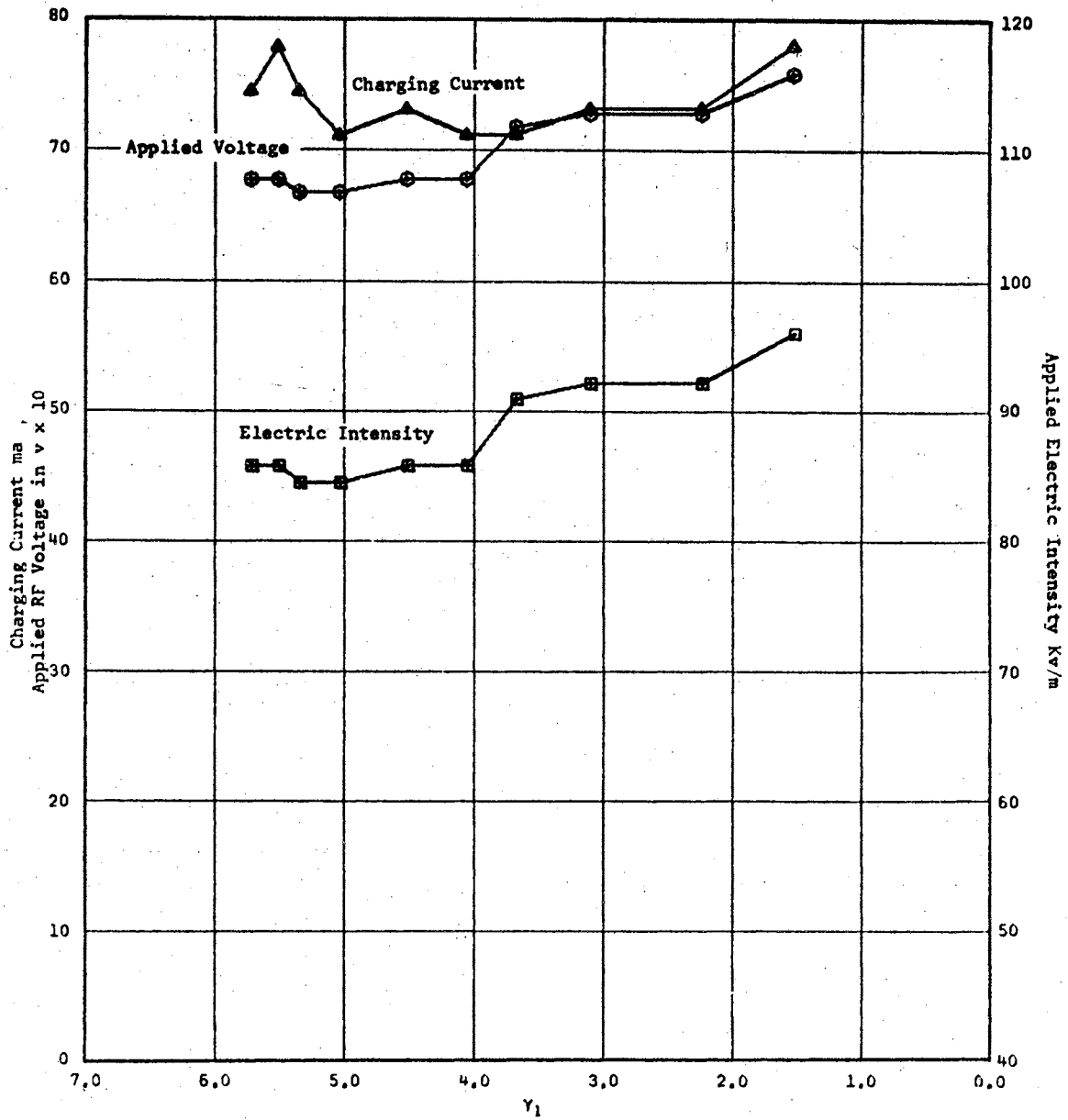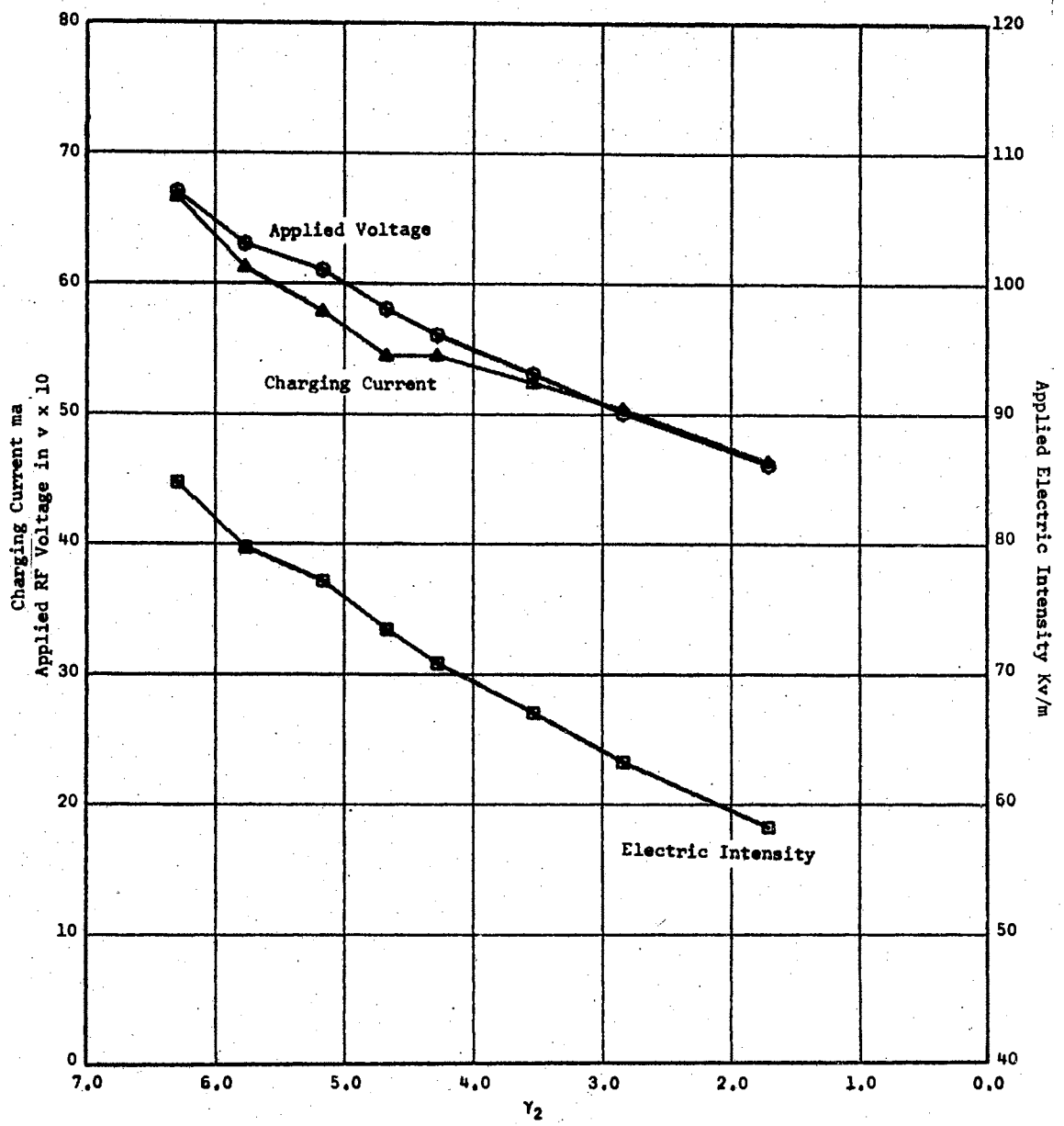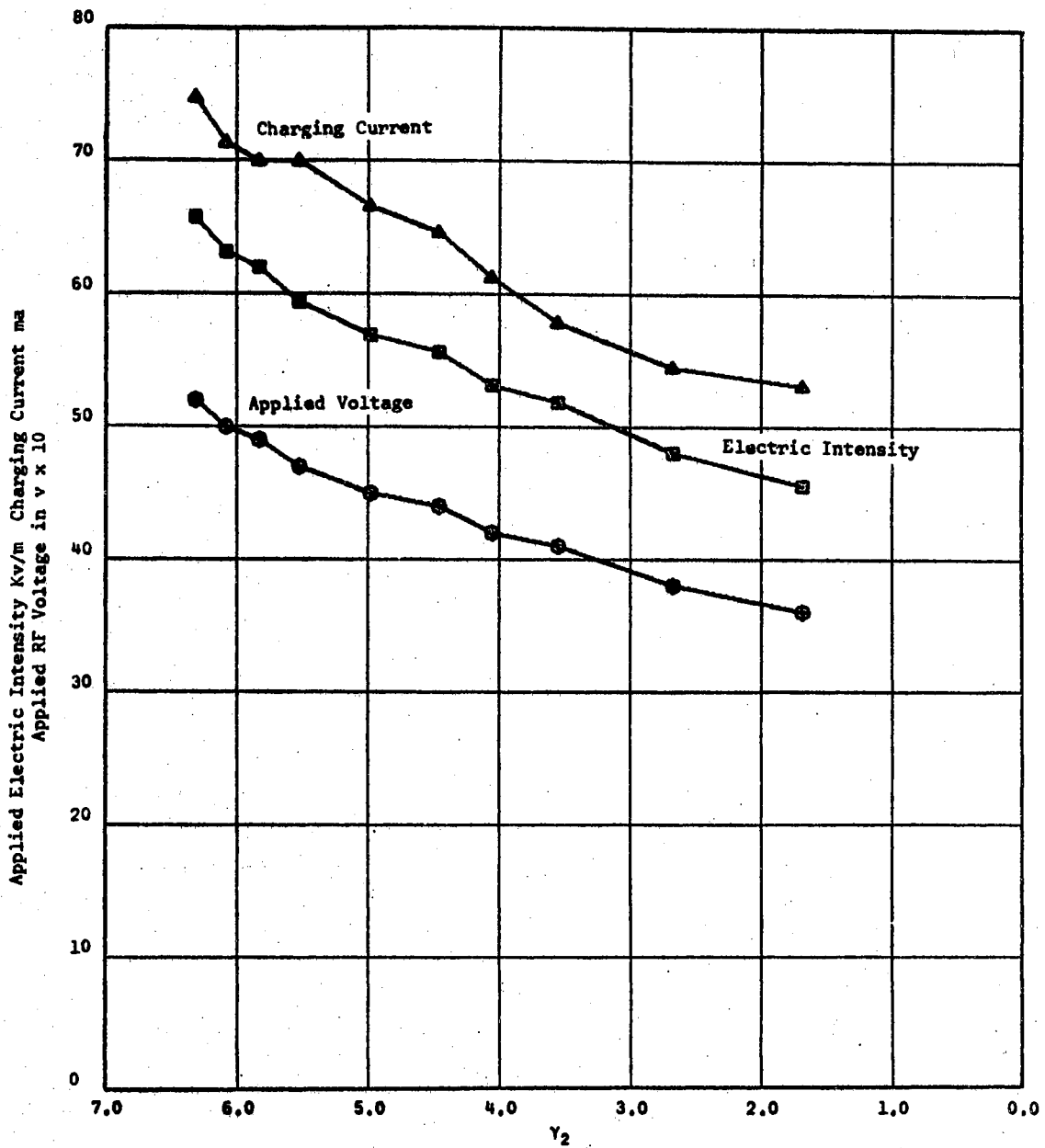
Figure 77c. Data taken June 20, 1966 at 15 MH_z with the Aluminum Cell, D = 0.002794 meters
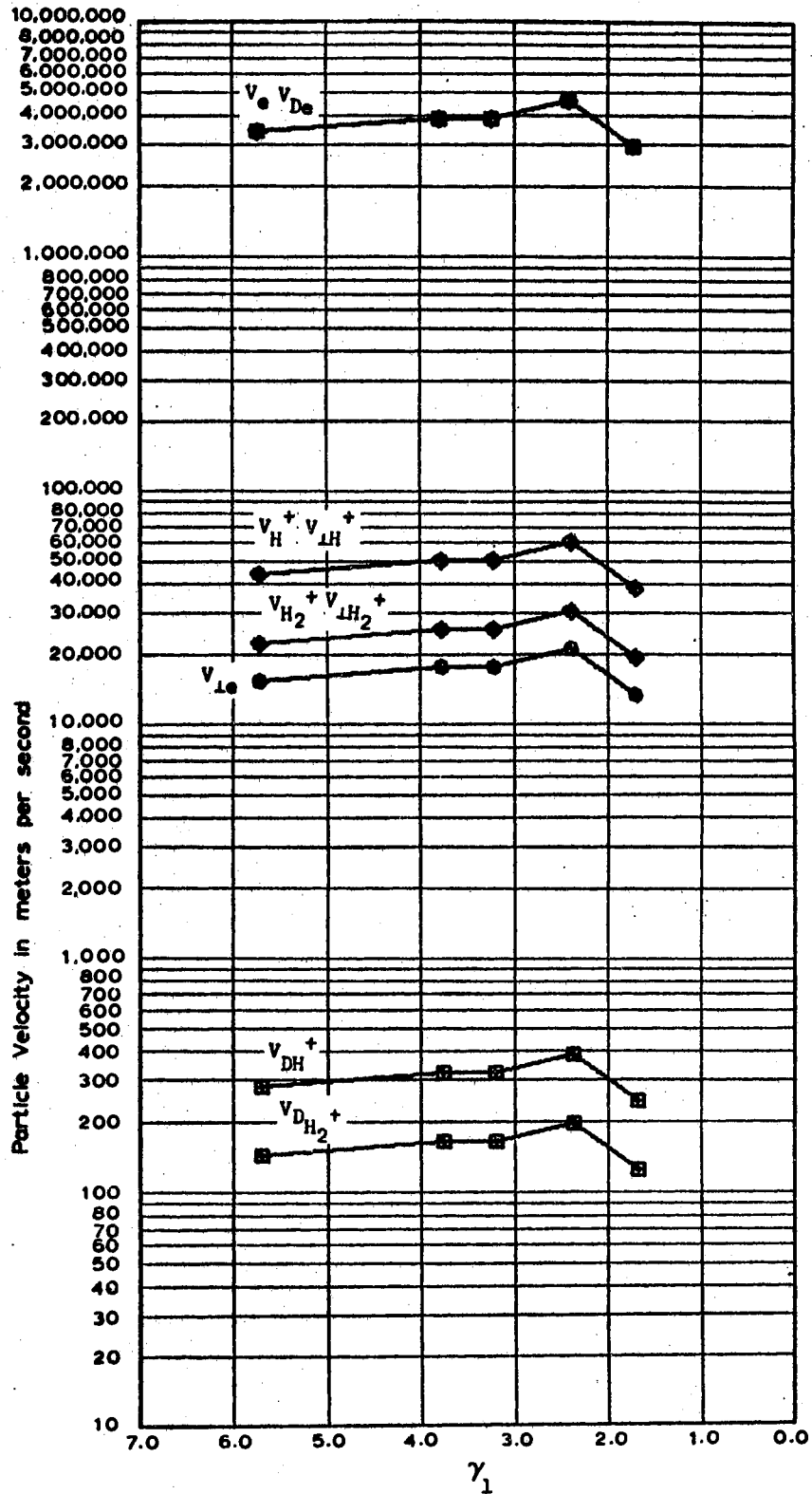
Figure 77d. Data taken June 20, 1966 at 15
MH with the Aluminum Cell,
$D \stackrel{Z}{=} 0.002794$ meters
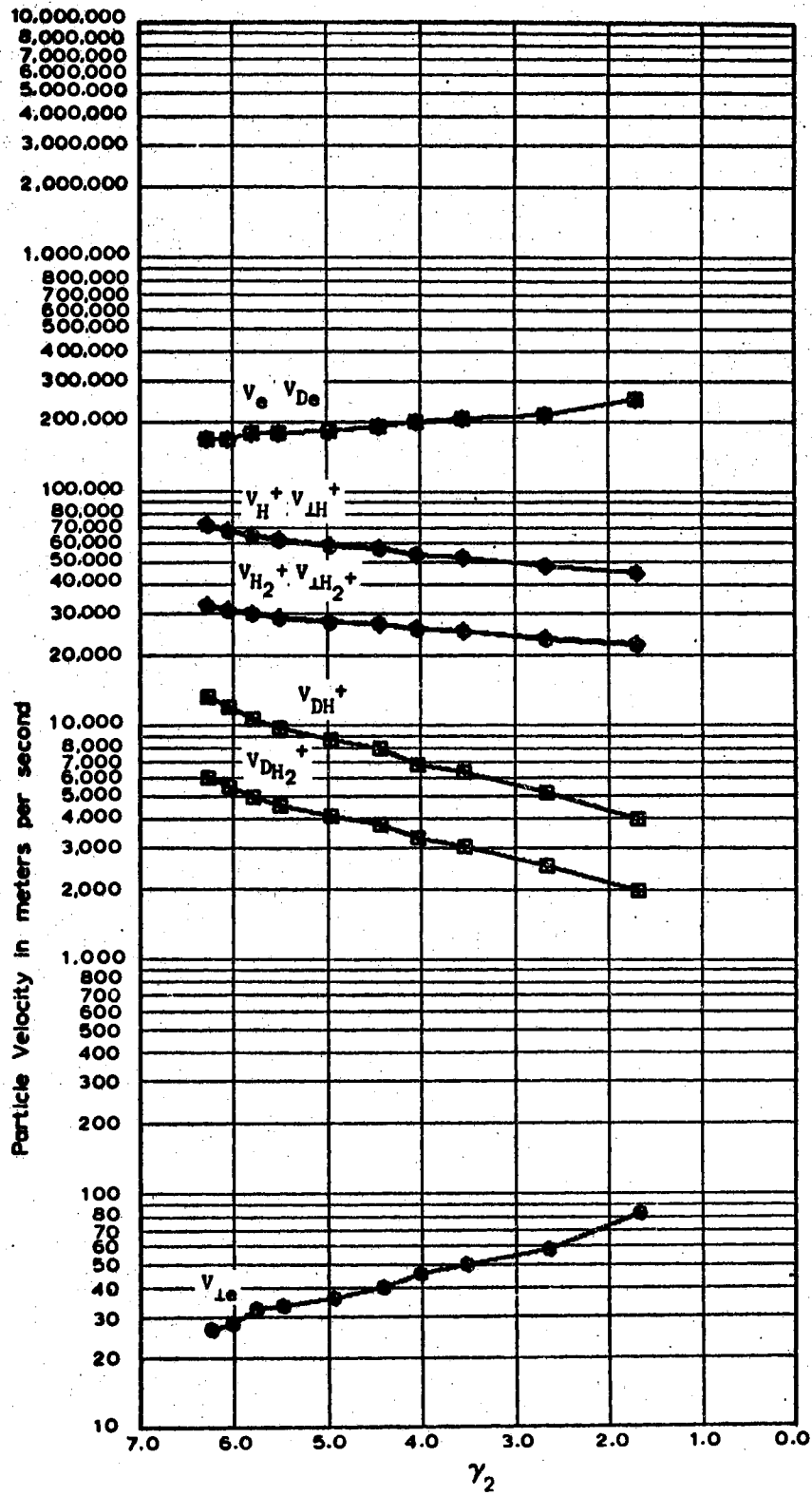
Figure 77e. Data taken June 20, 1966 at 15
MH$_z$ with the Aluminum Cell,
D $\cong$ 0.002794 meters
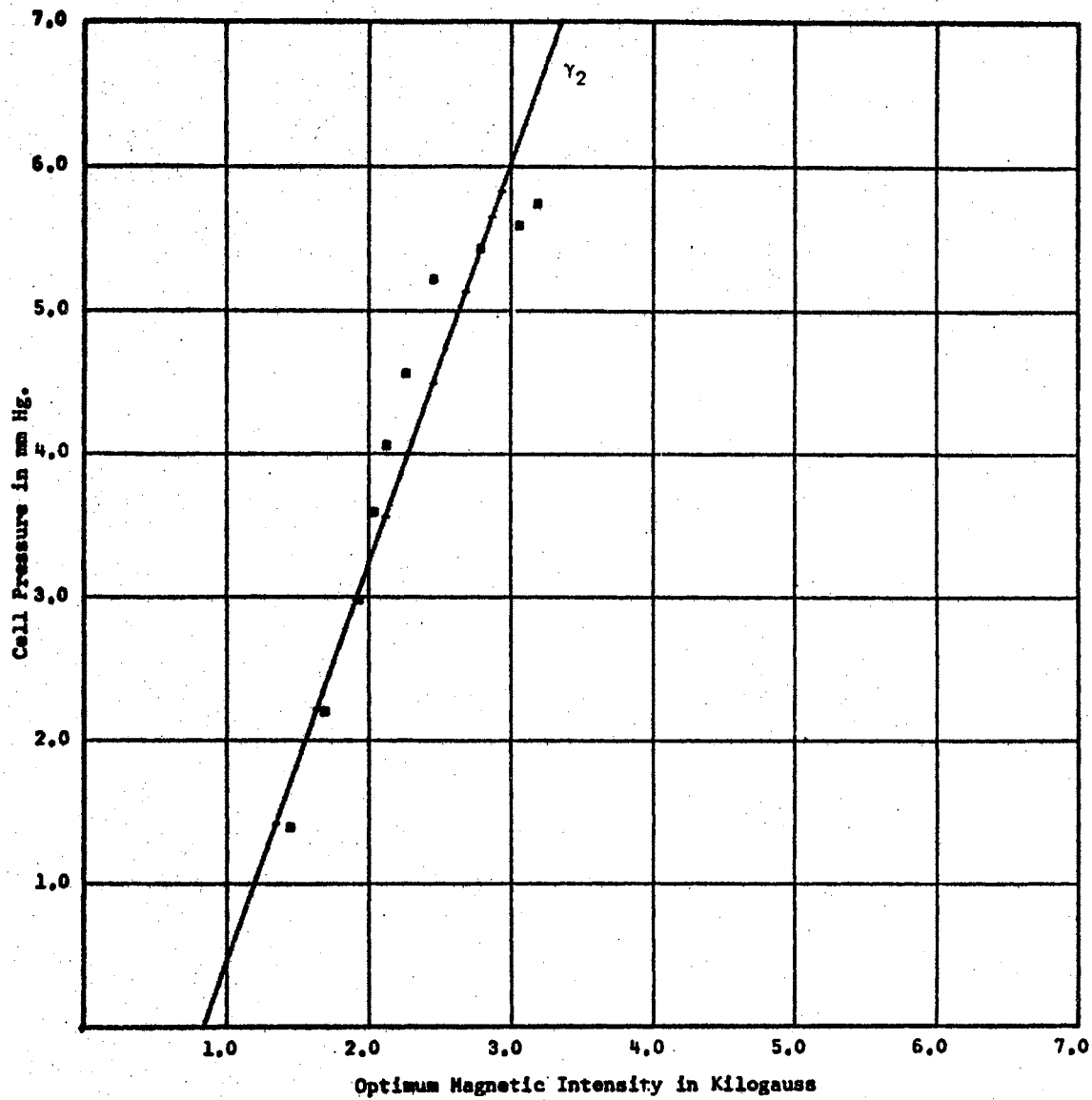
Figure 78a.   Data taken May 27, 1966 at 20 MH$_z$ with the Aluminum
Cell, D = 0.002794 meters
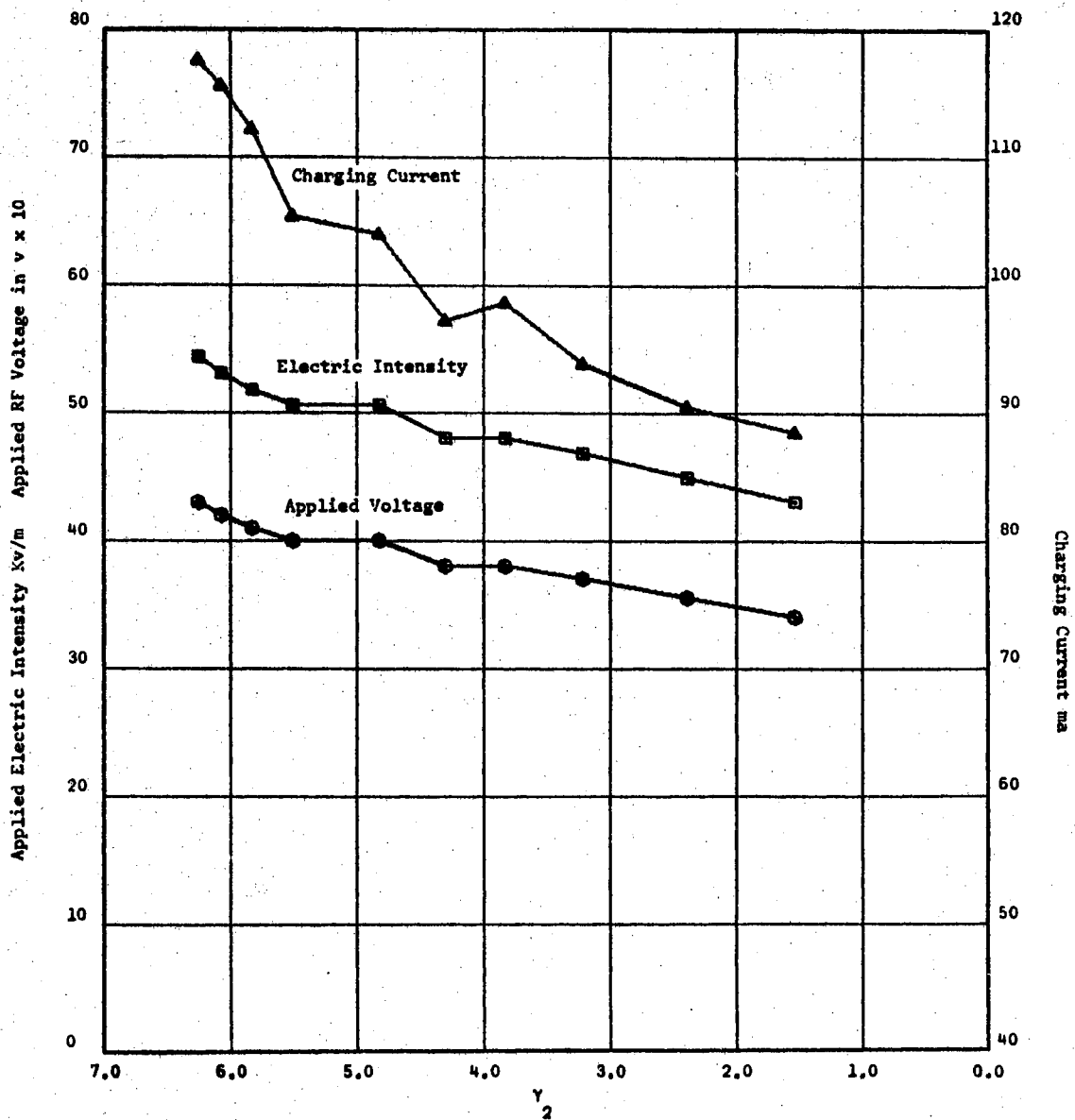
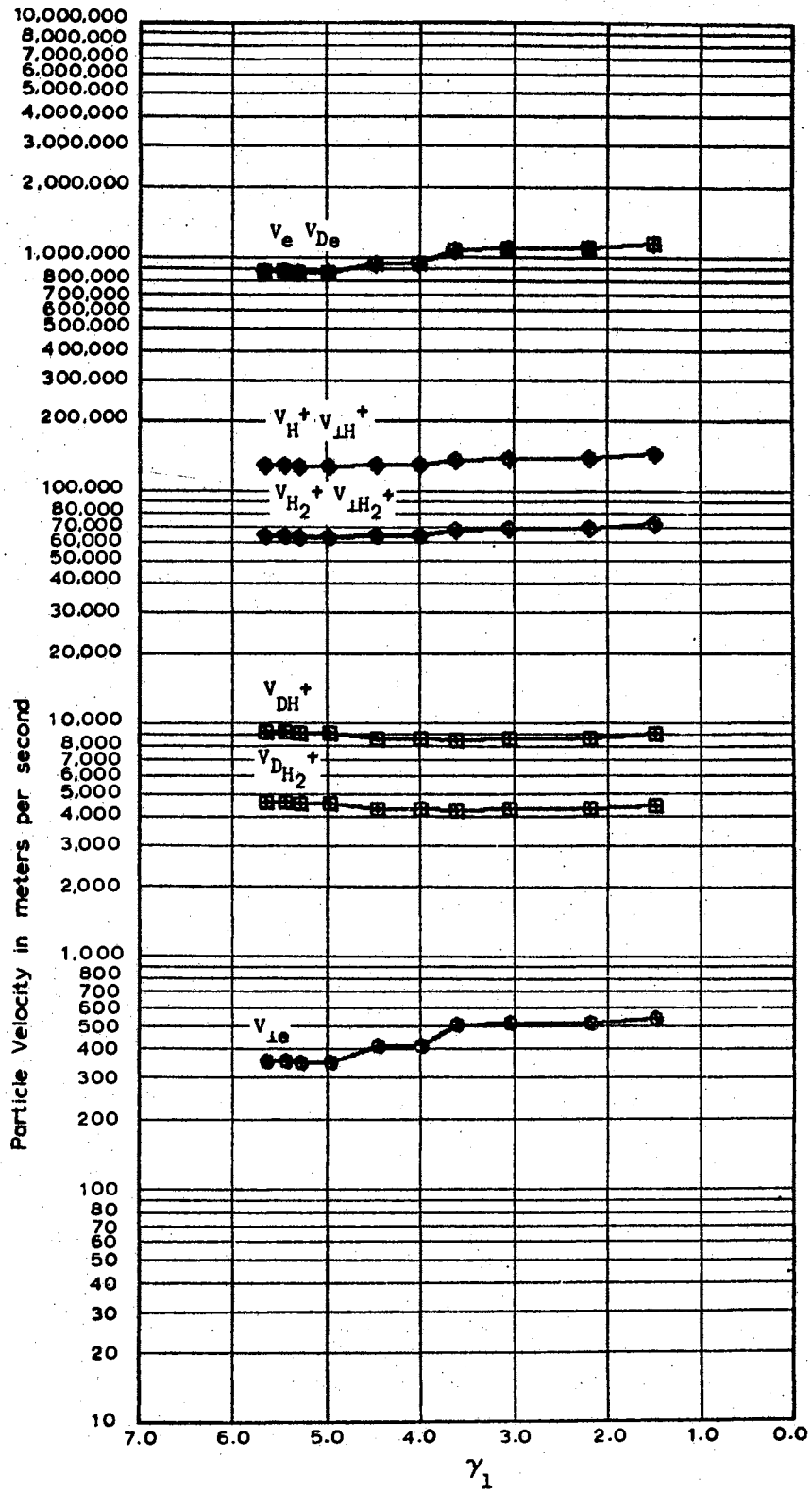Figure 78b. Data taken May 27, 1966 at 20 MH$_z$ with the Aluminum Cell, D = 0.002794 meters
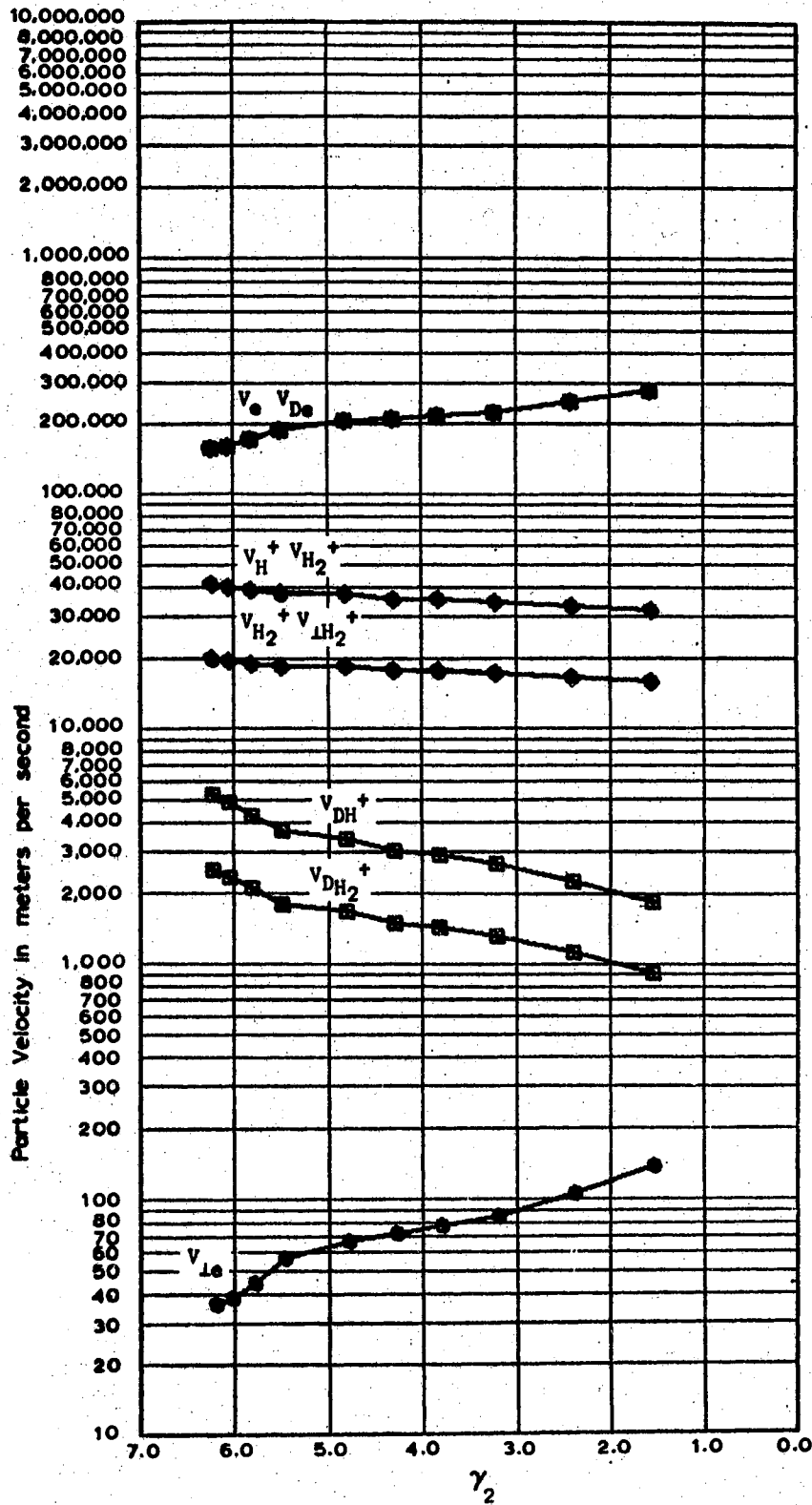
Figure 78c. Data taken May 27, 1966 at 20 MH$_z$ with the Aluminum Cell, D $\cong$ 0.002794 meters
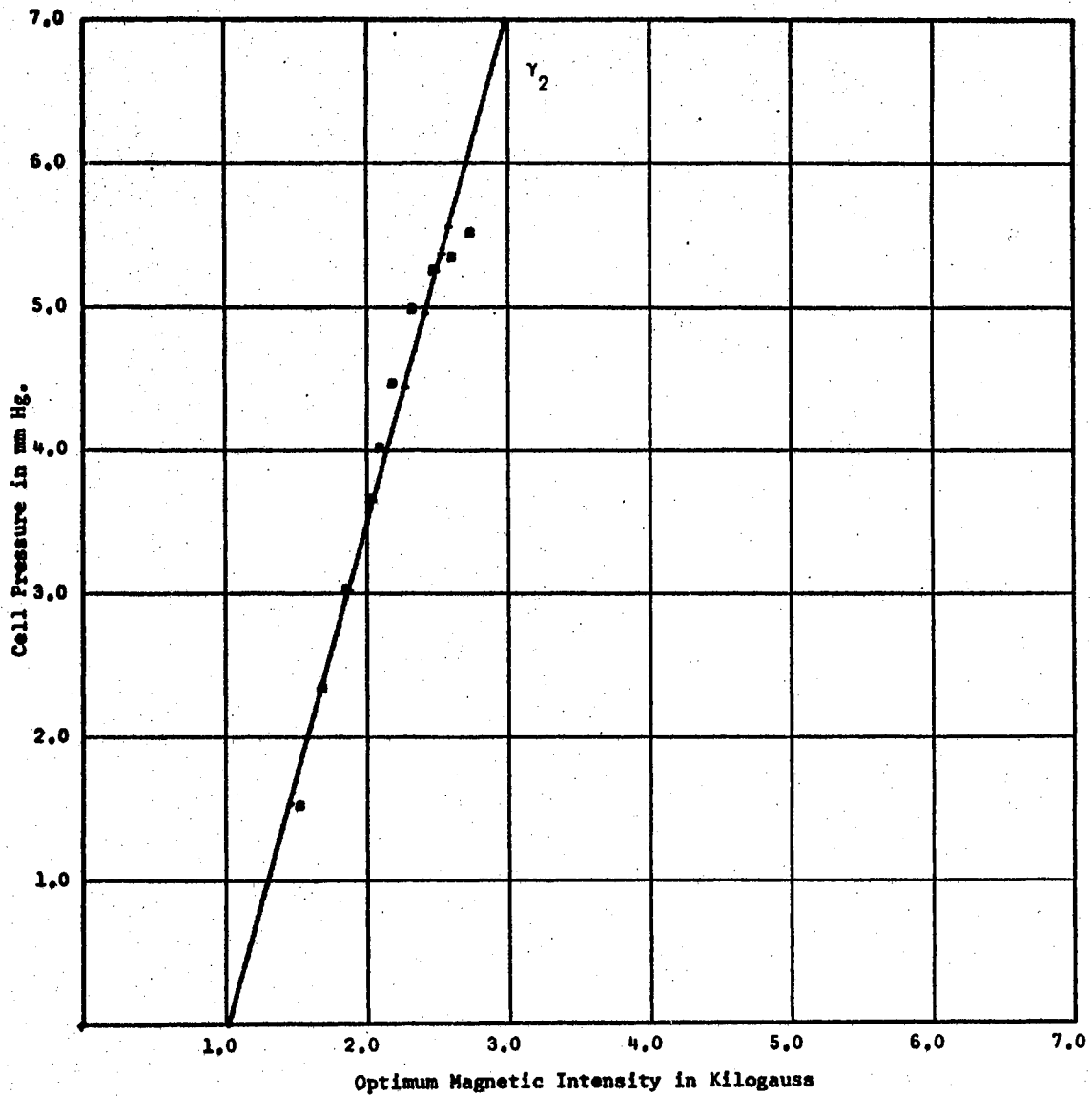
Figure 79a. Data taken June 13, 1966 at 20 MH$_z$ with the Aluminum Cell, D = 0.002794 meters
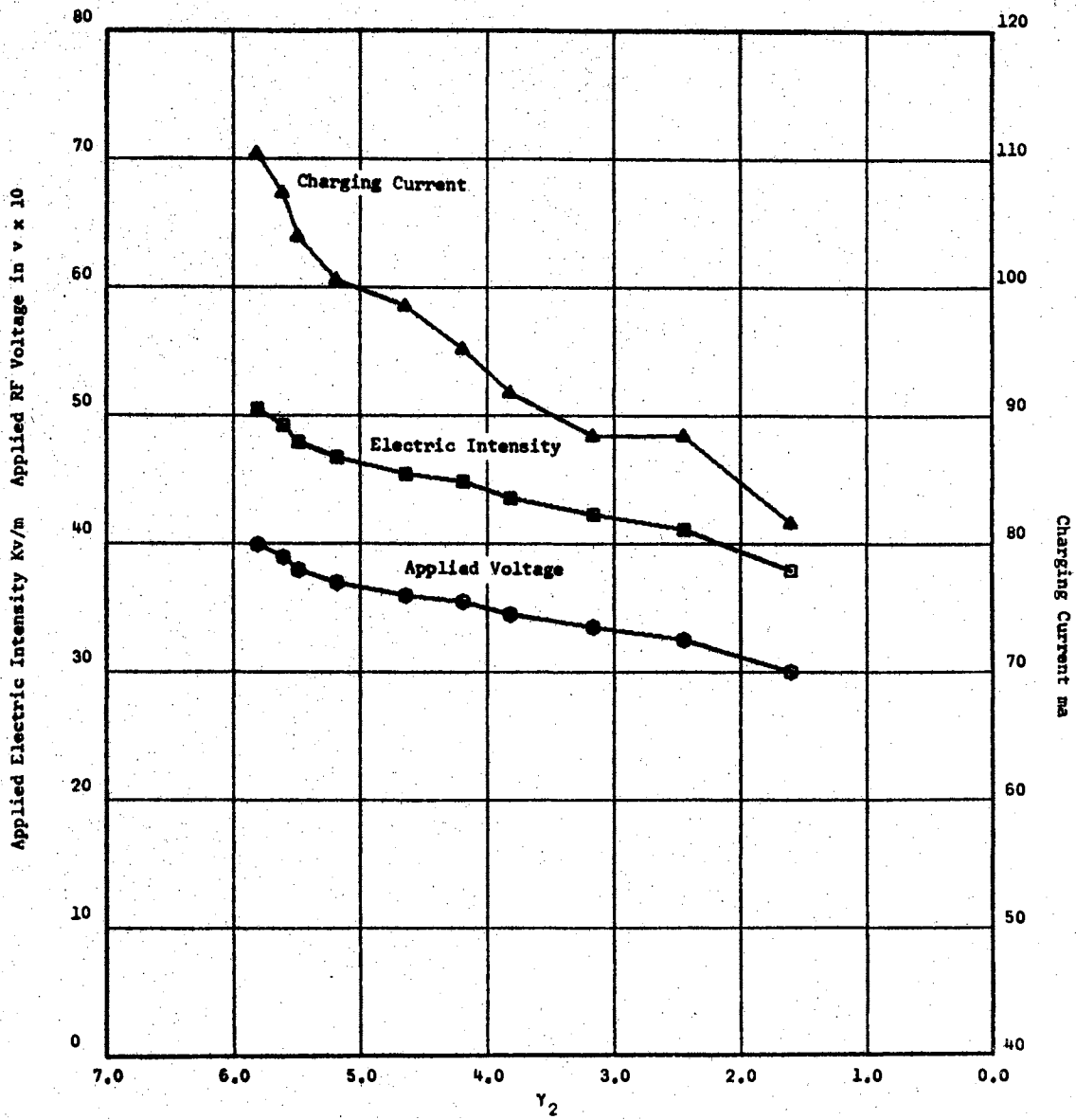
Figure 79b. Data taken June 13, 1966 at 20 MH$_z$ with the
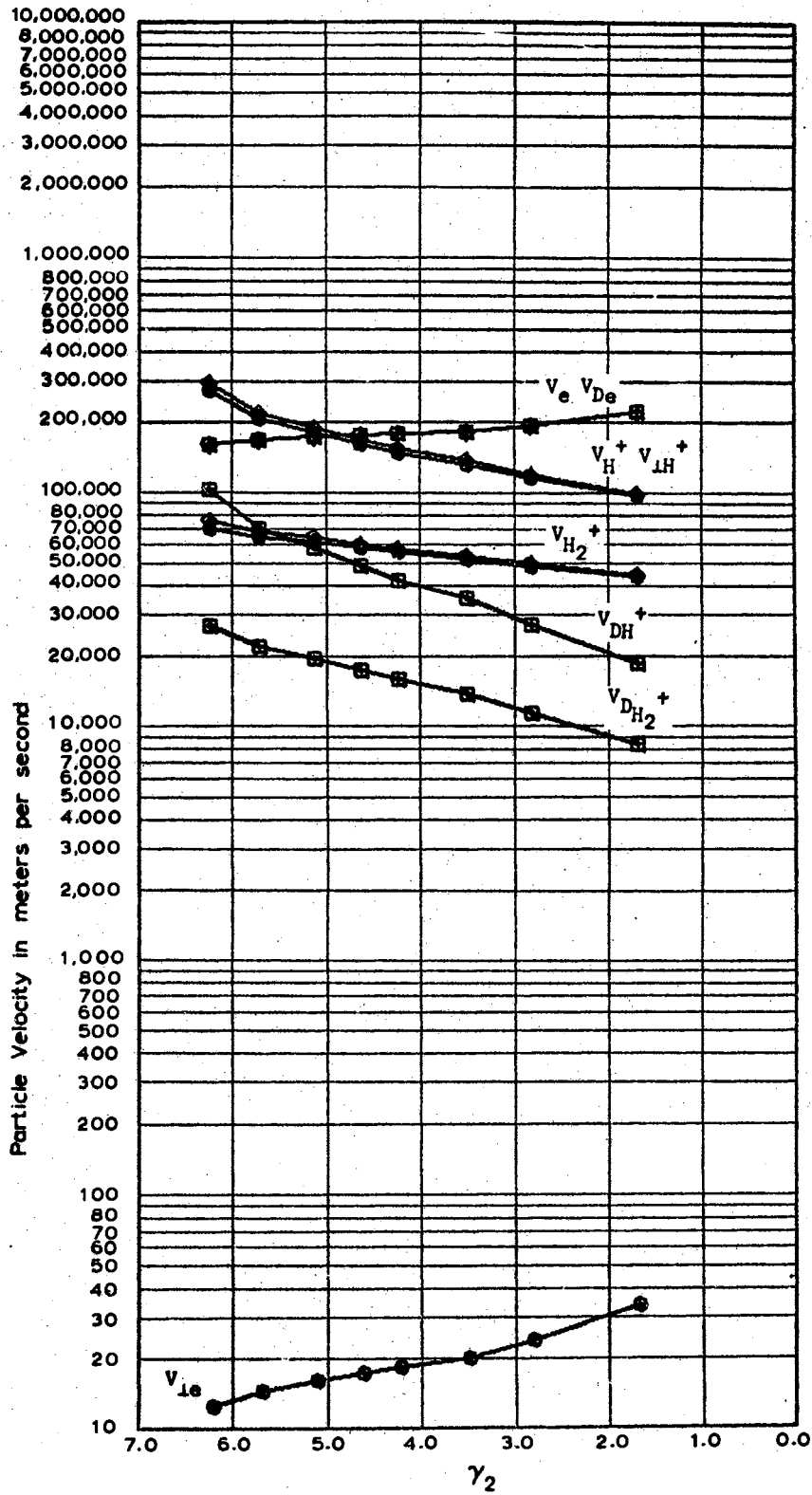Aluminum Cell, D = 0.002794 meters
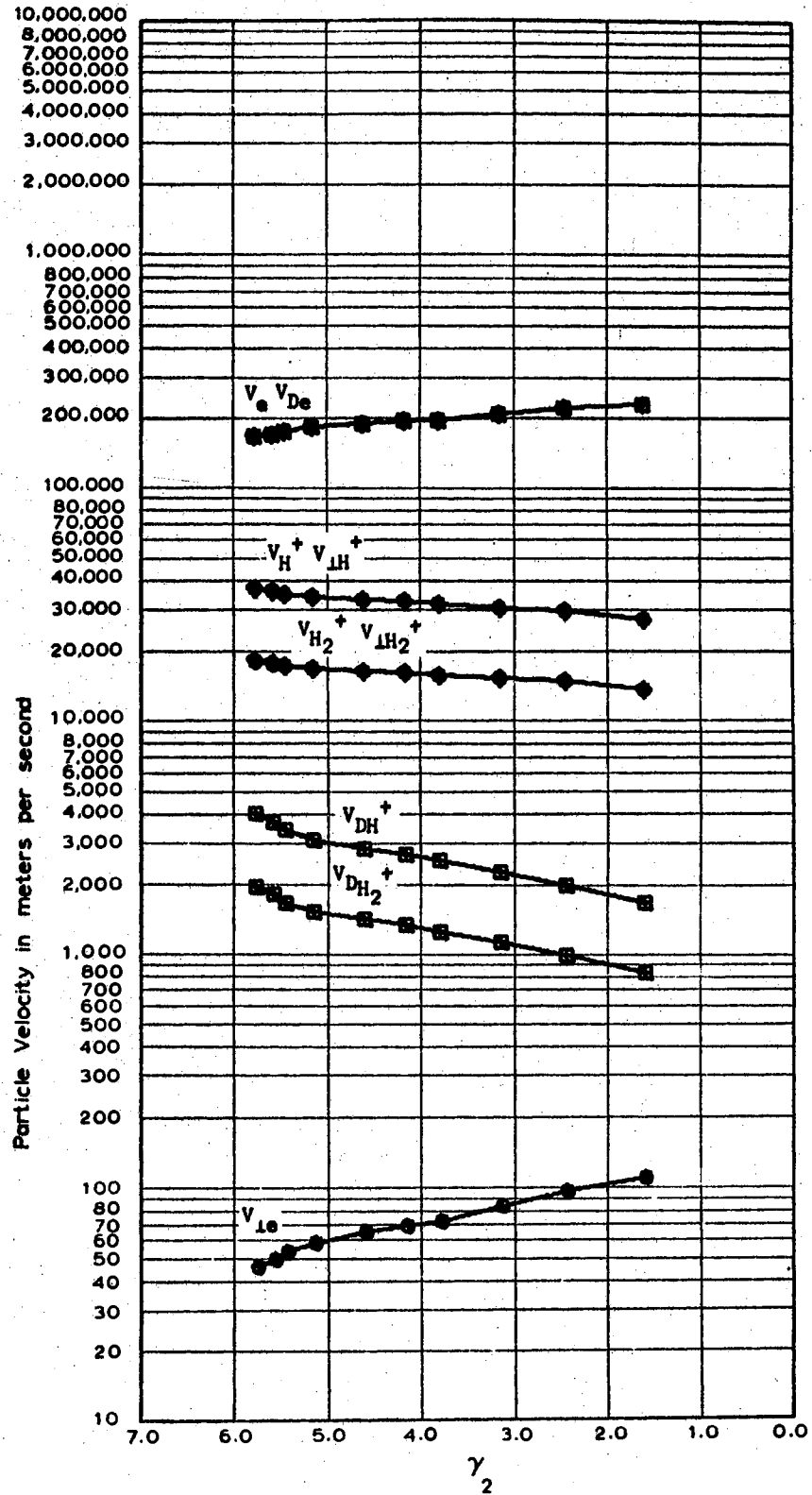
Figure 79c. Data taken June 13, 1966 at 20 MH$_z$ with the Aluminum Cell, D $\cong$ 0.002794 meters
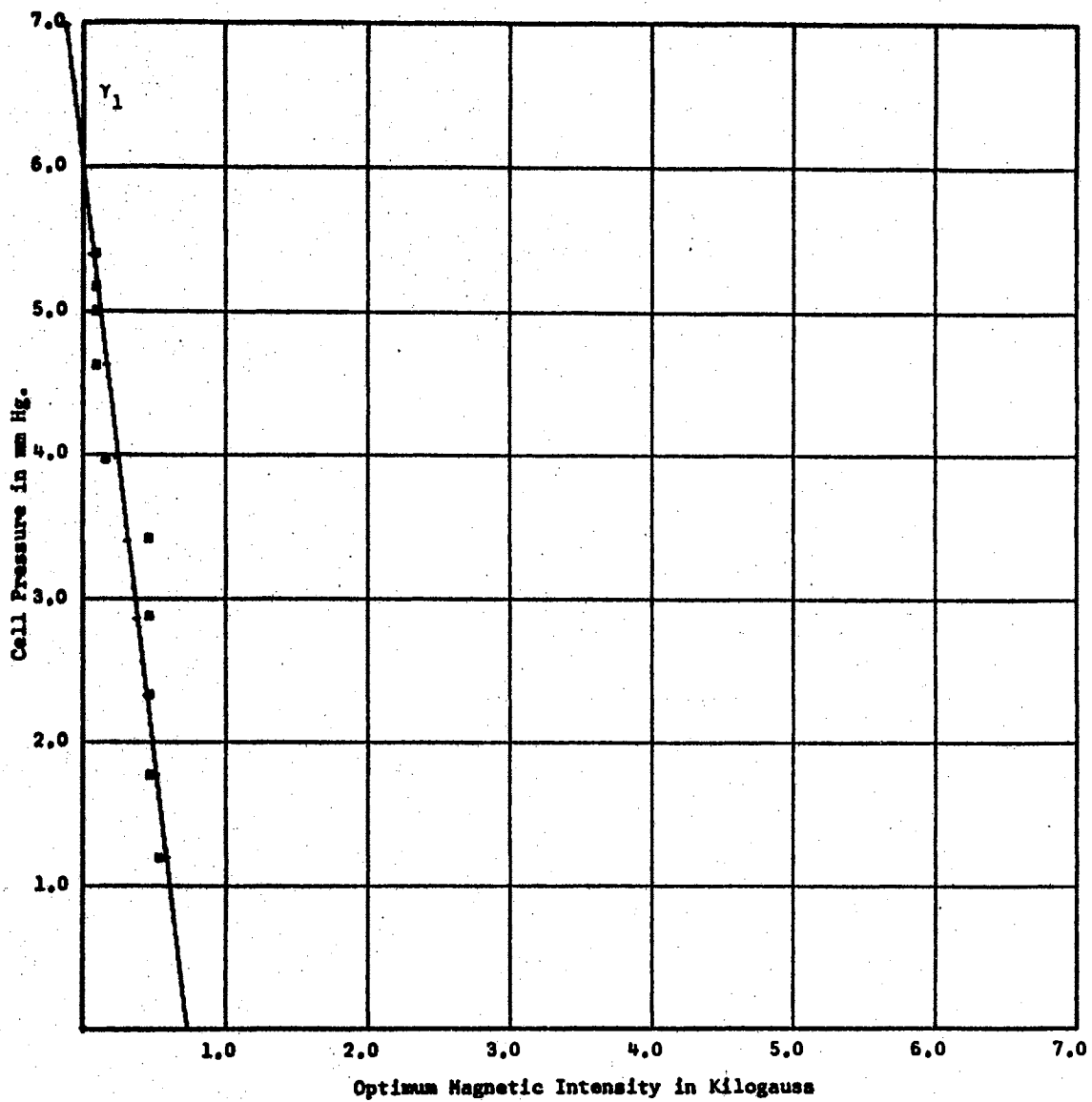
Figure 80a.   Data taken September 6, 1966 at 20 MH_z with the
Aluminum Cell No. 2, D = 0.0059309 meters
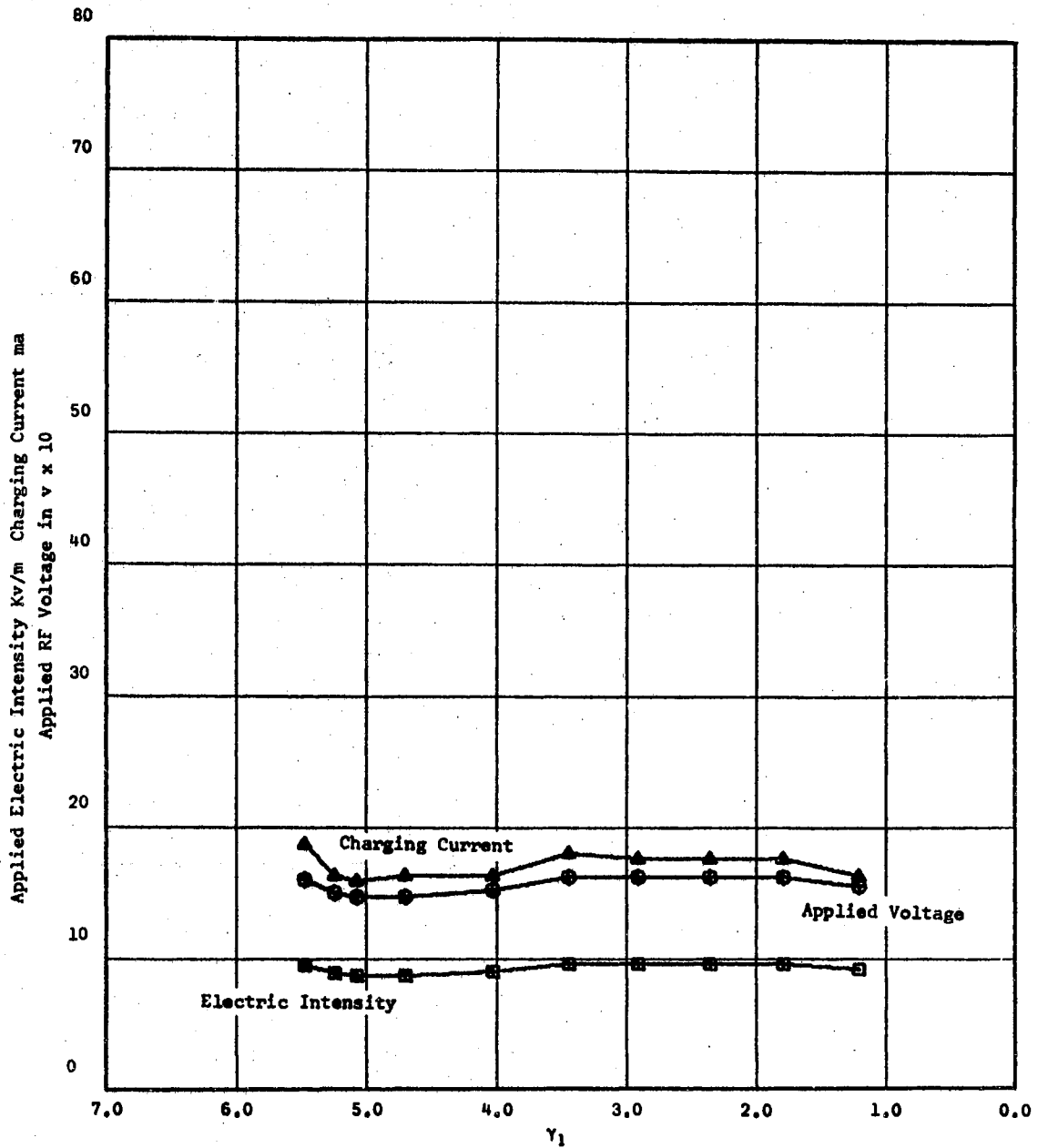
Figure 80b. Data taken September 6, 1966 at 20 MH$_z$ with Aluminum Cell No. 2, D = 0.0059309 meters
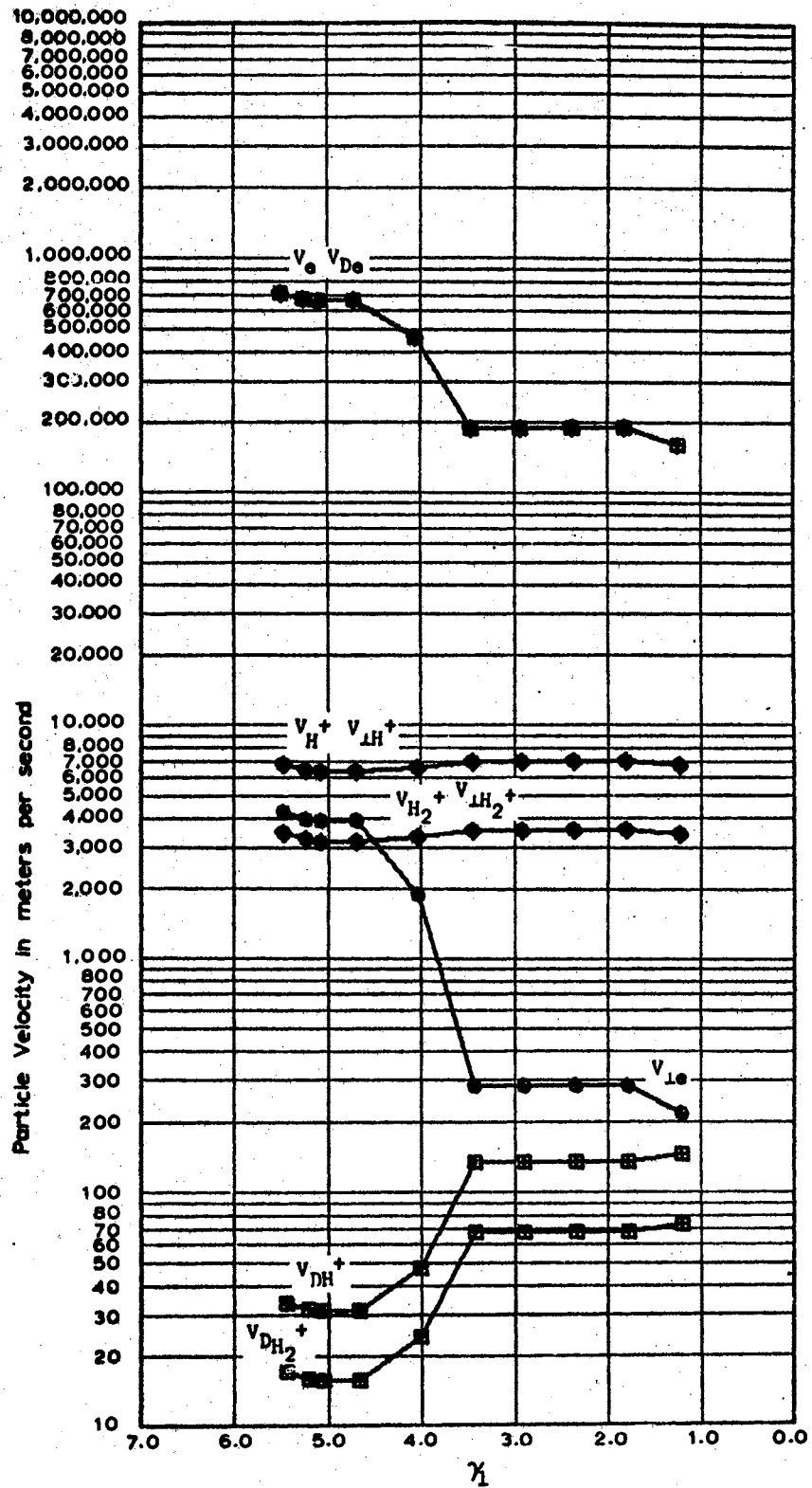
Figure 80c. Data taken September 6, 1966 at
20 MH with Aluminum Cell No.
2, D = 0.0059309 meters
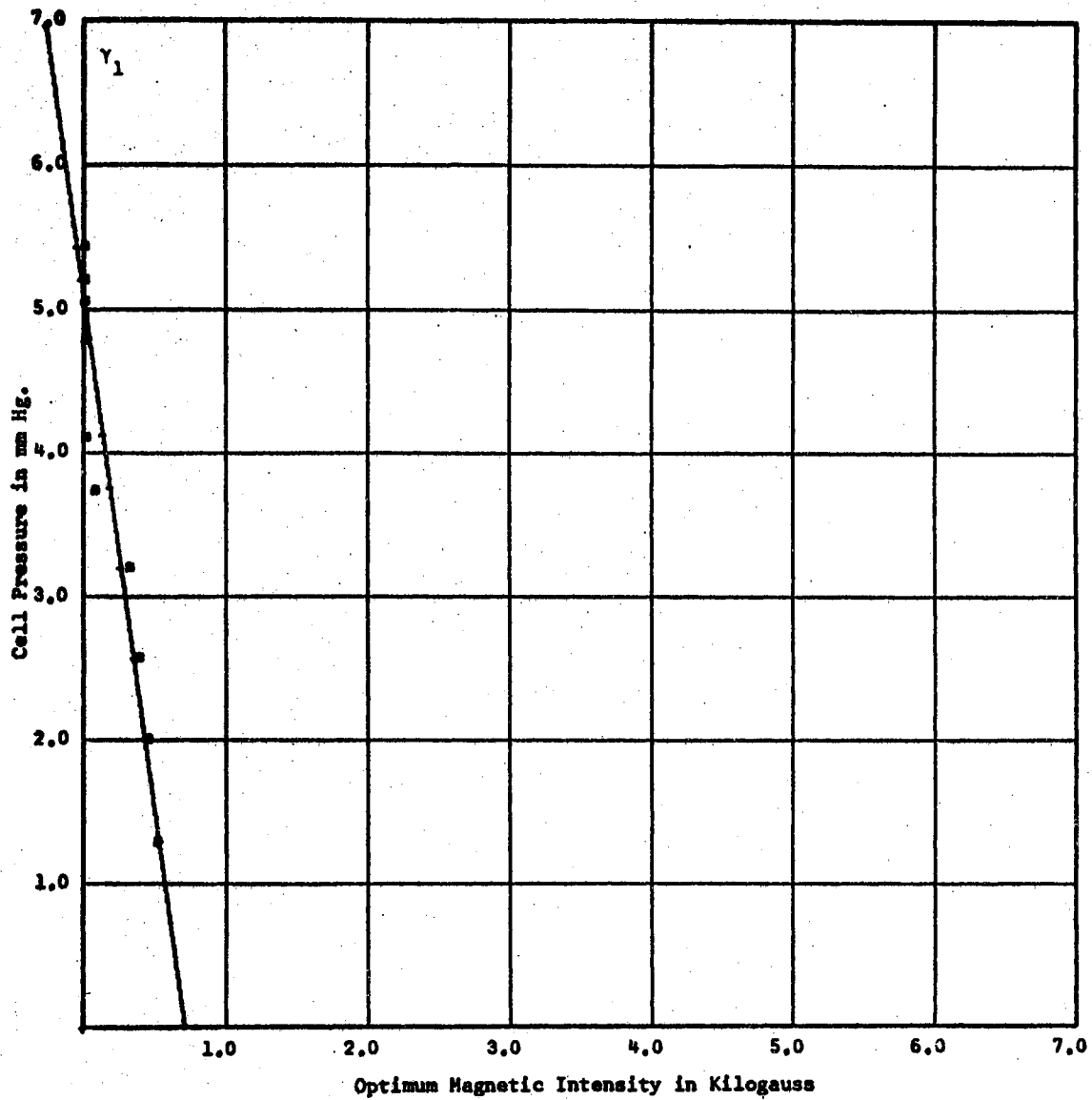
Figure 81a. Data taken September 9, 1966 at 20 MH_z with Aluminum Cell No. 2, D = 0.0059309 meters
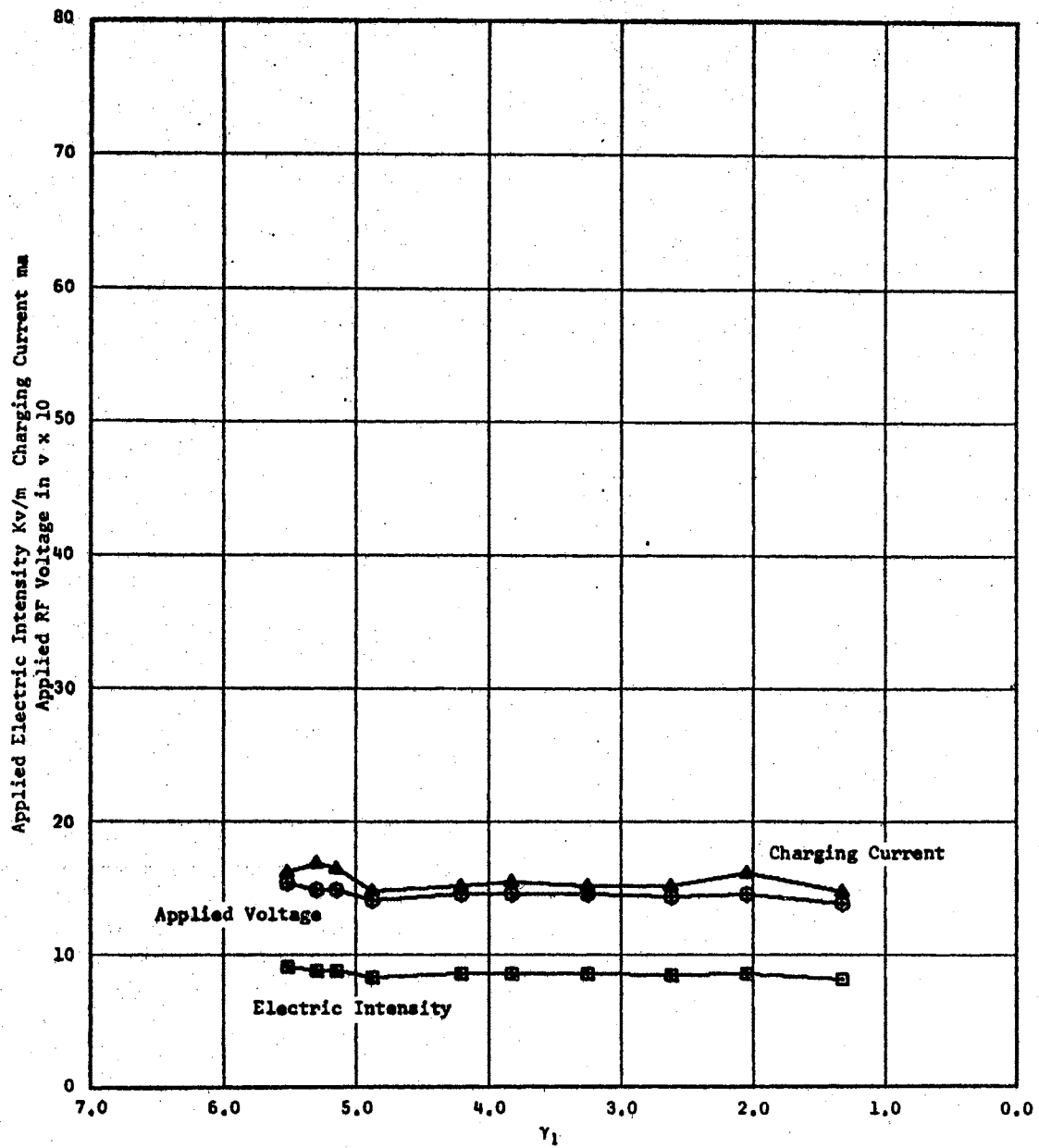
Figure 81b. Data taken September 9, 1966 at 20 MH$_z$ with
Aluminum Cell No. 2, D = 0.0059309 meters
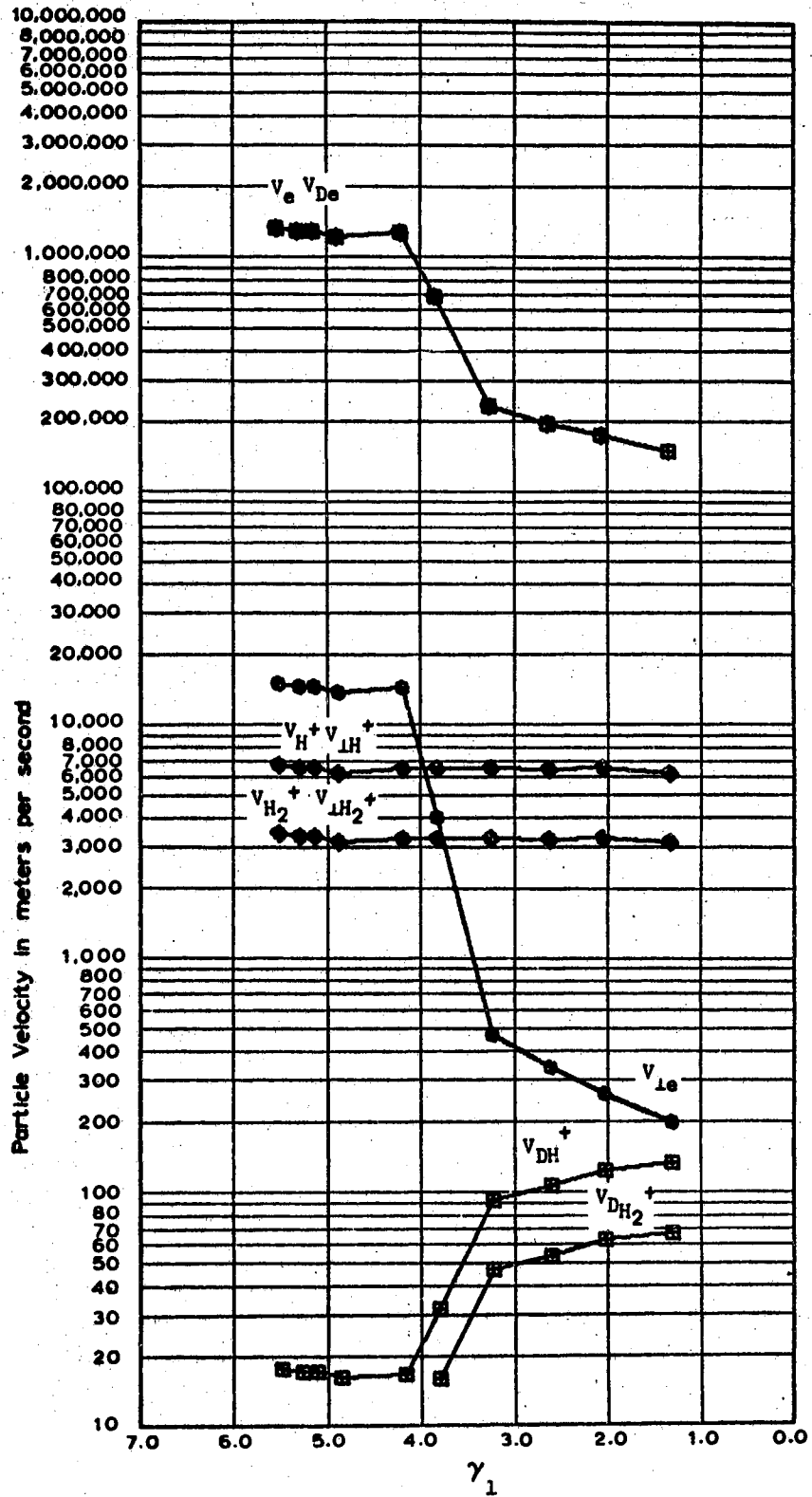
Figure 81c. Data taken September 9, 1966 at 20 MH_z with Aluminum Cell No. 2, D = 0.0059309 meters
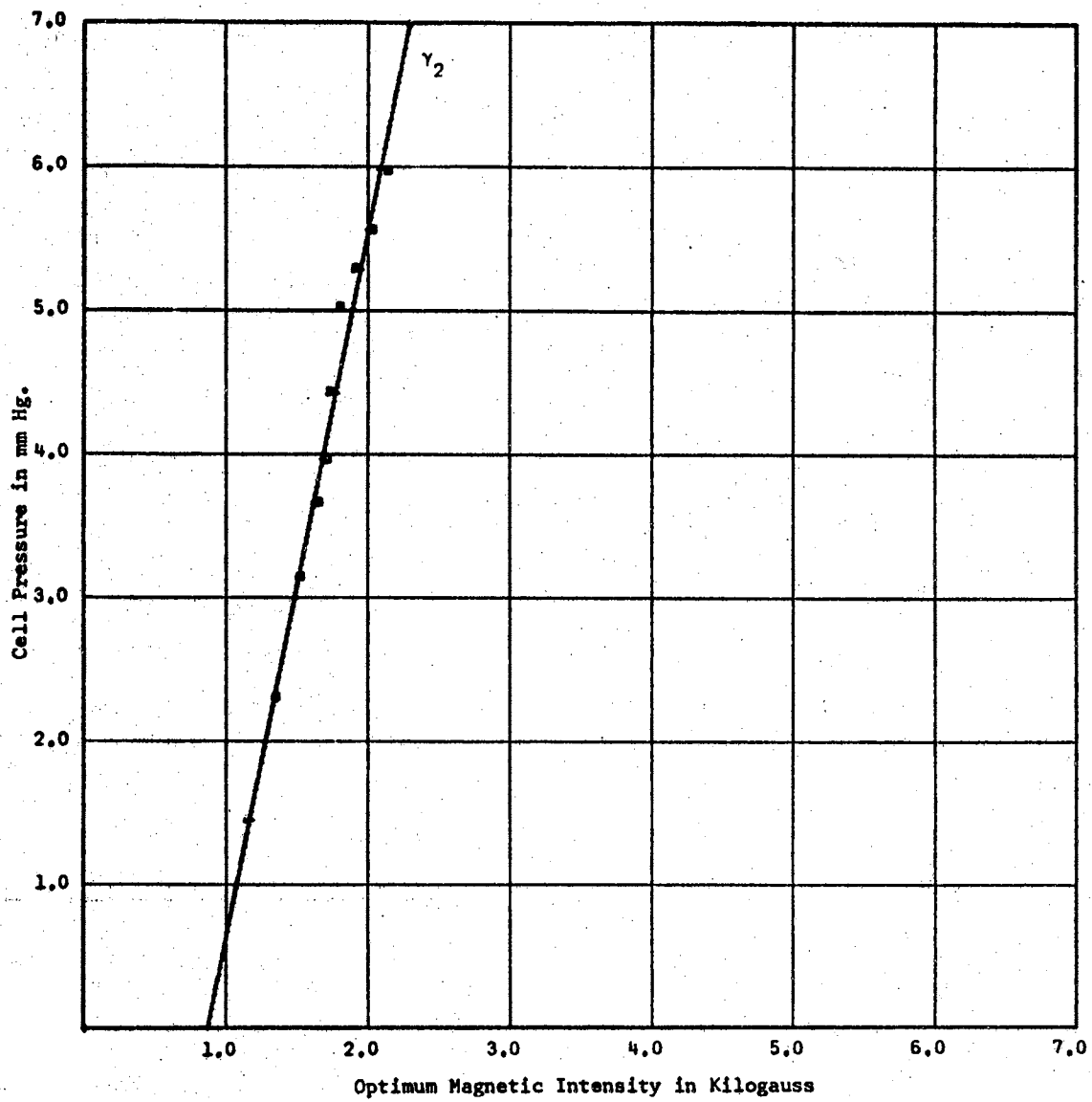
Figure 82a. Data taken June 10, 1966 at 25 MH_z with the Aluminum
Cell, D = 0.002794 meters
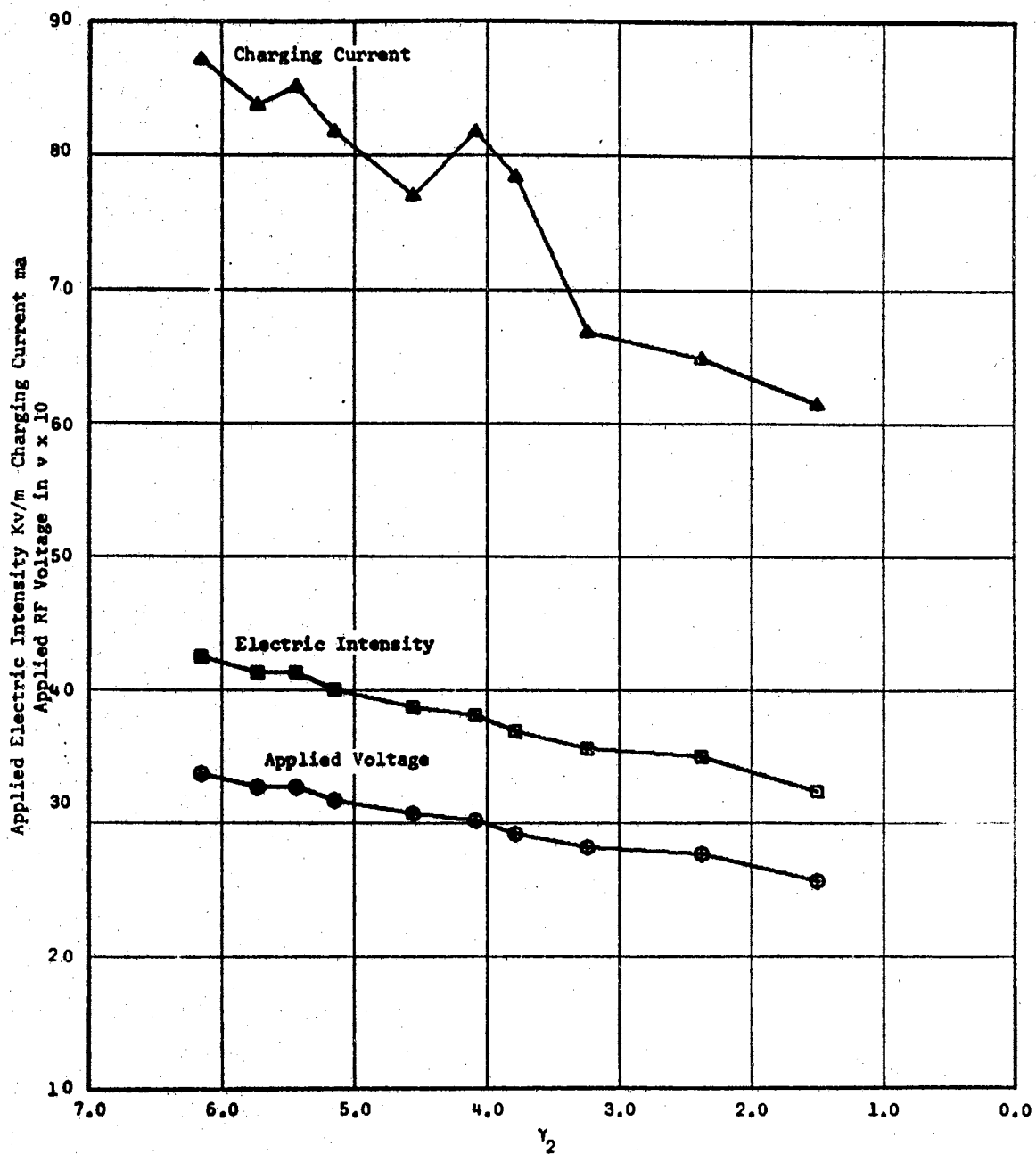
Figure 82b. Data taken June 10, 1966 at 25 MH$_z$ with the Aluminum Cell, D = 0.002794 meters
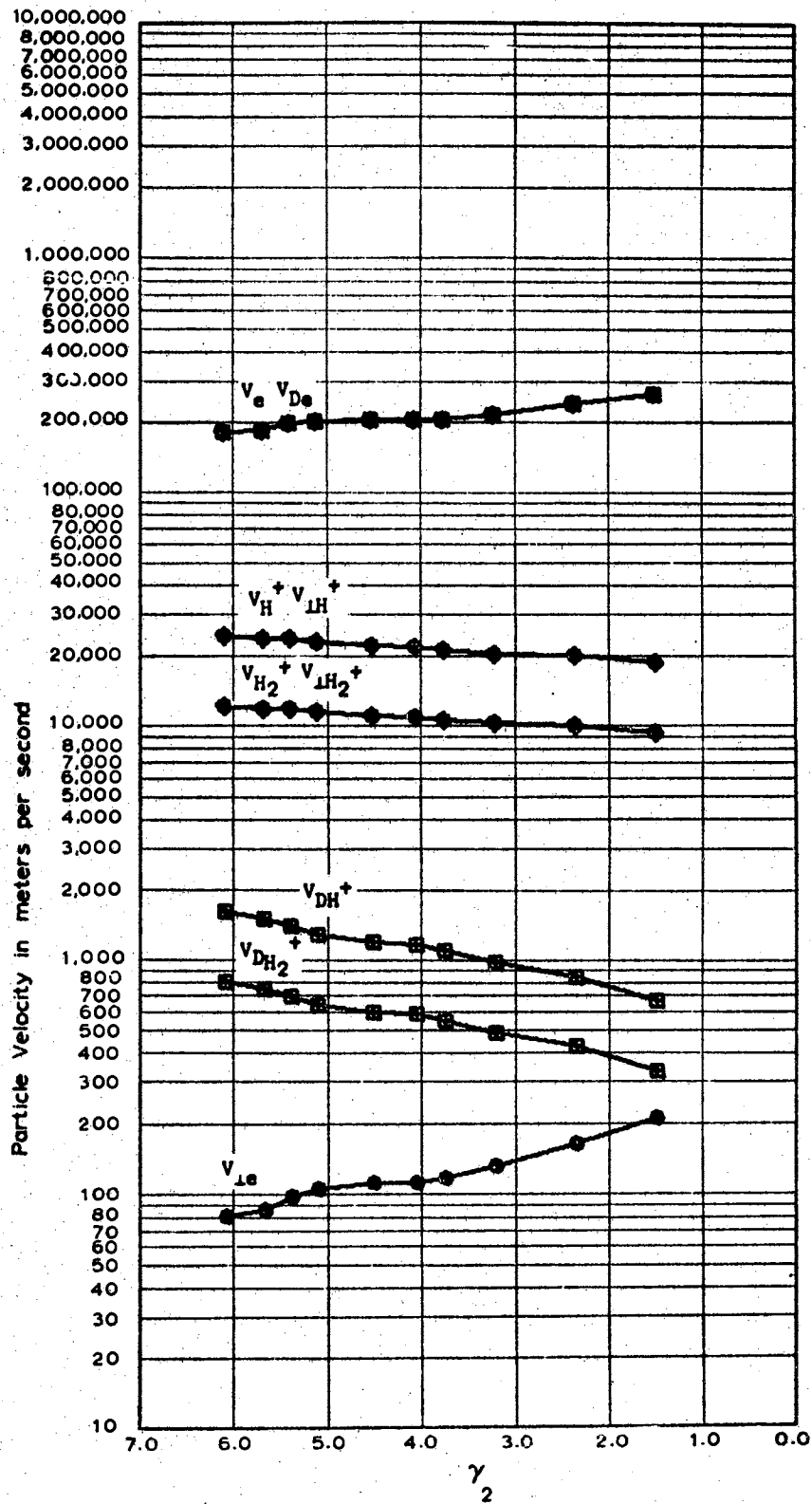
Figure 82c. Data taken June 10, 1966 at 25
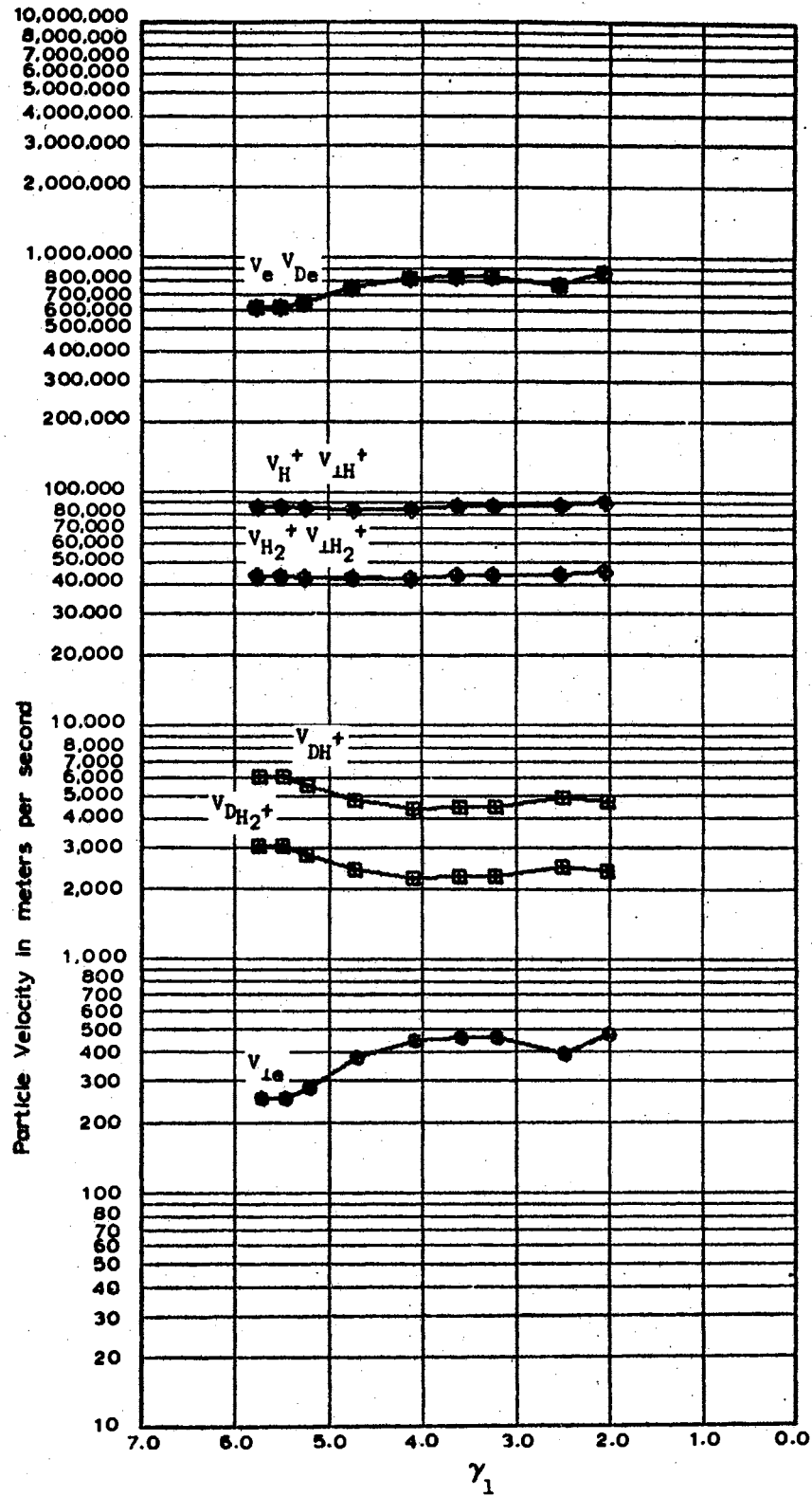MH$_z$ with the Aluminum Cell,
D = 0.002794 meters
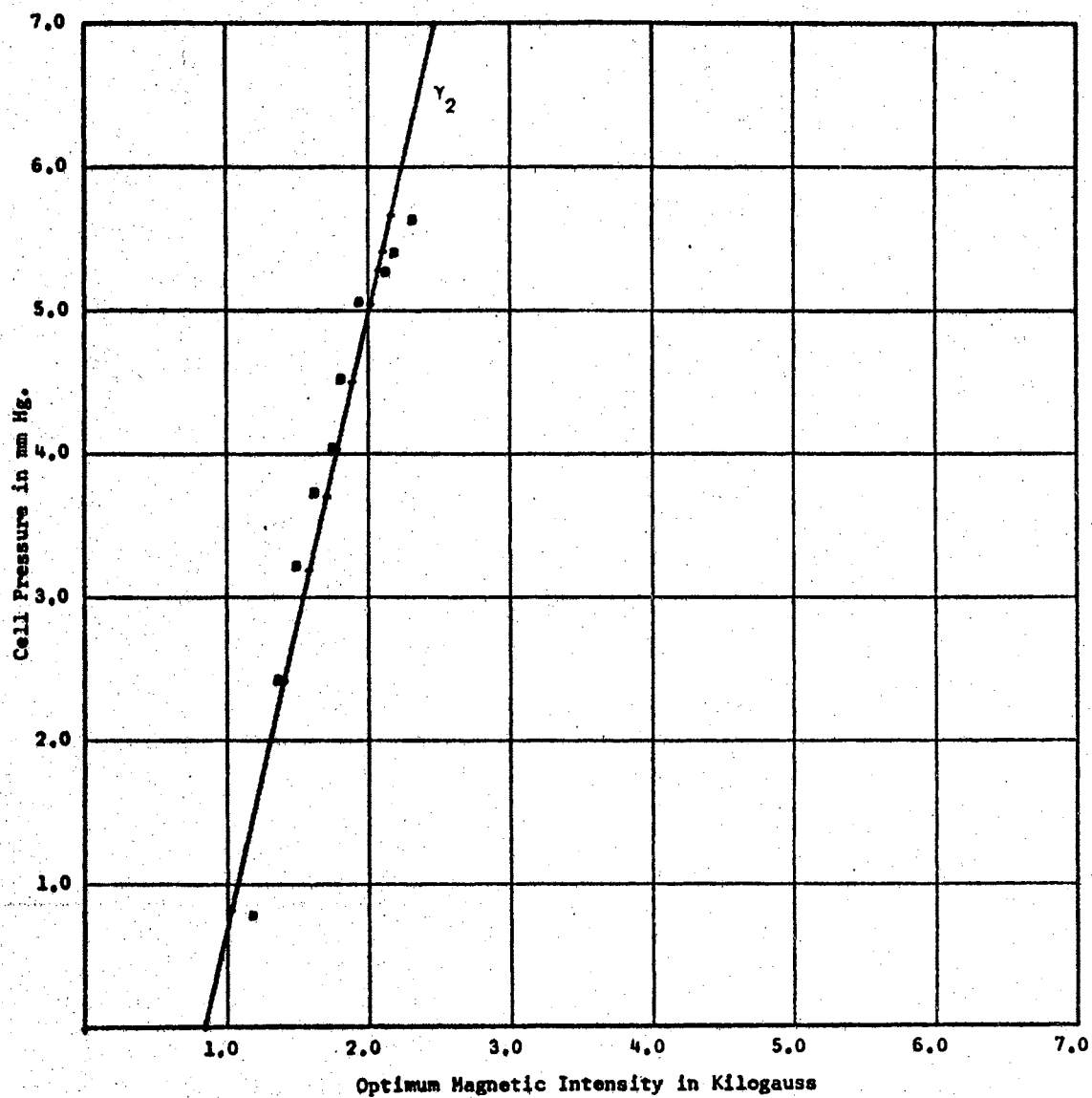
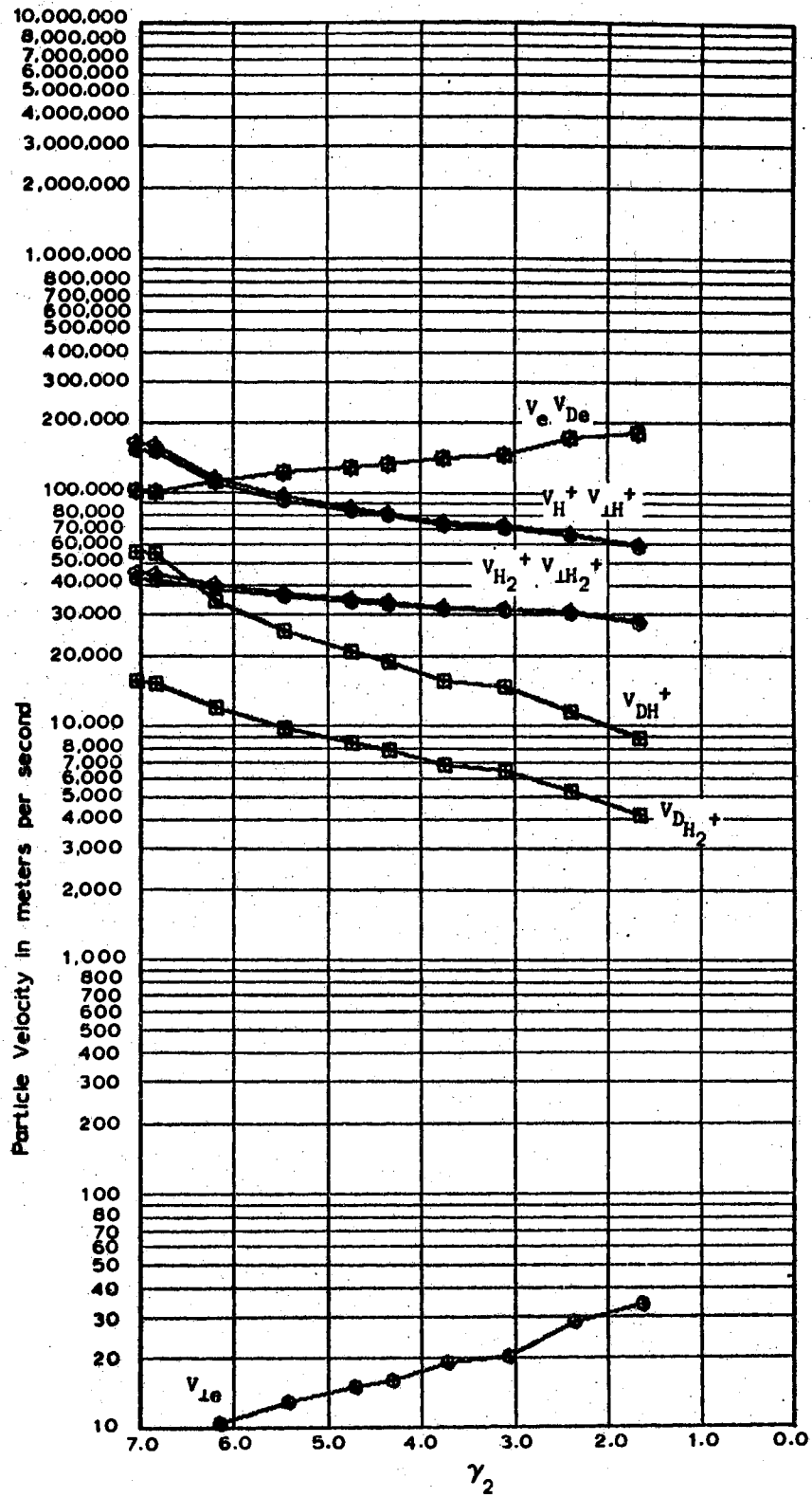Figure 83a. Data taken June 21, 1966 at 25 MH_z with the Aluminum Cell, D = 0.002794 meters
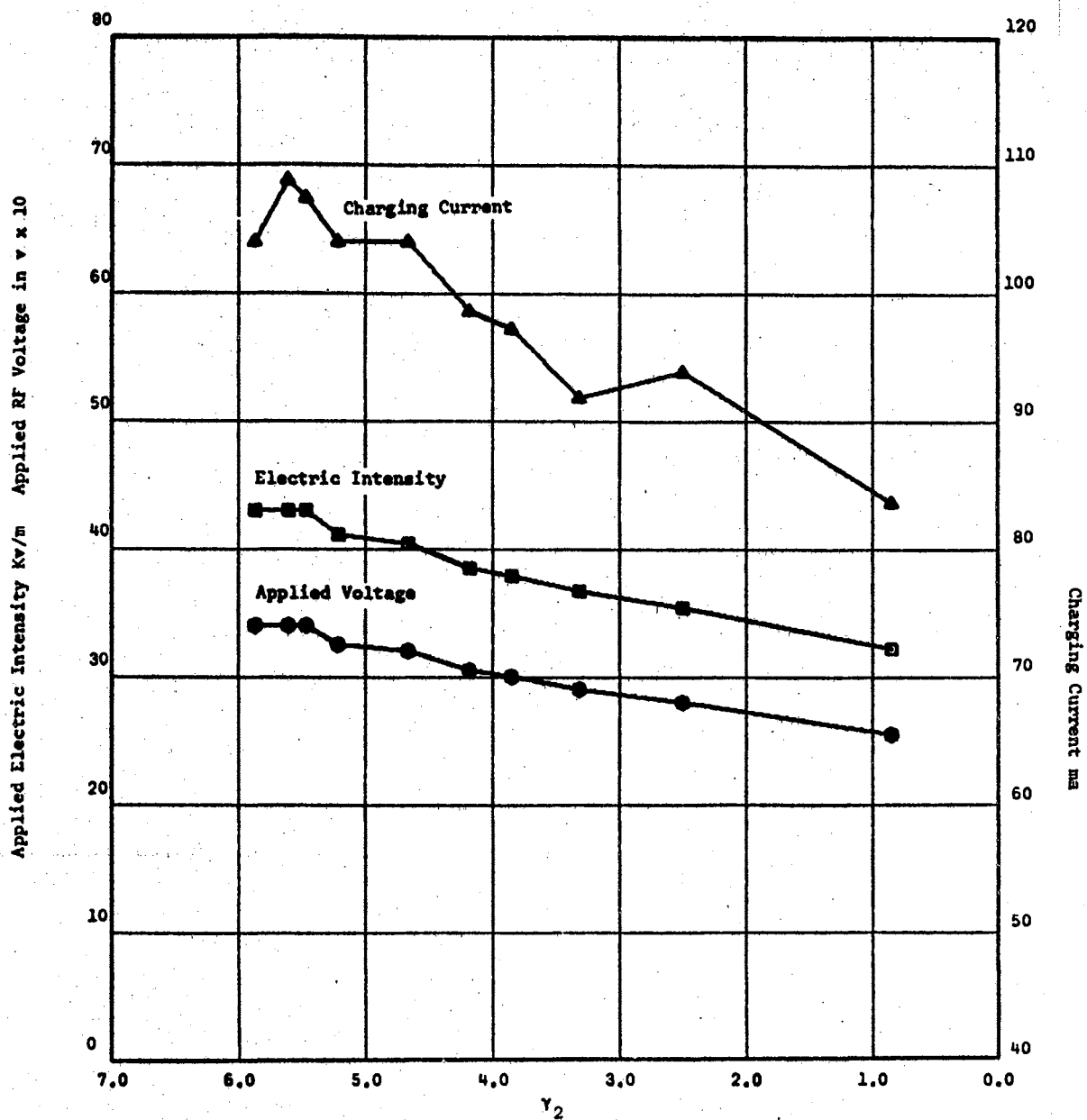
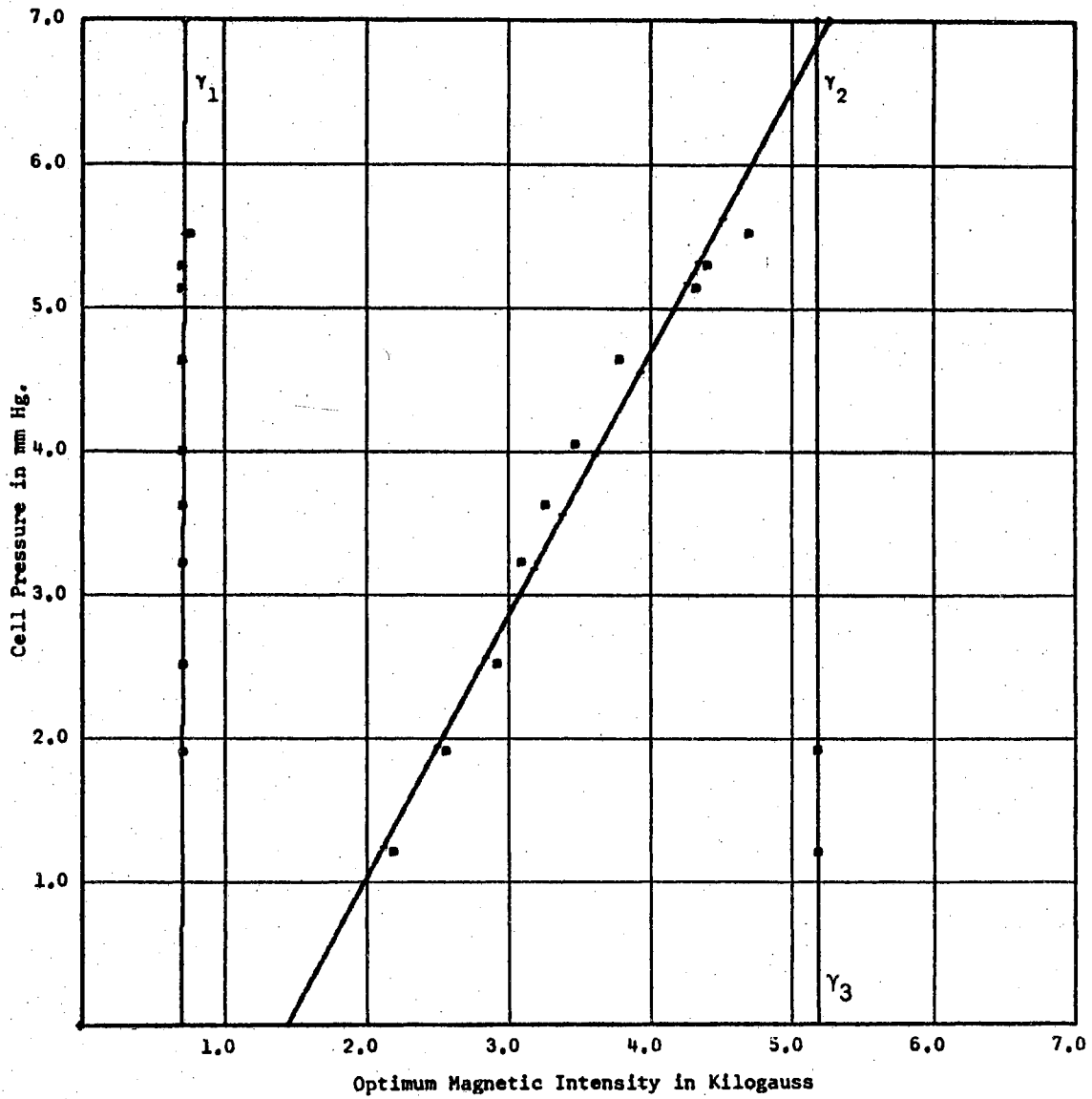Figure 83b. Data taken June 21, 1966 at 25 MH$_z$ with the Aluminum Cell, D = 0.002794 meters
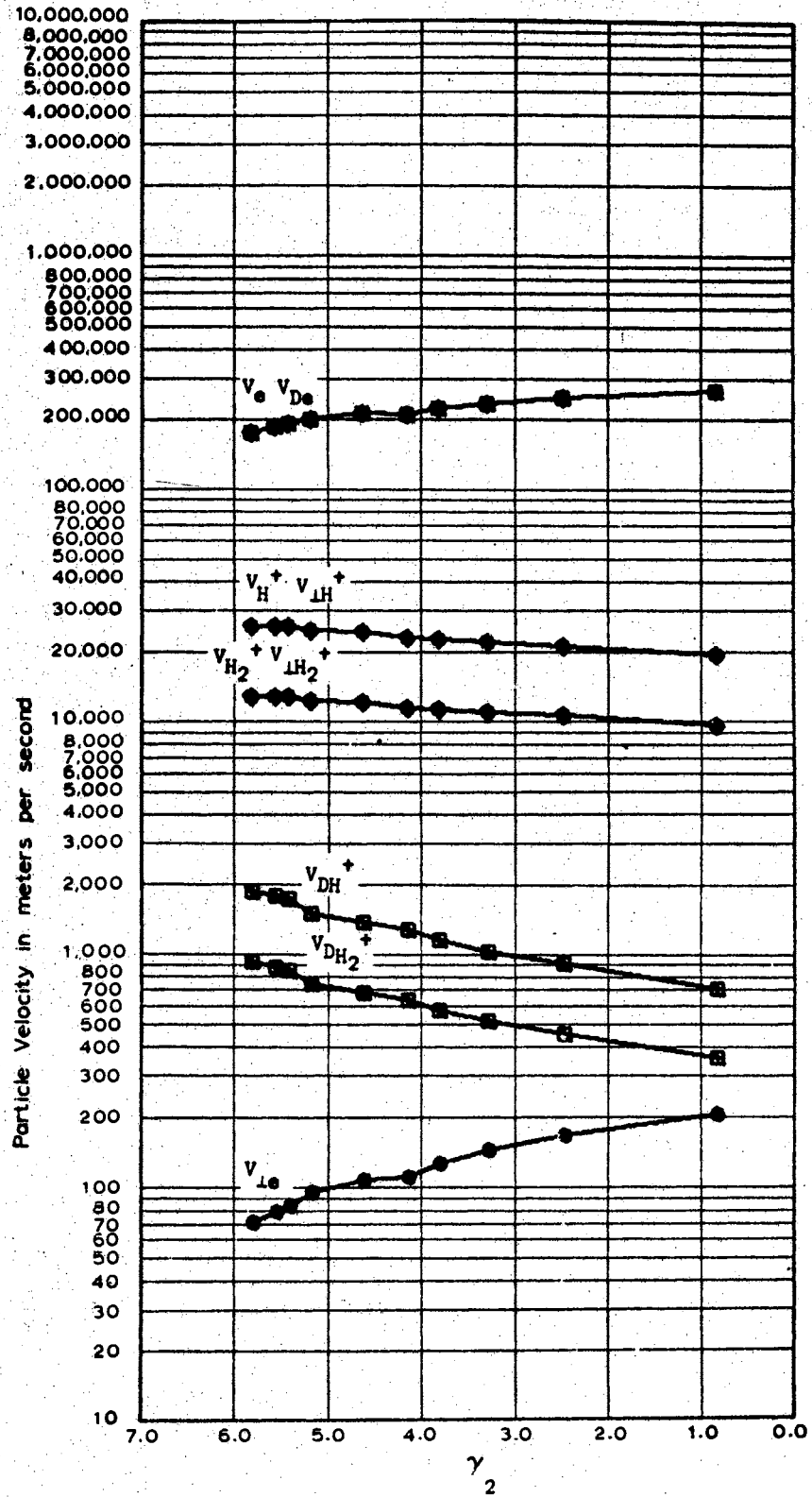
Figure 83c. Data taken June 21, 1966 at 25
MH$_z$ with the Aluminum Cell,
D $\cong$ 0.002794 meters

276
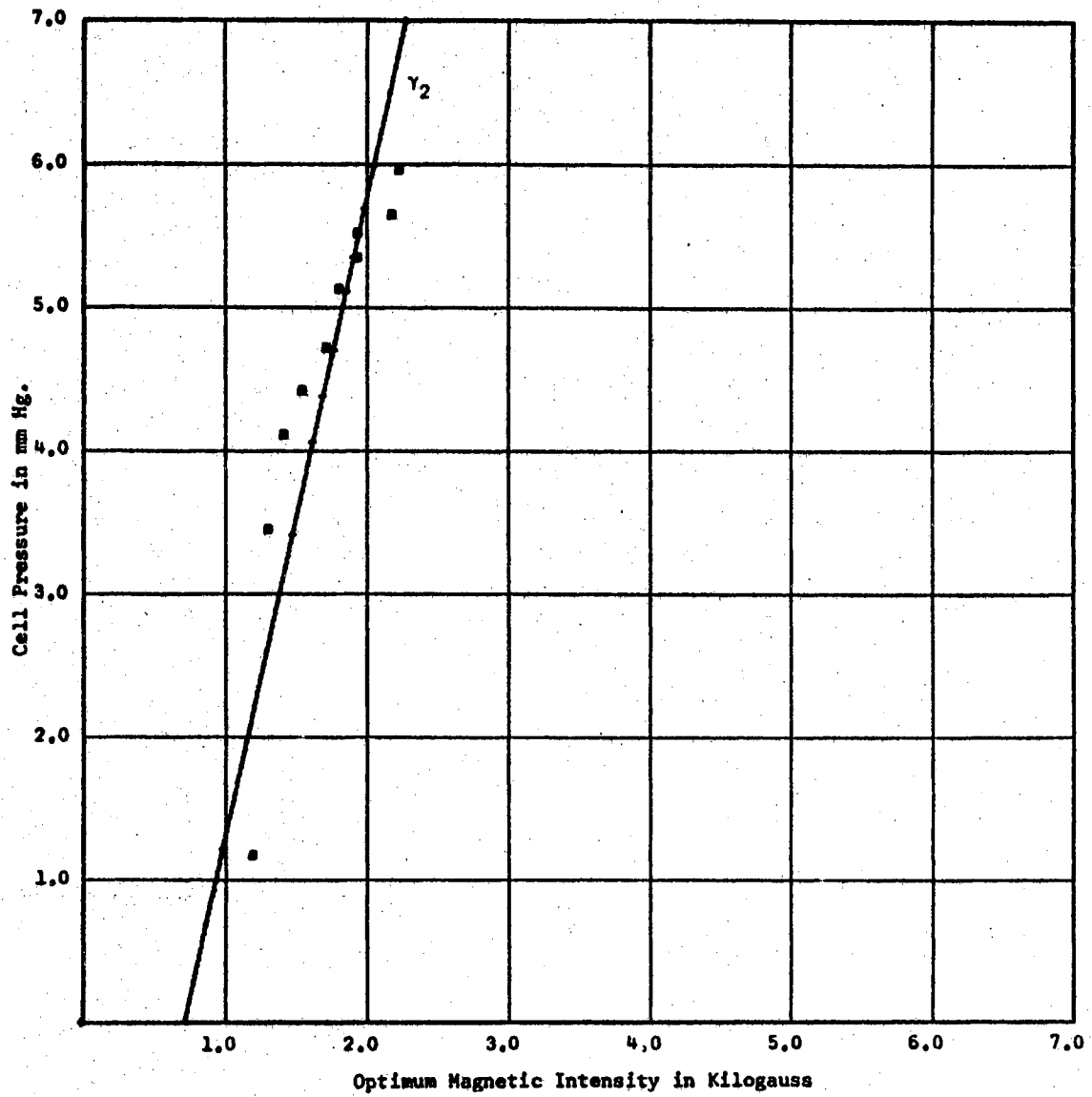
Figure 84a.   Data taken May 30, 1966 at 30 MH_z with the Aluminum
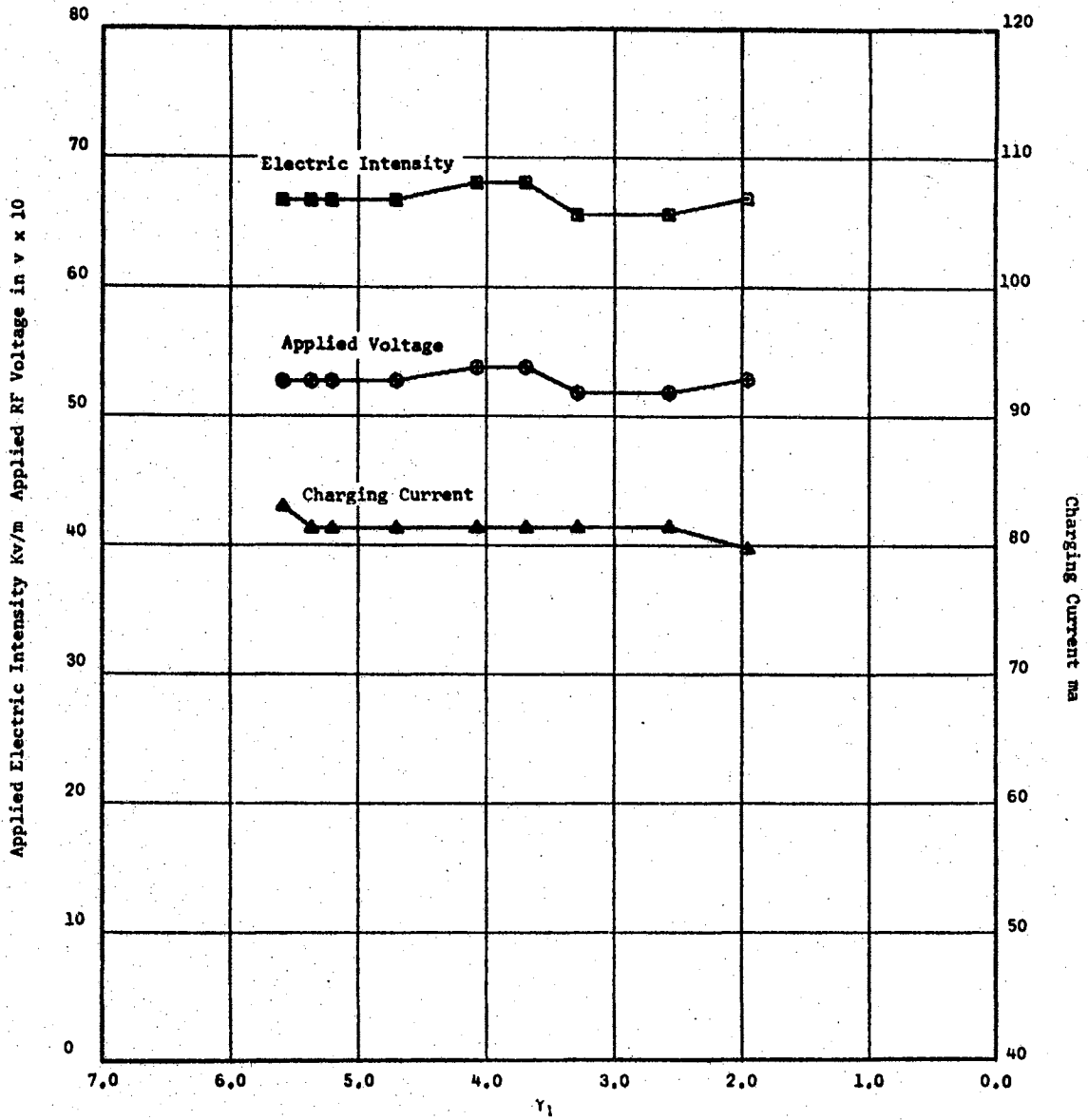Cell, D = 0.002794 meters
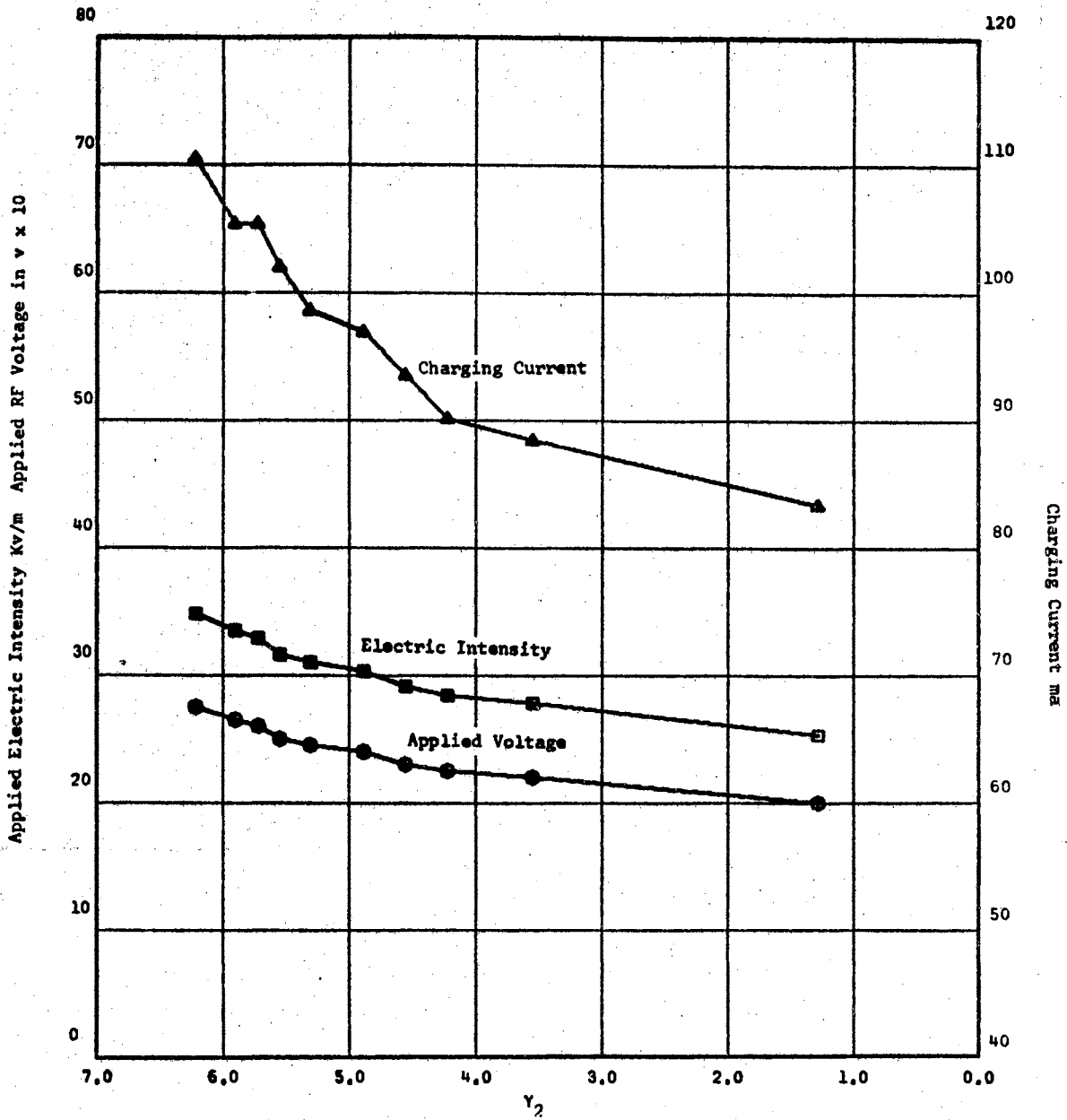
Figure 84b. Data taken May 30, 1966 at 30 MH$_z$ with the
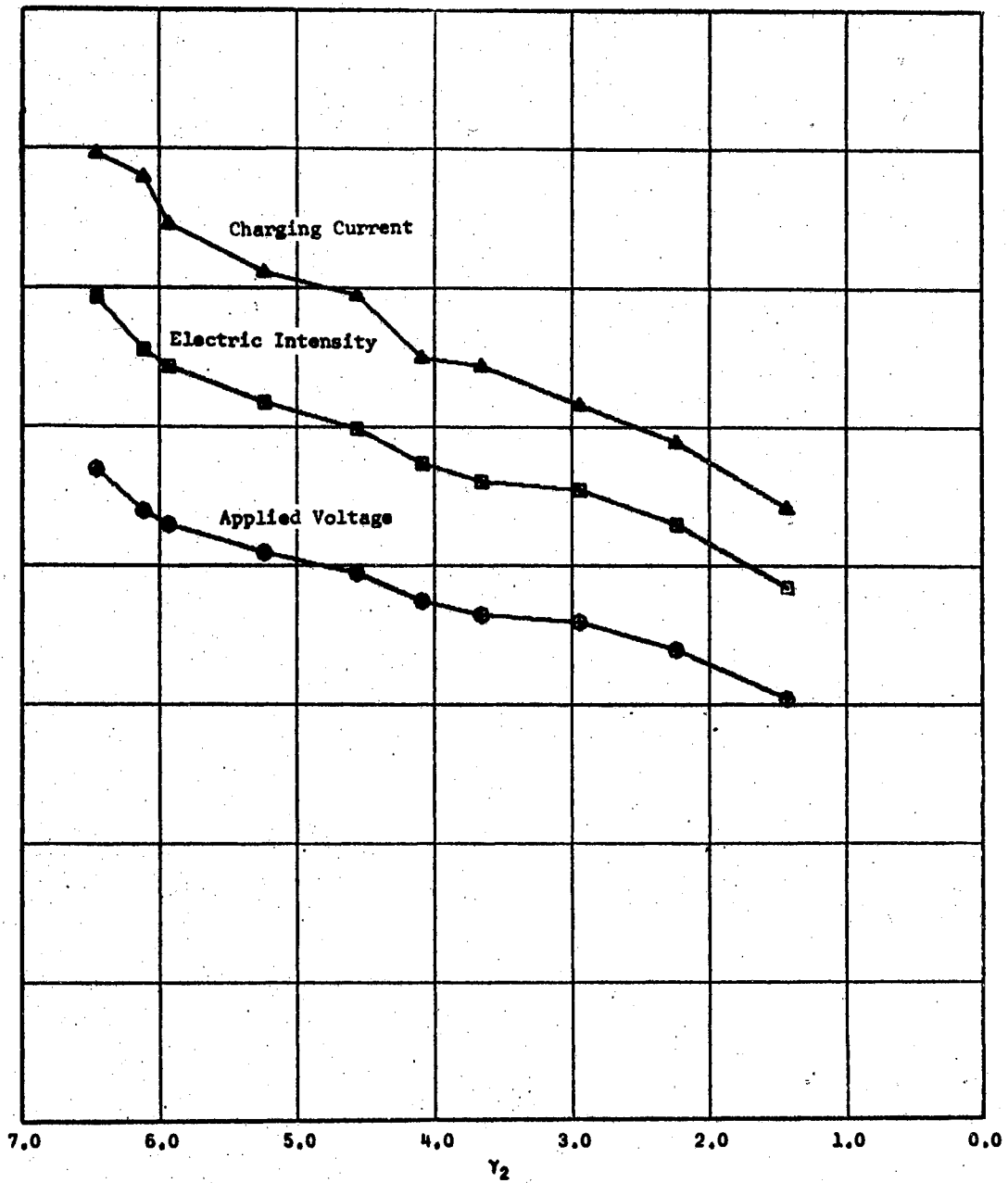Aluminum Cell, D = 0.002794 meters
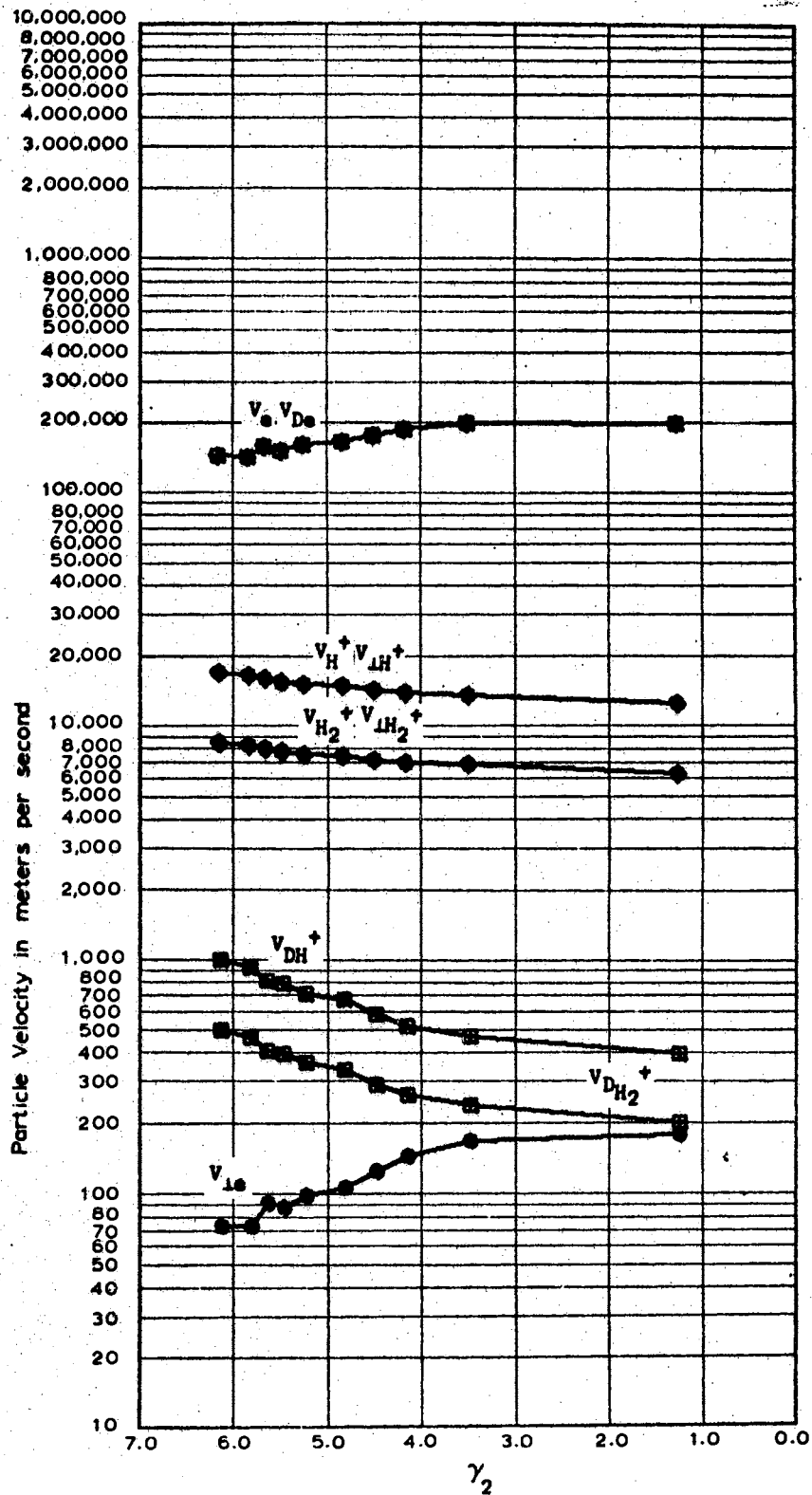
Figure 84c. Data taken May 30, 1966 at 30
MH$_Z$ with the Aluminum Cell,
D $\cong$ 0.002794 meters
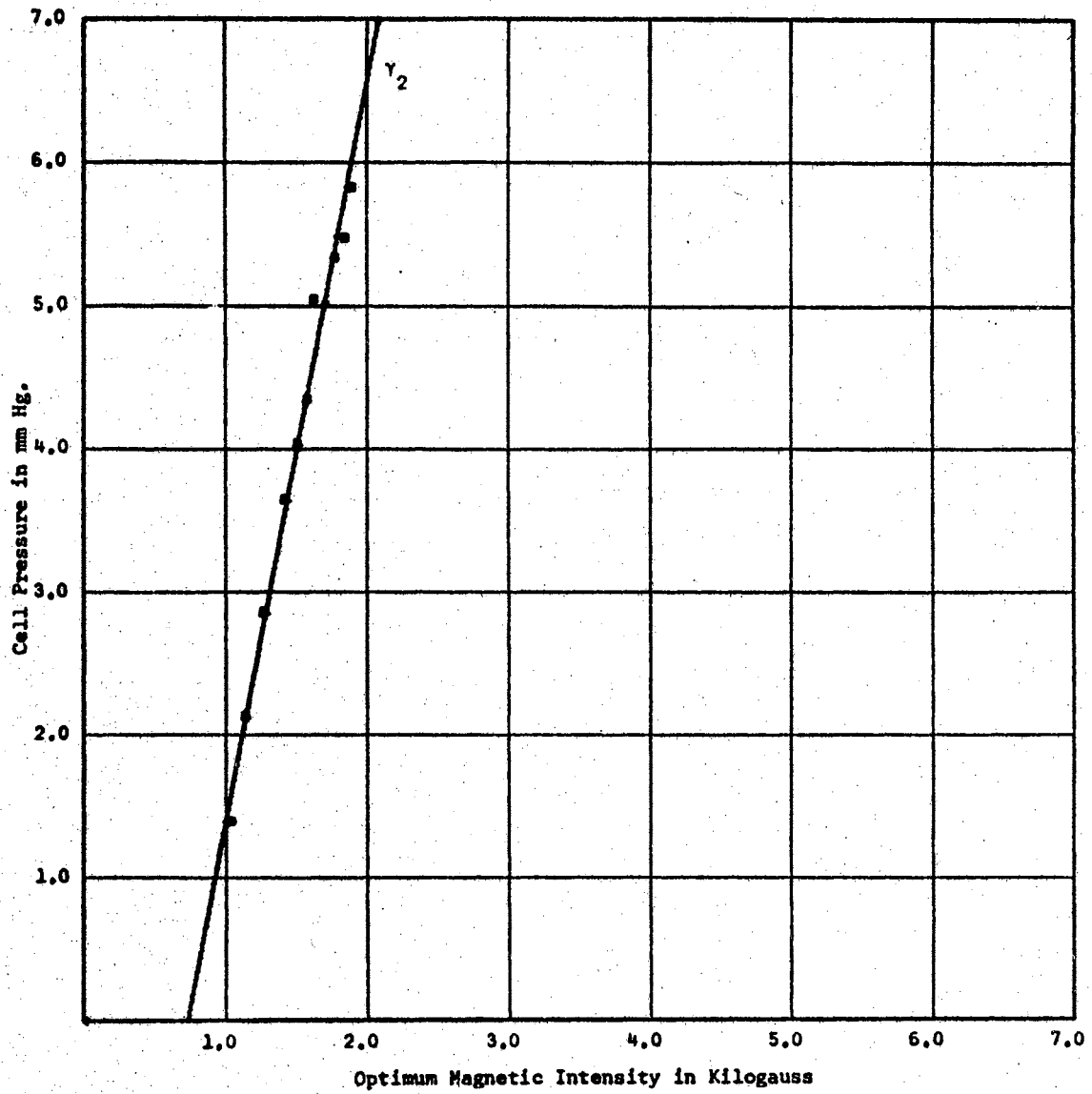
Figure 85a. Data taken June 9, 1966 at 30 MH$_z$ with the Aluminum Cell, D = 0.002794 meters
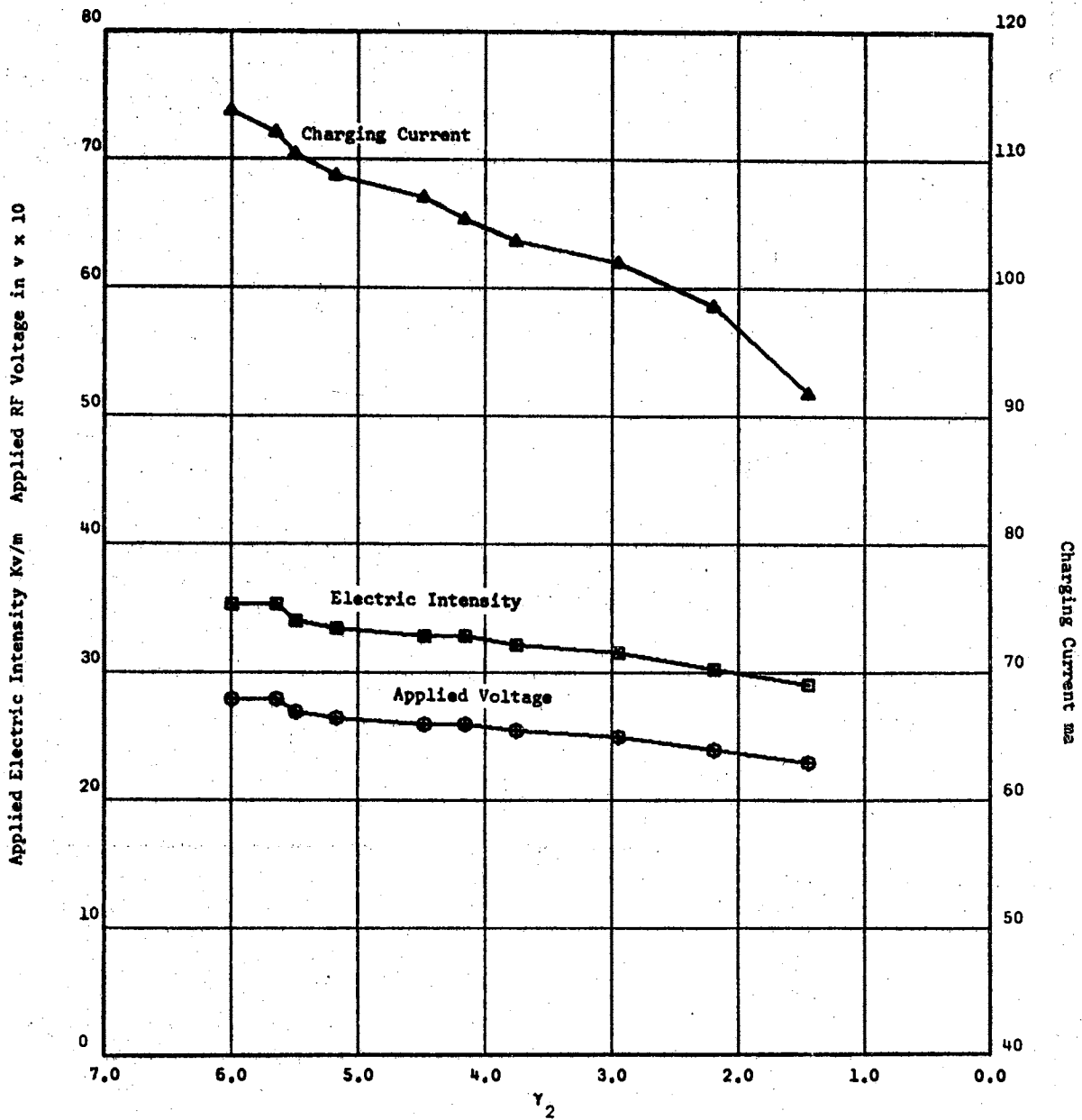
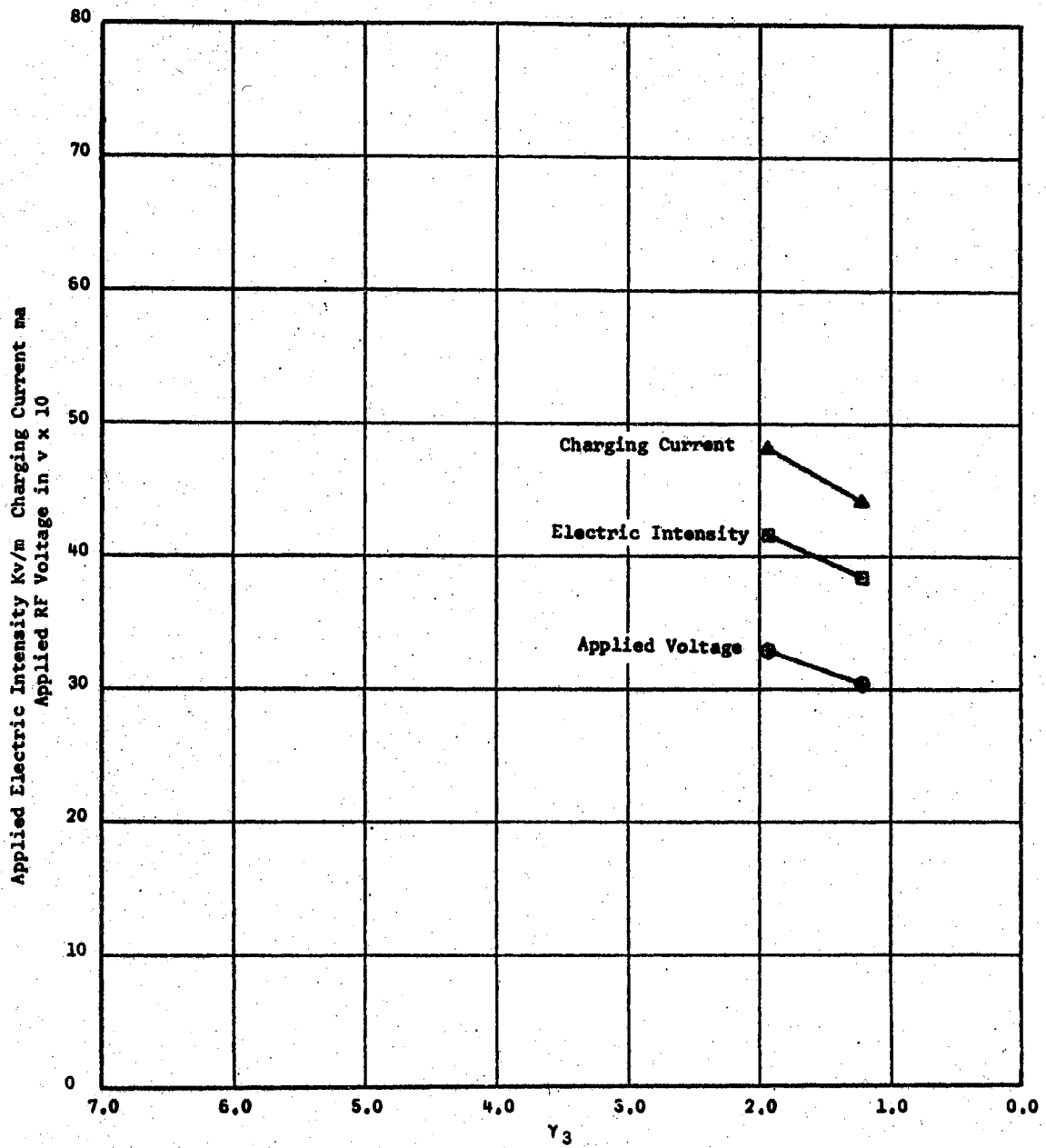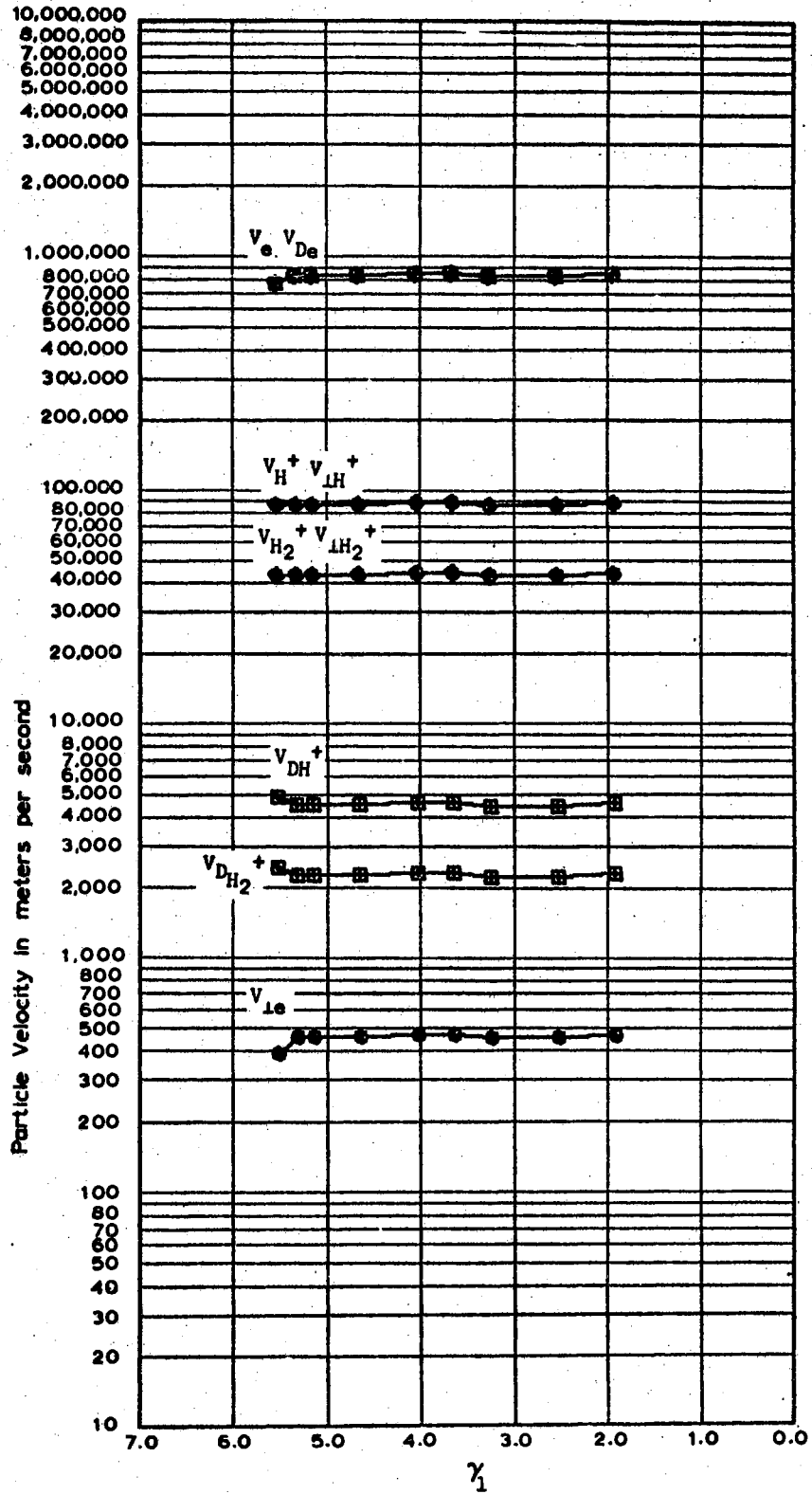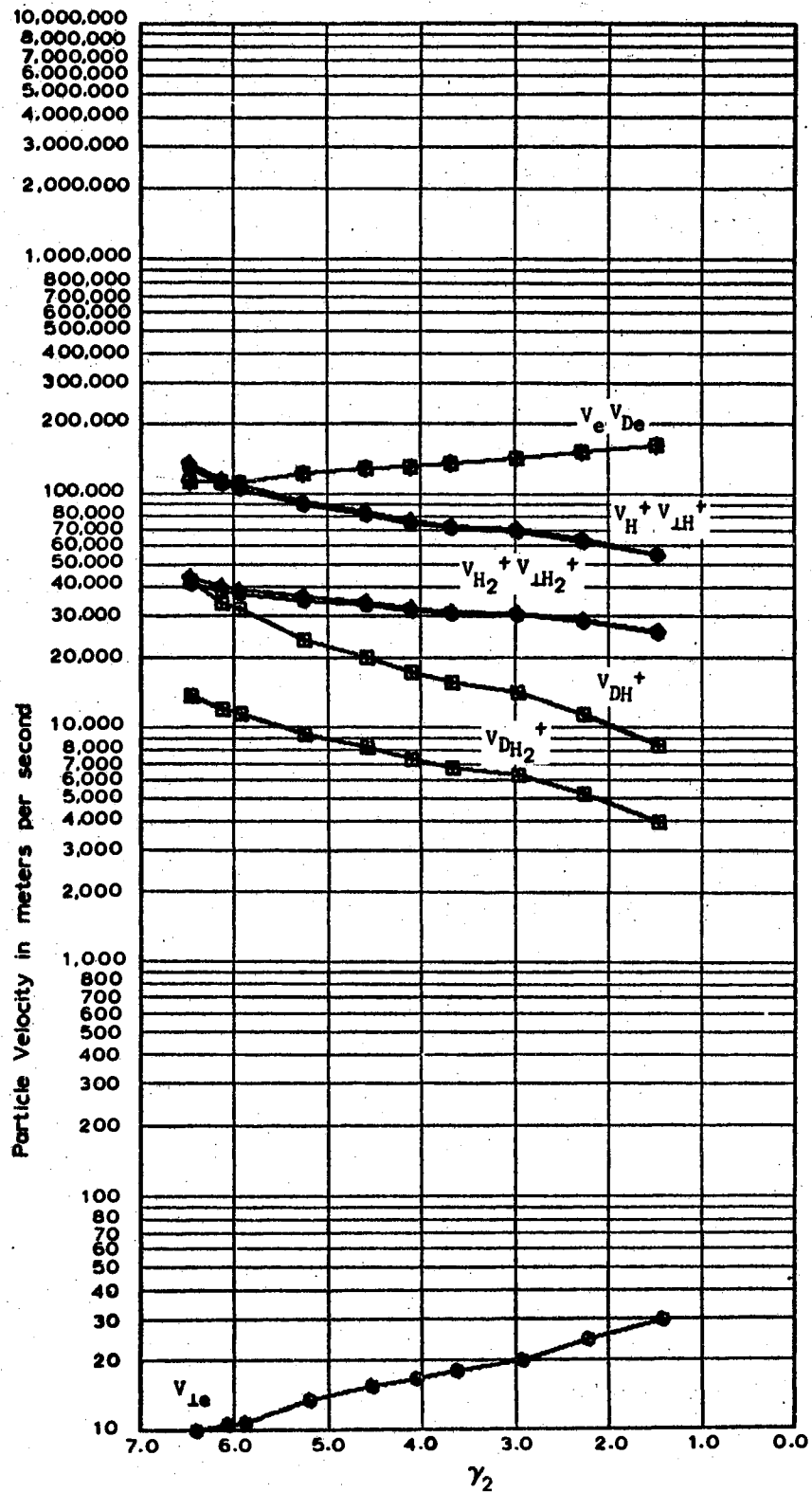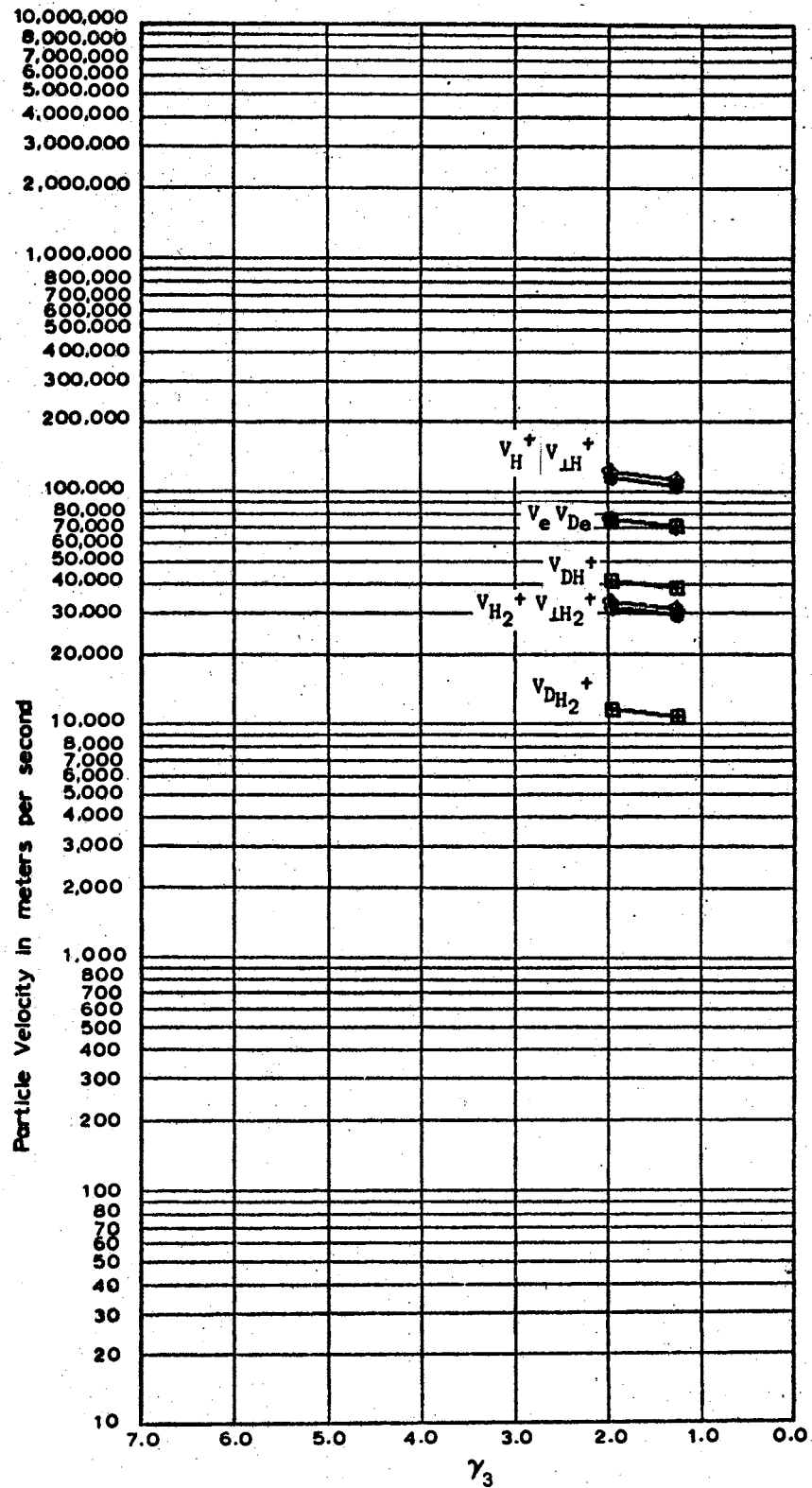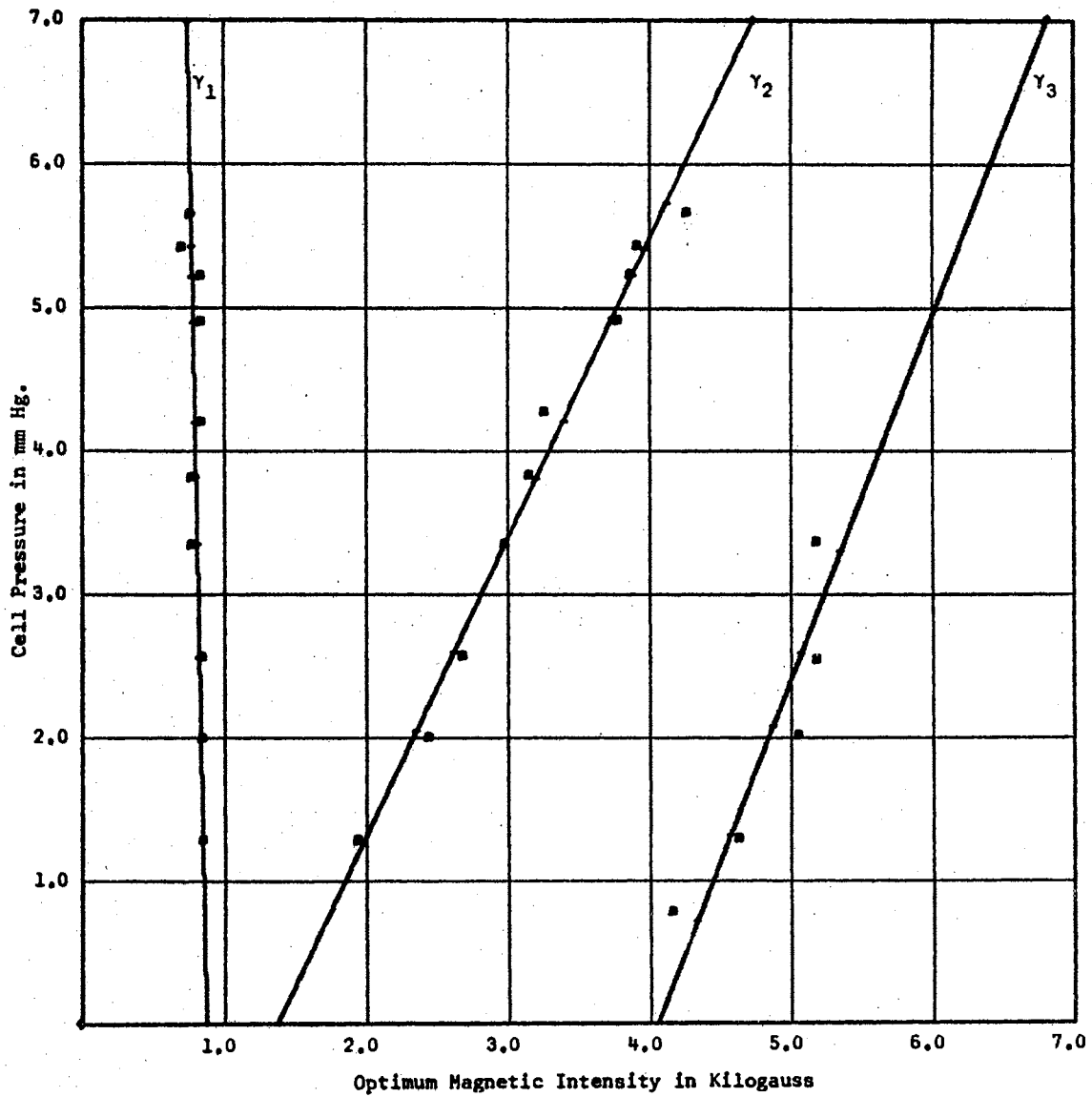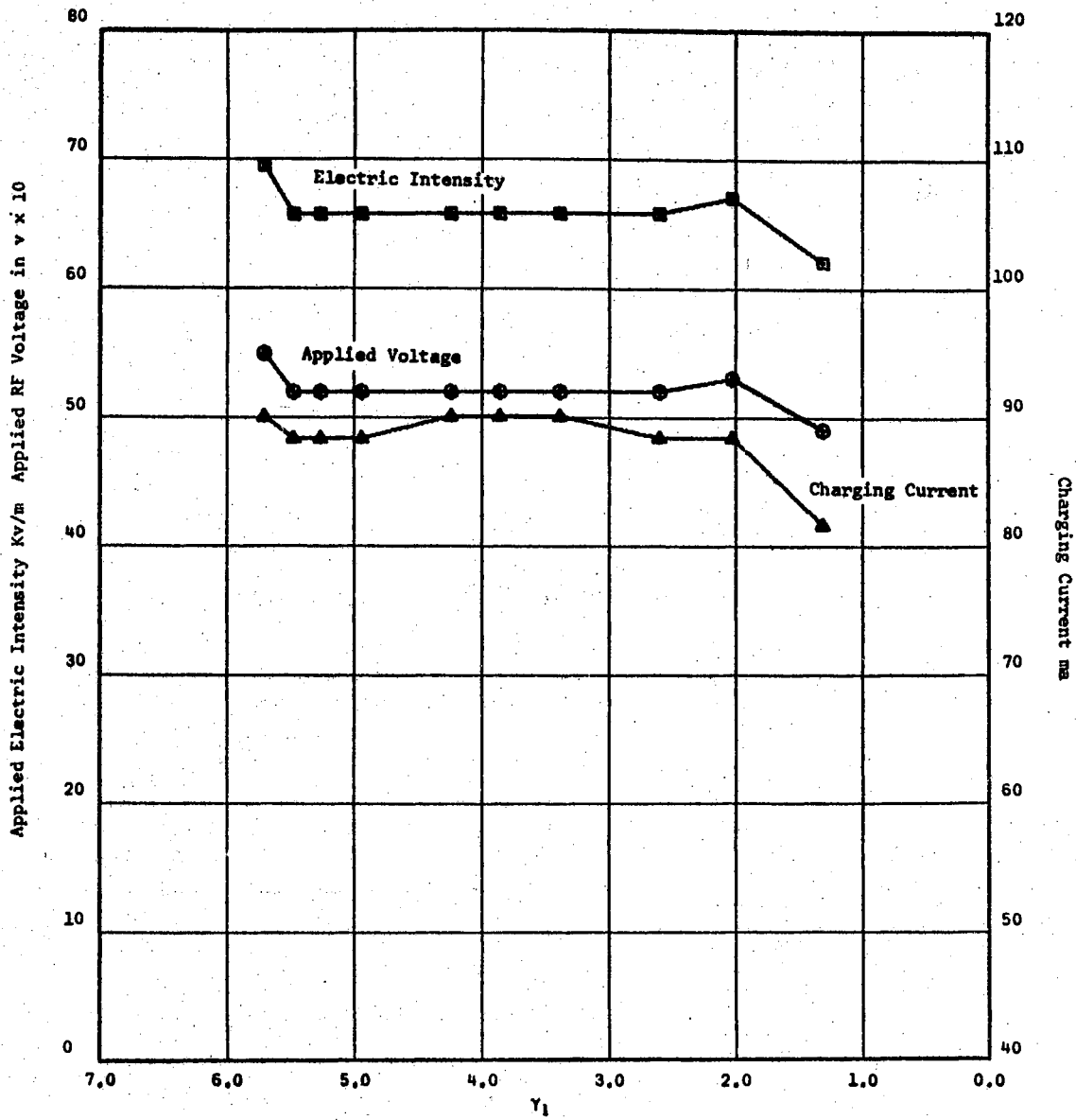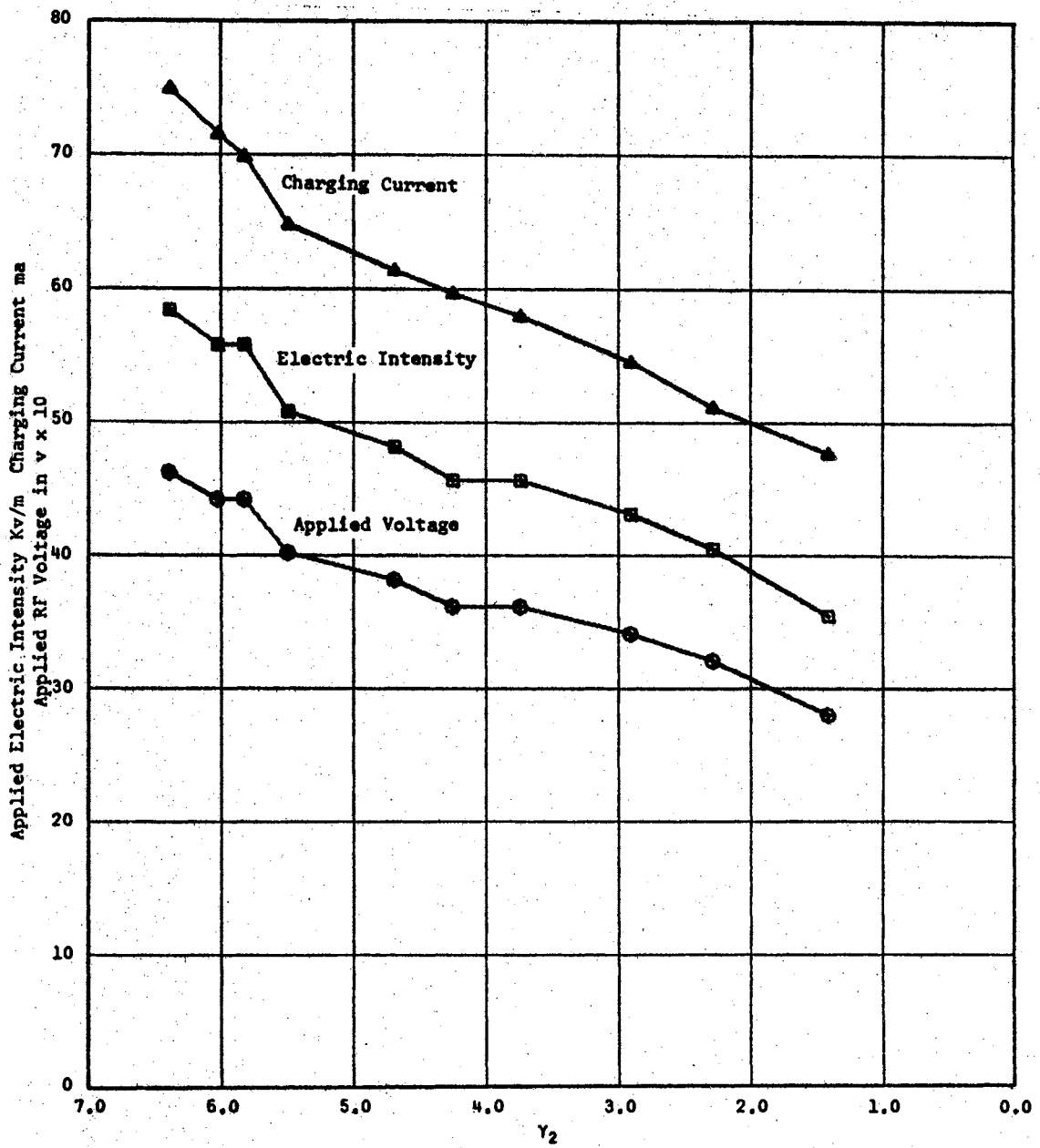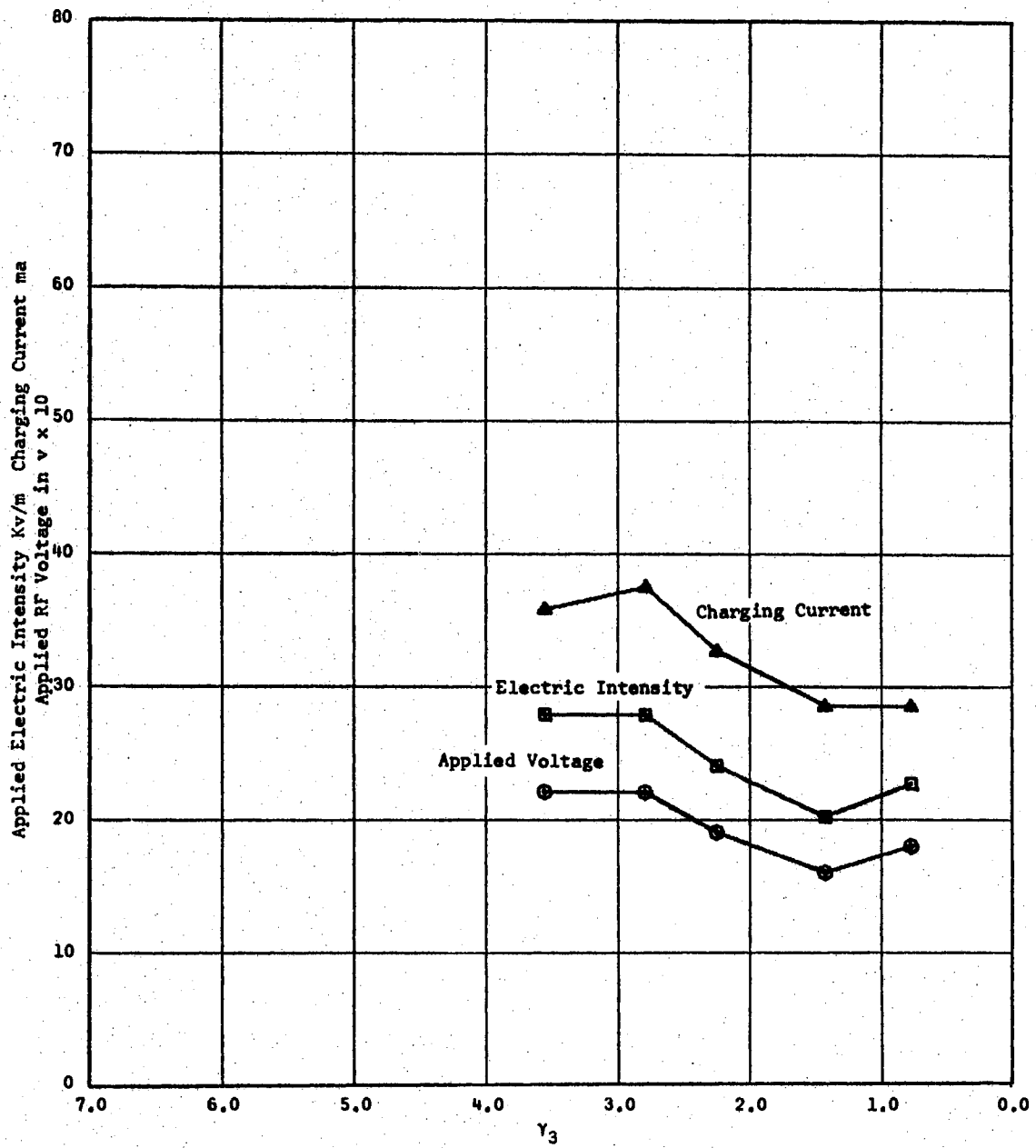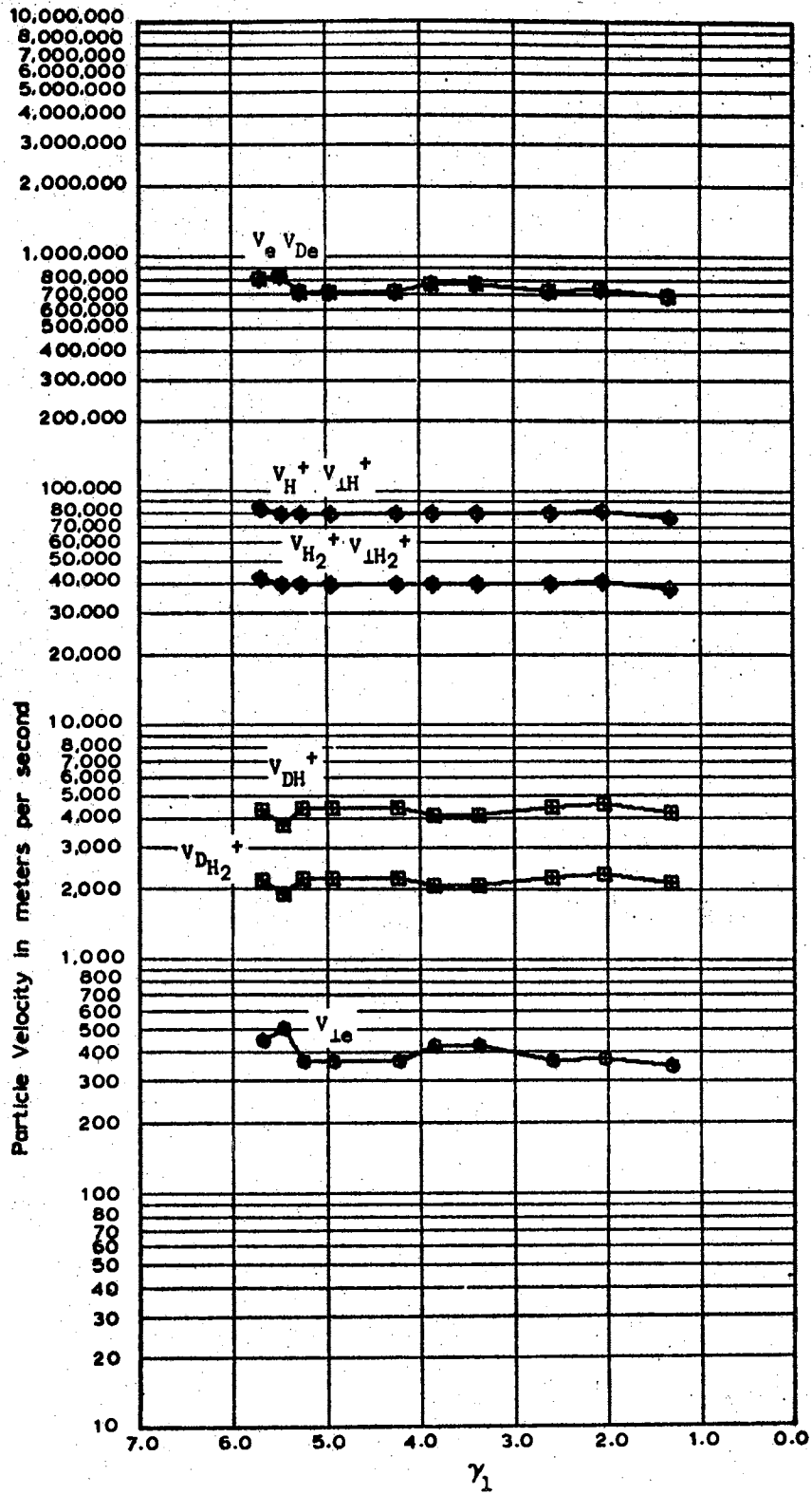Figure 85b. Data taken June 9, 1966 at 30 MH_z with the Aluminum Cell, D = 0.002794 meters
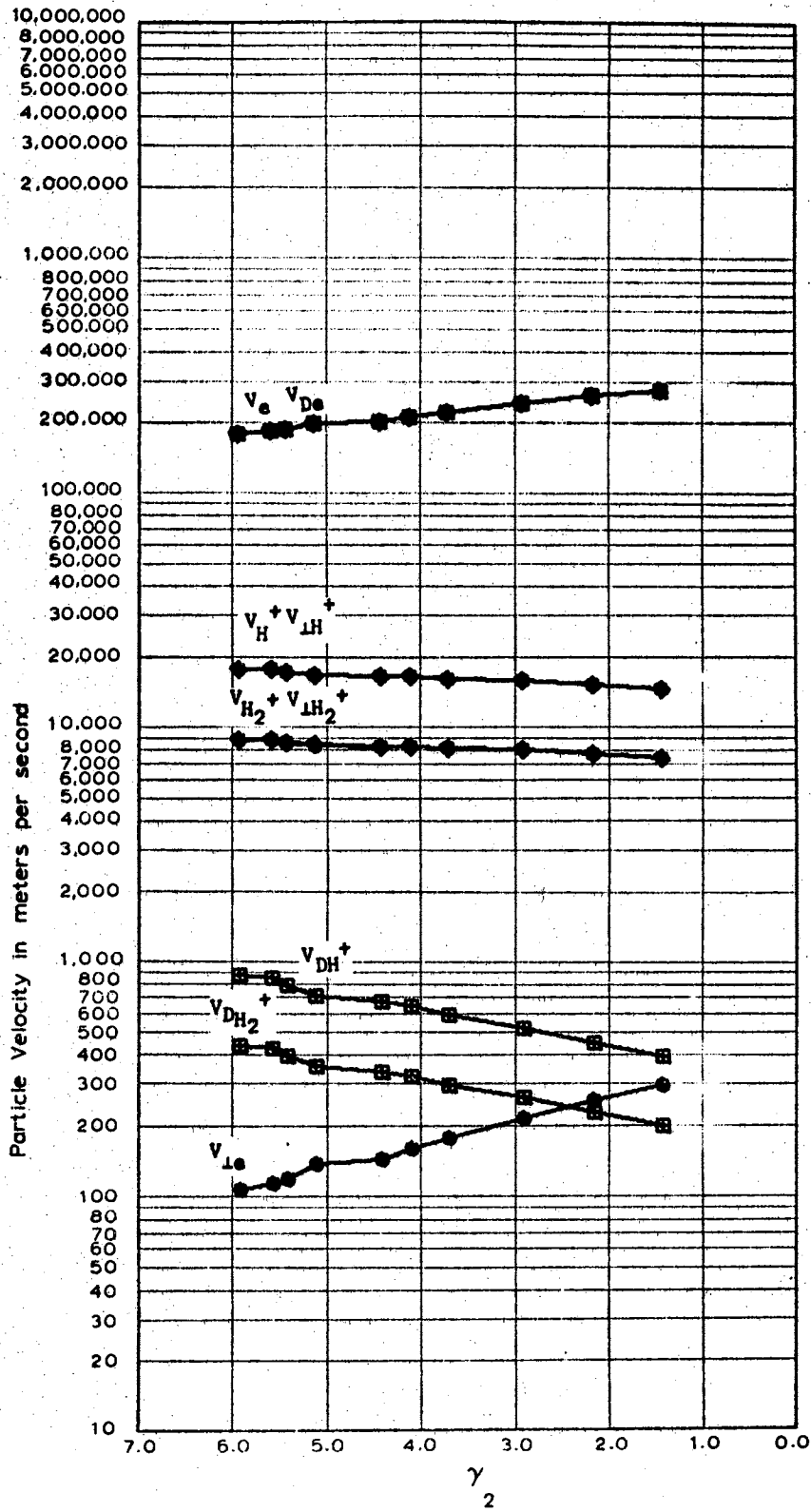
Figure 85c. Data taken June 9, 1966 at 30 MH$_z$ with the Aluminum Cell, D $\cong$ 0.002794 meters

CHAPTER VI

DISCUSSION AND CONCLUSIONS

As illustrated in Figures 40 through 62, pages 76 through 184

of the preceding chapter, the measured data up to approximately 9 MH_z

appears to fit the simple analysis presented in Chapter II to a

reasonable degree. This is evidenced by the velocity plots, where it

is seen that the electron velocity components V_e and V_{D_e} are substan-

tially greater than the other components along the γ_1-line, while

the $V_H{}^+$ components and/or the $V_{H_2^+}$ components are the larger along

the γ_2-line. A feature of these graphs which is not explained by

the theory is that the molecular ion, $H_2{}^+$, rather than the atomic

ion, H^+, is in the vicinity of gyromagnetic resonance along the

γ_2-line at the 3 and 4 MH_z frequencies. The vicinity of gyromagnetic

resonance is indicated by a steep slope at high values on the velocity

curve, e.g., Figure 45 e., page 99. The computer, of course, cannot

compute an infinity, so the facility for truncating the poles in the

velocity curves was built into the program. Then, poles indicating

gyromagnetic resonance appear as triangular spikes in the curves,

such as $V_H{}^+$ in Figure 54 e., page 144. At 5 MH_z we see the indication

of a transition from $H_2{}^+$ to H^+ in Figures 49 e. and 50 e., pages 119

and 124. Here, the indication is that $H_2{}^+$ is the higher velocity

particle at lower values of $\bar{B}$ and pressure while H^+ is the faster

at higher values of $\bar{B}$ and pressure. At 6 MH_z, this transition appears

282

to be complete, since as indicated by Figures 51 e. and 52 e., pages

129 and 134 respectively, H^+ is the higher velocity particle. We

know of no reason why one should predict that the gas would behave in

this manner. However, the above observations from the velocity plots

does appear to clear up what was previously thought to be a discrepancy

in the theory. Assuming the γ_2-line to always be due to the H^+ particle,

one would predict on the basis of Equations 2.13, 2.18, and 2.20 of

Chapter II that the γ-lines should become increasingly farther apart

with increasing excitation frequency. However, as Figures 40 a., 41 a.,

42 a., . . , . . ., 52 a., indicate, this is not the case. This may

well be due to inability to distinguish between a γ_2-line brought

about by a H^+ collision mechanism and a γ_3-line brought about by a

H_2^+ collision mechanism in this frequency region because of sensitivity

limitations in the measuring apparatus. On the other hand, it is

equally possible that the two collision mechanisms are so intermingled

here that no clear cut distinction can be made. At any rate, a

study of the velocity plots does appear to explain why the γ-lines

tend to become closer rather that farther apart with increasing

frequency.

The effects of primary electrode spacing were discussed in

Chapter IV and attributed to space charge, which has been neglected

in the theory. One may view the effect upon the velocity computations

well in the 7 MH_z plots, Figures 53 to 59, pages 135 to 165, where

measurements were performed with a variety of electrode spacings. For

spacings up to about 4 millimeters, the gyromagnetic resonance of the

H^+ particle appears on the γ_2-line, as indicated by Figure 52 e.,

page 134. However, at spacings of approximately 6 millimeters the

electron is computed to be the faster particle on the γ_2-line, as indicated by Figure 59 e., page 169. Several effects not accounted for in the computations are possibly coming into play here. First, the presence of a space charge would make the true value of electric intensity much different than the computed value used in the velocity computations. Further, it may be that the character of the space charge, such as stratification, etc., changes with electrode spacing so that even relative comparisons of velocity changes with electrode spacings cannot be made. Then, there is the question of the uniformity of the applied electric intensity. Increasing the electrode spacing will naturally affect the uniformity of the applied electric intensity in an adverse manner, but we have no way of determining to what degree and, in addition, no estimate as to what effects to expect with field non-uniformities. It is problematical as to whether this is a true indication of changes in the velocity patterns with change in electrode spacing, or merely a failure in the mathematical model to take a sufficient number of variables into account.

At 9 MH_z we begin to again observe a transition between H^+ and the electron along the γ_2-line, as indicated by Figures 63 e. and 64 e., pages 189 and 194. Here, the H^+ velocity is computed to be the larger for the lower values of $\overline{B}$ and pressure while the electron velocity is greater for larger values of $\overline{B}$ and pressure. Since this occurs at the approximate 2 millimeters electrode spacing, we have more faith in the indication here than the similar effect at 7 MH_z discussed above. The 10 MH_z data, Figures 65 e. and 66 e., pages 199 and 204, shows this same characteristic along the γ_2-line. At 11 MH_z, Figures 67 a. to 68 g., pages 215 to 216, we begin to pick up a third

γ-line. This appears at the extreme limit of the magnet's capability and, consequently, was missed in taking the first set of data, so it does not appear in Figure 67. The points shown on the γ_3-line in Figure 68 a. are much in doubt due to the limitations of the magnet and the slope of the line is to be taken as definitely in error. At 12 MH$_z$, Figures 69 a. to 70 g., pages 217 to 230, the γ_3-line is well established. The computed indication is that the electron velocity is larger throughout these measurements with the H$^+$ velocity being nearly as great on the γ_3-line. This is somewhat diverse to what would be expected in the way of charged particle velocities in terms of the theory.

As the excitation frequency increases, we begin to lose γ-lines within the range that data can be taken with the present system. At 13 and 14 MH$_z$, Figures 71 a. to 75 c., pages 231 to 249, we begin to lose the γ_1-line. This is thought to be due to the insensitivity of the magnet to small changes at very low values of supply current. At 15 MH$_z$, Figures 76 a. to 77 e., pages 250 to 257, we tend to lose both the γ_1 and γ_3-lines. This trend continues for the remainder of the data, out to 30 MH$_z$, and is thought to be due to limits in range and control of the magnet at both the high and low extremes of its scale. The electron velocity is computed to be the larger throughout this range in excitation frequencies. An exception to this velocity pattern is found in the data taken at 20 MH$_z$. The data taken at approximately 3 millimeter electrode spacings, Figures 78 a. to 79 c., pages 258 to 263, does follow the general pattern described above, but upon increasing the spacing to about 6 millimeters, Figure 80, pages 264 and 266, the data appears to be in the form of a γ_1-line.

Note also that the electron velocity is substantially greater than that computed for the data at the lesser electrode spacing which conforms to the notion of a γ_1-line.

On the basis of the observations discussed above, it is concluded that the simple theory presented in Chapter II is more applicable to the lower excitation frequencies and lesser primary electrode spacings. At frequencies up to about 9 MH_z, the computation of applicable frequencies of gyration does give a reasonable indication of the optimum values of magnetic intensity. However, at the higher excitation frequencies, 9 MH_z and above, the gyration frequencies cannot be construed to give anything more than a coincidental indication of optimum magnetic intensity. As discussed in Chapter IV, it is believed that the neglection of any space charge is the most serious defect in the theory. Efforts have been made to correct this defeat, but the theoretical problem appears to be most difficult and experimental methods for probing the region between the primary electrodes, other than the rough secondary electrode measurements discussed in Chapter IV, are not feasible due to the restrictive dimensions of the cell geometry. It has been suggested that this discrepancy at the higher frequencies might be due to the excitation frequency becoming sufficiently close to the plasma frequency as to instigate another resonance phenomenon. However, assuming that the degree of ionization is of the order of 10^{-4}, a typical value for a slightly ionized gas, one estimates an electron plasma frequency in the vicinity of 9 GH_z and above for the pressures employed in this study. On the same basis, plasma frequencies for the positive ions H^+, H_2^+, and H_3^+ are estimated to range from 100 to a few hundred MH_z. Since the degree of

ionization would have to be very much less than the above assumption
in order to bring the plasma frequencies down to the vicinity of the
excitation frequencies, it is considered unlikely that plasma frequency
plays an important part in these measurements.

Despite the limitations in the theory it is believed to be
sufficient, when taken in conjunction with the measured data, to be
of much aid in the formative stages of conception of non-conventional
energy sources. Such devices would naturally employ their own peculiar
electrode and field structures which could deviate considerably from
the geometry of the ionization cells employed in this study. For
this reason, it is recommended with one possible exception that further
studies of this nature of the ionization properties of hydrogen should
follow rather than precede the conception of such an application. In
this way, the more detailed theory and data could be closely tied to
the application. The complexities of the ionization processes are such
as to lead one to believe that this would generally be found essential
to success. The exception to this recommendation is as follows:
It might be found profitable to conduct an experimental study in the
microwave region of excitation frequencies where one could feasibly
create a "super-resonant" condition with the excitation, gyration,
and plasma frequencies all being the same. The argument against
this proposal is that microwave power is more difficult and extremely
expensive to generate, consequently it is difficult to see any appli-
cation of such a study to the field of energy conversion.

A SELECTED BIBLIOGRAPHY

1. Thomson, Sir J. J. and G. P. Thomson, "Conduction of Electricity Through Gases", Cambridge University Press, Third Edition, Vol. 1 (1928).

2. Townsend, J. S., "The Conductivity Produced in Gases by the Motion of Negatively-charged Ions", Nature, No. 1606, Vol. 62, August (1900), pp. 340.

3. Harrison, M. A. and R. Gabelle, "Simultaneous Measurement of Ionization and Attachment Coefficients", Physical Review, Second Series, No. 1, Vol. 91, July (1953), pp. 1-7.

4. Rose, D. J., "Townsend Ionization Coefficient for Hydrogen and Deuterium", Physical Review, Second Series, No. 2, Vol. 104, October (1956), pp. 273-277.

5. DeBitetto, D. J. and L. H. Fisher, "Townsend Ionization Coefficients and Uniform Field Breakdown in Hydrogen and Nitrogen at High Pressures", Physical Review, No. 5, Vol. 104, December (1956), pp. 1213-1220.

6. Haydon, S. C. and A. G. Robertson, "Ionization Coefficients for Hydrogen in Crossed Electric and Magnetic Fields", Proceedings 5th International Conference on Ionization Phenomena in Gases, Munich, (1961), pp. 75-84.

7. DeBittetto, D. J. and L. H. Fisher, "Second Townsend Coefficient in Oxygen at High Pressures", Physical Review, No. 2, Vol. III, July (1958), pp. 390-394.

8. Franck, J. and G. Hertz, Phys. Ges., 16:12 (1914); Phys. Zeits, 17:409 (1916); also discussion in H. E. White, Introduction to Atomic Spectra, McGraw-Hill (1934), pp. 92.

9. Rothe, et. al., "Electron Impact Ionization of Atomic Hydrogen and Atomic Oxygen", Physical Review, No. 2, Vol. 125, January (1962), pp. 582-583.

10. Teller, E., Z. Physik, Vol. 61, (1930), pp. 458: Hettler, W. and F. London, Z. Physik, Vol. 46, (1927), pp. 47, Vol. 47 (1928), pp. 835, Vol. 51, (1929), pp. 805: Wang, S. C. Physical Review, Vol. 31 (1928), pp. 579: Coolidge, A. S. and H. M. James, Journal of Chemical Physics, Vol. 1 (1933), pp. 825: Coulson, C. A., Transactions of the Faraday Society, Vol. 33, (1937),

pp. 1473; Slater, J. C., Quantum Theory of Matter, (1951).

11. Gould, L. and L. W. Roberts, The Breakdown of Air at Microwave Frequencies, Microwave Assoc., Inc., MA-1 (1955).

12. Gould, L., NAVSHIPS INDEX NO. NE-111616 (1956).

13. Cambel, A. B., Plasma Physics and Magnetofluidmechanics, McGraw-Hill, (New York, 1963), pp. 92.

APPENDIX

COMPUTER PROGRAMS

The velocity computations and all plotting of the Optimum Magnetic
Intensity Mapping displayed in Chapter V was accomplished by means
of digital computers. The raw data was first processed by the IBM
7040 to obtain listings of optimum magnetic intensity, pressure,
applied voltage and electric intensity, charging current and the
various charged particle velocities. This program is very much
routine, based on Equations 2.13 through 2.25 of Chapter II. The
principal problems experienced were in programming the magnet calibra-
tion and the correction of vacuum gauge readings to true pressure for
hydrogen. Polynomial curve fitting techniques were employed to program
the magnet calibration, using the library programs available. The
results obtained in fitting the calibration curve for a 8.5 cm gap
are shown in Figure 86. Referring to Figure 87, it is seen that the
fifth power polynomial gives the closer fit to the measured calibration
curve over the entire range of interest. Greater and lesser powers
give greater deviations from the measured curve, so the fifth power
was used in writing the computer program. However, the polynomial
curve fitting techniques failed to suffice for the correction of
vacuum gauge readings. Finally, it was discovered that the pressure
correction nomogram supplied with the instrument plotted as essentially
straight lines on a log-log graph. Then, writing the logarithmic
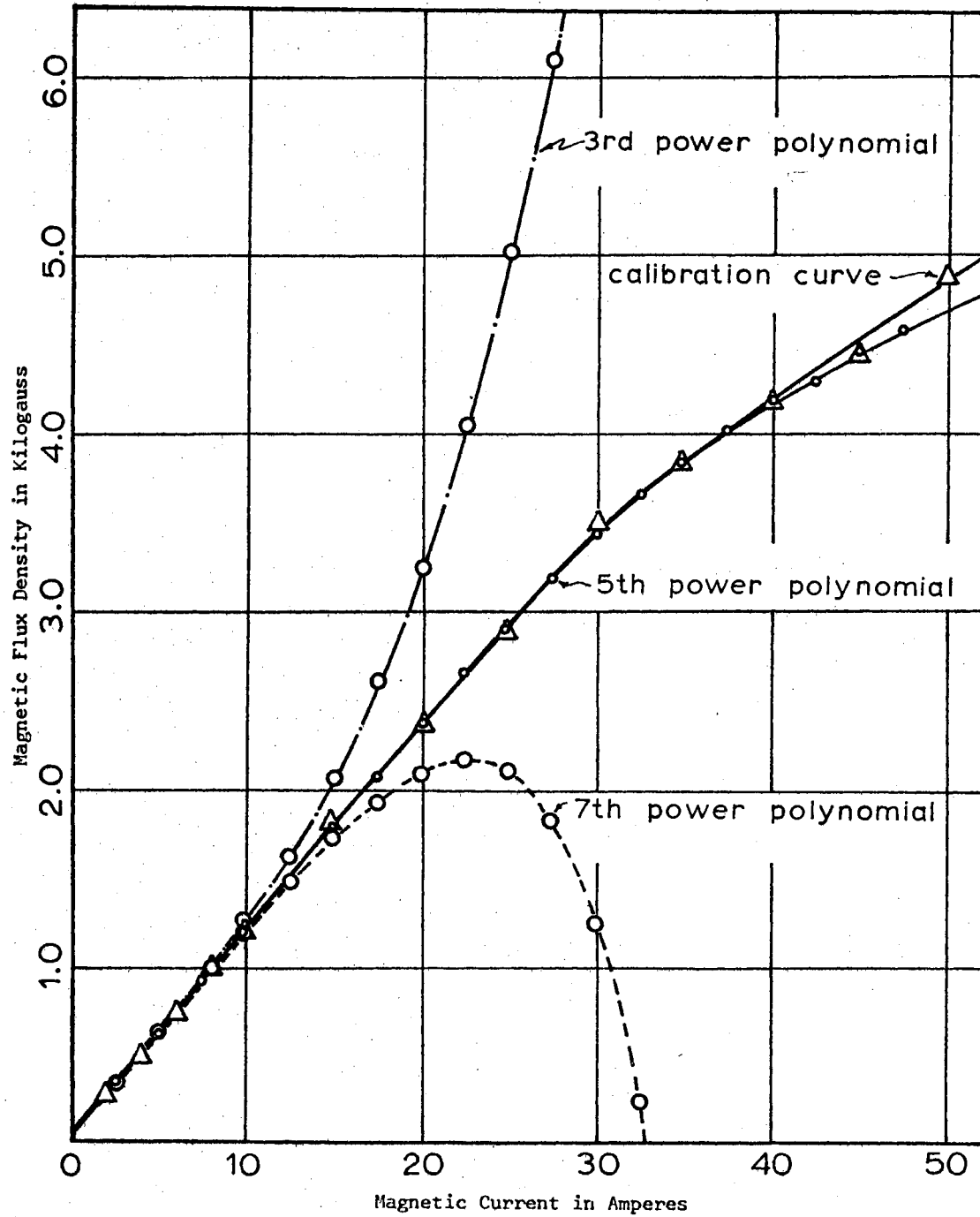
Figure 86. Computed Polynomial Curve Fit of the Magnet
Calibration
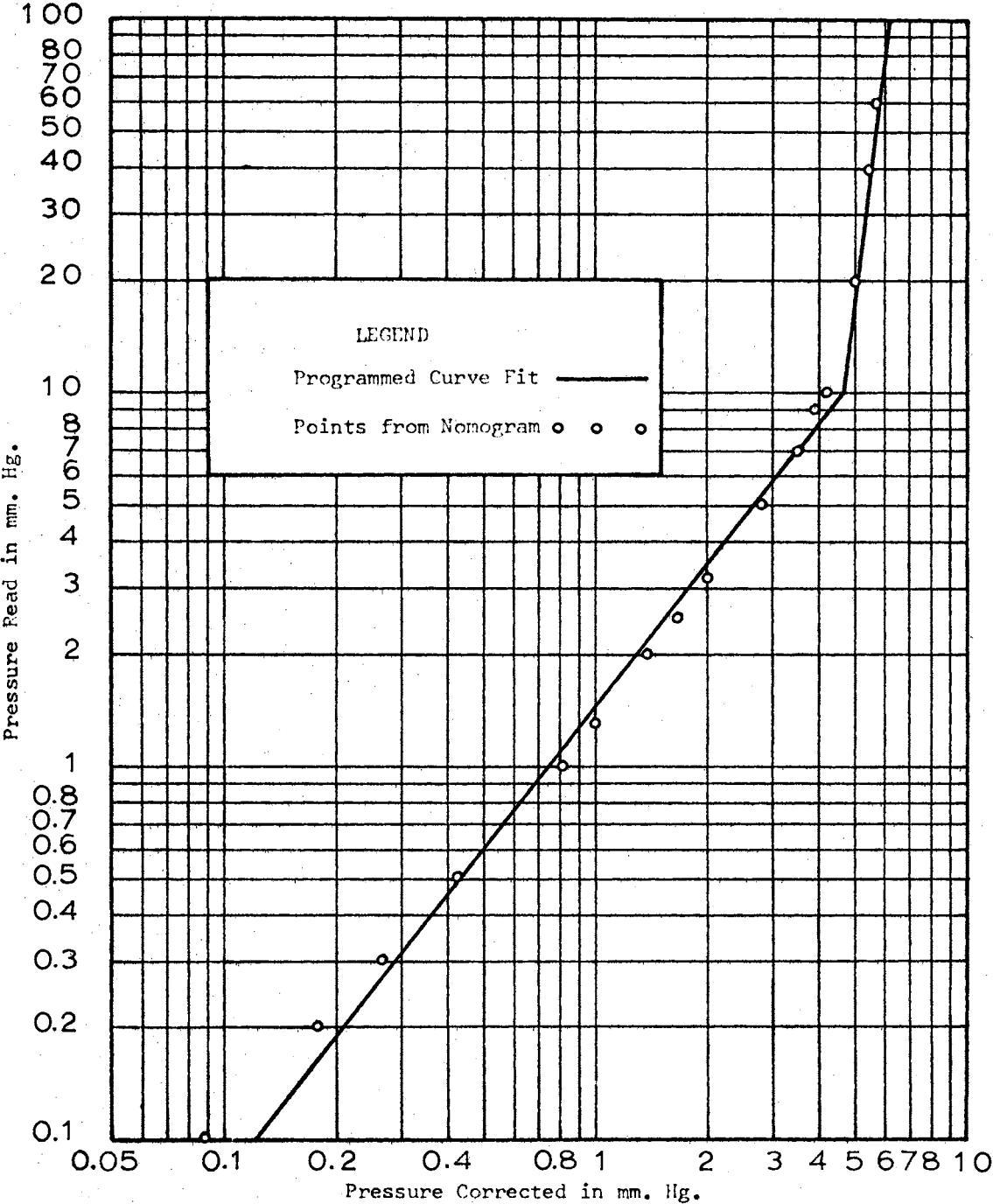
Figure 87. Log-Log Curve Fit of Pressure Correction

equations of the straight lines and programming these into the computer

resulted in the degree of fit indicated in Figure 87. Undoubtedly,

additional effort using the computer could increase the degree of fit

of the magnet calibration and pressure correction curves over that shown

in Figures 86 and 87, but the accuracy of the experimental data was not

considered sufficient to justify this effort.

The complete computer program for processing the raw data is

given on the five sheets of Table I. A sample readout of an output

from this program is shown in Table II. The first block of entries

in Table II, starting with the third card, is the input data to the

program. This is in the following order: excitation frequency in

MH_z, primary electrode spacing in meters, resistance of the rf load

(current sampling resistance) in ohms, the control number 0.0, the

number of data points, and the number 0. The following card lists the

coefficients B_1, B_2, ... B_6 for the 5th power polynomial fit of

the magnet calibration. Its format is 6F10.0. The fifth card in

this listing contains the powers and coefficients for the pressure

correction. The format is 4F10.0 and the numbers read in are P0,

P10, C0 and C10, where for P_{read} < 10 mm Hg,

$$P_{corrected} = (1.0/C0)*(P_{read})**(1.0/P0).$$

For P_{read} > 10 mm Hg, the form of the equation remains the same, but

the coefficients C10 and P10 are used in place of C0 and P0. The

remaining cards list the data taken during the operation of the

ionization cell. The format is 6F10.0 and the values read in are;

magnet current in amperes, the pressure read on gauge tube no. 4 (see

Figure 4) in mm Hg, the pressure on gauge tube no. 3 in mm Hg, mass

TABLE I

IBM 7040 PROGRAM FOR PROCESSING THE RAW DATA

```
$ID           A-0001 C CHEN
$JOB               C CHEN                              7303-51000
$IBJOB DKNAME  NODECK
$IBFTC DKNAME  NODECK
3         DO 630 N=1,2
4         READ(5,220) F,D,R,G,M,K
5         READ(5,221) B1,B2,B3,B4,B5,B6
6         READ(5,222) P0,P10,C0,C10
          DIMENSION A(50,30)
7         K=K+1
10        READ(5,225) CURB,XX1,XX2,FLOW,CUR,V
15        B= B1*(CURB**5)+B2*(CURB**4)+B3*(CURB**3)+B4*(CURB**2)+B5*CURB+B6
19        Y= 1.0/P0
20        Z= 1.0/P10
21        IF(XX1-10.0) 22,22,24
22        XX1C= ((1.0/C0)*XX1)**Y
23        GO TO 25
24        XX1C= ((1.0/C10)*XX1)**Z
25         IF(XX2-10.0) 26, 26, 28
26        XX2C= ((1.0/C0)*XX2)**Y
27        GO TO 30
28        XX2C= ((1.0/C10)*XX2)**Z
30        P=(XX1C+XX2C)/2.0
35        E= (V/D)*0.3536
40        CURTX= (353.6*CUR)/R
45        W=2.0*(3.1416*F)
50        WGE= (17.6*(10.**4)*B)
55        WGH1= 9.6*B
60        WGH2= WGH1/2.0
65        BWEB= B/10.0
70        VDE=E/BWEB
75        V1E=VDE*(F/(2.8*(10.0**4)))*(1.0/B)
80        VETOT= SQRT((VDE**2) + (V1E**2))
85        ENEE= 0.5*(VETOT**2)*9.11/(10.0**31)
90        AMIS=((WGH1**2)/(W**2))-1.0
95        AB= ABS(AMIS)
100       IF(AB-((2.0*B)/(W**2))) 125,125,105
105       V1H1= (15.3/F)*(E/AMIS)
110       VDH1= V1H1*(.77/F)*B
115       VH1TO= SQRT((VDH1**2) + (V1H1**2))
120       ENEH1= .5*(VH1TO**2)*1.6733/(10.0**27)
125       C= ((WGH2**2)/(W**2))-1.0
130       CB= ABS(C)
135       IF(CB-(B/2.0)*(1.0/W**2)) 165,165,140
140       V1H2= (7.7/F)*(E/C)
145       VDH2= V1H2*(.77/F)*B
150       VH2TO= SQRT((VDH2**2) + (V1H2**2))
155       ENEH2= .5*(VH2TO**2)*2.3466/(10.0**27)
160       I=K
165       A(I,1)=F
```

I (Continued)

```
          A(I,2)=B
          A(I,3)=E
          A(I,4)=P
          A(I,5)=FLOW
          A(I,6)=CURTX
170       A(I,7)=F
          A(I,8)=B
          A(I,9)=ENEE
          A(I,10)=VETOT
          A(I,11)=V1E
          A(I,12)=VDE
175       IF(AB-((2.0*B)/(W**2))) 180,180,190
180       A(I,13)=G
          A(I,14)=F
          A(I,15)=B
          A(I,16)=WGH1
          A(I,17)=AMIS
          A(I,18)=G
185       GO TO 195
190       A(I,13)=F
          A(I,14)=B
          A(I,15)=ENEH1
          A(I,16)=VH1TO
          A(I,17)=V1H1
          A(I,18)=VDH1
195       IF(CB-(B/2.0)*(1.0/W**2)) 200,200,210
200       A(I,19)=G
          A(I,20)=F
          A(I,21)=B
          A(I,22)=WGH2
          A(I,23)=C
          A(I,24)=G
205       GO TO 215
210       A(I,19)=F
          A(I,20)=B
          A(I,21)=ENFH2
          A(I,22)=VH2TO
          A(I,23)=V1H2
          A(I,24)=VDH2
215       IF(K.NE.M) GO TO 7
255       I=0
256       I=I+1
260       DO 298 J=1,3
265       MY= 5+ (6*J)
270       MYES= 6+(6*J)
275       IF(A(I,MYES).EQ.G) GO TO 298
280       ANGLE= ATAN(A(I,MY)/A(I,MYES))
285       L=24+J
290       IF(A(I,MY)-0.0) 295,295,297
295       A(I,L)= ANGLE+3.1416
```

I (Continued)

```
296      GO TO 298
297      A(I,L)= ANGLE
298      CONTINUE
299      IF(I.NE.M) GO TO 256
400      WRITE(7,325)
405      WRITE(7,315)
410      WRITE(7,376) A(1,1)
         WRITE(7,380)
415      WRITE(7,335)
         L=0
         I=0
420      I=I+1
         L=I+1
425      WRITE(7,300) A(I,4),A(I,5),A(I,2),A(I,3),A(I,6)
         IF(A(I,4).GT.A(L,4)) GO TO 600
426      IF(L.NE.M) GO TO 420
         WRITE(7,300) A(L,4),A(L,5),A(L,2),A(L,3),A(L,6)
430      WRITE(7,310)
435      WRITE(7,315)
440      WRITE(7,375) A(1,1)
445      WRITE(7,316)
         WRITE(7,380)
450      WRITE(7,320)
         L=0
         I=0
455      I=I+1
         L=I+1
460      WRITE(7,305) A(I,4),A(I,10),A(I,25),A(I,11),A(I,12),A(I,9)
         IF(A(I,4).GT.A(L,4)) GO TO 610
461      IF(L.NE.M) GO TO 455
         WRITE(7,305) A(L,4),A(L,10),A(L,25),A(L,11),A(L,12),A(L,9)
465      WRITE(7,310)
470      WRITE(7,315)
475      WRITE(7,375) A(1,1)
480      WRITE(7,317)
         WRITE(7,380)
495      WRITE(7,320)
         L=0
500      K=0
505      K=K+1
         L=K+1
510      IF(A(K,13).EQ.G) GO TO 525
515      WRITE(7,305) A(K,4),A(K,16),A(K,26),A(K,17),A(K,18),A(K,15)
         IF(A(K,4).GT.A(L,4)) GO TO 615
         IF(L.EQ.K) GO TO 535
516      IF(L.NE.M) GO TO 505
         K=L
         GO TO 510
525      WRITE(7,340) A(K,4),A(K,14),A(K,15),A(K,16),A(K,17)
         IF(A(K,4).GT.A(L,4)) GO TO 615
```

I (Continued)

```
        IF(L.EQ.K) GO TO 535
        IF(L.NE.M) GO TO 505
        K=L
        GO TO 510
530     GO TO 505
535     WRITE(7,310)
540     WRITE(7,315)
545     WRITE(7,375) A(1,1)
550     WRITE(7,318)
        WRITE(7,380)
555     WRITE(7,320)
        L=0
560     K=0
565     K=K+1
        L=K+1
570     IF(A(K,19).EQ.G) GO TO 585
575     WRITE(7,305) A(K,4),A(K,22),A(K,27),A(K,23),A(K,24),A(K,21)
        IF(A(K,4).GT.A(L,4)) GO TO 620
        IF(L.EQ.K) GO TO 630
576     IF(L.NE.M) GO TO 565
        K=L
        GO TO 570
585     WRITE(7,340) A(K,4),A(K,20),A(K,21),A(K,22),A(K,23)
        IF(A(K,4).GT.A(L,4)) GO TO 620
        IF(L.EQ.K) GO TO 630
        IF(L.NE.M) GO TO 565
        K=L
        GO TO 570
590     GO TO 565
600     WRITE(7,381)
        WRITE(7,335)
        GO TO 426
610     WRITE(7,381)
        WRITE(7,320)
        GO TO 461
615     WRITE(7,381)
        WRITE(7,320)
        GO TO 516
620     WRITE(7,381)
        WRITE(7,320)
        GO TO 576
630     CONTINUE
        CALL EXIT
340     FORMAT (5H POLE,3F10.3,2E17.7)
220     FORMAT (4F10.0,2I10)
221     FORMAT (6F10.0)
222     FORMAT (4F10.0)
225     FORMAT (6F10.0)
300     FORMAT(4X F10.2,F12.2,F12.3,F15.2,F10.2)
305     FORMAT (F6.2,F12.1,F11.3,F12.1,F14.1,E15.5)
```

I (Continued)

```
310    FORMAT (18X 37H VELOCITY AND ENERGY COMPUTATIONS FOR/)
315    FORMAT (31X 9H HYDROGEN /)
316    FORMAT(23X 26H CALCULATIONS FOR ELECTRON ///)
317    FORMAT(23X 28H CALCULATIONS FOR ATOMIC ION ///)
318    FORMAT(21X 31H CALCULATIONS FOR MOLECULAR ION ///)
320    FORMAT (2X 2H P,6X 8H V TOTAL,5X 6H ANGLE,5X 8H V PERP.,
       25X 8H V DRIFT,6X 7H ENERGY)
325    FORMAT ( 25X 22H EXPERIMENTAL DATA FOR /)
335    FORMAT(7X 9H PRESSURE,2X 10H MASS FLOW,5X 2H B,13X 2H E,
       26X 8H CURRENT)
375    FORMAT(28X F6.3,11H MEGACYCLES /)
376    FORMAT(28X F6.3,11H MEGACYCLES ///)
380    FORMAT(23X 17H GAMMA-ONE VALUES /)
381    FORMAT(/ 23X 17H GAMMA-TWO VALUES /)
       END
$ENTRY
$IBSYS
```

TABLE II

SAMPLE READOUT OF OUTPUT FROM RAW DATA PROCESSING PROGRAM

```
          1    10    4
        DATA TAKEN JULY 9 . 1966 AL CELL R=52.0 OHMS D=.002794 METERS
6.0          .002794    52.0        0.0                    14              0
.00          .00000034 -.00004922.00134888 .11554310 .06476900
 1.25         8.35       1.48        .0000273
6.5          2.4        1.55       10.0        6.0         730.0
5.5          4.1        2.5        20.0        5.8          710.0
5.5          6.1        3.5        30.0        5.7         700.0
5.5          8.5        4.6        40.0        5.6         690.0
5.5          9.0        5.0        50.0        5.6         690.0
5.7         20.0        7.0        70.0        5.6         690.0
5.7         33.0       10.0       100.0        5.8         710.0
5.8         57.0       17.0       150.0        5.9         710.0
6.2         83.0       24.0       200.0        6.0         720.0
6.2        150.0       43.0       300.0        6.1         740.0
22.5         2.4        1.55       10.0        4.2         530.0
30.0         4.1        2.5        20.0        4.8         600.0
40.0         6.1        3.5        30.0        5.2         640.0
45.0         8.5        4.5        40.0        5.5         680.0
```

EXPERIMENTAL DATA FOR
HYDROGEN
6.000 MEGACYCLES

GAMMA-ONE VALUES

PRESSURE	MASS FLOW	B	E	CURRENT
1.25	10.00	0.860	92386.54	40.80
1.89	20.00	0.733	89855.40	39.44
2.55	30.00	0.733	88589.83	38.76
3.26	40.00	0.733	87324.27	38.08
3.44	50.00	0.733	87324.27	38.08
4.25	70.00	0.758	87324.27	38.08
4.98	100.00	0.758	89855.40	39.44
5.33	150.00	0.771	89855.40	40.12
5.56	200.00	0.822	91120.97	40.80
5.97	300.00	0.822	93652.11	41.48

GAMMA-TWO VALUES

PRESSURE	MASS FLOW	B	E	CURRENT
1.25	10.00	2.874	67075.16	28.56
1.89	20.00	3.692	75934.14	32.64
2.55	30.00	4.565	80996.42	35.36
3.24	40.00	4.905	86058.70	37.40

II (Continued)

VELOCITY AND ENERGY COMPUTATIONS FOR
HYDROGEN
6.000 MEGACYCLES

CALCULATIONS FOR ELECTRON

GAMMA-ONE VALUES

P	V TOTAL	ANGLE	V PERP.	V DRIFT	ENERGY
1.25	1074413.1	0.000	267.7	1074413.0	0.52581E-18
1.89	1225554.2	0.000	358.2	1225554.2	0.68415E-18
2.55	1208292.9	0.000	353.1	1208292.8	0.66502E-18
3.26	1191031.6	0.000	348.1	1191031.5	0.64615E-18
3.44	1191031.6	0.000	348.1	1191031.5	0.64615E-18
4.25	1151376.8	0.000	325.3	1151376.7	0.60384E-18
4.98	1184750.0	0.000	334.7	1184750.0	0.63935E-18
5.33	1165323.9	0.000	323.8	1165323.9	0.61856E-18
5.56	1108852.7	0.000	289.1	1108852.7	0.56006E-18
5.97	1139654.2	0.000	297.2	1139654.1	0.59161E-18

GAMMA-TWO VALUES

P	V TOTAL	ANGLE	V PERP.	V DRIFT	ENERGY
1.25	233398.2	0.000	17.4	233398.2	0.24813E-19
1.89	205699.2	0.000	11.9	205699.2	0.19273E-19
2.55	177428.4	0.000	8.3	177428.4	0.14340E-19
3.24	175460.6	0.000	7.7	175460.6	0.14023E-19

VELOCITY AND ENERGY COMPUTATIONS FOR
HYDROGEN
6.000 MEGACYCLES

CALCULATIONS FOR ATOMIC ION

GAMMA-ONE VALUES

P	V TOTAL	ANGLE	V PERP.	V DRIFT	ENERGY
1.25	248952.0	4.602	-247449.9	-27306.4	0.51853E-16
1.89	238455.4	4.619	-237406.8	-22338.0	0.47573E-16
2.55	235096.8	4.619	-234063.0	-22023.4	0.46242E-16
3.26	231738.3	4.619	-230719.3	-21708.8	0.44930E-16
3.44	231738.3	4.619	-230719.3	-21708.8	0.44930E-16
4.25	232397.7	4.615	-231304.6	-22513.4	0.45186E-16
4.98	239133.8	4.615	-238009.1	-23166.0	0.47844E-16
5.33	239483.5	4.614	-238319.5	-23582.9	0.47984E-16
5.56	244346.8	4.607	-242999.2	-25626.5	0.49952E-16
5.97	251134.2	4.607	-249749.2	-26338.3	0.52766E-16

GAMMA-TWO VALUES

P	V TOTAL	ANGLE	V PERP.	V DRIFT	ENERGY
1.25	392521.9	4.359	-368273.6	-135823.3	0.12891E-15
1.89	1841752.0	4.270	-1664422.3	-788510.6	0.28380E-14
2.55	681325.1	1.041	587870.8	344400.8	0.38838E-15
3.24	463089.5	1.009	391915.0	246687.1	0.17942E-15

II (Continued)

VELOCITY AND ENERGY COMPUTATIONS FOR HYDROGEN
6.000 MEGACYCLES

CALCULATIONS FOR MOLECULAR ION

GAMMA-ONE VALUES

P	V TOTAL	ANGLE	V PERP.	V DRIFT	ENERGY
1.25	120729.6	4.602	-120001.1	-13242.3	0.17102E-16
1.89	116842.0	4.619	-116328.2	-10945.5	0.16018E-16
2.55	115196.3	4.619	-114689.7	-10791.3	0.15570E-16
3.26	113550.7	4.619	-113051.3	-10637.2	0.15128E-16
3.44	113550.7	4.619	-113051.3	-10637.2	0.15128E-16
4.25	113655.6	4.615	-113121.0	-11010.3	0.15156E-16
4.98	116949.9	4.615	-116399.9	-11329.5	0.16048E-16
5.33	117005.4	4.614	-116436.7	-11522.0	0.16063E-16
5.56	118888.6	4.607	-118232.9	-12468.7	0.16584E-16
5.97	122191.0	4.607	-121517.2	-12815.1	0.17518E-16

GAMMA-TWO VALUES

P	V TOTAL	ANGLE	V PERP.	V DRIFT	ENERGY
1.25	105930.5	4.359	-99386.6	-36654.9	0.13166E-16
1.89	138407.6	4.270	-125081.3	-59256.5	0.22477E-16
2.55	181932.9	4.182	-156977.9	-91964.6	0.38836E-16
3.24	213927.8	4.151	-181048.1	-113959.0	0.53696E-16

flow in std. cc/min., peak to peak value of the waveform across the

current sampling resistance in volts, and the peak to peak value of

the applied voltage in volts. The separation into γ-line values is

accomplished by the arrangement of these data cards. They should

begin with the low magnet current and low mass flow readings and progress

through the highest mass flow readings before introducing the upper

magnet current values. The program employs a DO loop to allow the

running of any number of data sets at one time. This is controlled

by appropriately indexing in statement no. 3 of the program.

The output from the raw data processing program is divided into

four parts, as shown in Table II. The first part groups the processed

experimental data in accordance with the γ-lines. Cell pressure is

listed in mm Hg, mass flow in std. cc/min., optimum magnetic intensity

B in kilogauss, applied electric intensity E in volts per meter and

charging current in milliamperes. The optimum magnetic intensity

and applied electric intensity values are appropriately substituted

into equations 13 through 25 of Chapter II to order to compute the

charged particle velocities shown in the remaining parts of Table II.

These following three parts group the velocity computations for the

electron, the atomic ion, and the molecular ion respectively in

accordance with the γ-lines. The velocities are listed in meters per

second and minus signs are used to indicate that the direction of

a particular velocity component is opposite to that of the same

component for an electron. The angle of total velocity is measured

in radians with respect to the electron drift velocity component,

V_{D_e}, and energies computed on the basis of $\frac{1}{2}mv^2$ are listed in Newton-

meters. The discovery, discussed in Chapter IV, that the applied

voltage tends to a constant independent of the electrode spacing largely destroys any significance that this later computation may have had otherwise and consequently, it was ignored in plotting the data.

All of the graphs shown in Chapter V were drawn by a combination of the IBM 1620 digital computer with disc storage and the Calcomp 565 automatic plotter with liquid ink conversion. The liquid ink conversion proved to be essential in order to obtain satisfactory photographic reproduction. The program for making the data plots is given in the eight sheets of Table III and consists of five linked sub-programs which were stored on the disc. The total output from the IBM 7040 raw data processing program, as shown in Table II, for example, constitutes the input data to this program. The essential steps written into the program of Table III are as follows: (1) read in the data, (2) plot cell pressure versus optimum magnetic intensity and then compute least squares fits to these points so as to form the γ-lines, (3) scale off the γ-lines to form the abscissa of the following graphs, (4) plot applied voltage, electric intensity, and charging current as a function of the appropriate γ-variable, (5) scale the computed velocity components logarithmically and plot as a function of the appropriate γ-variable.

TABLE III

IBM 1620 PROGRAM FOR LEAST-SQUARES FITTING THE

Y-LINES AND DATA PLOTTING

```
340003200701360003200702490240251196361300102
ZZJOB
ZZFOR
*LDISKPROG1
      ODIMENSION IND(11),A(15),B(15),C(15),D(15),E(15),GXX(2),HXX(2),
     1DISTO(15),DISTT(15)
      COMMON N1,N2,IND,GXX,HXX,DISTO,DISTT
      READ 101,INDEX,N1,N2
      READ  102, DUMMY,DUMYY,DUYYY,DYYYY,YYYYY,DDDDD,DUDUD,UUUUU
      PRINT 102, DUMMY,DUMYY,DUYYY,DYYYY,YYYYY,DDDDD,DUDUD,UUUUU
      DEFINE DISK (10,70)
      FIND (INDEX)
      DO 2 I=1,3
    2 READ 102, DUMMY
      IND(1)= INDEX
      RECORD (INDEX) N1,N2
      IND(2)= INDEX
C  READ AND RECORD VOLTAGES
      DO 10 I=1,N1
   10 READ 106, A(I)
      RECORD (INDEX) (A(I),I= 1,N1)
      IF (N2) 16,16,12
   12 DO 14 I= 1,N2
   14 READ 106, A(I)
      IND(3)= INDEX
      RECORD (INDEX) (A(I), I= 1, N2)
   16 IND(4)= INDEX
      DO 18 I=1,11
   18 READ 102, DUMMY
C  READ AND RECORD PRESSURE  MASS FLOW  B  E  CURRENT
      DO 20 I= 1, N1
   20 READ 109, A(I),B(I),C(I),D(I),E(I)
      RECORD (INDEX) (A(I),B(I),C(I),D(I),E(I),I=1,N1)
      IF (N2) 30,30,21
   21 DO 22 I= 1,4
      DO 22 I= 1,4
   22 READ 102, DUMMY
   24 IND(5)= INDEX
      DO 26 I=1,N2
   26 READ 109, A(I),B(I),C(I),D(I),E(I)
      RECORD (INDEX) (A(I),B(I),C(I),D(I),E(I),I=1,N2)
   30 DO 50 M=1,3
      MM= 2*M+4
      IND(MM)= INDEX
      DO 31 I=1,13
   31 READ 102, DUMMY
      DO 32 I=1,N1
   32 READ 112, A(I),B(I),C(I),D(I),E(I)
      RECORD (INDEX) (A(I),B(I),C(I),D(I),E(I),I=1,N1)
      IF (N2) 50,50,33
```

III (Continued)

```
 33 DO 34 I= 1,4
    DO 34 I=1,4
 34 READ 102, DUMMY
 36 MM= 2*M+5
    IND(MM)= INDEX
    DO 38 I= 1,N2
 38 READ 112, A(I),B(I),C(I),D(I),E(I)
    RECORD (INDEX) (A(I),B(I),C(I),D(I),E(I),I=1,N2)
 50 CONTINUE
101 FORMAT(5X,I5,3X,I2,3X,I2)
102 FORMAT(20A4)
106 FORMAT(25X,25X,F10.4)
109 FORMAT (4X,F10.2,F12.2,F12.3,F15.2,F10.2)
112 FORMAT (6X,F12.1,F11.3,F12.1,F14.1,E15.5)
    CALL LINK(PROG2)
    END
```

III (Continued)


```
ZZFOR
*LDISKPROG2
     ODIMENSION IND(11),A(15),B(15),C(15),D(15),E(15),GXX(2),HXX(2),
     1DISTO(15),DISTT(15)
      COMMON N1,N2,IND,GXX,HXX,DISTO,DISTT
      DEFINE DISK (10,70)
      FIND(IND(1))
      CALL PLOT (201,0.0,7.0,7.0,7.0,0.0,7.0,7.0,7.0)
      M= 1
      J= N1
   20 PS= 0.0
      BS= 0.0
      PQ= 0.0
      PB= 0.0
      IF(M-1) 50,50,60
   50 INDE= IND(4)
      GO TO 70
   60 INDE= IND(5)
   70 FETCH(INDE)(A(I),B(I),C(I),D(I),E(I),I=1,J)
      DO 22 I=1,J
      CALL PLOT (0,C(I),A(I))
      PUNCH TAPE 82
   82 FORMAT(23H96601111333355557777922)
      PS= PS+A(I)
      BS= BS+C(I)
      PQ=PQ+A(I)**2.
   22 PB= PB+A(I)*C(I)
      AN=J
      DE= AN*PQ-PS**2.
      H= (BS*PQ-PS*PB)/DE
      G= (AN*PB-BS*PS)/DE
      BEND= 7.0*G+H
      PEND = 7.0
      IF (BEND-7.0) 31,31,30
   30 BEND = 7.0
      PEND= (7.0-H)/G
   31 CALL PLOT (0,H,0.0)
      CALL PLOT (9,BEND,PEND)
      GXX(M)= G
      HXX(M)= H
      GO TO (40,42),M
   40 IF(N2-2) 42,41,41
   41 M= 2
      J= N2
      GO TO 20
   42 CALL PLOT (99)
      CALL PLOT (9,0.0,0.0)
      CALL LINK(PROG3)
      END
```

III (Continued)

```
ZZFOR
*LDISKPROG3
      ODIMENSION IND(11),A(15),B(15),C(15),D(15),E(15),GXX(2),HXX(2),
     1DISTO(15),DISTT(15)
       COMMON N1,N2,IND,GXX,HXX,DISTO,DISTT
       DEFINE DISK (10,70)
       M= 1
       J= N1
   12 G=GXX(M)
       H= HXX(M)
       ABC= 1.0+ G**2.
       RV= 1.0/SQRTF(ABC)
       RH= G*RV
       CALL PLOT (201,0.0,7.0,7.0,7.0,0.0,7.0,7.0,7.0)
       IF (M-1) 50,50,60
   50 INDE= IND(4)
       GO TO 70
   60 INDE= IND(5)
   70 FETCH(INDE)(A(I),B(I),C(I),D(I),E(I),I=1,J)
       DO 20 I= 1,J
       BB = (G*(G*H-A(I))+C(I))/ABC
       PP=(G*(G*A(I)+H-C(I)))/ABC
       DISTN= SQRTF((C(I)-BB)**2.+(A(I)-PP)**2.)
       PPROJ= DISTN*RV
       BPROJ= DISTN*RH+H
       CALL PLOT (90,BPROJ,PPROJ)
       PUNCH TAPE 82
   82 FORMAT (10H0337777339)
       IF(M-1)  51,51,61
   51 DISTO(I)= DISTN
       GO TO 20
   61 DISTT(I)= DISTN
   20 CONTINUE
       GO TO (21,23),M
   21 IF (N2-2) 23,22,22
   22 M= 2
       J= N2
       GO TO 12
   23 CALL PLOT (7)
       PRINT 102
  102 FORMAT(20HNEW PAPER THEN START)
       PAUSE
       CALL LINK(PROG4)
       END
```

III (Continued)


```
ZZFOR
*LDISKPROG4
      ODIMENSION IND(11),A(15),B(15),C(15),D(15),E(15),GXX(2),HXX(2),
     1DISTO(15),DISTT(15)
      COMMON N1,N2,IND,GXX,HXX,DISTO,DISTT
      DEFINE DISK (10,70)
      CALL PLOT (201,0.0,12.0,12.0,12.0,0.0,7.0,7.0,7.0)
C  READ IN DATA OF E AND CURRENT FOR GAMA ONE OR TWO
      M=1
      J=N1
      INDE=IND(4)
   70 FETCH (INDE)(A(I),B(I),C(I),D(I),E(I),I=1,J)
C  SCALE THE DATA AND PLOT
      DO 1 I=1,J
      IF (D(I)-80000.0) 1,1,2
    1 CONTINUE
      GO TO 4
    2 DO 3 I=1,J
    3 D(I)= D(I)-40000.0
      PRINT 103
    4 DO 5 I= 1,J
      IF (E(I)-80.0) 5,5,6
    5 CONTINUE
      GO TO 8
    6 DO 7 I= 1,J
    7 E(I)=E(I)-40.0
      PRINT 104
    8 IF (M-1) 51,51,61
   51 DO 10 I=1,J
   10 A(I)=DISTO(I)
      GO TO 71
   61 DO 12 I=1,J
   12 A(I)= DISTT(I)
   71 DO 14 I=1,J
      D(I)=D(I)/10000.
      CALL PLOT (0,D(I),A(I))
      PUNCH TAPE 84
   84 FORMAT(44H966660111111111333333333555555557777777777922220)
   14 CONTINUE
      CALL PLOT (99)
      DO 16 I=1,J
      E(I)=E(I)/10.
      CALL PLOT (0,E(I),A(I))
      PUNCH TAPE 85
   85 FORMAT (36H977701111143434434676676761111193330)
   16 CONTINUE
      CALL PLOT (99)
C  READ IN DATA OF VOLTAGE FOR GAMA ONE OR TWO
      IF (M-1) 52,52,62
   52 INDE= IND(2)
      GO TO 72
```

III (Continued)

```
   62 INDE= IND(3)
   72 FETCH (INDE) (A(I),I=1,J)
C  SCALE THE DATA AND PLOT
      DO 91 I= 1,J
      IF (A(I)-800.0) 91,91,92
   91 CONTINUE
      GO TO 9
   92 DO 93 I= 1,J
   93 A(I) =A(I)-400.0
      PRINT 105
  103 FORMAT (12HE SHIFTED 40   )
  104 FORMAT (18HCURRENT SHIFTED 40)
  105 FORMAT(18HVOLTAGE SHIFTED 40)
    9 IF (M-1) 53,53,63
   53 DO 20 I=1,J
   20 B(I)= DISTO(I)
      GO TO 73
   63 DO 22 I= 1,J
   22 B(I)= DISTT(I)
   73 DO 24 I=1,J
      A(I)= A(I)/100.
      CALL PLOT (0,A(I),B(I))
      PUNCH TAPE 87
   87 FORMAT (42H97777701212323343454556567677878181933333330)
   24 CONTINUE
      CALL PLOT (7)
      PRINT 102
  102 FORMAT(20HNEW PAPER THEN START)
      PAUSE
      IF (N2-2) 36,32,32
   32 IF(M-1) 34,34,36
   34 M= 2
      J= N2
      CALL PLOT (201,0.0,12.0,12.0,12.0,0.0,7.0,7.0,7.0)
      INDE= IND(5)
      GO TO 70
   36 CALL LINK(PROG5)
      END
```

III (Continued)

```
ZZFOR
*LDISKPROG5
      ODIMENSION IND(11),A(15),B(15),C(15),D(15),E(15),GXX(2),HXX(2),
     1DISTO(15),DISTT(15)
      DEFINE DISK (10,70)
      COMMON N1,N2,IND,GXX,HXX,DISTO,DISTT
      M= 1
      J= N1
      MM= 6
    9 CALL PLOT (201,0.0,12.2,8.23,12.2,0.0,7.0,4.385,7.0)
      PRINT 200
  200 FORMAT(8HBLUE PEN)
   10 INDE= IND(MM)
      FETCH (INDE) (A(I),B(I),C(I),D(I),E(I),I=1,J)
      PAUSE
      CALL PLOT (99)
      DO 20 I= 1,J
      A(I)= ABSF(A(I))
      A(I)= A(I)/10.0
      IF (A(I)-1.0) 20,60,60
   60 A(I)= LOGF(A(I))
      CALL PLOT (0,A(I),DISTO(I))
      PUNCH TAPE 150
   20 CONTINUE
      CALL PLOT (99)
      DO 22 I= 1,J
      C(I)= ABSF(C(I))
      C(I)= C(I)/10.0
      IF(C(I)-1.0) 22,62,62
   62 C(I)= LOGF(C(I))
      CALL PLOT (0,C(I),DISTO(I))
      PUNCH TAPE 151
   22 CONTINUE
      CALL PLOT (99)
      DO 24 I= 1,J
      D(I)= ABSF(D(I))
      D(I)= D(I)/10.0
      IF (D(I)-1.0) 24,64,64
   64 D(I)= LOGF(D(I))
      CALL PLOT (0,D(I),DISTO(I))
      PUNCH TAPE 152
   24 CONTINUE
      CALL PLOT (99)
      GO TO (41,42,43,44,45),M
   41 PRINT 201
  201 FORMAT(9HBLACK PEN)
      M= 2
      MM= 8
      GO TO 10
   42 PRINT 202
  202 FORMAT (7HRED PEN)
```

III (Continued)

```
      M= 3
      MM= 10
      GO TO 10
   43 IF(N2-2) 8888,50,50
   50 IF (MM-11) 55,8888,8888
   55 M= 4
      MM= 7
      CALL PLOT (7)
      PRINT 102
  102 FORMAT(20HNEW PAPER THEN START)
      PAUSE
      J= N2
      DO 30 I= 1,J
   30 DISTO(I)= DISTT(I)
      GO TO 9
   44 M= 5
      MM= 9
      PRINT 201
      GO TO 10
   45 MM= 11
      PRINT 202
      M= 3
      GO TO 10
  150 FORMAT(34H977777022222444446666688889333330)
  151 FORMAT(34H96670811213233435455657677871932220)
  152 FORMAT(44H9666601111111113333333335555555577777777922220)
 8888 CALL PLOT (7)
      CALL EXIT
      END
ZZZZ
```

VITA

James Russell McDougal

Candidate for the Degree of

Doctor of Philosophy

Thesis: A STUDY OF THE IONIZATION PROPERTIES OF HYDROGEN IN THE
PRESENCE OF RELATIVELY STRONG MAGNETIC FIELDS

Major Field: Electrical Engineering

Biographical:

Personal Data: Born near Osawatomie, Kansas, March 21, 1929, the
son of Thomas J. and Neva L. McDougal.

Education: Graduated from Lane High School, Lane, Kansas, in
1947; received the Bachelor of Science Degree in Electrical
Engineering from the University of Kansas in February, 1952;
received the Master of Science Degree (Kōgaku Shushi) in
Electrical Communications Engineering from the Tohoku
University, Sendai, Japan, in March, 1955; completed require-
ments for the Doctor of Philosophy Degree in May, 1968.

Professional Experience: From March, 1952, to April, 1955, was
a Lieutenant in the United States Army Corps of Engineers
with assignments as an Electrical Engineering Officer except
for the period November, 1952, to July, 1953, when in Korea.
Industrial experience includes the period June 10, 1957, to
September 2, 1961, at the Boeing Company, Wichita, Kansas,
as a Research Engineer in the Antenna and Microwave Group.
Was employed as an Assistant Professor at the University of
Wichita, Kansas, from September, 1961, to September, 1964;
also, was retained as a part-time consultant by the Boeing
Company during this period. Employed by the School of
Electrical Engineering of Oklahoma State University as an
Instructor from September, 1964, to November, 1967; and as
an Assistant Professor since November, 1967.

Professional Organizations: Member of the Institute of Electrical
and Electronics Engineers and Antennas and Propagation
Professional Group, The Institute of Electrical Communications
Engineers of Japan, Eta Eta Kappa, Sigma Tau, and Scabbard
and Blade.